15 December 2006 | $10

Science

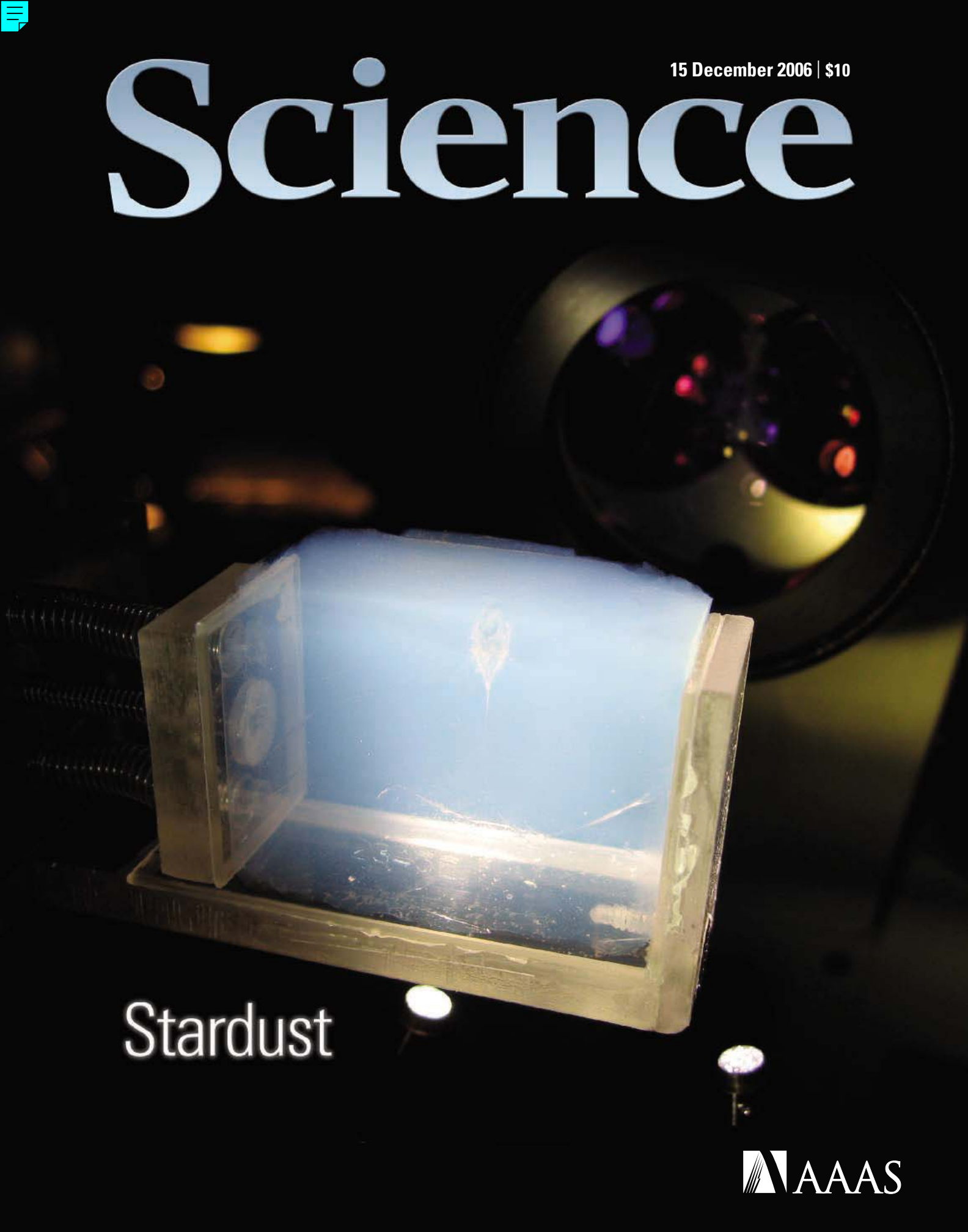

Stardust

AAAS

Volume 314, Issue 5806

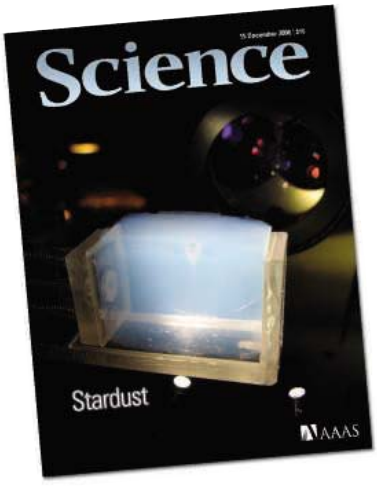

COVER

A large particle of comet dust collected by the NASA Stardust mission generated a carrot-shaped track in a 3-cm-deep silica tile as it was captured. Like the thousands of other particles returned by the mission, this one decelerated from high speed inside the silica aerogel. See the special section beginning on page 1707.

Image: NASA Stardust Team

DEPARTMENTS

EDITORIAL

SPECIAL SECTION

Stardust

INTRODUCTION

PERSPECTIVES

RESEARCH ARTICLE

REPORTS

1707

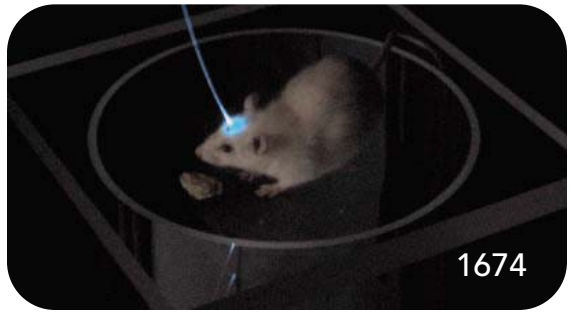

1674

NEWS OF THE WEEK

NEWS FOCUS

CONTENTS continued **>>**

Science

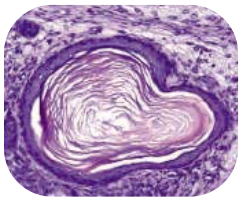

SCIENCE EXPRESS

www.sciencexpress.org

LETTERS

BOOKS *ET AL.*

POLICY FORUM

PERSPECTIVES

ASSOCIATION AFFAIRS

TECHNICAL COMMENT ABSTRACTS

ANTHROPOLOGY

REVIEW

OCEANS

BREVIA

IMMUNOLOGY

RESEARCH ARTICLE

GENETICS

REPORTS

ASTRONOMY

CONTENTS continued >>

REPORTS *CONTINUED...*

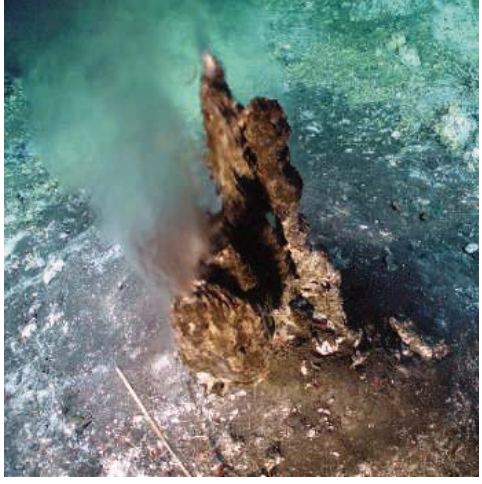

AAAS
ADVANCING SCIENCE, SERVING SOCIETY

SCIENCE (ISSN 0036-8075) is published weekly on Friday, except the last week in December, by the American Association for the Advancement of Science, 1200 New York Avenue, NW, Washington, DC 20005. Periodicals Mail postage (publication No. 484460) paid at Washington, DC, and additional mailing offices.

Domestic individual membership and subscription (51 issues): $139 ($74 allocated to subscription). Domestic institutional subscription (51 issues): $650; Foreign postage extra: Mexico, Caribbean (surface mail) $55; other countries (air assist delivery) $85. First class, airmail, student, and emeritus rates on request. Canadian rates with GST available upon request, GST #1254 88122. Publications Mail Agreement Number 1069624. **Printed in the U.S.A.**

Change of address: Allow 4 weeks, giving old and new addresses and 8-digit account number. **Postmaster:** Send change of address to AAAS, P.O. Box 96178, Washington, DC 20090–6178. **Single-copy sales:** $10.00 current issue, $15.00 back issue prepaid includes surface postage; bulk rates on request.

CONTENTS continued >>

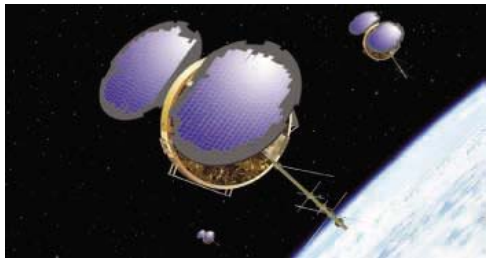

Bumpy ride for satellites.

SCIENCE**NOW**

www.sciencenow.org DAILY NEWS COVERAGE

Heads Up for Space Junk!
Atmospheric warming could increase threats to orbiting spacecraft.

Nuclear Winter Lite
Even a small exchange of WMD could create significant climate effects.

Perfect Hair Is in the Genes
Mice with messy fur provide insights into how a well-ordered mane develops.

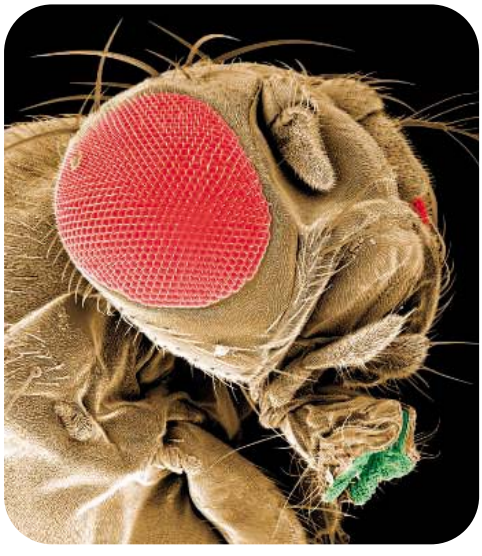

Fly eye organization, a result of noise.

SCIENCE'S **STKE**

www.stke.org SIGNAL TRANSDUCTION KNOWLEDGE ENVIRONMENT

PERSPECTIVE: Intermediate Filaments as Signaling Platforms
H.-M. Pallari and J. E. Eriksson
Novel roles for intermediate filaments depend on their ability to sequester or act as scaffolds for signaling molecules.

REVIEW: From Fluctuations to Phenotypes—The Physiology of Noise
M. S. Samoilov, G. Price, A. P. Arkin
In both single-celled organisms and multicellular organisms, stochastic changes in gene expression lead to different cellular fates.

Put your goals in writing.

SCIENCE **CAREERS**

www.sciencecareers.org CAREER RESOURCES FOR SCIENTISTS

EUROPE: Mastering Your Ph.D.—Setting Goals for Success
P. Gosling and B. Noordam
Committing concrete goals to paper will help you avoid feeling overwhelmed by the tasks ahead.

US: NIH Names First Postdoc Winners
A. Fazekas
NIH Pathways to Independence Award winners hope the honor will make it easier to become independent scientists.

US: Tooling Up—Be Politically Astute, But Don't Play Politics
D. Jensen
You can't avoid politics in the workplace, but you can stay above the fray.

Separate individual or institutional subscriptions to these products may be required for full-text access.

K. lactis Protein Expression Kit from New England Biolabs

YEAST PROTEIN EXPRESSION MADE EASY

The *K. lactis* Protein Expression Kit provides a simple method to clone and express your gene of interest in the yeast *Kluyveromyces lactis*. This system offers many advantages over bacterial systems and eliminates the methanol containing medium and antibiotic requirements of *Pichia pastoris*. With easy-to-use protocols and highly competent *K. lactis* cells included, this system can take you from bench top to large scale production with ease.

Advantages:

- High yield protein expression
- Rapid high cell density growth
- Methanol-free growth media
- Plasmid integration enhances stability
- Acetamide selection enriches for multi-copy integrants, enhancing yield
- Tight control of gene expression enables expression of toxic genes
- Access to eukaryotic protein folding and glycosylation machinery
- Simultaneous expression of multiple proteins
- Ease-of-use for those inexperienced with yeast systems
- Yeast competent cells included
- No license required for research use

***K. lactis* Protein Expression Kit** **E1000**

Kit components sold separately

***K. lactis* GG799 Competent Cells** **C1001**

pKLAC1 Vector **N3740**

	K. lactis	*P. pastoris*
High yield expression	✓	✓
Rapid high cell density growth	✓	✓
Yeast Competent Cells Included	✓	
Methanol-free growth media	✓	
Antibiotic-free Selection	✓	
Enhanced multi-copy integration	✓	
Protein folding and glycosylation	✓	✓
Expression of genes toxic to *E. coli*	✓	✓

Quick comparison of *K. lactis* and *P. pastoris* expression systems.

For more information and international distribution network, please visit www.neb.com

- **New England Biolabs Inc.** 240 County Road, Ipswich, MA 01938 USA 1-800-NEB-LABS Tel. (978) 927-5054 Fax (978) 921-1350 info@neb.com
- **Canada** Tel. (800) 387-1095 info@ca.neb.com
- **Germany** Tel. 0800/246 5227 info@de.neb.com
- **UK** Tel. (0800) 318486 info@uk.neb.com
- **China** Tel. 010-82378266 beijing@neb-china.com

NEW ENGLAND BioLabs® Inc.
the leader in enzyme technology

EDITED BY STELLA HURTLEY AND PHIL SZUROMI

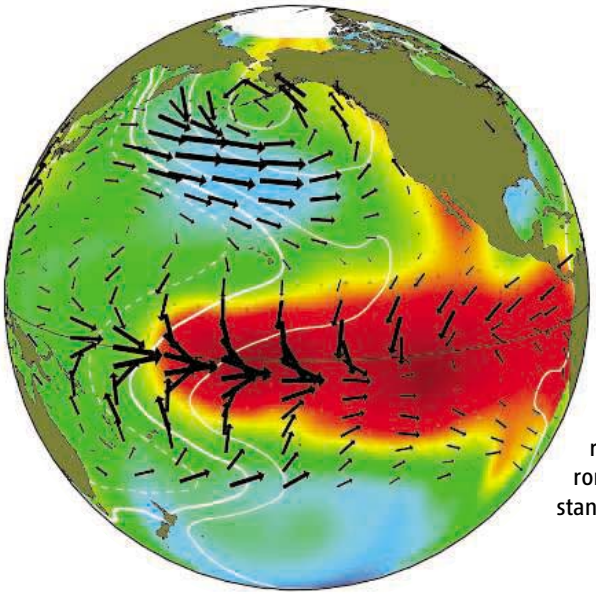

El Niño Integrated

The El Niño–Southern Oscillation, or ENSO, is the most energetic of all of the large-scale, quasi-periodic, ocean-atmosphere climate oscillations that happen on human time scales. Although ENSO occurs in and above the Pacific Ocean, nearly every region of Earth is affected by changes in weather, ecosystems, and the global carbon cycle. **McPhaden *et al.*** (p. 1740) review the physics of ENSO, and its most important environmental and socioeconomic impacts, in order to understand it as an "integrating" concept in earth science.

Rubidium-Rich Stars

When stars get old, they swell into giants. At the bottom of their convecting zones, heavy elements, such as rubidium and strontium, are produced through the s process by slow nuclear reactions involving the capture of neutrons. In hot stars that are several times more massive than the Sun, theory predicts that the neutrons generated by conversion of ^{22}Ne to ^{25}Mg should produce large amounts of the long-lived isotope ^{87}Ru, but little of this material has been observed. **García-Hernández *et al.*** (p. 1751, published online 9 November; see the Perspective by **Boothroyd**) have found the missing Rb in 60 asymptotic giant branch stars in our Galaxy. These stars have levels of ^{87}Ru that are 10 to 100 times greater than that of the Sun but are only three to eight times more massive. The discovery points to metallicity differences in nucleosynthesis reactions in the late stages of the evolution of intermediate-mass stars, and also has implications for isotopic anomalies observed in some presolar grains found in meteorites.

Stalking the Quantum Spin Hall Effect

In the quantum spin Hall effect (QSHE), coupling between the orbital and spin angular momentum of an electron on the edges of a bulk insulating state creates a conduction state that allows charge flow in only one direction. It does not require any external magnetic field (whose presence would break time-reversal symmetry), and it has been suggested that the helical edge states could conduct without dissipation. Although graphene exhibits characteristics of this state, its small energy gap complicates experimental observations. **Bernevig *et al.*** (p. 1757; see the Perspective by **Kane and Mele**) present theoretical work proposing that HgTe/CdTe quantum-well structures should be a more robust QSHE system, and present a outline of how the effect could be experimentally detected.

Coaxial Organic Photoconductor

In an organic photovoltaic devices, separate electron donor and acceptor layers harvest charge carriers created by absorption of photons. **Yamamoto *et al.*** (p. 1761; see the Perspective by **Würthner**) have self-assembled coaxial nanotubes from molecules that contain a large electron-donating aromatic core (hexabenzocoronene) on which is appended, via a long, flexible linker, an electron-accepting trinitrofluoronene group. These nanowires are 16 nanometers in diameter and several micrometers in length. When cast as films on electrodes, the nanotubes show large changes in conductivity (on-off ratios in excess of 10^4) when irradiated with ultraviolet-visible light. The nanotubes avoid formation of a nonconducting charge-transfer complex that was seen in an alternate microfiber morphology of these same molecules.

Grow, Stamp, Stack

The assembly of complex electronic and communication circuitry requires the assembly of several layers of dissimilar materials, and methods such as wafer bonding and epitaxial growth can deposit layers of thin films for the production of complex three-dimensional structures. However, for preformed nanomaterials, such carbon nanotubes or semiconductor nanowires, or materials with limited thermal stability, alternative assembly strategies will be needed for their controlled deposition. **Ahn *et al.*** (p. 1754) have produced nanometer-scale semiconducting materials and then printed them with an additive stamping process. The printing process works well on both rigid and flexible substrates and produces high-quality, robust electronic systems.

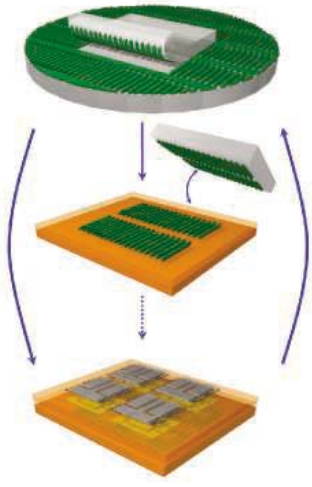

Mitochondrial Footprint of Human Migrations

Modern humans are thought to have dispersed out of Africa along a single southern path—from the Horn of Africa across Bab-el-Mandeb (the Gate of Tears) to the Arabian Gulf and then along the coasts of the Indian Ocean to Southeast Asia and Australasia, a migration route consistent with the known distribution of mitochondrial DNA (mtDNA) genetic markers. Curiously, haplotypoes M1 and U6, which are closely related of some of the predominantly Asian halogroups, are specifically found in North and East Africa. **Olivieri *et al.*** (p. 1767) sequenced a wide-ranging series of M1 and U6 mtDNA genomes and found that populations

Continued on page 1655

CREDITS (TOP TO BOTTOM): MCPHADEN *ET AL.*; AHN *ET AL.*

Thank you

to all of the sponsors and supporters of the 2007 AAAS Annual Meeting

SUBARU

Roche Pharmaceuticals

P&G beauty

L'ORÉAL

NATIONAL SCIENCE FOUNDATION

MERCK

THE SCIENCE CHANNEL

SUPPORTERS

Lawrence Livermore National Laboratory

European Commission

New Zealand Ministry of Research, Science, and Technology

Exploratorium

To become an exhibitor or sponsor of the meeting contact
Jill C. Perla
Manager of Marketing, Exhibits, and Sponsors
E-mail: jperla@aaas.org
Phone: 202-326-6736
Web site: http://www.aaasmeeting.org

In addition, generous funding for AAAS Awards was provided by Johnson & Johnson Pharmaceutical Research & Development L.L.C., GE Healthcare, and Affymetrix.

AAAS
ADVANCING SCIENCE, SERVING SOCIETY

Continued from page 1653

bearing these markers must have arisen in southwestern Asia and then returned to North and East Africa some 40,000 to 45,000 years ago, at a time when changes in climate created fragmented deserts in these areas. Ancestral M1 and U6 populations apparently moved through the Levant when populations from this area were moving into Europe.

Plankton Extinctions in Acidic Oceans

At the Paleocene-Eocene Thermal Maximum (~55 million years ago), rapid increases in atmospheric CO_2 levels in excess of 1000 parts per million by volume (about three times current levels) raised global temperatures by more than 5°C and caused marine and terrestrial extinctions. **Gibbs *et al.*** (p. 1770) used several high-resolution cores to examine the effects of this event on plankton and found little ecological basis for the extinctions. Most of the taxa that went extinct were rare taxa, and these did so rapidly, within the first 10,000 years or so of the event. Despite any effects of the high CO_2 levels on acidifying the oceans, there was no preferential extinction of plankton relying on calcium carbonate structures.

P[acman] P[romotes] T[ransformation]

About 20 years ago, the development of transgenic methods that used P element transformation greatly facilitated gene analysis in *Drosophila melanogaster*. However, the method limits the size of DNA fragments for insertion and can only target specific sites in the genome. **Venken *et al.*** (p. 1747, published online 30 November) now develop a tool, termed P[acman], that allows site-specific insertion of DNA fragments of more than 100 kilobases. The method will facilitate structural and functional analyses of any *Drosophila* gene and will permit tagging of proteins in vivo.

Injectable Virulence

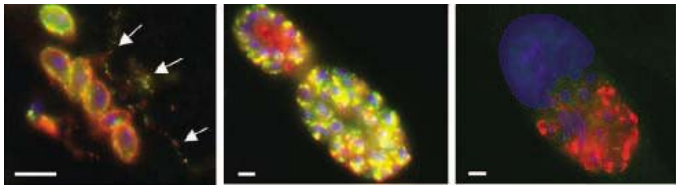

CREDIT: TAYLOR *ET AL.*

Little is known about the molecular determinants of virulence in eukaryotic pathogens like *Toxoplasma gondii* and malaria. Progress has been hampered by inefficient genetic tools, large genomes, and complex life cycles. Using forward genetic analysis, **Taylor *et al.*** (p. 1776) and **Saeij *et al.*** (p. 1780) show that a few clustered genes on a single chromosome control the dramatic difference seen in the virulence of natural lineages of the parasite *T. gondii*. The most important of these genes encodes a conserved serine/threonine kinase that is injected into the host cell. Although this process is reminiscent of type III secretion in bacteria, it is mechanistically and evolutionarily distinct.

Quieting the Brain at Birth

Birth entails a multitude of transitions. Studying rats, **Tyzio *et al.*** (p. 1788) have identified yet one more, a link between oxytocin exposure and the switch in how certain brain neurons fire. The neurotransmitter GABA (γ-aminobutyric acid) is usually excitatory in fetal brain neurons but inhibitory once they mature. Exposure to oxytocin during parturition causes a switch from excitation to inhibition in GABA signaling. This quieting of neuronal activity may serve to protect the brain against transient hypoxia during birth.

Climbing the Gradient

During chemotaxis, cells respond to tiny changes in the concentration of chemoattractant molecules and move toward their source. **Chen *et al.*** (p. 1792; see the Perspective by **Linden**) show that in addition to receptors for the chemoattractant peptide *N*-formyl-Met-Leu-Phe (fMLP), human neutrophils use two other receptor systems to promote appropriate cell migration. Neutrophils exposed to a concentration gradient of fMLP released adenosine triphosphate (ATP) at the leading edge of the cell. The released ATP appeared to act in an autocrine manner and stimulated purinergic receptors to provide a signal required for proper orientation of the cell.

HUMAN FRONTIER SCIENCE PROGRAM (HFSP)

12 quai St. Jean, 67080 STRASBOURG Cedex, FRANCE

E-mail: grant@hfsp.org
Web site: http://www.hfsp.org

OPPORTUNITIES FOR INTERDISCIPLINARY RESEARCH

The Human Frontier Science Program (HFSP) supports **international** collaborations in basic research with emphasis placed on *novel*, **innovative** and **interdisciplinary** approaches to fundamental investigations in the life sciences. Applications are invited for grants to support projects on **complex mechanisms of living organisms**.

CALL FOR LETTERS OF INTENT FOR RESEARCH GRANTS: AWARD YEAR 2008

The HFSP research grant program aims to stimulate novel, daring ideas by supporting collaborative research involving biologists together with scientists from other disciplines such as chemistry, physics, mathematics, computer science and engineering. Developments in these as well as emerging disciplines such as computational biology and nanoscience open up new approaches to understanding the complex mechanisms underlying biological functions in living organisms. Preliminary results are not required in research grant applications. Applicants are expected to develop new lines of research through the collaboration; projects must be distinct from applicants' other research funded by other sources. HFSP supports only international, collaborative teams, with an emphasis on encouraging scientists early in their careers.

International teams of scientists interested in submitting applications must first submit a letter of intent online via the HFSP web site. The guidelines for potential applicants and further instructions are available on the HFSP web site (www.hfsp.org).

Research grants provide 3 years support for teams with 2 – 4 members, with not more than one member from any one country, unless an additional member is absolutely necessary for the interdisciplinary nature of the project. A local or national **interdisciplinary** collaboration, as a component of an international team, will be considered as 1.5 team members for budgetary purposes (see below). The principal applicant must be located in one of the member countries* but co-investigators may be from any other country. Clear preference is given to **intercontinental** teams.

TWO TYPES OF GRANT ARE AVAILABLE:

Young Investigators' Grants are for teams of scientists who are all within 5 years of establishing an independent laboratory and within 10 years of obtaining their PhDs.

Program Grants are for independent scientists at all stages of their careers, although the participation of younger scientists is especially encouraged.

Depending on team size, successful teams will receive from $250,000 to $450,000 per year for the whole team.

Important Deadlines:
Compulsory pre-registration for password: 22 MARCH 2007
Submission of Letters of Intent: 03 APRIL 2007

**Members are Australia, Canada, the European Union, France, Germany, India, Italy, Japan, New Zealand, the Republic of Korea, Switzerland, the United Kingdom and the United States.*

Keith Alverson is director of the Global Ocean Observing System and head of Ocean Observations and Services at the IOC of UNESCO, 1 rue Miollis, 75732 Paris, Cedex 15, France. E-mail: k.alverson@unesco.org.

D. James Baker is a former undersecretary for Oceans and Atmosphere and administrator of the National Oceanic and Atmospheric Administration and is currently a consultant at the IOC of UNESCO.
E-mail: djamesbaker@comcast.net

Taking the Pulse of the Oceans

UNDERSTANDING HUMAN IMPACT ON THE GLOBAL ENVIRONMENT REQUIRES ACCURATE AND integrated observations of all of its interconnected systems. Increasingly complex models, running on ever more powerful computers, are being used to elucidate dynamic links among the atmosphere, ocean, earth, cryosphere, and biosphere. But the real requirement for integrated Earth system science is a systematic, sustained record of observations, starting from as early as we can get quantitative information and extending reliably into the future. In particular, the ocean is critically undersampled both in space and time, and national and intergovernmental observational commitments are essential for progress.

Ocean basins cover most of the planet and are filled with circulating turbulent fluid whose behavior can be modeled only by approximation. For instance, we talk of a "conveyor belt," but this is an unrealistic cartoon of actual turbulent circulation, which by transporting heat and fresh water affects the planet's climate. Knowledge about the true variability of the circulation remains elusive because long-term systematic observations are lacking.

Any seafarer knows that although one can look up from the deck of a ship and see the Moon clearly through 100 km of atmosphere, one cannot look down and see further than 1 m. Because the ocean is opaque to all wavelengths of electromagnetic radiation, Earth-observing satellites can't see below the surface either. Thus, much of the ocean must be observed from a patchwork of drifting and moored buoys, neutrally buoyant floats, coastal installations, and ship-based measurements.

Great recent progress has been made with each of these individual observing-system components. The launch of the 1250th drifting surface buoy in Halifax Harbor last year completed a network that is vital for tropical storm track prediction. The rapidly expanding international network of Argo floats has rewritten our knowledge of the temperature and salinity of the upper oceans. Moored buoy arrays in the tropics have made seasonal climate and El Niño prediction a real possibility. With tide gauges reporting in real time, not only can we predict coastal inundation hazards, but we can also disentangle the myriad processes involved in changing global sea level. Although observing the ocean is challenging, in particular cases it can be done well.

CREDIT: FADLAN ARMAN SYAM/AP

For 15 years, a global ocean-observing system under the auspices of the Intergovernmental Oceanographic Commission (IOC) of the United Nations' Educational, Scientific, and Cultural Organization (UNESCO) has been meeting important needs of global society. However, surprisingly little progress has been made toward a truly global system with long-term funding commitments. Lacking such a system and commitments, critical scientific hypotheses will remain untested.

The IOC is now working with the Global Earth Observation System of Systems (GEOSS) to identify national focal points for ocean observation efforts and to integrate these efforts into a truly global system. Unfortunately, there is still no plan for sustaining individual measurement programs, for integrating them into a coherent observing system, or for supporting them with stable funding. With a few notable exceptions, substantial multilateral government support for coordination and integration remains elusive.

To address this flaw, we propose the development of a UNESCO convention that commits nations to sustaining an integrated ocean-observing system that will lead to better understanding of the ocean and at the same time enable the provision of hazard warnings, monitoring of climate change, and management of marine and coastal resources. UNESCO's IOC stands ready to broker the development of such a convention. Preliminary discussions, including completion of the initial GEOSS tasks in ocean observation, begin at the next meeting of the Intergovernmental Committee for the Global Ocean Observing System in June 2007 in Paris. Will your nation be at the table?

– Keith Alverson and D. James Baker

10.1126/science.1135358

Congratulations, Dr. Mello!

The Nobel Prize in Medicine for 2006:
awarded to Craig C. Mello, PhD,
and his colleague Andrew Fire, PhD,
for their discoveries related to RNA interference.

QIAGEN

WWW.QIAGEN.COM

A cleaning session.

ECOLOGY

Feasting on Fish

Like drivers at a carwash, coral reef fish queue at cleaning stations to have parasites, slime, and broken scales nibbled away by smaller fish and by shrimps. These species interactions are interesting for their tropical ubiquity and the diversity of species that can be found as clients and cleaners. Although some cleaners are obligate professionals, others are dilettantes and adopt this life-style intermittently.

Floeter *et al.* have compiled data from around the tropics to tease out the selection pressures acting on these interactions. The basic emerging relationship is that, owing to abundance, the more common, planktivorous, and gregarious species take up most of the cleaner's time. Client size doesn't seem to be very important, nor does professionalism, when it comes to dealing with carnivores that might eat the fish or shrimp that is cleaning them. Hence, this study adds to a growing body of evidence suggesting a central role for abundance in structuring species interactions. Guimarães *et al.* have also looked at cleaning mutualisms. They document a pattern of nestedness, dominated by a core of a few, very busy cleaner species that service a wide variety of clients, with less popular cleaners and clients, both of which interact with core species but not each other, lounging on the periphery. — CA

J. Anim. Ecol. 10.1111/j.1365-2656.2006.01178x (2006); *Biol. Lett.* 10.1098/rsbl.2006.0562 (2006).

CHEMISTRY

Treacherous Tetrahedron

The relative strength of the triple bond in N_2 renders compounds with three or more catenated nitrogen atoms unstable, often explosively so. Banert *et al.* have succeeded in the careful preparation and isolation of the nitrogen-rich, dangerously explosive tetraazidomethane, $C(N_3)_4$, as a colorless liquid at room temperature. The stable, readily available trichloroacetonitrile molecule proved the most convenient precursor, affording the product after an 18-hour reaction with sodium azide in acetonitrile solvent. Cycloadducts with three and four equivalents of cyclooctyne could be isolated in ~5% yield and were characterized crystallographically. Reaction with norbornene, however, yielded unusual tetrazole derivatives in place of expected 1,3-dipolar cycloaddition adducts. Despite the compound's instability, the authors acquired clean ^{13}C and ^{15}N nuclear magnetic resonance spectra, as well as vibrational and mass spectral data, and an estimated boiling point of 165°C. Both Brønsted and Lewis acids accelerated exchange with free azide. — JSY

Angew. Chem. Int. Ed. **45**, 10.1002/anie.200603960 (2006).

BIOMEDICINE

An Absorbing Tale

Folate is a water-soluble vitamin that plays a critical role in metabolism. Because humans cannot synthesize it biochemically, they must obtain it by ingestion from folate-rich dietary sources. Maternal folate deficiency has been associated with an elevated risk of neural tube defects in the developing embryo, which can lead to malformations of the spine (such as spina bifida), skull, and brain. Because of these public health issues, there is considerable interest in understanding the specific molecular mechanisms that the body uses to absorb folate from food.

Through a combination of database mining, cell biology, and human genetic analysis, Qiu *et al*. have identified a transporter protein that appears to be responsible for the intestinal absorption of folate. Previously isolated as heme carrier protein HCP1, the proton-coupled folate transporter (PCFT) was expressed in the small intestine, bound folate with high affinity, and transported folate efficiently into cultured cells at the low pH that characterizes the intestinal milieu. An inactivating mutation in the corresponding gene was identified as the molecular culprit in a family with hereditary folate malabsorption. — PAK

PCFT (green) localizes to the plasma membrane.

Cell **127**, 917 (2006).

PSYCHOLOGY

Me *et al.*

An established and unsurprising characteristic of people working within teams is that each individual believes that he or she makes a disproportionately large contribution to the group output, so that the summed estimates are greater than the whole. These self-appraisals can be tempered if individuals are encouraged to regard what other team members do, and this shift in perceptions is thought to be conducive to group harmony and satisfaction.

Caruso *et al.* have looked more closely at whether structural heterogeneity within teams might influence perceptions and feelings in other-regarding situations. In studies gauging the self-contribution estimates of coauthors of 150 published papers (and their enjoyment of those collaborations) and experimentally manipulating the perceived and objective contributions to group projects, they found that workers who believed that they had done more (and those who actually had done more) were less satisfied, relative to those who had done less, when asked to consider the contributions of their teammates, in part because they became more aware of inequalities when taking a broader perspective. An additional

Continued on page 1661

CREDITS (TOP TO BOTTOM): GERALD ALLEN.; QIU *ET AL.*, *CELL* **127**, 917 (2006)

Continued from page 1659

finding is that this deleterious and unintended consequence of encouraging other-regarding behavior was largely mitigated in a competitive setting, where the allocation of rewards acknowledged individual rather than group performance, as exemplified in authorship order. — GJC

J. Pers. Soc. Psychol. **91**, 857 (2006).

CHEMISTRY

Brightening Tumor Analysis

In order to better understand the growth of cancerous tumors, clinicians may evaluate hundreds of samples for the expression of certain proteins, ideally in a quantitative fashion. Current methods of analysis tend to be only semi-quantitative, however, because the fluorescence signals generated from dyes may be distorted by tissue autofluorescence and photobleaching, and moreover, immunochemistry techniques can suffer from the imprecision of scoring by visual inspection. Ghazani *et al.* use semiconductor nanocrystals, or quantum dots (QDs), to implement a quantitative analysis technique. In contrast to fluorescent dyes, QDs have much brighter fluorescence signals and are less prone to photobleaching. The QDs in this case are bioconjugated for specific antigens, and the output fluorescence of a full array can be measured using optical spectroscopy. Efficient algorithms facilitate subtraction of tissue autofluorescence, as well as other automated corrections. Thus, intensity values can be used to give accurate, sensitive, and quantitative measurements for a range of protein markers. — MSL

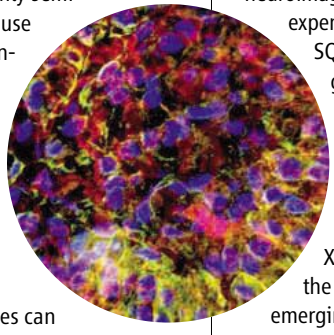

Antigen detection by QD fluorescence.

CREDIT: GHAZANI *ET AL.*, *NANO LETT.* **6**, 10.1021/NL062111N (2006)

Nano Lett. **6**, 10.1021/nl062111n (2006).

APPLIED PHYSICS

Warming Up Neuroimaging

Superconducting quantum interference devices, or SQUIDs, are remarkably sensitive instruments for detecting small magnetic fields. When placed in an array in a helmet-like structure, they can even be used to detect the minute magnetic fields given off by the human brain. However, these neuroimaging machines tend to be large and expensive, in part because they require the SQUIDs to be held constantly at cryogenic liquid helium temperatures.

Recent work has shown that certain atomic gases are also sensitive to small magnetic fields and can be used to detect the fields given off by the heart. By refining this technique, Xia *et al.* have succeeded in measuring the hundredfold-weaker magnetic signals emerging from the brains of human test subjects. A cloud of potassium atoms isolated in a gas cell is optically excited, effectively rendering each atom an individual compass needle. The presence of a magnetic field then causes the atoms to precess, which in turn induces optical rotation of a probe beam used to quantify the field. The measurement matches the sensitivity of the low-temperature SQUIDs without the need for cryogenic cooling. — ISO

Appl. Phys. Lett. **89**, 211104 (2006).

Science stke AAAS

www.stke.org

<< Stimulating Close Encounters

Phagocytes engulf microbes by enveloping them in a patch of membrane that invaginates to form a phagosome; this then fuses with a lysosome, which contributes the enzymes that destroy the internalized pathogen. Trivedi *et al*. exposed mouse macrophages to latex beads to investigate how immunoglobulin G (IgG)–class antibodies, which stimulate phagocytosis, might promote the latter stages of this process. When macrophages incubated with beads coated with either bovine serum albumin or IgG at 15°C (allowing bead engulfment but not fusion) were warmed to 37°C, the association of IgG-coated beads with phagolysosomes was faster than that of the albumin-coated beads. Cytosol from cells transfected with human Fcγ receptor (making them phagocytic) and incubated with IgG beads promoted phagosome-lysosome interactions more effectively than that from unexposed cells, an effect enhanced by transfection of the cells with protein kinase C (PKC). Inhibition of PKC abolished the stimulatory effect of IgG, and further pharmacological analysis indicated that IgG stimulated the actin-dependent tethering or docking (or both) of phagosomes and lysosomes. Thus, facilitation of phagosome-lysosome attachment by way of PKC appears to be one mechanism whereby IgG signaling stimulates phagocytosis. — EMA

Proc. Natl. Acad. Sci. U.S.A. **103**, 18226 (2006).

www.sciencemag.org

Science

1200 New York Avenue, NW
Washington, DC 20005
Editorial: 202-326-6550, FAX 202-289-7562
News: 202-326-6500, FAX 202-371-9227

Bateman House, 82-88 Hills Road
Cambridge, UK CB2 1LQ
+44 (0) 1223 326500, FAX +44 (0) 1223 326501

Subscription Services For change of address, missing issues, new orders and renewals, and payment questions: 866-434-AAAS (2227) or 202-326-6417, FAX 202-842-1065. Mailing addresses: AAAS, P.O. Box 96178, Washington, DC 20090-6178 or AAAS Member Services, 1200 New York Avenue, NW, Washington, DC 20005

Institutional Site Licenses please call 202-326-6755 for any questions or information

Reprints: Author Inquiries 800-635-7181
Commercial Inquiries 803-359-4578
Corrections 202-326-6501

Permissions 202-326-7074, FAX 202-682-0816

Member Benefits Bookstore: AAAS/BarnesandNoble.com bookstore www.aaas.org/bn; Car purchase discount: Subaru VIP Program 202-326-6417; Credit Card: MBNA 800-847-7378; Car Rentals: Hertz 800-654-2200 CDP#343457, Dollar 800-800-4000 #AA1115; AAAS Travels: Betchart Expeditions 800-252-4910; Life Insurance: Seabury & Smith 800-424-9883; Other Benefits: AAAS Member Services 202-326-6417 or www.aaasmember.org.

science_editors@aaas.org	(for general editorial queries)
science_letters@aaas.org	(for queries about letters)
science_reviews@aaas.org	(for returning manuscript reviews)
science_bookrevs@aaas.org	(for book review queries)

Published by the American Association for the Advancement of Science (AAAS), *Science* serves its readers as a forum for the presentation and discussion of important issues related to the advancement of science, including the presentation of minority or conflicting points of view, rather than by publishing only material on which a consensus has been reached. Accordingly, all articles published in *Science*—including editorials, news and comment, and book reviews—are signed and reflect the individual views of the authors and not official points of view adopted by the AAAS or the institutions with which the authors are affiliated.

AAAS was founded in 1848 and incorporated in 1874. Its mission is to advance science and innovation throughout the world for the benefit of all people. The goals of the association are to: foster communication among scientists, engineers and the public; enhance international cooperation in science and its applications; promote the responsible conduct and use of science and technology; foster education in science and technology for everyone; enhance the science and technology workforce and infrastructure; increase public understanding and appreciation of science and technology; and strengthen support for the science and technology enterprise.

Information for Contributors

See pages 102 and 103 of the 6 January 2006 issue or access www.sciencemag.org/feature/contribinfo/home.shtml

EDITOR-IN-CHIEF **Donald Kennedy**
EXECUTIVE EDITOR **Monica M. Bradford**
DEPUTY EDITORS **R. Brooks Hanson, Barbara R. Jasny, Katrina L. Kelner**
NEWS EDITOR **Colin Norman**

Editorial supervisory senior editor Phillip D. Szuromi; **senior editor/perspectives** Lisa D. Chong; **senior editors** Gilbert J. Chin, Pamela J. Hines, Paula A. Kiberstis (Boston), Marc S. Lavine (Toronto), Beverly A. Purnell, L. Bryan Ray, Guy Riddihough, H. Jesse Smith, Valda Vinson, David Voss; **associate editors** Jake S. Yeston, Laura M. Zahn; **online editor** Stewart Wills; **associate online editor** Tara S. Marathe; **book review editor** Sherman J. Suter; **associate letters editor** Etta Kavanagh; **information specialist** Janet Kegg; **editorial manager** Cara Tate; **senior copy editors** Jeffrey E. Cook, Cynthia Howe, Harry Jach, Barbara P. Ordway, Jennifer Sills, Trista Wagoner; **copy editors** Lauren Kmec, Peter Mooreside; **editorial coordinators** Carolyn Kyle, Beverly Shields; **publication assistants** Ramatoulaye Diop, Chris Filiatreau, Joi S. Granger, Jeffrey Hearn, Lisa Johnson, Scott Miller, Jerry Richardson, Brian White, Anita Wynn; **editorial assistants** Maris M. Bish, Emily Guise, Patricia M. Moore; **executive assistant** Sylvia S. Kihara; **administrative support** Maryrose Police

News senior correspondent Jean Marx; **deputy news editors** Robert Coontz, Jeffrey Mervis, Leslie Roberts, John Travis; **contributing editors** Elizabeth Culotta, Polly Shulman; **news writers** Yudhijit Bhattacharjee, Adrian Cho, Jennifer Couzin, David Grimm, Constance Holden, Jocelyn Kaiser, Richard A. Kerr, Eli Kintisch, Andrew Lawler (New England), Greg Miller, Elizabeth Pennisi, Robert F. Service (Pacific NW), Erik Stokstad; Rhituparna Chatterjee (intern); **contributing correspondents** Barry A. Cipra, Jon Cohen (San Diego, CA), Daniel Ferber, Ann Gibbons, Robert Irion, Mitch Leslie, Charles C. Mann, Evelyn Strauss, Gary Taubes, Ingrid Wickelgren; **copy editors** Linda B. Felaco, Rachel Curran, Sean Richardson; **administrative support** Scherraine Mack, Fannie Groom **bureaus:** Berkeley, CA: 510-652-0302, FAX 510-652-1867, New England: 207-549-7755, San Diego, CA: 760-942-3252, FAX 760-942-4979, Pacific Northwest: 503-963-1940

Production director James Landry; **senior manager** Wendy K. Shank; **assistant manager** Rebecca Doshi; **senior specialists** Jay Covert, Chris Redwood; **specialist** Steve Forrester **Preflight director** David M. Tompkins; **manager** Marcus Spiegler; **specialist** Jessie Mudjitaba

Art director Kelly Buckheit Krause; **illustrators** Chris Bickel, Katharine Sutliff; **senior art associates** Holly Bishop, Laura Creveling, Preston Huey; **associate** Nayomi Kevitiyagala; **photo editor** Leslie Blizard

***Science* International**

Europe (science@science-int.co.uk) **editorial: international managing editor** Andrew M. Sugden; **senior editor/perspectives** Julia Fahrenkamp-Uppenbrink; **senior editors** Caroline Ash (Geneva: +41 (0) 222 346 3106), Stella M. Hurtley, Ian S. Osborne, Stephen J. Simpson, Peter Stern; **associate editor** Joanne Baker **editorial support** Alice Whaley; Deborah Dennison **administrative support** Janet Clements, Phil Marlow, Jill White; **news: international news editor** Eliot Marshall **deputy news editor** Daniel Clery; **correspondent** Gretchen Vogel (Berlin: +49 (0) 30 2809 3902, FAX +49 (0) 30 2809 8365); **contributing correspondents** Michael Balter (Paris), Martin Enserink (Amsterdam and Paris), John Bohannon (Vienna)

Asia Japan Office: Asca Corporation, Eiko Ishioka, Fusako Tamura, 1-8-13, Hirano-cho, Chuo-ku, Osaka-shi, Osaka, 541-0046 Japan; +81 (0) 6 6202 6272, FAX +81 (0) 6 6202 6271; asca@os.gulf.or.jp; **asia news editor** Richard Stone +66 2 662 5818 (rstone@aaas.org) **japan news bureau** Dennis Normile (contributing correspondent, +81 (0) 3 3391 0630, FAX 81 (0) 3 5936 3531; dnormile@gol.com); **china representative** Hao Xin, + 86 (0) 10 6307 4439 or 6307 3676, FAX +86 (0) 10 6307 4358; cindyhao@gmail.com; **south asia** Pallava Bagla (contributing correspondent +91 (0) 11 2271 2896; pbagla@vsnl.com)

Africa Robert Koenig (contributing correspondent, rob.koenig@gmail.com)

EXECUTIVE PUBLISHER **Alan I. Leshner**
PUBLISHER **Beth Rosner**

Fulfillment & Membership Services (membership@aaas.org) **director** Marlene Zendell; **manager** Waylon Butler; **systems specialist** Andrew Vargo; **customer service supervisor** Pat Butler; **specialists** Laurie Baker, Tamara Alfson, Karena Smith, Vicki Linton, Latoya Casteel; **circulation associate** Christopher Refice; **data entry supervisor** Cynthia Johnson; **specialists** Tomeka Diggs, Tarrika Hill, Erin Layne

Business Operations and Administration director Deborah Rivera-Wienhold; **business manager** Randy Yi; **senior business analyst** Lisa Donovan; **business analyst** Jessica Tierney; **financial analyst** Michael LoBue, Farida Yeasmin; **rights and permissions: administrator** Emilie David; **associate** Elizabeth Sandler; **marketing: director** John Meyers; **marketing managers** Darryl Walter, Allison Pritchard; **marketing associates** Julianne Wielga, Mary Ellen Crowley, Catherine Featherston, Alison Chandler, Lauren Lamoureux; **international marketing manager** Wendy Sturley; **marketing/member services executive:** Linda Rusk; **japan sales** Jason Hannaford; **site license sales: director** Tom Ryan; **sales and customer service** Mehan Dossani, Kiki Forsythe, Catherine Holland, Wendy Wise; **electronic media: manager** Lizabeth Harman; **assistant manager** Lisa Stanford **production associates** Nichele Johnston, Kimberly Oster

Advertising director worldwide ad sales Bill Moran

Product (science_advertising@aaas.org); **midwest** Rick Bongiovanni: 330-405-7080, FAX 330-405-7081 • **west coast/w. canada** Teola Young: 650-964-2266 **east coast/e. canada** Christopher Breslin: 443-512-0330, FAX 443-512-0331 • **uk/europe/asia** Julie Skeet: +44 (0) 1223-326-524, FAX +44 (0) 1223-325-532 **japan** Mashy Yoshikawa: +81 (0) 33235 5961, FAX +81 (0) 33235 5852 **traffic manager** Carol Maddox; **sales coordinator** Deiandra Simms

Commercial Editor Sean Sanders: 202-326-6430

Classified (advertise@sciencecareers.org); **u.s.: recruitment sales manager** Ian King: 202-326-6528, FAX 202-289-6742; **u.s./industry:** Darrell Bryant: 202-326-6533; **midwest/canada:** Daryl Anderson: 202-326-6543; **northeast:** Allison Millar: 202-326-6572; **southeast:** Fernando Junco: 202-326-6740; **west:** Katie Putney: 202-326-6577; **sales coordinators** Erika Bryant; Rohan Edmonson, Shirley Young; **international: sales manager** Tracy Holmes: +44 (0) 1223 326525, FAX +44 (0) 1223 326532; **sales** Christina Harrison, Svitlana Barnes; **sales assistant** Kellie Jones; **japan:** Jason Hannaford: +81 (0) 52 757 5360, FAX +81 (0) 52 757 5361; **advertising production operations manager** Deborah Tompkins; **associates** Christine Hall; Amy Hardcastle; **publications assistants** Robert Buck; Mary Lagnaoui

AAAS Board of Directors retiring president, chair Gilbert S. Omenn; **president** John P. Holdren; **president-elect** David Baltimore; **treasurer** David E. Shaw; **chief executive officer** Alan I. Leshner; **board** Rosina M. Bierbaum; John E. Dowling; Lynn W. Enquist; Susan M. Fitzpatrick; Alice Gast; Thomas Pollard; Peter J. Stang; Kathryn D. Sullivan

AAAS
ADVANCING SCIENCE, SERVING SOCIETY

A New Look at Leonardo

What do the mountains in the background of the *Mona Lisa* reveal about Leonardo da Vinci's knowledge of erosion? What can high-tech scanners tell us about his other work? Find out at the nifty exhibit Universal Leonardo from the University of the Arts London. One section explores how Leonardo's writings, sketches, and paintings reflect his view of the world, where all things—from the motion of water to the curling of hair—are connected through the geometrical rules that govern nature.

Another highlight is an investigation of what different imaging techniques have uncovered about the history of Leonardo's 1501 painting *Madonna of the Yarnwinder*. For instance, a profilometric analysis, which uses a laser to map the painting's tiny variations in height, shows that some restorers "repaired" undamaged sections, such as the child's right cheek. An ultraviolet scan (above) also reveals touchups on the infant's calf and hip.
>> www.universalleonardo.org

AVOIDING WHALE-SHIP HITS

The London-based International Maritime Organization was expected to vote last week to shift shipping lanes off the Massachusetts coast in order to protect whales.

The decision is based on a 4-year effort by scientists to map the distribution of baleen whales 50 kilometers off Boston Harbor. Currently, hundreds of baleens, including the endangered North Atlantic right whale, feed on fish and plankton in the Stellwagen Bank National Marine Sanctuary. But roughly one whale per year is struck by the 200 shipping vessels that pass through the harbor monthly, and scientists say the recovery of the right whale, thought to number only 350, is hampered by these accidents, as well as by ships' fishing nets.

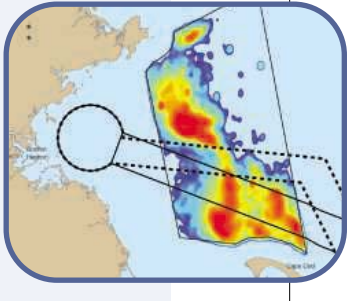

By poring over 25 years of whale observations, U.S. government and sanctuary researchers found that the current shipping lane passes directly through a high-density region of whale feeding (red area on map). So they proposed to shift the lane up to 16 km north (dotted line) and to narrow it by 20%, to 7.4 km. The Boston Harbor Pilot Association fears that the narrower lane will lead to more ship collisions, but others say it is safe given the precision afforded by Global Positioning Systems.

The change would add only 15 minutes to the trip and prevent most whale strikes, what Stellwagen's Craig McDonald calls "an enormous conservation benefit for a minimal cost."

The Tastes of Happiness?

Depression doesn't just put a lid on feelings. Many depressed people also complain of blunted taste sensations, a finding that has been hard to explain.

Diminished levels of certain types of brain neurotransmitters may be the reason, according to researchers at the University of Bristol in the U.K. The group, led by physiologist Lucy Donaldson, has shown that healthy volunteers who received a selective serotonin reuptake inhibitor, which increases serotonin levels in the brain, became supersensitive at detecting sweet and bitter tastes. Those who received an antidepressant that enhances noradrenaline became more sensitive to sour and bitter, the researchers reported last week in the *Journal of Neuroscience*.

The dampening of taste is probably not happening in the brain itself, as some have thought, Donaldson says: "Our hypothesis is that this is happening at the level of the taste buds." Although serotonin and noradrenaline are both known to be involved in taste signaling, the connection between mood and taste-bud activity is new. "It may be feasible to use a simple [taste] test to see what kind of medication people should be given," says Donaldson, who plans to repeat the experiment with depressed subjects to see whether they are more insensitive to sweet or sour tastes.

"I'm very excited by this paper," says taste researcher Stephen Roper of the University of Miami Miller School of Medicine in Florida, who adds that it "confirms and extends" the connection between serotonin and taste transmission.

Cloning Thumbs-Up in Oz

Australia last week became the latest in a handful of countries to explicitly approve the practice of therapeutic cloning—otherwise known as somatic cell nuclear transfer (SCNT)—for scientists working with human embryonic stem cells.

By a vote of 82 to 62, the House of Representatives in Canberra defied the country's political leadership, including Prime Minister John Howard, and endorsed a vote by the Senate last month, ending a 4-year ban on SCNT. The new law requires destruction of SCNT-created embryos within 14 days. It also adds a restriction: Insertion of human genetic material into animal eggs is not allowed.

Australian scientists are "elated" at the development, which may enable them to generate genetically tailored populations of stem cells to study diseases, says stem cell researcher Alan Trounson of Monash University in Melbourne.

The new law should also boost attendance at the 5th annual meeting of the International Society for Stem Cell Research, which will be held in Cairns, Australia, in June.

CREDITS (TOP TO BOTTOM): OPIFICIO DELLE PIETRE DURE, FLORENCE, FOR UNIVERSAL LEONARDO; C. BICKEL/*SCIENCE*; NOAA/STELLWAGEN BANK NMS/NMFS; WILEY, THOMPSON & MERRICK (UNPUBLISHED DATA)

Give Knowledge

It's not too late to order —
Say Happy Holidays all year. Give *Science* each week.

Special Gift Subscription Rate*
Professional $99 Postdoc/Student $50

Give 51 issues of *Science* along with the same yearlong benefits of AAAS membership that you enjoy.

You'll give colleagues a career boost and students an academic leg-up. You'll intrigue and enlighten friends; educate and entertain family members. And you'll add new supporters for the AAAS international, public policy, education, and career programs that advance science and serve society.

Make your holiday shopping list today—go to:

promo.aaas.org/giftnov
or call 1-866-434-AAAS (2227)

When you give *Science*, you receive our popular AAAS shirt.

Science
AAAS

*New members only. International orders will receive *Science* digital edition — to place an order outside the U.S., go to promo.aaas.org/giftn.

EDITED BY YUDHIJIT BHATTACHARJEE

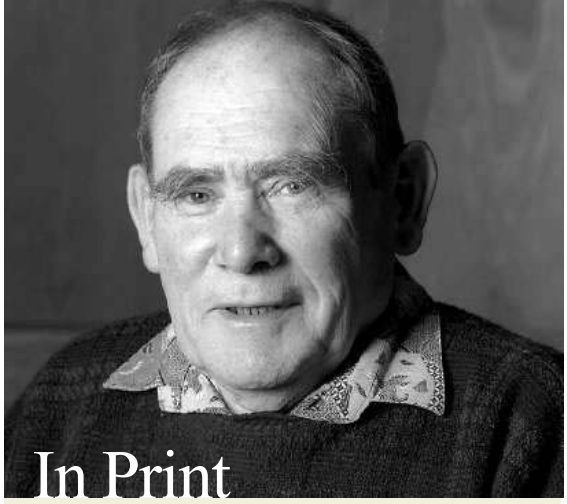

In Print

GLOBETROTTER. A prominent Japanese newspaper has criticized British Nobelist Sydney Brenner for spending only a fraction of his time in Japan despite drawing a $160,000 annual salary as full-time head of the planned Okinawa Institute of Science and Technology (OIST). But Japanese officials say Brenner's doing a great job no matter where he is.

The *Yomiuri Shimbun* calculated that the 79-year-old molecular biologist has spent only 63 days in Japan since being appointed to the position 15 months ago. That's not surprising given Brenner's multiple research and administrative appointments in the United States, United Kingdom, and Singapore.

Kiyoshi Kurokawa, science adviser to Japan's prime minister and chair of OIST's board of governors, admits that the paper's tally is "roughly correct." But "it is simply amazing to consider what he has been doing for us," says Kurokawa, who notes that Brenner's stipend is far below international standards. "*Yomiuri* has missed the point and is dwelling on a minuscule technicality." Brenner did not respond to an e-mail seeking comment.

Got a tip for this page? E-mail people@aaas.org

Data Point >>

HIGHER STAKES. Despite an increase in the U.S. National Science Foundation's (NSF's) budget, winning a grant from the agency is a lot tougher now than it was 6 years ago. But while the success rate for applicants has dropped from 30% in 2000 to a current level of 21% because of a 47% jump in applications and little growth in the number of awards made, scientists who succeed are getting grants that, on average, are 41% larger than in 2000 (see graph).

"In 2002, we said that if we had to choose between success rates and grant size, grant size should win," noted National Science Board member Ray Bowen after a recent presentation by an internal working group examining the issue.* "So in a sense, we asked for what has happened."

NSF hopes to survey recent grantees early next year to learn more about the factors driving the rise in applications. One factor could be a growth in solicitations for proposals in particular areas. The working group also found that the average winning scientist now submits 2.2 proposals compared to 1.7 a decade ago. At the same time, young scientists are keeping pace: Some 60% receive their first NSF grants within 5 years of their doctoral degrees, the same as a decade ago, and 73% get one within 7 years.

* www.nsf.gov/od/opp/opp_advisory/briefings/oct2006/nsf_prop_study.pdf

More Moolah, Tougher Chances

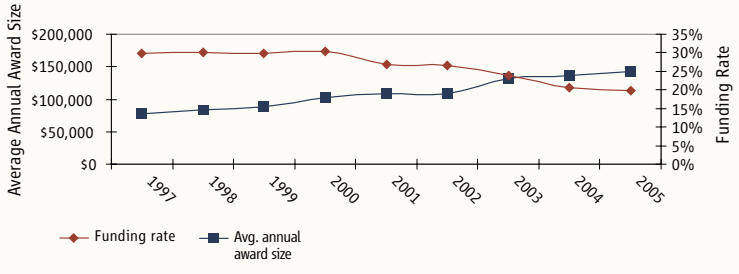

RISING STARS

A WIN-WIN. Education pays. Just ask Oak Ridge National Laboratory (ORNL) biologist Nagiza Samatova. This month, three Tennessee high school students she has been mentoring received $100,000 as the winning team in the annual Siemens Competition in Math, Science, and Technology. And their

research helped her win an $800,000 grant from the lab.

Scott Molony, Steven Arcangeli, and Scott Horton (left to right)—seniors at Oak Ridge High School—spent nearly 6 months in Samatova's lab identifying genes and biochemical pathways useful for microbial ethanol production. They were so successful that Samatova won an ORNL-run, peer-reviewed grant competition that gave her enough money over the next 2 years to keep the students working on the project and also hire additional staff. "It's not a miracle," she adds. "It's the families and school system; they gave us extremely good material."

Siemens gives away $2 million each year to outstanding students. Dmitry Vaintrob of South Eugene High School in Oregon won this year's top individual prize, a $100,000 college scholarship.

IN BRIEF

CHANGE AT EMBO. Frank Gannon, executive director of the European Molecular Biology Organization (EMBO), plans to retire from his post in mid-2007. In his 12 years as leader of the 1100-member society, Gannon introduced initiatives to nurture young researchers, launched two journals, *EMBO Reports* and *Molecular Systems Biology*, and expanded the society's influence on policymaking. A search for a new executive director is on.

HONORED. Nobelist Joshua Lederberg and Nathan Sharansky, a mathematician and prominent Soviet dissident, are among 10 individuals who will receive the U.S. National Medal of Freedom this year. The full list is available at www.whitehouse.gov.

CREDITS (TOP TO BOTTOM): SALK INSTITUTE FOR BIOLOGICAL STUDIES/GETTY IMAGES; ADAPTED FROM NSF; SIEMENS FOUNDATION

France's new planet hunter
1671

Evolution of milk tolerance
1672

Power shortage. Brookhaven's nuclear accelerator may not be able to afford its next run.

U.S. RESEARCH SPENDING

Scientists Feel the Pain as 2007 Budget Outlook Grows Dark

The Republican Congress adjourned last week without passing a 2007 budget for most federal agencies, choosing instead to extend a temporary spending measure until 15 February. And this week, the incoming Democratic leadership announced plans to apply current spending levels for the entire fiscal year, which ends 30 September, so that it can make a fresh start on the 2008 budget. Those decisions will put the squeeze on many research agencies and the scientists funded by them.

"There are no good options available to us to complete the unfinished work of the Republican Congress," declared Representative David Obey (D–WI) and Senator Robert Byrd (D–WV), incoming chairs of the appropriations committees in the House and Senate, in an 11 December statement. "After discussions with our colleagues, we have decided to dispose of the Republican budget leftovers by passing a yearlong joint resolution. We will do our best to make whatever limited adjustments are possible … to address the nation's most important policy concerns."

The yearlong resolution, if adopted once the new Congress convenes next month, would limit agency spending to the lowest of what either the House or Senate has already approved or what the agency received for the 2006 fiscal year. The biggest scientific loser would be the Administration's proposed American Competitiveness Initiative (ACI), which calls for a 10-year doubling of research at the Department of Energy's (DOE's) Office of Science, the National Science Foundation (NSF), and the in-house National Institute of Standards and Technology labs.

But some agencies are already feeling the effects of the delayed passage of their 2007 budgets. DOE's Brookhaven National Laboratory in New York, for example, may have to cancel the next run of its Relativistic Heavy Ion Collider if the lab doesn't receive its budget by 1 February. That's because a delay will push the next 20-week session into the summer months, when the cost of electricity is prohibitive. Some scientists in the Sea Grant program funded by the National Oceanic and Atmospheric Administration (NOAA) could miss the boat, as delays in the scheduled 1 February awarding of some 50 grants could prevent them from obtaining ship time or hiring the next crop of graduate students. ▶

High and dry? The budget snafu could delay NOAA's plans to outfit a research vessel with a new robotic submersible like this one.

CREDIT: BROOKHAVEN NATIONAL LABORATORY; MYSTIC AQUARIUM/IFE

Congress Extends Tax Credits for Industry

On its way out the door, Congress gave the U.S. business community a parting gift for the holidays: $16 billion in tax credits for money it spends on research and development. Legislators extended the current credit for 2 years and broadened the number of eligible firms.

First enacted in 1981, the R&D tax credits cover corporate investment in everything from drugs to automobile parts. Last year, U.S. companies claimed $5.2 billion in credits. But companies couldn't count on the tax break: It's been extended 11 times and last expired on 31 December 2005.

Businesses and, this year, the White House have long lobbied for a permanent credit. But lobbyists say they are grateful for the extension, which is retroactive to 2006. "At least we got out of it with the best result we could," says Washington, D.C.–based business lobbyist David Peyton.

Under the current rules, companies can claim a credit if research spending rose over previous years as a ratio of revenue. The new bill simply provides a credit for any increase in R&D alone, a change that Monica McGuire of the National Association of Manufacturers in Washington, D.C., hopes will double or triple the number of companies able to claim a credit, which will "make the U.S. more competitive."

The congressional move has its critics, however, including Citizens for Tax Justice in Washington, D.C. The nonprofit says the system is already too "open-ended" and "heavily abused" by corporations for expenditures unrelated to innovation.

–ELI KINTISCH

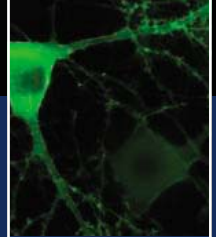

Nervous glow
1674

Past and future of Russian science
1677

Stop/go in nuclear science
1678

And investigators with funding from the National Institutes of Health have been told to expect only 80% of what NIH initially committed for the next year of their multiyear grant.

"It was unfortunate that Congress couldn't get its work done," says John Marburger, the president's science adviser. "It's especially disappointing that it left without an ACI appropriation," he adds, noting that spending panels in the House and Senate separately came close to matching the president's request. "At least they passed the tax package [see sidebar, p. 1666], which was the most expensive part of ACI, although we would like to see it made permanent."

Federal research officials say their watchword is caution as they await final word on their 2007 budgets. "We're being very conservative with pay lines and the size of awards," says Norka Ruiz Bravo, head of NIH's external research program. The Administration requested no increase for NIH in 2007, and a last-minute bump-up seems unlikely despite its widespread support in Congress (see sidebar, right). Whatever happens, NIH Director Elias Zerhouni has three priorities: "Maintain our ability to fund new investigators, support the first competing renewal of first-time grantees, and preserve the capacity of outstanding PIs [principal investigators] who have no other support." But he admits that there's no magic formula for achieving those goals within a steady-state budget. "The pain is real," he says.

NSF Director Arden Bement says that "the results would be dire" if Congress sticks to a yearlong spending resolution. The administration had requested an 8% boost, and Congress seemed inclined to go along—the House approved the full request, and a Senate spending panel came close. But without an increase, he warned, mandatory pay raises for staff and the rising cost of materials for new facilities would require cuts in existing programs.

At some agencies, those cuts are already being made. The 2007 NOAA budget passed by the House is, at $3.4 billion, half a billion dollars smaller than its 2006 budget. The $380 million Office of Oceanic and Atmospheric Research, for example, which handles much of the agency's extramural grants, will likely need to delay the next round of Sea Grant awards. Office chief Richard Spinrad says the delay is especially hard on young investigators with few grants from other agencies.

That's also the case at DOE's Jefferson accelerator lab in Virginia, which is limping along on a budget that was cut by 10% in 2006. That puts a squeeze on planning for an upgrade to its main machine, including experiments at lower energies that are often the lifeblood of young academic scientists vying for tenure. Even if the cuts are eventually restored, "it's going to be hard to do all the work necessary for the short-term experiments and to prepare for the upgrade," says nuclear physicist Ronald Gilman. **–JEFFREY MERVIS**

With reporting by Eli Kintisch and Erik Stokstad.

CREDIT: MARTY KATZ

Congress Endorses Bigger NIH Budget, Director's Fund

Applauded. Elias Zerhouni calls NIH reauthorization a "vote of confidence."

The National Institutes of Health (NIH) received a big pat on the back last week from the outgoing Republican Congress. In the waning hours of its final session, the 109th Congress approved legislation that authorizes higher budgets for NIH and spells out how the agency should conduct its business. Although the bill doesn't actually provide any new money, agency officials and the biomedical community hope that it will help them make the case for a bigger NIH budget with the new, Democrat-controlled Congress.

"We've been under a lot of scrutiny in the past few years, about how we operate and what we did with the recent doubling [of NIH's budget]," says NIH Director Elias Zerhouni. "So I see this as a reaffirmation of what we have been doing."

The 3-year reauthorization calls for NIH to receive budget increases of 6% and 8% in 2007 and 2008, respectively. It creates a common fund for novel ideas and trans-NIH projects—a mechanism that is already up and running as part of Zerhouni's Roadmap Initiative—and calls for its share to grow to 5% of NIH's total funding as the overall budget rises. (NIH is staring at a possible flat budget in 2007 after a cut last year.) The bill, which President George W. Bush is expected to sign shortly, also sets in motion a review of NIH's current structure of 27 institutes and centers, with a report to Congress in 18 months.

Although federal agencies get their money from annual appropriations, authorization bills give legislators a chance to address pressing problems as well as to fine-tune an agency's programs. A big problem for NIH in recent years has been its bungled oversight of interactions between intramural scientists and managers and industry, which led to several egregious examples of financial conflicts of interest (*Science*, 11 February 2005, p. 824). Legislators have also been curious about how well NIH had spent a 5-year doubling of its budget that ended in 2003—especially whether its administrative structure was up to snuff.

The bill (H.R. 6164) was a priority for Representative Joe Barton (R–TX), outgoing chair of the House Energy and Commerce Committee, which held several contentious hearings on those topics. Passed overwhelmingly by the House in September, the bill contained a 5%-a-year boost for NIH and would have required the common fund to get half of any NIH increase. Voting last week, the Senate removed the mandatory 50–50 split and upped the annual increases, changes that Barton accepted reluctantly in return for setting a minimum size for the common fund, now roughly 1.3% of NIH's $28 billion budget.

Biomedical lobbyists say they much prefer the Senate version that prevailed. The House bill would have restricted the ability of appropriators to target spending, notes Jon Retzlaff of the Federation of American Societies for Experimental Biology in Bethesda, Maryland. "If they wanted to add $100 million for some research program, they would need to give NIH $200 million," he says. In an era of tight budgets, say Retzlaff and others, such a split would siphon off money needed to preserve existing programs and awards to individual investigators.

Zerhouni acknowledges that the reauthorization isn't a substitute for a budget increase. But he says it would be "cynical" to dismiss it entirely. "I'd rather have a bill that says we need more dollars than no bill at all. It's really a big vote of confidence for us." **–J. D. M.**

PLANETARY SCIENCE

A Dry View of Enceladus Puts a Damper on Chances for Life There

With the discovery last year of a great plume of water rising from the south pole of Saturn's icy moon Enceladus, astrobiologists had a new potential home for life in the solar system. Liquid water is the scarcest requirement for life, and the plume's striking resemblance to the Old Faithful geyser back on Earth seemed to imply subsurface pools. But an alternative explanation for the Enceladus plume, proposed on page 1764, would create the Old Faithful look without a drop of liquid water and therefore with no possibility of life.

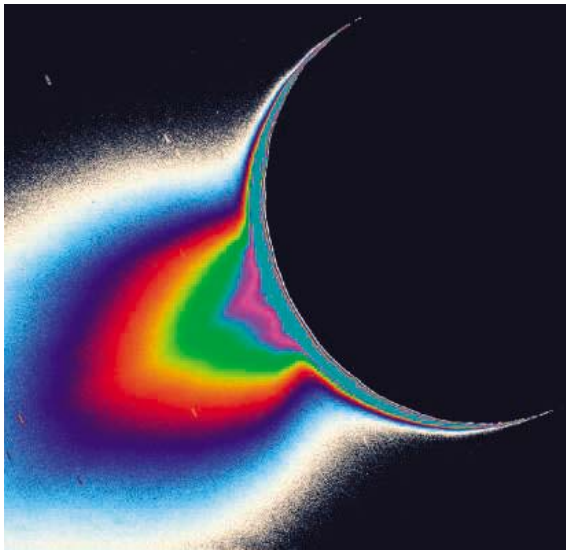

A dry gusher? The plume of Enceladus (color-coded here for density) may be driven by gas-laden ice rather than boiling water.

The concept of an Earth-like geyser on Enceladus emerged from early observations by the Cassini spacecraft orbiting Saturn, reported in the 10 March issue of *Science* (p. 1422). Each second, about a bathtub's worth of water in the form of water vapor and tiny ice particles soared hundreds of kilometers above the airless moon from a relatively "warm" (145 kelvin) spot on the surface. Cassini team members concluded in one paper that liquid water as little as 7 meters beneath the surface could be boiling as it encountered lower pressures. That would generate vapor and frozen droplets that jet out from crevices in the moon's icy crust.

There was one snag, says Susan Kieffer, a geological fluid dynamicist at the University of Illinois, Urbana-Champaign, who has studied the dynamics of Old Faithful. On reading an accompanying Cassini paper, Kieffer and her colleagues learned that the spacecraft's mass spectrometer had detected considerable amounts of carbon dioxide, methane, and nitrogen in the plume. That was odd, they thought, because nothing like those amounts of methane and nitrogen could possibly dissolve in the water. Although water couldn't hold the gases, water ice could, by trapping individual gas molecules within the "cages" of ice's own crystal structure.

The existence of such clathrates on Enceladus had been hypothesized 20 years ago. Kieffer and her colleagues reasoned that if clathrates lurked beneath a several-kilometer-deep crust of water ice, and tectonic activity created fractures in the crust, the pressure release would drive explosive decomposition of the clathrate. The required gases would gush out, along with ice particles that would sublimate enough water vapor to reproduce the observed plume composition. Their rough calculations support that scenario.

"It's a noble and proper attempt to account for the gases," says planetary meteorologist Andrew Ingersoll of the California Institute of Technology in Pasadena, a member of the Cassini team. But "it's not as simple as" uncorking some clathrates, he says. There are many details in the physics, such as how much water vapor ice particles could yield, that he needs to understand before taking back a potential habitat for life.

–RICHARD A. KERR

INTERNATIONAL AFFAIRS

Iranians Fume Over a Closed SESAME

A scientific project that hopes to be a calming influence in the Middle East has instead increased tensions between two important countries in the region. At issue is the failure of 35 Iranian scientists to obtain Egyptian visas for a recent meeting in Alexandria of researchers hoping to work on the Synchrotron Light for Experimental Science and Applications in the Middle East (SESAME) project.

Eight countries are now members of a consortium creating a home for a synchrotron, donated by Germany, at a site 32 kilometers outside Amman, Jordan (*Science*, 26 November 2004, p. 1465). The machine, a first for the region, is intended to serve starting in 2010 as both a platform for research and a model for peaceful cooperation. Eight countries—Jordan, Bahrain, Cyprus, Egypt, Israel, Pakistan, Palestine, and Turkey—are already members, and the Iranian parliament is expected to vote sometime next year on a proposal to formally join a project in which its scientists have participated since 2001.

But that vote could be influenced by what happened after the Iranians applied for visas to attend the 5-day Alexandria meeting, held the last week of November. The scientists say they never heard from the Egyptian embassy in Tehran after submitting their visa applications at least 6 weeks beforehand. "If this is not hostile treatment, I don't know what is," says Reza Mansouri, a physicist at Sharif University in Tehran and one of two Iranian representatives on the SESAME council. Iranian contingents have attended four previous user meetings held elsewhere in the region, but Mansouri fears that the latest incident will bolster opposition in parliament to any collaboration.

Egyptian authorities deny snubbing the delegation. The Iranian scientists simply did not apply early enough, says Egypt's science minister, Hany Helal. "It is exactly the same when an Egyptian submits a request for a visa to [go to] the U.S. or a European country," says Helal.

The council, which met in Jordan last week (Mansouri stayed home in protest), seems willing to give Egypt the benefit of the doubt. "It appears that the Iranians were given incorrect advice by the Egyptian embassy," says Herman Winnick, a physicist at the Stanford Linear Accelerator Center in Palo Alto, California, who helped initiate the project a decade ago and remains an adviser. "It's extremely unfortunate." Winnick says he hopes the incident will not prevent Iran from becoming a member country. **–YUDHIJIT BHATTACHARJEE**

CREDIT: NASA/JPL

SCIENTIFIC MISCONDUCT

Online Sleuths Challenge *Cell* Paper

When scientists at National Chung Hsing University in Taichung, Taiwan, published a microbiology paper in the 20 October issue of *Cell*, local media hailed the event, noting that it was the first report in the prestigious journal by an all-Taiwan group. One newspaper quoted the university president as saying that the "findings will rewrite textbooks." That local pride, however, was premature: After anonymous online sleuths raised questions about image manipulation in the paper, a university investigating committee has recommended that Ban-Yang Chang, the corresponding author, retract the paper.

In an e-mail to *Science*, Yu-Chan Chao, dean of the College of Life Sciences at the university, calls the episode an "unfortunate case." But Chao went on to say that Chang's team had provided "repeatable data suggesting that their overall conclusions were correct and reproducible."

The *Cell* paper, which questioned prevailing views of how transcription of a gene's DNA begins in bacteria, was challenged publicly on 16 November when an anonymous posting appeared on an electronic bulletin board run by Chinese students in the United States. The posting alleged that starting with figure 2 of the paper, "several dozen western lanes appeared to be copied and pasted." The board has been abuzz with discussions about the study since then. Another poster claimed to have used "difference blending," a feature of the image software Adobe Photoshop, to compare the upper parts of lanes in the high-resolution version of panel C of figure 2 of the *Cell* paper and concluded that they were almost identical.

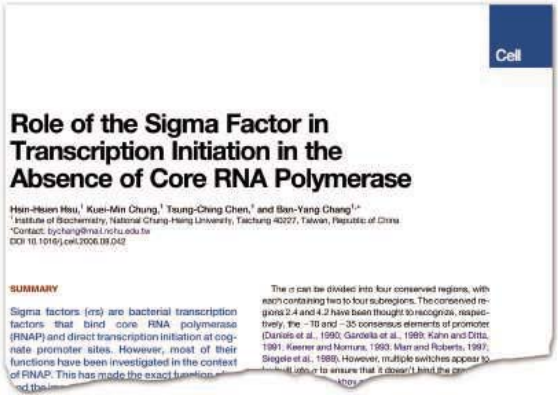
Cell

Role of the Sigma Factor in Transcription Initiation in the Absence of Core RNA Polymerase

Hsin-Hsien Hsu,[1] Kuei-Min Chung,[1] Tsung-Ching Chen,[1] and Ban-Yang Chang[1,*]

[1] Institute of Biochemistry, National Chung-Hsing University, Taichung 40227, Taiwan, Republic of China

*Contact: bychang@mail.nchu.edu.tw

DOI 10.1016/j.cell.2006.09.042

SUMMARY

Sigma factors (σs) are bacterial transcription factors that bind core RNA polymerase (RNAP) and direct transcription initiation at cognate promoter sites. However, most of their functions have been investigated in the context of RNAP. This has made the exact function

The σ can be divided into four conserved regions, with each containing two to four subregions. The conserved regions 2.4 and 4.2 have been thought to recognize, respectively, the −10 and −35 consensus elements of promoter (Daniels et al., 1990; Gardella et al., 1989; Kahn and Ditta, 1991; Keener and Nomura, 1993; Marr and Roberts, 1997; Siegele et al., 1989). However, multiple switches appear to

Paper suspect. Internet bulletin board posters discussed possible image manipulation of figures in this *Cell* article.

A subsequent reply on the board attributed to Chang denied any wrongdoing. And in an e-mail to *Science* last week, before the university investigation, Chang denied that images in the paper had been manipulated and stated that the "conclusion we made for the *Cell* paper is true on the basis of our data."

The paper dealt with the role of a transcription factor called sigma factor, a subunit of the RNA polymerase (RNAP) complex that transcribes DNA into messenger RNA. Sigma factor "melts" double-stranded DNA, separating the two strands to provide access for the polymerase, but it was thought to need the help of the core part of the RNA polymerase complex to bind to DNA. Chang's team, however, claimed to find that a truncated version of sigma factor could bind and open up DNA, without help from the core RNAP. A commentary in the same issue of *Cell* noted that the study adds "a twist to our current understanding of transcription initiation."

After Chang's online rebuttal, bulletin-board posters said they would contact Michael Rossner, managing editor of the *Journal of Cell Biology* and an expert on detecting image manipulation. Rossner confirmed to *Science* by e-mail that he was familiar with the case and "agree[s] with the students that some of the images are indeed questionable." *Cell* also received word of the allegations and started an investigation, confirmed Emilie Marcus, the journal's executive editor. (As *Science* went to press, *Cell* had not published a retraction, and Chang had not confirmed that he was retracting the paper.)

Last Friday, Chung Hsing University convened a committee, which consisted of two university vice presidents, the dean of the College of Life Sciences, and two top scientists from outside the university, to investigate the alleged manipulation. They advised Chang to retract the paper, Chao wrote. "The university will take this as a serious lesson for ethics education at all the colleges in the future," he added.

There may be more lessons to come. Bulletin-board posters have challenged figures in another paper by Chang's team that was published online 16 October by the *Journal of Biological Chemistry*.

–HAO XIN

French Vote With Their Euros

PARIS—In what is widely seen as a rebuke to clergy members' position on biomedical ethics, French citizens had pledged more than €101 million when this year's edition of the Téléthon closed on Sunday night, topping last year's record close. Some Roman Catholic bishops had sharply criticized the Téléthon, a fundraiser for genetic neuromuscular diseases, for supporting stem cell research and genetic studies that are at the basis of prenatal tests and preimplantation diagnostics (*Science*, 8 December, p. 1525).

Independently, a parliamentary committee unanimously adopted a report last week that advocates loosening France's 2004 bioethics law, which includes restrictive rules for research with human embryos. The report also says the ban on so-called therapeutic cloning should be lifted. The current law is slated for review in 2009, but the report recommends changing it as early as next year. It also suggests a series of ethical guidelines for egg donation.

–MARTIN ENSERINK

Greenpeace 1, Patenting Cells 0

BERLIN—German stem cell researchers fear that medical innovation will suffer after a court annulled the first German patent for a human stem cell–related invention. Scientists are allowed to use—but not create—human embryonic stem (ES) cells in Germany for basic research, but the court decided 5 December that patents cannot be granted, citing moral concerns. The court's decision is the culmination of a 7-year legal battle between University of Bonn cell biologist Oliver Brüstle and the German branch of Greenpeace, which argues that it is immoral to use cells created through the destruction of human embryos to turn a profit.

Brüstle was granted a German patent in 1999 for a method of converting ES cells into nerve cells for potential applications in treating neurological trauma and disease. Greenpeace challenged that patent in court soon after. The decision "will further weaken any attempt to develop stem cell–based therapies in Germany," says Hans Schöler, a stem cell biologist at the Max Planck Institute for Molecular Biomedicine in Münster. "Which [foreign] industrial partner will be interested to team up with someone who does not have a patent?" Brüstle plans an appeal soon.

–JOHN BOHANNON

SEISMOLOGY

Do Early Tremors Give Sneak Preview of Quake's Power?

Seismologists can give residents of earthquake zones a few seconds' warning of a coming quake—enough time to shut down nuclear reactors and slow high-speed trains—by analyzing the first waves the quake produces. But key information has been missing. "We know in a few seconds where an earthquake occurs, but we cannot predict the magnitude," says Paul Rydelek of the National Research Institute for Earth Science and Disaster Prevention in Tsukuba, Japan. Now, Italian researchers say the same waves can reveal how strong the tremor will be, allowing a more appropriate disaster response. Some experts are skeptical, but Marie-Paule Bouin of the Institute for the Physics of the Globe in Paris finds the data presented by the Italian team "convincing enough" to be looked at seriously.

Hopes flattened. A rescuer passes a school destroyed by a 2002 quake in southern Italy. Early warning systems hope to give several seconds' alarm.

The first earthquake signals to arrive at a seismic station are the primary or p-waves, which are compression waves like sound in air. P-waves travel fast, about 6 kilometers per second, but they do not carry the destructive force of the secondary or s-waves: shear waves that cause the ground to oscillate. S-waves travel at 3.5 kilometers per second and, depending on the distance to the epicenter, can arrive several seconds later.

Early Earthquake Warning (EEW) systems work by spreading seismic detectors over earthquake-prone regions and using fast digital processing to give a few seconds' warning of a coming quake (*Science*, 24 December 2004, p. 2178). By combining the signals received at several stations, an EEW can estimate the position of the epicenter, but judging the magnitude of the quake is trickier. Seismologists can get a rough estimate from the frequency of the early p-waves. But Aldo Zollo and his colleagues at the University of Naples and the National Institute of Geophysics and Volcanology in Rome think the amplitude, or strength, of the p-wave can give a better indication of the tremor's destructive power.

The Italian researchers analyzed records from seismic stations sited less than 50 kilometers from the epicenters of 207 earthquakes that occurred between 1976 and 1999 in the Mediterranean area. The magnitudes of the quakes ranged from 4 to 7.4. The team compared the peak amplitude of the first 2 seconds of the p-waves to the amplitude of the s-wave in their sample and found that both quantities correlate closely enough with the quake's magnitude to be useful in EEW systems.

To use that information to gauge the magnitude of an impending quake, forecasters would need to know the distance to the epicenter. In a real-life situation, that information might not arrive in time, but Zollo thinks future EEWs will be able to supply it. "As the wavefront propagates in the network, you measure the amplitudes and compare the results of each station with the quantities measured at the other stations in the network," he says. In this way, the network will quickly zero in on the location of the epicenter and the magnitude of the event, in time to trigger alarms at sites farther away seconds before the destructive s-waves arrive.

Predicting earthquakes is a notoriously tricky business, and other researchers have expressed some skepticism over Zollo's claims of better warnings. Because Zollo and his team did not study quakes with a magnitude greater than 7.5, their technique may not apply to the most destructive events, says François-Henri Cornet of the Institute for the Physics of the Globe. "The conditions of the propagation of seismic wavefronts change at these magnitudes," he says. Earthquakes also don't always develop in a tidy, symmetrical way. "The seismic wavefronts are often anisotropic, or are projected strongly in one direction, which can introduce errors," admits Zollo.

Errors aside, some researchers don't think it is possible to predict the magnitude of an earthquake, which depends on the total rupture length, by looking at seismic waves produced during its initial moments. "Once an earthquake begins, it will proceed essentially as a series of dominoes being knocked over. Sometimes the domino chain will stop, and at other times it will continue to go for a long distance," says William Ellsworth of the U.S. Geological Survey in Menlo Park, California. Whether the start of the chain holds clues to its ultimate length "is still an open question," he says.

Zollo argues that the initial amplitude peak of the p-wave does carry such clues. "The probability that a fracture grows to a larger size scales with the initial energy available. The stopping mechanisms become less efficient for earthquakes with an initially high energy," he says. Rydelek, however, remains skeptical. "I would like to see the physics that links these first seconds to the rupture propagation over the whole fracture," he says. "You can have twists and turns in the fault, and stress variability, and these really determine how big the earthquake gets, not the initial slip."

–ALEXANDER HELLEMANS

Alexander Hellemans is a writer in Paris, France.

CREDIT: MARIO LAPORTA/REUTERS

ASTRONOMY

France to Launch First Exoplanet Hunter

PARIS—The 200 or so planets discovered to date around other stars are all big balls of gas similar to Jupiter or Saturn. Earth-bound telescopes aren't sensitive enough to detect small, rocky planets like Earth that could harbor life. But all that should change at the end of this month when COROT, a space observatory built by France, is lofted into orbit. COROT will survey large areas of the sky, monitoring thousands of stars at a time for tiny telltale dips in brightness that reveal a planet passing in front of its star. "COROT will tell us about rocky planets in the very inner orbits. [It] will tell us that they exist. We are really looking forward to seeing its data," says William Borucki of NASA Ames Research Center at Moffett Field, California.

COROT, to be placed in a polar orbit by a Soyuz launcher, cost $46 million to build and is equipped with a 30-centimeter telescope and four charge-coupled device (CCD) array detectors. Two of the arrays are optimized to detect the tiny brightness changes of a transiting planet. Whereas Earth-based telescopes can measure changes in a star's luminosity of about 1%, good enough for them to detect Jupiter-size planets, COROT's detectors will be sensitive to changes of 0.01%. "Because of the absence of [Earth's] turbulent atmosphere, we can obtain a much higher photometric precision," says Pierre Barge of the Astrophysics Laboratory of Marseille and leader of the COROT exoplanet working group. When looking at very small stars, COROT will be able to pick out the dimming of starlight by an Earth-sized planet, Barge says. "Around stars like our sun, COROT will be able to detect planets twice the size of the Earth."

COROT will start out focusing on the galactic center, which is rich in stars, and will switch to point in the opposite direction before the sun comes into the telescope's field of view after a year of observation. Researchers will monitor about 60,000 stars, Barge says, and they hope to discover a few hundred warm, Jupiter-like planets and between 5 and 50 rocky ones.

COROT's other two CCD arrays have a faster sampling rate and are designed to spot seismic oscillations in stars. Many stars, our sun included, experience vibrations, which reveal themselves as tiny fluctuations in the luminosity of the star. "We use similar observation techniques to the one for looking for planets," says Annie Baglin of the Observatory of Paris at Meudon, COROT's principal investigator. Stellar oscillations, which can each last from a few seconds to several hours, are now an important tool in stellar research. "From the oscillation frequencies of a star, we can learn about its geometry, its mass, and its internal structure," says Meudon's Eric Michel, head of the COROT seismology group.

Although other orbiting observatories have studied stellar vibrations, COROT hopes to get better results with its larger telescope and with a novel method using the telescope's CCD arrays to keep the telescope steady. When making observations, researchers ensure that there are several bright stars with precisely known positions always in the telescope's field of view. "These stars become the anchors on which we hook the satellite," says Baglin.

Unblinking eye. COROT will look for planets passing in front of stars.

CREDIT: CNES

COROT will set the scene for the next space observatory that will look for rocky planets: NASA's Kepler mission, due to be launched in November 2008. It will be equipped with a 1-meter telescope and will observe the same area of sky unblinkingly for up to 6 years so that it can detect longer-period rocky planets farther from their stars, where conditions for life are better. "We will look at 100,000 stars like the sun, so we expect to find dozens of Earths in the inhabitable zone," says Borucki, Kepler's principal investigator.

–ALEXANDER HELLEMANS

Alexander Hellemans is a writer in Paris, France.

Onward, Uncreatively Named Telescopes

The European Southern Observatory (ESO) has set its sights on building the largest telescope in history: a 42-meter behemoth named the European Extremely Large Telescope (E-ELT). This week, the ESO Council gave the green light for a €57 million final design study, due to be completed in 3 years. The €800 million instrument could be ready in 2017. The E-ELT, which sports five large mirrors, will be sited in 2008; potential homes include Chile and Tibet. Meanwhile, U.S. astronomers are embarking on a smaller Thirty Meter Telescope (TMT), due to be completed in 2016. "I look forward to close cooperation with them," says TMT manager Gary Sanders.

–GOVERT SCHILLING

A Shot in the Arm for Biodefense

Congress has voted to create a new agency within the U.S. Department of Health and Human Services that will spend $1 billion over the next 2 years to speed private development of vaccines for bioterror and disease. Two years in the making, the nascent Biomedical Advanced Research and Development Agency has been criticized for its secrecy provisions and the possibility that funding it would sap existing research budgets (*Science*, 4 November 2005, p. 755). But research organizations did not actively oppose the measure, which passed this week with more robust information-sharing requirements. White House approval is expected soon.

–ELI KINTISCH

Getting the Lead Out

The U.S. Environmental Protection Agency (EPA) has asked an advisory panel to chew on an idea that is already giving some environmentalists heartburn. Last week, EPA announced that it is considering removing a standard requiring that levels of airborne lead not exceed 1.5 $\mu g/m^3$. EPA has not revised this standard since 1978, even though it is required to do so every 5 years, and the lead battery industry wants the standard to be dropped. In 2004, lawyers representing residents near a Missouri smelter sued EPA for not revising the standard. The agency lost the court battle last year and now faces a 2008 deadline for updating the standard. In a draft document released last week, EPA said the dramatic decline in lead pollution from reducing the lead in gasoline, plus other regulatory actions, might mean that no standard is needed. EPA's Clean Air Scientific Advisory Committee is scheduled to vet the proposal in February.

–ERIK STOKSTAD

HUMAN EVOLUTION

There's More Than One Way to Have Your Milk and Drink It, Too

The adage that milk does a body good may be true for American celebrities wearing milk mustaches in ad campaigns: Many Americans and northern Europeans descend from cattle herders and carry an ancient mutation that allows them to tolerate milk at any age. But milk gives cramps and diarrhea to roughly half the world's adults, especially in Asia and West Africa. That's why lactose tolerance has been held up as a classic example of human evolution, in which some people inherited the trait to digest milk, and some didn't.

Now, an international team reports a revealing twist on this evolutionary story. In this week's issue of *Nature Genetics*, researchers describe three new genetic variants that arose independently in groups of Africans; each variant allows carriers to drink milk and eat dairy products as adults. The study shows that lactose tolerance evolved more than once in response to culture, says team leader Sarah Tishkoff of the University of Maryland, College Park.

It's also an elegant example of how evolution can find several solutions to the same problem, especially in the face of strong selection, says molecular anthropologist Kenneth Weiss of Pennsylvania State University in State College. "There is not just one way to tolerate milk but several ways," he says. "It's very nice work because it shows that evolution isn't just about picking one gene and driving it."

The textbook tale of lactose tolerance runs this way: All humans digest mother's milk as infants. But for most of human history, weaned children didn't drink milk. So they shut down the enzyme lactase, which breaks lactose into sugars. With the domestication of cattle 9000 years ago, it became advantageous to digest milk, and lactose tolerance evolved in people who raised cattle.

In 2002, researchers identified a genetic mutation that regulates the expression of lactase and allows Finns and other northern Europeans to drink milk as adults. But researchers were surprised that the mutation appeared at lower frequency in southern Europe and the Middle East, and it was missing in most African pastoralists.

Tishkoff organized a team to collect blood samples from 470 Tanzanians, Kenyans, and Sudanese from 43 ethnic groups. Her team sequenced the DNA of 110 individuals who also were tested for milk tolerance.

Dairy queen. Some members of the Pokot people of Kenya carry three distinct mutations that allow adults to digest milk.

They found three new mutations in the same stretch of DNA as the European variant. The mutations turned up in varying frequencies in the Maasai and other Nilo-Saharan populations in Tanzania and Kenya, in Afro-Asiatic–speaking Kenyans, and in the Beja from Sudan; some people had all three mutations. People with any of the variants had higher blood sugar levels after drinking milk, a sign that lactose was being digested.

The researchers also found that the most common variant arose as recently as 3000 to 7000 years ago and spread rapidly. "This is extremely significant because it shows the speed with which a genetic mutation can be selected," says zooarchaeologist Diane Gifford-Gonzalez of the University of California, Santa Cruz. Indeed, the data suggest that humans who could digest milk had a huge reproductive advantage. "This is the strongest signature of recent positive selection yet observed," says Tishkoff.

The new data may also help explain why people tolerate milk to varying degrees. The ability to drink milk is "not a qualitative trait that you have or you don't," says Weiss. Tishkoff thinks there are yet more variants, and her team is seeking them.

–ANN GIBBONS

REGULATORY POLICY

EPA Draws Fire Over Air-Review Revisions

In a controversial move, the U.S. Environmental Protection Agency (EPA) has changed the way it reviews its health standards for six of the most widespread and dangerous air pollutants. Agency officials say the decision, announced last week, is designed to speed the notoriously slow process of revising these standards. But critics charge that the real intent is to give political appointees more control—an allegation that a powerful senator has vowed to investigate.

EPA's National Ambient Air Quality Standards (NAAQS) have enormous consequences, influencing the regulation of vehicles, industry, and agriculture in many ways. Under the Clean Air Act, the standards must be based on scientific evidence to protect human health and the environment, without regard to cost. The pollutants—including ozone, lead, and soot—must be reviewed every 5 years.

Fast lane. EPA says it wants to update air-quality standards more quickly, but critics see a political smokescreen.

Many observers believe the new review process has its roots in a political contretemps from a year ago, when Administrator Stephen Johnson ignored recommendations from staff scientists and the Clean Air Scientific Advisory Committee (CASAC) that a soot standard be tightened (*Science*, 6 January, p. 27). "It ▶

CREDITS (TOP TO BOTTOM): JIBRIL B. HIRBO; TOM GANNAM/AP PHOTO

was a PR fiasco for the Administration," claims Frank O'Donnell of the nonprofit Clean Air Watch in Washington, D.C., who thinks the Administration's goal with this revision is to prevent agency scientists from ever again making politically unpalatable recommendations. Just a week before the embarrassing episode, he notes, Johnson's deputy had asked for a "top-to-bottom review" of how EPA reviews the air standards.

Everyone agrees that the process is slow and cumbersome. EPA often misses the 5-year deadline, is sued by environmentalists, and ends up releasing incomplete or inadequate analyses. According to the new plan, a massive science review will be replaced with a slimmed-down "integrated science assessment," which could be finished and reviewed more quickly. In general, this is seen as a good move.

Other major changes are less welcome. High-level policymakers will now be involved early on to help identify "policy-relevant science issues," such as which dose-response model to use for turning observational data into an air standard. The current chair of CASAC—Rogene Henderson of the Lovelace Respiratory Research Institute in Albuquerque, New Mexico—thinks the purpose is to let upper-level management guide the analyses in ways that would make the recommended standards acceptable to the EPA administrator. In an earlier interview, George Gray, EPA's chief scientist, who helped design the new process, denied that the intent was political. "This is about efficiency," he said.

In another change, CASAC will no longer review early drafts of policy assessments; it will see them only after they're released for public comment as proposed rules—along with industry and other groups. "This is a huge step backward," says Philip Johnson of NESCAUM, a nonprofit association of air-quality agencies in Boston. He sees the changes as marginalizing CASAC and making it easier for the administrator to ignore its advice. But Henderson is more sanguine. "This won't interfere with duties of CASAC to be an honest broker of the science," she says.

U.S. Senator Barbara Boxer (D–CA), the new chair of the Senate Committee on Environment and Public Works, called the new air review process "a dangerous turn" and pledged to make it "a top priority for oversight in the 110th Congress." The changes will apply immediately to the review of the ozone standard, for which a proposed decision is due in March, and the lead review, which is just beginning. **–ERIK STOKSTAD**

CREDIT: UNNY ESKINDER DEBEBE

ARMS CONTROL

Little Progress at Bioweapons Talks

At least nobody slammed the door shut. That's the good news, participants say, after a 3-week international conference to review the international treaty banning biological weapons. The meeting ended in Geneva, Switzerland, on Friday with a low-key consensus statement: The participants basically agreed to keep talking. But outside observers say the meeting failed in its real ambition: to beef up the 34-year-old Biological and Toxin Weapons Convention (BTWC). A protocol to start verifying compliance, which the United States firmly rejected 5 years ago, wasn't even on the table. And conflicts about technology transfer hampered progress on other fronts.

Marathon. The 3-week session on weapons control heard from U.N. Secretary-General Kofi Annan and conference president Masood Khan of Pakistan (*center*).

The BTWC, a treaty that bans development, production, and stockpiling of biological weapons, has always been a work in progress. Just four pages long, it provides no mechanisms to monitor compliance or investigate countries suspected of cheating. At so-called Review Conferences, held every 5 years, member states have long discussed ways to strengthen the convention. The need to do so became painfully clear in the early 1990s, when defectors revealed a vast Soviet program to weaponize smallpox and anthrax.

But negotiations launched in 1995 to create a verification protocol for the BTWC collapsed in 2001, in part because the United States feared that allowing international experts to inspect biotech facilities might give away defense or industry secrets (*Science*, 20 July 2001, p. 414). In the resulting disarray, the Fifth Review Conference in 2001 failed to agree on a final declaration.

Since then, countries have searched for other ways to strengthen the convention. They held three intersessional meetings about issues such as disease surveillance and codes of conduct for scientists. And they have floated a number of new ideas for shoring up the convention at the Sixth Review Conference. By Friday, however, it had become clear that few plans to strengthen the treaty had made it to the finish line. One obstacle was an action plan, introduced by Iran and adopted by the countries of the Non-Aligned Movement to reinforce an article of the BTWC that promotes the transfer of technology for peaceful purposes.

Such stipulations give developing countries an incentive to participate, says Jonathan Tucker, a Fulbright Scholar at the German Institute for International and Security Affairs in Berlin. But developing countries overreached, says Finnish delegate Kari Kahiluoto, who spoke on behalf of the European Union, by demanding support for public health programs, vaccines, and drugs—issues that don't belong in an arms-control deal, he says. The United States also balked at the prospect that easing export controls on dual-use biotechnology equipment could increase biological weapons proliferation, adds Tucker. Iran and others in turn shot down a U.S.–backed plan to ensure that countries enshrine the treaty in national laws and regulations.

The intersessional meetings will continue until the next Review Conference in 2011, and the list of topics has been expanded slightly. There's a plan to recruit more countries to the convention. And members will finance a new three-person support team in Geneva. But these are "very modest" improvements, says Alan Pearson of the Center for Arms Control and Non-Proliferation in Washington, D.C. Indeed, says Tucker, "It shows how dysfunctional this process has become that we're excited about such small steps." But in negotiations like these, Kahiluoto says, "you can't even take a modest outcome for granted."

–MARTIN ENSERINK

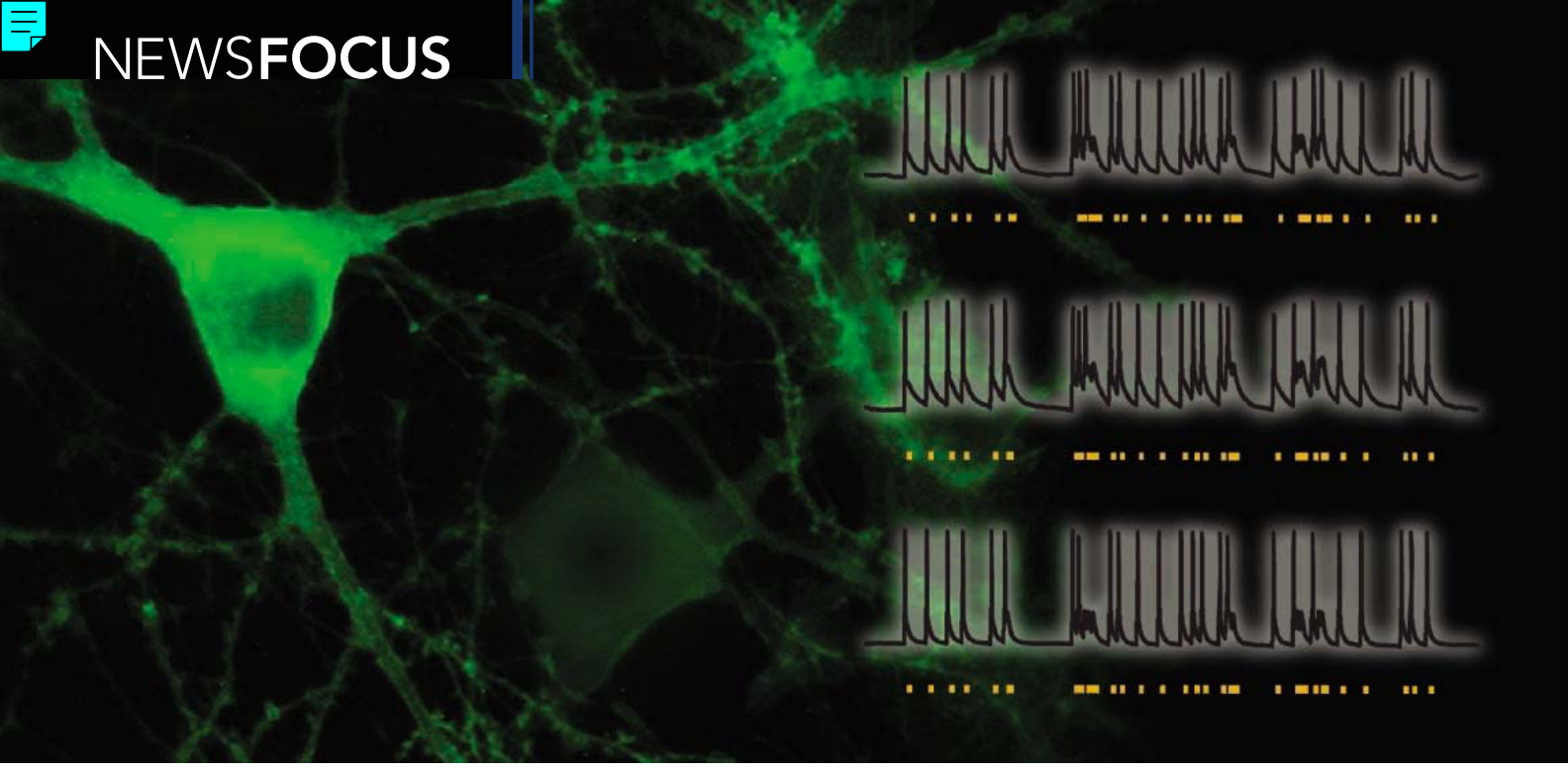

Emerging methods that combine genetics and optics have neuroscientists glowing about the possibilities

Shining New Light on Neural Circuits

WHEN RESEARCHERS FROM YALE university reported last year that they'd used a laser to activate neurons in fruit flies and in turn control the insects' behavior, even Jay Leno thought it was cool. In a skit, the *Tonight Show* host pretended to use a remote-controlled fly to harass President George W. Bush during a speech. "I thought it was actually quite funny," says Gero Miesenböck, the neuroscientist who led the study. A video clip of Leno's skit elicited chuckles when Miesenböck played it during a presentation at October's meeting of the Society for Neuroscience in Atlanta, Georgia.

But the neuroscientists who packed the crowded lecture hall hadn't come for laughs. Miesenböck's talk was part of a symposium on "optogenetics," an emerging field that combines tools from optics and genetics to visualize and stimulate the nervous system. Several of the new methods, such as the one Miesenböck developed for the fly experiments, use genetic manipulations to confer light sensitivity on specific groups of neurons, making it possible to control their activity with pulses of light. Many neuroscientists say such stimulation methods represent powerful new tools for investigating neural circuits. "I think it's really exciting," says Liqun Luo, a neurobiologist at Stanford University in Palo Alto, California, who attended the symposium. "It's at the cutting edge."

> "All you have to do is express this one protein, and **now you can control the activity of the neurons with light."**
>
> —Edward Callaway, Salk Institute for Biological Studies

Currently, several new photostimulation methods are in various stages of development, and scientists are just beginning to use them to address questions about brain function. But down the road—way down the road—some researchers envision exciting clinical applications. One idea is to replace the metal electrodes used for deep-brain stimulation in patients with Parkinson's disease and other disorders with fiber-optic probes that carry light deep inside the brain to boost the activity of only those neurons that need it.

Lighting up

Using light to manipulate the nervous system is not a new idea. In the past 20 years, researchers have done many experiments with neurotransmitters bound to molecules that change shape in response to light. Such "caged" neurotransmitters are inactive, but a pulse of laser light sets them free to activate their usual receptors. Glutamate, the brain's chief excitatory neurotransmitter, has become a particularly popular tool in caging experiments. Glutamate uncaged with lasers can stimulate synapses with precise temporal and spatial control; a team from Princeton University reported last year in *Nature Methods* that they had done this at up to 20,000 different locations in an excised slice of brain tissue. There are drawbacks, however. Because almost all neurons respond to glutamate, it's virtually impossible to target only neurons of a particular type. And the precise spatial control requires a stationary target—a nonstarter for researchers who want to study behavior in intact animals.

Miesenböck's fly experiments circumvent these problems. Together with graduate student Susana Lima, Miesenböck inserted a rat gene that encodes an ion channel into flies. Fly neurons normally don't make this cell membrane portal, which opens in response to ATP, the energy-storage molecule involved in cell metabolism. Using standard genetic engineering tools, Lima and Miesenböck created several fly strains that

CREDIT: FENG ZHANG AND KARL DEISSEROTH/STANFORD

Precision firing. A hippocampal neuron (green) loaded with ChR2 channels fires in response to flashes of light (yellow dots).

expressed the ATP-gated channel only in specific classes of neurons. Then they injected caged ATP into the flies. When liberated by a flash of light, the ATP opened the channels in the modified neurons and allowed sodium and calcium ions to rush in, thereby prompting the neurons to fire a burst of electrical impulses. Because only neurons made to express the channel could respond to light, precise aim wasn't necessary; a fly-sized spotlight did the trick.

In one strain of fruit flies, Lima and Miesenböck put the ATP-gated channel in just two neurons out of the roughly 100,000 in the fly's nervous system, the so-called giant fiber neurons that control the fly's escape reflex. A brief flash of light made these insects jump and frantically flap their wings. In another strain, the researchers restricted the channel to neurons that make the neurotransmitter dopamine. Stimulating these neurons with light made the flies more active and increased the time they spent exploring their enclosure, Lima and Miesenböck reported in the 8 April 2005 issue of *Cell*; it was this study that inspired Leno's skit.

These fly findings are consistent with the idea, suggested by many earlier studies, that dopamine helps animals predict rewards and punishments, Miesenböck says. One possibility, he explains, is that activating dopaminergic neurons increases exploratory behavior because flies interpret the dopamine burst as a signal that something good—or bad—is nearby. His team is now working on ways to target the ATP-gated channel to different subsets of the fly's 150 or so dopaminergic neurons so that their roles in exploratory and other types of behaviors can be investigated.

Ball and chain

Richard Kramer of the University of California (UC), Berkeley, has been investigating ways to make neurons sensitive to light by modifying other ion channels. In 2004, Kramer, neuroscientist Ehud Isacoff, and chemist Dirk Trauner, both also at UC Berkeley, described modified potassium channels that open and close when exposed to different wavelengths of light. Their approach makes use of an unusual feature of a molecule called azobenzene. In visible light, an azobenzene molecule is relatively straight and measures about 17 angstroms from end to end. When illuminated by ultraviolet light (UV), however, it folds in the middle, shortening the distance between the two ends to about 10 angstroms.

To take advantage of this shape change, Kramer and colleagues incorporated azobenzene into a molecular ball and chain that attaches to the extracellular side of a common variety of potassium channel. First, they tweaked the potassium channel gene to create a favorable binding site and expressed the altered channels in transgenic mice. Then they bathed slices of brain tissue from these mice in a solution containing the ball and chain, which has three components. The ball is a quaternary ammonium ion that can fit snugly into the channel's pore and prevent the flow of potassium ions. Next comes an azobenzene molecule and then a compound called maleimide that links the azobenzene to the potassium channel. When azobenzene is in its long state, the chain is just long enough to allow the ammonium ball to plug the pore. But when a pulse of UV light converts azobenzene to its shorter, bent configuration, the ammonium plug is pulled from the pore and potassium can flow freely into the neurons.

Opening potassium channels typically inhibits neural firing, so in the 2004 work, UV light acted something like an off switch on neurons equipped with the azobenzene-modified channels. Kramer and company recently created a light-controlled on switch for neurons by further tweaking the potassium channel gene so that the protein admits sodium ions as well. When these modified channels are lit up with UV light, sodium rushes into neurons and excites them, the researchers reported in the November 2006 issue of the *Journal of Neurophysiology*.

The UC Berkeley group has also added an azobenzene photoswitch to glutamate receptors, ubiquitous ion channels in neurons that normally open in response to glutamate.

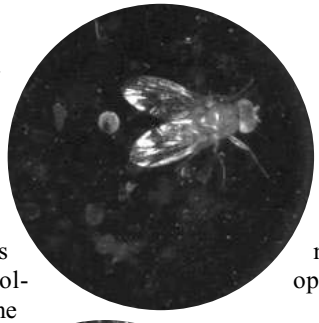

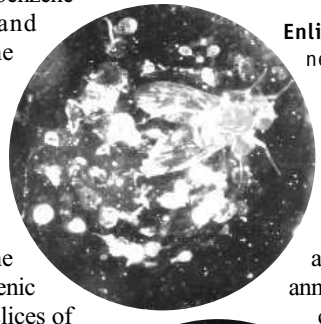

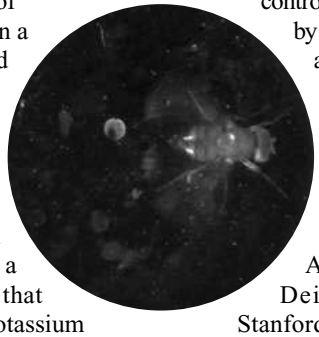

Enlightening. In a fly with light-sensitive neurons (*top*), a flash of light (*middle*) triggers an escape response, flapping wings (*bottom*).

They described the receptors in the January 2006 issue of *Nature Chemical Biology*. Kramer, Isacoff, and Trauner will be part of a newly announced center for studying the optical control of biological function. Funded by the National Institutes of Health and run jointly by UC Berkeley and Lawrence Berkeley National Laboratory, the center is part of NIH's nanomedicine initiative.

Help from algae

Across San Francisco Bay, Karl Deisseroth and colleagues at Stanford have developed yet another optogenetics approach, based on a light-sensitive ion channel found in a unicellular green alga. Called channelrhodopsin-2 (ChR2), the channel opens in response to light, allowing positively charged ions to pass through its pore. The photosynthetic algae use ChR2 to orient to light. Expressing the gene for ChR2 in neurons makes them fire when exposed to light, Deisseroth and colleagues first reported in the September 2005 issue of *Nature Neuroscience*.

With this approach, there's no need for extra steps such as adding caged ATP or azobenzene to neurons. "It's a very simple system because all you have to do is express this one protein, and now you can control the activity of the neurons with light," says Edward Callaway, a neuroscientist at the Salk Institute for Biological Studies in San Diego, California. And unlike the ATP-gated channels and the azobenzene photoswitch, the ChR2 system can trigger neural firing within just a few milliseconds of being hit by a laser beam. That makes it possible to deliver light pulses that drive the neurons in precisely controlled patterns that mimic the normal chatter of neural activity, explains

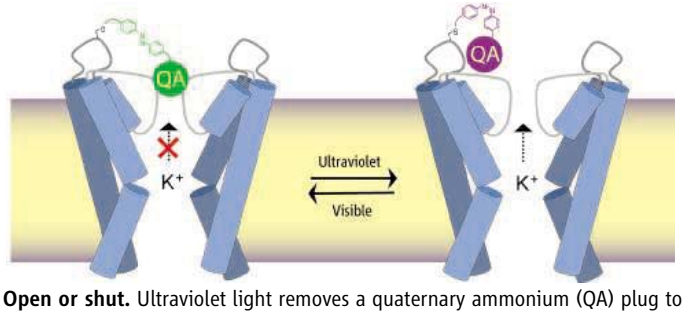

Open or shut. Ultraviolet light removes a quaternary ammonium (QA) plug to open a light-sensitive potassium channel.

CREDITS: (TOP) SUPP. MATERIAL FROM S. Q. LIMA AND G. MIESENBÖCK, *CELL* **121**, 141–152 (2005); (BOTTOM) R. H. KRAMER *ET AL.*, *NATURE CHEMICAL BIOLOGY* **1**, 7 (2006)

Gary Westbrook, a neuroscientist at Oregon Health & Science University in Portland. "I think the biggest advantage of channelrhodopsin is the ability to stimulate with such high time resolution," he says.

Westbrook's lab intends to express ChR2 in newborn neurons in the mouse hippocampus to study how these cells communicate with mature neurons as they integrate themselves into preexisting neural circuits (*Science*, 17 February, p. 938). "We don't know anything about the output of that population of cells," Westbrook says.

Other labs are also using the ChR2 system. At the recent neuroscience meeting, Guoping Feng of Duke University in Durham, North Carolina, presented preliminary work he's done in collaboration with Deisseroth and George Augustine at Duke. Feng and colleagues have created two strains of transgenic mice, one that expresses ChR2 in the output cells in a specific layer of the cerebral cortex and another that expresses the light-sensitive channel in mitral cells in the olfactory bulb. These efforts have convinced Feng that the method "works really well in vivo." Ultimately, he hopes to use the ChR2 system to investigate neural circuits involved in addiction and compulsive behavior. "Many neurological diseases are diseases of specific subtypes of neurons," he says. "This will give us a way to target specific neurons to understand their function in the circuitry of the brain."

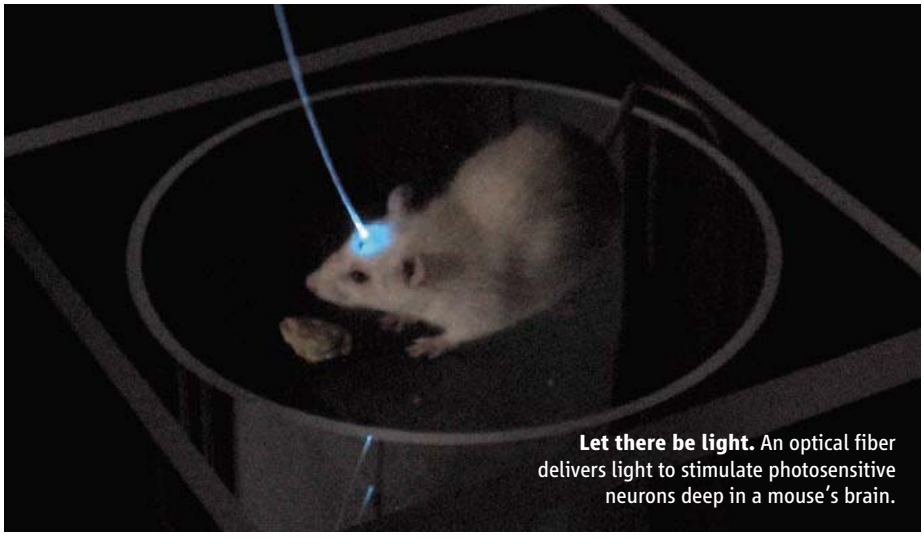

Let there be light. An optical fiber delivers light to stimulate photosensitive neurons deep in a mouse's brain.

At the neuroscience meeting, Deisseroth presented preliminary work that further illustrates the potential. He used a virus to put ChR2 into neurons in a slice of mouse hippocampus, genetically tagged the same neurons with a fluorescent dye so that they were visible under a microscope, and used a fluorescent indicator of calcium flux to monitor their activity. The ability to simultaneously see, stimulate, and record the activity of neurons with light is a powerful combination for investigating the connectivity of neural circuits, he and others say.

Clinical vision?

The new optogenetics techniques should provide more sophisticated options for exploring the neural underpinnings of behavior, Miesenböck says. Although neuroscientists have long used metal electrodes to manipulate neural activity, it's nearly impossible to use electrodes to stimulate a distributed population of neurons simultaneously, he explains. "The dopamine experiment in the fly would have been impossible with electrodes because you have about 150 cells arranged in different clusters," Miesenböck says.

Not that there are no obstacles. The main one at present, several researchers say, is the ability to deliver the required genes to specific classes of neurons. "All these methods rely on the ability to direct gene expression to a particular cell type," says Callaway. "I think 5 or 10 years ago, we all thought that was going to be really easy, but it hasn't proven so easy to do." Another hurdle is getting light to deep-lying parts of the nervous system; so far, the techniques have only been used in slices of brain tissue and areas close to the surface of the brain in live animals.

This last obstacle may not be insurmountable, however. Deisseroth's lab has been experimenting with using flexible optical fibers to stimulate ChR2-bearing neurons deep in the brains of awake, behaving mice. Off-the-shelf fiber optics are sufficient for stimulation alone, Deisseroth says, but more elaborate experiments that combine stimulation with recording and imaging—such as the ones he described in brain slices—may also be possible in live animals before long. And at the neuroscience meeting, Stanford applied physicist Mark Schnitzer showed off a microendoscope small enough to fit on the head of a freely moving mouse. The thumbnail-sized device weighs less than 4 grams, and its fiber-optic probes can reach any structure in the mouse brain. So far, Schnitzer's group has been using the device for imaging cells labeled with fluorescent dyes, but he says there's no reason it couldn't also be used to stimulate light-sensitive neurons.

Far in the future, it's conceivable that fiber-optic light stimulation could replace deep brain stimulation via electrodes, a method currently under investigation for Parkinson's disease, depression, epilepsy, and other disorders. "An electrode stimulates all the cell types" that happen to be near its tip, Deisseroth says. "It's generally understood that that will contribute to side effects and reduce the efficacy." A better solution, he says, would be to target the stimulation to certain classes of cells. But Deisseroth cautions that "a lot of things have to fall into place for this to happen," not the least of which is resolving the serious safety concerns about gene therapy in humans.

Another potential clinical application is restoring sight in people with retinal degeneration. In the 6 April 2006 issue of *Neuron*, researchers led by a team at Wayne State University in Detroit, Michigan, reported encouraging results from an experiment in which they used a virus to deliver the ChR2 gene to retinal ganglion cells in mice whose retinas lack photoreceptor cells. Retinal ganglion cells are normally insensitive to light. But adding ChR2 made them respond to light and made the animals' visual cortices responsive to visual stimuli. (Kramer's team has been experimenting with ways to add a photoswitch to these cell's natural ion channels by chemical means alone rather than introducing foreign genes.)

There's no reason the future clinical applications of photostimulation methods would have to be limited to the nervous system, Kramer adds. He can imagine doctors one day using fiber-optic probes to examine the heart and other organs—using light to perturb a few specific cells that had been temporarily made light-sensitive by genetic or other means and recording a physiological response. Kramer is quick to add that any such clinical payoffs are a long way off: "It's so far out there who knows if it will ever happen," he says. But when it comes to basic neuroscience research, he and others are confident that the new optogenetics methods have a bright future. **–GREG MILLER**

CREDIT: ALEX ARAVANIS AND KARL DEISSEROTH/STANFORD

PROFILE: VITALY GINZBURG

After a Lifetime in Russian Science, Concern for the Future

In his 90th year, Vitaly Ginzburg sees promise in Russian science but says, "I don't like very much what is happening now in our country"

MOSCOW—If anyone ever wanted proof that intellectual capacity is not limited by physical space, it can be found in the office of Vitaly L. Ginzburg, the Nobel laureate. The room is long and narrow—smaller than the wardrobe closet of a New Russian. It is so narrow, in fact, that plaster has been knocked out of a wall in two places by the desk chair, which cannot be pushed back far enough to sit down or get up comfortably. And Ginzburg, who celebrated his 90th birthday in October, is a tall man.

Creature comforts have always been an extravagance at the P. N. Lebedev Physical Institute of the Russian Academy of Sciences, where Ginzburg carried out much of his prizewinning theoretical studies of superconductivity. Formulas still are worked out for all to see on a wide green chalkboard that hangs in a central corridor.

These days, Ginzburg's office is unused. Yellow Post-it notes hang, dusty, from cabinet doors. Cracks in the windows are covered with packing tape. Debris from the ceiling is scattered over stacks of papers and books on the windowsill. A calendar says 2003—the year Ginzburg was awarded the Nobel Prize in physics with two others, Alexei A. Abrikosov and Anthony J. Leggett, for their contributions concerning two phenomena in quantum physics: superconductivity and superfluidity. In the 1950s, Ginzburg helped develop a theory on the behavior of superconductors—metals, alloys, ceramic compounds—in a magnetic field, laying the groundwork for further studies on so-called Type 2 superconductors, which pass electricity without resistance at higher, more practical temperatures. They are used, for example, in magnetic resonance imagining and particle acceleration. Not long after receiving the prize, Ginzburg was diagnosed with Waldenstrom macroglobulinemia, an extremely rare cancer of the blood that is treatable but incurable. He lived and worked for nearly 2 years in a hospital bed.

Bright moment. Born in tsarist times, Ginzburg worked on the hydrogen bomb and received the Nobel Prize in 2003 for theoretical studies of superconductivity.

CREDIT: STEFAN LINDBLOM/CORBIS

Late last summer, he was told that he had recovered enough to go home. "If my secretary tries to say that I'm doing well, don't believe her," says Ginzburg, a good-humored man who, nevertheless, characterizes himself as "rather grave."

Ginzburg sleeps and works in his airy study in a spacious Moscow apartment that is teeming with houseplants. The time he once spent undergoing treatment he now spends writing in light-blue flannel pajamas at a large wooden desk, above which hang two photographs: one of his wife, Nina, and the other of the two of them out on the town. He calls the office regularly. "He doesn't want to lose contact with the outside world," says his secretary, Svetlana Volkova, who types the essays and letters that he writes, longhand, at all hours. The words are often scrawled in pencil in large letters, because he has yet to learn how to use a computer. He delights in the freedom enjoyed by theoretical physicists; he says they "possess a singular possibility to engage in a very wide spectrum of problems, since it is easy to move from one to the other on paper."

Ginzburg is concerned with the worsening state of democracy in Russia, the creeping influence of religion in education, and the effects of what he calls "pseudosciences," such as astrology. He is also concerned with euthanasia; he thinks the terminally ill should be allowed to die if they choose. He tries to keep up with research in physics, particularly superconductivity at warmer temperatures. "I also think a lot about my own fate," he says. "I am grateful that they succeeded in giving me the prize before I died."

Ginzburg focuses much of his energy commenting on the future of the Russian Academy of Sciences, the 282-year-old institution that, in exchange for government pledges to spend more money on salaries and laboratory equipment, recently ceded much of its autonomy to the state (*Science*, 10 November, p. 917). He may be the most prominent of a group of critics who claim that the Kremlin has been empowered to sell off the academy's assets—an "idiotic" plan, he thinks. "Undoubtedly, science in Russia has fallen behind. Essentially, some 20 years have been lost," he says. "We cannot catch up to America, or even England. But, overall, it is possible to do good work here. A large number of highly qualified people remain." The government should increase financing for the sciences, he says, but without favoring applied over fundamental research, or converting the institution into what is effectively a governmental department.

Although Ginzburg has been immobilized by illness, his assistants are keen to point out that his moral barometer is robust. "Please understand that I am a democrat at heart, and, of course, I don't very much like what is happening now in our country. … But I am not a political activist. I don't say all that I feel, as they would likely jail me," he says, laughing. Still, he cannot be said to be biting his tongue.

He characterizes as a "return to the time of Stalin" the arrests since the late 1990s of scientists by the Federal Security Service. The charges, which Ginzburg and many other scientists consider to be flimsy, are that they sold state secrets. He rails against attacks on atheists, such as himself, by those who wish to bring church teachings into public schools and universities. He also denounces major newspapers, such as *Izvestia*, for publishing horoscopes, which he calls "pure hokum."

Often he is asked what he has done with the roughly $350,000 in Nobel Prize money, an enormous sum in a country where experienced researchers are being promised 30,000 rubles ($1150) a month by 2008. He says that he has put the money away for the college educations of his two great-grandchildren, a twin boy and girl living in Princeton, New Jersey.

He sold his country house to help pay for medical treatment and likens his fate to that of two great Soviet physicists, Igor Y. Tamm and Lev D. Landau, both Nobel laureates with whom he worked. (Like Tamm, Ginzburg was recruited to help design the first Soviet nuclear bombs, but by a stroke of luck, he says in his Nobel autobiography, his low security rating kept him in Moscow, away from the Arzamas-16 military site.) Although he is proud to have followed in the footsteps of Tamm and Landau as a physicist, he says he is reluctant to be following "their path [to the grave]." He recounts their deaths in an essay on the Web site of a magazine for which he is editor, *Uspekhi Fiziki*, or *Advances in Physics*, which has been in existence since 1918.

Tamm, who suffered from amyotrophic lateral sclerosis, or Lou Gehrig's disease, used to say that he was attached to a respirator like "a bug on a pin" in a specimen case. Landau died over the course of 6 years after sustaining painful injuries in a car accident. Ginzburg, saying he has a low tolerance for pain, recently laid bare his wishes in an essay titled, "On the Right to Die." "From the very beginning of my illness, I have dreamed about death, but, of course, a painless death," he writes.

He published the piece online in a relatively obscure publication, he says, to avoid being accused of encouraging euthanasia, a crime in Russia. "I have done all that I can. Within several months at the end of successful treatment, I most likely will have written, in my [90] years, a mere handful of articles and letters. It is absurd to suffer such long months for that. It brings me to recall the joke that goes, 'Why do you exercise?' The answer: 'To die healthy!'"

Civil society, he says, is not sufficiently developed in Russia to enact a right-to-die law anytime soon. So he continues to write the essays and letters for which he has concluded that life is not worth living.

Increasingly, he has been publishing interviews and essays in the magazine *Zdravy Smysl*, or *Common Sense*—something that he says is missing from public discourse in his country. "What else can I do?" he says. "For now, living is in the cards."

–BRYON MACWILLIAMS

Bryon MacWilliams is a writer in Moscow.

CREDIT: RIKEN

NUCLEAR PHYSICS

Japan Gets Head Start in Race to Build Exotic Isotope Accelerators

A new facility begins to explore the structure of the nucleus as Europe awaits two machines and the United States revises its plans

WAKO, JAPAN, AND ROSEMONT, ILLINOIS— Sometime this month, a warning siren will clear personnel out of the bowels of a massive concrete building in Wako, a city just east of Tokyo. Then, the world's most powerful cyclotron will propel a stream of uranium ions at a carbon target. The resulting smashup will produce radioactive nuclei that have never existed outside a supernova. Such fleeting exotic bits of matter should help unify a fragmented theory of the nucleus, reveal the origins of the heavier elements, and provide clues to why the universe contains so much more matter than antimatter.

Data from the $380 million Radioactive Isotope Beam Factory (RIBF) at the Institute of Physical and Chemical Research (RIKEN) in Wako "will allow us to form a new framework for nuclear physics," says Hiroyoshi Sakurai, chief nuclear physicist at RIKEN's Nishina Center for Accelerator-Based Science, which built and will operate the machine. Richard Casten, a nuclear physicist at Yale University, agrees that knowledge sifted from the atomic shards "will be transformational in our understanding of nuclei."

But Japanese physicists aren't the only ones staking a claim to this fertile turf. RIBF is the first in a new generation of exotic isotope accelerators. Researchers in Germany and France hope to have machines ready to power up in 2010 and 2011, respectively. Meanwhile, a U.S. National Research Council (NRC) report released last week makes the case for building the most powerful machine of all. U.S. researchers hope the report will jump-start a project, once known as the Rare Isotope Accelerator (RIA), that stalled last year after the U.S. Department of Energy (DOE) ordered researchers to cut in half the projected $1 billion cost. "This report helps get the project unstuck by more clearly defining the science that can be done with it and the international situation," says Michael Turner, a cosmologist at the University of Chicago and chief scientist at DOE's Argonne National Laboratory in Illinois, one of two institutions vying for the machine.

Accounting for more than 99.9% of an atom's mass and less than a billionth of its volume, the nucleus is a knot of protons and neutrons. Nature provides 260 stable nuclei, and researchers have glimpsed 10 times that number of unstable ones. But machines that produce even more would provide new insights into the structure of the nucleus.

For example, since the 1940s, physicists have known that nuclei with certain "magic" numbers of protons or neutrons appear to be more stable than might otherwise be expected. However, recent findings suggest that the known magic numbers—2, 8, 20, 28, 50, 82, and 126—may not apply to nuclei with an extreme excess or deficiency of

Revving up. Japan's new exotic isotope accelerator should come on line within weeks.

neutrons, says Takaharu Otsuka, a theoretical physicist at the University of Tokyo. An exotic isotope accelerator could search for new magic numbers for highly unstable nuclei and help physicists develop a more comprehensive theory of the nucleus.

Experiments at RIBF will also allow researchers to "take on the challenge" of elucidating stellar processes, says Yasushige Yano, head of the Nishina Center. Scientists believe that half elements heavier than iron are created somewhere within supernovae by a phenomenon known as the R-process, in which nuclei become bloated with neutrons. The resulting neutron-rich nuclei then decay into the familiar stable elements. But physicists don't know precisely how, or even where, the R-process takes place. Studying fleeting neutron-laden nuclei in the lab should help remedy that situation, says Otsuka.

An exotic isotope accelerator might even help explain why the universe is rich in matter and essentially devoid of antimatter. Physicists believe that the imbalance emerged in the infant universe thanks in part to a slight asymmetry between matter and antimatter known as charge-parity (CP) violation, which has been observed only in two types of exotic particles called mesons. According to the standard model of particle physics, such asymmetry could be reflected in the properties of certain exotic nuclei, such as the distribution of electric charge within them. So those nuclei might reveal other sources of CP violation to probe one of the larger mysteries in the cosmos.

To pursue such goals, RIBF links an existing linear accelerator, or linac, and cyclotron with two new conventional cyclotrons and a superconducting ring cyclotron that together will accelerate even the heaviest nuclei up to 70% of light speed. The heavy nuclei will blast through a target of lighter ones and be ripped apart, like a car crashing into a steel post—a process called in-flight fragmentation. The exotic nuclei will be sorted into secondary beams and analyzed or smashed into still other nuclei.

But some of the science may have to wait for more funding. Although the beamline is ready, RIKEN lacks money for instrumentation and experiments. Some projects will start next year, but more complete instrumentation won't be in place until 2008, says Sakurai.

Still, that timetable gives RIKEN a big head start on the competition. Researchers at France's heavy-ion lab, GANIL in Caen, are working on SPIRAL2, a linac that will also produce exotic isotopes by in-flight fragmentation. SPIRAL2 will also smash light nuclei into heavy ones in a solid target to chip the target nuclei apart—a technique known as isotope separation online (ISOL). Meanwhile, researchers at Germany's GSI heavy-ion research center in Darmstadt await a green light to build the sprawling international Facility for Antiproton and Ion Research (FAIR), a synchrotron lab that will produce exotic isotopes, among other things. FAIR will create the nuclei by in-flight fragmentation and will accelerate them to far higher energies. GSI officials are hammering out an agreement with international partners, and construction could start next year.

Researchers in the United States hope that the NRC report will help them get back in the game. In 1999, nuclear physicists proposed using a high-energy, high-throughput linac to create RIA, a dream machine that would have excelled in every technique. In 2003, RIA tied for third on a list of 28 projects DOE hoped to complete within 20 years, and researchers anticipated construction starting as early as 2008. Argonne and Michigan State University in East Lansing were vying to host the machine.

But in February, DOE put the pricey project on hold and asked for something cheaper (*Science*, 24 February, p. 1082). DOE and the National Science Foundation (NSF) had already requested an NRC review of the science that RIA could do, and the Argonne and Michigan State teams suggested building a shorter linac with half the energy (but twice the beam current) and eliminating experimental stations. Last week, the review committee presented its analysis of the more modest proposal to members of NSF and DOE's Nuclear Science Advisory Committee (NSAC) at a meeting outside Chicago.

Even the smaller-scale machine would be worth building, the committee concluded. "There is a persuasive case for the science that can be done with this machine," says committee co-chair John Ahearne, a physicist with the scientific society Sigma Xi in Research Triangle Park, North Carolina. That conclusion takes into account the foreseeable competitors, says co-chair Stuart Freedman, an experimental physicist at the University of California, Berkeley, who noted that "without a facility like this, this part of the [U.S. nuclear physics] community likely would not survive."

The report cheered rare-isotope researchers. "It's very positive, very encouraging," says Konrad Gelbke, director of the NSF-funded National Superconducting Cyclotron Laboratory at Michigan State. Donald Geesaman, a physicist at Argonne, says the report provides "validation of the importance of the science from a broader community" than just exotic-isotope researchers. Researchers now hope construction can begin in 2011 for a start-up in 2016.

Physicists still have a long way to go to transform their idea into a machine, however. First up is a design for the vaguely defined facility. Unlike RIA, the new machine won't do it all. Argonne researchers favor the ISOL approach, whereas Michigan State physicists favor in-flight fragmentation. Both groups would also pursue a novel scheme called reacceleration, catching isotopes in a tank of gas and then feeding them into a second accelerator. This spring, an NSAC subcommittee will weigh in on the matter.

Then there's the question of finding $500 million to pay for the machine. Last year, DOE submitted to Congress a 5-year plan "that involves growth in the bottom line of the Office of Science, and this [facility] is part of the plan," says Dennis Kovar, director of the DOE nuclear physics program. Whether the new Congress will go along, however, remains to be seen.

–DENNIS NORMILE AND ADRIAN CHO

Rare opportunity. The U.S. rare-isotope community needs a machine like the one proposed at Michigan State University to stay competitive, says Stuart Freedman, co-chair of a recent review panel.

CREDITS: NSCL; (INSET) A. CHO/*SCIENCE*

PICTURE YOURSELF AS A AAAS SCIENCE & TECHNOLOGY POLICY FELLOW!

Advance your career and serve society by plugging the power of science into public policy. Year-long Science & Technology Policy Fellowships offer opportunities in six thematic areas: Congressional • Diplomacy • Energy, Environment, Agriculture & Natural Resources • Global Stewardship • Health, Education, & Human Services • National Defense & Global Security.

Work in Dynamic Washington, D.C.
Since 1973, AAAS Fellows have been applying their expertise to federal decision-making processes that affect people in the U.S. and around the world. A broad range of assignments is available in the U.S. Congress and executive branch agencies.

Join a Network of Nearly 2,000 Fellows.
AAAS Fellows benefit from a growing and diverse network of colleagues. Applicants must hold a PhD or equivalent doctoral-level degree in any physical, biological, medical/health, or social science, or any engineering discipline. Individuals with a master's degree in engineering and three years of post-degree professional experience also may apply. Federal employees are not eligible and U.S. citizenship is required.

Apply Now!
The application deadline for the 2007-2008 Fellowships is 20 December 2006. Fellowships are awarded in the spring and begin in September. Stipends range from $67,000 to $87,000, depending on experience.
To apply: fellowships.aaas.org

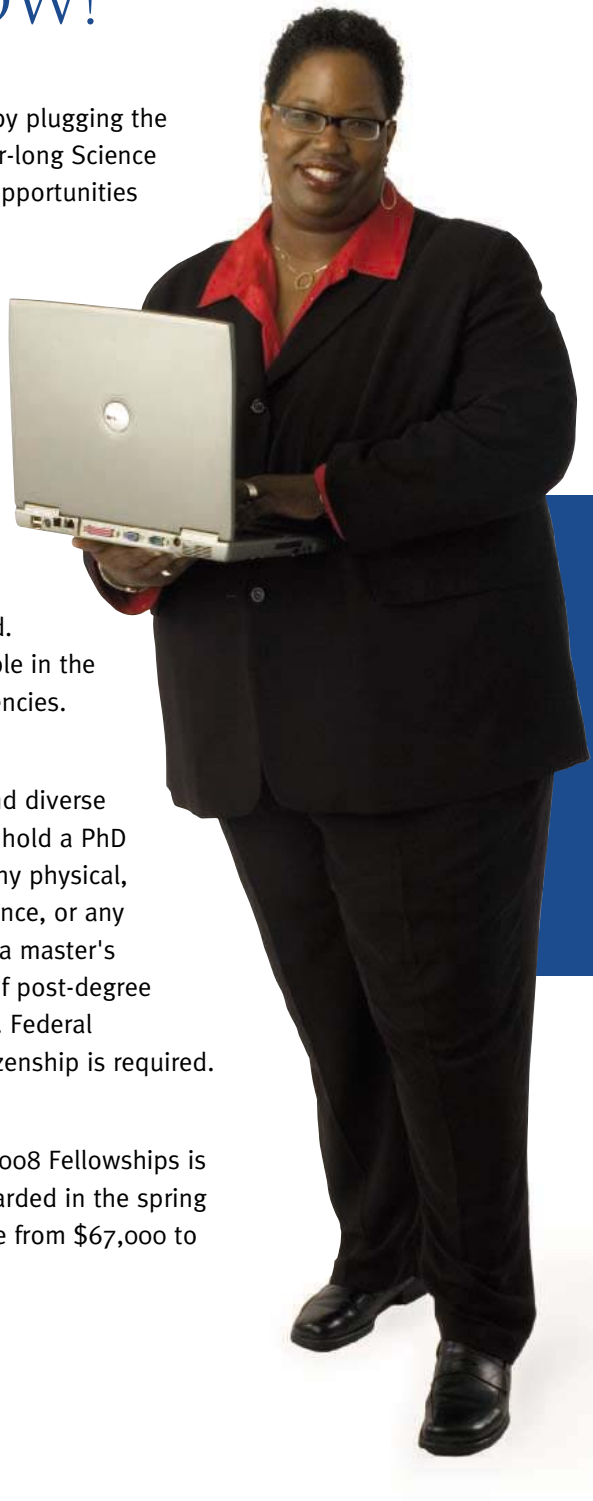

Enhancing Public Policy, Advancing Science Careers

Stephanie Adams, PhD

Interdisciplinary Engineering, Texas A&M University.

2005-2006 AAAS Fellow at the National Science Foundation, Division of Engineering Education and Centers.

Currently associate professor and assistant dean for research at the Department of Engineering at the University of Nebraska-Lincoln, which granted her a two-year Interpersonnel Agreement (IPA).

AAAS
ADVANCING SCIENCE, SERVING SOCIETY

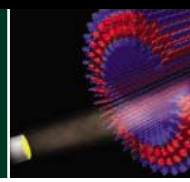

LETTERS

edited by Etta Kavanagh

Retraction

WE WISH TO RETRACT OUR REPORT "DUAL SIGNALING REGULATED BY calcyon, a D1 dopamine receptor interacting protein" (*1*). In this Report, enhanced D1 dopamine receptor (D1R)–stimulated intracellular Ca^{2+} release was attributed to a direct interaction with calcyon, a novel protein isolated in a yeast two-hybrid screen (Y2H) using the D1R C-terminal tail as bait. Resequencing of the cDNA clone obtained in the Y2H screen resolved a particularly GC-rich region upstream of the calcyon start codon that had been misread before and indicated that the calcyon coding sequence is out of frame with the GAL4 activation domain. In view of this, we conducted other in vitro studies and found that calcyon and D1Rs do not directly interact. Further, we also determined that although D1Rs do stimulate intracellular Ca^{2+} release after priming of cells (*1*) or neurons with G_q-linked receptor agonists (*2*), calcyon does not significantly enhance this response. The ability of calcyon and D1Rs to co-immunoprecipitate when co-expressed in cells as reported (*1*) presumably stems from the association of both proteins with clathrin-coated vesicles (*3*, *4*). Likewise, calcyon is co-expressed in a number of D1R–positive neurons in brain and, like D1Rs, is found in dendritic spines. Thus, the isolation of the calcyon clone in a Y2H screen with D1Rs appears to have been adventitious. We must therefore retract this Report. We sincerely regret that we did not discover these errors before publishing. The third author of the Report, Steven Eubanks, has graduated from Medical College of Georgia and could not be located to sign the Retraction. The fifth author, Patricia Goldman-Rakic, is now deceased.

NELSON LEZCANO,[1] LADISLAV MRZLJAK,[3] ROBERT LEVENSON,[4] CLARE BERGSON[2]

[1]Department of Neurology, [2]Department of Pharmacology and Toxicology, Medical College of Georgia, Augusta GA 30912, USA. [3]Section of Neurobiology, Yale School of Medicine, New Haven, CT 06510, USA. [4]Department of Pharmacology, Pennsylvania State College of Medicine, Hershey, PA 17033, USA.

References and Notes

1. N. Lezcano *et al.*, *Science* **287**, 1660 (2000).
2. N. Lezcano, C. Bergson, *J. Neurophysiol.* **87**, 2167 (2002).
3. R. G. Vickery, M. Von Zastrow, *J. Cell Biol.* **144**, 31 (1999).
4. J. Xiao, R. Dai, L. Negyessy, C. Bergson, *J. Biol. Chem.* **281**, 15182 (2006).
5. R. Dai and J. Xiao are gratefully acknowledged for their work in discovering the errors and correcting the results.

Honey Bees and Humans: Shared Innovation

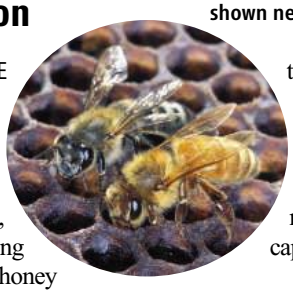

A European honey bee (right; *Apis mellifera*) is shown next to an Africanized honey bee.

CREDIT: SCOTT BAUER, USDA AGRICULTURAL RESEARCH SERVICE, WWW.FORESTRYIMAGES.ORG

IN HER DISCUSSION OF THE sequencing of the genome of the honey bee ("Honey bee genome illuminates insect evolution and social behavior," 27 Oct., p. 578), E. Pennisi concludes by noting that "[i]n a few respects, the honey bee shares more similarities with humans than with the other insects whose genomes have been sequenced," pointing to presumably ancient genes that were "lost in a few lines."

There is another remarkable property that honey bees share with humans, perhaps reflecting a common innovation. Karl von Frisch was awarded the Nobel Prize in 1973 for his work illuminating the capacity of *Apis mellifera* to use the sun's position as a point of reference and identify the direction and distance of nectar outside the hive through a tail-wagging "dance" that is to some extent genetically based and to some extent learned. He showed that the dance has a slightly different form in bees in different locations and that bees can adapt to local conditions. So far, the Honeybee Genome Sequencing Consortium has not identified a genetic source for this capacity shared with humans.

DAVID W. LIGHTFOOT

Assistant Director, National Science Foundation, Directorate of Social, Behavioral and Economic Sciences, Arlington, VA 22230, USA. E-mail: dlightfo@nsf.gov

Climate Change Hearings and Policy Issues

THE RANDOM SAMPLES ITEM "AS EARTH warms, Congress listens" (6 Oct., p. 29) ends with a proclamation by the National Resources Defense Council's David Doniger that climate change hearings "don't do anything." Although Doniger's frustrations are understandable, his lament misses a crucial point: In fact, it is precisely what climate hearings actually do that so badly hinders policy progress.

Climate change hearings are held because the issue is deeply divisive. As Nobelist Herbert Simon reminded us, "when an issue becomes highly controversial—when it is surrounded by uncertainties and conflicting values—then expertness is very hard to come by, and it is no longer easy to legitimate the experts" (*1*). Studies of discourse in these settings, including my own analysis of examples from the last 15 years (*2*–*4*), show, for example, that discussions of uncertainty have had the dual effect of justifying increased research funding while delaying policy decisions—a win for both the scientists and the politicians!

Scientists must recognize that when they testify at such hearings, they are participating in a political event, not a scientific one. When issues are highly polarized, a hearing may be a useful tool for adding to the public record or building support for a particular policy

position, but it should not be seen as a way to impose scientific rationality on politics.

RYAN M. MEYER

Consortium for Science Policy and Outcomes, Arizona State University, Tempe, AZ 85287–4401, USA.

References

1. H. A. Simon, *Reason in Human Affairs* (Stanford Univ. Press, Stanford, CA, 1983), p. 97.
2. S. Shackley, P. Young, S. Parkinson, B. Wynne, *Clim. Change* **38**, 159 (1998).
3. J. van der Sluijs, J. van Eijndhoven, S. Shackley, B. Wynne, *Social Stud. Sci.* **28**, 291 (Apr. 1998).
4. R. Meyer, *Perspect. Public Affairs* **3**, 85 (Spring 2006).

Cost-Benefit Analysis of the RFA

THE U.S. NATIONAL INSTITUTES OF HEALTH issues requests for applications (RFA) to solicit proposals on a specific topic. While a well-designed RFA can have significant benefit to the scientific enterprise and support the mission of the Institute, a poorly designed RFA can produce a significant loss of scientific effort.

The benefit of an RFA can be estimated by multiplying the number of teams funded by the duration of support. The costs associated with an RFA are more diffuse, but just as real. Teams prepare proposals, diverting effort from ongoing projects. Reviewers evaluate proposals, again diverting effort. University staff review budgets and deal with regulatory approval, increasing overhead rates. Institute staff attend study sections and prepare summary statements, consuming resources. Our conservative estimate is that each proposal costs two months of team effort in preparation and review.

Unfortunately, some RFAs have much greater cost than benefit. As a recent example, the National Institute for Biomedical Imaging and Bioengineering issued a "Quantum Projects" RFA. In response, 89 proposals were received with only one grant funded. The benefit of this RFA was support for three years of scientific effort. The cost of this RFA was nearly 15 years of lost effort. This RFA resulted in a net loss of 12 years of scientific effort

Institutes can improve the cost-benefit ratio of RFAs. Sufficient resources must be invested to ensure that the RFA has net benefit. RFAs must be focused and Institutes should employ pre-proposals to screen applications and minimize the number of full proposals required for preparation and review. (Pre-proposals are used by NSF and also a few NIH programs. They are much shorter and require much less effort than a full proposal.) Finally, Institutes should publish the number of proposals received and the number of grants funded to guide response to future RFAs.

NORMAN J. DOVICHI[1] AND STEVEN A. SOPER[2]

[1]Department of Chemistry, University of Washington, Seattle, WA 98195–1700, USA. [2]Department of Chemistry, Louisiana State University, Baton Rouge, LA 70803, USA.

Data Mining on the Web

WE READ WITH GREAT INTEREST THE PERspective "Creating a science of the Web" by T. Berners-Lee *et al.* (11 Aug, p. 769). We agree that evolving Web technologies enable the creation of novel structures of information, whose properties and dynamics can be fruitfully studied. More generally, we would like to point out that the Web is a specific phenomenon associated with the increasing prevalence of information being digitized and linked together into complicated structures. The complexity of these structures underscores the need for systematic, large-scale data mining both to uncover new patterns in social interactions and to make discoveries in science through connecting disparate findings. For this vision to be realized, we have to develop a new science of practical data mining focusing on questions answerable with the existing digital libraries of information. In particular, today, free-text search (as embodied by Google) is the primary means of mining the Web, but there are many kinds of information requests it cannot handle. Queries combining general, standardized annotation about pages (such as from the semantic Web) with free-text search within them are often not supported—e.g., doing a full-text search of all biophysics blogs emanating just from governmental institutions within 100 miles of Chicago. Furthermore, it would be useful to develop ways of leveraging the small amounts of highly structured information in the semantic Web as "gold-standard training sets" to help bootstrap the querying and clustering of the large bodies of unstructured information on the Web as a whole. Thus, the science of the Web should enumerate the range of information requests that can be fruitfully made and the kinds of information infrastructure and data-mining techniques needed to fulfill them.

ANDREW SMITH[1] AND MARK GERSTEIN[2]

[1]Department of Computer Science, [2]Albert Williams Professor of Biomedical Informatics, Yale University, New Haven, CT 06520, USA.

Response

WE AGREE WITH SMITH AND GERSTEIN'S VIEW that data mining is among the many important areas of research that are considering the Web as an object of scientific inquiry. They are correct in pointing out the importance of "text mining," the basis of current Web search, for providing new Web capabilities. However, with the increasing amount of directly machine-readable data that are available on the Web (coming from, for example, database-producing equipment such as modern scientific devices and data-oriented applications), it is also clear that text mining needs to be augmented with new data technologies that work more directly with data and metadata. Data mining is also an excellent case in point for the main focus of our Perspective in relation to the interdisciplinary nature of the emerging science of the Web. Analytic modeling techniques will be needed to understand where Web data reside and how they can best be accessed and integrated. Engineering and language development are needed if we are to be able to perform data mining without having to pull all the information into centralized data servers of a scale that only the few largest search companies can currently afford. In addition, data mining provides not just opportunities for better search, but also real policy issues with respect to information access and user privacy, especially where multiple data sources are aggregated into searchable forms.

TIM BERNERS-LEE,[1] WENDY HALL,[2] JAMES HENDLER,[3]* NIGEL SHADBOLT,[2] DANIEL J. WEITZNER[1]

[1]Computer Science and Artificial Intelligence Laboratory, Massachusetts Institute of Technology, Cambridge, MA 02139, USA. [2]School of Electronics and Computer Science, University of Southampton, Southampton SO17 1BJ, UK. [3]Computer Science Department, University of Maryland, College Park, MD 20742, USA.

*To whom correspondence should be addressed. E-mail: hendler@cs.umd.edu

Letters to the Editor

Letters (~300 words) discuss material published in *Science* in the previous 6 months or issues of general interest. They can be submitted through the Web (www.submit2science.org) or by regular mail (1200 New York Ave., NW, Washington, DC 20005, USA). Letters are not acknowledged upon receipt, nor are authors generally consulted before publication. Whether published in full or in part, letters are subject to editing for clarity and space.

Using Models to Manage Carnivores

THE NEWS FOCUS ARTICLE "THE CARNIVORE comeback" (M. Enserink, G. Vogel, 3 Nov., p. 746) illustrates the difficulty of conserving free-ranging predators in highly anthropic landscapes such as Europe. Because large carnivores can cause heavy damages to livestock as well as threaten human beings, it is critical that management policies are flexible enough to allow for some removals while keeping

populations viable (*1*).

Although the use of models for carnivore management has not been widespread (*2*), it is now possible to build realistic demographic models for species with complex social systems like the wolf, thanks to the recent emergence of modeling techniques that incorporate patterns at the individual level (*3*). Designing efficient adaptive management schemes—i.e., implementing policies as experiments—should be achieved through a wider use of such models.

Management recommendations would be much improved and accepted by the public if they were based on population modeling rather than on expert opinion consensus. Because models are logical constructions based on falsifiable assumptions, their recommendations can be invalidated, whereas expert opinions are verbal constructions difficult to refute. Fisheries management has made an extensive use of population models, and there is no valid reason why they should not apply to terrestrial carnivores.

GUILAUME CHAPRON AND RAPHAËL ARLETTAZ

Zoological Institute–Conservation Biology, University of Bern, Baltzerstrasse 6, Bern, Switzerland.

References

1. J. Robbins, *Conserv. Practice* **6**, 28 (2005).
2. M. Kelly, *Trends Ecol. Evol.* **17**, 394 (2002).
3. V. Grimm *et al.*, *Science* **310**, 987 (2005).

TECHNICAL COMMENT ABSTRACTS

COMMENT ON "Early Domesticated Fig in the Jordan Valley"

Simcha Lev-Yadun, Gidi Ne'eman, Shahal Abbo, Moshe A. Flaishman

Kislev *et al*. (Reports, 2 June 2006, p. 1372) described Neolithic parthenocarpic fig fruits and proposed that they derive from trees propagated only by cuttings and thus represent the first domesticated plant of the Neolithic Revolution. Because parthenocarpic fig trees naturally produce both seeded and seedless fruits and are capable of spontaneous reproduction, we argue that the finds do not necessarily indicate cultivation, nor horticulture predating grain crops.

Full text at www.sciencemag.org/cgi/content/full/314/5806/1683a

RESPONSE TO COMMENT ON "Early Domesticated Fig in the Jordan Valley"

Mordechai E. Kislev, Anat Hartmann, Ofer Bar-Yosef

We suggest that parthenocarpic or fertile fig branches were planted along with staples like wild barley in the early Neolithic villages of Gilgal and Netiv Hagdud. In contrast to the repeated sowing of wild barley, we argue that planting branches of selected fig trees constitutes a form of domestication. The simplicity of fig tree propagation likely contributed to its domestication before cereal crops.

Full text at www.sciencemag.org/cgi/content/full/314/5806/1683b

CORRECTIONS AND CLARIFICATIONS

Reports: "Boryllithium: isolation, characterization, and reactivity as a boryl anion" by Y. Segawa *et al.* (6 Oct., p. 113). Reference 28 for preparation of a free anionic gallium species substituted with diisopropylphenyl groups should cite R. J. Baker, R. D. Farley, C. Jones, M. Kloth, D. M. Murphy, *J. Chem. Soc. Dalton Trans.* **2002**, 3844 (2002). The current reference [E. S. Schmidt, A. Jockisch, H. Schmidbaur, *J. Am. Chem. Soc.* **121**, 9758 (1999)] describes preparation of tert-butyl-substituted anionic gallium species. Additionally, in table S1 of the supporting online material, the parameter "params" in the second column (headed **3-DME**) should be "384" rather than "155."

Policy Forum: "Genomics and medicine at a crossroads in Chernobyl" by G. S. Ginsburg *et al.* (6 Oct., p. 62). In the first paragraph, in line 11, the phrase "1.1-billion-ton temporary 'sarcophagus'" should instead read "1.1-million-ton temporary 'sarcophagus.'"

Special Section on Migration and Dispersal: News: "Follow the footprints" by K. Unger (11 Aug., p. 784). In the article, tapirs are described as "piglike." Although to the uninitiated observer, tapirs seem piglike, they are actually more closely related to horses and rhinos.

MILITARY RESEARCH

Dr. DARPA—Or How the Pentagon Learned to Stop Worrying and Love…

Michael Shermer

In Stanley Kubrick's 1964 film *Dr. Strangelove or: How I Learned to Stop Worrying and Love the Bomb*, the character Brigadier General Jack D. Ripper reflected on the opinion on war expressed by the World War I French Premier Georges Clemenceau: "He said war was too important to be left to the generals. When he said that, 50 years ago, he might have been right. But today, war is too important to be left to politicians. They have neither the time, the training, nor the inclination for strategic thought. I can no longer sit back and allow communist infiltration, communist indoctrination, communist subversion and the international communist conspiracy to sap and impurify all of our precious bodily fluids."

Read Al Qaeda for communist and homeland security for precious bodily fluids to see how life imitates art, although today we have allowed scientists into the war room (where no fighting is allowed). This is equally problematic, for scientists are subject to the same cognitive biases as these other cohorts. In fact, even smart people like scientists believe weird things, because they are highly skilled at rationalizing beliefs that they arrived at for nonsmart reasons (*1*). And after two decades of investigating weird beliefs on the borderlands of scientific credulity, I know pseudoscience when I see it.

Imaginary Weapons
A Journey Through the Pentagon's Scientific Underworld
by Sharon Weinberger
Nation, New York, 2006. 304 pp. $26. ISBN 1-56025-849-7.

"Pseudoscience" is also the verdict rendered by the former chief scientist at the U. S. Arms Control and Disarmament Agency, Peter Zimmerman, to Sharon Weinberger, an investigative journalist and the editor of *Defense Technology International*, when she inquired in 2003 about the Pentagon's top-secret superweapon, the hafnium bomb. "One knows bad science and after a while learns to recognize it as such," Zimmerman explained. Weinberger's query led her into the Pentagon's "scientific underworld" that "starts the moment a military official tosses aside science and proceeds with some idea too far out to believe." The further down the rabbit hole she went, the weirder things got. Rockets based on antimatter physics, psychic spies who employ extrasensory perception–like "remote viewing" to find missing soldiers and hidden weapons, and *Star Trek*–like research on "teleportation physics" and "warp drive metrics" are just a few of the goofier projects Weinberger encountered in her search. "I would learn that Pentagon officials enter the underworld of science, never again to leave. That's when things can go terribly, terribly wrong."

The imagined bomb. Martin Stickley claimed that "stimulated isomer energy release" would produce a two-kiloton explosive yield from a five-inch-diameter grenade.

Imaginary Weapons is Weinberger's gripping account of her investigation into a terribly wrong idea: a two-kiloton "nuclear hand grenade" based on highly questionable physics involving an unstable atomic nucleus, an isomer called hafnium-178. This isomer bomb was sold to the Pentagon as a vital weapon in the war on terror, a weapon that could melt human flesh through a powerful burst of gamma rays, penetrate underground concrete bunkers, and cause an entire city block to disappear in one fatal blast.

To determine the feasibility of the hafnium bomb, Zimmerman was charged with directing a secret group of elite scientists called the Jasons. Their verdict was unequivocal, as Weinberger explains: "Hafnium couldn't be made into a bomb for a host of scientific and technical reasons: it was too radioactive to be around; it was too expensive to produce; and there was no way to get the chain reaction needed for an explosion." In fact, it couldn't even pass the "snicker test," Zimmerman noted. "It was, in the truest sense of the word," Weinberger concludes, "an imaginary weapon."

Then how did the Pentagon come to believe in it? Here's how: (i) Adopt a high risk–taking philosophy. In the Pentagon's Defense Advanced Research Projects Agency (DARPA)—charged with developing the secret weapon—"impossible" is just the sort of project their scientists are supposed to undertake; in fact, "DARPA hard" refers to technological challenges considered beyond the capability of the military's other research and development laboratories. (ii) Remove the normal checks and balances that accompany scientific research. Within DARPA, notes Weinberger, the agency's "science and technology projects are shielded from the periodic oversight and cost audits that plague the Pentagon's more expensive weapons." (iii) Ignore negative results. Whereas in normal science failures are learning opportunities, in DARPA "no one remembers the failure," reports Tony Tether, head of the agency in 2002. "DARPA is *Groundhog Day*. We do things over and over and over again." (iv) Favor short-term thinking. DARPA's policy is that program managers are not allowed to serve for more than four years. Although this prevents the ossification suffered by other federal agencies top-heavy in lifelong bureaucrats, it means that long-term projects will be passed over.

With this milieu of credulity in place, Weinberger shows, "all it took was a used dental x-ray machine, a few die-hard supporters, some farfetched claims of a new arms race, and the Pentagon thought it was on its way to the next superbomb." Given the power of the hindsight bias (whose vision is always 20/20), is it fair to task the Pentagon for not heeding the warning signs? Yes, concludes Weinberger. The signs were too numerous and too substantial: the failure to replicate key experiments; the increasingly elaborate reasons offered by hafnium-bomb supporters to explain away experimental failures; ignoring the negative assessment of the project by the Jason scientists and instead listening only to supporters; the fact that no one in the nuclear physics community outside of the bomb group believed that hafnium could be triggered with x-rays; and, therefore, the concoction by hafnium proponents of an elaborate conspiracy theory alleging actions against them by the "scientific elite."

The story of how DARPA convinced the Pentagon to quit worrying and love the hafnium bomb presents an important lesson in healthy skepticism. Weinberger's account in *Imaginary Weapons* offers a warning about excessive credulity that should be heeded by scientists and policy-makers alike—for nature will not bend to political predilections.

The reviewer is at *Skeptic* magazine, 2761 North Marengo Avenue, Altadena, CA 91001, USA. E-mail: mshermer@skeptic.com

Reference

1. M. B. Shermer, *Why People Believe Weird Things: Pseudoscience, Superstition, and Other Confusions of Our Time* (Holt, New York, ed. 2, 2002).

10.1126/science.1132058

CREDIT: COURTESY SHARON WEINBERGER

EXHIBITS: GENETICS

From a Monk in His Garden

R. Scott Winters

Part-time researcher. Mendel (2nd from right, back row; holding a *Fuschia*) and his fellow friars at the Abbey of St. Thomas (photograph *c.* 1862) were required to teach in public schools.

Very little evidence remains of the life of Gregor Mendel, the Augustinian friar who elucidated the mechanism of particulate inheritance. Working alone in the garden of a small abbey in what is now the Czech Republic, this enigmatic schoolteacher solved one of the most pressing and long-standing controversies in biology. In doing so, he bolstered Charles Darwin's emerging theory of evolution through natural selection and laid the foundations for the field of study that would become genetics. However, the significance of Mendel's findings—first presented in 1865—was not appreciated until the early 1900s, when his research was independently rediscovered by the botanists Carl Correns, Hugo de Vries, and Erich von Tschermak-Seysenegg. In the interim years, nearly all evidence of Mendel's seminal work was lost as his contemporaries focused their attention on his subsequent role as abbot rather than researcher.

Many of the relics of Mendel's life are currently on display at the Field Museum in Chicago as part of *Gregor Mendel: Planting the Seeds of Genetics*. The exhibition, the most complete popular presentation of Mendel to date, presents him through his personal effects and his place in the continuum of research on heredity. Nearly all of the included Mendel artifacts are on loan from the Mendelianum and the Abbey of St. Thomas and are being displayed for the first time outside of Brno, Czech Republic. Following its appearance in Chicago, the exhibit will travel through 2008 to Columbus, Memphis, Philadelphia, and Washington, D.C.

Gregor Mendel: Planting the Seeds of Genetics

developed by the Field Museum, the Vereinigung zur Förderung der Genomforschung in Vienna, Austria, and the Mendel Museum in Brno, Czech Republic

The Field Museum, Chicago, through 1 April 2007.
www.fieldmuseum.org/mendel/

Although modest in size, the exhibit attempts to provide a full perspective of Mendel within the historical context of science. The first, and stronger, of the exhibit's two parts offers a detailed picture of the friar as scientist. Mendel is portrayed as an astute researcher and devoted naturalist, a polymath who saw connections between disparate scientific fields. Highlights of the exhibit include Mendel's eyeglasses, microscope, telescope, gardening tools, and annotated copy of Darwin's *On the Origin of Species*. Given the rarity and frailty of Mendel artifacts, it is not surprising that the exhibit relies heavily upon facsimile documents (such as reproductions of the two surviving pieces of his notebooks) rather than the originals. Mendel's personal effects and photos are augmented with displays intended to evoke the locus of his labors, such as a photomural of the library at the Abbey of St. Thomas.

The second half of the exhibit sketches the course of genetic research since Mendel. The focus here is on luminaries such as Thomas Hunt Morgan (who discovered chromosomal inheritance through his studies of fruit flies) and Barbara McClintock (who demonstrated the existence of mobile genetic elements in maize), but controversies such as eugenics are also acknowledged. Refreshingly, these vignettes remain true to Mendel's primary inquiry: the properties of inheritance of living organisms. As such, the section emphasizes genetics in the context of evolutionary and biodiversity studies (spotlighting two of the Field Museum's researchers) as opposed to the medical applications of genetics (which have been highlighted in several popular exhibitions). Interleaved throughout the exhibit is a series of contemporary works of art inspired by Mendel's research.

We have only a poor understanding of how this amateur scientist unlocked one of the most important secrets in the history of science. His thoughts, ideas, and inspiration remain opaque, and we do not know how the germ of his idea came to fruition. Although the exhibit *Gregor Mendel* comprehensively presents what remains of its subject's life, we are still left with only an enigmatic picture of the person.

10.1126/science.1134959

The reviewer is in the Division of Oncology, Children's Hospital of Philadelphia, 34th Street and Civic Center Boulevard, Philadelphia, PA 19104, USA. E-mail: winters@genome.chop.edu

MILITARY RESEARCH

An Elite Source of Advice

Peter Zimmerman

In 1959 a team of first-rank American physicists made the U.S. Department of Defense an offer it would not refuse. The physicists proposed the creation of a new animal in the defense advice zoo. It would not be a Federal Contract Research Center (a public research institute hired by government agencies to carry out research and development and to provide engineering support) but also not just a bunch of independent consultants chasing small contracts. The new organization, Jason, was to become a self-perpetuating group of top scientists who would tackle important scientific and technical issues during a lengthy summer residency in enjoyable parts of the country and discuss other topics at fall and spring meetings in the Washington, D.C., area. By 1960, the idea was funded.

Among the earliest scientists recruited to the group were Marvin ("Murph") Gold-

The reviewer is in the Department of War Studies, King's College London, Strand Campus, London WC2R 2LS, UK. E-mail: peter.zimmerman@kcl.ac.uk

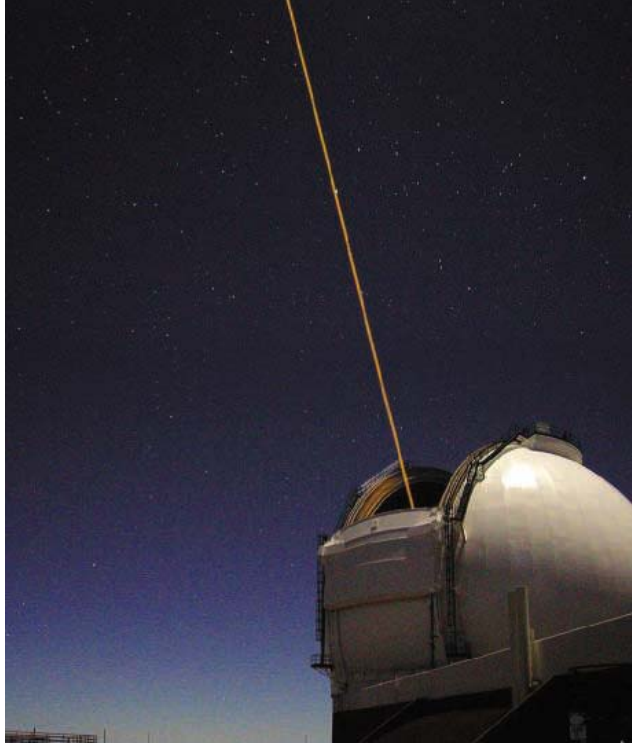

A source of guidance. The adaptive optics system of the Keck II telescope on Mauna Kea uses a sodium laser guide star.

berger, Murray Gell-Mann, and Kenneth Watson. Eleven present and future Nobel Laureates would join over the years. Jason is quietly approaching its 50th birthday, and yet it seems to be almost unknown, even among the science community—and, more remarkably, even among the media that cover the Defense Department. Jason likes it that way. Thus the account Ann Finkbeiner (a freelance writer who teaches in the graduate science writing program at Johns Hopkins University) offers in *The Jasons* will be revealing to most readers.

Full disclosure: I know many members of Jason, have been a guest at a number of Jason meetings, and even commissioned a Jason study on the feasibility of the "hafnium bomb," a study mentioned at the very end of the book.

There is no public list of the members of Jason, past or present. The project office in McLean, Virginia, gives out very little information. Few if any Jasons (the word refers both to the group and to the individual members) brag of their affiliation on their Web sites or their curriculum vitae. The group's reticence probably goes back to their earliest days of controversy, during the Vietnam War. As Finkbeiner admirably details in her book, the first dedicated to a thorough study of the Jasons, the group figured prominently, although anonymously, in the Pentagon Papers through its 1966 report "The Effects of U.S. Bombing in North Vietnam."

Instead of continuing strategic bombing of the North for no measurable gain, Jason advocated cutting the Ho Chi Minh Trail with a combination of systems including sensors on the ground, relay aircraft overhead, strike aircraft at the ready, and a computer to fuse the sensor data. Had all of the recommendations of this Jason report been followed, it seems likely that conventional bombing of North Vietnam would have been phased out with significant savings of both American and Vietnamese lives. The report's technical centerpiece, the "McNamara Line," was an operational failure, but it led directly to modern smart weapons.

The Jasons
The Secret History of Science's Postwar Elite
by Ann Finkbeiner
Viking, New York, 2006. 336 pp. $27.95, C$39. ISBN 0-670-03489-4.

When its title was leaked, the report backfired on Jason, inflicting tactical—if not strategic—harm on the organization and its members. Many Jasons were identified by peace activists and became the targets of abuse (and occasionally of serious threats to their personal safety and that of their families). The legacy of reticence continues today in the refusal of the organization to name its members and in the reluctance of Jasons themselves to name other members or to talk about the group. (Although one prominent Jason, atomic physicist Will Happer of Princeton, credits being trapped in the anti-Jason rioting at Columbia University with convincing him to join the group.)

Finkbeiner dwells on what she indicates is a difference between "blue-collar" Jasons who stick to hard science, and "white-collar" members who are also policy advocates in the mold of Jasons Richard Garwin and Sidney Drell. White-collar scientists combine work on highly classified projects with vigorous programs of public speaking and discussions with Congress and members of the executive branch. I doubt that this distinction is useful; all Jasons I contacted while preparing this review said that they are unfamiliar with the collar code.

Jason started out as a bunch of high-powered physicists spending summers doing interesting but very applied physics. It has metamorphosed over the years and now includes biologists, chemists, computer scientists, and engineers, a reflection of the long-term changes in the problems the United States faces. Finkbeiner's elegant recording of this transition, one of the book's best parts, is done in part through interviews with nonphysicist Jasons, particularly "Dr. X" (an anonymous biochemist) and "Professor Y" (a woman who trained as a chemist but works as a condensed matter physicist).

This mutability of Jason and the diverse interests of its members has kept the group vital (alive) and vital to the security of the United States. Finkbeiner informs the reader that Jason long ago fragmented into subgroups that focus on such topics as arms control, nuclear weapons, biological challenges, missile defense, and naval warfare. But Jason's defining attribute is the group's ability to find very smart people in many fields, educate them about fields they do not know, and then get them to tackle very hard problems in back-of-the-envelope ways that often result in solutions that truly are good enough for government work. A list of Jason's greatest accomplishments includes demonstrating that the United States could accept a zero-yield nuclear test ban without risk to its stockpile, showing that anti–intercontinental ballistic missile defense was unlikely to work, and developing the sodium laser artificial star used to guide the adaptive optics that make the current generation of very large optical telescopes possible.

If there is an obvious flaw in *The Jasons*, it is that the group restricted the author's access and she accepted those ground rules. The book is not an investigative report; Finkbeiner interviewed only those Jasons who agreed to talk with her and carefully concealed the identities of all who asked not to be named. It is disappointing that the Jasons never let her watch them in action. As a result, Finkbeiner completely misses out on just how much fun they have at their work and how enjoyable it is to watch them listen, probe, and occasionally skewer one program or another.

Finkbeiner has given us an unprecedented look at the inside of Jason. No other group of scientific advisers has been so useful to the United States for so many decades. Some day a historian of science should be given the opportunity to write a wider-ranging and more analytic study of Jason and its accomplishments. Although that probably cannot be done without access to classified information, the unclassified heart of the matter can, as many official nuclear histories have shown, still make fascinating reading. Until such a study appears, Finkbeiner's absorbing and intelligent appraisal of Jason should be read by anyone interested in the interactions between science and national security.

10.1126/science.1132057

EPIDEMIOLOGY

Ensuring Safe Drinking Water in Bangladesh

Excessive levels of arsenic in drinking water is a vast health problem in Southeast Asia. Several viable approaches to mitigation could drastically reduce arsenic exposure, but they all require periodic testing.

M. F. Ahmed,[1] S. Ahuja,[2] M. Alauddin,[3] S. J. Hug,[4] J. R. Lloyd,[5] A. Pfaff,[6] T. Pichler,[7] C. Saltikov,[8] M. Stute,[9,10] A. van Geen[10]*

In the early 1980s, K. C. Saha from the School of Tropical Medicine in Kolkata attributed skin lesions in West Bengal, India, to exposure to arsenic in groundwater pumped from shallow tube wells (*1*). Despite these findings, millions of tube wells have been installed across the Bengal Basin, the geological formation that includes West Bengal and Bangladesh, and across river floodplains and deltas in southern Asia.

The popularity of tube wells reflects the reduced incidence of diarrheal disease when drinking groundwater, instead of untreated surface water, and the modest cost of installation (about 1 month of household income). Today, perhaps 100 million people in India, Bangladesh (see figure, right), Vietnam, Nepal, and Cambodia (and possibly other countries) are drinking water with arsenic concentrations up to 100 times the World Health Organization (WHO) guideline of 10 μg per liter (*2*–*4*). Whereas technologies for treating either surface water or groundwater periodically receive considerable attention, the record to date suggests that more widespread testing of wells to identify those aquifers that do not require treatment is presently far more promising.

Arsenic can occur in groundwater naturally, without an anthropogenic source. There is broad agreement that arsenic release into groundwater of the Bengal Basin is facilitated by microbial metabolism of organic matter contained in river floodplain and delta deposits (*3*–*6*). Elevated concentrations of arsenic in Bangladesh groundwater probably predate agricultural practices that could plausibly have caused the composition of groundwater to change, such as the use of phosphate fertilizer or large groundwater withdrawals for irrigation (*3*, *7*). This does not rule out the possibility that irrigation is affecting the distribution and mobilization of arsenic today (*7*–*9*). Although there are remaining questions, current understanding of the occurrence of arsenic is sufficient to direct national strategies for lowering exposure.

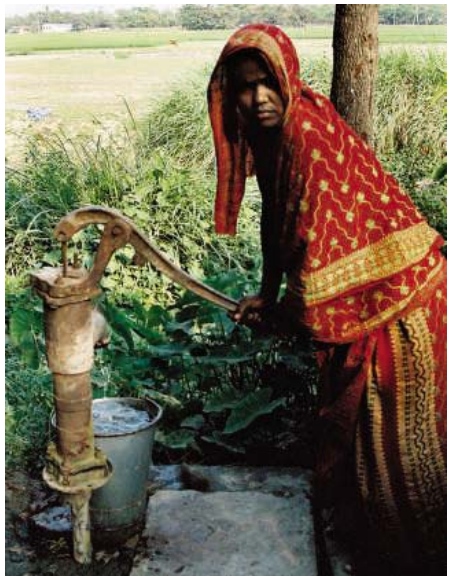

Woman using a tube well in Araihazar, Bangladesh.

CREDIT: AMY SCHOENFELD

After studies established the scale of the problem (*2*, *3*), a massive campaign was initiated in Bangladesh in 1999 to test tube wells in the most affected portions of the country. The field kits that were used had limitations, but were reliable enough (*10*) to identify the vast majority of tube wells that did not meet the local standard for arsenic in drinking water of 50 μg per liter. By 2005, the spouts of 1.4 million cast-iron pumps that draw groundwater with >50 μg per liter arsenic according to the field test had been painted red. Another 3.5 million wells with up to 50 μg per liter arsenic had been painted green (*11*). Such testing did not reduce the rate of private well installations, at least within areas that have been recently resurveyed (*12*, *13*). Sadly, most tube wells that were installed after the national testing campaign remain untested today.

The two interventions that have so far most effectively lowered human exposure in Bangladesh rely on the spatial heterogeneity of the distribution of arsenic in groundwater, which is controlled principally by the local geology (*3*, *14*). Testing alone had the biggest impact as ~29% of the millions of villagers informed that their tube well was elevated in arsenic have changed their water source (see the chart on page 1688). Large variations in the proportion of well-switching across villages reflect in part the availability of safe wells that are within walking distance. A recent comparison has shown, however, that both additional education and periodic reinforcement of the message that arsenic is a health hazard can overcome existing obstacles to nearly double the proportion of switching (*12*, *13*).

The intervention with the second largest impact (~12% of users with unsafe wells) has been the installation of tens of thousands of deep wells by the government and by nongovernmental organizations. Such wells supply groundwater from deeper, usually older, aquifers that generally do not contain elevated levels of arsenic (*3*, *14*, *16*). They are often shared or community wells that require walking ~100 m several times a day. Yet these wells can be very popular when placed in a central location that, for instance, does not discourage use by women. These community installations have also had an indirect impact because numerous households followed suit by reinstalling their own well to greater depth (*12*, *13*).

In 2004, Bangladesh issued a National Policy for Arsenic Mitigation (NPAM) accompanied by a more detailed Implementation Plan for Arsenic Mitigation (*17*). Well-switching was recognized by the NAPM in the sense that alternative water supply was not proposed for villages where <40% of tube wells are unsafe. However, the NPAM considered deep tube wells a low-priority option. Instead, the document encouraged a return to the use of surface or very shallow groundwater without paying sufficient attention to the increased likelihood of exposure to microbial pathogens.

Five other mitigation approaches promoted by the NPAM have had a limited impact, each reaching <1% of the population at risk (see the chart on page 1688). The early record of

[1]Bangladesh University of Engineering and Technology, Dhaka -1000, Bangladesh. [2]Ahuja Consulting, Calabash, NC 28467, USA. [3]Department of Chemistry, Wagner College, Staten Island, NY 10301, USA. [4]Department of Water Resources and Drinking Water, Swiss Federal Institute of Aquatic Science and Technology (Eawag), CH-8600 Duebendorf, Switzerland. [5]School of Earth, Atmospheric and Environmental Sciences, University of Manchester, Manchester M13 9PL, UK. [6]Earth Institute, Columbia University, New York, NY 10027, USA. [7]Department of Geology, University of South Florida, Tampa, FL 33620, USA. [8]Environmental Toxicology, University of California, Santa Cruz, Santa Cruz, CA 95064, USA. [9]Department of Environmental Sciences, Barnard College, Columbia University, New York, NY 10027, USA. [10]Lamont-Doherty Earth Observatory of Columbia University, Palisades, NY 10964, USA.

*Correspondence to: avangeen@ldeo.columbia.edu

arsenic removal from groundwater by adsorption and/or coprecipitation is mixed. Failures have arisen from inadequate removal due to the challenging composition of the groundwater, logistical difficulties in ensuring proper maintenance, and inconvenience to the users (*18*). Since four arsenic-removal technologies have been provisionally approved for marketing, however, treatment may become more widespread. Dug wells are used by thousands of villagers. Although the shallowest aquifers tapped by these wells are typically low in arsenic, a full-scale return to this traditional technology is hampered by concerns regarding the microbial quality of the water and the need for regular maintenance (*16*). Treatment of pond or river water by sand filtration, a priority in the 2004 NPAM, appears less promising. Ponds often directly receive human waste from surrounding latrines and are increasingly used for aquaculture. Also, as industry develops throughout rural Bangladesh, sand filtration alone is unlikely to guarantee a treatment suitable for human consumption. Rainwater harvesting by individual households can provide safe drinking water. Its main drawbacks are the potential for microbial contamination and the high cost of storage sufficient for Bangladesh's 8-month dry season. Last, piped-water supply is frequently touted as the solution to the arsenic problem. The high capital and maintenance costs of such systems relative to those of individual tube wells, however, is likely to restrict this approach to urban areas or the most affluent villages.

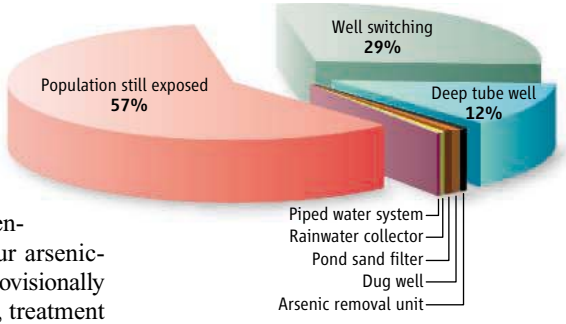

Impact of arsenic mitigation in Bangladesh (SOM Text). The initially exposed population has been estimated at 28 to 35 million relative to the local standard of 50 μg per liter arsenic in drinking water (*3*).

Recommendations

More than half of the population in Bangladesh at risk from arsenic is still exposed (see chart, above). To reach a greater fraction of the population, we urge a revision of the NPAM to (i) stimulate the periodic monitoring of water quality no matter the mitigation option, (ii) encourage rather than discourage the wise use of deep aquifers that are low in arsenic, and (iii) include the newly demonstrated effects of arsenic on the mental development of children in information campaigns (*19*).

Periodic field testing of numerous point sources of drinking water would be an enormous challenge for any government. We recommend consideration of alternative programs for well testing, in particular a national certification program to license and monitor entrepreneurs offering commercial field testing to villages. Ideally, test results should indicate actual concentrations. Households have used this information to reduce arsenic exposures even without access to a safe well. The cost of testing tube wells for arsenic is significant (~$1 per test) but is even higher for other water-supply options that require water treatment, because the performance of such systems is more likely to vary over time. Dug wells, for instance, should be tested monthly for microbial contamination, which is a considerably more difficult measurement than a field test for arsenic.

As the population of Bangladesh continues to grow, many shallow wells are likely to become contaminated with human, agricultural, and industrial waste. In addition, groundwater pumped from a majority of shallow tube wells is naturally elevated in manganese, another constituent of increasing health concern because of its neurological effects (*3*, *20*). Several field kits are available to determine whether a well meets the WHO guideline of 0.4 mg per liter for manganese. The systematic use of these field kits for testing shallow and deep wells should be considered, even if the health implications of exposure to manganese present in groundwater are not yet fully understood.

Groundwater from deep wells is a good source of drinking water in many parts of Bangladesh because it does not require treatment. Deep wells nevertheless should be tested at least once a year, as a small fraction are likely to fail over time. Presently, not even deep wells installed by the government are periodically tested for arsenic. One source of confusion has been that the depth to older aquifers that are systematically low in arsenic varies from <30 m to >200 m across the country and can vary even between adjacent villages (*3*, *21*). Thus, the depth to aquifers that are low in arsenic must be determined at the village level and attempts to establish the depth to low-arsenic aquifers over larger areas are misguided.

We believe that significant contamination of deep aquifers with arsenic is unlikely unless large amounts of water are withdrawn for irrigation (*22*). Managing irrigation is therefore important. Although the incorporation of arsenic into rice that has been grown on shallow groundwater appears to be limited (*23*, *24*), potential long-term effects of irrigating with groundwater that is elevated in arsenic should be monitored.

In summary, water testing must be drastically expanded in Bangladesh. Eight years after a major arsenic conference in Dhaka, millions of people continue to drink groundwater containing toxic levels of arsenic. Without discouraging any option, the NPAM should be revised soon after the upcoming elections to expand the scale of those interventions that have been most effective to date.

References and Notes

1. A. K. Chakraborty, K. C. Saha, *Indian J. Med. Res.* **85**, 326 (1987).
2. R. K. Dhar *et al.*, *Curr. Sci.* **73**, 48 (1997).
3. D. G. Kinniburgh, P. L. Smedley, Eds., vol. 2 of *Arsenic Contamination of Ground Water in Bangladesh, Final Report* (BGS Technical Report WC/00/19, British Geological Survey, Keyworth, UK, 2001).
4. L. Charlet, D. A. Polya, *Elements* **2**, 91 (2006).
5. R. Nickson *et al.*, *Nature* **395**, 338 (1998).
6. F. S. Islam *et al.*, *Nature* **430**, 68 (2004).
7. S. Klump *et al.*, *Environ. Sci. Technol.* **40**, 243 (2006).
8. M. L. Polizzotto *et al., Proc. Natl. Acad. Sci. U.S.A.* **102**, 188819 (2005).
9. C. F. Harvey *et al.*, *Chem. Geol.* **228**, 112 (2006).
10. A. van Geen *et al., Environ. Sci. Technol.* **39**, 299 (2005).
11. Bangladesh Arsenic Mitigation Water Supply Program, www.bamwsp.org/Survey%20Results.htm.
12. A. Opar *et al. Health Place* **13**, 164 (2007).
13. A. Schoenfeld, thesis, Columbia University, New York, NY (2006), www.ldeo.columbia.edu/~avangeen/arsenic/.
14. P. Ravenscroft *et al.*, *Hydrogeol. J.* **13**, 727 (2005).
15. M. M. H. Sarker, M. A. Matin, A. Hassan, M. R. Rahman, "Report on development of arsenic decision support system" [Center for Environmental and Geographic Information Services, United Nations Children's Fund (UNICEF), Dhaka, Bangladesh, 2005].
16. M. F. Ahmed *et al.*, *Risk Assessment of Arsenic Mitigation Options (RAAMO)* [Arsenic Policy Support Unit (APSU), Dhaka, Bangladesh, 2005], www.apsu-bd.org/.
17. National Policy for Arsenic Mitigation, 2004, www.sdnpbd.org/sdi/policy/doc/arsenic_policy.pdf.
18. M. A. Hossain *et al.*, *Environ. Sci. Technol.* **39**, 4300 (2005).
19. G. A. Wasserman *et al.*, *Environ. Health Perspect.* **112**, 1329 (2004).
20. G. A. Wasserman *et al.*, *Environ. Health Perspect.* **114**, 124 (2006).
21. A. Gelman *et al., Risk Anal.* **24**, 1597 (2004); see also www.ldeo.columbia.edu/welltracker/.
22. Y. Zheng *et al.*, *Geochim. Cosmochim. Acta* **69**, 5203 (2005).
23. P. N. Williams *et al.*, *Environ. Sci. Technol.* **39**, 5531 (2005).
24. A. van Geen *et al., Sci. Total Environ.* **367**, 769 (2006).
25. This paper is the outcome of discussions following a symposium on arsenic in South Asia, convened by S. Ahuja, at the 2006 American Chemical Society meeting. We are grateful to K. M. Ahmed, G. Howard, R. Johnston, D. Kinniburgh, K. Radloff, P. Ravenscroft, P. Smedley, and R. Wilson for their helpful input. This is Lamont-Doherty Earth Observatory contribution 6989.

Supporting Online Material

www.sciencemag.org/cgi/content/full/314/5805/1687/DC1
SOM Text

10.1126/science.1133146

CELL BIOLOGY

Purinergic Chemotaxis

Release of adenosine 5′-triphosphate from immune cells in response to membrane deformation implicates purinergic signaling in cell migration during host defense responses.

Joel Linden

Adenosine 5′-triphosphate (ATP) provides energy currency for cells, harboring energy in its chemical bonds that can be utilized when ATP is metabolized. The negative charge of the triphosphate groups renders the molecule impermeable to lipid bilayers, so ATP usually remains within cells. However, ATP can be released and rapidly metabolized to adenosine 5′-diphosphate (ADP) adenosine 5′-monophosphate (AMP), and adenosine. Excepting AMP, these purines participate in autocrine signaling (affecting the cell that secreted them) and paracrine signaling (affecting nearby target cells) by binding to various purinergic receptors on the cell surface. On page 1792 of this issue, Chen *et al.* (*1*) show that ATP is released during cell migration. Specifically, as a neutrophil moves toward an attracting stimulus, rapid and transient release of ATP further enforces its directional movement by autocrine signaling via ATP and adenosine receptors. This purinergic signaling circuit appears to amplify the migratory response elicited by chemoattractants.

In neurons as well as in platelets and mast cells of the immune system, ATP or ADP (especially in platelets) is contained in granules that are released to the extracellular space in response to specific chemical or electrical stimuli. But in other cell types, including endothelial and epithelial cells, ATP that is not associated with dense granules is released in response to membrane-deforming stimuli such as shear stress and hypotonic conditions. Cell swelling, in response to hypotonicity, can trigger a 1000-fold increase in ATP release from epithelial cells within 1 μm of the cell surface (*2*). Similar release can boost cell proliferation, as observed in prostate cancer cells (*3*).

Neutrophils, the leukocytes that play a central role in host defense by engulfing and destroying foreign microorganisms, also secrete ATP when they become activated and start migrating toward chemotactic peptides released by invading pathogens. This ATP release appears to require hemichannels at the cell surface (*4*). Chen *et al*. observed that ATP is released predominantly from the deformed protruding region at the front end (known as the leading edge) of a migrating neutrophil as it moves toward *N*-formyl-methionyl-leucyl-phenylalanine (fMLP), a chemoattractant molecule secreted by certain pathogens. Treatment of neutrophils with apyrase, which hydrolyzes secreted ATP, nearly abolished chemotaxis, indicating that production and response to an ATP gradient is critical for initiating chemotaxis. Apyrase also reduced the fMLP-stimulated oxidative burst that contributes to the ability of neutrophils to kill pathogens. To the extent that adenosine is generated upon the addition of apyrase, it will also influence neutrophil chemotaxis and the oxidative burst. Although a small increase in the concentration of ATP was detected in buffer containing cells that were stimulated to undergo chemotaxis, a much larger increase in ATP—concentrations exceeding 1 μM—was detected in a localized area near the leading-edge membrane, as visualized by fluorescence microscopy.

Enzymes that metabolize ATP that are present in the cell's plasma membrane, with catalytic domains oriented extracellularly (ectoenzymes), play important roles in regulating the normal immune response to pathogens or tissue damage. In many cell types, including platelets, endothelial cells, and neutrophils, nucleoside triphosphate diphosphohydrolase-1/CD39 and ecto-5′-nucleotidase/CD73 dephosphorylate ATP and ADP to AMP. AMP is then converted to adenosine by CD73 or other enzymes. The importance of this extracellular purinergic flux in controlling inflammation is apparent in mice genetically engineered to lack CD39 (*5*, *6*) or CD73 (*7*). In these animals, activation of inflammatory cells such as platelets, macrophages, and neutrophils, and their adhesion to the vascular endothelium, are enhanced. ATP released from the leading edge of migrating neutrophils is metabolized by CD39 to generate AMP (*1*, *4*). Neutrophils have little CD73, but this enzyme is abundant on endothelial cells and lymphocytes. Chen *et al.* find evidence that an exogenous adenosine gradient causes the polarized localization and activation of A3 adenosine receptors at the leading edge of migrating neutrophils. The effect of this adenosine gradient is to increase the speed of chemotaxis. Consistent with this observation, the authors report a reduction in chemotaxis speed by pharmacological blockade of the A3 receptor. The results suggest that intravenous administration of an A3 agonist could inhibit neutrophil chemotaxis—and thus prevent unwanted inflammation—by providing a nondirectional, rather than a directional, chemotactic stimulus.

But there is a balance to this purinergic circuitry (see the figure). In addition to A3 adenosine receptors, neutrophils also express A2A adenosine receptors, which are not concentrated at the leading edge. When activated,

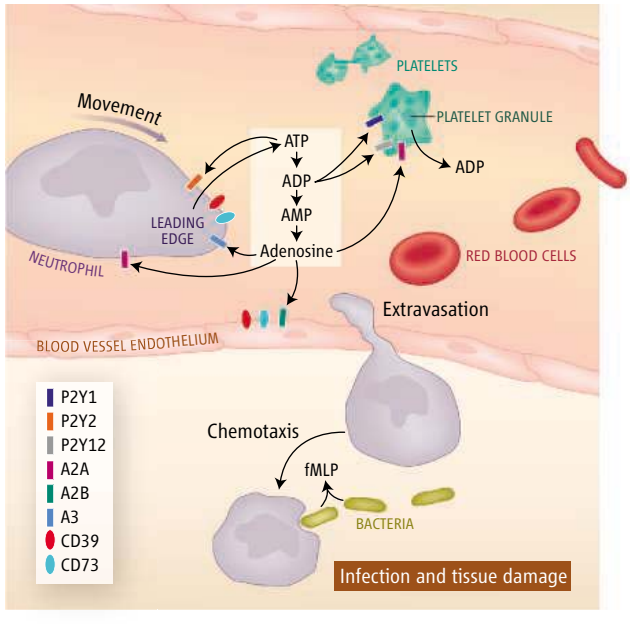

Purinergic signaling circuitry. The inflammatory response to infection or tissue damage depends on the coordination of adenine nucleotide metabolism and signaling among many cell types via purinergic receptors that recognize ATP, ADP, or adenosine. A neutrophil migrating toward a chemotactic stimulus (fMLP) releases ATP from its leading edge. ATP is dephosphorylated by ectoenzymes (CD39 and CD73) to ADP and adenosine. Gradients of ATP and adenosine initiate and accelerate directional chemotaxis via P2Y2 and A3 adenosine receptors, respectively, on neutrophils. Other adenosine receptors (A2A and A2B) inhibit neutrophil chemotaxis and adhesion to endothelial cells, as well as platelet aggregation.

The author is in the Department of Medicine, University of Virginia, Charlottesville, VA 22908, USA. E-mail: jlinden@virginia.edu

these G_s protein–coupled receptors block chemotaxis by stimulating cyclic AMP production, which blocks neutrophil adhesion and extravasation through the vascular endothelium. Activation of A2B, another adenosine receptor on endothelial cells, also decreases endothelial permeability (*4*). Adenosine also inhibits platelet aggregation and the release of granular ADP by binding to platelet A2A receptors. This counteracts the effects of ADP receptors (P2Y1 and P2Y12) that are also found on platelets. Clearly, purine release, signaling pathways, and metabolism among neutrophils, platelets, lymphocytes, and endothelial cells must be coordinated to allow platelet aggregation as well as neutrophil adhesion, extravasation, and chemotaxis.

The findings of Chen *et al.* indicate that extracellular purinergic gradients are at work to orient and regulate neutrophil chemotaxis. Because connexin 43 hemichannels have been implicated in the release of ATP from neutrophils (*4*), it will be of interest to determine if such channels are selectively activated on the leading edge of neutrophils and other cells during chemotaxis. Activation of the small GTP-binding protein Rho A, and actin reorganization, are known to participate in neutrophil shape change and movement in response to fMLP. These molecules may contribute to signaling responses downstream of activated purinergic signaling receptors. The findings of Chen *et al.* also suggest that the regulation of purinergic receptors and purinergic ectoenzymes, as well as the movement of cells that express ectoenzymes on their surface, can trigger a rapid and dynamic change in the local concentration of purines to influence the adhesion and movement of inflammatory cells.

References

1. Y. Chen *et al.*, *Science* **314**, 1792 (2006).
2. S. F. Okada, R. A. Nicholas, S. M. Kreda, E. R. Lazarowski, R. C. Boucher, *J. Biol. Chem.* **281**, 22992 (2006).
3. R. Nandigama, M. Padmasekar, M. Wartenberg, H. Sauer, *J. Biol. Chem.* **281**, 5686 (2006).
4. H. K. Eltzschig *et al.*, *Circ. Res.* **99**, 1100 (2006).
5. J. J. Wu, L. E. Choi, G. Guidotti, *Mol. Biol. Cell* **16**, 1661 (2005).
6. C. Goepfert *et al.*, *Circulation* **104**, 3109 (2001).
7. P. Koszalka *et al.*, *Circ. Res.* **95**, 814 (2004).

10.1126/science.1137190

ASTRONOMY

Heavy Elements in Stars

Abundances of elements produced in stars four to eight times the mass of the Sun indicate a different dominant nuclear reaction mechanism than in lower-mass stars.

Arnold I. Boothroyd

Almost all elements heavier than helium are produced in stars. Nuclear fusion reactions can produce elements up through iron, but most heavier elements result from a series of neutron absorption reactions (interspersed with radioactive decays of unstable neutron-rich isotopes). Some isotopes can only be produced by an extremely rapid, intense burst of neutrons (the r process). Others require slow neutron absorption (the s process), with neutron fluxes low enough that each unstable neutron-rich nucleus has time to decay before the next neutron is likely to be absorbed. Via the s process, stars in the mass range between $M_\odot$ and $8M_\odot$ (where $M_\odot$ is the mass of the Sun) produce roughly half of all elements heavier than iron (*1*). For stars with mass less than about $3M_\odot$, numerous observations of s-process element abundances have been reported (*2*–*5*). On page 1751 of this issue, García-Hernández *et al.* (*6*) report observations of s-process elements in stars with mass greater than $4M_\odot$. This result challenges our understanding of how such stars evolve but also may explain some of the puzzling isotope abundances found in the universe.

Near the end of its lifetime, a star in the mass range $M_\odot$ to $8M_\odot$ reaches the asymptotic giant branch (AGB) stage, as a cool red giant hundreds of times the size of the Sun and thousands of times more luminous. At this stage, the star's core (roughly the size of Earth) of extremely dense carbon and oxygen is surrounded by a helium-burning shell; very slightly farther out is a hydrogen-burning shell (which produces most of the star's luminosity), and outside this is the tenuous hydrogen-rich envelope (almost entirely convectively mixed) that reaches to the star's surface. A strong stellar wind grows even stronger as the star's luminosity increases. When mass loss from this stellar wind has stripped off the bulk of the envelope, the star ends up as a white dwarf.

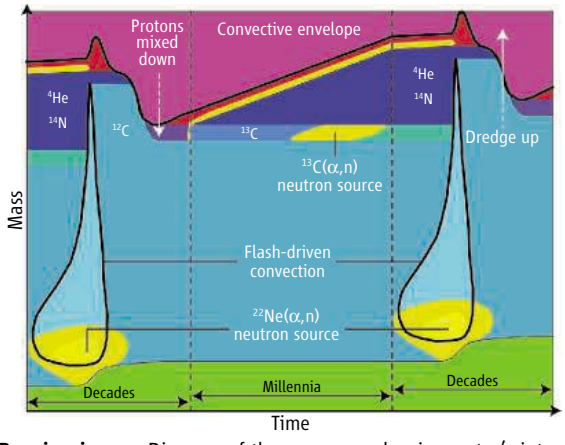

Burning issues. Diagram of the s process, showing a star's intershell region over a period that includes two helium shell flashes. The time scales are appropriate for a star of several solar masses (note compressed scale between the vertical dashed lines). The vertical coordinate is in terms of mass, rather than radial distance (because the latter varies with time). Nuclear burning is indicated in yellow, hydrogen-rich regions in red (magenta for the convective envelope, which is largely offscale), helium-rich regions in blue (cyan for convective regions), and the carbon-oxygen core (largely offscale) in green. Thick black lines indicate boundaries of convective regions.

Neutron reactions are crucial to heavy-element production in AGB stars. As shown in the figure, hydrogen burning via the carbon-nitrogen-oxygen (CNO) cycle (yellow region at the base of the hydrogen-rich envelope) leaves behind ashes composed of helium with a little ^{14}N (dark blue). Periodically, helium burning ignites (bright yellow outside the carbon-oxygen core) in a violent transient event known as a helium shell flash. Some of the helium is burned to ^{12}C; most of the ^{14}N is burned to ^{22}Ne, some of which burns via the ^{22}Ne(α,n) reaction (that is, the isotope ^{22}Ne absorbs an α particle and emits a neutron), producing neutrons for s processing. The flash drives a temporary convective region (cyan) that mixes the nucleosynthesized elements throughout most of the intershell region, leaving behind a region that is still largely helium but also contains a large amount of ^{12}C and some s-process elements (slate blue). The flash also causes the intershell region to expand and cool, extinguishing the hydrogen-burning shell. Envelope convection retreats momentarily, then reaches

The author is at the Canadian Institute for Theoretical Astrophysics, University of Toronto, Toronto, Ontario, M5S 3H8, Canada. E-mail: boothroy@cita.utoronto.ca

inward, engulfing part of the intershell region and dredging up nucleosynthesized elements to the star's surface; there they can be observed and are ejected into the interstellar medium by the stellar wind. After the helium shell flash dies away, hydrogen burning reignites, burning steadily until the next helium shell flash.

Another s-process neutron source results from incomplete mixing at the base of the convective envelope. During dredge-up, a little hydrogen (protons) is mixed some distance into the helium- and carbon-rich region below (purple region in the figure). When hydrogen burning reignites, these protons burn some of the ^{12}C to ^{13}C, leaving a ^{13}C pocket (sky blue). This pocket eventually gets hot enough for the $^{13}C(\alpha,n)$ reaction, yielding s-process elements (blue-green region). These are engulfed by intershell convection from the next helium shell flash and mixed throughout the intershell region (part of which is then dredged up to the stellar surface).

Theoretical mixing models are not good enough to predict the size of the ^{13}C pocket; in addition, rotational shear may yield further mixing in this region, in a manner that is likewise poorly understood (*1, 5*). The $^{22}Ne(\alpha,n)$ neutron source is easier to model, but this nuclear reaction rate is rather uncertain. The number of neutrons (and the amount of ^{12}C) produced are also affected by uncertainties in modeling the base of the flash-driven convective region (*1*). Fortunately, there are observational constraints.

The $^{22}Ne(\alpha,n)$ reaction produces a relatively high neutron density for a brief period (a few years). Even when neutron absorption yields an unstable isotope, this may absorb still another neutron before decaying unless its half-life is quite short. In contrast, the ^{13}C pocket yields a lower density of neutrons (over a much longer time period). Neutron-rich isotopes with relatively long half-lives have time to decay before they are likely to absorb another neutron, leading to a pattern of s-process isotopic and elemental abundances that differs from the pattern produced by the $^{22}Ne(\alpha,n)$ neutron source. In AGB stars with mass less than $4M_{\odot}$, s-process abundance observations indicate that the $^{13}C(\alpha,n)$ neutron source dominates (*1–5*). However, more massive stars burn hotter and faster, and the strong temperature sensitivity of the $^{22}Ne(\alpha,n)$ reaction rate suggests that it should be more important there. The observations of García-Hernández *et al.* (*6*) show that in fact the $^{22}Ne(\alpha,n)$ neutron source dominates in such stars. Not only do they demonstrate that these stars are sources of isotopes (such as ^{87}Rb) that are not produced in lower-mass stars; their observations also place new constraints on the physical processes involved, which will be beneficial to models of stars of all masses.

Our understanding of the s process is growing as a result of improvements in the theoretical models and in the observations that constrain them. We can look forward to a time when we will have a full understanding of how slow neutron capture produces elements from krypton to lead in giant stars.

References

1. F. Herwig, *Annu. Rev. Astron. Astrophys.* **43**, 435 (2005).
2. M. Busso, R. Gallino, G. J. Wasserburg, *Annu. Rev. Astron. Astrophys.* **37**, 239 (1999).
3. M. Busso *et al.*, *Astrophys. J.* **557**, 802 (2001).
4. C. Abia *et al.*, *Astrophys. J.* **559**, 1117 (2001).
5. J. C. Lattanzio, M. A. Lugaro, *Nucl. Phys. A* **758**, 477c (2005).
6. D. A. García-Hernández *et al.*, *Science* **314**, 1751 (2006); published online 9 November 2006 (10.1126/science.1133706).

10.1126/science.1136842

MICROBIOLOGY

Ramping Up the Heat on Nitrogenase

A heat-tolerating archaeon from a deep-sea vent can convert N_2 into molecules usable by other organisms. This finding of nitrogen-fixing ability has implications from ecology to biotechnology.

Douglas G. Capone*

On page 1783 of this issue, Mehta and Baross (*1*) describe a hyperthermophilic methanogen that can fix nitrogen (N_2). The authors isolated the organism from a deep (~1500 m) hydrothermal vent. Like other nitrogen-fixing bacteria and archaea, it uses the nitrogenase enzyme to tap the vast reservoir of dissolved N_2 gas for its nutritional needs for nitrogen. The discovery is noteworthy for several reasons: It establishes a new temperature maximum of 92°C for an active biological nitrogenase system, with biotechnological potential; it provides evidence for a new environment in which nitrogen fixation may occur; and it establishes yet another role for archaea in the marine nitrogen cycle. Furthermore, genomic analysis of this organism may provide important clues to the early evolution of the nitrogenase enzyme system.

Enhanced online at www.sciencemag.org/cgi/content/full/314/5806/1691

Hot-vent environments have piqued the imagination of scientists since their discovery in the 1970s. The biological diversity of these exotic and remote environments (see the figure) is largely sustained by chemoautotrophic microbes, which live on reduced inorganic chemical species released from vent fluids and thereby largely satisfy the carbon and energetic demands of the entire community (*2*). However, biological nitrogen fixation may also be operative in deep-vent environments (*3*). The organism found by Mehta and Baross, called FS406-22, provides further substance to this possibility.

Thus, nitrogen fixation may be a primary

CREDIT: NOAA VENTS PROGRAM

Life at a deep-sea vent. Hot hydrothermal vent fluid pours out of Vixen anhydrite chimney, located south of Axial caldera on the edge of an older (pre-1987) lava flow.

The author is in the Department of Biological Sciences, University of Southern California, Los Angeles, CA 90089, USA. E-mail: capone@usc.edu

*Present address: Laboratoire d'Oceanographie de Villefranche, 063234 Villefranche sur Mer, France.

source of nitrogen, a critical nutrient, in hydrothermal communities. Substantial nitrogen fixation would further increase the nutritional independence of these exotic ecosystems from from the surfaceof the ocean,where light drives the photosynthesis-based primary productionthat feeds the major marine food webs. The biogeochemical importance of nitrogen fixation in hot-vent communities must therefore be evaluated directly. The identification of novel sites of marine nitrogen fixation (such as hot vents, which are broadly distributed throughout the deep sea) may also help to determine the magnitude of oceanic nitrogen fixation, which is currently poorly constrained (*4*, *5*).

A large proportion of the microbial populations of the sea are archaea (largely of the Crenarchaeota lineage) (*6*, *7*). However, the physiological and ecological role of these organisms has remained elusive. Recent findings have shown that many marine Crenarchaeota have the ammonium monooxygenase gene and may in fact dominate marine nitrification, the biological oxidation of ammonium using oxygen as the electron acceptor (*8*). Nitrogen fixation in archaea was first reported in 1984 (*9*), and in 2003, Mehta *et al*. (*10*) retrieved the first marine archaeal *nifH* sequences from deep-sea environments, including a hot-vent system (*nifH* is a gene from the nitrogenase operon that codes for one of the enzymes of the nitrogenase complex, dinitrogenase reductase). The current report thus confirms a second role for archaea in the nitrogen cycle of the sea.

FS406-22 has an optimal growth temperature of 90°C and fixes dinitrogen at temperatures of up to 92°C, smashing the previous record of 64°C held by *Methanothermococcus thermolithotrophicus* (*11*) by a comfortable 28°C margin. Enzymes with high thermal stabilities have found broad use in molecular biology and biotechnology. Given the importance of nitrogen fixation in global agriculture and the creative exploitation of novel organisms by the biotechnology industry, a heat-stable nitrogenase system is likely to find a useful industrial application.

Recent analyses have suggested that nitrogenase may have first arisen either before the divergence of the three main branches of life (*12*) or, alternatively, more recently in a thermophilic archaeon (*13*). On the basis of genetic analysis of several of the structural and regulatory genes of the *nif* operon, as well as several related genes, Mehta and Baross argue that their archaeal nitrogen-fixing isolate may be representative of some of the earliest lineages of nitrogen fixation, thus lending support to the first scenario.

For a number of well-characterized enzyme systems of Archaea and Bacteria living at mesophilic temperatures (10° to 30°C), which use molybdenum at the active site, the analog enzyme in hyperthermophiles has replaced molybdenum with tungsten (*14*). Will FS406-22 reveal the first tungsten-based nitrogenase? And, for that matter, if the earliest precursors of life were hyperthermophiles, did tungsten enzyme catalysis predate catalysis based on molybdenum? A few more questions to ponder.

References

1. M. P. Mehta, J. A. Baross, *Science* **314**, 1783 (2006).
2. H. W. Jannasch, C. O. Wirsen, *Bioscience* **29**, 592 (1979).
3. G. H. Rau, *Nature* **289**, 484 (1981).
4. L. A. Codispoti, *Biogeosci. Discuss.* **3**, 1203 (2006).
5. N. Gruber, in *The Ocean Carbon Cycle and Climate*, M. Follows, T. Oguz, Eds. (Kluwer, Dordrecht, the Netherlands, 2004), pp. 97–148.
6. J. Fuhrman, K. McCallum, A. A. Davis, *Nature* **356**, 148 (1992).
7. E. DeLong, *Proc. Natl. Acad. Sci. U.S.A.* **89**, 5685 (1992).
8. C. Wuchter *et al.*, *Proc. Natl. Acad. Sci. U.S.A.* **103**, 12317 (2006).
9. P. A. Murray, S. H. Zinder, *Nature* **312**, 284 (1984).
10. M. P. Mehta, D. A. Butterfield, J. A. Baross, *Appl. Environ. Microbiol.* **69**, 960 (2003).
11. N. Belay, R. Sparling, L. Daniels, *Nature* **312**, 286 (1984).
12. J. Raymond, J. L. Siefert, C. R. Staples, R. E. Blankenship, *Mol. Biol. Evol.* **21**, 541 (2004).
13. F. D. Ciccarelli *et al.*, *Science* **311**, 1283 (2006).
14. A. Kletzin, M. W. W. Adams, *FEMS Microbiol. Rev.* **18**, 5 (1996).

10.1126/science.1136980

PHYSICS

A New Spin on the Insulating State

Charles L. Kane and Eugene J. Mele

Theory suggests a practical method for producing a novel insulating state of matter.

Electrical insulators are usually appreciated for their ability to do nothing. Such materials either trap or restrict the motion of free charges in matter. This is useful in all kinds of applications, ranging from the wiring in your home to directing the flow of electrons in the tiny circuits of your iPod. Now, on page 1757 of this issue, Bernevig *et al*. have proposed a new kind of two-dimensional insulator, which permits the flow of charge only at its edges (*1*). This may lead to the development of a new kind of solid-state electronic device.

An insulator has an energy gap separating filled and empty bands of electronic states, and thus is electrically inert because a finite energy is required to dislodge an electron. In the 1960s, Kohn characterized the insulating state in terms of the sensitivity of electrons inside the material to effects on the sample boundary (*2*). His insight was that the electrons of an insulator can be regarded as occupying localized orbitals (see the figure), so that they are insensitive to perturbations on the boundary.

The presence of a bulk energy gap does not guarantee that electrons have this "nearsighted" property. A counter example is provided by the quantum Hall state of a two-dimensional electron gas in a perpendicular magnetic field. In the quantum Hall effect, an energy gap results from the quantization of the closed circular orbits that electrons follow in a magnetic field. The inside of a quantum Hall system is thus inert like an insulator. However, at the boundary of the material a different type of motion occurs, which allows charge to flow in one-dimensional edge states. These edge states are unique in that they allow for charge to flow in one direction only. This makes them insensitive to scattering from impurities and explains the observed precise quantization of the Hall resistance.

Because both have a bulk energy gap, the insulating state and the quantum Hall state appear similar. The difference was explained by Thouless *et al*. (*3*), who generalized Kohn's notion of boundary sensitivity to show that an occupied band is characterized by an integer topological index. This index, n, distinguishes the insulating state ($n = 0$) from the quantum Hall state ($n \neq 0$) in a manner similar to the way that the mathematical "genus" of a solid body—which counts the number of holes—distinguishes a marble from a donut or a coffee cup. For quantum Hall states, the conducting edge states are a consequence of this topological structure.

Recently a new class of topological insulators has been predicted to be possible at zero magnetic field. This occurs because electrons have a quantum property called spin, which can have two possible polarizations, "up" and "down." In 2005, we showed theoretically that a single two-dimensional sheet of graphite, called graphene, has a small energy gap that

The authors are in the Department of Physics, University of Pennsylvania, Philadelphia, PA 19104. E-mail: kane@physics.upenn.edu

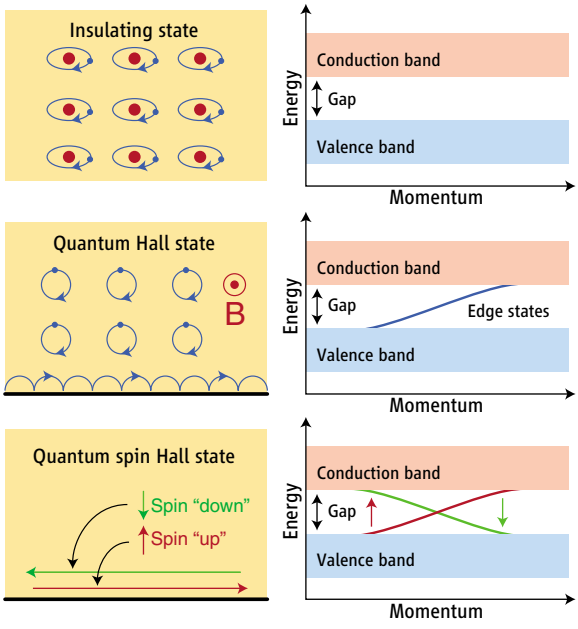

States of matter. (Top) Electrons in an insulator are bound in localized orbitals (left) and have an energy gap (right) separating the occupied valence band from the empty conduction band. (**Middle**) A two-dimensional quantum Hall state in a strong magnetic field has a bulk energy gap like an insulator but permits electrical conduction in one-dimensional "one way" edge states along the sample boundary. (**Bottom**) The quantum spin Hall state at zero magnetic field also has a bulk energy gap but allows conduction in spin-filtered edge states.

arises from the interaction between the electrons' spin and orbital degrees of freedom (*4*). The resulting electronic state is inert in the bulk like an insulator, but has conducting edge states. We found that a new topological invariant distinguishes this state from a conventional insulator and guarantees the presence of those edge states (*5*). In the simplest picture, the edge states are spin-filtered in that electrons with spin-up propagate in one direction, whereas electrons with spin-down propagate in the opposite direction. In this sense, this state exhibits a quantum spin Hall effect.

The quantum spin Hall effect will be hard to observe in graphene because carbon's weak spin-orbit interaction makes the energy gap quite small and susceptible to thermal fluctuations. The new proposal by Bernevig *et al.* is exciting because it solves this problem and provides a feasible method for observing the quantum spin Hall effect. They considered a semiconductor heterostructure consisting of a thin layer of HgTe sandwiched between crystals of CdTe. Their convincing theoretical analysis shows that in an appropriate range of layer thickness this two-dimensional structure should exhibit a robust quantum spin Hall effect. HgTe, CdTe, and their alloys are a well-studied family of semiconductor materials with strong spin-orbit interactions. The proposed device can be made with current technology, thanks to decades of experience in the growth of high-quality semiconductor structures.

In addition to providing a venue for a new fundamental state of matter, the structure proposed by Bernevig *et al.* may be of practical interest because it provides a method for the electrical manipulation of spins and spin currents with little or no dissipation. The experimental demonstration of the quantum spin Hall effect would be an important step in this direction.

References

1. B. A. Bernevig, T. L. Hughes, S.-C. Zhang, *Science* **314**, 1757 (2006).
2. W. Kohn, *Phys. Rev.* **133**, A171 (1964).
3. D. J. Thouless, M. Kohmoto, M. P. Nightingale, M. den Nijs, *Phys. Rev. Lett.* **49**, 405 (1982).
4. C. L. Kane, E. J. Mele, *Phys. Rev. Lett.* **95**, 226801 (2005).
5. C. L. Kane, E. J. Mele, *Phys. Rev. Lett.* **95**, 146802 (2005).

10.1126/science.1136573

CHEMISTRY

Generating a Photocurrent on the Nanometer Scale

Scientists have devised a nanometer-scale analog of the bulk photoconductors used in copiers and laser printers.

Frank Würthner

Photocopiers and laser printers play an important role in our day-to-day life, but we rarely pay attention to how these devices work. They rely on photoconductors, which are insulators in the dark but become conductive under light illumination. About three decades ago, environmentally more benign organic photoconductors replaced the toxic inorganic selenium alloy (*1*). The photoconductors in use today are bilayer systems consisting of a charge-generating layer and a charge-transporting layer (*1*).

On page 1761 of this issue, Yamamoto *et al.* describe a nanometer-scale analog of such bulk photoconductors. They report well-defined self-assembled coaxial nanowires, in which hexabenzocoronene (HBC) layers are laminated by trinitrofluorenones (TNF) (see the figure) (*2*). Like their macroscopic counterparts, these nanowires are insulators in the dark but generate a photocurrent upon irradiation with ultraviolet or visible light.

Earlier attempts to create supramolecular organic photoconductors have mainly focused on columnar liquid-crystalline materials (*3*–*5*). Müllen and colleagues have shown that HBC-based columnar liquid crystals can achieve charge carrier mobilities three orders of magnitude higher than those of commercially available amorphous organic materials (*4*). Recently, Percec *et al.* have reported more complex photoconducting columnar liquid crystals, in which the active units (carbazoles and TNFs) are confined in the center of the columns (*5*).

These studies aim to create a highly organized, higher-mobility bulk material that can replace existing low-molecular-weight organic photoconductors or can be used in other applications, such as field-effect transistors. In contrast, the coaxial nanowires described by Yamamoto *et al.* are not primarily targeted for implementation in existing technologies. Rather, the incentive for this work comes from the desire to create nanometer-scale functional supramolecular entities. Such entities are ubiquitous in nature, for example in photosynthesis, where different self-assembled units interact to accomplish light harvesting, charge separation, and water oxidation in the confined space of a membrane (*6*). The tubular organization of the HBC molecules in the system of Yamamoto *et al.* (see the figure) has a striking similarity to

The author is at the Institute of Organic Chemistry and the Wilhelm Conrad Röntgen Research Center of Complex Material Systems, University of Würzburg, 97074 Würzburg, Germany. E-mail: wuerthner@chemie.uni-wuerzburg.de

the light-harvesting antennae in green sulfur bacteria (*7*).

Yamamoto *et al.* show that subtle changes in external parameters have a pronounced impact on the nanometer-scale morphology of their structures, which in turn determines the photofunctional properties (*2*). At high concentration, brown microfibers composed of HBC-TNF charge-transfer complexes are formed. In contrast, self-assembly at lower concentration affords yellow coaxial nanowires that consist of segregated layers of graphitic HBCs and electron-accepting TNFs (see the figure). Only these nanowires exhibit the desired photoconductive properties. In contrast, the close contacts (indicated by the brown color) between the electron-rich HBCs and the electron-poor TNFs in microfibers rapidly quench the photoinduced charge-separated state, thus prohibiting the photocurrent.

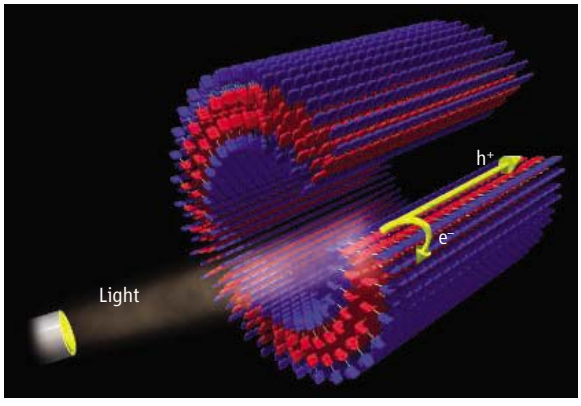

A nanometer-scale analog of bulk photoconductors. The coaxial supramolecular nanowire reported by Yamamoto *et al.* forms through self-assembly of HBC (red) and TNF (blue) molecules. Illumination with ultraviolet or visible light leads to the generation of electrons (e^-) and holes (h^+), followed by hole transport through the HBC layer (*2*).

This work marks a breakthrough in the emerging field of supramolecular electronics (*8*, *9*). The pivotal aspects of supramolecular electronics are (i) synthesis of molecular building blocks that contain photo- and redox-active components (here, HBC and TNF); (ii) self-assembly of such building blocks, directed by external parameters such as solvent or temperature, to afford functional nanometer-scale entities (here, a photoconducting supramolecular nanowire); and (iii) connection of these entities to electrodes to enable characterization of the desired physical properties (here, photoconductivity).

The implementation of self-assembled organic nanoelectronic materials—such as the coaxial nanowires reported by Yamamoto *et al.*—into existing commercial microelectronics technology poses severe challenges. However, such materials may enable a new technology based on self-assembled nanometer-scale electronic circuits. Such nanodevices may even be able to communicate with biological systems that have similar dimensions and are based on similar organizing principles.

A closer look at the coaxial nanowire of Yamamoto *et al.* reveals a defined interface between electron-rich p-type semiconducting HBCs and electron-poor n-type semiconducting TNFs. The system can thus be understood as a nanometer-scale version of a bulk p-n heterojunction (*10*)—the most important functional unit of solar cells. Therefore, this assembly should, in principle, be able to convert light energy into electricity that can drive a supramolecular machine. Future developments based on this and related nanometer-scale photofunctional assemblies may open up new perspectives for nanodevices.

References

1. R. O. Loutfy *et al., Pure Appl. Chem.* **60**, 1047 (1988).
2. Y. Yamamoto *et al., Science* **314**, 1761 (2006).
3. D. Adam *et al., Nature* **371**, 141 (1994).
4. A. M. van de Craats *et al., Adv. Mater.* **11**, 1469 (1999).
5. V. Percec *et al., Nature* **417**, 384 (2002).
6. T. Pullerits, V. Sundström, *Acc. Chem. Res.* **29**, 381 (1996).
7. T. S. Balaban, H. Tamiaki, A. R. Holzwarth, *Top. Curr. Chem.* **258**, 1 (2005).
8. A. P. H. J. Schenning, E. W. Meijer, *Chem. Commun.* **2005**, 3245 (2005).
9. M. R. Wasielewski, *J. Org. Chem.* **71**, 5051 (2006).
10. F. Würthner *et al., J. Am. Chem. Soc.* **126**, 10611 (2004).

10.1126/science.1136984

NEUROSCIENCE

The Impact of Invisible Stimuli

Invisible stimuli that are irrelevant to a task are more disturbing than visible distractors because of failed communication in regions of the brain that normally supress such responses.

Petra Stoerig

Sigmund Freud's groundbreaking work first demonstrated that a large part of our conscious mental life is governed by motives and memories that are not, or are no longer, accessible to conscious insight. Events that can no longer be consciously remembered also guide the behavior of neurological patients, as famously shown by Édouard Claparède's amnesic patient. The patient could not recall that her doctor had once painfully pricked her with a needle when shaking her hand, but nonetheless refused to shake his hand again (*1*). Information that fails to reach awareness can also guide behavior in neurological patients who, as a result of lesions of the brain's sensory cortices, are completely unaware of its existence. Evidence for such "implicit" processing has come from studies of vision, audition, touch, emotion, and action (*2*), and has also been well documented in healthy people. On page 1786 of this issue, a report by Tsushima and colleagues adds a new twist to the slowly unfolding story of the impact of implicit processes and offers a brain-based explanation (*3*).

Imagine performing a task that requires full attention. If you had to do so in a normal office environment, rather than a sound-proof lab, you would likely predict that telephones ringing and people rushing by your desk would distract you more than would imperceptible stimuli irrelevant to your task. Tsushima *et al*. investigated the influence of the strength of distracting stimuli on task performance (see the figure). Contrary to expectation, they report that subthreshold distracting stimuli—that is, weak stimuli that are irrelevant to the task being performed—have a greater impact than strong, easily noticeable distractors. The authors used a rapid visual presentation task in which healthy participants had to detect two digits that appeared very briefly in a central stream of six letters. This stream of alphanumeric symbols was surrounded by an annulus of randomly moving dots. Different proportions of these dots—0 to 20%—moved coherently in the same direction (the "signal") during the trials. The larger the proportion of these coherently moving dots (the larger the motion coherence ratio of the task-irrelevant background), the more motion one perceives. Although higher motion coherence should have impaired digit identification more than lower coherence—after all, motion tends to capture attention, even inadvertently—performance was signif-

The author is at the Institute of Experimental Psychology, Heinrich-Heine-Universität, 40225 Düsseldorf, Germany. E-mail: stoerig@uni-duesseldorf.de

icantly worse at 5% coherence ratios than at 20%, where task performance was statistically similar to that observed at 0% coherence. At 5% coherence, the task-irrelevant motion had the most pronounced effect on digit identification, although the subjects were unable to discriminate the direction of the motion signal at this low coherence ratio, even when this was their only task.

Moreover, magnetic resonance imaging revealed that the human motion complex hMT+, the brain's visual cortical area that responds preferentially to moving stimuli, was more strongly activated at 5% coherence than at higher coherence ratios. Because stronger stimuli commonly evoke both earlier and stronger cortical responses than weak ones (*4*, *5*), this result is surprising. The authors relate it to the inverse relationship

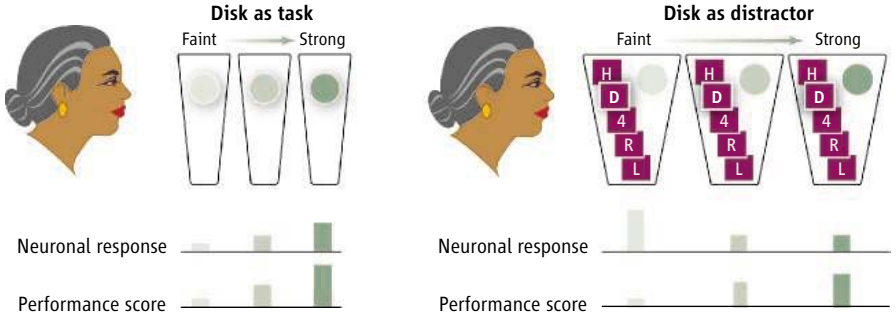

Distraction paradox. (**Left**) When attention is focused on stimuli that vary in strength (gray disks), faint stimuli evoke weaker neuronal responses than stronger ones, and task performance improves with stimulus strength. (**Right**) When a different task, such as the identification of digits in a rapidly presented stream of letters, has to be performed, digit identification is better with a strong distracting stimulus than with a weak, imperceptible one.

they observed between activity in hMT+ and in the lateral prefrontal cortex, an area thought to play an important role in inhibiting the influence of irrelevant signals. They suggest that because of the weakness of the 5% coherent motion signal, this cortical region fails to effectively inhibit the hMT+ response. Because it fails to "notice" the hMT+ response, the lateral prefrontal cortex fails to intervene, so that the weak motion distractor can exert its disruptive effect on performance, unchecked.

Attention is thought to work through amplification of task-relevant information and/or suppression of task-irrelevant information. Here, an indiscriminately weak distracting signal seems to slip under the inhibitory guard, and disrupts task performance more than a much stronger distracting signal would. Would the same result also be found in instances of "inattentional blindness" (*6*) where people fail to notice even very salient events that are irrelevant to the task they perform—like a person in a gorilla suit walking through a group of people playing ball (*7*)? Our astonishing ability to overlook the gorilla when we are focused on counting the number of passes the players make may depend on it being noticeable. Perhaps the counting of passes would suffer more if a barely noticeable event were to occur. Does attentional suppression require visibility?

If "invisibility" makes distractors more effective, does it make a difference whether it is due to the physical weakness of the signal, or to its inability to reach the subject's awareness? With subthreshold stimuli that are too weak to be detected, weakness and unawareness go hand in hand. But with strong, easily detectable stimuli, one could attempt to disentangle the relative effects of the subjects' unawareness from those of the stimulus' physical properties, provided one presents strong stimuli under conditions that render them almost or even entirely invisible.

Many studies have convincingly shown that we often fail to notice even salient events. "Masking," where the presence of one or more additional stimuli renders another stimulus invisible (*8*), is an example of such "experimental blindness" that might be adapted to learn whether a masked distractor would impair performance more than the masking stimulus alone. As both the masking stimulus and the masked stimulus are physically strong, manipulations of this kind could be used to elucidate whether it is the physical weakness of the distractor, or rather the subjects' unawareness of its presence, that is responsible for the pronounced effects that invisible stimuli appear to exert on task performance in healthy subjects. Furthermore, strong but task-irrelevant stimuli could be presented to neurological patients who, because of lesions of the sensory cortices, can no longer consciously perceive them, to learn whether these stimuli would disrupt their performance in an unrelated task despite being imperceptible. Both in healthy subjects and in patients with lesions in the visual cortex, the neural responses to physically strong stimuli that fail to reach awareness have been shown to be weaker than the neural responses that the same stimuli evoke when they are consciously perceived (*9*). Might such strong but imperceptible stimuli therefore also fail to be inhibited by attention? Should they prove to be more effective distractors than task-irrelevant stimuli that subjects can easily perceive, one could ask whether the lateral prefrontal cortex that Tsushima *et al*. call upon to explain the effect of their weak distractor also fails to exert its inhibiting effects on the neuronal response evoked by strong but imperceptible stimuli. If so, perhaps even the subconscious motives and memories that affect our behaviors in so many ways could eventually become attributed to failures in interareal neuronal communication of the kind described by the authors.

Since Freud, much evidence shows that we often fail to notice what is right before our eyes, that our brain responses precede conscious volition (*10*), and that we make patently false claims about our choices (*11*, *12*). Evidence like this is the reason why many have come to doubt our intuitive certainty regarding the causal role of consciousness (*13*). At the same time, we have learned that information that is no longer, or not at all, accessible to consciousness guides our behavior and affects the processing of stimuli of which we are aware. The results of Tsushima *et al*. go beyond confirming this. By showing that invisible stimuli may affect performance more effectively than stimuli that do reach awareness, they shift the balance yet further from conscious to unconscious processes.

References

1. É. Claparède, *Arch. Psychol.* **11**, 79 (1911).
2. B. de Gelder, E. de Haan, C. Heywood, Eds., *Out of Mind: Varieties of Unconscious Processes* (Oxford Univ. Press, Oxford, 2001).
3. Y. Tsushima, Y. Sasaki, T. Watanabe, *Science* **314**, 1786 (2006).
4. J. H. Maunsell, J. R. Gibson, *J. Neurophysiol.* **68**, 1332 (1992).
5. W. T. Newsome, E. B. Pare, *J. Neurosci*. **8**, 2201 (1988).
6. A. Mack, I. Rock, *Inattentional Blindness* (MIT Press, Cambridge, MA, 1998).
7. D. J. Simons, C. F. Chabris, *Perception* **28**, 1059 (1999).
8. H. Ögmen, B. Breitmeyer, *The First Half Second* (MIT Press, Cambridge, MA, 2006).
9. R. Marois, Y. Do-Joon, M. M. Chun, *Neuron* **41**, 465 (2004).
10. B. Libet, *Mind Time: The Temporal Factor in Consciousness* (Harvard Univ. Press, Cambridge, MA, 2004).
11. R. E. Nisbett, T. D. Wilson, *Psychol. Rev*. **84**, 231 (1977).
12. P. Johansson, L. Hall, S. Sikström, A. Olsson, *Science* **310**, 116 (2006).
13. D. M. Wegner, *The Illusion of Conscious Will* (Bradford/MIT Press, Cambridge, MA, 2002).

10.1126/science.1136956

PRESIDENTIAL ADDRESS

Grand Challenges and Great Opportunities in Science, Technology, and Public Policy

Gilbert S. Omenn

Science is about asking questions and finding credible ways to answer them. Scientists and engineers lay the foundation for practical applications of what is learned, and respond to needs in the broader society, as well as our own curiosity and passion for new knowledge. Economists have attributed more than half of the gains in gross national product and up to 85% of the gains in per capita income over the past several decades to advances in science and technology (*1*–*3*). Science works best in a culture that welcomes challenges to prevailing ideas and nurtures the potential of all of its people. Scientific ways of thinking and of re-evaluating one's views in light of new evidence help strengthen a democracy.

Many of us are confident that the scientific community could do even more if we are asked to do so and if we organize to accelerate work toward major goals for society. The AAAS theme, "Grand Challenges and Great Opportunities," helped frame the special 125th anniversary issue of *Science* on "What Don't We Know?" (*4*) and an excellent 2006 annual meeting.

The concept and promotion of Grand Challenges can help energize not only the scientific and engineering community, but also students, journalists, the public, and their elected representatives, to develop a sense of the possibilities, an appreciation of the risks, and an urgent commitment to accelerate progress. They can show the added value of further major investments in research and development and education at a time of intense competition for federal funds. They can help the United States sustain its competitive edge in a global economy, while helping other countries to make big gains at the same time.

Curiosity about the worlds around us is an innate feature of humans and a driving force for science. To a variable extent, we are all curious about both the world of nature and the nature of human societies. All species have mechanisms for exploring their environments. Regrettably, as young children progress and ask lots of questions, too many parents and teachers suppress that curiosity by ignoring or criticizing questions they cannot or are unwilling to answer. Instead, we should feed that curiosity and stimulate ourselves in the process.

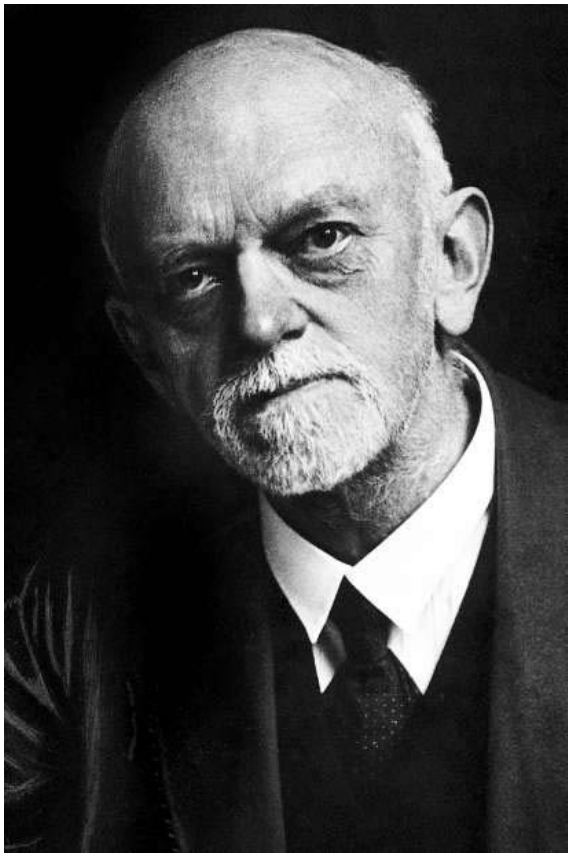

German mathematician David Hilbert

The author is in the Departments of Internal Medicine, Human Genetics, and Public Health and Center for Computational Medicine and Biology, University of Michigan, MI 48109–2218, USA. E-mail: gomenn@umich.edu

To demonstrate the historical roots and disciplinary breadth of the concept, I have selected Grand Challenges in three categories: (i) scientific and engineering fields, with examples from mathematics, physics, environmental sciences, and genomics; (ii) multidisciplinary research and development problems, illustrated with green chemistry for sustainability, energy security, control of global infectious diseases, and international efforts to reduce extreme poverty and hunger; and (iii) science and technology to enhance public understanding and decision-making about risks to health and to economic competitiveness. Finally, I will discuss some schemes for attracting people to Grand Challenges work.

Grand Challenges in Specific Fields

Mathematics. In 1900, a 38-year-old professor from Göttingen, Germany, David Hilbert, dared to define 23 "mathematical puzzles," which kept his contemporary and future colleagues busy for a century (*5*). As he said, "Who of us would not be glad to lift the veil behind which the future lies hidden; to cast a glance at the next advances of our science and at the secrets of its development during future centuries?…A mathematical problem should be difficult in order to entice us, yet not completely inaccessible, lest it mock at our efforts. It should be to us a guide post on the mazy paths to hidden truths, and ultimately a reminder of our pleasure in the successful solution."

The problems ranged from mathematical foundations and prime numbers to geometry, algebraic number theory, and topology. Nearly all have now been solved, or partially solved; each mathematician I consulted has his or her own tally! The solutions have generated additional challenging questions. A century later, the Clay Mathematics Institute of Cambridge, MA, has offered prizes of $1 million each for solutions to seven problems; one is a carryover from the original 23 (the Riemann Hypothesis).

Physics and astronomy. Last year we celebrated the centennial of Einstein's magical year of 1905, which saw his three stunning publications on photons, Brownian motion,

and special relativity (*6*). Only 11 years earlier, in 1894, a prominent physicist, Albert Michelson, had declared that physics was a mature field and that "[t]he future of physics lies in the 6th decimal place"—an extreme form of filling in the details! Two years later, Roentgen described ionizing radiation. Then came Einstein, Rutherford, Bohr, and the century of physics. Lists of Grand Challenges have become a part of the informal educational process in physics and related fields. As the late David Schramm noted (*7*), "The study of the very large (cosmology) and the very small (elementary particles) is coming together." In 2003, the National Research Council Board on Physics and Astronomy published a strategy for the intersection of physics and astronomy: *Connecting Quarks with the Cosmos: Eleven Science Questions for the New Century* (*7*). These questions sought to understand the creation of matter and energy at the initiation of the universe, the dark matter that pervades the cosmos, the dark energy that appears to be causing the expansion of the universe to accelerate, additional dimensions beyond four of space-time, strong-field gravitational physics, very-high-energy cosmic rays, neutrino mass, and extreme physics of black holes and magnetized neutron stars. Progress has been facilitated in the past two decades by the Hubble Space Telescope, an example of the crucial role of new technology in advancing scientific concepts and experiments.

Environmental sciences. The search for knowledge about the impact of human societies on our environment has gained in importance as rapid population growth and economic development intensify the stresses human beings place on the biosphere and ecosystems. Advances in biology, computer sciences, and techniques for sensing biological, physical, and chemical phenomena on, below, and above the Earth's surface could help us develop a more sustainable relationship with the Earth and its natural resources.

The National Science Foundation (NSF) commissioned a National Research Council report that selected eight Grand Challenges (Table 1) from 200 nominations (*8*). These were defined as "major scientific thrusts that are compelling for both intellectual and practical reasons, offer potential for major breakthroughs on the basis of recent advances in science and technology, and are feasible with current capabilities, given a serious infusion of resources." The criteria comprised probability of significant payoff, large scope, relevance to environmental issues, feasibility, timeliness, and requirement for multidisciplinary collaboration.

There is a lot of practical value in learning how natural systems work; how human activities and other influences perturb these systems; what causes these perturbations; how changes in one system affect other systems; and how knowledge may guide well-informed choices about means of transforming or restoring ecologic systems.

Genetics and genomics. The life sciences were fairly sleepy for a long time, with even dramatic observations about heredity and biochemistry making only a minor impression between 1860 and 1944. Then McCarty, MacLeod, and Avery's critical experiment showed that DNA, not proteins, carried the molecular message of inheritance. Within a decade, x-ray crystallography of DNA molecules by Rosalind Franklin and Maurice Wilkins and deductions about the role of hydrogen-bonding of antiparallel strands of DNA led James Watson and Francis Crick to propose in 1953 the double-helical structure for DNA and its functional implications. Once the triplet code was cracked, the pace accelerated remarkably, leading eventually to the Human Genome Project.

A mathematical problem should be difficult in order to entice us, yet not completely inaccessible, lest it mock at our efforts. It should be to us a guide post on the mazy paths to hidden truths, and ultimately a reminder of our pleasures in the successful solution.

–David Hilbert

When the Human Genome Project was proposed in 1986, it was ridiculed as impossible, absurd, mind-numbingly dull, even dangerous, according to those who feared that the 15-year, $3 billion estimated price tag would require sacrificing funds for individual research projects to the lure of "big science" (*9*). The U.S. Department of Energy charged ahead with enthusiastic support from its advisory committee and the Congress. The project was then denounced as a scheme for unemployed bombmakers! By 1988, however, a National Academy of Sciences (NAS) panel endorsed a stepped approach, mapping genes on the chromosomes, vastly improving sequencing technologies, and sequencing the smaller genomes of other organisms. These intermediate goals permitted multiple important successes, rather than a single target of finishing the human sequence. National Institutes of Health (NIH) Director James Wyngaarden enlisted Watson to head a special Office for Genome Research, and NIH quickly took the lead. In response to a congressional query about potential risks of genetic knowledge, Watson committed to allocate 3 to 5% of the funding for research and conferences on ethical, legal, and social implications of the Human Genome Project (ELSI).

Competition between Craig Venter's shotgun sequencing approach at the company Celera Genomics and the international public consortium (by then led by Francis Collins) at NIH with many international colleagues heightened public and political interest and accelerated the pace, overcoming major technical hurdles. By now, the sequencing effort, completed 2 years ahead of schedule, has transformed biomedical research. Additional large collaborative projects have analyzed single nucleotide polymorphisms (SNPs) and linked genes in haplotypes (the HapMap) for variation within populations and discovery of biomarkers of disease. Surprises include the relatively low number of genes in humans; the high frequency of splicing of genes or messenger RNAs; the generation of many more proteins than the number of original coding genes; the regulatory role of small interfering RNA molecules; and the significance of repeated triplet sequences in disrupting protein function and causing degenerative neurological diseases.

Proteomics, systems biology, and drug development. Grand Challenges abound in the new era of biology. One of the largest is the effort to detect and measure all of the proteins in cells and in the blood. Proteins are the major effector molecules of the cell—enzymes, receptors, antibodies, and structural proteins. Proteins undergo modifications that change their functions, a huge range of concentrations, and rapid changes in response to physiological processes, diseases, and pharmacological and nutritional stimuli. Proteomics is the study of all the proteins, in analogy to genomics, the study of all the genes. Characterization of a

proteome, for example, the plasma proteome (*10*), is more daunting than sequencing a genome, even though proteomics gets a head start from the gene sequence databases. One valuable outcome of such efforts will be the validation of proteins for clinical use as biomarkers of diseases.

The complementary Grand Challenge of systems biology (*11*) models the interconnected changes in the whole cell. Genes, messenger RNAs, proteins, protein complexes, and metabolites, plus the mechanisms that up-regulate or down-regulate in-dividual genes or proteins and the corresponding metabolic or signaling pathways in cell networks during development, ag-ing, disease, and recovery from disease, all must be represented. Computational tools for these efforts and for text and data mining are still in developmental stages. Modeling the pathways and networks inside cells and between cells is an exciting, open-ended domain. As part of the NIH Roadmap (see below), seven National Centers for Biomedical Computing have been funded through participation of nearly all of the NIH institutes. Results to be expected from such centers include such findings as a new class of fusion genes (TMPRSS2/ETS) that seem to be critical to development of prostate cancers (*12*).

The more we learn about the cellular complexity of tumors (*13*) and the complex interactions of receptor-mediated intracellular signaling pathways, the more we may need to redirect drug development research. Instead of seeking a "magic bullet" that targets a single receptor, pathway, or phenomenon, we may need to simultaneously attack two or more pathways, both for initial benefit and to prevent emergence of resistant cells. This situation may be analogous to multi-antibiotic regimens for microorganisms that are prone to develop resistance to therapy and may force a rethinking of clinical trials for U.S. Food and Drug Administration approvals.

Another challenge for drug development is the heterogeneity of patients and the heterogeneity among what appear to be similar tumors under the microscope. If a drug works well in only 10 to 20% of patients with lung cancers, for example, a pharmacogenomic test that identifies those patients and excludes the others would be better for the patient and those paying for the treatment. The challenge is to learn whether the same mechanism might account for some percentage of cancers of the colon, breast, pancreas, and prostate, so that the total number of cases that could be specifically and effectively treated becomes large, even though drug use is restricted to those able to respond.

Genomic and proteomic analyses are being applied also to the differentiation of embryonic stem cells into nerve, blood, and muscle cells. Understanding how stem cells develop is one of the most basic challenges in biology. Powerful new molecular methods will accelerate this work and, hopefully, its clinical applications.

1 Grand Challenges

Environmental Sciences

- Biogeochemical cycles (nutrient elements C, O, H, N, S, P and regulators K, Ca, Mb, Fe, Zn) and their perturbations
- Biological diversity and ecosystem functioning
- Climate variability—local and regional
- Hydrologic forecasting—floods, droughts, contamination
- Environmental changes as selection agents on pathogen virulence and host susceptibility to infections
- Markets, treaties, and rules to govern resource extraction and waste disposal
- Land use and land cover dynamics
- Reinventing the use of materials/nearly complete recycling

Grand Challenges in Multidisciplinary R&D

Chemical R&D for sustainability and energy security. The National Research Council Committee on Grand Challenges for Sustainability in the Chemical Industry in 2005 defined sustainability as "a path forward that allows humanity to meet current environmental and human health, economic, and societal needs without compromising the progress and success of future generations" (*14*). Their eight priorities are listed in Table 2.

This agenda is part of the Grand Challenge to mitigate the expected large-scale, adverse consequences of well-documented greenhouse gas accumulation and global climate change. The seventh item offers formidable thermodynamic challenges to combine basic and applied research to "decarbonize" our energy usage and change the environmental balance of carbon dioxide (CO_2) through uses of CO_2.

As advocated in a 1991 NAS report chaired by former Washington Governor Dan Evans, many of the climate-change mitigation actions should be pursued aggressively to decrease our dependence on oil and gas, even if climate change were not a problem. More than 30 years ago, I had the privilege of serving as a key staff person, while a White House Fellow assigned to the Atomic Energy Commission, for the report "Our Nation's Energy Future" (*15*). That report was a clarion call for technological advances in five domains. The first priority, reflecting the early payoff from all energy sources, was much higher efficiency in burning fuels, by using gas turbines and other innovative combined technologies; this is the technological counterpart to reduced use of energy and fuels. Next came more extensive recovery of oil and gas from established fields; clean coal technologies; safe operation of nuclear fission reactors and acceptable disposal of nuclear wastes; and finally, the longer-term technologies for solar, wind, geothermal, and nuclear-fusion energy sources. Regrettably, this agenda has remained fresh for three decades. It is past time to dedicate sustained effort. The urgency for energy security is greater than ever, as reflected in the world map of sources of most imported oil.

Given the rapid growth in energy demand by China, India, and other developing countries and continued growth in well-developed economies, we will need a broad array of energy sources with improved technologies for every aspect of their life cycle. As a generation of nuclear reactors is coming to the end of their expected lifetimes, our country must decide how to keep nuclear energy in our mix. As noted by my successor as AAAS President, John P. Holdren, we need a balanced portfolio of energy sources (*16*). Currently, about 20% of our electricity is generated from nuclear reactors. Nuclear energy and its radioactive wastes must be managed safely and at a competitive price.

A peculiar challenge for the United States is limited access to natural gas. As demand has increased as a result of residential and industrial heating switching to gas without increases in the numbers of pipelines or terminal facilities needed to supply this country, prices have increased, with special vulnerability from the concentration of facilities offshore near New Orleans. The chemical industry,

which depends on natural gas as a feedstock for major classes of chemicals, for decades was our leading generator of profitable exports, and later second only to airplanes. Now that industry has been hit with both high energy prices and high feedstock prices; companies are siting new facilities anywhere but in the United States. As noted in the *Wall Street Journal* (*17*), using precious natural gas for its lowest-value application (space heating) reflects disjointed energy policy at the national level both in the private sector and in government. Perhaps such a policy reflects inadequate input from chemists, chemical engineers, and economists.

Global infectious diseases. The Gates Foundation Grand Challenges in Global Health Initiative was launched in 2003 to harness the power of science and technology to dramatically improve health in the world's poorest countries (*18*). Its roots lie in the Great Neglected Diseases of Mankind Program of The Rockefeller Foundation from 30 years earlier. The initiative seeks scientific breakthroughs for preventing, treating, and curing diseases that annually kill millions of people, especially children, in developing countries.

The Gates Foundation looked for "a specific scientific or technological innovation that would remove a critical barrier to solving an important health problem in the developing world with a high likelihood of global impact and feasibility." Based on 1500 suggestions from more than 1000 scientists from around the world, 14 Grand Challenges were identified (Table 3). Awards for 43 projects, involving collaborators in 33 countries, were made in 2005 from a fund with nearly $500 million from the Gates Foundation, in collaboration with the Foundation for the National Institutes of Health, the Wellcome Trust, and the Canadian Institutes of Health Research. The Challenge has generated tremendous interest and high ex-pectations.

Solutions could transform health in the world's poorest countries by bringing state-of-the-art solutions to people who need them most. Some projects are focused on adapting existing health tools, like sophisticated laboratory tests, to novel technology platforms practical in settings of developing countries. Others seek to fundamentally redefine our understanding of how to prevent and treat disease, with entirely new vaccines and drugs. Many projects are applying cutting-edge technology that has never before been used to advance global health. For example, the challenge to "improve nutrition" includes work of the Donald Danforth Plant Research Center on cassava, a staple crop with excellent nutritive value, plus value as a biomass fuel source, should there be excess production. Some of these same technologies will be helpful for diseases now at epidemic levels in the United States, including hepatitis C and HIV/AIDS.

The U.N. Millennium Development Goals for 2015. The U.N. Millennium Goals aim to combine science and technology, community organization, empowered women, and donor interest after an unprecedented political commitment at the United Nations in 2000 to overcome the most extreme problems of poverty and hunger in various regions of the world (*19, 20*). The goals are people-centered, time-bound, measurable, and, hopefully, achievable with sustained political support.

The U.N. partnership for development (Table 4) would have an open trading and financial system; tariff and quota-free access for their exports; enhanced debt relief; more generous official development assistance for countries targeting poverty reduction; special efforts for landlocked and small-island developing states; decent, productive work for youth; access to affordable essential drugs; and modern technology, especially Internet and telecom.

At the AAAS R&D Policy Forum in April 2005, Lael Brainerd of The Brookings Institution presented a comprehensive plan for engagement of all categories of science and technology development in this mission. Jeffrey Sachs and many others addressed these goals at the AAAS 2006 Annual Meeting. However, recent progress has been extremely uneven; there is very good improvement in Asia and East Asia, but considerable worsening in sub-Saharan Africa.

2 Grand Challenges

Chemistry for Sustainability

- Green chemistry to reduce waste streams, by substitution and catalytic efficiencies
- Life cycle analysis to compare total environmental impact of products and processes
- Toxicology of fate and effects of all chemical inputs and outputs
- An energy mix of fuels from multiple renewable sources
- Chemical feedstocks from renewable sources, especially biomass
- Reduced energy intensity of chemical processing
- Separation, sequestration, and utilization of carbon dioxide
- Science literacy and education about sustainability throughout the public

Science & Technology to Help Address Societal Risks

Chemical hazards. A well-developed framework has been created since 1970 to identify potential hazards, characterize the risks, and propose actions to reduce risks associated with human or ecosystem exposures to chemicals. In many cases, there is uncertainty from hazard identification studies whether a particular chemical causes harm or not, especially for humans. Even when there is indisputable evidence of adverse health effects at high exposures in rodents, or in highly exposed workers, risk assessors are generally asked to estimate the risks at exposures far below levels at which such effects can be observed. Thus, it is no surprise that experts disagree, but the public and the media often find such admissions unsatisfactory. A decade ago a Presidential/Congressional Commission on Risk Assessment and Risk Management examined the many scientific and policy aspects of regulation of chemicals and proposed a comprehensive framework (see the figure on p. 1703). The special features were the insistence on early, proactive engagement of stakeholders and the guidance to put each problem into a public health context (*21, 22*). "Context" means moving beyond analysis of just one chemical in one environmental medium (air, water, soil, food) for one health effect (cancer, birth defect, etc), as required by individual statutes, to a comprehensive public health analysis. There are many approaches to the complementary challenges of risk communication and risk management, but the critical element is hearing and responding to the questions people want addressed. Affected people often have more pragmatic suggestions for how to reduce risks than do experts or regulators who assume worst-case scenarios. Experts further complicate the message when risks are stated with indefensible precision (like "2.437×10^{-4} upper-bound

CREDIT (PHOTO): GETTY

lifetime risk"). Accurate communication about probabilities is difficult for most people, including health care professionals who get questions from patients. Lay people regularly challenge risk assessors to examine the chemical soups that we breathe, drink, eat, and touch. It is feasible and useful to test real-world mixtures like diesel exhaust and polluted air (*21, 22*).

Diet and hormones. Diet poses one of the most confusing challenges regarding human health. I led a large cancer-prevention trial with 18,314 men and women at high risk for lung cancers due to cigarette smoking with or without occupational exposure to asbestos. We tested whether daily doses of the vitamins beta-carotene and vitamin A could reduce the incidence of lung cancers. The stunning results were that there was no benefit and, further, there was harm—increases in the rates of lung cancers and rates of overall deaths and cardiovascular deaths (*23, 24*). A complementary study of beta-carotene in 29,000 smokers in Finland showed no benefit and similar harm (*25*). These findings stimulated a new generation of laboratory research on underlying carcinogenic mechanisms.

The Women's Health Initiative was a huge trial with 160,000 women launched in the early 1990s by the NIH to study possible benefits of a reduction of total fats in the diet on heart disease, breast cancer, and colon cancer risks. No such benefits were demonstrated (*26*). Most likely, certain kinds of fats are harmful, while others are fine. The same trial found net harm for most women from the long-term use of hormone-replacement therapy (*27*). The new evidence was frustrating for patients, juicy for journalists, and irritating to doctors, who thought they had been giving well-founded guidance to their patients. The resulting call for individualized decision-making is a logical, but challenging, task in a busy doctor's office.

Microbial hazards: Influenza. At the 2005 AAAS annual meeting, U.S. Centers for Disease Control (CDC) Director Julie Gerberding warned of the risks of a lethal influenza pandemic like the 1918 flu that claimed at least 20 million—probably 50 million—lives when the world's population was one-fourth of the number today. During the past 2 years, H5N1 flu strains have been causing infections and deaths in millions of chickens and other birds. By February 2006 several dozen human deaths from avian flu had been reported, primarily in China, Vietnam, and Thailand. Birds are afflicted in Nigeria, Turkey, and several European and former Soviet Union countries. Living intimately with infected birds is the main route of infection for the relatively few humans affected so far.

Control requires timely and open cooperation among nations. Remarkable improvements in rapid PCR (polymerase chain reaction)–based testing for H5N1 viruses in birds and humans now permit real-time monitoring and much more effective surveillance, timely culling of poultry, and potential timely use of vaccines and antiviral drugs, where available, if needed. Nevertheless, experts are anxious and determined that we step up our preparations, contingencies, and political will (*28, 29*).

University of Chicago and Aspen Institute cosmologist David Schramm

Are we ready? The World Health Organization, the NIH, CDC, and Department of Homeland Security in the United States, and counterpart agencies in other countries, are doing many things right. The grand challenge is to understand what is required for an avian flu strain to mutate sufficiently to be transmitted from birds to humans and from humans to humans, and to be lethal in humans. These questions are being actively investigated. The 1918 virus has been reconstituted, and new vaccine production methods that bypass the months-long, nonstorable preparation of viral antigen in chicken eggs seem promising, but will take years to test fully. Adjuvants are being tested in combination with the viral antigen(s) to try to reduce the dose of vaccine required, thereby covering many more people with the same supply. Legal, ethical, and organizational aspects are being explored, including involvement of the Council on Foreign Relations and the Royal Institution World Assembly. A pandemic in which large numbers of health care personnel would fall ill could become chaotic and catastrophic. Finally, the competition among nations and within nations for access to drugs and vaccine in shortage circumstances could become ugly. In sum, this is a really big hazard, with quite uncertain probabilities and unknown timing.

Countering terrorism. Immediately after the September 11, 2001, terrorist attacks on America, the NAS undertook an urgent, multifaceted analysis of what science and technology, broadly engaged, could do in *Making Our Nation Safer: The Role of Science and Technology in Countering Terrorism* (*30*). The Academies did not wait for a request or a contract for a long-term study. The leadership recognized that the nation needed the scientific community to step forward and create a blueprint for a comprehensive program that would take advantage of available technologies and ongoing R&D, and also invest in new R&D and technology assessment. One element was the capability to create psychological profiles of potential terrorists. This timely report of multiple working groups was welcomed by the Bush Administration, and helped ensure high-level positions for R&D and for technology in the eventual Department of Homeland Security. Unfortunately, the recommendations have been applied incompletely since the first year.

The risk of bioterrorism became real in October 2001, when anthrax spores were mailed to congressional offices and contaminated several postal facilities. In response, our country has made a large, appropriate investment in the sciences of counterbioterrorism. One of the most sensitive issues about microorganisms with high toxicity for humans or plant crops or agriculturally important animals is whether some kinds of research should be secret and not

CREDIT: M. GILSON/COURTESY OF THE UNIV. OF CHICAGO

published in the open scientific literature. Sharing methods, databases, and strains greatly facilitates collaborative research advances, at the same time raising fears.

A dramatic example is the reconstitution of the influenza virus thought to have been responsible for the 1918 pandemic. We need such knowledge and techniques to accelerate development of new influenza vaccines in a race against the spread of the virus across the world. But potent new technologies raise the dual specter of inadvertent release and of deliberate misuse by terrorist states, organizations, or even individuals. For examples, RNA interference (the discovery that won the 2006 Nobel Prize in Physiology or Medicine) that can silence specific genes; synthetic biology to produce novel proteins; nanomaterials; and informatics permit specific modifications of microorganisms and potentially of human targets unimaginable just a few years ago. The National Academies report *Globalization, Biosecurity, and the Future of the Life Sciences* (*31*) documented extensive life-sciences research around the world. It focused on these technologies.

Disaster resilience. Even before Hurricanes Katrina and Rita hit the Gulf Coast, the National Research Council Disasters Roundtable convened its 12th Workshop in 2004 and published in 2005 *Creating a Disaster-Resilient America* (*32*). They defined Grand Challenges as "fundamental problems in S&T whose solution can be advanced by coordinated and sustained investments in research, education, communication, and application of knowledge and technology." Such investments would aim to reduce the loss of life and property from natural, technological, and human-induced disasters. The emphasis is predictive capability and preparedness to minimize effects of disasters. Examples are building codes in earthquake-prone regions in California, which greatly reduced casualties in the San Francisco Bay area in 1989, compared with a similar-magnitude earthquake in Georgia of the former Soviet Union that claimed about 100 times as many lives that same year; the trans-Alaska oil pipeline's successful design that withstood a magnitude 7.9 quake in the Denali Fault in November 2002; and the buildings in Washington State that sustained only very limited damage after the magnitude 6.8 Nisqually earthquake in February 2001.

In general, we have been foolish to permit, and even to financially assist, return of displaced populations to floodplains and earthquake-prone regions. We clearly lack comprehensive planning and the political will to prevent recurrences of these disasters. Maybe we don't marshal the scientific and engineering evidence at timely points in the process. Along the Mississippi River, one might inquire how well the building codes and emergency preparedness plans protect against major consequences from long-awaited earthquakes in this region. The Mid America Earthquake Center at the University of Illinois–Urbana/Champagne has an active program in this area. The underlying principle, of course, is Benjamin Franklin's expression, "An ounce of prevention is worth a pound of cure." How true that might have been in New Orleans!

Katrina and the aftermath. As emphasized in the Disaster Resilience report and demonstrated tragically soon afterward in New Orleans, disaster mitigation requires integrated, long-term processes that combine technical with organizational, social, and economic dimensions to deliver the four R's: robustness, redundancy, rapidity, and resourcefulness. The hurricane-associated floods and their aftermath revealed the consequences of neglected engineering upgrades and lack of preparedness and coordination at all levels of government. They also laid bare deep-seated social, economic, and political disparities along racial lines. We repeat history and do not learn its lessons. The Great Flood of 1927 that inundated parts of many states along the Mississippi River might have prepared us to prevent the New Orleans debacle.

Comprehensive scientific and engineering guidance and strategic national investment should restore the protective wetlands south of New Orleans; unfortunately, these wetlands had been permitted to recede over many years, which reduced the area's capacity to withstand flood surges. Meanwhile, the Mecca for Music and the Arts mega-project proposed by New Orleans native Wynton Marsalis and the Bring Back New Orleans Cultural Committee may help rekindle the spirit of the city and its special place in the cultural heritage of our country.

Risks to the economy. Senators Lamar Alexander and Jeff Bingaman during 2005 tapped the scientific community for urgent recommendations on how to enhance our economic competitiveness. The resulting report from the National Academies, *Rising Above The Gathering Storm* (*1*), recommends that billions of dollars be invested for better teaching of math and science and for sustained growth in federal support of R&D, including an Advanced Research Projects Agency–Energy program. It also calls for easing access of foreign scientists to this country as visitors, students, and permanent residents, and continuation and expansion of the tax credit for R&D by corporations. Together with the Council on Competitiveness, this report galvanized bipartisan proposals in the Congress. The AAAS Board wrote to President Bush urging action. Thus, it was gratifying to hear the president support math and science teaching, increased budgets for physical sciences, and renewal of the expiring R&D tax credit (*33*). The education component would begin to address the "quiet crisis" Shirley Ann Jackson discussed in her 2005 AAAS presidential address (*34*): projected extreme shortages of well-prepared women and men to pursue careers in science and engineering, just as the knowledge-based world economy demands high skills.

The study of the very large (cosmology) and the very small (elementary particles) is coming together.

–David Schramm

Despite the catchy title of Tom Friedman's book, *The World Is Flat*, we are a long way from a level playing field globally or within any country. Nevertheless, the effects of globalization, instant communication, and outsourcing of tasks have created grave uncertainty about the competitiveness of our companies and our workforce for the long term. Freeman Dyson told the University of Michigan graduates in 2004 that—just like France, Spain, and Great Britain—America's time as the dominant country in the world will be limited. My response is that a cooperative future should be our goal, rather than a future dominated by one new economic or military superpower.

Anti-science attacks. Ever since Darwin's original writings, the intersection of various religious beliefs about the origins of the world and of humans with observations of natural selection for reproductive advantage has stimulated speculation, debate, and periods of intense conflict. The literature on this subject is rich and fascinating. For examples, Ursula Goodenough has written of the *Sacred Depths of Nature* and "the epic of evolution" (*35*), and Randolph Nesse and George Williams have addressed *Why We Get Sick* from the viewpoint of evolutionary biology (*36*, *37*).

Some of our problems arise from misunderstandings about specific words. In science, the term "theory" carries connotations of elegance and a strong evidentiary basis. The "theory" of evolution is ranked together with the theory of gravitation. To most laypersons, however, "theory" is closer to "speculation." Thus, we should recognize by now that it is a diversionary battle to insist on explaining the meaning of "theory" when we should be explaining the meaning of evolution and of natural selection. Darwin used the phrase "descent with modification," but the sound-bite of "survival of the fittest" has long conjured up images unrelated to reproductive fitness. Finally, when applied to evolution, the terms "random" and "chance" can irritate those who celebrate the remarkable designs in nature, however they arose. The results of natural selection are not random; it is mutations that may arise in random fashion, although not all mutations are equally likely at the molecular level.

The good news is that we are successfully turning the attacks on the teaching of evolution to our advantage, helping many more people, including scientists, to learn more about evolution and, more broadly, learning more about scientific ways of thinking. In 1984 and 1999, the NAS issued reports on *Science and Creationism* and in 1998 on *Teaching about Evolution and the Nature of Science*. An update will be issued in 2007. Evolution is the most important single concept in biology and is essential to understanding geology and astronomy.

Evolution is an ongoing process, highlighted as the 2005 Breakthrough of the Year by *Science* (*38*) in recognition of new results that show natural selection in action. In our own academic community of Ann Arbor and the adjacent blue-collar city of Ypsilanti, Michigan, this year's combined Community Reads book selection is *The Beak of the Finch* by Jonathan Weiner (*39*). The book has engaged thousands of local people in seminars and courses on the theme of Revolutions in Science: the people, theories, explanations and discoveries that challenged our thinking and changed the world. Weiner describes the work of Rosemary and Peter Grant, modern evolutionists painstakingly studying 13 species of Darwin's finches for 33 years on the island of Daphne Major in the Galápagos. They are doing what Darwin could not do—going back to the Galápagos year after year, seeing there what Darwin did not imagine could be seen at all in brief periods of time.

Darwin marshaled an enormous amount of evidence that evolution has occurred, but he never saw it happen. He was in the Galápagos (for just 5 weeks) only once during his 5-year voyage on the H.M.S. *Beagle*. In *On the Origin of Species*, he described natural selection as "silently and insensibly working, whenever and wherever opportunity offers…We see nothing of these slow changes in progress…we see only that the forms of life are now different from what they formerly were" (*40*). Evolutionists are now observing evolution of species in real time on isolated island laboratories around the globe.

The power of direct observation and the testing of hypotheses drive us to challenge unexpected findings until they cannot be explained away. Such logical thinking is the opposite of learning a catechism. The pressure on teachers to ignore evolution or lump it with a particular religious view of "creation science" or its reincarcation "intelligent design" is harmful. It first neglects the beliefs and views of many other religions and cultures and then usurps the already-limited time to interest children and their families in the math and science essential to their being prepared for good jobs and effective citizenry in the knowledge-based, technological economy of this new century. The AAAS Board has taken a strong stand in denouncing anti-science legislation and mixing of religion and science in the science classroom.

We now have a comprehensive verdict on the matter of the teaching of evolution in the schools from Judge John E. Jones III of the U.S. District Court in Pennsylvania in the case of *Kitzmiller et al. v. Dover School District et al.* (*41*). He made clear that intelligent design is a direct descendant of creation science and should have no standing in a science classroom. I strongly share that view. I would add that many scientists are themselves religious and compartmentalize their professional activities and their religious beliefs. As Daniel Boorstin quoted Goethe in *The Seekers—The Story of Man's Continuing Quest to Understand His World*, "When we do science, we are pantheists; when we do poetry, we are polytheists; when we moralize, we are monotheists." The AAAS has been very active in these matters, including a highly successful Forum with and for high school science teachers, *Evolution on the Front Line*, and the AAAS Dialogue on Science, Ethics, and Religion (DoSER).

3 Grand Challenges

Global Health

Improve childhood vaccines
- Create effective single-dose vaccines useful soon after birth
- Prepare vaccines that do not require refrigeration
- Develop needle-free delivery systems

Create new vaccines
- Devise reliable tests for live-attenuated vaccines in model systems
- Solve how to design antigens for effective protective immunity
- Learn which immunological responses are protective

Control insects that transmit disease agents
- Develop a genetic strategy to deplete or incapacitate a disease-transmitting insect population
- Develop an analogous chemical strategy

Improve nutrition
- Create a full range of optimal, bioavailable nutrients in a single staple plant

Improve drug treatment of infectious diseases
- Discover drugs and delivery systems that minimize emergence of drug-resistant microorganisms

Cure latent and chronic infection
- Create therapies to cure latent infections
- Create immunological methods that can cure latent infection

Measure health status accurately and economically in developing nations
- Develop technologies that permit quantitative assessment of population health
- Develop technologies that allow assessment of individuals for multiple conditions or pathogens at point of care

Mobilizing for Grand Challenges

All Americans are familiar with the highest-visibility Grand Challenges of recent decades.

CREDIT (PHOTOS): PHOTOS.COM

They had well-defined, readily understood, time-limited goals and support from the highest levels politically: Franklin Roosevelt's assignment to develop and test a nuclear bomb in the Manhattan Project before the Nazis did so; John F. Kennedy's call in 1961 "to put a man on the moon and bring him safely home by the end of the decade"; and the sequencing of the Human Genome DNA within 15 years.

Less visible Grand Challenges have included directed research under the Defense Advanced Research Project Agency (DARPA), founded after Sputnik in 1958, which has been judged so often successful that proposals periodically emerge to try similar high-risk, high-payoff, highly directed approaches in energy R&D and in biomedical research; the construction of major physics and astronomy facilities to advance particle physics and studies of the universe; and the War on Cancer, which set out in 1971 to enhance survival and prevent new cancers, an elusive target, despite quite remarkable growth in knowledge about cancer biology and some dramatically effective therapies.

All of these initiatives had clear R&D priorities backed up by substantial, sustained investments by the federal government and by universities, companies, and states committed to shared goals.

NIH Roadmap. In the biomedical domain, the NIH and the biomedical research community supported by NIH have met high standards for excellence and progress in generating knowledge and in bringing physical sciences, engineering, and informatics together with the new biology. The aim now is to achieve a more predictive, personalized, and preventive system of health care, especially for complex common diseases. Both a NAS committee (*42*) and the NIH Director, Elias Zerhouni, concluded that NIH as a whole could do more than NIH as a loose federation of 27 institutes and centers, mostly focused on different sets of diseases. Thus, the NIH has launched an institutional experiment, starting with just 0.5% of the $28-billion NIH budget in 2004, called the NIH Roadmap for Medical Research (*43*). The Roadmap recognizes revolutionary changes in the underlying science and technology, risk factors and treatments that in-fluence multiple different common diseases that are investigated by different institutes of the NIH, and barriers to translating results in the laboratory into studies and results in patients. The Roadmap is organized to exploit new pathways to discovery (genomics, proteomics, computational biology), to re-engineer the clinical research enterprise (integrating training, clinical research centers, clinical research, and innovations in clinical care), and to build highly interdisciplinary research teams to achieve scale and complexity in research, while preserving the investigator-initiated foundation of biomedical and behavioral research.

Meanwhile, the not-for-profit Howard Hughes Medical Institute, which directly supports 320 of the world's most outstanding scientists, has adopted a complementary strategy for "big science" to meet the Grand Challenge of exploiting multidisciplinary approaches to disease processes. Their 700-acre Janelia Farms Research Center in Virginia features advanced instrumentation, powerful computational capability, and a very active visiting scientists program. Their models are the famously productive Medical Research Centers of Great Britain and the Bell Labs in their heydays.

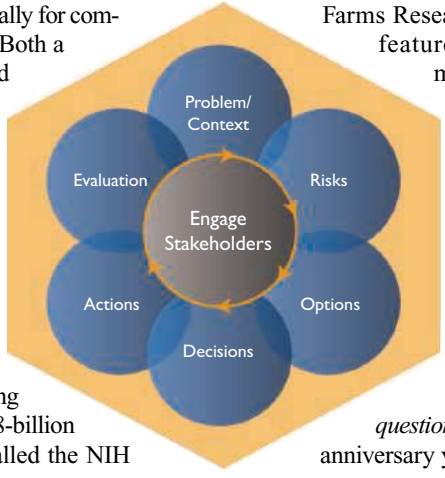

Commission's Six-Stage Framework for Risk Management. Note the central role of stakeholders in setting the context and guiding the technical assessments. The arrow is removed from stage six so as not to encourage "paralysis by analysis." [Adapted from (*21*)]

4 Grand Challenges

UN Development Goals for 2015

- Eradicate extreme poverty and hunger
- Achieve universal primary education for boys and girls
- Promote gender equality and empower women
- Reduce child mortality rate before age 5 by two-thirds
- Improve maternal health and reduce mortality ratio by 75%
- Combat HIV/AIDS, malaria, and other diseases
- Ensure sustainability, increasing access to safe drinking water
- Develop a global partnership for development

Posing challenging questions. To celebrate the 125th anniversary year of *Science*, the editors created a 1 July 2005 special issue with 125 questions about "What Don't We Know?" (*4*). These questions cover a great diversity of challenges in various fields. Like Hilbert's puzzles, these questions should stimulate scientists in numerous fields to step up, take some risks, and reach beyond the horizon.

Much broader questions arise from the policy and social ends of the spectrum. Why do we accept combustion methods that waste the majority of the energy generated? Why do we tolerate excessive use of depletable fossil fuels, especially in light of global warming? Why are we paralyzed about nuclear energy over questions of safer operations and management of highly radioactive wastes?

Why do we tolerate the poor performance of our educational system? We know that there are excellent school systems and individual schools, teachers, principals, and students that perform at outstanding levels. The AAAS Project 2061 on Science Literacy for All Americans has provided, in collaborations with science teacher organizations, standard-setting groups, and selected school districts, spectacular materials for schools to utilize. The Congress enacted the No Child Left Behind Act. Yet we seem to be failing to achieve higher performance, let alone excellence, on any significant scale in this diverse country.

What can we do to bring fresh ideas to our persistent failure to emphasize prevention and health promotion and to achieve universal coverage in our health care system (*44*)? Can our research yield credible designs to reduce the burden of employer-based health insurance costs, especially for companies competing globally?

Internationally, we face the consequences of lack of curiosity and ignorance about people of different cultures, different religions, and different world views. How can we change this situation in settings ranging from our K-12 (kindergarten through 12th grade) and higher-education communities to our national intelligence apparatus?

Prizes. In addition to the well-known Nobel Prize, the Lasker Awards, the Wolf

Prize, the General Motors Cancer Prizes, and our own awards at the AAAS annual meeting recognize research excellence. A memorable award was the Waterman Award, for work by a scientist before age 35, to Richard Muller of the Lawrence Berkeley Laboratory in 1978. He had completed three groundbreaking projects in the separate fields of astrophysics, optics, and radio-dating. The award cited the fact that his projects were so far beyond conventional wisdom and contemporary knowledge that his peer-reviewed research grant proposals had been rejected by several agencies, including NSF, which made the award! Muller had been supported on institutional funds at the Lawrence Berkeley National Laboratory by the director, Walter Alvarez, who recognized enormous potential and compelling ideas in a young scientist.

Special prizes can bring public attention to a challenge. A classic example is the enormous prize offered by the British Parliament in 1712 for a practical measure of longitude (*45*). The Ansari Project X offered $10 million to the first team to achieve space flight with private funds; the winner was a group assembled by Paul Allen, who probably responded to the competition more than the money! A DARPA challenge required robots to be designed to traverse difficult terrain; none succeeded in the first year, apparently due to misperceiving creosote plants as boulders, but four did so in the second round. The seven Clay Mathematics Prizes are awaiting solutions. Remarkably, the first recognized to be solved, the Poincaré Conjecture, by Grigori Perelman of St. Petersburg, led to complications from the rules requiring peer-reviewed publication and then rejection of the funds by the reclusive mathematician (*46*). The Methusaleh Foundation has posted a $3 million reward for a dramatic increase in longevity in an experimental animal model. An Eli Lilly Company spinoff, Innocentive Inc., uses the Internet to pose problems for scientists or engineers anywhere on the planet to solve, with specific payoffs from $5000 to $100,000 for those first to submit a documented solution or product that meets the explicit criteria of their client. The Grainger Challenge Prize for Sustainability, administered by the National Academy of Engineering, offers $1 million, $200,000, and $100,000 prizes for the best low-cost household devices to make arsenic-contaminated drinking water safe in developing countries (*47*).

Closing Remarks

In tight budget times, the peer-review process for research funding becomes more cautious than ever, requiring more so-called preliminary data until the project is nearly done before it is proposed. This situation disadvantages young people seeking their first grants and established scientists with fresh ideas. A public process of eliciting and publicizing Grand Challenges in various fields may be an antidote to this overly conservative trend (*48*). We should dare to study hard problems, individually when feasible, and in teams when the challenge demands multidisciplinary effort.

As an organization with many effective, but largely unconnected, programs and activities, I think the AAAS could play a larger role in this process, partly by taking advantage of the activities and outputs of our own programs, committees, sections, and affiliates. The NAS have demonstrated that they can step up on urgent matters, with the Counter-Terrorism report in 2002 and *Rising Above The Gathering Storm* in 2005. In their own fields, the scientific and engineering societies could do the same and join to address broader challenges.

I am certain the public and the media will be interested. And I am hopeful that young people will understand better what we do and what we hope to achieve in science and technology as they consider their own career prospects. Finally, I hope we can entice our political leaders, regionally and nationally, to call upon the scientific community to step up on these and other Grand Challenges.

References and Notes

1. National Academies, *Rising Above the Gathering Storm: Energizing and Employing America for a Brighter Ecnomic Future* (National Academies Press, Washington, DC, 2005).
2. K. M. Murphy, R. H. Topel, Eds., *Measuring the Gains From Medical Research: An Economic Approach* (Univ. of Chicago Press, Chicago, 2003).
3. *Exceptional Returns: The Economic Value of America's Investment in Medical Research* (Funding First/Lasker Foundation, New York, 2001); see www.laskerfoundation.org/reports.
4. 125th Anniversary issue, *Science* **309**, 75 (2006).
5. D. Hilbert, *Nachricht. Konigl. Ges. Wiss. Gottingen*, 253 (1900); see http://aleph0.clarku.edu/~djoyce/hilbert/problems.html.
6. D. Gross, in *The Legacy of Einstein's Science*, The Science Network, 2005; see www.tsntv.org/Events/EinsteinLegacy.
7. National Research Council, *Grand Challenges in Physics and Astronomy: Connecting Quarks with the Cosmos* (National Academies Press, Washington, DC, 2003).
8. National Research Council, *Grand Challenges in Environmental Sciences* (National Academies Press, Washington, DC, 2001).
9. L. Roberts, *Science* **291**, 1182 (2001).
10. G. S. Omenn *et al.*, *Proteomics* **5**, 3226 (2005).
11. L. Hood, J. R. Heath, M. E. Phelps, B. Lin, *Science* **306**, 640 (2004).
12. S. A. Tomlins *et al.*, *Science* **310,** 644 (2005).
13. D. Hanahan, R. A. Weinberg, *Cell* **100**, 57 (2000).
14. National Research Council, Board on Chemical Sciences and Technology, *Sustainability in the Chemical Industry: Grand Challenges and Research Needs* (National Academies Press, Washington, DC, 2005).
15. U.S. Atomic Energy Commission, *Our Nation's Energy Future* (Germantown, MD, December 1973).
16. J. P. Holdren *et al.*, *Ending the Energy Stalemate: A Bipartisan Strategy to Meet America's Energy Challenges* (National Commission on Energy Policy, Washington, DC, 2004).
17. J. J. Fialka, R. Gold, "Chilly reception: Fears of terrorism crush plans for liquified gas terminals," *Wall Street Journal*, 14 May 2004, p. A1.
18. H. Varmus *et al.*, *Science* **302**, 398 (2003); see www.gatesfoundation.org/GlobalHealth.
19. United Nations, *U.N. Millennium Development Goals* (United Nations, New York, 2005); J. D. Sachs, *The End of Poverty: Economic Possibilities for Our Time* (Penguin Press, New York, 2005).
20. C. K. Prahalad, *The Fortune at the Bottom of the Pyramid: Eradicating Poverty Through Profits* (Wharton School Publishing, Philadelphia, 2006).
21. Presidential/Congressional Commission on Risk Assessment and Risk Management, *Framework for Environmental Health Risk Management* (Government Printing Office, Washington, DC, 1997); see www.riskworld.com/Nreports/ NR5ME001.HTM.
22. G. S. Omenn, *Public Health Rep.* **111**, 514 (1996).
23. G. S. Omenn *et al.*, *N. Engl. J. Med.* **334**, 1150 (1996).
24. G. S. Omenn, *Annu. Rev. Public Health* **19**, 73 (1998).
25. The Alpha-Tocopherol, Beta-Carotene (ATBC) Cancer Prevention Study Group, *N. Engl. J. Med.* 330, 1029 (1994).
26. R. L. Prentice *et al.*, *Am. J. Epidemiol.* **162**, 404 (2005).
27. J. E. Rossouw *et al.*, *J. Am. Med. Assoc.* **288**, 321 (2002).
28. Institute of Medicine, Forum on Microbial Threats. *The Threat of Pandemic Influenza: Are We Ready?* (National Academies Press, Washington, DC, 2005).
29. A. S. Fauci, *Nature* **435**, 423 (2005).
30. National Academies, *Making Our Nation Safer: The Role of Science and Technology in Countering Terrorism* (National Academies Press, Washington, DC, 2002).
31. National Research Council, *Globalization, Biosecurity, and The Future of the Life Sciences* (National Academies Press, Washington, DC, 2006).
32. National Research Council, Disasters Roundtable, *Creating a Disaster Resilient America: Grand Challenges in Science and Technology* (National Academies Press, Washington, DC, 2005).
33. A. I. Leshner, G. S. Omenn, *Science* **311**, 741 (2006).
34. S. A. Jackson, *Science* **310**, 1634 (2005).
35. U. Goodenough, *The Sacred Depths of Nature* (Oxford Univ. Press, Oxford, 1998).
36. R. M. Nesse, G. C. Williams, *Why We Get Sick: The New Science of Darwinian Medicine* (Times Books, New York, 1995).
37. R. M. Nesse, S. C. Stearns, G. S. Omenn, *Science* **311**, 1071 (2006).
38. E. Culotta, E. Pennisi, *Science* **310**, 1878 (2005).
39. J. Weiner, *The Beak of the Finch: A Story of Evolution in Our Time* (Vintage Books, New York, 1995).
40. C. Darwin, *On the Origin of Species* (Barnes & Noble, New York, 2004; orig. published 1859).
41. *Kitzmiller et al. v. Dover School District et al.* (U.S. District Court for the Middle District of Pennsylvania, 26 December 2005).
42. National Research Council, *Enhancing the Vitality of the National Institutes of Health: Organizational Change to Meet New Challenges* (National Academies Press, Washington, DC, 2003).
43. http://nihroadmap.nih.gov
44. F. Bloom, *Science* **300**, 1680 (2003).
45. D. Sobel, *Longitude: The True Story of a Lone Genius Who Solved the Greatest Problem of His Time* (Penguin Books, New York, 1995).
46. S. Begley, "Major math problem is believed solved by reclusive Russian," *Wall Street Journal*, 21 July 2006, p. A9.
47. www.nae.edu/NAE/grainger.nsf
48. G. M. Lamb, "Grand challenges spur grand results," Christian Science Monitor, 12 January 2006.

10.1126/science.1135003

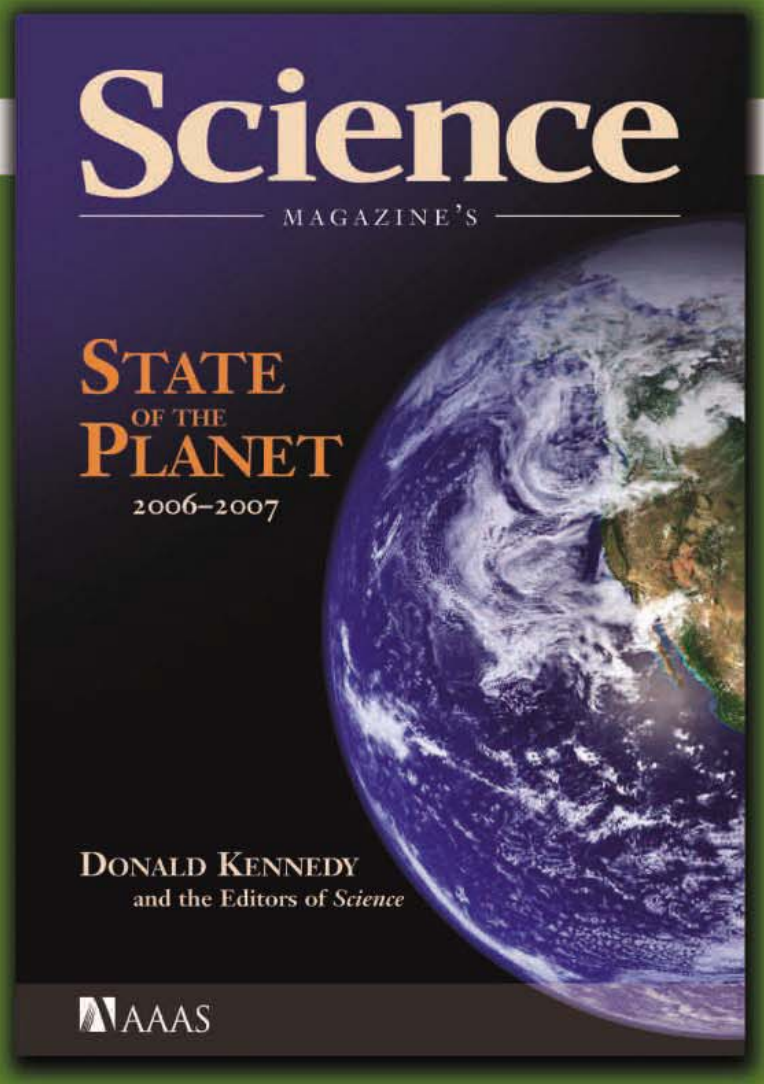

Science Magazine's
State of the Planet 2006-2007

Donald Kennedy, Editor-in-Chief, and the Editors of *Science*

The American Association for the Advancement of Science

The most authoritative voice in science, *Science* magazine, brings you current knowledge on the most pressing environmental challenges, from population growth to biodiversity loss.

COMPREHENSIVE • CLEAR • ACCESSIBLE

ISLANDPRESS

Science
AAAS

islandpress.org

Happy Holidays

Wishing you a joyous, peaceful, and healthy holiday season and New Year.

Science
AAAS

INTRODUCTION

Look into the Seeds of Time

COMETS ARE FABLED HARBINGERS OF DOOM, BUT MANY OF US WILL REMEMBER more fondly the peaceful visits of comets Hayakutake and Hale-Bopp to our skies in 1996 and 1997. These wanderers of our solar system spend most of their time in its cold outer reaches, only occasionally venturing near Earth's orbit. As they veer close to the Sun, ice and dust from their small nuclei are swept out by the radiation and solar wind into a fuzzy halo, or coma, and a long tail.

Comets are thought to harbor relatively pristine detritus from the rubble disk out of which the planets grew. In just over a year, two space missions have given us a close look at the materials that make up different comets. First, Deep Impact fired a projectile into the nucleus of comet 9P/Tempel 1, ejecting a huge plume that was studied remotely (see *Science*, 14 October 2005). Now, as described in this issue, Stardust has retrieved direct samples of the coma of comet 81P/Wild 2.

Comet Wild 2 originally hails from the Kuiper belt, beyond Neptune, but was recently perturbed into an orbit between Mars and Jupiter that is within the reach of spacecraft. After its launch in 1999, Stardust sneaked up on the comet in 2004, then returned its precious cargo to Earth in a capsule on 15 January 2006. Bringing back materials from a known extraterrestrial source, as with the Apollo samples from the Moon, is critical for deciphering the history of our solar system and interpreting our other extraterrestrial samples: meteorites and cosmic dust particles.

Stardust's goal rested largely on two technical achievements. First the spacecraft had to be slowed so that it could engage with the comet. A clever trajectory enabled it to pass within 240 km of the nucleus at a speed of just 6 km/s, albeit six times faster than a bullet. To catch the comet particles, a special lightweight material called aerogel was developed and molded into a detector grid. Aerogel, the lightest solid known, is a foamed glass that has the density of air (see the cover). Particles were gently brought to a standstill as they tunneled through it without much heating or alteration, leaving carrot-shaped tracks. Thousands of tiny particles were trapped, most of them smaller than a micrometer in size.

Analysis of the tiny samples by many international teams shows that many particles are mixtures of minerals, mostly silicates. The lack of amorphous grains is one surprise, because such materials are seen in interstellar space. Isotopically, the comet specks resemble rocks from the inner solar system; virtually no grains that pre-date the Sun were seen. A single grain contains minerals produced at high temperatures, in a region close to the Sun, and with isotope ratios similar to those of some meteorites. Thus, material has been mixed across the solar system, from the innermost portion to the outer regions of the Kuiper belt where this comet originated.

Although this mixing makes it difficult to explain comet histories, it also means that the Stardust samples might tell us much more about how planets formed. The first rock samples brought back to Earth from anywhere beyond the Moon, the tiny Stardust grains may contain the building blocks of the entire solar system.

–JOANNE BAKER

Stardust

CONTENTS

Science

CREDIT: NASA

PERSPECTIVE

Whence Comets?

Michael F. A'Hearn

Recent advances in cometary science have indicated the importance of mixing of materials in the disk where the planets of our solar system formed. Now, the results from the Stardust Discovery Mission unambiguously show that even more extensive and earlier mixing of the material took place, raising new challenges for theories of the protoplanetary disk and the formation of comets.

Twenty years ago, there was tremendous interest in the return of comet P/Halley. Although that return was somewhat disappointing compared with its closer previous return in 1910, it was scientifically a tremendous apparition. Primarily this was because the advance knowledge of its return allowed scientists to plan both Earth-based observing programs and to design the first space missions to a comet. The first spacecraft to fly past a comet was actually intended to study the solar wind but was diverted to pass through the tail of comet Grigg-Skjellerup in late 1985. For comet Halley, however, an entire armada of spacecraft—Suisei, Sakigake, Vega 1, Vega 2, and Giotto—flew past the comet in March 1986. The dramatic breakthroughs in our understanding of comets triggered great interest, largely because comets hold unique clues to the origin of our own planetary system. Nevertheless, it took 15 years before the next missions were under way.

Deep Space 1 flew past comet Borrelly in 2001, heralding a suite of complementary missions to very different comets: Stardust flew past comet 81P/Wild 2 in January 2004, Deep Impact excavated 10,000 tons of material from comet Tempel 1 in July 2005, and Stardust returned to Earth the grains that it had collected from comet Wild 2 in January 2006. These missions, coupled with recent dynamical studies, have caused a major rethinking of the origin of comets.

There is no doubt that comets did not form in orbits even remotely similar to the ones in which we now observe them (Fig. 1). Our classical picture has been that the majority of short-period comets (the Jupiter family, of which Borrelly, Wild 2, and Tempel 1 are members) formed from solids that condensed beyond Neptune in the cold Kuiper belt. Over the 4.5-billion-year age of the solar system, the comets gradually spread among the giant planets, with some of them ending up in orbits that are visible from Earth.

The long-period comets (and some short-period comets, including Halley), on the other hand, formed from solids that condensed closer to the Sun and at higher temperatures. Forming in among the giant planets, these comets were ejected out to the Oort cloud (extending halfway to the Sun's nearest neighbor, alpha Centauri) and then much later perturbed into orbits that are also visible from Earth. Recently, dynamicists have shown that the trans-Neptunian objects in what is now called the scattered disk (discovered in the 1990s and containing objects in eccentric orbits extending beyond the classical Kuiper belt) complicate this picture dramatically. The scattered disk feeds comets into both the Jupiter family and the Oort cloud [and thus into the group of Halley-type comets (*1*, *2*)]. So mixing of comet families complicates the picture.

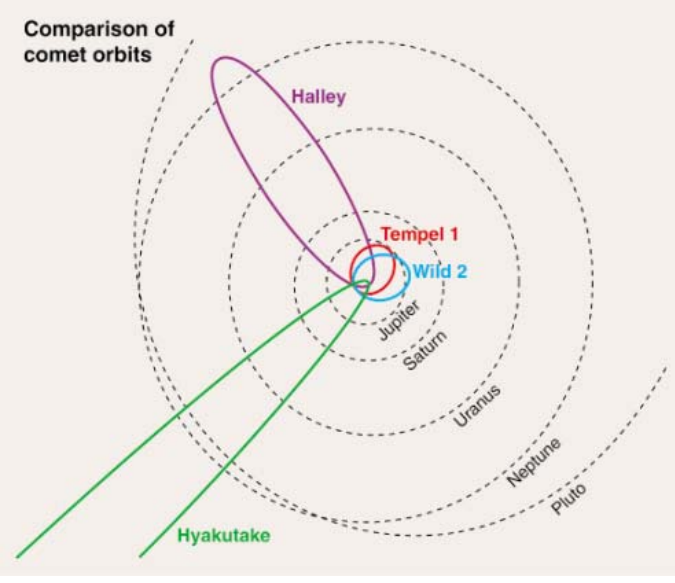

Fig. 1. Schematic showing the orbits of comets (T. Farnham, University of Maryland). Wild 2 and Tempel 1 are Jupiter family comets (originally from the Kuiper belt in the classical picture); Halley is the prototype of the Halley-class comets (originally from Oort cloud); Hyakutake is a comet coming from the Oort cloud. The classical Kuiper belt would be circular orbits just outside the orbits of Neptune and Pluto. The scattered disk consists of elongated orbits with perihelia in as close as Uranus and aphelia at 50 to 100 AU (up to about three times Neptune's orbit).

The nuclei of even the three Jupiter family comets visited by spacecraft are surprisingly diverse in their shapes and in their surface topography (Fig. 2). Comet Borrelly has a bend, like a banana's shape (*3*, *4*), Wild 2 is more ellipsoidal (*5*), and Tempel 1 has surfaces that are nearly planar (*6*). All three show signs of layering, although it is most obvious in the high-resolution images of Tempel 1 (*6*, *7*), that may reflect the original formation scenario (*8*). The gas coming out of Tempel 1 (*9*) showed great heterogeneity, consistent with the idea that the nucleus is made of cometesimals (smaller chunks) of different composition. These results can be interpreted as suggesting extensive radial mixing of cometesimals in the outer parts of the early solar system, rather than formation of cometary nuclei from cometesimals condensed at a uniform distance from the proto-Sun. This means that it will be somewhat harder to pin down the locations about which comets can give us clues to formation.

The Stardust results presented in this issue provide dramatic evidence for much more extensive radial mixing at an even earlier stage in the formation. They show, perhaps most importantly, that nearly all of the crystalline silicate grains, which have been known for some time to exist in comets, must have formed in the solar system very close to the proto-Sun rather than being circumstellar or other presolar grains that were transported from the interstellar medium and directly incorporated. Only one circumstellar grain was found, showing that material is preserved from the interstellar medium but that, at least among the refractory grains, it is only a small fraction of the material near the surface of a comet. Although this mixing of near-Sun condensates with preserved circumstellar grains has been suggested before as an important part of cometary formation, we now have clear evidence that this mixing must be taken into account in any theory of our solar system.

The Stardust results also show significant differences when compared with the results from Tempel 1. At a basic level, the size distribution of impacted Wild 2 grains is different

Department of Astronomy, University of Maryland, College Park, MD 20742–2421, USA. E-mail: ma@astro.umd.edu

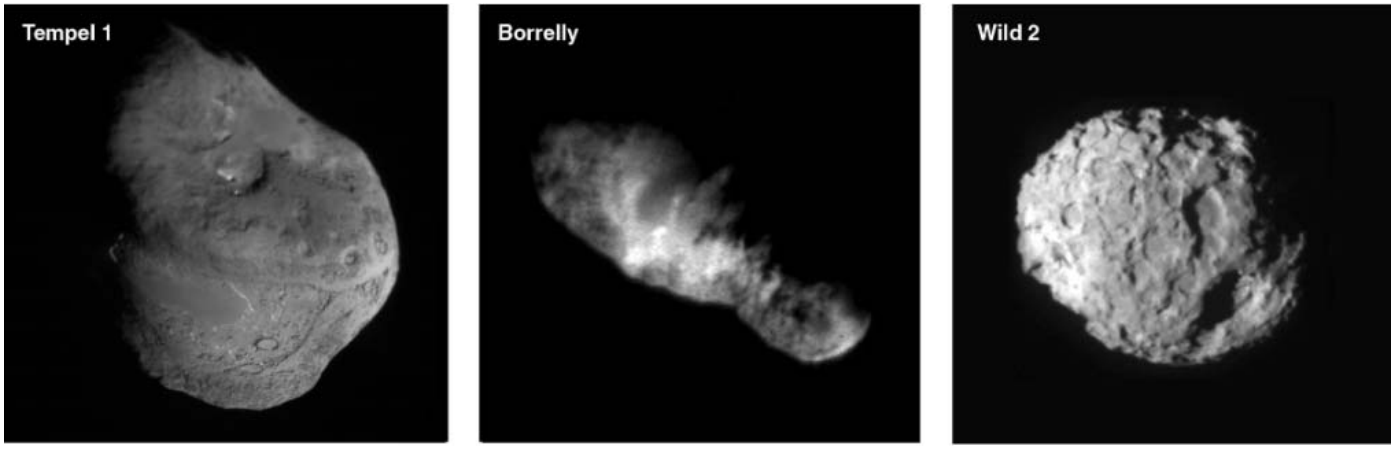

Fig. 2. Cometary nuclei visited in the last decade: (**left**) Tempel 1 (NASA, University of Maryland, and Deep Impact Team), (**middle**) Borrelly [NASA, Jet Propulsion Laboratory (JPL), and Deep Space 1 Team], and (**right**) Wild 2 (NASA, JPL, and Stardust Team). The longest dimensions are 8 km for Borrelly, 6 km for Tempel 1, and 5.5 km for Wild 2. Note the differences in overall shape, even though all are comparable in size. The smooth areas on Tempel 1 are low, whereas the only smooth area on Borrelly is topographically high. On Wild 2, the smooth areas are at the bottoms of circular depressions. The circular features on Wild 2 have a morphology that is very different from those on Tempel 1.

from that inferred for the ejecta from the impact onto Tempel 1 (*10*), different from that of the particles seen at Halley, and even different from that deduced from the Dust Flux Monitor Instrument on Stardust itself as it flew through the coma of Wild 2. Perhaps more significantly, there are differences in the types of particles inferred for Wild 2 and Tempel 1. What does all this mean for the origin of comets? Are these differences between two comets, both the compositional and grain-size differences reported here and the large-scale morphological differences, related to their somewhat different orbital histories—Wild 2 having only recently been perturbed into the inner solar system, whereas Tempel 1 has been in the inner solar system far longer? Or are these differences due to mixing of comets from different reservoirs into the population of Jupiter family comets? Or do they merely represent different mixing ratios for the cometesimals that made up the cometary nuclei?

Stardust has certainly brought us plenty of food for thought. Combining the Stardust results with those from other recent comet missions will keep the theoreticians working for some time, while we hope for visits to other comets in the future.

References

1. M. Duncan, H. Levison, L. Dones, in *Comets II*, M. C. Festou, H. U. Keller, H. A. Weaver, Eds. (Univ. of Arizona Press, Tucson, AZ, 2004), pp. 193–204.
2. J. A. Fernández, T. Gallardo, A. Brunini, *Icarus* **172**, 372 (2004).
3. R. L. Kirk, E. Howington-Kraus, L. A. Soderblom, B. Giese, J. Oberst, *Icarus* **167**, 54 (2004).
4. J. Oberst *et al.*, *Icarus* **167**, 70 (2004).
5. R. L. Kirk *et al.*, *Lunar Planet. Sci.* **XXXVI**, 2244 (2005).
6. P. C. Thomas *et al.*, in preparation.
7. M. F. A'Hearn *et al.*, *Science* **310**, 258 (2005); published online 8 September 2005 (10.1126/science.1118923).
8. M. J. S. Belton *et al.*, *Icarus*, in press; published online 7 November 2006 (10.1016/j.icarus.2006.09.05).
9. L. M. Feaga, M. F. A'Hearn, J. M. Sunshine, O. Groussin, T. L. Farnham, in preparation.
10. C. M. Lisse *et al.*, *Science* **313**, 635 (2006); published online 12 July 2006 (10.1126/science.1124694).

10.1126/science.1137083

PERSPECTIVE

NASA Returns Rocks from a Comet

Don S. Burnett

Cometary particles returned by the Stardust Discovery Mission are primarily silicate materials of solar system origin. Some of the grains were formed at high temperatures close to the Sun, but then transported far out to the Kuiper belt region of the solar system before being incorporated in the comet.

Until now, extraterrestrial materials available for study have come from the inner solar system, including meteorites that have fallen from the sky and the returned lunar samples. Meteorites include unequivocal samples of Mars and the Moon as well as an impressive variety of asteroidal materials.

Department of Geological and Planetary Sciences, California Institute of Technology, Pasadena, CA 91125, USA. E-mail: burnett@gps.caltech.edu

The Stardust Discovery Mission has, for the first time, returned cometary materials for analyses in terrestrial laboratories. Initial results are reported in this issue of *Science*. Launched in 1999, the Stardust spacecraft encountered comet P81/Wild 2 in January 2004, passing through the dust cloud surrounding the cometary nucleus and capturing an estimated 1000 particles in the size range of 5 to 300 micrometers (*1*). These were successfully returned to Earth in January 2006.

Wild 2 is a Jupiter family comet; evidence suggests that it formed in the Kuiper belt of objects beyond the orbit of Neptune and was then diverted into the inner solar system by orbital perturbations from Neptune and Jupiter. Thanks to Stardust, we now have material to study from a body that unequivocally originated in the outer regions of the solar system.

In the inner solar system, volatile constituents, primarily H_2O, sublimate from a comet nucleus. Dust grains imbedded in the ices are swept out with the outflowing gas, becoming part of a large cloud of gas and dust, or coma. The cometary dust is there for the taking—the challenge is to capture the particles without destroying both the dust and the spacecraft in the process. Two clever technological achievements led to the success of Stardust: (i) design of a spacecraft trajectory by Chen-Wan Yen (Jet Propulsion Laboratory) that produced a relatively low encounter velocity of 6.1 km/s and (ii) development of an aerogel capture medium by Peter Tsou (Jet Propulsion Laboratory).

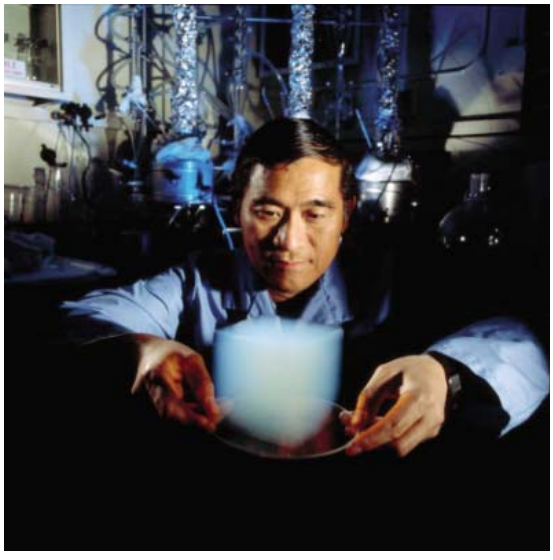

Fig. 1. A cube of the aerogel capture medium used by Stardust. [Photo: Jet Propulsion Laboratory]

Aerogel is a highly porous silica foam that has a density comparable to that of air (Fig. 1). The low density slows down impacting particles gradually, allowing them to escape melting and/or vaporization. The capture event leads to millimeter-sized tracks (Fig. 2). Most material is left as fragments along the walls of the track, but there is usually an intact terminal particle.

Sample return missions result in major scientific progress because terrestrial laboratories use the latest technology and eliminate the limitations imposed by remote spacecraft instrument operations. This is amply demonstrated by the results reported in this issue. An incredible array of analytical firepower has been unleashed to unlock the secrets of Wild 2. Some of the instruments have diameters that are kilometers in size. Yet, the amount of cometary material consumed in this work is a negligible part of the 1 to 10 micrograms of material returned.

The Wild 2 samples recovered by Stardust are small rocks. None of the particles studied represents a single mineral; all are mixtures of minerals, typically submicrometer in size. Fortunately, we have the capability to at least begin the studies of such complex samples. The most abundant minerals are the crystalline silicate minerals, olivine and pyroxene, along with troilite (FeS) (*2*). These are very stable phases, common in planetary materials; however, finding them here is somewhat surprising because many expected that cometary material would be similar to interstellar material, in which most silicates are believed to be amorphous. In contrast, cometary amorphous material in the returned samples is rare or nonexistent, although it is worth noting that aerogel melting produced silica glass, and silica glass mixed with cometary materials makes the identification of cometary amorphous material difficult (*2*).

Two major conclusions can be drawn from the Stardust analyses, one anticipated and one unexpected. As anticipated, isotopic analyses could determine whether cometary materials were made in the solar system or were aggregated presolar materials. Stars synthesize elements heavier than Li with wildly varying isotopic compositions, and rare circumstellar grains of such material have been recovered from meteorites. However, with important exceptions, the isotopic compositions of elements are very homogeneous in inner solar system materials, and it is widely accepted that this homogenization occurred in situ, within the solar system. Stardust isotopic data reveal a few isotopically anomalous presolar grains, but most appear isotopically indistinguishable from inner solar system materials. The Wild 2 rocks are solar system rocks (*3*).

The unanticipated result was the discovery of a single grain made of high-temperature minerals found in meteoritic Ca- and Al-rich inclusions (CAIs) (*2*), which are products of gas-solid separation at high temperatures only possible in the inner solar system very close to the Sun. Moreover, the Stardust CAI has the same distinctive oxygen isotopic composition as that found in meteoritic CAIs (*3*). It appears inescapable that, during the formation of the solar system, materials formed near the Sun were mixed as far out as the Kuiper belt and there incorporated into objects which eventually became comets. Such mixing has been proposed but observational proof was lacking (*4*).

There is considerable interest in carbonaceous matter from comets. A large number of essentially pure C grains (known as CHON particles for the elements observed in them) were observed in the comet Halley flybys (*5*), but such grains are very rare in Stardust samples studied to date (*2*, *6*, *7*). Nevertheless, the impacts released labile cometary organic compounds (*7*), and further study of these is of considerable importance.

The large number of authors of the present papers is typical—and appropriate—for the initial results of big projects. However, the Stardust papers are relatively unique in that essentially all of the coauthors collected data, which allowed the application of many different techniques. Redundant verification by independent techniques is difficult in big projects and prohibitively expensive in many cases. Here, not only have a large number of scientists participated in Stardust analyses, but the data they produced can be independently verified to be correct. Anomalous results will quickly be checked.

Fig. 2. A millimeter-long track of a Wild 2 particle in aerogel. The particle entered at the wide end. The force of impact broke up the particle; consequently, each black dot is a small cometary rock. [Image: JPL]

The results reported here are only the first chapter in unlocking the secrets of Wild 2. The samples are available, and they will be preserved as they await more detailed study by both current techniques and more advanced analytical techniques yet to be developed, some of which may be inspired by the availability of Wild 2 material.

References

1. D. E. Brownlee *et al.*, *Science* **314**, 1711 (2006).
2. M. E. Zolensky *et al.*, *Science* **314**, 1735 (2006).
3. K. D. McKeegan *et al.*, *Science* **314**, 1724 (2006).
4. F. Shu, H. Shang, T. Lee, *Science* **271**, 1545 (1996).
5. J. Kissel *et al.*, *Nature* **321**, 280 (1986).
6. L. P. Keller *et al.*, *Science* **314**, 1728 (2006).
7. S. A. Sandford *et al.*, *Science* **314**, 1720 (2006).

10.1126/science.1137084

RESEARCH ARTICLE

Comet 81P/Wild 2 Under a Microscope

Don Brownlee,[1] Peter Tsou,[2] Jérôme Aléon,[3,4] Conel M. O'D. Alexander,[5] Tohru Araki,[6] Sasa Bajt,[7] Giuseppe A. Baratta,[8] Ron Bastien,[9] Phil Bland,[10,11] Pierre Bleuet,[12] Janet Borg,[13] John P. Bradley,[14] Adrian Brearley,[15] F. Brenker,[16] Sean Brennan,[17] John C. Bridges,[18] Nigel D. Browning,[19,20] John R. Brucato,[21] E. Bullock,[22] Mark J. Burchell,[23] Henner Busemann,[5] Anna Butterworth,[24] Marc Chaussidon,[25] Allan Cheuvront,[26] Miaofang Chi,[14] Mark J. Cintala,[27] B. C. Clark,[26] Simon J. Clemett,[28] George Cody,[29] Luigi Colangeli,[21] George Cooper,[30] Patrick Cordier,[31] C. Daghlian,[32] Zurong Dai,[14] Louis D'Hendecourt,[13] Zahia Djouadi,[13] Gerardo Dominguez,[33] Tom Duxbury,[2] Jason P. Dworkin,[34] Denton S. Ebel,[35] Thanasis E. Economou,[36] Sirine Fakra,[37] Sam A. J. Fairey,[38] Stewart Fallon,[14] Gianluca Ferrini,[39] T. Ferroir,[40] Holger Fleckenstein,[41] Christine Floss,[42] George Flynn,[43] Ian A. Franchi,[44] Marc Fries,[29] Z. Gainsforth,[24] J.-P. Gallien,[45] Matt Genge,[46] Mary K. Gilles,[47] Philipe Gillet,[40] Jamie Gilmour,[48] Daniel P. Glavin,[34] Matthieu Gounelle,[49,10] Monica M. Grady,[18] Giles A. Graham,[14] P. G. Grant,[14] Simon F. Green,[18] Faustine Grossemy,[13] Lawrence Grossman,[36,50] Jeffrey N. Grossman,[51] Yunbin Guan,[52] Kenji Hagiya,[10] Ralph Harvey,[53] Philipp Heck,[54] Gregory F. Herzog,[55] Peter Hoppe,[54] Friedrich Hörz,[56] Joachim Huth,[54] Ian D. Hutcheon,[4] Konstantin Ignatyev,[57] Hope Ishii,[14] Motoo Ito,[58] Damien Jacob,[59] Chris Jacobsen,[60] Stein Jacobsen,[61] Steven Jones,[2] David Joswiak,[1] Amy Jurewicz,[62] Anton T. Kearsley,[10] Lindsay P. Keller,[56] H. Khodja,[47] A.L. David Kilcoyne,[37,47] Jochen Kissel,[63] Alexander Krot,[64] Falko Langenhorst,[65] Antonio Lanzirotti,[66] Loan Le,[67] Laurie A. Leshin,[68] J. Leitner,[69] L. Lemelle,[40] Hugues Leroux,[70] Ming-Chang Liu,[71] K. Luening,[17] Ian Lyon,[48] Glen MacPherson,[22] Matthew A. Marcus,[37] Kuljeet Marhas,[72] Bernard Marty,[73] Graciela Matrajt,[1] Kevin McKeegan,[71] Anders Meibom,[48] Vito Mennella,[74] Keiko Messenger,[9] Scott Messenger,[58] Takashi Mikouchi,[75] Smail Mostefaoui,[76] Tomoki Nakamura,[77] T. Nakano,[78] M. Newville,[66] Larry R. Nittler,[5] Ichiro Ohnishi,[79] Kazumasa Ohsumi,[80] Kyoko Okudaira,[81] Dimitri A. Papanastassiou,[82] Russ Palma,[83,84] Maria E. Palumbo,[8] Robert O. Pepin,[84] David Perkins,[26] Murielle Perronnet,[56] P. Pianetta,[57] William Rao,[85] Frans J. M. Rietmeijer,[15] François Robert,[49] D. Rost,[22] Alessandra Rotundi,[86] Robert Ryan,[2] Scott A. Sandford,[87] Craig S. Schwandt,[13] Thomas H. See,[88] Dennis Schlutter,[83] J. Sheffield-Parker,[89] Alexandre Simionovici,[54] Steven Simon,[50] I. Sitnitsky,[90] Christopher J. Snead,[24] Maegan K. Spencer,[96] Frank J. Stadermann,[42] Andrew Steele,[29] Thomas Stephan,[69] Rhonda Stroud,[89] Jean Susini,[14] S. R. Sutton,[50,66] Y. Suzuki,[91] Mitra Taheri,[87] Susan Taylor,[92] Nick Teslich,[14] Kazu Tomeoka,[77] Naotaka Tomioka,[77] Alice Toppani,[3,14] Josep M. Trigo-Rodríguez,[93,94] David Troadec,[68] Akira Tsuchiyama,[95] Anthony J. Tuzzolino,[34] Tolek Tyliszczak,[35,45] K. Uesugi,[96] Michael Velbel,[97] Joe Vellenga,[26] E. Vicenzi,[22] L. Vincze,[98] Jack Warren,[9] Iris Weber,[69] Mike Weisberg,[99] Andrew J. Westphal,[24] Sue Wirick,[41] Diane Wooden,[87] Brigitte Wopenka,[72,100] Penelope Wozniakiewicz,[10] Ian Wright,[18] Hikaru Yabuta,[29] Hajime Yano,[81] Edward D. Young,[71] Richard N. Zare,[96] Thomas Zega,[81] Karen Ziegler,[71] Laurent Zimmerman,[25] Ernst Zinner,[42] Michael Zolensky[56]

The Stardust spacecraft collected thousands of particles from comet 81P/Wild 2 and returned them to Earth for laboratory study. The preliminary examination of these samples shows that the nonvolatile portion of the comet is an unequilibrated assortment of materials that have both presolar and solar system origin. The comet contains an abundance of silicate grains that are much larger than predictions of interstellar grain models, and many of these are high-temperature minerals that appear to have formed in the inner regions of the solar nebula. Their presence in a comet proves that the formation of the solar system included mixing on the grandest scales.

Stardust was the first mission to return solid samples from a specific astronomical body other than the Moon. The mission, part of the NASA Discovery program, retrieved samples from a comet that is believed to have formed at the outer fringe of the solar nebula, just beyond the most distant planet. The samples, isolated from the planetary region of the solar system for billions of years, provide new insight into the formation of the solar system. The samples provide unprecedented opportunities both to corroborate astronomical (remote sensing) and sample analysis information (ground truth) on a known primitive solar system body and to compare preserved building blocks from the edge of the planetary system with sample-derived and astronomical data for asteroids, small bodies that formed more than an order of magnitude closer to the Sun. The asteroids, parents of most meteorites, formed by accretion of solids in warmer, denser, more collisionally evolved inner regions of the solar nebula where violent nebular events were capable of flash-melting millimeter-sized rocks, whereas comets formed in the coldest, least dense region. The samples collected by Stardust are the first primitive materials from a known body, and as such they provide contextual insight for all primitive meteoritic samples. About 200 investigators around the world participated in the preliminary analysis of the returned samples, and the papers in this issue summarize their findings.

Observations. During its 2 January 2004 flyby, 234 km from the surface of comet Wild 2, Stardust collected more than 10,000 particles in the 1-to 300-μm size range that were returned to Earth on 15 January 2006 (*1*). Flyby images showed at least 20 collimated jets of solid particles streaming into space from widely distributed small sources (*2*). The collected particles are expected to be a representative sampling of the nonvolatile component of the interior of the comet. Wild 2 is a Jupiter family comet (JFC) currently on an orbit that approaches the orbits of both Jupiter and Mars. Like other JFCs, this ~4.5-km-diameter body is believed to have formed in the Kuiper belt, exterior to the orbit of Neptune, and only recently entered the inner regions of the solar system where solar heat causes "cometary activity," processes mainly driven by the sublimation of water ice that lead to the loss of gas, rocks and dust at rates of tons per second. As a JFC, the most likely history of Wild 2 is that it formed beyond Neptune, where it spent nearly all of its life orbiting in the Kuiper belt. A close encounter with Jupiter on 10 September 1974 placed it in its current orbit, but its journey from the Kuiper belt to the inner solar system probably took millions of years and multiple encounters with outer planets. As a JFC, its orbit will change, and it has an expected dynamical lifetime of ~10^4 years before it either hits a larger object or is ejected from the solar system (*3*). The active lifetime will be shorter because of mass loss or disintegration.

The particles ejected by the comet and collected by Stardust should be the same materials that accreted along with ices to form the comet ~4.57 billion years ago when the Sun and planets formed. The original accreted materials included both fine nebular particles and compounds from the disruption of large bodies (*4*). Cometary activity has caused Wild 2 to lose its original surface, and for this and other reasons it is believed that all of the particles ejected by the comet date back to the formational period of the solar system history and not to recent solar system processes. Exposed to space for hours before collection, solar heating at 1.86 AU probably volatilized ice components during transit from Wild 2 to the spacecraft, although it is possible that some ice could have been retained

in the largest particles. The fact that particles ranging down to submicron size were ejected by such a gentle process as ice sublimation indicates that the collected material from Wild 2 had not been lithified and altered in Wild 2 by internal processes such as heating, compaction, or aqueous alteration. These processes did act on original asteroidal materials, altering them into relatively dense and strong rocks that could survive entry into the atmosphere, impact the ground and be found as meteorites.

Collection of particles. Most of the samples were collected in silica aerogel, a porous glass composed of nanometer-sized silica particles with bulk density that was made to vary from <0.01 g/cm^3 at the impact surface to 0.05 g/cm^3 at 3-cm depth. In addition to aerogel, about 15% of the total collection surface was aluminum, the frame used to hold aerogel. Impact on this metal produced bowl-shaped craters lined with melted, and in some cases unmelted, projectile residue. The craters provide important information that is complementary to the primary aerogel collection medium. The impacts into aerogel produced deep, tapered cavities (tracks) with shapes varying with the nature of the impacting particle (Fig. 1). All but a few of the impact tracks contain deeply penetrating particles. Nonfragmenting particles produced carrot-shaped tracks with length/diameter ratios of >25, whereas fragmenting particles produced tracks with bulbous upper regions and sometimes multiple roots. In many cases, as described by Hörz *et al*. (*5*), it appears that the particles consisted of aggregates that separated into fragments on impact. The smaller fragments stopped in the upper (bulbous) region of the tracks, whereas the larger fragments traveled deeper into the aerogel. The upper parts of the hollow tracks are lined with relatively large amounts of melted aerogel with dissolved projectile, the mid-regions contain less melt and more preserved projectile material along with compressed aerogel, and the lower regions contain largely unmelted comet fragments at the track ends. In the majority of cases, the deepest penetrating particles are solid mineral grains or rocks composed of multiple components. To date, no terminal particles have been found that

[1]Department of Astronomy, University of Washington, Seattle, WA 98195, USA. [2]Jet Propulsion Laboratory, California Institute of Technology, Pasadena CA 91109–8099, USA. [3]Centre de Spectrometrie Nucleaire et de Spectrometrie de Masse, Bat 104, 91405 Orsay Campus, France. [4]Glenn T. Seaborg Institute, Lawrence Livermore National Laboratory, Livermore, CA 94550, USA. [5]Department of Terrestrial Magnetism, Carnegie Institution, Washington, DC 20015–1305, USA. [6]Department of Physics, North Carolina State University, Raleigh, NC 27695, USA. [7]Lawrence Livermore National Laboratory, 7000 East Avenue, L-210, Livermore, CA 94550, USA. [8]Istituto Nazionale di Astrofisica, Osservatorio Astrofisico di Catania, Via Santa Sofia 78, 95123 Catania, Italy. [9]Engineering Science Contract Group, NASA Johnson Space Center, Houston, TX 77058, USA. [10]Department of Mineralogy, Natural History Museum, London, SW7 5BD, UK. [11]Impact and Astromaterials Research Centre, Department of Earth Sciences and Engineering, Imperial College of Science, Technology, and Medicine, Prince Consort Road, London, SW7 2AZ, UK. [12]European Synchrotron Research Facility, Grenoble, France. [13]Institut d'Astrophysique Spatiale, Campus, 91405 Orsay Cedex, France. [14]Institute for Geophysics and Planetary Physics, Lawrence Livermore National Laboratory, Livermore, CA 94550, USA. [15]Department of Earth and Planetary Sciences, University of New Mexico, MSC 03-2040, Albuquerque, NM 87131–0001, USA. [16]Johann Wolfgang Goethe Universitat, Frankfurt, Germany. [17]Stanford Linear Accelerator Center, Menlo Park, CA 94025, USA. [18]Planetary and Space Sciences Research Institute, The Open University, Walton Hall, Milton Keynes MK7 6AA, UK. [19]Department of Chemical Engineering and Materials Science, University of California–Davis, Davis, CA 95616, USA. [20]Materials Science and Technology Division, Chemistry and Materials Science Directorate, Lawrence Livermore National Laboratory, Livermore, CA 94550, USA. [21]INAF, Osservatorio Astronomico di Capodimonte, Via Moiariello 16, 80131 Napoli, Italy. [22]Smithsonian Institution, Washington DC, USA. [23]School of Physical Sciences, University of Kent, Canterbury, Kent CT2 7NH, UK. [24]Space Sciences Laboratory, University of California, Berkeley, CA 94720–7450, USA. [25]Centre de Recherches Petrographiques et Geochimiques, 15 rue Notre Dame des Pauvres, BP 20, 54501 Vandoeuvre lès Nancy, France. [26]Lockheed Martin Space Systems, Littleton, CO 80125, USA. [27]Astromaterials Research and Exploration Science, NASA Johnson Space Center, Houston, TX 77058, USA. [28]ERC, Inc., NASA Johnson Space Center, Houston, TX 77058 USA. [29]Geophysical Laboratory, Carnegie Institution of Washington, Washington, DC 20015 USA. [30]Exobiology Branch, NASA Ames Research Center, Moffett Field, CA 94035, USA. [31]Laboratoire de Structure et Propriétés de l'Etat Solide, Bat C6, Université des Sciences et Technologies de Lille, 59655 Villeneuve d'Ascq, France. [32]Dartmouth College, Hanover, NH 03755, USA. [33]Department of Chemistry and Biochemistry, University of California San Diego, 9500 Gilman Drive, La Jolla, CA 92093–0356, USA. [34]Goddard Center for Astrobiology, NASA Goddard Space Flight Center, Greenbelt, MD 20771, USA. [35]Department of Earth and Planetary Sciences, American Museum of Natural History, New York, NY 10024, USA. [36]Laboratory for Astrophysics and Space Research, Enrico Fermi Institute, University of Chicago, 933 East 56th Street, Chicago, IL 60637, USA. [37]Advanced Light Source, Lawrence Berkeley National Laboratory, Berkeley, CA 94720–8225, USA. [38]Centre for Astrophysics and Planetary Sciences, University of Kent, Canterbury, Kent CT2 7NH, UK. [39]Novaetech s.r.l., Napoli, Italy. [40]Laboratoire de Sciences de la Terre, Ecole Normale Superieure de Lyon, 46, allee d'Italie, 69007, Lyon, France. [41]Physics and Astronomy Department, SUNY at Stony Brook, Stony Brook, NY 11794–3800, USA. [42]Laboratory for Space Sciences, CB1105, Washington University, St. Louis, MO 63160–4899, USA. [43]Department of Physics, SUNY, Plattsburgh, NY 12901, USA. [44]Open University, Milton Keynes MK7 6AA, UK. [45]Laboratoire Pierre Süe, CEA-Saclay 91191 Gif sur Yvette, France. [46]Impact and Astromaterials Research Centre, Department of Earth Sciences and Engineering, Imperial College of Science Technology and Medicine, London, SW7 2AZ, UK. [47]Chemical Science Division, Lawrence Berkeley National Laboratory, Berkeley, CA 94720–8225, USA. [48]School of Earth, Atmospheric and Environmental Sciences, University of Manchester, Manchester, M13 9PL, UK. [49]Museum National d'Histoire Naturelle, Laboratoire d'Etude de la Matiere Extraterrestre, USM 0205 (LEME), Case Postale 52, 57, rue Cuvier, 75005 Paris, France. [50]Department of the Geophysical Sciences, University of Chicago, 5734 South Ellis Avenue, Chicago, IL 60637, USA. [51]United States Geological Survey, 954 National Center, Reston, VA 20192, USA. [52]Division of Geological and Planetary Sciences, California Institute of Technology, Pasadena, CA 91125, USA. [53]Geology Department, Case Western Reserve University, Cleveland, OH 44106, USA. [54]Max Planck Institute for Chemistry, Particle Chemistry Department, P.O. Box 3060, 55020 Mainz, Germany. [55]Rutgers University, Piscataway NJ, USA. [56]Astromaterials Research and Exploration Science, NASA Johnson Space Center, Houston, Texas 77058, USA. [57]Stanford Synchrotron Radiation Laboratory, Stanford Linear Accelerator Center, Menlo Park, CA 94025, USA. [58]Robert M. Walker Laboratory for Space Science, Astromaterials Research and Exploration Science Directorate, NASA Johnson Space Center, Houston, TX 77058, USA. [59]Laboratoire de Structure et Propriétés de l'Etat Solide, Bat C6, Université des Sciences et Technologies de Lille, 59655 Villeneuve d'Ascq, France. [60]Physics and Astronomy Department, SUNY at Stony Brook, Stony Brook, NY 11794–3800, USA. [61]Department of Earth and Planetary Sciences, Harvard University, 20 Oxford Street, Cambridge, MA 02138, USA. [62]Center for Meteorite Studies, Arizona State University, m/c 1404, Tempe AZ 85287,USA. [63]Max Planck Institut for Solar System Research, Max-Planck-Strasse 2, 37191Katlenburg-Lindau, Germany. [64]Hawaii Institute of Geophysics and Planetology, University of Hawaii, Honolulu, HI 96822, USA. [65]Institute of Geosciences, Friedrich-Schiller-University Jena, Burgweg 11, D-07749 Jena, Germany. [66]Center for Advanced Radiation Studies, University of Chicago, Chicago, IL 60637, USA. [67]Jacobs Sverdrup, ESCG, Houston, TX 77058, USA. [68]Sciences and Exploration Directorate, NASA Goddard Space Flight Center, Greenbelt, MD 20771, USA. [69]Institut für Planetologie, Westfälische Wilhelms-Universität, Münster, Germany. [70]Université Lille, Lille, France. [71]Department of Earth and Space Sciences, University of California Los Angeles, Los Angeles, CA 90095–1567, USA. [72]McDonnell Center for the Space Sciences, Department of Physics, Washington University, St. Louis, MO 63130, USA. [73]Centre de Recherches Petrographiques et Geochimiques, 15 rue Notre Dame des Pauvres, BP 20, 54501 Vandoeuvre lès Nancy, France. [74]INAF, Osservatorio Astronomico di Capodimonte, Via Moiariello 16, 80131 Napoli, Italy. [75]Department of Earth and Planetary Science, University of Tokyo, Hongo, Bunkyo-ku, Tokyo 113-0033, Japan. [76]Museum National d'Histoire Naturelle, Laboratoire d'Etude de la Matiere Extraterrestre, 57 rue Cuvier, 75005, Paris, France. [77]Kyushu University, Fukuoka, Japan. [78]Advanced Industrial Science and Technology, Geological Survey of Japan, Ibaragi, Japan. [79]Department of Earth and Planetary Sciences, Faculty of Science, Kobe University, Nada, Kobe 657-8501, Japan. [80]Institute of Materials Structure Science, Tsukuba-shi, Ibaraki-ken, 305, Japan. [81]Japan Aerospace Exploration Agency, Institute of Space and Astronautical Science, 3-1-1 Yoshinodai, Sagamihara, Kanagawa, 229-8510, Japan. [82]Science Division, Jet Propulsion Laboratory, 4800 Oak Grove Drive, Pasadena, CA 91109, USA. [83]Department of Physics and Astronomy, Minnesota State University, 141 Trafton Science Center N, Mankato, MN 56001, USA. [84]School of Physics and Astronomy, University of Minnesota, Minneapolis, MN 55455, USA. [85]Savannah River Ecology Lab, Aiken, SC 29801, USA. [86]Dip. Scienze Applicate, Università degli Studi di Parthenope, Napoli, Italy. [87]Astrophysics Branch, NASA Ames Research Center, Moffett Field, CA 94035, USA. [88]Engineering Science Contract/Barrios Technology, Astromaterials Research and Exploration Science/Johnson Space Center, Houston, Texas 77258–8447, USA. [89]U.S. Naval Research Laboratory, Washington, DC 20375, USA. [90]State University of New York, Plattsburgh, NY 12901, USA. [91]Japan Synchrotron Radiation Institute, Hyougo, Japan. [92]Engineer Research and Development Center, Cold Regions Research and Engineering Laboratory, Hanover, NH 03755, USA. [93]Institute of Space Sciences Institut d'Estudis Espacials de Catalunya, CSIC, Universitat Autònoma de Barcelona, Campus UAB, 08193 Bellaterra (Barcelona), Spain. [94]Institut d'Estudis Espacials de Catalunya (IEEC), Ed. Nexus, Gran Capità, 2-4, 08034 Barcelona, Spain. [95]Department of Earth and Space Science, Osaka University, 1-1 Machikaneyama-cho, Toyonaka, 560-0043, Japan. [96]Department of Chemistry, Stanford University, Stanford, California 94305–5080, USA. [97]Department of Geological Sciences, Michigan State University, East Lansing, MI 48824–1115, USA. [98]Ghent Univ, Ghent, Belgium. [99]Physical Sciences, Kingsborough Community College (CUNY), Brooklyn, NY 11235, USA. [100]Department of Earth and Planetary Sciences, Washington University, St. Louis, MO 63130-4899, USA.

*To whom correspondence should be addressed. E-mail: brownlee@astro.washington.edu

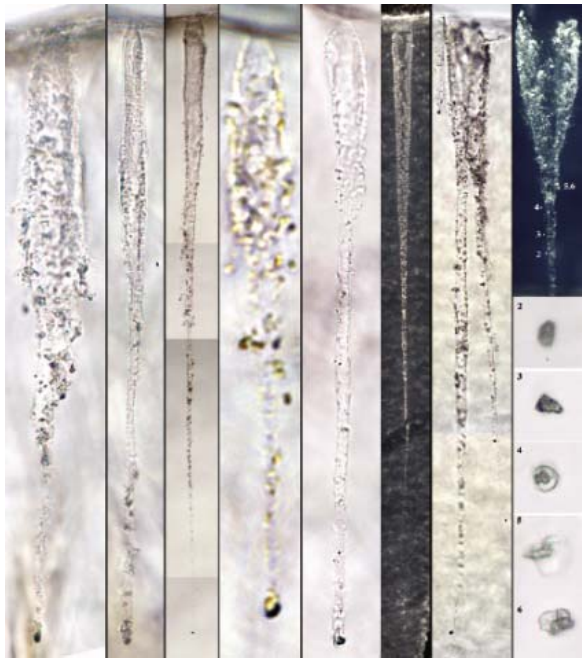

Fig. 1. Optical images of deceleration tracks of eight comet particles in aerogel that entered at the top and terminated at the base. Left to right, the track names and their lengths are T59 (0.35 mm), T58 Noni (0.29 mm), T61 (1.6 mm), T72 Gea (0.12 mm), T71 Surya (0.22 mm), T38 Tara (3.2 mm), T27 Sitara (>2 mm), and T25 Inti (2 mm). The thinner tracks suffered very little fragmentation that leads to substantial production of side tracks. The break in the T38 track is due to sample preparation, and the upper bulb of T25 widened a bit when it was intentionally flattened. All of the other tracks have their original shapes. The squares below T25 (Inti) are magnified images of five of the major 5- to 12-μm particles. The tip of the track containing the 20-μm terminal particle was removed before the track image was taken. The terminal particle as well as many of the other fragments are isotopically and mineralogically linked CAIs, exotic refractory components in primitive meteorites that may have formed very close to the young Sun.

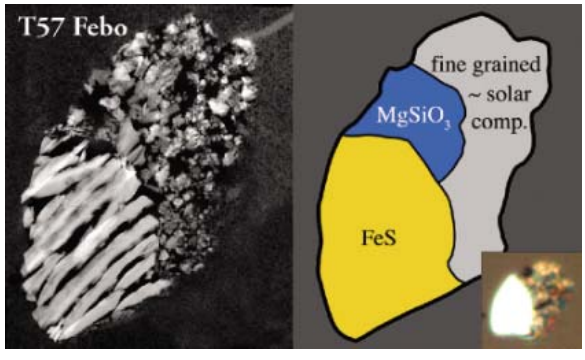

Fig. 2. The 8-μm terminal particle of T57 (Febo), a bifurcated track >1.4 mm long. The left image is a high-angle annular darkfield (HAADF) image of a 70-nm-thick microtome section of the particle. The images combined with x-ray spectral analysis show that the particle has three major components. The sulfide pyrrhotite on the left, a 3-μm enstatite grain in the upper middle, and fine-grained porous aggregate material with approximately chondritic elemental composition (Mg, Al, Si, S, Ca, Cr, Mn, Fe, Ni ~ solar ratios) dominates the right half of the image. The particle's smooth exterior contour is probably due to abrasion during passage through aerogel, although the particle contains only trace amounts, at most, of adhering aerogel. The survival of fine-grained chondritic composition material as a major part of a terminal particle is unusual, and its survival may have been aided by shielding; it may have been in the lee of the large sulfide. The small inset image shows a reflected-light view of the "potted butt," the sample that remains after removing microtome sections.

are entirely composed of submicron chondritic composition (Mg,Al,Si,S,Ca,Fe,Ni ratios = solar) materials similar to the material that dominates interplanetary dust and the matrix of primitive carbon-rich meteorites, although such material has been seen attached to terminal particles (Fig. 2).

All the particles were modified to some degree by capture, and recognizing and developing a better understanding of the effects is important for understanding the properties of the cometary samples. High-speed capture left some components in excellent condition, whereas others were severely altered. In general, components larger than micron-size were often well preserved, whereas smaller or finer-grained components were strongly modified. The most extreme modifications observed were the cases of vesicular silica in the upper regions of track walls that contain only a percentage of projectile material, usually Mg, Al, Ca, Mn, and Fe in roughly solar relative proportions, dissolved into previously molten aerogel. This glass usually contains large numbers of submicron beads of FeNi sulfide or metal, immiscible phases that could not dissolve in silica. These materials were clearly heated above the ~2000 K melting point of silica, and this is the possible fate of many of the submicron components that stopped in the upper regions of tracks.

Despite laboratory simulation studies and aerogel capture of meteoroids in space, the capture effects on bona fide comet dust at 6 km/s were unknowable before the encounter because of the unknown nature of cometary materials and the technical limitations of accelerating loosely bound aggregates like those implied by studies of interplanetary dust particles (IDPs) and meteors. Simulations at 6 km/s were done with a variety of solid particles that could be accelerated, and there was a moderate amount of experience with capture of actual meteoroids by orbiting spacecraft (*5*, *6*). All of these projects showed that solid particles >10 μm could be captured in reasonably good condition consistent with the Stardust mission findings. These projects showed that even temperature-sensitive materials such as hydrated silicates and materials that melt at ~600°C could be captured in good shape with only minor alteration except at particle surfaces where they were sometimes coated with a thin layer of melted aerogel. The juxtaposition of melted and unmelted material indicates extremely high temperature gradients at particle surfaces. Particles impacted Stardust at 6.1 km/s and were stopped on time scales ranging from a microsecond to less than a nanosecond depending on the particle size and the collection media. At nanosecond interaction times, the thermal wave produced by contact with molten aerogel at temperatures >2000 K does not penetrate deeply into captured particles (Fig. 3). Although the smallest components were often strongly heated, those over a micron in size appear to have been protected by their own thermal inertia.

The range of effects inside aerogel tracks can be crudely understood in terms of velocity-dependent heating. If an ideal nonfragmenting particle simply sweeps up aerogel in its path, accelerating it to the particle velocity and then releasing it, the particle's speed will decrease by 1/e every time it sweeps up its own mass of aerogel. In this simplified model, the speed (v) of a 10-μm density 3-g/cc particle in 0.01 g/cc (ρ) aerogel decreases to 2.2 km/s after 3 mm, 0.8 km/s at 6 mm, and stops at about 1 cm when the dynamic pressure ($\sim\rho v^2$) is matched by the aerogel's compression strength. The power generated varies as v^3, and at 3-mm and 6-mm depth it would be 5% and 0.2%, respectively, of the power generated at the point of entry. Entering projectiles generate a spray of molten aerogel that forms and lines track walls, but this process rapidly declines with depth. Aerogel along the track walls varies from molten at the entry to compressed in the mid-range and then is little affected as the track actually narrows to the projectile diameter near the track's end. Actual tracks of particles made by 10 μm silicates are about 1 mm long, which implies somewhat faster deceleration than in this crude model. Deceleration of actual particles can be greater if the

column cross-section of aerogel that is accelerated is larger than the projectile cross-section or less if intercepted aerogel is not accelerated to the projectile velocity. Additional complications include build-up and shedding of caps (*7*) of compressed or melted aerogel and general fragmentation.

Context. The work on the Stardust mission samples has only recently begun, but the first laboratory studies of comet samples have already provided considerable insight into (i) the formation of comets, (ii) the origin of crystalline silicates around stars that form planets, and (iii) large-scale mixing in the solar nebula and, by inference, mixing in circumstellar accretion disks that form planets around other stars. There have been various suggestions for the origin of comets, but the most widely held view is that they are mixtures of ice and interstellar grains, specifically submicron-sized core-mantle grains (*8*, *9*). Complicating factors to this model include infrared spectral evidence that comets, particularly long-period comets, contain crystalline silicates (*10*, *11*), whereas silicates observed in the interstellar medium are almost entirely noncrystalline (*12*, *13*), a state commonly attributed to radiation processes. The standard explanation for this is that crystalline silicates in comets were produced by annealing, the devitrification of glass or amorphous silicates at elevated temperature. For common silicates and appropriate time scales, this process requires temperatures of 800 K or more and is inconsistent with the environment that produced comets containing ices that condensed below 40 K. Bockelée-Morvan *et al*. (*14*) suggested that the annealing of amorphous silicates occurred in hot inner regions of the solar nebula and were carried outward by turbulent mixing, potentially a very effective transport process (*15*). Modeling suggests that turbulent mixing can cause large-scale radial mixing on 10^4-year time scales. Although mixing is a prediction of several solar system formation models, the radial variations of the properties of minor planets as well as larger-scale variation of solar system bodies suggest that the solar nebula was not well mixed.

A major portion of the Stardust mission particles larger than a micron is composed of the silicate minerals olivine and pyroxene (Figs. 2 to 4). The presence of these two phases has also been indicated by infrared data from other comets, in particular in Hale-Bopp (*11*) and Tempel 1, the comet impacted by the Deep Impact mission (*16*). Like all minerals, and by definition of the word mineral, these are crystalline solids. There are also amorphous silicates in some of the samples, but it is not yet clear whether these existed before collection or were produced during the capture. Isotopic work on these samples is just beginning, but it is evident that the majority of the large crystalline silicates collected by Stardust have solar isotopic compositions and not the anomalous ones expected and seen in interstellar grains. At this early stage, it appears that a major fraction of the micron and larger silicates in Wild 2 were produced in our solar system. It is also remarkable that so many of the impacting comet particles contained at least a few relatively large solid grains, an order of magnitude larger than the size of typical interstellar grains (*17*). In addition to silicates and abundant sulfides, the collected comet samples contain organic materials (*18*) even in the submicron size range (Fig. 5).

The range of compositions of olivine and pyroxene grains in the Stardust mission samples, particularly with regard to the minor elements, indicates a reasonable similarity to components found in interplanetary dust and some primitive unequilibrated meteorites (*19*). Extensive work has been done on these meteoritic materials, and there has been vigorous debate about which grains are primary condensates from hot regions of the solar nebula and which ones are fragments of highly processed materials such as chondrules, objects composed of crystals, and glass formed by rapid crystallization of a melt. In stark contrast to astronomical interpretations, studies of meteoritic materials have not suggested that these phases formed by annealing of presolar amorphous silicates. The detailed quantitative evaluation of a large set of silicates collected by Stardust has yet to be done, but the isotopic composition, minor element composition, and even the range of Fe/Si does not appear to be compatible with an origin by annealing of radiation-damaged interstellar silicates. Specifically, many of the olivines are nearly Fe free and yet have moderately high abundances of Al, Ca, Cr, and sometimes Mn. There is no model or set of experiments that suggest that such compositions would form from plausible amorphous interstellar materials. The composition of the grains collected by Stardust provides both a rich source of new

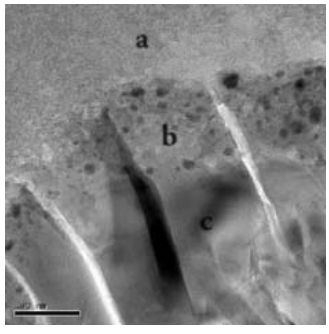

Fig. 3. Conventional brightfield transmission electron microscope image of a microtome section of an Fo99 (Mg/Mg + Fe atomic ratio = 0.99) olivine grain showing a 100-nm-thick alteration rim produced during high-speed capture. The rim (b) contains nanophase FeNi metal and sulfide grains resulting from the interaction of the grain with a thin flow of material containing Fe, Ni, and S, presumably a mix of melted silica aerogel and comet materials. Below the thin rim (c), the grain appears to be perfectly preserved; above the rim (a) is unmodified aerogel in which the particle was captured.

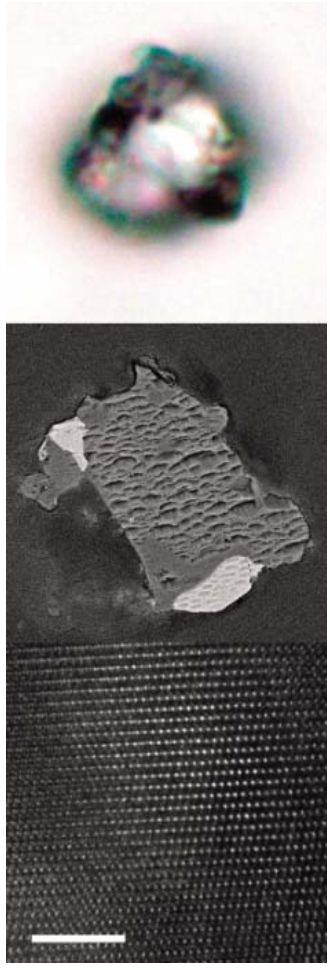

Fig. 4. Three images of the 8-μm terminal particle at end of the >2-mm-long track 27 (Sitara), also shown in Fig. 1. The top is an optical image showing parent central grain (that is also birefrigent) with two attached opaque phases. Other focus depths show additional opaques inside the grain. The middle image is an SEM backscattered electron (BSE) image of the flat surface ("potted butt") of the particle mounted in acrylic after several dozen 70-nm slices had been removed with a diamond microtome. The image brightness is proportional to mean atomic weight and this, along with x-ray spectral measurements, shows that the particle is a solid rock composed of at least four phases. The two bright regions are sulfides; one is pyrrhotite $Fe_{1-x}S$, and the other is pentlandite, a Ni-rich sulfide. The central gray region marked by aligned "chatter pits" from the diamond knife is enstatite. The smooth gray regions are an undetermined crystalline Mg silicate that contains Na, Al, and Ca at abundances of several percent. The bottom image shows the enstatite grain observed in a microtome section at near atomic-scale resolution. Scale bar, 5 nm).

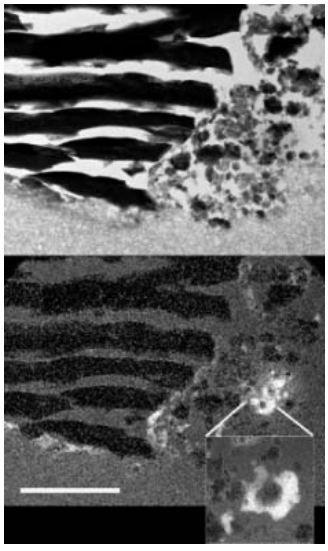

Fig. 5. Energy-filtered TEM images of the lower region of the T57 (Febo) slice shown in Fig. 2 (scale bar, 1 μm). The top image is a zero-loss image made with electrons that did not lose energy during passage through the sample, and the lower image displays the carbon distribution. The carbon image was made with the standard three-window method that combines images taken in energy passbands above and below the 285-ev carbon edge. The sulfide on the left is carbon free, but regions of carbon are seen both as submicron components in the fine-grained chondritic component on the right and as partial rims on the sulfide grain. Isotopic measurements made at Johnson Space Center have shown considerable ^{15}N enrichment in the carbon-rich region shown in the expanded window.

information for determining the origin of silicates in comets formed at the edge of the solar nebula and a superb means of assimilating and fostering new understanding of the sometimes incompatible inferences from the extraterrestrial sample and astronomical communities.

Radial mixing in the solar nebula. Perhaps the most straightforward result of the Stardust analysis program is information for large-scale mixing in the solar nebula. The comet samples collected by Stardust do contain presolar materials, the initial building materials of the solar system, but they clearly are not just a collection of submicron interstellar grains. The collection contains abundant high-temperature minerals such as forsterite (Mg_2SiO_4) and enstatite ($MgSiO_3$). It also contains at least one particle that is mineralogically and isotopically linked to meteoritic calcium- and aluminum-rich inclusions (CAIs). CAIs are the oldest samples of the solar system, they are systematically enriched in ^{16}O, and they contain abundant minerals that condense at temperatures higher than the 1400 K condensation temperature of forsterite. Meteoritic CAIs are thought to have formed in the hottest portion of the solar nebula. A popular model for the ^{16}O enrichment involves photochemical self-shielding processes that may have occurred mainly in the innermost regions of the solar nebula, well inside the orbit of Mercury (*20*). These apparent inner solar system materials in the comet must have been transported beyond the orbit of Neptune by a process that was capable of moving particles at least as large as 20 μm. The existence of such a process provides a fundamental constraint on models of the solar nebula. Particles could have been transported from the center to the outer edge of the nebula in two different ways: (i) ballistic transport above the nebular midplane or (ii) turbulent transport in the midplane. Although it was widely believed that comets were isolated from inner solar system materials, there have been several suggestions that such transport was possible. Bockelée-Morvan *et al*. (*14*) and others predicted such transport based on turbulent mixing in the solar nebula disk, and Shu *et al*. (*21*) predicted that even quite large particles could be launched by an outflow called the X-wind from a region that was very close to the young Sun and ballistically transported above the midplane of the nebular disk. Shu and colleagues specifically predicted that the X-wind model would transport CAIs from near the Sun to the edge of the solar system where Wild 2 formed.

Comparison with Deep Impact results. The Deep Impact mission also provided important information about the composition of dust from another Jupiter family comet. A portion of the Deep Impact spacecraft impacted comet 9P/Tempel 1 liberating ~10^6 kg of debris that was observed in the infrared. Many of the spectra have superb signal-to-noise ratios and show numerous features caused by emission from submicron grains. The Deep Impact data was used to estimate the mineralogical make-up of the comet by synthesizing the observed spectra as a mixture of spectra of various laboratory compounds (*16*). The model composition expressed as relative weighted surface area is ferrosilite ($FeSiO_3$) 33, forsterite (Mg_2SiO_4) 31, amorphous olivine [$(Mg,Fe)_2SiO_4$] 17, niningerite [(Mg,Fe)S] 15, smectite nontronite (a hydrated silicate) 14, diopside ($CaMgSi_20_6$) 12, orthoenstatite ($MgSiO_3$] 10, fayalite (Fe_2SiO_4) 9, siderite ($FeCO_3$) 5, amorphous pyroxene [$(Mg,Fe)SiO_3$] 4, and magnesite ($MgCO_3$) 3. Of these minerals, only forsterite was found in Wild 2 at abundances above a few percent. The inferred presence of MgFe sulfides, the oxymoron phases amorphous olivine and pyroxene, as well as carbonates and hydrated silicates are clearly at odds with the sample return data. To date, no compelling evidence has been seen in the samples for either the presence of these phases or their thermal decomposition products. For example Mg-, Ca-, or Fe-bearing carbonates, even if they decomposed during capture, would be converted to oxides by strong heating and would be readily observed if they had existed in Stardust samples. Iron sulfides are abundant components in Wild 2, but FeMg sulfides have not been seen, they are not present in IDPs, and they are exceedingly rare in primitive meteorites. The Deep Impact modeling included components of amorphous olivine and pyroxene, yet noncrystalline silicates with these stoichiometric compositions are not seen except perhaps as trace occurrences in Wild 2, IDPs, or meteorites. The most notable difference between the results of the two missions is the presence of carbonates and hydrated silicates, phases whose existence in meteorites is usually attributed to formation by hydrothermal alteration inside a wet parent body. Extraterrestrial hydrated silicates have been collected in meteoroids impacting aerogel on Earth-orbiting spacecraft and in laboratory simulation experiments (*22*, *23*), but they have not been seen in Stardust samples. If abundant hydrated silicates >200 nm existed in Wild 2, there should be clear evidence of them in the analyzed samples.

There are several possible explanations for the differences between the conclusions of the two missions. The comets may be different, the sampling regions are different, the size-range sampled is somewhat different, the laboratory materials that were chosen to match the observations may not be appropriate analogs for submicron cometary materials that are both ancient and complex, and numerous factors may complicate the combination of more than a dozen different components to accurately infer the mineralogical composition of a complex natural material. Comets are collections of materials that accreted to form them. It is possible that some comets contain hydrated silicates from the nebula or from the break-up of larger (>100 km) bodies that experienced internal heating, melting of ice, and aqueous alteration of silicates. The Tempel 1 sampling site was near two large features that look like impact craters, and it is conceivable that hydrated silicates could have formed inside Tempel 1 by hydrothermal processes caused by these events. Unlike Tempel 1, Wild 2 does not show clear evidence for classic impact craters, implying that its ancient cratered surface, and possible impact-modified material, has been lost due to cometary activity. As previously mentioned, Stardust is believed to have sampled particles ejected from dozens of ice-bearing subsurface regions that have never been sufficiently heated to cause the separation of the fine-grained mix of submicron dust and ice, let alone hydrothermal alteration processes that can form hydrated silicates.

Remarks. The Stardust mission has provided us large numbers of particles that were at the edge of the solar system at the time of its formation. Efforts have just begun to compare these with meteoritic samples: meteorites, ~0.1-mm micrometeorites (*24*), and 10-μm interplanetary dust. The total mass of collected comet material is actually equivalent to several hundred thousand of the nanogram IDPs that have been intensively studied in the laboratory for the past 35 years. We anticipate that the comet samples and their comparison with meteoritic samples will provide important boundary conditions for models of the origin of the solar

system, the origin of silicate minerals around stars, and mixing in circumstellar disks. The mineral grains and components that we have seen in the comet are analogous to glacial erratics; they clearly did not form in the environment they were found in. Each particle is a treasure that provides clues on its place of origin and mode of transport. In many cases, it appears that they formed in the center of the solar nebula, and many of the larger particles are rocks composed of several minerals. Although better estimates will come from continued studies, initial investigations indicate that on the order of 10% or possibly more of the comet's mass was transported outward from the inner regions of the solar nebula as particles larger than a micron. The solar nebula may not have been well mixed, but the Stardust mission results show that there was abundant radial transport of solids on the largest spatial scales. One of the most surprising findings has been that we have seen many of these materials before. The distribution of minor element compositions of minerals, such as forsterite, indicate a link to the rare forsterite fragments found in primitive meteorites. Meteorite studies indicate that these high-temperature phases, serving as tracers, were distributed to varying degrees, sometimes as very minor components, across the inner parts of the solar nebula (*25*–*27*). From the work on Stardust samples, it now appears that components like forsterite and CAIs, formed in the hottest regions of the solar nebula, were transported over the entire solar nebula.

Comets have always been notable because of their contents of frozen volatiles but they are now additionally notable because of their content of exotic refractory minerals. The information on materials and mixing from the Stardust mission provide a new window of insight into the origin of solid grains that form disks around stars and lead to the formation of planetary bodies. This is a window that is explored with electron microscopes, mass spectrometers, synchrotrons, and a host of other modern instruments to provide information at levels of detail that were not previously imagined. The best available instruments and methods on the planet were used in this study, and it is expected that additional studies coupled with advances in analytical capabilities will continue to reveal important secrets about the origin and evolution of the solar system that are contained in these few thousand particles recovered from comet Wild 2.

References and Notes

1. D. E. Brownlee *et al.*, *Science* **304**, 1764 (2004).
2. Z. Sekanina *et al.*, *Science* **304**, 1769 (2004).
3. H. F. Levison, M. J. Duncan, *Icarus* **127**, 13 (1997).
4. D. R. Davis, P. Farinella, *Icarus* **125**, 50 (1997).
5. F. Horz *et al.*, *Science* **314**, 1716 (2006).
6. F. Horz *et al.*, *Icarus* **147**, 559 (2000).
7. G. Dominguez *et al.*, *Icarus* **172**, 613 (2004).
8. J. M. Greenberg, in *Comets*, L. L. Wilkening, Ed. (Univ. of Arizona Press, Tucson, 1982), pp. 131–163.
9. J. M. Greenberg, *Astron. Astrophys.* **330**, 375 (1998).
10. M. S. Hanner *et al.*, *Astrophys. J.* **425**, 274 (1994).
11. D. H. Wooden *et al.*, *Astrophys. J.* **517**, 1034 (1999).
12. F. Kemper, W. J. Vriend, A. G. G. M. Tielens, *Astrophys. J.* **609**, 826 (2004).
13. J. Dorschner *et al.*, *Astron. Astrophys.* **300**, 503 (1995).
14. D. Bockelée-Morvan *et al.*, *Astron. Astrophys.* **384**, 1107 (2002).
15. J. N. Cuzzi, S. S. Davis, A. R. Dobrovolskis, *Icarus* **166**, 385 (2003).
16. C. Lisse *et al.*, *Science* **313**, 635 (2006).
17. J. S. Mathis *et al.*, *Astrophys. J.* **217**, 425 (1977).
18. S. A. Sandford *et al.*, *Science* **314**, 1720 (2006).
19. Unequilibrated meteoritic materials have not experienced substantial diffusion of atoms between components, usually due to heating, that causes phases such as olivine to have the same elemental composition. The wide range of Fe/Mg ratios in Wild 2 olivine as well as the Ni content of sulfides show that the comet is at least as unequilibrated as the very rare and least equilibrated meteorites.
20. R. N. Clayton, *Nature* **415**, 860 (2002).
21. F. H. Shu *et al.*, *Astrophys. J.* **548**, 1029 (2001).
22. K. Okudaira, *36th Annual Lunar and Planetary Science Conference* **36**, 1832 (2005).
23. G. A. Graham *et al.*, *Dust in Planetary Systems*, Proceedings of the conference held 26 to 28 September 2005 in Kaua'i, Hawaii. LPI Contribution No. **1280**, 56 (2005).
24. C. Engrand *et al.*, *Meteoritics Planet. Sci.* **41**, 5237 (2006).
25. E. R. D. Scott, A. N. Krot, *Astron. Soc. Pacific Conf. Ser.* **341**, 15 (2005).
26. A. Pack, H. Palme, J. M. G. Shelley, *Geochim. Cosmochim. Acta* **69**, 3159 (2005).
27. S. Simon, L. Grossman, *Meteoritics Planet. Sci* **38**, 813 (2003).

28. The Stardust sample analysis team is grateful to NASA for funding and supporting the mission and to the hundreds of other team members that were involved in design, construction, flying, and recovery of the mission. The team, from 100 organizations, gratefully acknowledges their supporting institutions.

3 October 2006; accepted 17 November 2006
10.1126/science.1135840

REPORT

Impact Features on Stardust: Implications for Comet 81P/Wild 2 Dust

Friedrich Hörz,[1]* Ron Bastien,[2] Janet Borg,[3] John P. Bradley,[4] John C. Bridges,[5] Donald E. Brownlee,[6] Mark J. Burchell,[7] Miaofang Chi,[4] Mark J. Cintala,[1] Zu Rong Dai,[4] Zahia Djouadi,[3] Gerardo Dominguez,[8] Thanasis E. Economou,[9] Sam A. J. Fairey,[7] Christine Floss,[10] Ian A. Franchi,[5] Giles A. Graham,[4] Simon F. Green,[5] Philipp Heck,[11] Peter Hoppe,[11] Joachim Huth,[11] Hope Ishii,[4] Anton T. Kearsley,[12] Jochen Kissel,[13] Jan Leitner,[14] Hugues Leroux,[15] Kuljeet Marhas,[10] Keiko Messenger,[2] Craig S. Schwandt,[2] Thomas H. See,[2] Christopher Snead,[16] Frank J. Stadermann I,[10] Thomas Stephan,[14] Rhonda Stroud,[17] Nick Teslich,[4] Josep M. Trigo-Rodríguez,[18,19] A. J. Tuzzolino,[9] David Troadec,[20] Peter Tsou,[21] Jack Warren,[2] Andrew Westphal,[16] Penelope Wozniakiewicz,[12] Ian Wright,[5] Ernst Zinner[10]

Particles emanating from comet 81P/Wild 2 collided with the Stardust spacecraft at 6.1 kilometers per second, producing hypervelocity impact features on the collector surfaces that were returned to Earth. The morphologies of these surprisingly diverse features were created by particles varying from dense mineral grains to loosely bound, polymineralic aggregates ranging from tens of nanometers to hundreds of micrometers in size. The cumulative size distribution of Wild 2 dust is shallower than that of comet Halley, yet steeper than that of comet Grigg-Skjellerup.

Stardust's sample collector exposed SiO_2-based aerogel and aluminum foil to the flux of particles emanating from comet Wild 2 as the spacecraft's trajectory took it to within 234 km of the comet's surface (*1*). The cometary dust grains collided with these surfaces at 6.1 km s^{-1}, producing hypervelocity craters in the aluminum and deep penetration tracks in the highly porous, low-density aerogel (*2*) (fig. S1). Even the most cursory inspection of these surfaces reveals an unexpected diversity in the morphologies and sizes of both craters and tracks.

Detailed morphologic analysis of these impact features and comparison with experimental impacts produced by a suite of well-characterized projectiles was undertaken during the preliminary examination of Stardust to evaluate the common view that cometary solids are fluffy, highly porous objects (*3*). Also, the size distribution of Wild 2 dust can be deduced from the size distribution of the impact features and compared with those for other comets, such as Halley (*4*). In addition, attempts were made to analyze the compositions of molten projectile residues inside craters, as detailed by Zolensky *et al.* and Flynn *et al.* (*5*, *6*).

Stardust's fixed encounter speed of 6.1 km s^{-1} is well within the performance limits (~7 km s^{-1}) of small-caliber, light-gas guns, allowing direct laboratory simulation of Stardust's impact features (*7*–*9*). This is in stark contrast to earlier dust-collection experiments in low Earth orbit, which included aluminum (*10*) and SiO_2-based aerogel (*11*, *12*). Figure 1 compares experimental craters into Al_{1000} targets with those observed on Stardust foils and shows that detailed crater morphology reflects the physical properties of the impactor(s). It also illustrates

notable diversity among Stardust craters brought about by impactors that range from dense objects, such as nonporous silicates of ~3 g cm^{-3}, to highly porous aggregates with bulk densities as low as 0.3 g cm^{-3} (*8*). Detailed cross-sections through representative Stardust craters are shown in fig. S2 to quantify some of these morphologic characteristics, such as widely varying depth-to-diameter ratios and variable scales of surface roughness, which reflect particle density and structure.

We inferred the modal mineralogy of Wild 2 dust from the scanning electron microscopy (SEM) and energy dispersive spectrometer analyses of the molten residues in about 200 craters with diameters of <5 μm (Fig. 2A). Composite projectiles containing variable amounts of olivine, pyroxene, and Fe-sulfide are the most common (56%), and essentially monomineralic particles composed of primarily one of these three major phases make up an additional 36%. These major projectile types dominate at all crater sizes (Fig. 2B). Polymineralic impactors dominate even the smallest craters, some of which are <100 nm in size (Fig. 1F). This implies that individual components contributing to these tiny aggregates must be only tens of nanometers in size, finer than those of typical interplanetary dust particles (*13*). According to Kearsley *et al.* (*7*, *8*), most craters summarized in Fig. 2 are the result of submicrometer-sized impactors; all dust grains analyzed by Zolensky *et al*. and Flynn *et al*. (*5*, *6*) were an order of magnitude larger before impact. All analyses, however, suggest that small and large particles from Wild 2 are composed of a similar, if not identical, suite of minerals.

The penetration tracks in aerogel also displayed a wide range of morphologies. We distinguished three major groups: Type A tracks are carrot-like, with long, slender, continuously tapering walls. In contrast, type B tracks have more bulbous cavities, from which either one or a small number of slender tracks emerge, and resemble turnips with single or multiple roots. Type C tracks consist only of a bulbous, rather stubby cavity. We compared experimental tracks in aerogel formed at about 6 km s^{-1} with those from Stardust (Fig. 3). It seems evident from the laboratory simulations that the type A tracks were made by relatively cohesive impactors, whereas type B tracks resulted from poorly consolidated, fine-grained materials containing competent, coarse components. The fine-grained materials decelerate more rapidly and disperse radially with great efficiency to form a bulb, compared with the more massive and dense components that penetrate deeply. Alternatively, as illustrated by the lizardite experiment in Fig. 3C, the sudden release of copious volatiles could also contribute to bulb formation. However, there is no evidence to date for volatile rich materials in Wild 2 dust (*5*, *6*).

Quantitative measurements of the largest cavity diameter and maximum track length of all tracks in some 20 harvested tiles are illustrated in fig. S3. These measurements provide a quantitative basis for separating the three major track types, yet their transitions are highly gradational. These measurements also reveal that track morphology is size dependent: Most tracks less than 200 μm in length are type A, whereas most of the largest structures are type B; type C tracks are rare at all sizes.

In analogy to interstellar particles, small (<1 μm) and fluffy, highly porous particles are commonly thought to be typical for comets (*3*), but our observations indicate that such particles are only part of a broad continuum that also includes cohesive and dense objects. Particle size is highly variable as well and includes aggregates from <100 nm to >100 μm. This diversity in physical properties is unexpected for particles from a single comet, yet recent modeling of the light-scattering properties of the dust from comet Hale-Bopp also suggests a mixture of fluffy and dense particles (*14*).

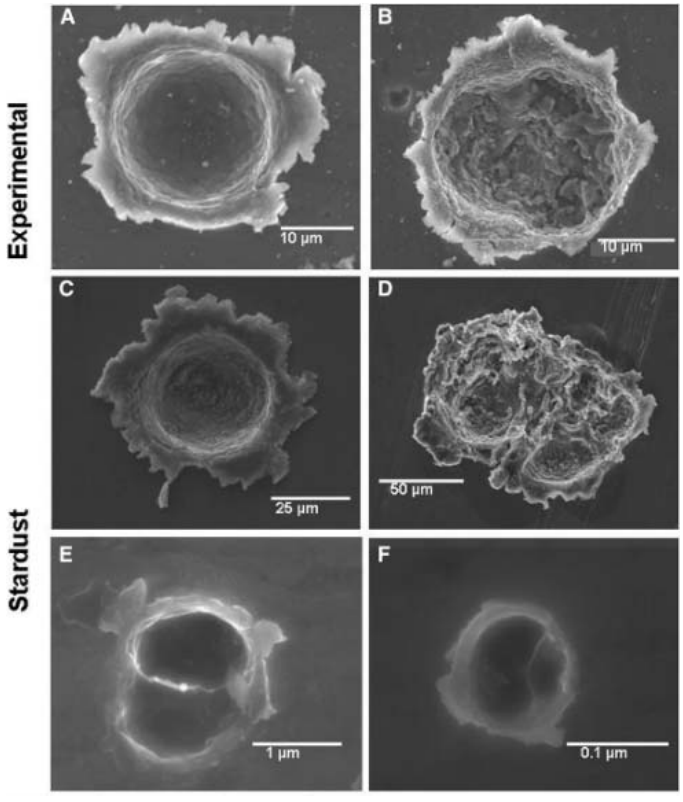

Fig. 1. Comparison of experimental craters (formed at ~6.1 km s^{-1}) and Stardust impacts. (**A**) Experimental crater made by a soda-lime glass sphere. (**B**) Experimental crater produced by an irregular fragment of powdered Allende meteorite. Notably, a crater's plan view grossly mirrors projectile shape. The physically homogeneous glass impactor produced a smooth floor, whereas the Allende crater is rugged, reflecting the fine-grained texture of Allende's matrix. (**C**) Fairly deep, bowl-shaped Stardust crater, suggestive of an equant, dense impactor [identified as Mg-rich silicate (*5*)]. (**D**) Compound, shallow Stardust crater characterized by irregular outlines and overlapping depressions that are separated by discrete septa. Such structures are the result of impactors with distinctly heterogeneous mass distributions, suggestive of aggregate particles with low bulk densities. Similarly, Stardust craters (**E**) and (**F**) are the products of aggregate impactors with discrete mass centers.

[1]Astromaterials Research and Exploration Science, NASA Johnson Space Center, Houston, TX 77058, USA. [2]Engineering Science Contract Group, NASA Johnson Space Center, Houston, TX 77058, USA. [3]Institut Astrophysique Spatiale, 91405 Orsay Cedex, France. [4]Institute for Geophysics and Planetary Physics, Lawrence Livermore National Laboratory, Livermore, CA 94550, USA. [5]Planetary and Space Sciences Research Institute, The Open University, Walton Hall, Milton Keynes MK7 6AA, UK. [6]Department of Astronomy, University of Washington, Seattle, WA 98195, USA. [7]Centre for Astrophysics and Planetary Sciences, University of Kent, Canterbury, Kent CT2 7NH, UK. [8]Department of Chemistry and Biochemistry, University of California San Diego, La Jolla, CA 92093–0356, USA. [9]Laboratory for Astrophysics and Space Research, Enrico Fermi Institute, University of Chicago, Chicago, IL 60637, USA. [10]Laboratory for Space Sciences, CB1105, Washington University, St. Louis, MO 63160–4899, USA. [11]Max Planck Institute for Chemistry, Particle Chemistry Department, Post Office Box 3060, 55020 Mainz, Germany. [12]Department of Mineralogy, The Natural History Museum, London SW7 5BD, UK. [13]Max Planck Institut for Solar System Research, 37191 Katlenburg-Lindau, Germany. [14]Institut für Planetologie, Westfälische Wilhelms-Universität Münster, 48149 Münster, Germany. [15]Laboratoire de Structure et Propriétés de l'Etat Solide, BAT C6, Université de Lille, F-59655 Villeneuve d'Ascq, France. [16]Department of Physics, University of California, Berkeley, CA 94720, USA. [17]Naval Research Laboratory, Code 6360, Washington, DC 20375, USA. [18]Institute of Space Sciences, Institut d'Estudis Espacials de Catalunya–CSIC, 08193 Barcelona, Spain. [19]Institut d'Estudis Espacials de Catalunya, 08034 Barcelona, Spain. [20]Insitut d'Electronique de Microélectronique et de Nanotechnologies, Université de Lille, F-59655 Villeneuve d'Ascq, France. [21]Jet Propulsion Laboratory, California Institute of Technology, Pasadena CA 91109–8099, USA.

*To whom correspondence should be addressed. E-mail: friedrich.p.horz@jsc.nasa.gov

Traywide scanning of all foils and aerogel surfaces at modest optical resolutions produced inventories of all large craters (with crater diameters $D_c > 20$ μm) and tracks (track diameters $D_t > 100$ μm) on the entire collector (*15*). The largest crater was 680 μm in diameter, and the widest track had a bulb diameter of 9.6 mm; the deepest track was 21.9 mm long. Their spatial distribution (fig. S4) suggests uneven, possibly nonrandom location of impact sites. In addition, detailed SEM analyses of individual foils reveal occasionally distinct clustering of craters (fig. S5). Similarly, individual aerogel cells show groups of small tracks that indicate distinctly off-normal trajectories, potentially representing secondary ejecta from the collision of dust with the upper surface of Stardust's collisional Whipple shield. However, none of the 250 craters and tracks analyzed by the entire preliminary examination effort indicates the presence of spacecraft debris (*5*, *6*, *16*). This raises the possibility that the observed clustering had natural causes. Particle fragmentation within cometary comae does not seem uncommon (*17*) and has been suggested specifically for Wild 2 (*18*) to explain the distinctly spiked impact rates observed by Stardust's Dust Flux Monitor Instrument (DFMI) (*19*). Current observations are insufficient to distinguish between these scenarios, and the projectile clustering on Stardust remains poorly understood.

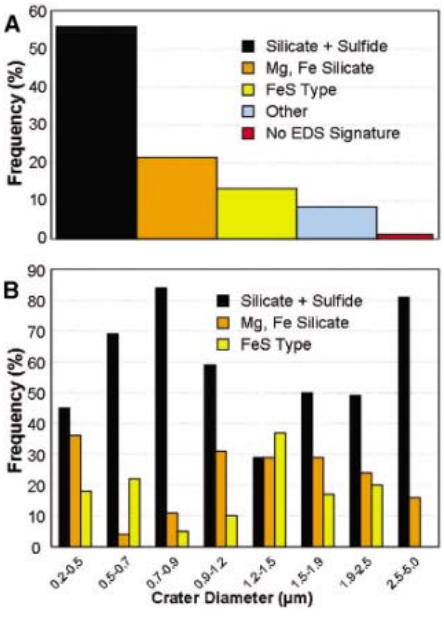

Fig. 2. Relative frequency of mineralogically distinct projectiles inferred from SEM and energy dispersive spectrometer analyses of projectile residues found as discontinuous and somewhat lumpy liners of shock-molten material on the floors and walls of Stardust foil craters. (**A**) Summary of all analyses. (**B**) Projectile composition as a function of crater diameter.

We next turned to the size frequency and fluence of Wild 2 dust based on the size frequency of craters and tracks and their areal density (number per square meter). The detailed crater and track counts are shown in fig. S6. The areal density of craters varies among individual foils by three orders of magnitude at $D_c > 10$ μm. The areal density of tracks varies as well, but only by one order of magnitude. This could relate to the scale of observation and integration, typically 8 cm^2 for individual aerogel tiles, but only 5 mm^2 (or less) for each foil. Regardless, the highly variable areal densities of both crater and tracks mandate a particle environment that is heterogeneous at scales ranging from millimeters squared to centimeters squared.

To obtain the size distribution of Wild 2 particles, we generated individual distribution curves for D_c and D_t that faithfully represent the relative size frequency of craters or tracks over the entire observational size range. Obviously, the traywide surveys define the large features, and the most thoroughly documented foils [8, 20, 37, and 52 (fig. S6)] and cells 12 and 23 were averaged for the small crater and track populations. These diameter data were then converted into spherical impactors (*20*). The results are plotted in Fig. 4. The independent crater and track calibrations seem to agree well for projectile diameters $D_p < 50$ μm, but they deviate at larger sizes. This is an artifact, because we assumed all measurements of D_t to be associated with type A tracks, akin to the experimental calibrations (*20*); bulbous track cavities most likely require smaller impactors than do carrot-shaped tracks at the same D_t, considering the pronounced, radial expansion of fine-grained materials. For this reason, we consider the crater-derived data more reliable at present.

A least-squares fit through the crater data only (inset in Fig. 4), results in a log-log slope of $D_p = -1.72$ and thus a mass slope of –0.57. This disagrees with the averaged slope of –0.85 for particles <50 μm measured by DFMI (*19*). However, the latter found large temporal and mass-dependent variations in this mass index from <–0.3 to –1.15 (*21*). The DFMI mass index of approximately –0.5 at $D_p > 50$ μm, including absolute fluence, is compatible with the collector observations, but we have no ready explanation as to why the two approaches produce seemingly discrepant results at the smaller sizes for comet Wild 2. The mass distribution of comet Halley (*4*) varies with particle size (and distance from the nucleus) but is steeper (~–1.0)

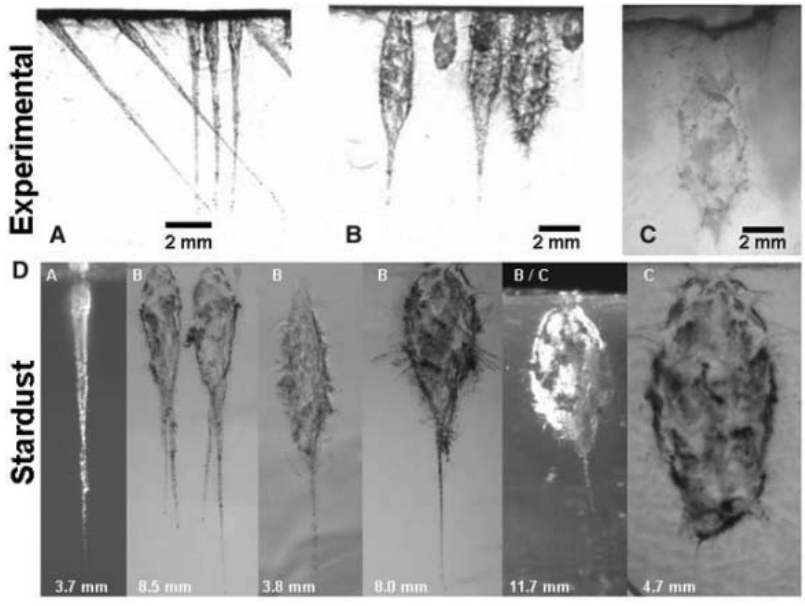

Fig. 3. Comparison of experimental aerogel tracks at 5 to 6 km s^{-1} with representative Stardust features. (**A**) Carrot-shaped tracks (type A) produced by two separate experiments, which used spherical glass projectiles that collided with the aerogel target at angles of 90° and 45° to the surface, thus demonstrating that tracks preserve some trajectory information. (**B**) Bulbous tracks resulting from glass projectiles embedded in a matrix of modestly compacted, very fine (cocoa) powder; the latter partly disaggregated during launch, producing poorly defined clods. Some of these clods contained glass beads that penetrated deeply to form slender termini (type B tracks), whereas others were composed of fine-grained powder only, resulting in type C tracks. (**C**) Bulbous track produced by a volatile-rich projectile (lizardite; containing 15% H_2O). (**D**) Stardust tracks that show, from left to right, the transition from slender (type A) to bulbous features with (type B) or without (type C) slender terminal portions. The total length of the Stardust tracks is given in millimeters.

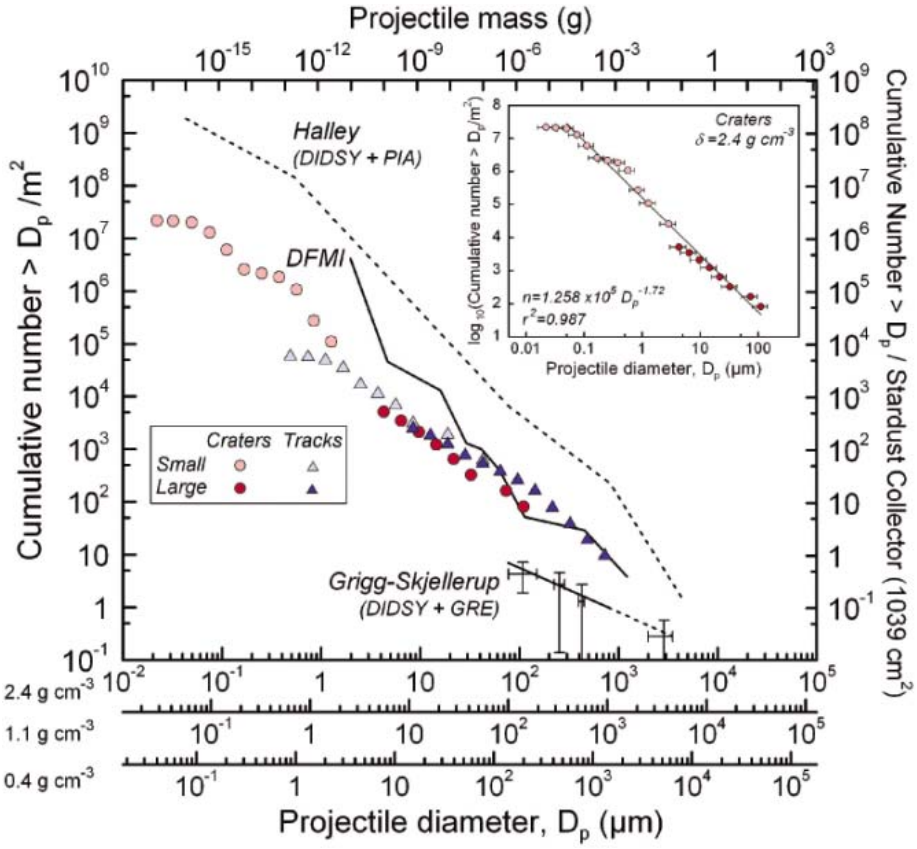

Fig. 4. Size distribution of Wild 2 dust, derived from the measurement of crater and track diameters (fig. S6) and impact calibration experiments (*7*, *20*) that used soda-lime glass (2.4 g cm^{-3}). The 1.1 and 0.4 g cm^{-3} scale bars apply only to craters (*8*), because current track calibrations are limited to soda-lime glass. Also plotted are the measurements of DFMI (*21*), which suggest a substantially steeper average slope than the collector observations. For comparison, in situ spacecraft observations for comets Halley [Dust Impact Detection System (DIDSY) and Particle Impact Analyzer (PIA)] (*4*) and Grigg-Skjellerup [DIDSY and Giotto Radio Science Experiment (GRE)] (*22*) are included. All spacecraft observations were modeled as spherical objects of 2.4 g cm^{-3}, and absolute fluence was adopted from Green *et al.* (*21*). (Inset) Least-square fit through all projectile diameter data, excluding the two points at the smallest sizes.

than that of Stardust over the region measured by both. Wild 2 dust thus seems deficient in small particles compared with that of Halley. The mass index for comet Griggs-Skjellerup, however, is –0.31 (*22*), at about D_p > 100 μm, suggesting fewer small particles than observed by Stardust.

Using the projectile size distribution and fluence of Fig. 4, we calculated a total mass of ~3 × 10^{-4} g of comet material that encountered the entire Stardust collector, yet the actual mission yield could be smaller as a result of impact-induced mass loss. Obviously, most mass is contained in only a few particles that are >100 μm, yet thousands of individual craters and tracks were retrieved that contain residues of Wild 2 dust massive enough to be analyzed individually by state-of-the-art instruments. Such analyses are just beginning.

References and Notes

1. D. E. Brownlee *et al.*, *Science* **304**, 1764 (2004).
2. Total exposed surface area was 1039 cm^2 for aerogel and 152 cm^2 for the Al foils (Al$_{1100}$; 100 μm thick).
3. J. M. Greenberg, A. Li, *Space Sci. Rev.* **90**, 149 (1999).
4. J. A. M. McDonnell, P. L. Lamy, G. S. Pankiewicz, in *Comets in the Post-Halley Era, Vol. 2*, R. L. Newburn *et al.*, Eds. (Kluwer Academic, Norwell, MA, 1991), pp. 1043–1073.
5. M. E. Zolensky *et al.*, *Science* **314**, 1735 (2006).
6. G. J. Flynn *et al.*, *Science* **314**, 1731 (2006).
7. A. T. Kearsley *et al.*, *Meteorit. Planet. Sci.* **41**, 167 (2006).
8. A. T. Kearsley *et al.*, *Meteorit. Planet. Sci.*, in press; preprint available at http://xxx.lanl.gov/abs/astro-phys/0612013.
9. M. J. Burchell *et al.*, *Annu. Rev. Earth Planet. Sci.* **34**, 385 (2006).
10. A. S. Levine, Ed., *LDEF—69 Months in Space, Third Post-Retrieval Symposium*, Williamsburg, VA, 8 to 12 November 1993 (NASA Conference Publication 3275, 1993).
11. F. Hörz, T. H. See, M. E. Zolensky, R. P. Bernhard, J. L. Warren, *Icarus* **147**, 559 (2000).
12. The impact velocities for these low Earth orbit instruments are basically unknown, but mean velocities are 15 to 17 km s^{-1} and thus beyond light-gas gun capabilities. Impact angles are random in low Earth orbit, but they were constant and normal to the collector surfaces for Stardust.
13. F. J. M. Rietmeijer, in *Planetary Materials*, vol. 36 of *Reviews in Mineralogy*, J. J. Papike, Ed. (Mineralogical Society of America, Washington, DC, 1998), pp. 2.1–2.95.
14. J. Lasue, A. C. Levasseur-Regourd, *J. Quant. Spectros. Radiat. Transfer* **100**, 220 (2006).
15. The collector-wide surveys are complete and included all craters with D_c > 20 μm (n = 63) and all tracks of D_t > 100 μm (n = 256). All SEM observations combined refer to a cumulative foil surface of <2 cm^2 (<2% of the collector surface); all detailed track data (e.g., fig. S3) refer to about 20 aerogel tiles, in part incomplete, and thus ~13% of the total aerogel collector surface.
16. S. A. Sandford *et al.*, *Science* **314**, 1720 (2006).
17. P. M. Edenhofer *et al.*, *Astron. Astrophys.* **187**, 712 (1987).
18. B. C. Clark *et al.*, *J. Geophys. Res.* **109**, 10.1029/2004JE002319 (2004).
19. A. J. Tuzzolino *et al.*, *Science* **304**, 1776 (2004).
20. All calibration experiments were conducted at 6.0 to 6.2 km s^{-1} and used projectiles 10 to 100 μm in size and Stardust "flight spare" Al foils and density-graded aerogel targets. Experiments by Kearsley *et al.* in (*7*) used spherical projectiles of soda lime-glass (2.4 g cm^{-3}), whereas polymethylmethacrylate (1.1 g cm^{-3}) and hollow glass spheres (0.4 g cm^{-3}) were used by Kearsley *et al.* in (*8*). Least-squares fits through the measured crater diameters (lip-crest to lip-crest) yielded the empirical constants K in the general relationship of $D_c = KD_p$. Corresponding experiments into Stardust aerogel are ongoing and presently limited to glass beads that produce carrot-shaped type A tracks (*23*); bulbous tracks remain uncalibrated, because they can be produced presently only by clods of fine-grained material of undefined size or mass.
21. S. F. Green *et al.*, *J. Geophys. Res.* **109**, 10.1029/2004JE002318 (2004).
22. J. A. M. McDonnell *et al.*, *Nature* **362**, 732 (1993).
23. M. J. Burchell, personal communication.

24. The encounter of comet Wild 2 by Stardust was the fourth flight project of NASA's Discovery Mission Program. Numerous individuals in government, academia, and industry contributed to the design, manufacture, launch, cruise, fly-by, and safe return of the payload to Earth. In addition, the research reported here was generously supported by our home institutions and national funding agencies.

Supporting Online Material

www.sciencemag.org/cgi/content/full/314/5806/1716/DC1
SOM Text
Figs. S1 to S6
References

29 September 2006; accepted 10 November 2006
10.1126/science.1135705

REPORT

Organics Captured from Comet 81P/Wild 2 by the Stardust Spacecraft

Scott A. Sandford,[1*] Jérôme Aléon,[2,3] Conel M. O'D. Alexander,[4] Tohru Araki,[5] Saša Bajt,[6] Giuseppe A. Baratta,[7] Janet Borg,[8] John P. Bradley,[6] Donald E. Brownlee,[9] John R. Brucato,[10] Mark J. Burchell,[11] Henner Busemann,[4] Anna Butterworth,[12] Simon J. Clemett,[13] George Cody,[14] Luigi Colangeli,[10] George Cooper,[15] Louis D'Hendecourt,[7] Zahia Djouadi,[8] Jason P. Dworkin,[16] Gianluca Ferrini,[17] Holger Fleckenstein,[18] George J. Flynn,[19] Ian A. Franchi,[20] Marc Fries,[14] Mary K. Gilles,[21] Daniel P. Glavin,[16] Matthieu Gounelle,[22] Faustine Grossemy,[8] Chris Jacobsen,[18] Lindsay P. Keller,[23] A. L. David Kilcoyne,[21,24] Jan Leitner,[25] Graciela Matrajt,[9] Anders Meibom,[22] Vito Mennella,[10] Smail Mostefaoui,[22] Larry R. Nittler,[4] Maria E. Palumbo,[7] Dimitri A. Papanastassiou,[26] François Robert,[22] Alessandra Rotundi,[27] Christopher J. Snead,[12] Maegan K. Spencer,[28] Frank J. Stadermann,[29] Andrew Steele,[14] Thomas Stephan,[25] Peter Tsou,[26] Tolek Tyliszczak,[21,24] Andrew J. Westphal,[12] Sue Wirick,[18] Brigitte Wopenka,[30] Hikaru Yabuta,[14] Richard N. Zare,[28] Michael E. Zolensky[31]

Organics found in comet 81P/Wild 2 samples show a heterogeneous and unequilibrated distribution in abundance and composition. Some organics are similar, but not identical, to those in interplanetary dust particles and carbonaceous meteorites. A class of aromatic-poor organic material is also present. The organics are rich in oxygen and nitrogen compared with meteoritic organics. Aromatic compounds are present, but the samples tend to be relatively poorer in aromatics than are meteorites and interplanetary dust particles. The presence of deuterium and nitrogen-15 excesses suggest that some organics have an interstellar/protostellar heritage. Although the variable extent of modification of these materials by impact capture is not yet fully constrained, a diverse suite of organic compounds is present and identifiable within the returned samples.

Comets are small bodies that accreted in the outer solar system during its formation (*1*) and thus may consist of preserved samples of the "starting materials" from which the solar system was made. Organic materials are expected to be present in cometary samples (*2*) and may include molecules made and/or modified in stellar outflows, the interstellar medium, and the protosolar nebula, as well as by parent-body processing within the comet. The presence of organic compounds in comets and their ejecta is of astrobiological interest because their delivery to early Earth may have played an important role in the origin of life on Earth (*3*).

An overview of the Stardust mission and the collection and recovery of Wild 2 samples is provided elsewhere (*4*, *5*). We describe the results obtained from the returned samples by the Stardust Organics Preliminary Examination Team (PET). Samples were studied using a wide range of analytical techniques, including two-step laser desorption laser ionization mass spectrometry (L^2MS), liquid chromatography with UV fluorescence detection and time of flight mass spectrometry (LC-FD/TOF-MS), scanning transmission x-ray microscopy (STXM), x-ray absorption near-edge spectroscopy (XANES), infrared and Raman spectroscopy, ion chromatography with conductivity detection (IC), secondary ion mass spectrometry (SIMS), and time-of-flight SIMS (TOF-SIMS) (*6*). These techniques provide a wealth of information about the chemical nature and relative abundance of the organics in the samples. Our results are compared with organic materials found in primitive meteorites and interplanetary dust particles (IDPs) collected in the stratosphere, as well as to astronomical and spacecraft observations of comets.

Despite some uncertainties associated with the presence of contaminants and alteration of the samples during the capture process, considerable information about the nature of the organics in the samples can be determined.

Some organic-containing contaminants are present in the returned sample collectors, but they are of low enough abundance or are sufficiently well characterized that they can be distinguished from the organics in the cometary materials in the returned samples (*6*). For example, the aerogel collector medium, which consists predominantly of amorphous SiO_2, contains from a quarter to a few weight percent C. However, nuclear magnetic resonance studies indicate that this C is largely in the form of simple Si-CH_3 groups easily distinguishable from the cometary organics described below. It should be noted that not all the collected organics in the samples will be fully representative of the original cometary material because some may have been modified during impact with the aerogel collectors. There is evidence that at least some organic compounds were generated or altered by impact heating of this material (*6*).

Multiple experimental techniques demonstrate that the samples contain polycyclic aromatic hydrocarbons (PAHs). L^2MS spectra obtained from individual particles and in aerogel along impact tracks split lengthwise show PAHs and their alkylated derivatives. Two distinct types of PAH distributions along tracks can be distinguished from the low backgrounds of PAHs present in the aerogel (figs. S1 and S2). In some cases, benzene and naphthalene (1- to 2-ring PAHs, including alkylation out to several CH_3 additions) are observed in the absence of moderate mass 3- to 6-ring PAHs (fig. S1). These distributions are uncharacteristic of meteorites and IDPs but resemble pyrolysis products of meteoritic macromolecular organics and are observed in high-power laser L^2MS measurements of preflight and Stardust Witness aerogel tiles (*6*), raising the question about how many of the lower mass PAHs originate from impact processing of C original to the aerogel.

The second type of PAH population shows complex distributions that resemble those seen in

[1]Astrophysics Branch, NASA-Ames Research Center, Moffett Field, CA 94035, USA. [2]Glenn T. Seaborg Institute, Lawrence Livermore National Laboratory, Livermore, CA 94550 USA. [3]Centre de Recherches Pétrographiques et Géochimiques, Vandoeuvre-les-Nancy, France. [4]Department of Terrestrial Magnetism, Carnegie Institution, Washington, DC 20015–1305, USA. [5]Department of Physics, North Carolina State University, Raleigh, NC 27695, USA. [6]Institute of Geophysics and Planetary Physics, Lawrence Livermore National Laboratory, Livermore, CA 94550, USA. [7]Istituto Nazionale di Astrofisica, Osservatorio Astrofisico di Catania, Via Santa Sofia 78, 95123 Catania, Italy. [8]Institut d'Astrophysique Spatiale, Campus, 91405 Orsay Cedex, France. [9]Department of Astronomy, University of Washington, Seattle, WA 98195, USA. [10]INAF, Osservatorio Astronomico di Capodimonte, Via Moiariello 16, 80131 Napoli, Italy. [11]School of Physical Sciences, University of Kent, Canterbury, Kent CT2 7NH, UK. [12]Space Sciences Laboratory, University of California at Berkeley, Berkeley, CA 94720–7450, USA. [13]Expense Reduction Consulting, Inc., NASA Johnson Space Center, Houston, TX 77058, USA. [14]Geophysical Laboratory, Carnegie Institution of Washington, Washington, DC 20015, USA. [15]Exobiology Branch, NASA-Ames Research Center, Moffett Field, CA 94035, USA. [16]Goddard Center for Astrobiology, NASA-Goddard Space Flight Center, Greenbelt, MD 20771, USA. [17]Novaetech s.r.l., Città della Scienza, via Cordoglio 57d, 80124 Napoli, Italy. [18]Physics and Astronomy Department, State University of New York at Stony Brook, Stony Brook, NY 11794–3800, USA. [19]Department of Physics, State University of New York at Plattsburgh, Plattsburgh, NY 12901, USA. [20]Planetary and Space Sciences Research Institute, Open University, Milton Keynes, MK7 6AA, UK. [21]Chemical Science Division, Lawrence Berkeley National Laboratory, Berkeley, CA 94720–8225, USA. [22]Laboratoire d'Etude de la Matiere Extraterrestre, Muséum National d'Histoire Naturelle, Paris, France. [23]NASA, Johnson Space Center, Houston, TX 77058, USA. [24]Advanced Light Source, Lawrence Berkeley National Laboratory, Berkeley, CA 94720–8225, USA. [25]Institut für Planetologie, Westfälische Wilhelms-Universität Münster, Wilhelm-Klemm-Strasse 10, 48149 Münster, Germany. [26]Science Division, Jet Propulsion Laboratory, 4800 Oak Grove Drive, Pasadena, CA 91109, USA. [27]Dipartimento Scienze Applicate, Università degli Studi di Napoli "Parthenope," Napoli 80133, Italy. [28]Department of Chemistry, Stanford University, Stanford, CA 94305–5080, USA. [29]Department of Physics and McDonnell Center for the Space Sciences, Washington University, St. Louis, MO 63130, USA. [30]Department of Earth and Planetary Sciences and McDonnell Center for the Space Sciences, Washington University, St. Louis, MO 63130–4899, USA. [31]Astromaterials Research and Exploration Science, NASA, Johnson Space Center, Houston, TX 77058, USA.

*To whom correspondence should be addressed. E-mail: ssandford@mail.arc.nasa.gov

meteorites and IDPs (fig. S2A). For example, track 16 has a surface covered relatively uniformly with aromatic molecules. The organic mass distribution in this track was intermediate between typical spectra from primitive chondrites and individual IDPs. In the 78 to 300 atomic mass unit (amu) range, the predominant observed species are naphthalene ($C_{10}H_8$) (2 rings, 128 amu), phenanthrene ($C_{14}H_{10}$) (3 rings, 178 amu), and pyrene ($C_{16}H_{10}$) (4 rings, 202 amu), along with their alkylated homologs extending up to at least C_4-alkyl. This distribution strongly resembles that of matrix material in the Murchison carbonaceous chondrite and some IDPs (*7*). However, additional peaks not accounted for by simple 2-, 3-, and 4-ring C_n-alkyl-aromatics imply a more diverse suite of organics than found in Murchison. Peaks at 101, 112, 155, and 167 amu, inconsistent with simple PAHs, were observed when an attenuated laser photoionization pulse was used to minimize photofragmentation. These peaks could be due to O- and N-substituted aromatic species having hetero-functionality external to the aromatic structure, that is, not N- or O-heterocyclics. Similar mass peaks have been observed in several IDPs (*7*). The similarity to IDPs extends to masses beyond 300 amu; several track spectra show mass envelopes extending up to 800 amu with both odd and even mass peaks (fig. S2B). Such high-mass envelopes in IDPs have been attributed to polymerization of smaller aromatics within the samples by radiation processing during their extended exposure to interplanetary space or heating during atmospheric entry. Modification of the original PAH population by heating may also explain the higher mass envelopes observed in these Stardust impact tracks.

PAHs were also seen by TOF-SIMS analyses of a terminal particle extracted from aerogel (track 44, grain 4), a dissected aerogel keystone with a particle track split down the middle (track 21), and residues found in a large crater on Al foil C2009N. All PAHs were correlated to the presence of grains or the impact feature (fig. S3, B and C). Cometary samples from track and terminal particles typically show a steep decrease in PAH abundances with increasing number of C atoms in TOF-SIMS data, but this dependence is weaker for the crater residue (fig. S3A). This fractionation may be due to preferential loss of smaller PAHs during impact on the foil compared with the less violent deceleration into aerogel.

Aromatic materials are also seen using Raman spectroscopy. Raman spectra, acquired for 12 Stardust particles extracted from tracks 13 (1 particle), 17 (2 particles), and 35 (9 particles), are dominated by two broad bands centered at ~1360 Δcm^{-1} and ~1580 Δcm^{-1} (Fig. 1). These "D" and "G" bands, respectively, are characteristic of "disordered carbonaceous material"—graphite-like sp^2-bonded carbon in the form of condensed carbon rings. Relative peak sizes, peak positions, and widths of the D and G bands reflect the degree of disorder of the material and can provide constraints on the degree of thermal metamorphism experienced by organic materials (*8*, *9*).

The Raman spectra of the 12 Stardust particles are qualitatively similar to those of many IDPs and primitive meteorites (Fig. 1 and fig. S4), indicating the presence of relatively unmetamorphosed organic matter. The G-band parameters of the Stardust samples span the range observed in IDPs and meteorites (Fig. 1B). It is not clear whether this variation reflects heterogeneity in the cometary samples or variable processing during aerogel impact. However, the presence of points in the upper left of the plot indicates that at least some organics were captured with relatively little alteration. A variety of carbonaceous materials exhibit the D and G bands, including disordered graphite, large PAHs, and "kerogens" (aromatic moieties linked together in a disordered manner). These materials contain condensed aromatic rings but differ in chemical composition. In addition to C and H, meteoritic macromolecular organics contain substantial amounts of O, N, and S, both in the aromatic rings and in cross-linked side chains. Raman spectra can reflect such compositional differences in the overall fluorescent background of the spectrum. Many Raman spectra of Stardust particles are characterized by very high and increasing backgrounds similar to the spectra obtained from type II kerogen, some deuterium-rich IDPs (*10*), and primitive meteorites, indicating that the samples may be rich in noncarbon heteroatoms such as N, as confirmed by XANES and SIMS results [see below and (*11*)]. In a few cases, aromatic materials have also been identified by infrared (IR) spectroscopy (*6*).

IR spectra taken from tracks and individual extracted particles provide evidence for the presence of other, nonaromatic chemical functional groups. IR spectra of particles and tracks often contain absorption features at 3322 cm^{-1} (–OH), 3065 cm^{-1} (aromatic CH), 2968 cm^{-1} ($–CH_3$), 2923 cm^{-1} ($–CH_2–$), 2855 cm^{-1} ($–CH_3$ and $–CH_2–$), and 1706 cm^{-1} (C=O) (Fig. 2 and figs. S5 and S6) (*12*). When present, these features are particularly intense along the track walls. IR reflectance spectra of individual grains removed from impact tracks and pressed into Au substrates exhibit similar absorption features. One particle (track 35, grain 26) also showed a weak 2232 cm^{-1} band possibly due to –C≡N stretching vibrations. Raman spectra of three Stardust samples (track 35, grain 30; track 35, grain 32; and track 41, grain 7) are also consistent with the presence of alkane-type saturated hydrocarbons (fig. S4). Combined, these spectra data indicate the presence of aromatic, aliphatic, carboxylic, and N-containing functional groups.

The observed $–CH_2–$ (2923 cm^{-1})/$–CH_3$(2968 cm^{-1}) band-depth ratios in the returned samples is typically ~2.5 (*12*). This band-depth ratio is similar to the average value from IR spectra of anhydrous IDPs (*13*) but considerably larger than that seen in macromolecular material in primitive carbonaceous chondrites (~1.1) and the diffuse interstellar medium (ISM) (1.1 to 1.25). This suggests that the aliphatic moieties in Wild-2 particles are longer or less branched than those in the diffuse ISM. The

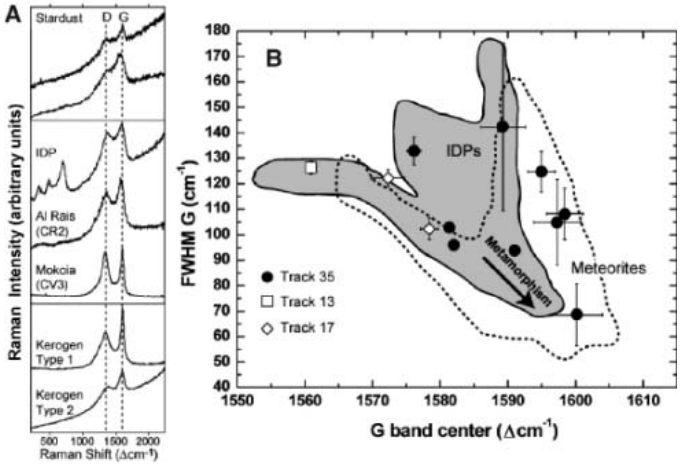

Fig. 1. (**A**) Raman spectra of Stardust particles from track 35, grain 30 and track 13, grain 1 (top pair) compared with the spectra of organics from extraterrestrial (middle three) and terrestrial (bottom pair) carbonaceous materials with different fluorescence backgrounds. All exhibit D and G bands characteristic of disordered sp^2-bonded carbon. The phyllosilicate bands below 1000 cm^{-1} in the IDP spectrum have not been seen in Stardust samples. (**B**) The G band position and width [full width at half maximum (FWHM)] of a material reflect its degree of thermal metamorphism and "structural ordering." The boundaries show the range of values from more than 40 chondritic meteorites (unshaded area with dashed outline) and 40 IDPs (shaded area with solid outline) analyzed in PET Raman laboratories (*9*, *10*, *29*). Analyzed Stardust particles (points) span the entire range seen in IDPs and meteorites. Organics in highly thermally metamorphosed meteorites plot to the lower right. The presence of Stardust points in the upper left indicates that at least some of the cometary organics are very primitive and were captured with relatively little alteration. One Stardust sample shows an unusually low G-band position (below 1570 cm^{-1}), suggesting diamond-like carbon that has been amorphized, for example, due to particle irradiation (*30*). One-sigma error bars represent measurement reproducibility and do not include estimates of possible interlaboratory biases.

band depth ratio of ~2.5 corresponds to a functional group ratio of $–CH_2–/–CH_3$ ~ 3.7 in the Wild 2 samples, assuming typical intrinsic band strengths for these features (*14*). The ratio of aromatic to aliphatic C–H is quite variable, with C–H stretching aromatic/aliphatic optical depth ratios ranging from below the detection limit to ~0.1 (*6*).

C,N,O-XANES analyses of thin sections of individual grains confirm the presence of 1s-π* transitions consistent with variable abundances of aromatic, keto/aldehydic, and carboxyl moieties, as well as amides and nitriles (Fig. 3A). XANES data suggest that considerably less H- and C-substituted sp^2-bonded C (olefinic and aromatic) is present than in highly primitive chondritic organic matter. Aliphatic C likely contributes to spectral intensity around 288 eV in most of the particles. One particle (particle 1 in Fig. 3A) has remarkably simple C chemistry, consistent with a predominance of alcohol and/or ether moieties. However, the XANES data generally indicate complex molecular structures variably rich in heteroatoms O and N and, compared with the macromolecular material in primitive meteorites, containing additional materials that are relatively poor in aromatic and olefinic C. The high abundances of heteroatoms and the low concentration of aromatic C in these organics differ greatly from the acid insoluble organic matter in meteorites and, in terms of thermal processing, appear to be more primitive.

XANES provides quantitative estimates of atomic O/C and N/C ratios present in the various functional groups identified (*6*). Care must be taken to account for O from any associated silicates or aerogel. Figure 3B shows that five of six organic-rich particles are richer in the heteroatoms O and N relative to both chondritic organic matter and the average composition of comet P/Halley particles measured by Giotto (*15*). The values are, however, qualitatively similar to the average O/C and N/C reported for stratospheric IDPs (*16*). Particles with such high O/C and N/C ratios are likely to be relatively labile [see below and (*6*)].

Particles 2 and 3 are particularly rich in N and exhibit abundant amide C in their XANES spectra (Fig. 3A). The presence of N-containing compounds is further suggested by studies of collector aerogel using LC-FD/TOF-MS. Although PET attention has largely focused on impacts in the aerogel and Al foils, Stardust may have returned a "diffuse" sample of gas-phase molecules that struck the aerogel directly or that diffused away from grains after impact. To test this possibility, samples of flight aerogel were carried through a hot water extraction and acid hydrolysis procedure (*17*) to determine if primary amine compounds were present in excess of those seen in controls.

With the exception of methylamine (MA) and ethylamine (EA), all amines detected in Stardust aerogel samples cell 2054, aerogel fragment 4 (hereafter C2054,4) and cell 2086, aerogel fragment 1 (hereafter C2088,1) were also present in the witness coupon aerogel sample (WCARMI1CPN,9). The absolute abundances of MA and EA are much higher, and the molar ratio of MA to EA in Stardust comet–exposed aerogel (C2054,4: 1.0 ± 0.1; C2086,1: 1.8 ± 0.2) is distinct from preflight aerogel (flight spare aerogel cell E243-13C, unflown: 10 ± 3) (*6*). The absence of MA and EA in the aerogel witness coupon suggests that these amines are cometary in origin. The concentrations of MA and EA in C2054,4 (0.6 to 2.2 parts per million) were similar to those present in C086,1, which was not located adjacent to a par-

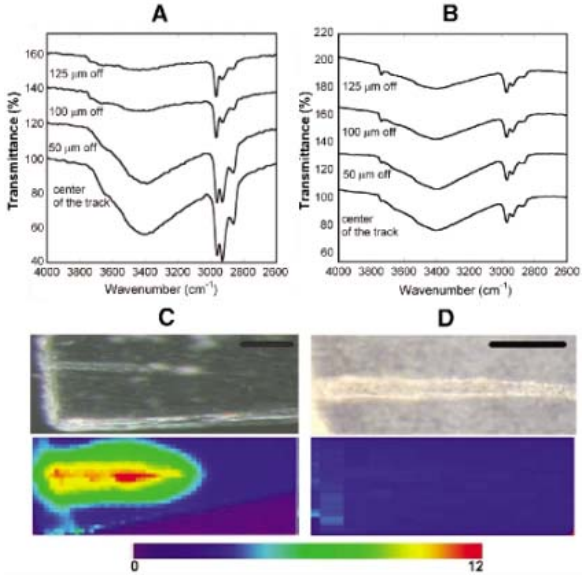

Fig. 2. IR transmittance spectra obtained along a line perpendicular to cometary impact tracks (**A**) track 59 and (**B**) track 61. In addition to aerogel features, the spectra of track 59 (A) display peaks at 3322 (broad), 2968, 2923, 2855, and 1706 cm^{-1} (not shown), both inside the track and extending outward into the aerogel. (B) track 61 exhibits only the aliphatic CH stretching feature dominated by the 2968 cm^{-1} peak and (Si-O) bands (not shown) characteristic of the flight aerogel. The optical images of the same tracks, with corresponding maps to the same scale showing the intensity distribution of the 2923 cm^{-1} peak ($–CH_2–$), are displayed in (**C**) and (**D**). The false-color image scale shown at the bottom is used in both maps, and the black scale bars correspond to 100 μm. In both cases, the entrance of the cometary particle is on the left side. The false-color map in (C) shows an increase in intensity of the 2923 cm^{-1} $–CH_2–$ peak in and near the track. The distributions of other organics peaks are similar. In contrast, the second track shown in (D) shows almost uniform distribution of the peak area centered at 2923 cm^{-1}; that is, the track shows only the features of aerogel.

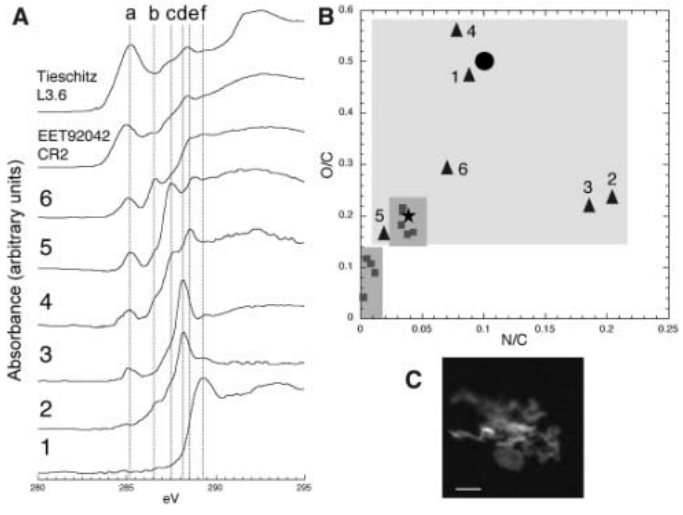

Fig. 3. (**A**) C-XANES spectra of six thin-section samples (1 to 6) compared with spectra of primitive (EET92042, CR2) and moderately processed (Tieschitz, L3.6) chondritic organic matter. Samples are 1, track 16, grain 1, mount 10; 2, track 35, grain 16, mount 4; 3, track 22, grain 1, mount 5; 4, track 35, grain 32, mount 10; 5, track 35, grain 32, mount 8; and 6, (track 13, grain, mount 5) (samples 4 and 5 are different thin sections of the same grain). Specific organic functional groups are highlighted (dashed lines a to f). a, C=C at ~285.2 eV; b, C=C–O at ~286.5 eV; c, C=O at ~287.5 eV; d, N–C=O at 288.2 eV; e, O–C=O at 288.6 eV; and f, C–O at 289.5 eV. Sample chemistry ranges enormously, with sp^2-bonded carbon varying from nonexistent in sample 1 to modest in samples 5 and 6 (relative to chondritic organic matter). (**B**) Atomic O/C and N/C for samples 1 to 6 derived from C,N,O-XANES analysis (black triangles) are compared with chondritic organic matter (gray squares, where the higher values correspond to petrologic type 1 and 2 and the lower values are type 3). Average values for comet Halley particles and stratospheric IDPs (*15*, *16*) are marked by a black star and a large solid circle, respectively. (**C**) An example of a sample thin section from track 35, grain 32, mount 8 (spectrum 5) revealed as a high-resolution (40-nm pixel size) STXM optical density image (scale bar, 1 μm) on the carbon 1s absorption edge.

ticle track, suggesting that these amines, if cometary, originate from submicron particles or gas that directly impacted the collector. Glycine is also present in samples C2054,4 and C086,1 at relative abundances that exceed those found in controls. This may indicate that a cometary component for this amino acid is also present. Compound-specific isotope measurements will be necessary to constrain the origin of these amines. No MA, EA, or glycine was detected in non–acid-hydrolyzed aerogel extracts. This suggests that these amines are present in an acid-soluble bound form rather than as a free primary amine. These results are consistent with the XANES detection of an amine-rich organic polymer in some of the recovered particles.

Raman (Fig. 1B), XANES (Fig. 3), and isotopic (*11*) data all demonstrate that the distribution of organics (overall abundance, functionality, and relative elemental abundances of C, N, and O) is heterogeneous both within particles and between particles. The STXM XANES results show variations in the physical distribution of these materials within particles, and the IR mapping of particle tracks (Fig. 2) shows the presence of organic features in some impact tracks but not others. The degree to which these variations represent heterogeneity in the original samples versus differences in impact processing is currently not fully constrained. On the whole, the chemical variations suggest that cometary organics do not represent an equilibrated reservoir of materials.

Most of the organic material in meteorites is in insoluble macromolecular phases. In contrast, the Stardust samples show evidence of abundant, relatively labile organics. In many cases, the organic components that produce the –OH, $–CH_3$, $–CH_2–$, and C=O IR absorption bands extend well beyond the visible edge of the track (Fig. 2). This suggests that the incoming particles contained organics that volatilized during impact and diffused into the surrounding aerogel. This material is unlikely to be due to impact-altered C from the aerogel because similar tracks are seen in the same aerogels that show no IR-detectable organics beyond those seen in the original aerogel (Fig. 2). All impacting particles had identical velocities, and tracks of similar length probably had similar impact energies. Consequently, similar amounts of organics would be expected in all tracks if this material came solely from reprocessing of C in the aerogel. Also, if impact-driven oxidation of C in the aerogel was occurring, the C=O band might be expected to be seen in and around all tracks, but this feature is only seen in tracks with the other organic features. Finally, locations near tracks show no deficits of the $–CH_3$ original to the aerogel, implying that the original C has not been substantially converted to other forms.

Hydrogen isotopic measurements were made by SIMS in fragments of five particles (*11*). D/H enrichments up to three times terrestrial were observed in three of five measured samples. D enrichments are often seen in meteoritic and IDP organics and are thought to be due to materials with an interstellar/protostellar chemical heritage (*18*–*20*). In all cases, the D-rich H is heterogeneously distributed within the samples and is associated with C, indicating it is organic. The elevated D/H ratios are comparable to those of many IDPs and meteoritic samples, although none of the cometary samples examined to date have shown ratios as extreme as the most anomalous values measured in some IDPs, meteorites, and some cometary coma gases.

Isotopic anomalies are also observed in C and N (*11*). As with IDPs and meteorites, these anomalies often appear in the form of "hot spots" that differ from the surrounding particle. NanoSIMS ion imaging demonstrates that N and S are associated with organic molecules (Fig. 4). The samples show a distribution of N/C ratios ranging from 0.005 to values approaching 1. Some particles exhibit the entire range of values, whereas others fall more uniformly at the high N/C end of the range, consistent with the XANES data (Fig. 3B). However, there are regions with high C content that are not rich in N. Sulfur is typically associated with C and N but is also distributed in small hot spots, presumably due to sulfides, which are commonly seen in the returned samples (*21*).

When observed, the D and/or ^{15}N enhancements provide clear evidence of a cometary origin for the organics and suggest that cometary organics contain a population with an interstellar/protostellar chemical heritage. Particles with measured isotopic anomalies are represented among the samples studied by other techniques by the Organics PET. For example, FC9,0,13,1,0 (track 13, grain 1) (particle 6 in Fig. 3) was examined by XANES, and track 13, particle 1; track 17, grain 1; and track 35, grain 25 were measured by Raman.

In terms of sample heterogeneity, the organics found in Stardust samples are similar to stratospheric IDPs and primitive meteorites. Like meteoritic organic matter, they contain both aromatic and nonaromatic fractions. However, the Stardust samples exhibit a greater range of compositions (higher O and N concentrations), include an abundant organic component that is poor in aromatics, and contain a more labile fraction. These latter two "components" could possibly be accounted for by a single population of organics. The nonaromatic fraction appears to be far more abundant, relative to aromatics, than is seen in meteorites. In general terms, the organics in Stardust samples are even more "primitive" than those in meteorites and IDPs, at least in terms of being highly heterogeneous and unequilibrated.

The Cometary and Interstellar Dust Analyzer (CIDA) TOF-MS instrument on the Stardust spacecraft detected very few particle impacts during the flyby (*22*). However, some of the returned mass spectra suggest the presence of particles with a nitrogen-rich chemistry and lower abundances of O, implying that nitriles or polycyanides may have been present (*22*). Although direct comparisons are not possible, studies of the samples confirm that N-rich components are present in the dust.

The presence of high O and N contents and the high ratios of $–CH_2–/–CH_3$ seen in the infrared data indicate that the Stardust organics are not similar to the organic materials seen in the diffuse ISM, which look more similar to the insoluble macromolecular material seen in primitive mete-

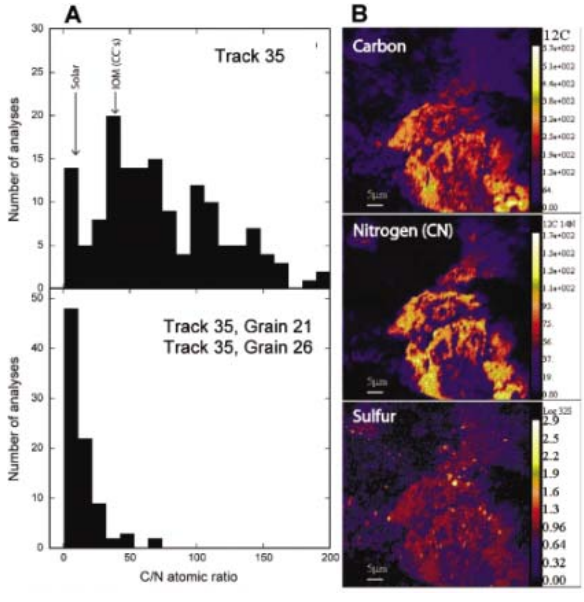

Fig. 4. Distribution of C and N. (**A**) Histograms of C/N ratios in organics in three different Stardust samples. One sample (top) shows a large spread in C/N, whereas two samples (bottom) have organics characterized by low C/N ratios, consistent with the presence of volatile organic molecules such as HCN or their polymer counterparts. (**B**) NanoSIMS images of the distribution of C, N, and S in a region of an aerogel sample from along track 35 containing cometary materials. The intensity of the signal increases from blue to red to bright yellow. C, N, and S distributions are clearly correlated, although considerable variations in their relative abundances are observed. S is also present in a population of hot spots that likely indicate the presence of sulfides. The color scale in the S map is logarithmic, in order to show the large difference in S count rates between the organics and the sulfides. The distribution of C and N is qualitatively similar in particles both with and without ^{15}N excesses. The location labeled IOM (CCs) in the upper left panel denotes the C/N ratio of the insoluble organic matter found in carbonaceous chondrites.

orites, but with even lower O/C ratios (*23*). This suggests that the Stardust organics are not the direct result of stellar ejecta or diffuse ISM processes but rather result from dense cloud and/or protosolar nebular processes. The high O and N contents, lower aromatic contents, and elevated $–CH_2–/–CH_3$ ratios are all qualitatively consistent with what is expected from radiation processing of astrophysical ices and the polymerization of simple species such as HCO, H_2CO, and HCN (*24*–*26*).

The Stardust samples clearly contain an organic component that is more labile than the materials seen in meteorites and IDPs. These labile materials may be absent from stratospheric IDPs because they are lost during atmospheric entry heating and/or are destroyed or modified by radiation during the IDPs' transit from parent body to Earth. Given the O- and N-rich nature of the Stardust materials, these labile organics could represent a class of materials that have been suggested as parent molecules to explain the extended coma sources of some molecular fragments like CN (*27*, *28*). The high O/C and N/C ratios of the samples fall well outside the range of most meteorites and, interestingly enough, reach higher values than those observed at comet Halley by the Giotto spacecraft (*15*). In this respect, some of the returned material appears to represent a new class of organics not previously observed in other extraterrestrial samples.

References and Notes

1. M. C. Festou, H. U. Keller, H. A. Weaver, Eds., *Comets II* (Univ. of Arizona Press, Tucson, AZ, 2004).
2. A. H. Delsemme, *Adv. Space Res.* **12**, 5 (1992).
3. C. F. Chyba, C. Sagan, *Nature* **355**, 125 (1992).
4. D. E. Brownlee *et al.*, *J. Geophys. Res.* **108**, E10, 8111, p. 1-1 (2003).
5. D. E. Brownlee *et al.*, *Science* **314**, 1711 (2006).
6. Materials and methods are available as supporting material on *Science* Online.
7. S. Clemett, C. Maechling, R. Zare, P. Swan, R. Walker, *Science* **262**, 721 (1993).
8. B. Wopenka, J. D. Pasteris, *Am. Mineral.* **78**, 533 (1993).
9. L. Bonal, E. Quirico, M. Bourot-Denise, G. Montagnac, *Geochim. Cosmochim. Acta* **70**, 1849 (2006).
10. B. Wopenka, *EPSL* **88**, 221 (1988).
11. K. D. McKeegan *et al.*, *Science* **314**, 1724 (2006).
12. L. P. Keller *et al.*, *Science* **314**, 1728 (2006).
13. G. Matrajt *et al.*, *Astron. Astrophys.* **433**, 979 (2005).
14. S. A. Sandford *et al.*, *Astrophys. J.* **371**, 607 (1991).
15. J. Kissel, F. R. Krueger, *Nature* **326**, 755 (1987).
16. G. J. Flynn, L. P. Keller, S. Wirick, C. Jacobsen, *Proceedings of the 8th International Conference on X-ray Microscopy*, IPAP Conf. Series **7**, 315 (2006).
17. D. P. Glavin *et al.*, *Meteorit. Planet. Sci.* **41**, 889 (2006).
18. S. Messenger, *Nature* **404**, 968 (2000).
19. J. Aléon, F. Robert, *Icarus* **167**, 424 (2004).
20. H. Busemann *et al.*, *Science* **312**, 727 (2006).
21. M. E. Zolensky *et al.*, *Science* **314**, 1741 (2006).
22. J. Kissel, F. R. Krueger, J. Silén, B. C. Clark, *Science* **304**, 1774 (2004).
23. Y. J. Pendleton, L. J. Allamandola, *Astrophys. J. Suppl. Ser.* **138**, 75 (2002).
24. M. P. Bernstein, S. A. Sandford, L. J. Allamandola, S. Chang, M. A. Scharberg, *Astrophys. J.* **454**, 327 (1995).
25. W. A. Schutte, L. J. Allamandola, S. A. Sandford, *Icarus* **104**, 118 (1993).
26. G. Strazzulla, G. A. Baratta, M. E. Palumbo, *Spectrochim. Acta A* **57**, 825 (2001).
27. M. J. Mumma, P. R. Weissman, S. A. Stern, in *Protostars and Planets III*, E. H. Levy, J. I. Lunine, M. S. Matthews, Eds. (Univ. of Arizona Press, Tucson, AZ, 1993), pp. 1171–1252.
28. G. Strazzulla, *Space Sci. Rev.* **90**, 269 (1999).
29. E. Quirico, J. Borg, P.-I. Raynal, G. Montagnac, L. D'Hendecourt, *Planet. Space Sci.* **53**, 1443 (2005).
30. G. A. Baratta *et al.*, *J. Raman Spectrosc.* **35**, 487 (2004).

31. The Stardust Organics Preliminary Examination Team is grateful to NASA for funding and supporting the mission and to the hundreds of other team members that were involved in design, construction, flying, and recovery of the mission. The Organics Team, from 31 organizations, gratefully acknowledges their supporting institutions.

Supporting Online Material

www.sciencemag.org/cgi/content/full/314/5806/1720/DC1
Materials and Methods
Figs. S1 to S9
References

3 October 2006; accepted 9 November 2006
10.1126/science.1135841

REPORT

Isotopic Compositions of Cometary Matter Returned by Stardust

Kevin D. McKeegan,[1*] Jerome Aléon,[2,3,4] John Bradley,[3] Donald Brownlee,[5] Henner Busemann,[6] Anna Butterworth,[7] Marc Chaussidon,[8] Stewart Fallon,[3,4] Christine Floss,[9] Jamie Gilmour,[10] Matthieu Gounelle,[11] Giles Graham,[3] Yunbin Guan,[12] Philipp R. Heck,[13] Peter Hoppe,[13] Ian D. Hutcheon,[3,4] Joachim Huth,[13] Hope Ishii,[3] Motoo Ito,[14] Stein B. Jacobsen,[15] Anton Kearsley,[16] Laurie A. Leshin,[17] Ming-Chang Liu,[1] Ian Lyon,[10] Kuljeet Marhas,[9] Bernard Marty,[8] Graciela Matrajt,[5] Anders Meibom,[11] Scott Messenger,[14] Smail Mostefaoui,[11] Sujoy Mukhopadhyay,[15] Keiko Nakamura-Messenger,[14,18] Larry Nittler,[6] Russ Palma,[19,20] Robert O. Pepin,[20] Dimitri A. Papanastassiou,[21] François Robert,[11] Dennis Schlutter,[20] Christopher J. Snead,[7] Frank J. Stadermann,[9] Rhonda Stroud,[22] Peter Tsou,[21] Andrew Westphal,[7] Edward D. Young,[1] Karen Ziegler,[1] Laurent Zimmermann,[8] Ernst Zinner[9]

Hydrogen, carbon, nitrogen, and oxygen isotopic compositions are heterogeneous among comet 81P/Wild 2 particle fragments; however, extreme isotopic anomalies are rare, indicating that the comet is not a pristine aggregate of presolar materials. Nonterrestrial nitrogen and neon isotope ratios suggest that indigenous organic matter and highly volatile materials were successfully collected. Except for a single ^{17}O-enriched circumstellar stardust grain, silicate and oxide minerals have oxygen isotopic compositions consistent with solar system origin. One refractory grain is ^{16}O-enriched, like refractory inclusions in meteorites, suggesting that Wild 2 contains material formed at high temperature in the inner solar system and transported to the Kuiper belt before comet accretion.

The isotopic compositions of primitive solar system materials record evidence of chemical and physical processes involved in the formation of planetary bodies ~4.6 billion years ago and, in some cases, provide a link to materials and processes in the molecular cloud that predated our solar system. The vast majority of isotopic analyses of extraterrestrial materials have been performed on chondritic (undifferentiated) meteorites, samples of asteroids that likely accreted at 2 to 4 astronomical units (AU) within the first few million years of solar system history. Comets formed in much colder regions of the protoplanetary disk and are widely considered to consist of more primitive matter than even the most unequilibrated meteorites.

Analyses of isotope compositions of comets are rare. Measurements of D/H, $^{13}C/^{12}C$, $^{15}N/^{14}N$, or $^{18}O/^{16}O$ have been made for a few abundant molecules in gases of several comet comae by ground-based spectroscopy (*1*–*3*) and of comet P/Halley by mass spectrometers on the Giotto spacecraft (*4*). Direct measurements of isotope compositions in the dust fraction of comets are limited to low-precision data from the Halley flyby (*5*). Isotopic measurements of stratosphere-collected interplanetary dust particles (IDPs) demonstrate the highly primitive nature of many anhydrous IDPs [e.g., (*6*, *7*)]; however, a cometary origin for specific individual particles cannot be ascertained. Here, we report laboratory analyses of the light "stable" isotopes of H, C, N, O, and Ne in individual grains, particle fragments, crater debris, and/or trapped volatile materials collected from comet 81P/Wild 2 and returned to Earth by the NASA Discovery Mission, Stardust.

The goals of the Isotope Preliminary Examination Team analyses are to provide first-order answers to questions relating to the provenance of Wild 2 dust: (i) Does the comet consist of a mechanical agglomeration of essentially unprocessed, or perhaps only thermally annealed, presolar materials? (ii) Do comets provide a well-preserved reservoir of circumstellar dust grains (*8*) with distinct nucleosynthetic histories (i.e., stardust)? (iii) Can isotopic signatures establish whether extraterrestrial organic materials are present above contamination levels? (iv) What are the

relations to known isotope reservoirs in meteoritic samples and in IDPs? (v) What are the implications for mixing and thermal processing in the early solar system? The preliminary examination has focused on the abundant light elements H, C, N, and O and on light noble gases because they have characteristic isotopic signatures that vary widely in solar system materials [e.g., (*9*)] and compositions that can often be linked to distinct astrophysical environments and/or processes.

Hydrogen isotopic compositions in bulk fragments of five Wild 2 particles (see supporting online material) range from values similar to those of terrestrial and chondritic particles, up to moderate D/H enhancements of about three times the D/H in mean ocean water (Fig. 1, table S1). Variations in δD within a particle are also observed with some "hotspots" having a δD up to 2200 ± 900 per mil (‰) (*10*). All the observed D enrichments are associated with carbon, although only one of the samples (T17) is dominated by carbonaceous material. Although overlapping the range of values observed for IDPs (*11*, *12*) and water in (Oort cloud) comets (*4*), the maximum D/H is well below that characteristic of a minor component of organic matter in anhydrous IDPs, especially of the low-density "cluster" type thought to be derived from comets (*13*). The maximum D/H values of Wild 2 grains are also far less than those measured in small hotspots of insoluble organic matter separated from carbonaceous chondrites (*14*) and in cometary HCN ice (*15*), which are both thought to have close affinities to organic material produced at very low temperatures in molecular cloud environments. It is not known if this relative paucity of highly D-enriched matter signifies an intrinsic difference between Wild 2 samples and macromolecular materials in IDPs and carbonaceous chondrites. It is also possible that D/H signatures were modified during impact. Because of the association with carbon and the lack of evidence for any hydrated minerals in Wild 2 particles, it is unlikely that D/H values can be ascribed to Wild 2 water.

Some cometary volatiles appear to have been captured. Helium, neon, and argon abundances, as well as $^{20}Ne/^{22}Ne$ ratios, were analyzed in two bulbous sections of an impact track that contains fragments of fine-grained impactor material mixed with melted aerogel along its periphery. Noble gases in a control sample (unexposed aerogel taken from the rear portion of a collector cell) are consistent with system blanks, indicating that flight aerogel does not contain a detectable background of noble gases. In contrast, aerogel fragments containing the impact track show excess He and Ne above blank levels by factors of 3 to 4 (table S2), suggesting that the very rapid time scales (<μs) for melting of aerogel during deceleration of comet particles helped trap indigenous cometary volatiles. This inference is supported by measured $^{20}Ne/^{22}Ne$ ratios, which are significantly higher than that in air. In a $^{22}Ne/^{20}Ne$ versus $^{4}He/^{20}Ne$ diagram (fig. S1), the data do not lie on a pure mixing trajectory between air and the solar composition but instead point toward a nonatmospheric end-member with a $^{4}He/^{20}Ne$ ratio lower than solar, consistent with expectations for comets due to preferential trapping of heavier noble gases in ice accreted at ~30 K (*16*).

Carbon and nitrogen isotope analyses were made by isotopic mapping with NanoSIMS instruments, measuring atomic ions of C^- and isotopologs of the intense CN^- beam, respectively. Microtomed particles extracted from aerogel, as well as Al-foil crater debris, were mapped with a spatial resolution of ~100 nm to search for isotopic anomalies that could identify circumstellar dust grains like the C- and N-rich phases (SiC, Si_3N_4, graphite) found in primitive meteorites (*17*). No circumstellar dust grains were definitively identified despite an intensive search comprising more than 20 slices and fragments from a dozen particles and ~5700 μm^2 of debris in and around six small (<2 μm) and four large (>50 μm) craters on Al-foil collectors. This result contrasts sharply with inferences of a population of nearly pure ^{12}C grains in comet Halley (*5*). One ~150-nm region from the bottom of a large Al-foil crater has an isotopic composition ($\delta^{13}C = 59 \pm 61‰$; $\delta^{15}N = -518 \pm 60‰$) that falls in a range consistent with "mainstream" presolar SiC grains (*17*); however, the grain was sputtered away before a mineral identification could be made. Another hotspot was enriched in ^{13}C ($\delta^{13}C = 964 \pm 219‰$) and depleted in ^{15}N ($\delta^{15}N = -415 \pm 94‰$), typical of mainstream SiC; however, the ion-emission area was not as localized as would be expected for a very small circumstellar grain and, moreover, showed a high abundance of nitrogen (inferred C/N ~ 3). This grain disappeared rapidly during analysis, as did a second spot with a low inferred C/N ratio ≈ 6 and low $\delta^{15}N \approx -350‰$. This behavior is consistent with sputtering of labile organic material. Notably, this isotopically light nitrogen component is rarely seen in IDPs (*7*, *18*), but within ~10% uncertainties, is consistent with estimates of the nitrogen isotopic composition in HCN gas from comet Hale Bopp (*19*) and of the solar composition based on analyses of the jovian atmosphere (*20*) and of solar wind implanted in lunar grains (*21*).

On a micrometer scale, all samples are homogeneous in both C and N isotope compositions and show no correlation between $\delta^{13}C$ and $\delta^{15}N$ (Fig. 2). Carbon isotopes fall in a particularly restricted range with most "bulk" $\delta^{13}C$ values falling between −20 and −50‰. This range is somewhat higher than recent estimates ($\delta^{13}C = -105 \pm 20‰$) of the solar carbon isotope composition (*22*), but is compatible with carbon isotopes in other primitive solar system matter including IDPs (*6*) and most organic matter in chondrites (*23*).

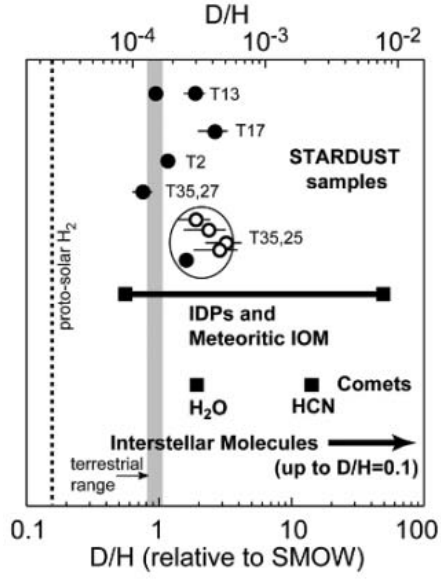

Fig. 1. Hydrogen isotopic compositions in bulk fragments (solid circles) of five Wild 2 particles and in micrometer-sized subareas of one particle (open circles) compared to SMOW and to ranges of laboratory measurements of D/H in IDPs and in insoluble organic matter (IOM) from chondritic meteorites. Also shown are an estimate for protosolar H_2 and ranges of D/H measured remotely for specific gaseous molecules from comets and for molecular clouds. Error bars are 1σ.

[1]Department of Earth and Space Sciences, University of California Los Angeles, Los Angeles, CA 90095–1567, USA. [2]Centre de Spectrometrie Nucleaire et de Spectrometrie de Masse, Bat 104, 91405 Orsay Campus, France. [3]Institute of Geophysics and Planetary Physics, Lawrence Livermore National Laboratory, Livermore, CA 94550, USA. [4]Glenn T. Seaborg Institute, Lawrence Livermore National Laboratory, Livermore, CA 94550, USA. [5]Department of Astronomy, University of Washington, Seattle, WA 98195, USA. [6]Department of Terrestrial Magnetism, Carnegie Institution of Washington, 5241 Broad Branch Road, NW, Washington, DC 20015, USA. [7]Space Sciences Laboratory, University of California, 7 Gauss Way, Berkeley, CA 94720–7450, USA. [8]Centre de Recherches Petrographiques et Geochimiques, 15 rue Notre Dame des Pauvres, BP 20, 54501 Vandoeuvre lès Nancy, France. [9]McDonnell Center for the Space Sciences, Department of Physics, Washington University, St. Louis, MO 63130, USA. [10]School of Earth, Atmospheric and Environmental Sciences, The University of Manchester, Manchester M13 9PL, UK. [11]Museum National d'Histoire Naturelle, Laboratoire d'Etude de la Matiere Extraterrestre, 57 rue Cuvier, 75005 Paris, France. [12]Division of Geological and Planetary Sciences, California Institute of Technology, Pasadena, CA 91125, USA. [13]Max-Planck-Institute for Chemistry, Particle Chemistry Department,].-].-Becherweg 27, D-55128 Mainz, Germany. [14]Robert M. Walker Laboratory for Space Science, Astromaterials Research and Exploration Science Directorate NASA Johnson Space Center, Houston, TX 77058, USA. [15]Department of Earth and Planetary Sciences, Harvard University, 20 Oxford Street, Cambridge, MA 02138, USA. [16]Impacts and Astromaterials Research Centre, Department of Mineralogy, Natural History Museum, Cromwell Road, South Kensington, London SW7 5BD, UK. [17]Sciences and Exploration Directorate, NASA Goddard Space Flight Center, Greenbelt, MD 20771, USA. [18]Jacobs Sverdrup, Houston, TX 77058, USA. [19]Department of Physics and Astronomy, Minnesota State University, 141 Trafton Science Center N, Mankato, MN 56001, USA. [20]School of Physics and Astronomy, University of Minnesota, 116 Church Street, SE, Minneapolis, MN 55455, USA. [21]Science Division, Jet Propulsion Laboratory, 4800 Oak Grove Drive, Pasadena, CA 91109, USA. [22]Code 6360, Naval Research Laboratory, Washington, DC 20375, USA.

*To whom correspondence should be addressed. E-mail: mckeegan@ess.ucla.edu

A wider range is observed for "bulk" nitrogen with many samples clustering near 0‰ (atmospheric) but others showing modest $\delta^{15}N$ enrichments of +100 up to ~500‰, similar to the range observed for anhydrous IDPs (*7*). On a submicrometer scale, more-extreme values are found with a maximum $\delta^{15}N$ of 1300 ± 400‰, similar to the highest values found in refractory organic matter in IDPs (*7*) and meteorites (*14*). Unlike IDPs, however, the Wild 2 samples display both low and high $\delta^{15}N$, indicating an unequilibrated mixture of a low-$\delta^{15}N$ (perhaps icy) component and a more refractory (high C/N) organic material with high $\delta^{15}N$ and isotopically "normal" carbon. The fact that most IDPs are characterized by ^{15}N excesses may reflect the instability of the more labile, low-$\delta^{15}N$ component during atmospheric-entry heating. Thus, the Wild 2 samples could represent a different type of organic material than that available for study through the stratospheric IDPs, although it is puzzling that the Wild 2 particles analyzed thus far appear to be deficient in total organic matter compared to most IDPs. This observation contradicts expectations of comets as being very rich in organic matter and may indicate that much of the Wild 2 organic matter did not survive the capture process as discrete phases still closely associated with silicate minerals.

Oxygen is the most abundant element in rocky planets, asteroids, and comets and exhibits distinctive isotopic compositions that are essentially unique to each class of planetary materials from the inner solar system (*24*). Although the isotopic variations that occur on planetary scales are relatively subtle (less than a few ‰), individual components of unequilibrated meteorites have oxygen isotope compositions varying by 50‰ or more in relative abundances of ^{16}O [e.g., (*9*)]. These isotopic variations are fairly systematic (*25*) and, together with planetary-scale variations, imbue oxygen with a unique diagnostic capability to indicate sample provenance (*24*). Orders-of-magnitude larger isotopic variations are observed in presolar oxide and silicate dust grains that condensed in the outflows of evolved, mass-losing stars and inherited specific isotopic compositions due to local nucleosynthetic processes (*26*). Few definitive data exist regarding oxygen isotope compositions in cometary materials. In situ measurements of water ice from comet Halley, made by the Giotto mission, yield $\delta^{18}O = 12 \pm 75$‰, but no measurement of $\delta^{17}O$ is available (*4*).

Oxygen isotope measurements of Wild 2 samples were made by mapping techniques to search for presolar grains and by focused probe SIMS on individual particle fragments to relate the comet samples to known classes of meteoritic materials. Of some 2 dozen particle fragments prepared as microtomed (<200 nm thick) sections from aerogel keystones, no candidate presolar grains were identified on the basis of extreme oxygen isotope anomalies (supporting online material). For several samples, the measurement of oxygen isotopes was compromised by mixing with melted aerogel, which could not be resolved even with the <100-nm spatial resolution of the NanoSIMS. Therefore, residues from impact craters in the Al-foil targets were also examined by high-resolution isotope mapping.

Thirty-seven small craters, between 320 nm and 1.5 μm in diameter, and four large craters (59, 72, 140, and >200 μm in diameter) were mapped, resulting in the identification of ~10^4 O-rich subareas. Only one presolar grain was found (Fig. 3). The ~250-nm grain is highly enriched in ^{17}O and slightly depleted in ^{18}O compared to solar system samples and has a composition of $^{17}O/^{16}O = (1.01 \pm 0.20) \times 10^{-3}$ and $^{18}O/^{16}O = (1.77 \pm 0.24) \times 10^{-3}$. This isotopic composition is typical for presolar oxide (and silicate) grains belonging to "group 1," thought to originate in red giant or asymptotic giant-branch stars (*26*). Unfortunately, the mineralogy of the grain could not be determined, although it is likely that it was a relatively refractory oxide or silicate.

High-precision oxygen isotope measurements were made in 5- to 10-μm spots of individual "terminal grains" separated from aerogel tracks and pressed into clean Au foil. Fragments from one enstatite-rich grain (T69) and one forsterite-rich grain (T22) have similar oxygen isotope compositions that plot slightly below the terrestrial mass-dependent fractionation (TF) line and to the low $\delta^{18}O$ side of the ^{16}O-mixing line that characterizes refractory components (calcium- and aluminum-rich inclusions, CAIs) in chondrites (Fig. 4; table S2). Although unlikely, we cannot exclude the possibility that the deviation of the T69 and T22 data from the CAI mixing line is due to minor contamination with aerogel (supporting online material). The oxygen isotopic compositions of these Mg-rich silicates from Wild 2 are compatible with those of most mafic silicate minerals from carbonaceous chondrite chondrules.

Oxygen isotopes were also measured in a polymineralic refractory grain (T25, "Inti") by means of both NanoSIMS mapping and higher-precision IMS 1270 spot measurements (supporting online material). The sample consists of a fine-grained mix of spinel, Al-rich diopside, melilite, and anorthite, with a minor component of perovskite (*27*). Although the NanoSIMS analyses resolve individual phases, it was not possible to avoid sampling multiple mineral phases during the IMS 1270 analyses (5-μm-diameter spot). The consistency of the data (Fig. 4) demonstrates that the sample is isotopically homogeneous with an ^{16}O-rich composition compared to most planetary materials ($\delta^{18}O \approx \delta^{17}O \approx -40$‰). Notably, this composition is virtually identical to that of a large population of CAIs and refractory oxide grains in chondrites (*9*). Similarly ^{16}O-enriched compositions have been observed for rare refractory IDPs collected in the stratosphere (*28*), but the relation between these particles and meteoritic CAIs has not been thoroughly investigated.

As an ensemble, the isotopic compositions of the light elements—H, C, N, O, and Ne—demonstrate that the dust of comet Wild 2 is an unequilibrated aggregate of material from different sources. The H, C, and N isotope compositions indicate the presence of several minor components that are isotopically fractionated to a large extent, probably reflecting chemical reactions at very low temperatures like those characteristic of molecular cloud or, possibly, Edgeworth-Kuiper belt environments. This is consistent with a general view of Jupiter family comets as having accreted from cold materials at the edge of the solar nebula.

Two observations, however, run counter to expectations: (i) The abundance of presolar grains appears to be low compared with that of primitive meteorites and IDPs, and (ii) the comet contains high-temperature silicate and oxide minerals with oxygen isotopic compositions essentially identical to those of analogous minerals in carbonaceous chondrites. The first observation could perhaps be explained as a preservation effect, i.e., loss of presolar materials during impact, yet the one presolar grain firmly identified was found in the residue of the largest impact crater so far investigated (the grain

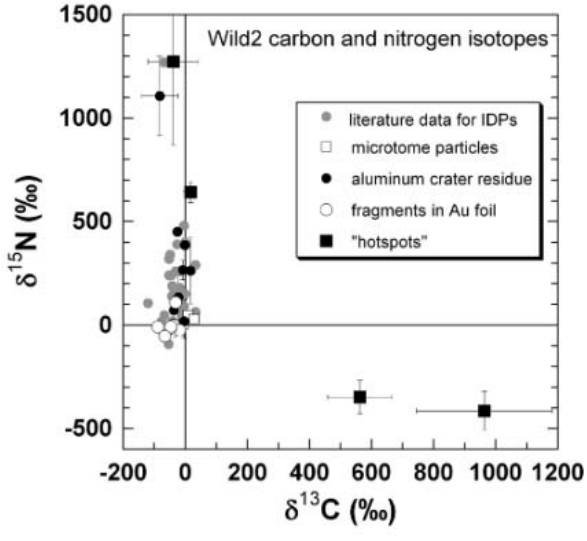

Fig. 2. Correlated carbon and nitrogen isotopic compositions of individual cometary grains compared with literature data (gray circles) for stratosphere-collected IDPs (*7*). Shown are average values for cometary grains prepared as microtome sections (open squares), for fragments extracted from aerogel and pressed into Au foil (open circles), and for residue in and surrounding craters in the Al foil collector (solid circles). Also shown are selected hotspots (solid squares) from the crushed samples. Error bars are 2σ.

actually punctured the Al foil). If similar grains were abundant, they should have been seen in or around other craters and in the aerogel as well. However, if most of the presolar material in Wild 2 consists of interstellar amorphous silicates rather than circumstellar mineral grains, then it is possible that these would not be recognized either because of too much mixing with aerogel or, in the case of residue in Al-foil craters, because they might not possess sufficiently anomalous oxygen isotopic compositions to be identified as nonsolar. On the other hand, the crystalline silicate and oxide minerals for which we have oxygen isotope data could not have formed by annealing (devitrification) of presolar amorphous silicates in the Kuiper belt. Not only is such an origin incompatible with the chemistry and mineralogy of these grains, but, because these grains differ markedly in their relative ^{16}O abundances, they also could not have formed from a single isotopic reservoir. The similarity in O-isotope composition between Wild 2 grains and materials from carbonaceous chondrites is pronounced. Identifying precisely what regions of the inner solar system may be sampled by this comet is clearly central to understanding the scale of radial mixing outward in the solar protoplanetary disk.

Most interstellar silicate dust is thought to be amorphous (*29*), and with recent recognition of the relatively large fraction of crystalline silicates in comets and in protostellar disks based on infrared spectral data [e.g., (*30*)], astronomers have postulated mixing of dust from inner warm regions, where ambient conditions are above glass transition temperatures, outward to Kuiper belt regions [e.g., (*31*, *32*)]. However, other observations suggest production of crystalline silicates (specifically forsterite) at large (>10 AU) stellar distances (*33*). That the CAI-like particle (Inti) has the same intrinsic oxygen isotopic properties as CAIs from all major classes of primitive meteorites argues strongly for an origin in the same source region as meteoritic CAIs (*9*). One possibility is that this region could be at the inner truncation of the accretion disk (<0.1 AU) where very high temperatures exist. Here, winds associated with bipolar outflows, driven by interactions of the young Sun with the accretion disk, can carry small refractory particles to large heliocentric distances where they can accrete together with cold, icy materials (*34*, *35*). Other models (*36*) invoke turbulent transport of hot inner nebula (silicate) dust out to zones of comet accretion, which could account for the carbonaceous chondrite-like isotopic compositions of Wild 2 olivine and pyroxene grains. We conclude that the coupled oxygen isotopic and mineralogic data are best understood as indicating that a large fraction of dust in comet Wild 2 is derived from chemically and thermally processed precursors from the inner solar system, consistent with predictions of the X-wind and other models (*34*–*36*) for the protosolar disk.

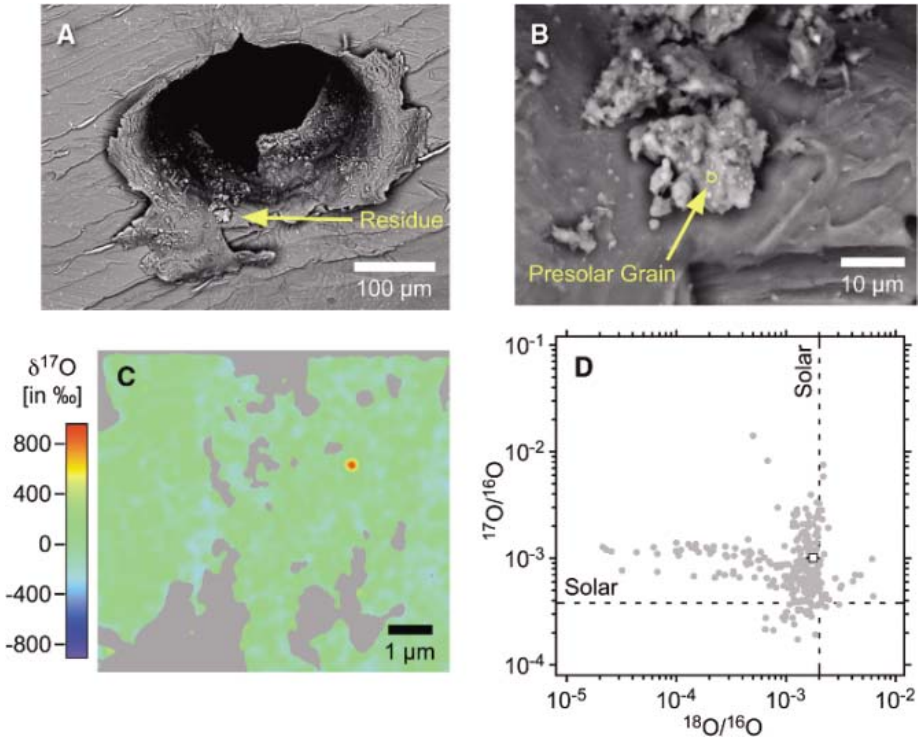

Fig. 3. Presolar grain discovered in residue of crater C2086W1. (**A**) Backscattered electron image of a crater which punctured the Al foil. (**B**) Electron image of projectile residue in crater lip. (**C**) False-color isotope map of $\delta^{17}O$ measured by high-resolution NanoSIMS. (**D**): Oxygen three-isotope plot of presolar grain (open square) compared to literature data for presolar oxide grains separated from meteorites. On this scale, all materials formed in the solar system plot at the intersection of the two dashed lines. Error bars are 1σ.

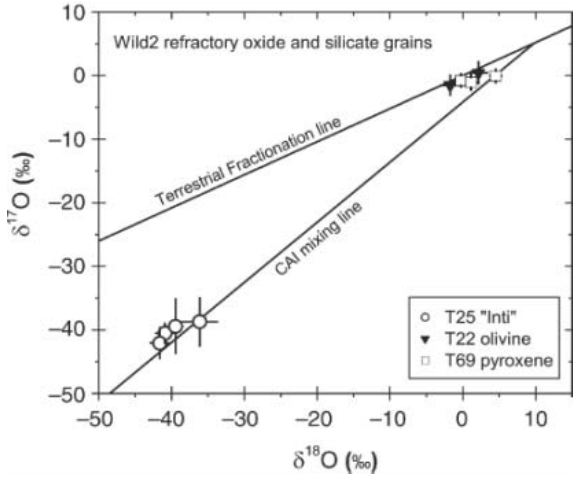

Fig. 4. Oxygen isotopic compositions of individual cometary grains. The terrestrial mass-dependent fractionation line (TF) and the CAI-mixing line are shown for reference. Error bars are 2σ.

References and Notes

1. D. Hutsemekers *et al.*, *Astron. Astrophys.* **440**, L21 (2005).
2. E. Jehin *et al.*, *Astrophys. J.* **613**, L161 (2004).
3. C. Arpigny *et al.*, *Science* **301**, 1522 (2003).
4. P. Eberhardt, M. Reber, D. Krankowsky, R. R. Hodges, *Astron. Astrophys.* **302**, 301 (1995).
5. E. K. Jessberger, *Space Sci. Rev.* **90**, 91 (1999).
6. S. Messenger, F. J. Stadermann, C. Floss, L. R. Nittler, S. Mukhopadhyay, *Space Sci. Rev.* **106**, 155 (2003).
7. C. Floss *et al.*, *Geochim. Cosmochim. Acta* **70**, 2371 (2006).
8. We differentiate, in principle, between different types of presolar materials: "circumstellar" dust grains formed as condensates in the ejecta of evolved stars—hence they are literally stardust—whereas presolar dust also includes dust particles that were formed or reprocessed in the interstellar medium. In practice, it is not clear if the latter could be recognized solely on the basis of isotopic compositions (given that radiometric dating is not yet possible).
9. K. D. McKeegan, L. A. Leshin, *Rev. Mineral. Geochem.* **43**, 279 (2001).
10. The delta notation expresses the relative deviation of a measured composition from that of a standard reference material in parts per thousand. Thus, $\delta D = [(D/H)_{sample}/(D/H)_{standard} - 1] \times 1000$ and similarly for $\delta^{13}C$, $\delta^{15}N$, and $\delta^{17}O$, etc. The conventional reference standards are used here: standard mean ocean water (SMOW) for

H and O, Pee Dee belemnite (PDB) for C, and air for N. Absolute values for these standards are defined as $(D/H)_{SMOW} = 1.556 \times 10^{-4}$; $(^{18}O/^{16}O)_{SMOW} = 2.0052 \times 10^{-3}$; $(^{17}O/^{16}O)_{SMOW} = 3.8288 \times 10^{-4}$; $(^{13}C/^{12}C)_{PDB} = 1.12372 \times 10^{-2}$; $(^{15}N/^{14}N)_{Air} = 3.6765 \times 10^{-3}$. Unless noted, reported uncertainty estimates are 2σ (standard error).
11. S. Messenger, R. M. Walker, in *Astrophysical Implications of the Laboratory Study of Presolar Materials*, T. J. Bernatowicz, E. K. Zinner, Eds. (American Institute of Physics, St. Louis, MO, 1997), AIP Conf. Proc. vol. 402, pp. 545–564.
12. J. Aléon, C. Engrand, F. Robert, M. Chaussidon, *Geochim. Cosmochim. Acta* **65**, 4399 (2001).
13. S. Messenger, *Nature* **404**, 968 (2000).
14. H. Busemann *et al.*, *Science* **312**, 727 (2006).
15. R. Meier *et al.*, *Science* **279**, 1707 (1998).
16. A. Bar-Nun, T. Owen, in *Solar System Ices*, B. B. Schmidt, C. De Bergh, M. Festou, Eds. (Kluwer, Norwell, MA, 1998), pp. 353–366.
17. D. D. Clayton, L. R. Nittler, *Annu. Rev. Astron. Astrophys.* **42**, 39 (2004).
18. J. Aléon, F. Robert, M. Chaussidon, B. Marty, *Geochim. Cosmochim. Acta* **67**, 3773 (2003).
19. D. C. Jewitt, H. E. Matthews, R. Meier, *Science* **278**, 90 (1997).
20. T. Owen, T. Encrenaz, *Space Sci. Rev.* **106**, 121 (2003).
21. K. Hashizume, M. Chaussidon, B. Marty, F. Robert, *Science* **290**, 1142 (2000).
22. K. Hashizume, M. Chaussidon, B. Marty, K. Terada, *Astrophys. J.* **600**, 480 (2004).
23. F. Robert, S. Epstein, *Geochim. Cosmochim. Acta* **46**, 81 (1982).
24. R. N. Clayton, *Annu. Rev. Earth Planet. Sci.* **21**, 115 (1993).
25. For example, CAIs are nearly always enriched in ^{16}O compared to chondrules, and carbonaceous chondrite materials are more ^{16}O-enriched than their petrologically similar counterparts (chondrules, matrix, etc.) in ordinary chondrites.
26. L. R. Nittler, in *Astrophysical Implications of the Laboratory Study of Presolar Materials*, T. J. Bernatowicz, E. K. Zinner, Eds. (American Institute of Physics, Woodbury, NY, 1997), pp. 59–82.
27. M. E. Zolensky *et al.*, *Science* **314**, 1735 (2006).
28. K. D. McKeegan, *Science* **237**, 1468 (1987).
29. F. Kemper, W. J. Vriend, A. Tielens, *Astrophys. J.* **609**, 826 (2004).
30. F. Molster, C. Kemper, *Space Sci. Rev.* **119**, 3 (2005).
31. J. Bouwman *et al.*, *Astron. Astrophys.* **375**, 950 (2001).
32. R. van Boekel *et al.*, *Nature* **432**, 479 (2004).
33. J. Bouwman, A. de Koter, C. Dominik, L. Waters, *Astron. Astrophys.* **401**, 577 (2003).
34. K. Liffman, M. Brown, *Icarus* **116**, 275 (1995).
35. F. H. Shu, H. Shang, T. Lee, *Science* **271**, 1545 (1996).
36. D. Bockelée-Morvan, D. Gautier, F. Hersant, J. M. Huré, F. Robert, *Astron. Astrophys.* **384**, 1107 (2002).
37. We thank D. Burnett and G. J. Wasserburg for helpful advice and encouragement during the Preliminary Examination. We acknowledge financial support from the NASA Cosmochemistry Program, the NASA Sample Return Laboratory Instrumentation and Data Analysis Program, the Stardust Participating Scientist Program, the NSF Instrumentation and Facilities Program, the Particle Physics and Astronomy Research Council, the Centre National d'Etudes Spatiales, the CNRS France Etats-Unis program, and the Région Lorraine. Aspects of this work were performed under the auspices of the U.S. Department of Energy by the University of California, Lawrence Livermore National Laboratory, under Contract No. W-7405-Eng-48. We also thank the scientists and engineers at the Jet Propulsion Laboratory and at Lockheed Martin Astronautics whose dedication and skill brought these precious samples back to Earth.

Supporting Online Material

www.sciencemag.org/cgi/content/full/314/5806/1724/DC1
Methods
Fig. S1 to S5
Tables S1 and S6

6 October 2006; accepted 17 November 2006
10.1126/science.1135992

REPORT

Infrared Spectroscopy of Comet 81P/Wild 2 Samples Returned by Stardust

Lindsay P. Keller,[1]* Saša Bajt,[2] Giuseppe A. Baratta,[3] Janet Borg,[4] John P. Bradley,[2] Don E. Brownlee,[5] Henner Busemann,[6] John R. Brucato,[7] Mark Burchell,[8] Luigi Colangeli,[7] Louis d'Hendecourt,[4] Zahia Djouadi,[4] Gianluca Ferrini,[9] George Flynn,[10] Ian A. Franchi,[11] Marc Fries,[6] Monica M. Grady,[11] Giles A. Graham,[2] Faustine Grossemy,[4] Anton Kearsley,[12] Graciela Matrajt,[5] Keiko Nakamura-Messenger,[13] Vito Mennella,[7] Larry Nittler,[6] Maria E. Palumbo,[3] Frank J. Stadermann,[14] Peter Tsou,[15] Alessandra Rotundi,[16] Scott A. Sandford,[17] Christopher Snead,[18] Andrew Steele,[6] Diane Wooden,[17] Mike Zolensky[1]

Infrared spectra of material captured from comet 81P/Wild 2 by the Stardust spacecraft reveal indigenous aliphatic hydrocarbons similar to those in interplanetary dust particles thought to be derived from comets, but with longer chain lengths than those observed in the diffuse interstellar medium. Similarly, the Stardust samples contain abundant amorphous silicates in addition to crystalline silicates such as olivine and pyroxene. The presence of crystalline silicates in Wild 2 is consistent with mixing of solar system and interstellar matter. No hydrous silicates or carbonate minerals were detected, which suggests a lack of aqueous processing of Wild 2 dust.

Comets are widely believed to be repositories of the building blocks of the solar system that include both presolar and early nebular matter. The nature of the organic and inorganic materials in comets is frequently inferred through the analysis and interpretation of features in their infrared (IR) spectra, especially the mid-IR (2.5 to 15 μm) and far-IR (15 to 100 μm) parts of the spectrum where organic materials and minerals have diagnostic bands. Ground-based and spacecraft observations of comet P/Halley provided new insights into the nature of comets, including their organic inventory (*1*) and mineralogy with the detection of crystalline olivine (*2*–*4*). In the past decade, IR spectroscopy as a method to study comets and objects outside our solar system has blossomed. The Infrared Space Observatory (ISO) obtained IR spectra over a wide spectral range (2.4 to 200 μm) tracing the widespread occurrence of crystalline silicates in many astrophysical objects including comets, young stars (e.g., Herbig Ae/Be stars), and evolved stars [(*5*) and references therein] following ground-based observations (*6*, *7*). The Spitzer Space Telescope has substantially extended and broadened that view. The inferred mineralogy of dust ejecta from the Deep Impact mission, which includes phases such as hydrous silicates and carbonate minerals, is already challenging long-held beliefs on the nature of comets (*8*). In addition, a large database (*9*, *10*) exists on the physical properties (e.g., composition, mineralogy, isotopic systematics, IR spectra) of cometary interplanetary dust particles (IDPs) collected in Earth's stratosphere. With bona fide samples of a specific comet now returned by the Stardust mission (*11*), the detailed analysis of these samples can be used to test the chemical and mineralogical composition of comets as determined from astronomical measurements, comet encounter missions (Giotto, Puma, Deep Impact), and laboratory analyses of cometary IDPs.

We present results obtained by Fourier transform infrared (FTIR) spectroscopy on materials from comet 81P/Wild 2 returned by the Stardust mission and compare them with astronomical data and laboratory results from primitive solar system materials. Indigenous organic matter from Wild 2 was collected by the Stardust mission and survived capture [see also (*12*)]. It is associated with discrete grains and as finely disseminated material within impact cavities in the aerogel collection medium. FTIR measurements of extracted grains and in situ measurements from individual impact tracks show absorption features in the C-H stretching region that are consistent with long-chain aliphatic hydrocarbons (Fig. 1). The IR feature consists of a strong CH_2 asymmetric stretch at ~2925 cm^{-1} and a weaker CH_3 asymmetric stretch at ~2960 cm^{-1}. A third aliphatic CH stretching band is seen near 2855 cm^{-1}. In pure aliphatic hydrocarbons, this region contains two distinct features due to the symmetric stretching vibrations of CH_3 and CH_2 groups. However, these two modes often become strongly blended when the aliphatic groups are bound to strongly perturbing

groups (e.g., aromatic molecules) (*13*, *14*). The Wild 2 spectra are consistent with the presence of aliphatic groups attached to other molecules. Weak carbonyl C=O and C–C bending vibrations also occur in spectra from several grains. Hydrogen isotopic measurements show that the organic-rich grain in Fig. 1 is moderately enriched in deuterium (*15*). The Stardust aerogel contains organic residue from its manufacture and shows CH_2 symmetric and asymmetric bands at ~2872 and ~2967 cm^{-1}, respectively, and a CH_3 asymmetric band at ~2928 cm^{-1}. The aerogel C-H feature is dominated by the CH_3 symmetric stretch band at ~2967 cm^{-1} and is distinct from the Wild 2 organic matter (Fig. 1). The aromatic CH feature at ~3050 cm^{-1} has been detected in two of the grains analyzed to date by IR spectroscopy, including grain C2054,0,35,16,0 (Fig. 2). Aromatic species have also been detected in Stardust samples by two-step laser desorption–laser ionization mass spectrometry, and a highly disordered graphitic carbon has been observed with Raman spectroscopy [the G bands are characteristic of aromatic carbon (*12*)].

The observed C-H feature in Stardust particles bears a close resemblance to the features seen in primitive IDPs in terms of peak shapes, positions, and the CH_2/CH_3 stretching band depth ratio (*14*, *16*, *17*). The observed CH_2/CH_3 band depth ratio in the Wild-2 particles is ~2.5 and is the same as the average value obtained from IR spectra of anhydrous IDPs. This ratio is clearly larger than that measured for the macromolecular material extracted from primitive carbonaceous chondrite meteorites such as Orgueil and Murchison, which have CH_2/CH_3 band depth ratios of ~1.1 (*16*, *18*, *19*). There are also large differences between the Wild 2 CH features and those observed in astronomical measurements (Fig. 1). The organic component of interstellar dust in the diffuse interstellar medium (ISM) is dominated by hydrocarbons (both aliphatic and aromatic forms) with little or no O in attached functional groups such as carbonyl and alcohols (*20*). The C-H stretching features of aliphatic hydrocarbons are observed along many lines of sight in the diffuse ISM (*13*, *18*, *21*–*24*) and show CH_2/CH_3 band depth ratios ranging from 1.1 to 1.25 (*13*, *21*), indicating that the aliphatic chains in Wild 2 particles and IDPs are longer (or less branched) than those in the diffuse ISM. The fact that the CH_2/CH_3 ratios of the cometary grains and the ISM grains are different suggests that the primary organic materials that formed in the ISM may have been processed before their incorporation into the parent body. Processing of Wild 2 organic matter is also supported by the higher O/C ratios of the Stardust samples relative to diffuse ISM organics (*12*).

Comparison of the Wild 2 C-H feature to that in other comets is difficult. Astronomical measurement of the C-H feature in most comets (*1*) is complicated because it represents a mixture of gas-phase species such as CH_3OH superimposed on absorption bands from solid grains (*25*). After subtraction of the gas-phase molecules, the remaining solid-phase carbonaceous material shows a strong contribution from the asymmetric CH_2 stretching vibration of aliphatic hydrocarbons (*25*), which is consistent with observations from the Wild-2 samples.

The extent to which the capture process modified Wild 2 organic matter is currently not fully understood. Certainly there has been redistribution of organic material along the walls and margins of the impact bulbs (*12*), and there is lack of petrographically recognizable carbonaceous material associated with many terminal particles (*26*). Labile organic material that is moderately deuterium-rich survived capture, and Raman spectroscopy data from the same grain are consistent with very primitive and poorly ordered carbonaceous material.

Amorphous silicates are the dominant silicate in the ISM and show a broad and featureless absorption band in the IR that has a maximum at 9.7 μm (*27*). The contribution of crystalline silicates such as olivine and pyroxene to this feature is estimated to be <2% (*28*, *29*). Amorphous silicates are also a major component of anhydrous IDPs, many of which are believed to have a cometary origin. The majority of amorphous silicates in IDPs occur as GEMS (glass with embedded metal and sulfides) grains (*30*). GEMS grains are typically 0.1 to 0.5 μm in diameter, contain variable amounts of nanophase FeNi metal and Fe sulfide grains as

[1]Astromaterials Research and Exploration Science Directorate, Mail Code KR, NASA-Johnson Space Center, Houston, TX 77058, USA. [2]Institute for Geophysics and Planetary Physics, Lawrence Livermore National Laboratory, Livermore, CA 94550, USA. [3]Istituto Nazionale di Astrofisica (INAF)–Osservatorio Astrofisico di Catania, Via Santa Sofia 78, 95123 Catania, Italy. [4]Institut d'Astrophysique Spatiale, 91405 Orsay Cedex, France. [5]Department of Astronomy, University of Washington, Seattle, WA 98195, USA. [6]Department of Terrestrial Magnetism, Carnegie Institution, Washington, DC 20015, USA. [7]INAF–Osservatorio Astronomico di Capodimonte, Via Moiariello 16, 80131 Napoli, Italy. [8]School of Physical Science, University of Kent, Canterbury, Kent CT2 7NR, UK. [9]Novaetech s.r.l., Piazza Pilastri 18, 80125 Napoli, Italy. [10]Physics Department, State University of New York, Plattsburgh, NY 12901, USA. [11]Open University, Milton Keynes MK7 6AA, UK. [12]Department of Mineralogy, Natural History Museum, London SW7 5BD, UK. [13]Engineering Science Contract Group, NASA Johnson Space Center, Houston, TX 77058, USA. [14]Laboratory for Space Sciences, Washington University, St. Louis, MO 63160, USA. [15]Jet Propulsion Laboratory, California Institute of Technology, Pasadena, CA 91109, USA. [16]Dipartimento di Scienze Applicate, Università degli Studi di Napoli "Parthenope," 80133 Napoli, Italy. [17]Astrophysics Branch, NASA-Ames Research Center, Moffett Field, CA 94035, USA. [18]Department of Physics, University of California, Berkeley, CA 94720, USA.

*To whom correspondence should be addressed. E-mail: lindsay.p.keller@nasa.gov

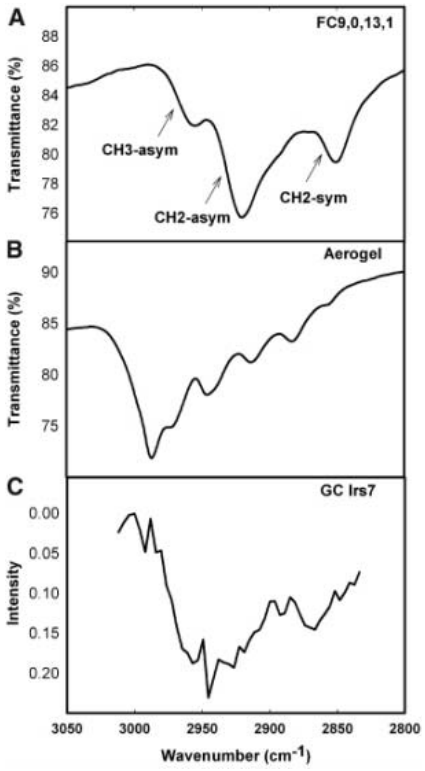

Fig. 1. (**A** and **B**) The C-H stretching features from grain FC9,0,13,1 (A) showing well-resolved CH_2 and CH_3 stretching features distinct from the CH_3-dominated feature from aerogel (B). (**C**) A C-H feature obtained through the diffuse ISM (*13*).

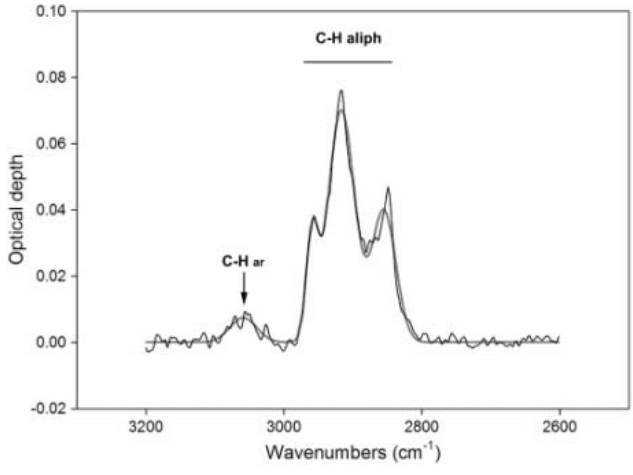

Fig. 2. The C-H stretch features of particle C2054,0,35,16,0 after continuum subtraction. The aromatic C-H feature is labeled C-H ar; the aliphatic C-H feature is labeled C-H aliph.

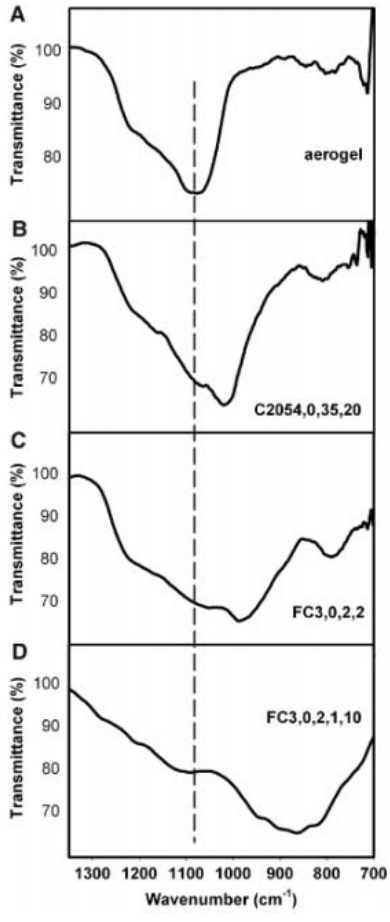

Fig. 3. The Si-O stretching feature in aerogel (**A**) compared to the range of amorphous silicate features observed in Wild-2 grains extracted from aerogel (**B** to **D**). The vertical dashed line marks the maximum absorption from aerogel.

inclusions in an amorphous silicate matrix, and have IR spectral properties in some cases similar to those of ISM amorphous silicates. One expectation based on the IDP results is that GEMS-like amorphous silicates might be similarly abundant in Wild 2. Indeed, despite complications due to overlap with the aerogel Si-O feature, the majority of Wild 2 particles analyzed to date (40 of 49) with IR spectroscopy are dominated by amorphous silicates whose maximum absorption feature occurs between 1050 and 850 cm^{-1} (Fig. 3). Electron microscopy (EM) observations show that the amorphous silicates in the Wild 2 particles contain abundant nanophase FeNi metal grains and FeNi sulfides dispersed in an amorphous Mg-silicate matrix (Fig. 4) that is in general similar to GEMS grains but differs in detail (*26*). The IR spectrum from the GEMS-like grains mapped in Fig. 4 is similar to that observed for GEMS in IDPs (*30*) and the silicate feature observed in the diffuse ISM (*28*). The x-ray maps in Fig. 4 show compositional heterogeneity at the ~0.1-μm scale similar to that in IDP GEMS grains that were not erased by the thermal pulse experienced during capture. However, TEM observations of many of these particles also show evidence for vesiculation of the amorphous silicate matrix and partial loss of sulfur that may indicate thermal alteration during capture or interaction with aerogel (*26*). Without coordinated transmission electron microscopy (TEM) and perhaps ion microprobe measurements, it is not possible to distinguish primary Wild 2 amorphous silicates from secondary glasses that may have been produced during capture from their FTIR spectra.

Extracted terminal particles and some of the grains extracted from the base of the impact "bulbs" show sharp features in mid- and far-IR spectra consistent with crystalline silicates. The silicates identified to date by IR include enstatite, olivine, and diopside with pyroxene predominating (6 of 8 grains). Similar trends are observed in anhydrous IDPs where pyroxene is more abundant than olivine (*31*). Far-IR measurements were obtained from terminal particles in aerogel keystones. Despite the thickness of aerogel, IR bands for enstatite, olivine, and diopside were observed. The one olivine-rich terminal particle lacked the strong 33-μm feature commonly observed in Mg-rich olivines (>Fo 90) such as those observed in comet Hale-Bopp (*32*) and young stellar objects and is consistent with a more Fe-rich olivine composition (~Fo 75). The IR spectral properties of Wild 2 particles show marked similarities to astronomical IR spectra from young stellar objects and comets but are distinct from the spectra of primitive meteorites, which are dominated by crystalline silicates, mainly olivine, or phyllosilicates in the CI and CM chondrites.

No definitive FTIR evidence for hydrated silicates or carbonates at the percent level has been observed to date in any of the extracted particles. We specifically searched for 3- and 6-μm structural OH bands and the distinctive carbonate band at 6.8 μm in the Wild 2 spectra. The possibility exists that thermal effects from capture may have destroyed fine-grained phyllosilicates and carbonates. However, this possibility is not supported by mineralogical analysis of the particles, because the thermal breakdown products of phyllosilicates and carbonates are readily recognized by TEM and have not been observed to date (*26*).

The presence of crystalline silicates in the Wild 2 samples indicates that this comet is not simply an assemblage of preserved ISM silicates, but rather is a mixture of presolar and solar system materials.

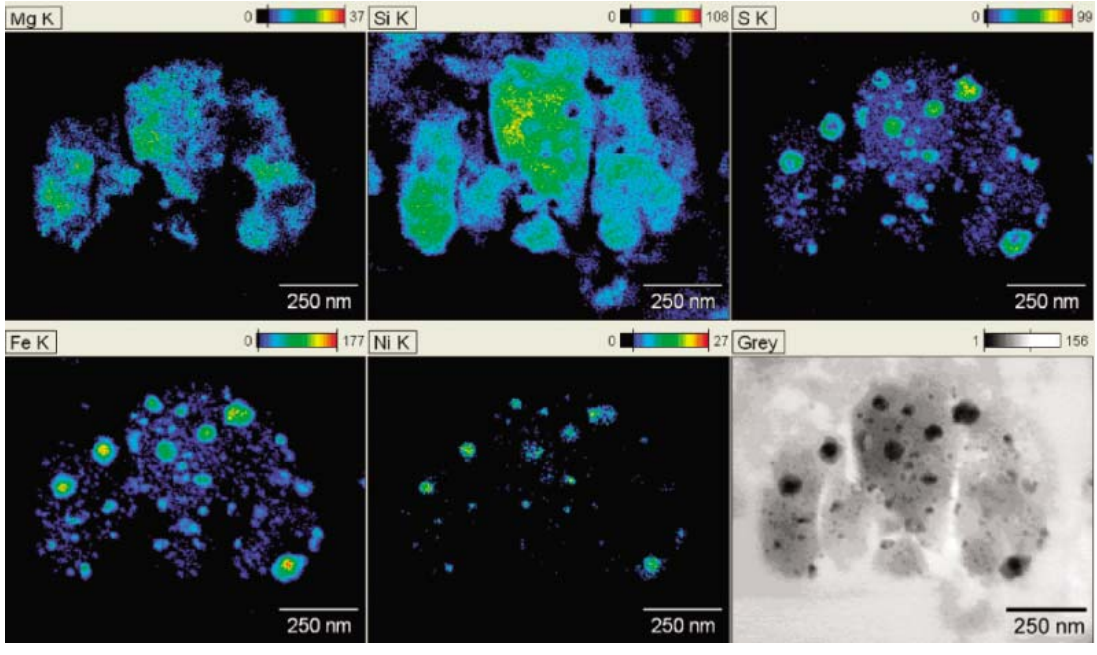

Fig. 4. Elemental x-ray (k-line) maps of a GEMS-like object from a thin section of grain C044, track 7, showing preserved chemical heterogeneity at the 0.1-μm scale typical of GEMS grains in IDPs (*33*). The Fe, Ni, and S maps show the locations of the nanophase FeNi metal and sulfide inclusions within the amorphous silicate matrix. The gray image is a bright-field TEM image of the GEMS-like object. The color scale in the element maps is x-ray counts.

References and Notes

1. M. J. Mumma, P. R. Weissman, S. A. Stern, In *Protostars and Planets III*, E. H. Levy, J. I. Lunine, M. S. Matthews, Eds. (Univ. of Arizona Press, Tucson, AZ, 1993), pp. 1172–1252.
2. J. D. Bregman *et al.*, *Astron. Astrophys.* **187**, 616 (1987).
3. J. D. Bregman *et al.*, *Astron. Astrophys.* **334**, 1044 (1988).
4. H. Campins, E. V. Ryan, *Astrophys. J.* **341**, 1059 (1989).
5. F. J. Molster, L. B. F. M. Waters, in *Astromineralogy, Lecture Notes in Physics*, T. K. Henning, Ed. (Springer, Berlin, 2003), pp. 121–170.
6. D. H. Wooden *et al.*, *Astrophys. J.* **517**, 1034 (1999).
7. D. E. Harker *et al.*, *Astrophys. J.* **580**, 579 (2002).
8. C. M. Lisse *et al.*, *Science* **313**, 635 (2006).
9. F. J. M. Rietmeijer, *Rev. Mineral.* **36**, 95 (1998).
10. J. P. Bradley, in *Treatise on Geochemistry,* vol. 1, H. D. Holland, K. K. Turekian, Eds. (Elsevier, Oxford, 2004), pp. 1121–1140.
11. D. E. Brownlee *et al.*, *Science* **314**, 1711 (2006).
12. S. A. Sandford *et al.*, *Science* **314**, 1720 (2006).
13. S. A. Sandford *et al.*, *Astrophys. J.* **371**, 607 (1991).
14. L. P. Keller *et al.*, *Geochim. Cosmochim. Acta* **68**, 2577 (2004).
15. K. D. McKeegan *et al.*, *Science* **314**, 1724 (2006).
16. G. J. Flynn, L. P. Keller, M. Feser, S. Wirick, C. Jacobsen, *Geochim. Cosmochim. Acta* **67**, 4791 (2003).
17. G. Matrajt *et al.*, *Astron. Astrophys.* **433**, 979 (2005).
18. P. Ehrenfreund, F. Robert, L. D'Hendencourt, F. Behar, *Astron. Astrophys.* **252**, 712 (1991).
19. A. Gardinier *et al.*, *Earth Planet. Sci. Lett.* **184**, 9 (2000).
20. Y. J. Pendleton, L. J. Allamandolla, *Astrophys. J. Suppl. Ser.* **138**, 75 (2002).
21. Y. J. Pendleton *et al.*, *Astrophys. J.* **437**, 683 (1994).
22. D. C. B. Whittet *et al.*, *Astrophys. J.* **490**, 729 (1997).
23. J. E. Chiar *et al.*, *Astrophys. J.* **537**, 749 (2000).
24. E. Dartois *et al.*, *Astron. Astrophys.* **423**, 549 (2004).
25. M. A. DiSanti *et al.*, *Icarus* **116**, 1 (1995).
26. M. E. Zolensky *et al.*, *Science* **314**, 1735 (2006).
27. J. Dorschner, T. Henning, *Astron. Astrophys. Rev.* **6**, 271 (1995).
28. F. Kemper, W. J. Vriend, A. G. G. M. Tielens, *Astrophys. J.* **609**, 826 (2004).
29. F. Kemper, W. J. Vriend, A. G. G. M. Tielens, *Astrophys. J.* **633**, 534 (2005).
30. J. P. Bradley *et al.*, *Science* **285**, 1716 (1999).
31. G. J. Flynn, L. P. Keller, *Workshop on Cometary Dust in Astrophysics*, LPI Contribution No. 1182, #6053 (2003).
32. J. Crovisier *et al.*, *Science* **275**, 1904 (1997).
33. L. P. Keller, S. Messenger, *Lunar Planet Sci.* **35**, 1985 (2004).

34. We thank L. Carr and R. Smith for providing key support for the far-IR measurements at the National Synchrotron Light Source, Brookhaven National Laboratory; M. Martin and Z. Hao at the Advanced Light Source, Lawrence Berkeley National Laboratory; and the personnel of Assing S.p.A. for their availability and technical assistance. Supported by grants from the NASA Cosmochemistry and Origins programs (L.P.K.) Some of this work was performed in part under the auspices of the U.S. Department of Energy by the Lawrence Livermore National Laboratory under contract W-7405-ENG-48. The Advanced Light Source is supported by the Office of Basic Energy Sciences, Materials Sciences Division, of the U.S. Department of Energy under contract DE-AC03-76F00098 at Lawrence Berkeley National Laboratory. The work was also supported by the Università di Napoli "Parthenope," INAF, and MIUR.

Supporting Online Material

www.sciencemag.org/cgi/content/full/314/5806/1728/DC1
SOM Text

2 October 2006; accepted 15 November 2006
10.1126/science.1135796

REPORT

Elemental Compositions of Comet 81P/Wild 2 Samples Collected by Stardust

George J. Flynn,[1]* Pierre Bleuet,[2] Janet Borg,[3] John P. Bradley,[4] Frank E. Brenker,[5] Sean Brennan,[6] John Bridges,[7] Don E. Brownlee,[8] Emma S. Bullock,[9] Manfred Burghammer,[2] Benton C. Clark,[10] Zu Rong Dai,[4] Charles P. Daghlian,[11] Zahia Djouadi,[3] Sirine Fakra,[12] Tristan Ferroir,[13] Christine Floss,[14] Ian A. Franchi,[7] Zack Gainsforth,[15] Jean-Paul Gallien,[16] Philippe Gillet,[13] Patrick G. Grant,[4] Giles A. Graham,[4] Simon F. Green,[7] Faustine Grossemy,[3] Philipp R. Heck,[17] Gregory F. Herzog,[18] Peter Hoppe,[17] Friedrich Hörz,[19] Joachim Huth,[17] Konstantin Ignatyev,[6] Hope A. Ishii,[4] Koen Janssens,[20] David Joswiak,[8] Anton T. Kearsley,[21] Hicham Khodja,[16] Antonio Lanzirotti,[22] Jan Leitner,[23] Laurence Lemelle,[13] Hugues Leroux,[24] Katharina Luening,[6] Glenn J. MacPherson,[9] Kuljeet K. Marhas,[14] Matthew A. Marcus,[12] Graciela Matrajt,[8] Tomoki Nakamura,[25] Keiko Nakamura-Messenger,[26] Tsukasa Nakano,[27] Matthew Newville,[22] Dimitri A. Papanastassiou,[28] Piero Pianetta,[6] William Rao,[29] Christian Riekel,[2] Frans J. M. Rietmeijer,[30] Detlef Rost,[9] Craig S. Schwandt,[26] Thomas H. See,[26] Julie Sheffield-Parker,[31] Alexandre Simionovici,[13] Ilona Sitnitsky,[1] Christopher J. Snead,[15] Frank J. Stadermann,[14] Thomas Stephan,[23] Rhonda M. Stroud,[32] Jean Susini,[2] Yoshio Suzuki,[33] Stephen R. Sutton,[22] Susan Taylor,[34] Nick Teslich,[4] D. Troadec,[24] Peter Tsou,[28] Akira Tsuchiyama,[35] Kentaro Uesugi,[33] Bart Vekemans,[20] Edward P. Vicenzi,[9] Laszlo Vincze,[36] Andrew J. Westphal,[15] Penelope Wozniakiewicz,[21] Ernst Zinner,[14] Michael E. Zolensky[19]

We measured the elemental compositions of material from 23 particles in aerogel and from residue in seven craters in aluminum foil that was collected during passage of the Stardust spacecraft through the coma of comet 81P/Wild 2. These particles are chemically heterogeneous at the largest size scale analyzed (~180 ng). The mean elemental composition of this Wild 2 material is consistent with the CI meteorite composition, which is thought to represent the bulk composition of the solar system, for the elements Mg, Si, Mn, Fe, and Ni to 35%, and for Ca and Ti to 60%. The elements Cu, Zn, and Ga appear enriched in this Wild 2 material, which suggests that the CI meteorites may not represent the solar system composition for these moderately volatile minor elements.

NASA's Stardust spacecraft collected dust particles from comet 81P/Wild 2, at an encounter speed of ~6.1 km/s, in silica aerogel capture cells and in impact craters (*1*). Analytical results from the aerogel and foils were combined to provide a more comprehensive elemental analysis of the Wild 2 particles.

The impacts in aerogel produced elongated cavities called tracks. Wedges of aerogel, called keystones (*2*), containing an entire track were extracted. The volume containing each track was analyzed by means of synchrotron-based x-ray microprobes (SXRMs), providing abundances for elements having an atomic number $Z \geq 16$ (S). One track was subsequently split open, exposing the wall for time-of-flight–secondary ion mass spectrometry (TOF-SIMS) analysis, detecting lower-Z elements, particularly Mg and Al. Because Si and O are the major elements in silica aerogel, neither element could be determined in the comet material in tracks. The residues in craters were analyzed by scanning electron microscopy using energy-dispersive x-ray (SEM-EDX) analyses and TOF-SIMS, providing other element abundances, including Mg and Si.

The SXRMs produce intense, focused beams of x-rays that completely penetrate a keystone, exciting fluorescence (*3*). Elemental analysis was performed on keystones containing 23 tracks, which were selected to sample the diversity on the collector, by seven research groups with the use of six different SXRMs (*4*). These tracks range in length from ~250 μm to almost 10,000 μm and vary in shape from conical to bulbous. The Fe content of the tracks varies from ~180 fg to 6.4 ng (table S3), comparable to the Fe in chondritic particles ranging from ~1 to ~30 μm in size. All 23 tracks were approximately normal to the aerogel surface, which was the arrival direction for particles collected from Wild 2 (*1*), whereas interplanetary particles, also collected, arrived over a wide range of orientations. Comets are thought to preserve dust from the early solar system, so we compared the Wild 2 dust to the elemental composition of the CI meteorites (CI) (*5*) because CI is thought to represent the nonvolatile composition of the solar system (*6*).

A map of the K-alpha fluorescence intensity for Fe from a conical track, track 19, shows that the incident particle deposited Fe along much of the entry path (Fig. 1), with only 3% of the total Fe contained in the terminal particle. The fraction of the total Fe detected in the terminal particle varies from track to track, ranging from almost 60% in one terminal particle to zero in two tracks having no detectable terminal particle. In most of the 23 tracks, most of the incident Fe mass is unevenly distributed along the track, indicating that the

particles are relatively weak. Their behavior during aerogel capture is most like that observed when grains from mechanically weak meteorites, such as Orgueil, are shot at high velocities into aerogel.

The spatial distributions of other elements in each track vary widely (*4*). Nickel is deposited along the entire length of track 19 (Fig. 1). The Ni/Fe ratio summed over the whole track is 0.041, which is within 50% of the CI ratio (0.058) (*5*). However, Ni/Fe is much lower (0.0062) in the terminal particle, demonstrating elemental heterogeneity. Zinc is concentrated along one edge of the track, with almost none detectable in the terminal particle, but ~80% of the total Cr is in the terminal particle.

The terminal particle and the 19 most intense element hot spots along track 19 were analyzed individually, with the use of much longer acquisition times than at each pixel in the maps. Most element/Fe ratios vary by more than two orders of magnitude from spot to spot along this track (Fig. 1). A "whole-track" composition for track 19 (Fig. 1) was determined by adding the element abundances from these 20 analyses. The S/Fe, Cr/Fe, Mn/Fe, and Ni/Fe ratios are similar to the CI values, but the moderately volatile elements Cu, Zn, Ga, and Se are higher than CI, and Ca and Ge are lower.

The whole-track composition for track 19 differs significantly from the composition of the terminal particle (Fig. 1), with the moderately volatile elements being much lower in the terminal particle. Many terminal particles have elemental compositions that are consistent with their being dominated by a single mineral, generally olivine, pyroxene, or sulfide, a result confirmed by mineralogical examination of some extracted particles (*7*). Thus, terminal particle analysis provides limited information on the bulk elemental composition of Wild 2.

No single mineral found in terrestrial or extraterrestrial material has a CI composition. So, a CI composition indicates that the particle is a mixture of compositionally diverse grains. The high variability of the 20 spot analyses along track 19 (Fig. 1) further indicates the particle was an aggregate of diverse grains. However, not all tracks demonstrate near-CI abundances (Fig. 2).

We determined the mean composition of the comet material by summing the measured abundance of each element over all 23 tracks (Table 1 and Fig. 3). The aerogel contains trace quantities of virtually all stable elements (*1*), and several elements are found in hot spots (fig. S1), complicating background subtraction (*4*).

The widespread distribution of compositionally diverse comet material and contamination along most tracks required the development of analytical strategies that provided the most comprehensive set of element analyses. Tracks were analyzed in different laboratories by means of two complementary methods. For some keystones, an entire fluorescence spectrum was collected, with the use of a long integration time, at each point in a raster scan over the whole track. Other keystones were analyzed by identifying "hot spots" in a quick scan and then dwelling for much longer times on these hot spots. The first technique provides more reliable data for elements in high abundance, whereas the second is more sensitive for trace elements. The mean, blank-corrected compositions obtained through the two techniques are very similar (fig. S6), indicating that any systematic differences between the two techniques are smaller than the statistical errors in each data set (*4*).

Iron was detected in all 23 tracks; Ni in 22; S in 21; Ca, Cr, Mn, and Cu in 20; Zn in 17; Ga in 14; and Ti and Se in 9 (table S3). When an element was not detected, its concentration was recorded as zero in calculating the central value and lower limit on the mean. This technique underestimates the central value of the mean for low-abundance elements. It also underestimates the lower limit, leading to an overly conservative confidence interval (*4*). The

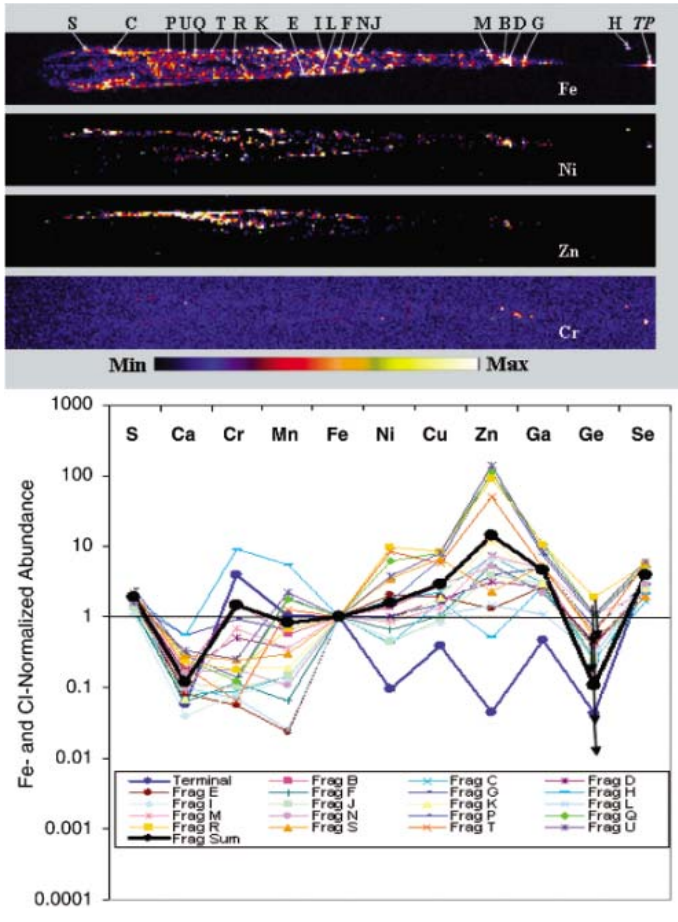

Fig. 1. X-ray fluorescence analysis results obtained on track 19, an 860-μm-long track. Maps of the Fe, Ni, Zn, and Cr fluorescence intensities were obtained with a step size of 3 μm per pixel and a dwell time of 0.5 s per pixel. The CI- and Fe-normalized element abundances for the terminal particle (TP) and the 19 most-intense element hot spots (letters B, C to N, P to U), whose positions are indicated on the Fe map, are plotted along with the whole-track average composition, determined by adding the element abundances from 19 spot analyses along the track and the analysis of the terminal particle. The horizontal line at 1 is the CI meteorite composition, which is thought to represent the mean solar system composition. Arrows indicate that all Ge analyses for these particles were upper limits.

[1]Department of Physics, State University of New York at Plattsburgh, 101 Broad Street, Plattsburgh, NY 12901, USA. [2]European Synchrotron Radiation Facility, Grenoble, France. [3]Institut d'Astrophysique Spatiale, Orsay, France. [4]Institute of Geophysics and Planetary Physics, Lawrence Livermore National Laboratory, Livermore, CA 94550, USA. [5]Institut für Mineralogy, Johann Wolfgang Goethe-Universität, Frankfurt, Germany. [6]Stanford Linear Accelerator Center, Menlo Park, CA 94025, USA. [7]The Open University, Milton Keynes, MK7 6AA, UK. [8]Department of Astronomy, University of Washington, Seattle, WA 98195, USA. [9]Department of Mineral Sciences, Smithsonian Institution, Washington, DC 20560, USA. [10]Lockheed Martin, Post Office Box 179, Denver, CO 80201, USA. [11]Dartmouth College, Hanover, NH 03755, USA. [12]Advanced Light Source, Lawrence Berkeley National Laboratory, Berkeley, CA 94720, USA. [13]École Normale Supérieure de Lyon, Lyon, France. [14]Washington University, St. Louis, MO 63130, USA. [15]Space Sciences Laboratory, University of California, Berkeley, CA 94720, USA. [16]Laboratory Pierre Süe, CEA/CNRS, Saclay, France. [17]Max Planck Institute for Chemistry, Mainz, Germany. [18]Department of Chemistry and Chemical Biology, Rutgers University, Piscataway, NJ 08854, USA. [19]NASA Johnson Space Center, Houston, TX 77058, USA. [20]Department of Chemistry, Universiteit Antwerpen, Antwerp, Belgium. [21]Department of Mineralogy, The Natural History Museum, London, SW7 5BD, UK. [22]The University of Chicago, Chicago, IL 60637, USA. [23]Institut für Planetologie, Universität Münster, 48149 Münster, Germany. [24]University Lille, Lille, France. [25]Kyushu University, Fukuoka, Japan. [26]Engineering and Science Contract Group/Jacobs Sverdrup, NASA Johnson Space Center, Houston, TX 77058, USA. [27]Geological Survey of Japan, National Institute of Advanced Industrial Science and Technology, Tsukuba, Japan. [28]Jet Propulsion Laboratory, California Institute of Technology, Pasadena, CA 91109, USA. [29]University of Georgia, Athens, GA 30602, USA. [30]Department of Earth and Planetary Sciences, University of New Mexico, Albuquerque, NM 87131, USA. [31]XRT Limited, Port Melbourne, Australia. [32]U.S. Naval Research Laboratory, Washington, DC 20375, USA. [33]Japan Synchrotron Radiation Research Institute/SPring-8, Hyougo, Japan. [34]Engineering Research and Development Center/Cold Regions Research and Engineering Laboratory, Hanover, NH 03755, USA. [35]Osaka University, Toyonaka, Japan. [36]Ghent University, Ghent, Belgium.

*To whom correspondence should be addressed. E-mail: george.flynn@plattsburgh.edu

CI-normalized whole-track element/Fe ratios (Fig. 2) exhibit variations of more than two orders of magnitude from track to track. Thus, a reliable mean composition can only be determined by averaging many tracks.

There are four major sources of error in the mean composition of the particles that produced the tracks: (i) the precision and accuracy of the analyses, (ii) absorption corrections in the capture medium and the particles themselves, (iii) the extent to which the material analyzed is representative of all the material in the initial particle, and (iv) uncertainty resulting from averaging only a small number of samples having extremely diverse compositions.

The SXRM abundances are accurate to ±20% for the elements having $Z \geq 24$ (Cr), and absorption corrections are small for elements having $Z \geq 20$ (Ca) (*4*). In no case can we be certain that we analyzed all the material from any incident particle. The extent to which vaporized material can be lost through the entry hole of a track has yet to be investigated. Vaporized material may also penetrate many track diameters through the aerogel, as observed for some organic matter in Wild 2 tracks (*8*). In addition, the spot analysis used for nine of the tracks only analyzed material in these hot spots. Nonetheless, the largest uncertainty in the mean composition is likely to result from the high degree of compositional heterogeneity among the particles (*4*). This uncertainty was estimated by means of a Monte Carlo method that assumes the particle sizes and compositions of the 23 measured tracks are characteristic of the entire dust population hitting the collector and determines 1 SD (1σ) and 2σ confidence limits from the distributions of elements in ensembles randomly picked from the observed data set (*4*).

Summing all 23 tracks, the Fe-normalized mean element abundances (Table 1) for Ca, Ti, Cr, Mn, Ni, Ge, and Se are consistent with CI values at the 2σ confidence level (Fig. 3). Because Ge and Se were detected in only a few particles, their central values and lower limits may be underestimated (*4*). Sulfur is depleted, and Cu, Zn, and Ga are enriched (Table 1).

One keystone, track 21, was dissected laterally to expose the track wall, and two slices were analyzed by TOF-SIMS (table S1). These analyses indicate that Mg/Fe, Al/Fe, Cr/Fe, and Mn/Fe are within 50% of CI (*4*).

Analysis of impact residue, which is abundant in all large craters in the Al foils examined, provides element-to-Si ratios. These Al foils contain indigenous Fe inclusions, occasional Si-rich inclusions, and a wide range of trace elements, but unambiguous impact residue was easily located in craters by both SEM-EDX and TOF-SIMS.

To assess element loss during crater production, we fired a variety of projectiles into Al1100 foil, the type flown on Stardust, with impact velocities of ~6 km/sec. In craters >50 μm in diameter, the loss of S, Na, Mg, Si, and Fe was small (*9*) (fig. S9), so analysis of residue in large craters is expected to provide a good sample of the composition of Wild 2 dust. Seven craters, each having a diameter >50 μm, were characterized by means of SEM-EDX (table S2).

The mass of each impacting particle, estimated through the crater-size calibration of Kearsley *et al.* (*10*) scaled by particle density appropriate for the mineralogy inferred from its chemical composition (*4*), ranges from 3 to 178 ng, with six having impactor masses of 17 ng or less (table S2). Only Mg, Si, and Fe were detected in all seven craters, Cr in four, Na in three, and P, K, Mn, and Ni in only two. Confidence limits on the mean abundances were modeled with the use of the same Monte Carlo technique used for the track data.

The CI- and Si-normalized mean composition for elements detected in four or more craters (Table 2) is within 50% of CI for Mg, Ca, and Fe. Depletions in S, Ca, Cr, and Fe, relative to that of Si, are significant at the 2σ confidence level (Fig. 4). The S depletion is consistent with the results

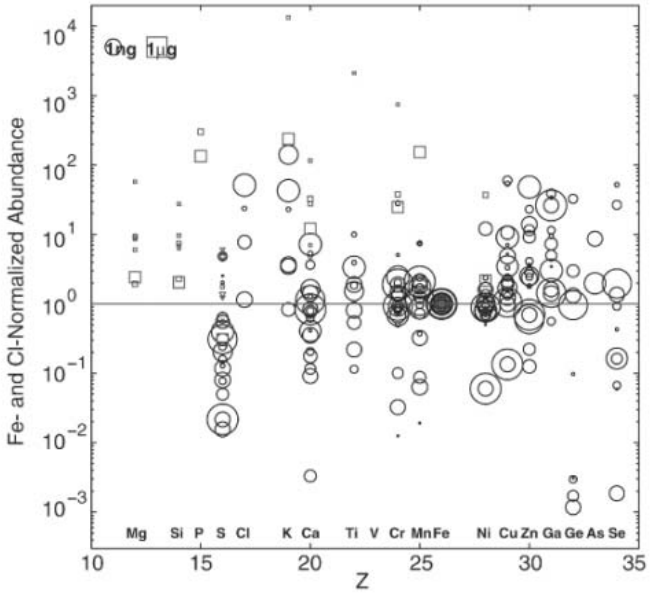

Fig. 2. CI- and Fe-normalized abundance for each element in each of the 23 whole tracks (circles) and in each of the seven crater residues (squares). The area of each data point is proportional to the cross section of an equant particle of equivalent mass. Because much larger masses were analyzed in the craters, there is a difference in the scale size of the two symbols by three orders of magnitude. There is a high degree of variability from track to track, with most elements varying by two orders of magnitude or more.

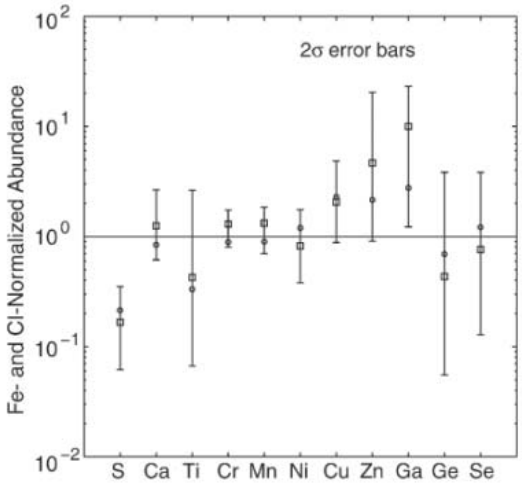

Fig. 3. CI- and Fe-normalized mean composition determined by summing the 23 whole-track analyses (squares) and by summing the same data set except for the particle having the highest Fe content (circles). One track contributed ~30% of the total Fe, but its inclusion does not distort the mean composition, because the mean excluding this track does not differ significantly from the 23-track mean. The vertical bars show the 2σ variation in the mean of a Monte Carlo simulation designed to assess the effect of this elemental diversity on the mean composition (*4*).

Table 1. Comparison of the mean composition of the material in the 23 tracks with the CI meteorite composition, with a CI- and Fe-normalized value of 1 indicating exact agreement between the total amount of that element detected in all the tracks and that expected if the particles had a CI composition. 1σ confidence limits are given.

Element	CI- and Fe-normalized abundance	1σ confidence limit (upper, lower)
S	0.17	+0.12, −0.06
Ca	1.25	+0.47, −0.43
Ti	0.42	+1.74, −0.23
Cr	1.30	+0.24, −0.31
Mn	1.32	+0.32, −0.37
Ni	0.82	+0.37, −0.24
Cu	2.06	+1.14, −0.69
Zn	4.60	+6.30, −3.10
Ga	10.00	+8.90, −7.50
Ge	0.43	+1.46, −0.22
Se	0.76	+1.51, −0.42

from the tracks. Higher Ca and Cr were found in the tracks (Fig. 3), but the 2σ confidence limits overlap for both elements in the track and crater analyses. Elements with less than four measurements were not reported in Table 2 because confidence limits were difficult to determine with so few detections, but the mean values obtained were Mn = 1.2 × CI, K = 0.7 × CI, Na = 1.6 × CI, and Ni = 0.2 × CI.

The residues in five of these craters were analyzed by TOF-SIMS (table S4). Calibration shots of mineral standards into Al foil demonstrate good agreement for most elements between TOF-SIMS analyses of impact residue and SEM-EDX analyses of unshot projectile material, but Na and K are sometimes higher in the TOF-SIMS analyses (fig. S11). The Si-normalized mean abundances (Fig. 4) are consistent with CI for Mg, Ca, and Ni, but there are small depletions for Cr and Fe, which are consistent with the SEM-EDX results. Lithium, Na, and K are enriched. Most of the Na and K detected by TOF-SIMS was found in a single crater (table S4), but SEM-EDX analysis of Na and K in residue in the same crater gives results that are an order of magnitude lower (table S2). This difference may result from SEM-EDX measuring micrometers into the residue, predominately at the crater bottom, whereas TOF-SIMS only measures material sputtered from the surface, mainly from the crater lip (*4*). The TOF-SIMS analyses in two different orientations show significantly different Na and K abundances (table S4), which suggests a very heterogeneous distribution, making it difficult to determine a mean abundance.

An SEM survey of the Al foils identified many smaller impact craters, generally <2 μm in diameter, corresponding to projectiles from ~20 to ~400 nm in diameter (*10*). SEM-EDX analysis of residue in several hundred small craters identified compositional groups that are consistent with impacting particles composed of silicates, sulfides, and mixtures of silicate and sulfide (*11*). However, the mass-frequency distribution of impacting particles (*11*) indicates that most of the mass collected at Wild 2 is in larger projectiles, so the total mass of material in the small craters is inadequate to substantially alter the mean element abundances measured on tracks and larger craters.

Table 2. Comparison of the mean composition of the material in the seven crater residues with the CI meteorite composition, with a CI- and Fe-normalized value of 1 indicating exact agreement. 1σ confidence limits are given.

Element	CI- and Si-normalized abundance	1σ confidence limit (upper, lower)
Mg	1.13	+0.22, −0.05
S	0.13	+0.40, −0.06
Ca	0.51	+0.12, −0.05
Cr	0.31	+0.31, −0.04
Fe	0.75	+0.05, −0.40

Sulfur is depleted in both the tracks and craters. The statistical significance of this depletion is high. Sulfur is highly variable in chondritic meteorites. Of the major elements, S shows the most extreme variation, being lower by a factor of five in ordinary chondrites than in CI meteorites. However, for the tracks, low-energy S fluorescence x-rays are attenuated by a few micrometers of a high-density mineral (e.g., Fe-sulfide) or compacted aerogel. Because most keystones are ~300 μm thick, a first-order correction, which assumed that all the S is shielded by ~150 μm of 20 mg/cm^3 of aerogel (*1*), would increase the abundance of S by no more than a factor of two, which does not provide consistency with CI at the 2σ level. However, some S is finely distributed in compacted or melted aerogel (*7*), possibly large enough to attenuate S fluorescence, and micrometer-size sulfide grains attenuate the S fluorescence, so the full effect of attenuation cannot be assessed without a detailed knowledge of the shape or size of aerogel and sulfide grains along each track. Selenium abundance is well correlated with S in meteoritic minerals. Although we detected Se in only 9 tracks, the mean Se abundance is nearly CI. If S and Se are correlated in the Wild 2 particles and have similar behavior during capture, then S in the whole-track data may be underestimated.

The size at which the composition of an aggregate converges to the average composition is an indication of the grain size of the material. Fine-grained, chondritic interplanetary dust particles (IDPs) of ~10 μm size (*12*), aggregates typically containing >10^4 grains, generally show only a factor-of-two variation in major elements and less than a factor-of-five variation in minor elements (*13*). Primitive chondritic meteorites, which contain much larger grains, show much greater variation in composition in samples up to millimeters in size. Because the largest track and the largest crater each have a composition significantly different from the mean (Fig. 2), Wild 2 dust is heterogeneous at the largest size scale of particle that we analyzed, showing greater compositional diversity than ~10 μm IDPs.

Before the Stardust mission, the only direct measurement of the elemental composition of comet dust came from impact-ionization mass spectrometers on the Giotto and VEGA spacecraft (*14*) that analyzed dust from comet 1P/Halley in 1986. The impact-ionization yields are uncertain, but the mean abundances of major refractory elements in Halley dust are reported to be within a factor of two of CI (*15*), although Fe, Cr, Mn, and Ni were depleted relative to Mg. These Halley results were based on the analysis of <1 ng of comet material.

The Wild 2 particles in the 23 keystones contain ~21 ng of Fe. Assuming the CI Fe content, the total mass of Wild 2 material in these tracks is ~115 ng. The crater residue resulted from the impact of ~215 ng of material (table S2). Taken together, we analyzed material from >300 ng of Wild 2 dust, several orders of magnitude more material than was analyzed at comet Halley. Even so, only 10% of the Stardust aerogel cells and a comparable fraction of the Stardust Al foils have been examined thus far. Comprehensive elemental analysis of the remaining material should provide a better mean S content and decrease the uncertainty in other element abundances.

The composition data on Wild 2 particles are generally consistent with but greatly extend the measurements at comet Halley because of the larger sample mass that we analyzed, coupled with the ability to analyze this material with the use of high-sensitivity instruments in state-of-the-art laboratories on Earth. The Wild 2 material appears depleted in S and Fe relative to Si and enriched in the moderately volatile minor elements Cu, Zn, and Ga as compared to CI. Both of these effects were previously reported in the fine-grained, anhydrous IDPs (*16*, *17*), some of which have inferred atmospheric entry speeds that suggest a cometary origin (*18*). The CI meteorite element abundances are presumed to represent the solar nebula composition for nonvolatile elements because of the good agreement between CI abundances and the composition of the solar photosphere (*6*). However, the abundances of Cu, Zn, and Ga are not well determined in the solar photosphere (*6*), which suggests that the Wild 2 particles and the anhydrous IDPs may better reflect the composition of the solar nebula for these moderately volatile elements.

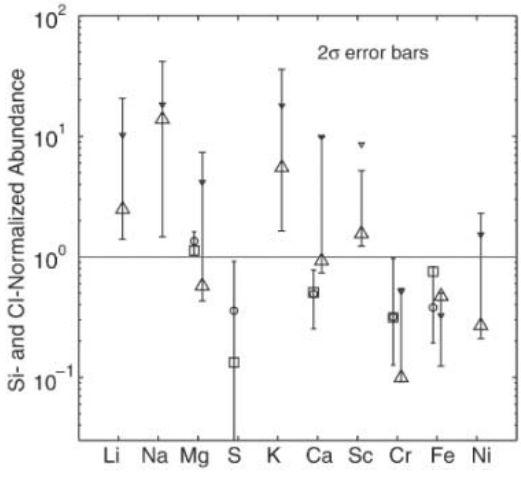

Fig. 4. CI- and Si-normalized average composition determined by summing the seven crater residue analyses (squares at Mg, S, Ca, Cr, and Fe) and by summing the same data set except for the largest crater (circles). The largest crater was produced by a particle having 82% of the total mass contributed by all seven particles, but the trend in the data is the same in both data sets, indicating that the mean composition is not significantly perturbed by the largest particle. TOF-SIMS results for five craters are also shown (large triangles at Li, Na, Mg, K, Ca, Sc, Cr, Fe, and Ni give the five-crater mean whereas the smaller triangles give the mean excluding the largest crater). The vertical bars show the 2σ statistical uncertainty (*4*).

References and Notes

1. P. Tsou *et al.*, *J. Geophys. Res.* **109**, E12S01 (2004).
2. A. J. Westphal *et al.*, *Meteorit. Planet. Sci.* **39**, 1375 (2004).
3. G. J. Flynn, F. Hörz, S. Bajt, S. R. Sutton, *Lunar Planet. Sci.* **XXVII**, 369 (1996).
4. See the supporting material on *Science* Online.
5. K. Lodders, *Astrophys. J.* **591**, 1220 (2003).
6. E. Anders, N. Grevese, *Geochim. Cosmochim. Acta* **53**, 197 (1989).
7. M. E. Zolensky *et al.*, *Science* **314**, 1735 (2006).
8. S. A. Sandford *et al.*, *Science* **314**, 1720 (2006).
9. A. T. Kearsley *et al.*, *Meteorit. Planet. Sci.*, in press.
10. A. T. Kearsley, M. J. Burchell, F. Hörz, M. J. Cole, C. S. Schwandt, *Meteorit. Planet. Sci.* **41**, 167 (2006).
11. F. Hörz *et al.*, *Science* **314**, 1716 (2006).
12. D. E. Brownlee, in *Properties and Interactions of Interplanetary Dust*, Proceedings of the Eighty-fifth Colloquium, Marseille, France, 9–12 July 1984 (Reidel, Dordrecht, Netherlands, 1985), pp. 143–147.
13. G. J. Flynn, S. R. Sutton, in *Proceedings of the 20th Lunar and Planetary Science Conference* (Lunar and Planetary Institute, Houston, TX, 1990), pp. 335–342.
14. J. Kissel, in *Advances in Mass Spectroscopy 1985, Proceedings of the 10th International Mass Spectrometry Conference*, Swansea, UK, 9–13 September 1985 (Wiley and Sons, Hoboken, NJ, 1986), pp. 175–184.
15. E. K. Jessberger, *Space Sci. Rev.* **90**, 91 (1999).
16. L. S. Schramm, D. E. Brownlee, M. M. Wheelock, *Meteoritics* **24**, 99 (1989).
17. G. J. Flynn *et al.*, in *Physics, Chemistry, and Dynamics of Interplanetary Dust*, B. Å. S. Gustafson, M. S. Hanner, Eds. (Astronomical Society of the Pacific, San Francisco, 1996), pp. 291–294.
18. D. E. Brownlee *et al.*, *Lunar Planet. Sci.* **XXIV**, 205 (1993).

19. Four synchrotrons used in this effort are national user facilities supported in part by the U.S. Department of Energy, Office of Science, Office of Basic Energy Sciences, under contract numbers (with managing institutions in parentheses) DE-AC02-05CH11231 (Advanced Light Source, University of California), DE-AC02-06CH11357 (Advanced Photon Source, University of Chicago Argonne, LLC), DE-AC02-98CH10886 (National Synchrotron Light Source, Brookhaven Science Associates), and DE-AC03-765F00515 (Stanford Synchrotron Radiation Laboratory, Stanford University). Experiments were performed at the BL47XU in the SPring-8 with the approval of the Japan Synchrotron Radiation Research Institute. The European Synchrotron Radiation Facility provided synchrotron radiation facilities. Stardust was the fourth flight project of NASA's Discovery Program.

Supporting Online Material

www.sciencemag.org/cgi/content/full/314/5806/1731/DC1
SOM Text
Figs. S1 to S11
Tables S1 to S4
References

10 October 2006; accepted 20 November 2006
10.1126/science.1136141

REPORT

Mineralogy and Petrology of Comet 81P/Wild 2 Nucleus Samples

Michael E. Zolensky,[1]* Thomas J. Zega,[2] Hajime Yano,[3] Sue Wirick,[4] Andrew J. Westphal,[5] Mike K. Weisberg,[6] Iris Weber,[7] Jack L. Warren,[8] Michael A. Velbel,[9] Akira Tsuchiyama,[10] Peter Tsou,[11] Alice Toppani,[12,13] Naotaka Tomioka,[14] Kazushige Tomeoka,[14] Nick Teslich,[12] Mitra Taheri,[2] Jean Susini,[15] Rhonda Stroud,[2] Thomas Stephan,[7] Frank J. Stadermann,[16] Christopher J. Snead,[5] Steven B. Simon,[17] Alexandre Simionovici,[18] Thomas H. See,[19] François Robert,[20] Frans J. M. Rietmeijer,[21] William Rao,[22] Murielle C. Perronnet,[1] Dimitri A. Papanastassiou,[23] Kyoko Okudaira,[3] Kazumasa Ohsumi,[24] Ichiro Ohnishi,[14] Keiko Nakamura-Messenger,[8] Tomoki Nakamura,[25] Smail Mostefaoui,[20] Takashi Mikouchi,[26] Anders Meibom,[20] Graciela Matrajt,[27] Matthew A. Marcus,[28] Hugues Leroux,[29] Laurence Lemelle,[18] Loan Le,[8] Antonio Lanzirotti,[30] Falko Langenhorst,[31] Alexander N. Krot,[32] Lindsay P. Keller,[1] Anton T. Kearsley,[33] David Joswiak,[27] Damien Jacob,[29] Hope Ishii,[12] Ralph Harvey,[34] Kenji Hagiya,[35] Lawrence Grossman,[17,36] Jeffrey N. Grossman,[37] Giles A. Graham,[12] Matthieu Gounelle,[20,33] Philippe Gillet,[18] Matthew J. Genge,[38] George Flynn,[39] Tristan Ferroir,[18] Stewart Fallon,[12] Denton S. Ebel,[40] Zu Rong Dai,[12] Patrick Cordier,[29] Benton Clark,[41] Miaofang Chi,[12] Anna L. Butterworth,[5] Donald E. Brownlee,[27] John C. Bridges,[42] Sean Brennan,[43] Adrian Brearley,[21] John P. Bradley,[12] Pierre Bleuet,[15] Phil A. Bland,[33,38] Ron Bastien[8]

The bulk of the comet 81P/Wild 2 (hereafter Wild 2) samples returned to Earth by the Stardust spacecraft appear to be weakly constructed mixtures of nanometer-scale grains, with occasional much larger (over 1 micrometer) ferromagnesian silicates, Fe-Ni sulfides, Fe-Ni metal, and accessory phases. The very wide range of olivine and low-Ca pyroxene compositions in comet Wild 2 requires a wide range of formation conditions, probably reflecting very different formation locations in the protoplanetary disk. The restricted compositional ranges of Fe-Ni sulfides, the wide range for silicates, and the absence of hydrous phases indicate that comet Wild 2 experienced little or no aqueous alteration. Less abundant Wild 2 materials include a refractory particle, whose presence appears to require radial transport in the early protoplanetary disk.

The nature of cometary solids is of fundamental importance to our understanding of the early solar nebula and protoplanetary history. Until now, we have had to study comets from afar using spectroscopy or settle for analyses of interplanetary dust particles (IDPs) of uncertain provenance. We report here mineralogical and petrographic analyses of particles derived directly from comet 81P/Wild 2.

All of the Wild 2 particles we have thus far examined have been modified in various ways by the capture process, in which cometary particles punched into the silica aerogel capture media, making various types of tracks and disaggregating into grains distributed along the tracks. All particles that may have been loose aggregates ("traveling sand piles") disaggregated into individual components, with the larger, denser components penetrating more deeply into the aerogel, making thin tracks with terminal grains (fig. S1). Individual grains experienced heating effects that produced results ranging from excellent grain preservation to melting (Fig. 1); such behavior was expected (*1*–*3*). What is remarkable is the extreme variability of these modifications and the fact that unmodified and severely modified materials can be found within 1 μm of each other, requiring tremendous local temperature gradients. Fortunately, we have an internal gauge of impact collection heating. Fe-Ni sulfides are ubiquitous in the Wild 2 samples and are very sensitive indicators of heating, and accurate chemical analyses can reveal which have lost S and which have not (and are therefore stoichiometric) (Fig. 2). Our surveys show that crystalline grains are found along the entire lengths of tracks, not just at track termini (fig. S1).

There appears to be very limited contamination from the spacecraft in the aerogel. Potential problems with secondary impacts (cometary grains striking the spacecraft, ricocheting, and splashing onto the aerogel) failed to materialize (*4*).

We have harvested samples from 52 tracks and have obtained a substantial understanding of the mineralogy of 26 of these. These tracks were chosen at random from those of average length. Analyses have also been performed on impact residues in seven aluminum foil craters >50 μm in diameter and on over 200 craters <5 μm in diameter (*5*). Crystalline materials are abundant in comet Wild 2 and many are coarse-grained relative to the submicrometer scales characteristic of many anhydrous IDPs and interstellar dust populations (*6*). Of the best-studied 26 tracks, 8 are dominated by olivine [$(Mg,Fe)_2SiO_4$] grains (tracks 1, 22, 26, 43, 57, 68, 71, and 77); 7 by low-Ca pyroxene [$(Mg,Fe)SiO_3$] (tracks 17, 20, 24, 27, 32, 41, and 69); 3 by a fairly equal amount of olivine and pyroxene (tracks 5, 10, and 35); and the remaining 8 by other minerals, mainly Fe-Ni sulfides. One of the latter tracks contains predominantly refractory minerals, one contains Na-silicate minerals, and five (tracks 36, 38, 42, 52, and 59) are dominated by ~5-μm-sized sulfide grains. These results suggest that crystalline materials are abundant in Wild 2.

In the seven large craters in aluminum foil that we examined, one contains only remnants of stoichiometric olivine, three are dominated by Mg-

silicates and sulfide, and two contain a mixture of mafic silicates and Na- and Ca-rich silicates. The last complex impact feature has overlapped bowl-shaped depressions containing residues with a heterogeneous collection of stoichiometric compositions, suggesting impact by an aggregate of micrometer-scale grains of Ca-rich clinopyroxene, Mg-rich pyroxene (probably enstatite), and a mixture of Fe-Ni sulfides, as well as grains composed of finely mixed silicate and sulfide. Just over half of the residue-bearing very small craters we examined contain mixtures of silicate and sulfur-bearing residue, whereas the others are mainly monomineralic olivine, pyroxene, and Fe-Ni sulfides, with occasional preservation of crystalline material.

Olivine, one of the most abundant minerals in the solar system (*7*–*9*), is present in the majority of Wild 2 particles. Its observed grain sizes range from submicrometer to over 10 μm. Wild 2 olivine has an extremely wide compositional range, from Fo_4 to Fo_{100} ["Fo" being the 100 × molar Mg/(Mg+Fe) ratio for olivine, just as "En" is the same ratio for low-Ca pyroxenes] (Fig. 3), with a pronounced frequency peak at Fo_{99}. Although it is possible that collection effects have biased surviving olivines to the most refractory, Mg-rich compositions, the abundance of Fe-rich olivine among the Wild 2 samples suggests that this effect has been minor. One olivine crystal in track 22 was found to display dramatic reverse chemical zoning, from the Fo_{70} core to the Fo_{92} rim. It is clear that these grains were not equilibrated during capture, because we would then observe a greatly reduced compositional range and a peak at a high Fe (low Fo value) concentration (*1*, *2*, *10*, *11*).

Wild 2 olivines include varieties with very elevated MnO, Al_2O_3, and Cr_2O_3 contents, up to 6.45, 0.71, and 1.46 weight %, respectively. About 25% of these Mn- and Cr-rich olivines contain <<1% FeO. Olivines with enrichments in these elements have been reported in carbonaceous chondrites, micrometeorites, and chondritic IDPs, though they are very rare (*12*–*16*). The compositions of the Mn- and Cr-rich olivines in the Wild 2 samples are similar to those in IDPs, carbonaceous chondrites, and unequilibrated ordinary chondrites (fig. S2). Many Wild 2 olivines contain inclusions of other phases, notably Fe-Cr-Ti oxides (including chromite), but thus far, melt inclusions have not been observed within any silicates. Olivine with low Fe and elevated Mn has been proposed to form from condensation in the protosolar nebula (*12*).

Wild 2 olivine-dominated grains are commonly polycrystalline, with some interstitial glass, which could be indigenous cometary glass. One fragment from the wall of the 1-cm-long track 35 was investigated by microtomography (*17*) and found to have a microporphyritic texture with olivine crystals (~Fo_{80}) set within lower-density fine-grained material, probably glass. From the manner in which the enclosing aerogel wraps around this particular grain without intruding into it, the glass appears to be indigenous. This fragment has an obvious igneous origin and resembles a microporphyritic chondrule. A terminal grain from track 26 consists of an intergrowth of fayalite (Fo_4) and tridymite, another texture observed in some chondrules.

Both low- and high-Ca pyroxenes are present among the Wild 2 grains, with the former being dominant. In some cases, synchrotron x-ray diffraction (SXRD) or selected-area electron diffraction

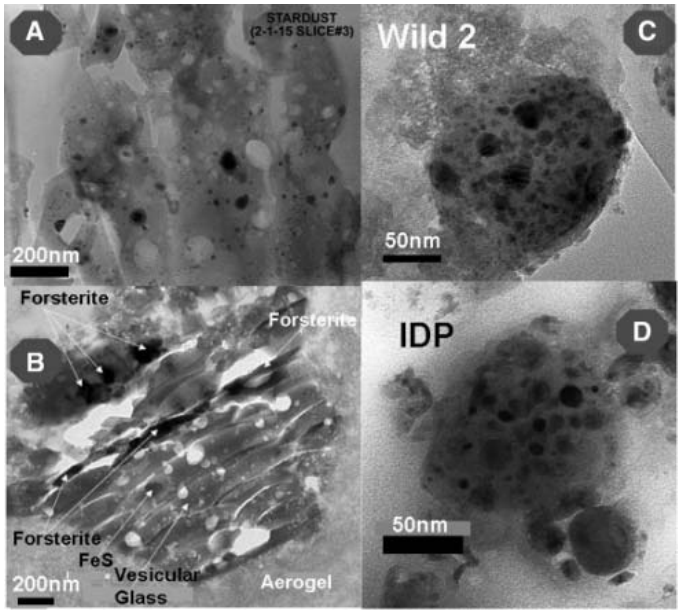

Fig. 1. Bright-field TEM images of Wild 2 grains. (**A**) View of the compressed and vesicular melted aerogel surrounding grains and lining track walls. Dark gray and black objects are admixed silicates, Fe-Ni metal, and Fe-Ni sulfides. (**B**) Captured Wild 2 grain composed predominantly of forsterite and Fe-sulfides, mantled by compressed-to-melted aerogel. (**C**) Glassy body from Wild 2 track 10, resembling a GEM; rounded dark inclusions are predominantly Fe-Ni metal, Fe-Ni sulfides, and ferromagnesian silicates. (**D**) GEM from an anhydrous chondritic IDP; rounded dark inclusions are predominantly Fe-Ni metal, Fe-Ni sulfides, and ferromagnesian silicates.

[1]Astromaterials Research and Exploration Science, NASA Johnson Space Center, Houston, TX 77058, USA. [2]Naval Research Laboratory, Code 6360, 4555 Overlook Avenue SW, Washington, DC 20375, USA. [3]JAXA-ISAS, 3-1-1 Yoshinodai, Sagamihara, Kanagawa 229-8510, Japan. [4]National Synchrotron Light Source, Brookhaven National Laboratory, Upton, NY 11973, USA. [5]Space Sciences Laboratory, University of California, 7 Gauss Way, Berkeley, CA 94720–7450, USA. [6]Department of Physical Sciences, Kingsborough Community College (CUNY), Brooklyn, NY 11235, USA. [7]Institut für Planetologie, Westfälische Wilhelms-Universität Münster, Wilhelm-Klemm-Strasse 10, 48149 Münster, Germany. [8]Jacobs Sverdrup, Engineering Science Contract Group, Houston, TX 77058, USA. [9]Department of Geological Sciences, 206 Natural Science Building, Michigan State University, East Lansing, MI 48824–1115, USA. [10]Department of Earth and Space Science, Osaka University, 1-1 Machikaneyama-cho, Toyonaka 560-0043, Japan. [11]Jet Propulsion Laboratory, M/S 183-501, 4800 Oak Grove Drive, Pasadena, CA 91109, USA. [12]Institute for Geophysics and Planetary Physics, Lawrence Livermore National Laboratory, Livermore, CA 94550, USA. [13]Centre de Spectrometrie Nucleaire et de Spectrometrie de Masse, Bâtiment 104, 91405 Orsay Campus, France. [14]Department of Earth and Planetary Sciences, Faculty of Science, Kobe University, Nada, Kobe 657-8501, Japan. [15]European Synchrotron Radiation Facility, Boîte Postale 220, 38043 Grenoble, France. [16]Department of Physics, Washington University, St. Louis, MO 63130, USA. [17]Department of Geophysical Sciences, The University of Chicago, 5734 South Ellis Avenue, Chicago, IL 60637, USA. [18]Laboratoire de Sciences de la Terre, Ecole Normale Superieure de Lyon, 46, Allee d'Italie, 69007 Lyon, France. [19]Engineering Science Contract/Barrios Technology, ARES/JSC, Houston, TX 77258–8447, USA. [20]Museum National d'Histoire Naturelle, Laboratoire d'Etude de la Matiere Extraterrestre, USM 0205 (LEME), Case Postale 52, 57 Rue Cuvier, 75005 Paris, France. [21]Department of Earth and Planetary Sciences, University of New Mexico, MSC 03-2040, Albuquerque, NM 87131–0001, USA. [22]Savannah River Ecology Lab, Aiken, SC 29801, USA. [23]Science Division, Jet Propulsion Laboratory, M/S 183-335, 4800 Oak Grove Drive, Pasadena, CA 91109, USA. [24]Institute of Materials Structure Science, Tsukuba-shi, Ibaraki-ken 305, Japan. [25]Department of Earth and Planetary Sciences, Faculty of Sciences, Kyushu University, Hakozaki, Fukuoka 812-8581, Japan. [26]Department of Earth and Planetary Science, University of Tokyo, Hongo, Bunkyo-ku, Tokyo 113-0033, Japan. [27]Department of Astronomy, University of Washington, Seattle, WA 98195, USA. [28]Advanced Light Source, Lawrence Berkeley National Laboratory, 1 Cyclotron Road, MS 2R2100, Berkeley, CA 94720, USA. [29]Laboratoire de Structure et Propriétés de l'Etat Solide, Bâtiment C6, Université des Sciences et Technologies de Lille, 59655 Villeneuve d'Ascq, France. [30]Consortium for Advanced Radiation Sources, The University of Chicago, Chicago, IL 60637, USA. [31]Institute of Geosciences, Friedrich-Schiller-University Jena, Burgweg 11, D-07749 Jena, Germany. [32]Hawaii Institute of Geophysics and Planetology, University of Hawaii, Honolulu, HI 96822, USA. [33]Impact and Astromaterials Research Centre, Department of Mineralogy, Natural History Museum, Cromwell Road, London, SW7 5BD, UK. [34]Department of Geology, Case Western Reserve University, Cleveland, OH 44106, USA. [35]Graduate School of Life Science, University of Hyogo, Koto 3-2-1, Kamigori, Ako-gun, Hyogo 678-1297, Japan. [36]Enrico Fermi Institute, The University of Chicago, 5640 South Ellis Avenue, Chicago, IL 60637, USA. [37]U.S. Geological Survey, 954 National Center, Reston, VA 20192, USA. [38]Impact and Astromaterials Research Centre, Department of Earth Sciences and Engineering, Imperial College of Science Technology and Medicine, Prince Consort Road, London, SW7 2AZ, UK. [39]Department of Physics, State University of New York, Plattsburgh, NY 12901, USA. [40]Department of Earth and Planetary Sciences, American Museum of Natural History, Central Park West at 79th Street, New York, NY 10024, USA. [41]Lockheed Martin Astronautics, Denver, CO 80201, USA. [42]Planetary and Space Sciences Research Institute, Open University, Milton Keynes, MK7 6AA, UK. [43]Stanford Linear Accelerator Center, Menlo Park, CA 94025, USA.

*To whom correspondence should be addressed. E-mail: michael.e.zolensky@nasa.gov

(SAED) patterns reveal low-Ca pyroxenes to be orthoenstatite, requiring slow cooling (*18*), but in the majority of cases we have only energy-dispersive x-ray analyses and are not certain whether we have ortho- or clinopyroxene. The compositional range displayed by the low-Ca pyroxene is also very extensive, from En_{52} to En_{100}, with a significant frequency peak centered at En_{95} (Fig. 3). Low-Ca pyroxene usually coexists with olivine, but the Mg/Fe ratios for coexisting phases are not always similar. Track 17 contains olivine in the range $Fo_{55–69}$, whereas associated low-Ca pyroxene is $En_{52–96}$. Flash heating during sample collection may account for this disparity, because olivine equilibrates faster than orthopyroxene under identical circumstances (*19*). Diopside occurs in several grains, usually in association with low-Ca pyroxene. A Ti-, Al-rich diopside is abundant within the calcium-, aluminum-rich inclusion (CAI)–like particle.

Sulfides are the only mineral group found in all extraterrestrial materials. Fe-Ni sulfides are also ubiquitous in the Wild 2 grains, grading from sulfides apparently melted and mixed with Fe-Ni metal, all the way to apparently unmodified FeS and pentlandite [$(Fe,Ni)_9S_8$] grains (fig. S3). Several tracks (such as track 59) have FeS- or pentlandite-dominated terminal grains. In this paper, we collectively refer to troilite (stoichiometric FeS) and pyrrhotite ($Fe_{1-x}S$) as FeS because the exact stoichiometry and structure are unknown in most instances. A plot of analyses of Wild 2 Fe-Ni sulfides (Fig. 2) shows that many have compositions close to that of FeS, with less than 2 atom % Ni. Only two pentlandite grains have been found. The complete lack of compositions in between these (intermediate solid solution compositions) suggests (but does not require) that FeS and pentlandite condensed as crystalline species [that is, did not condense as amorphous phases, which later became annealed (*20*)]. The remaining Fe-Ni sulfides (approximately half) have compositions that reflect progressive loss of S, because they trend from FeS directly toward the Fe apex. SAED patterns of these S-depleted phases show the presence of two different lattices: strong maxima for a Fe-Ni sulfide phase and a much finer pattern consistent with a metal phase, but which could be an oxide. Loss of S from Fe-Ni sulfides is almost certainly a result of capture heating and could be used to gauge the degree of capture modification of the enclosing Wild 2 grains. The two verified pentlandite crystals in only two Wild 2 tracks are intriguing because this phase is frequently an indicator of low-temperature metamorphism under oxidizing conditions and/or of aqueous alteration (*21*).

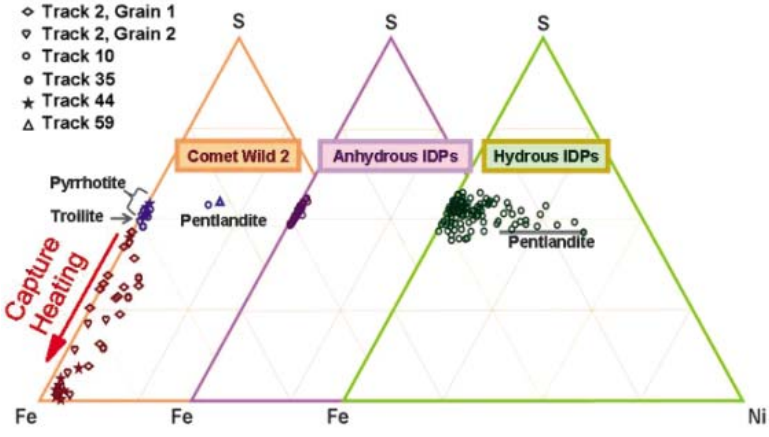

Fig. 2. Composition ranges of Fe-Ni sulfides from six grains from five Wild 2 particle tracks. Grains from track walls as well as track termini were analyzed. Most Wild 2 sulfides are probably a mixture of troilite and pyrrhotite, and two grains of pentlandite are present. Many sulfides plot with non-stoichiometric, low-S compositions reflecting capture heating. The corresponding composition ranges for hydrous and anhydrous chondritic IDPs (*21*) are also shown. Anhydrous chondritic IDPs contain only troilite and pyrrhotite, whereas the hydrous chondritic IDPs also have equally abundant Ni-rich sulfides, including pentlandite. With the exception of the two identified pentlandite crystals, the Wild 2 grains have the same Fe-Ni sulfide composition range as the anhydrous chondritic IDPs.

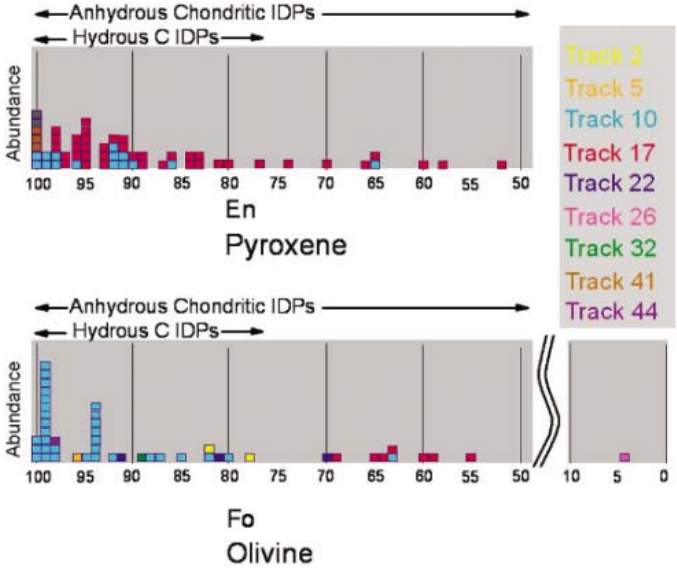

Fig. 3. Composition ranges of low-Ca pyroxene (En) and olivine (Fo) in grains from nine Wild 2 particles (tracks). Grains from track walls as well as track termini were analyzed, but predominantly the latter. The corresponding composition ranges for hydrous and anhydrous chondritic IDPs are also shown (*34*). The Wild 2 grains have the same olivine and low-Ca pyroxene composition ranges as the anhydrous chondritic IDPs, although the presence of mixed hydrous and anhydrous materials is compatible with these data.

Some of these are attached to Fe-Ni sulfides, suggesting a genetic relationship.

No evidence of phyllosilicates or indigenous carbonate has been seen in any Wild 2 samples. Despite the fact that substantial heating and structural modification accompanied the collection of many grains in the aerogel, we would have seen characteristic compositions, grain morphologies, and lattice fringes of phyllosilicates or carbonates had they

A Cu-Fe sulfide, probably cubanite ($CuFe_2S_3$), is present within terminal grains in at least two tracks (tracks 22 and 26). Cubanite is occasionally encountered in extraterrestrial materials, most commonly in carbonaceous chondrites. (Fe,Zn)S was found within a terminal grain from track 22. If it can be established that this phase is in equilibrium with FeS and metal, it may be appropriate to apply the sphalerite cosmobarometer to this particular particle (*22*).

Fe-Ni metal is present as nanoscale beads in significant quantities in most tracks, partly as a product of capture heating of Fe-Ni sulfides, but the high abundance of Ni in these shows that some of this metal is intrinsic to the comet particles. In addition, tracks 38 and 43 have ~5-μm-sized Fe-Ni metal terminal grains (Ni/Fe ~ 0.03), which appear to be indigenous cometary phases.

Some Wild 2 grains contain alkali-rich mineral assemblages, including phases in tracks 3 and 16 with compositions corresponding to K-feldspar (SAED patterns suggest a feldspar-like structure, but the exact phase is not known) and what appears to be eifelite [$KNa_2(MgNa)Mg_3Si_{12}O_{30}$] (track 56). Eifelite is in the osumilite mineral group, whose members have been reported in iron meteorites, as well as enstatite and ordinary chondrites (*23*), where they formed from a combination of igneous and metasomatic processes. In addition, alkali-rich silicate material is present in some of the larger craters in aluminum foil, but it has not been well characterized.

Transmission electron microscope (TEM) observations of some tracks revealed the presence of carbonaceous phases. In the terminal grain from tracks 10, 13, 27, 41, 57, and 58, there are submicrometer-sized subgrains of poorly crystalline carbon.

been present (*2*, *3*, *24*). Serpentine and Ca carbonates of the same sizes as in IDPs have been successfully captured in silica aerogel even at velocities 1 km/s higher than those experienced at Wild 2, in both laboratory simulations and actual IDP collection in Earth orbit aboard the Mir space station. In instances where phyllosilicates have been dehydrated, rendered amorphous, or recrystallized during capture in silica aerogel, characteristic grain morphologies and basal lattice spacings are formed, which signal the original mineralogy (*2*, *24*). Thus, the lack of these phases among the ~50 Wild 2 grains we have so far well characterized suggests that they could not have composed more than a few percent of the more coarse-grained fraction of captured Wild 2 samples.

Along most tracks are found abundant rounded, glassy silicate bodies containing submicrometer-sized beads of silicates, Fe-Ni sulfides, and Fe-Ni metal (Fig. 1, C and D). In some respects these bodies are similar to the bits of glass with embedded metal and sulfides (GEMS) common to most anhydrous chondritic IDPs (*6*), as well as one peculiar clast in the unequilibrated carbonaceous chondrite Ningqiang (*25*). It has been proposed that GEMS are among the most primitive of solar system materials, possibly recording the radiation environment of the early Sun or of a presolar environment (*6*).

The GEMS-like bodies in the tracks often stand out texturally from the typical and dominating aerogel capture medium in terms of composition, structure, and morphology. A composition comparison with true GEMS (Table 1) shows similarities but also important differences. For example, compared to the GEMS, the glassy bodies in the tracks have low Fe as compared to Mg and S (Table 1). Additionally, there exists a textural difference between GEMS and the Stardust glassy bodies. In GEMS, the inclusions are scattered about randomly and grade from nanometer- to submicrometer-sized objects (*6*). The glassy bodies in the aerogel tracks have coarser-grained inclusions and a tendency for these to be arranged in nonrandom patterns. Also, there are sometimes no distinct boundaries between the GEMS-like objects and the embedding aerogel. In addition, some of the metal grains in the Stardust glassy bodies have S-rich rims, which are not observed in GEMS. Because <5% of GEMS have isotopic compositions very different from terrestrial values (*26*), we have not been able to determine which, if any, of the glass bodies in the aerogel collectors are cometary "GEMS" and which might be formed as a result of the melting and intermingling of fine-grained cometary matter with aerogel during the capture process.

Table 1. Quantitative energy-dispersive x-ray spectral analyses (atomic %) of two GEMS-like objects embedded in the aerogel of track 35 (GEMS 1 and 2) compared with actual GEMS in a chondritic IDP and CI chondrite (CI) abundances.

Element (atom %)	GEMS-like 1 (60 nm in diameter)	GEMS-like 2 (100 nm in diameter)		GEMs in IDPs (*6*)			CI (*39*, *40*)
O	64.95	65.8	65.7	75.3	61.9	56.2	49.7
Mg	6.3	3.5	4.6	1.2	2.9	22.3	10.3
Si	26.4	28.4	26.0	19.1	16.9	13.3	11.5
S	1.75	1.65	2.7	1.2	6.1	3.2	5.7
Ca	0.1	0.1	0.15	Nd	0.15	nd	0.3
Cr	trace	trace	trace	0.2	0.3	0.1	0.3
Mn	0.1	0.1	0.15	0.1	nd	nd	0.2
Fe	0.3	0.2	0.5	2.2	11.1	4.2	20.0
Ni	0.1	0.1	0.2	0.4	nd	0.1	1.1
Al	nd	nd	nd	0.5	0.8	0.6	0.9

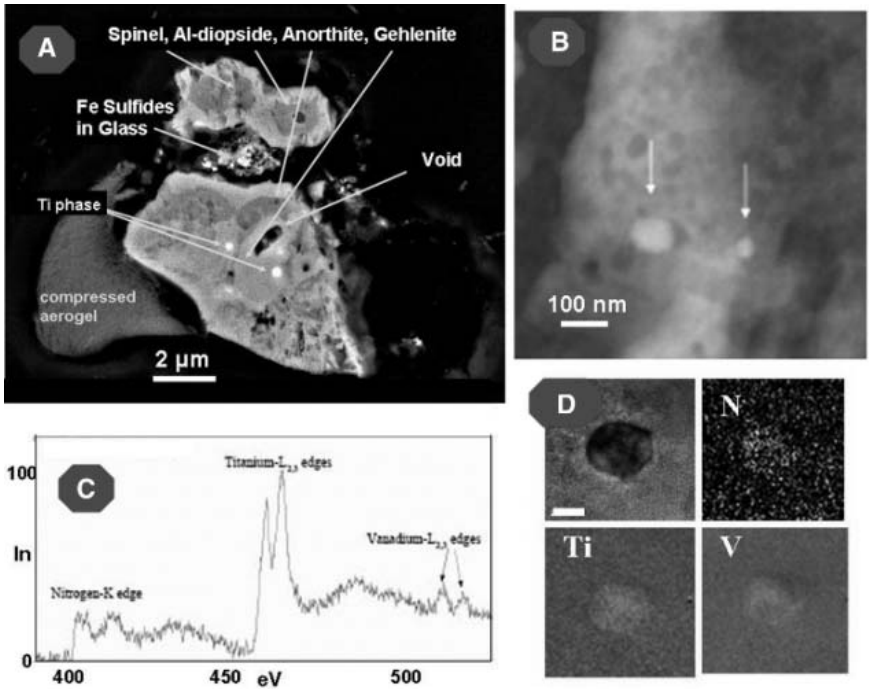

Fig. 4. The CAI-like grain from track 25. (**A**) Backscattered electron (BSE) image of the CAI-like grain from track 25, showing the gray shell of compressed-to-melted aerogel at lower left. (**B**) High-angle annular dark-field TEM image of two osbornite grains (arrows) within spinel. (**C**) EELS spectrum of an osbornite grain showing peaks for N, Ti, and V; scales represent intensity (In) and energy (in electron volts). (**D**) EELS element maps of an orbornite grain: BSE, N, Ti, and V. Scale bar, 40 nm.

One Wild 2 sample (track 25) has received special attention (Fig. 4) because it consists of very refractory minerals, including anorthite; a Ca-, Al-, Ti-rich clinopyroxene; gehlenite; spinel; corundum; FeS; V-bearing osbornite [(Ti,V)N]; and a phase that is probably perovskite. The osbornite occurs as sub–100-nm-sized grains within spinel, and its identification was carefully established by a combination of electron energy-loss spectroscopy (EELS) and SAED work; it may be associated with titanium oxide. The largest terminal grain from track 25 is ^{16}O-rich (*27*).

Track 25 yielded a terminal particle and at least four major subparticles, which have been characterized. These particles exhibit some similarities to and differences from the CAIs found in carbonaceous chondrites; in particular, they have mineralogies similar to CAIs in CV3 and CM2 chondrites (*5*) (CV3 and CM2 are among the most abundant types of carbonaceous chondrites), an important finding because the inclusions are known to be among the most primitive solar system objects (based on their mineralogy, reduced oxidation state, enrichments in refractory trace elements, isotopes, etc.).

The minerals within the Wild 2 CAI-like particle, especially the osbornite, require rather high temperatures for formation, possibly higher than 2000 K, depending on oxygen fugacity (*28*). According to equilibrium thermodynamic calculations, osbornite + spinel + Ca-rich clinopyroxene is a stable condensate assemblage in systems that are otherwise solar in composition only if their atomic C/O ratio lies between ~0.79 and ~0.97, which is well above the solar value of 0.5. The presence of a CAI-like particle in comet Wild 2 appears to require large-scale radial transport in the protoplanetary disk (*29*, *30*). Although the anorthite in this particle is too small for a meaningful search for evidence of ^{26}Al, this may prove possible in some refractory Wild 2 grains.

The recovered Wild 2 samples are mixtures of crystalline and amorphous materials. Analytical

electron microscopy (AEM) analysis of grains from the upper, often bulb-shaped, portions of tracks shows that they typically have widely varying compositions, sometimes similar to chondrites for most elements except Si, even in severely heated and melted regions (Table 1) (*31*). The crystalline grains observed among the upper portions of individual tracks are almost always submicrometer in grain size. These observations suggest that the materials captured in the upper portions of the tracks are, in general, much finer-grained than the material at the end of the slender, so-called stylus tracks that almost always project from the bulb-like upper tracks (fig. S1). AEM of very small craters on the aluminum foil also reveals crystalline olivine, pyroxene, and sulfides derived from separate submicrometer components within micrometer-sized particles. Synchrotron x-ray fluorescence (SXRF) analyses (*31*) suggest that 65 to 90% of the collected grains' mass is found in the upper portions of tracks, and only 10 to 35% is represented by the track termini grains. Our emerging model of the structure of the captured grains is that many were predominantly very fine-grained (submicrometer-sized) loosely bound aggregates with a bulk chondritic composition, most also containing much larger individual crystals (most commonly) of olivine, pyroxene, and Fe-Ni sulfides. Out of the ~70 tracks we have carefully photodocumented, only 2 appear to have no visible terminal grains, which indicates that practically all collected cometary particles contained some of these larger grains, which therefore probably served to nucleate the cometary particles. This view is supported by some of the larger crater morphologies observed on the Stardust Al foils, which have a multilobe appearance rather than being simple hemispherical craters (fig. S5) and can contain diverse subgrain compositions. This physical structure is consistent with several chondritic materials, most notably chondritic IDPs (*13*). In general, the captured Wild 2 grains are much finer-grained than the bulk of meteoritic matrix materials or IDPs.

Considering first the ferromagnesian mineral–dominated Wild 2 grains, the olivine and pyroxene crystals have the same range of Mg, Fe, Mn, and Cr compositions as those in anhydrous chondritic IDPs [with the exception of a single Fo_4 terminal grain (Fig. 3)] and are very similar to those in type 2 and some type 3 carbonaceous chondrites. The lack of hydrous phases among the Wild 2 samples precludes a common origin with type 1 or 2 chondrites. The type 3 carbonaceous chondrites (including primitive chondrites Acfer 094 and ALHA 77307) (*32*, *33*) and hydrous chondritic IDPs generally have narrower or somewhat equilibrated olivine and pyroxene compositional ranges (*34*). However, with the exception of the two pentlandite grains encountered in our examination, the Fe-Ni sulfide compositions of the Wild 2 grains are similar only to the anhydrous chondritic IDPs. Hydrous IDPs and all chondrites contain large amounts of pentlandite and low-Ni pentlandite (*21*). In addition, the absence of any identified aqueous alteration products in the Wild 2 grains (no phyllosilicates or indigenous carbonates, etc.) eliminates the hydrous chondritic materials from direct comparison.

No nuclear tracks (which are linear defects made by penetrating solar flare particles from the Sun) have yet been observed among Wild 2 samples. It is possible that the majority of these, if ever present, were annealed during capture, although some were observed in crater residue on the Long Duration Exposure Facility and in lunar silicate grains shot into aerogel (*35*).

In summary, the bulk of the Wild 2 samples appear to be weakly constructed mixtures of nanometer-scale grains with occasional much larger (>1 μm) ferromagnesian silicates, Fe-Ni sulfides, and Fe-Ni metal. The restricted compositional ranges of the sulfides and very wide range for silicates suggest that Wild 2 experienced little or no aqueous alteration. Of known extraterrestrial materials, the anhydrous chondritic IDPs and anhydrous micrometeorites are most similar to the Wild 2 grains, and in fact a cometary origin for anhydrous IDPs has been suspected for many years (*36*), whereas models of weakly constructed comet grains have been popular for years (*37*). The similarity of Wild 2 samples to some IDPs demands reexamination of the latter with new eyes, for there are some apparent differences. For example, Fe-Cr-Ti oxides have not been reported as inclusions in IDP olivines, nor has orthoenstatite been reported (*13*). The very wide ranges of olivine and low-Ca pyroxene compositions in Wild 2 require a wide range of formation conditions, including diverse temperatures and oxygen fugacities, probably reflecting different locations in the protoplanetary disk. It is critical to determine the role of annealing in cometary grain formation, but this cannot be done with the mineralogic data in hand.

The presence of a refractory particle resembling a meteoritic CAI among the Wild 2 grains raises many new questions. IDPs are believed to contain samples of both asteroids and comets, and wholly refractory IDPs were identified two decades ago (*31*, *32*) but have received very little attention. In mineralogical terms, the Wild 2 CAI-like particle appears similar to these poorly understood IDPs and is similar (though finer-grained) in various respects to CAI from CM, CR, and CH-CB carbonaceous chondrites. The presence of CAI-like material in a comet appears to require substantial radial transport of material across the early protoplanetary disk, as does the rather wide range of olivine and pyroxene compositions discussed above.

The lack of aqueous alteration products in Wild 2 samples is in clear contrast to the mineralogy reported for comet Tempel 1, based on Spitzer Space Observatory data in support of the Deep Impact mission (*9*). This mineralogical difference could be due to differences in the geological histories of Jupiter-family comets (*38*).

References and Notes

1. R. A. Barrett, M. E. Zolensky, R. Bernhard, *Lunar Planet. Sci.* **24**, 65 (1993).
2. F. Hörz, M. E. Zolensky, R. P. Bernhard, T. H. See, J. L. Warren, *Icarus* **147**, 559 (2000).
3. M. J. Burchell, G. Graham, A. Kearsley, *Annu. Rev. Earth Planet. Sci.* **34**, 385 (2006).
4. These issues are treated at greater length in the supporting material on *Science* Online.
5. F. Hörz *et al.*, *Science* **314**, 1716 (2006).
6. J. P. Bradley, *Science* **265**, 925 (1994).
7. E. K. Jessberger, A. Christoforidis, J. Kissel, *Nature* **332**, 691 (1988).
8. M. E. Lawler, D. E. Brownlee, S. Temple, M. M. Wheelock, *Icarus* **80**, 225 (1989).
9. C. Lisse *et al.*, *Science* **313**, 635 (2006).
10. J. Akai, *Proc. NIPR Symp. Antarct. Meteorites* **3**, 55 (1990).
11. M. E. Zolensky, W. H. Kinard, *Adv. Space Res.* **13**, 75 (1993).
12. W. Klöck, K. L. Thomas, D. S. McKay, H. Palme, *Nature* **339**, 126 (1989).
13. F. J. M. Rietmeijer, in *Planetary Materials*, J. J. Papike, Ed. (Mineralogical Society of America, Washington, DC, 1998), pp. 2-1–2-95.
14. M. Gounelle *et al.*, *Meteorit. Planet. Sci.* **37**, A55 (2002).
15. S. B. Simon, L. Grossman, *Meteorit. Planet. Sci.* **38**, 813 (2003).
16. M. K. Weisberg, H. C. Connolly, D. S. Ebel, *Meteorit. Planet. Sci.* **39**, 1741 (2004).
17. A. Tsuchiyama, *Lunar Planet. Sci. Conf.* **XXXVII**, abstract 2001 (2006).
18. W. A. Deer, R. A. Howie, J. Zussman, *Rock-Forming Minerals, Volume 2A, Single-Chain Silicates* (Longman, London, 1978).
19. J. Ganguly, V. Tazzoli, *Am. Mineral.* **79**, 930 (1994).
20. D. Vaughan, J. Craig, *Mineral Chemistry of Metal Sulfides* (Cambridge Univ. Press, Cambridge, 1978).
21. M. E. Zolensky, K. Thomas, *Geochim. Cosmochim. Acta* **59**, 4707 (1995).
22. M. N. Hutchison, S. D. Scott, *Geochim. Cosmochim. Acta* **47**, 101 (1983).
23. A. N. Krot, J. T. Wasson, *Meteoritics* **29**, 707 (1994).
24. R. A. Barrett, M. E. Zolensky, F. Hörz, D. J. Lindstrom, E. K. Gibson, *Proc. 19th Lunar Planet. Sci. Conf.* **22**, 203 (1992).
25. M. E. Zolensky *et al.*, *Meteorit. Planet. Sci.* **38**, 305 (2003).
26. S. Messenger, L. P. Keller, F. J. Stadermann, R. M. Walker, E. Zinner, *Science* **300**, 105 (2003).
27. K. D. McKeegan *et al.*, *Science* **314**, 1724 (2006).
28. D. Ebel, in *Meteorites and the Early Solar System II*, D. S. Lauretta, H. Y. McSween Jr., Eds. (Univ. of Arizona Press, Tucson, AZ, 2006), pp. 253–278.
29. F. Shu, H. Shang, A. E. Glassgold, T. Lee, *Science* **277**, 1475 (1997).
30. J. Cuzzi, S. Davis, A. Dobrovolskis, *Icarus* **166**, 385 (2003).
31. G. Flynn *et al.*, *Science* **314**, 1731 (2006).
32. A. J. Brearley, *Geochim. Cosmochim. Acta* **57**, 1521 (1993).
33. A. Greshake, *Geochim. Cosmochim. Acta* **61**, 437 (1997).
34. M. E. Zolensky, R. A. Barrett, *Meteoritics* **29**, 616 (1994).
35. P. Tsou *et al.*, *Lunar Planet. Sci. Conf.* **XXI**, 1264 (1990).
36. A. O. Nier, D. J. Shlutter, *Meteoritics* **28**, 675 (1993).
37. A. Li, M. Greenberg, *Astrophys. J.* **498**, L83 (1998).
38. D. E. Brownlee *et al.*, *Science* **314**, 1711 (2006).
39. E. Anders, M. Ebihara, *Geochim. Cosmochim. Acta* **46**, 2363 (1982).
40. In (*39*), carbon is ignored in the calculations and oxygen is calculated.

41. We thank the U.S. public for supporting the Stardust mission with valuable tax dollars and our many home institutions and funding agencies for making possible this concentrated 9-month-long analytical effort. The dedicated personnel of the Johnson Space Center Curation Facility were critical to our analytical efforts. We also thank our good friends at Lockheed Martin Space Systems for the wonderful spacecraft.

Supporting Online Material

www.sciencemag.org/cgi/content/full/314/5806/1735/DC1
Materials and Methods
Figs. S1 to S6
References

3 October 2006; accepted 20 November 2006
10.1126/science.1135842

ENSO as an Integrating Concept in Earth Science

Michael J. McPhaden,[1]* Stephen E. Zebiak,[2] Michael H. Glantz[3]

The El Niño–Southern Oscillation (ENSO) cycle of alternating warm El Niño and cold La Niña events is the dominant year-to-year climate signal on Earth. ENSO originates in the tropical Pacific through interactions between the ocean and the atmosphere, but its environmental and socioeconomic impacts are felt worldwide. Spurred on by the powerful 1997–1998 El Niño, efforts to understand the causes and consequences of ENSO have greatly expanded in the past few years. These efforts reveal the breadth of ENSO's influence on the Earth system and the potential to exploit its predictability for societal benefit. However, many intertwined issues regarding ENSO dynamics, impacts, forecasting, and applications remain unresolved. Research to address these issues will not only lead to progress across a broad range of scientific disciplines but also provide an opportunity to educate the public and policy makers about the importance of climate variability and change in the modern world.

The El Niño–Southern Oscillation (ENSO) cycle, a fluctuation between unusually warm (El Niño) and cold (La Niña) conditions in the tropical Pacific, is the most prominent year-to-year climate variation on Earth. El Niño and La Niña typically recur every 2 to 7 years and develop in association with swings in the Southern Oscillation, an atmospheric pressure pattern spanning the tropical Indian and Pacific Oceans that is intimately related to the strength of the Pacific trade winds. ENSO is unique among climate phenomena in its strength, predictability, and global influence, projecting beyond the tropical Pacific through atmospheric teleconnections that affect patterns of weather variability worldwide.

Major advances in ENSO research from the early 1980s to the mid-1990s included development of the ENSO observing system (*1*), theoretical understanding of the mechanisms responsible for the ENSO cycle and its global teleconnections (*2*, *3*), seasonal climate forecast models (*4*), and an elucidation of ENSO's human dimensions (*5*). Then, the extraordinary 1997–1998 El Niño focused worldwide attention on the ENSO cycle, its global impacts, and its socioeconomic consequences (*6*). Spurred by the enormity of this event, by some measures the strongest of the 20th century (*7*), interest in ENSO exploded in both the research community and the general public (*8*).

ENSO, with its cat's cradle of interconnected scientific and societal issues, has long been fertile ground for interdisciplinary research. Study of its causes and consequences takes on even greater importance today in view of efforts to develop informed policies for sustainable development and responsible stewardship of the environment. This article provides perspectives on recent advances, current trends, and present challenges in ENSO research and applications.

[1]NOAA/Pacific Marine Environmental Laboratory, Seattle, WA, USA. [2]International Research Institute for Climate and Society, Palisades, NY, USA. [3]National Center for Atmospheric Research, Boulder, CO, USA.

*To whom correspondence should be addressed. E-mail: michael.j.mcphaden@noaa.gov

ENSO Physics

A key feature of ocean-atmosphere interactions in the tropical Pacific is the positive feedback between trade wind intensity and zonal sea surface temperature (SST) contrasts referred to as the Bjerknes feedback (*9*). The trade winds normally pile up warm surface water in the western Pacific while upwelling colder water in the east from below the surface along the equator and off the west coast of South America. The resulting east-west surface temperature contrast reinforces an east-west air pressure difference across the basin that in turn drives the trades.

During El Niño, the trade winds weaken along the equator as atmospheric pressure rises in the western Pacific and falls in the eastern Pacific. Anomalous warming in the central and eastern Pacific ensues as warm water in the western Pacific migrates eastward and upwelling is reduced (Fig. 1). The Bjerknes feedback now runs in reverse, with weakened trade winds and SST warming tendencies along the equator reinforcing one another as El Niño develops.

Weakened trade winds at the onset of El Niño generate basin-scale waves in sea level, upper ocean currents, and temperatures that rapidly propagate eastward and westward along the equator. These waves initially support the growth of anomalously warm SSTs. However, after transiting the basin and reflecting off the eastern and western boundaries, they act in concert with upwelling favorable waves generated by wind forcing at the height of El Niño to eventually shut off the warming (*2*). Equatorial wave-induced cooling thus represents a delayed negative feedback that brings about the demise of El Niño and, if strong enough, the initiation of La Niña. The combination of Bjerknes and equatorial wave feedbacks controls the magnitude and duration of individual ENSO events and the interval between them. The mean seasonal cycle also acts as a pacemaker for ENSO, with the largest SST anomalies typically occurring near the end of the calendar year.

This basic conceptual framework for understanding ENSO does not imply that it is a purely cyclic phenomenon. The fluctuation between warm and cold events exhibits considerable irregularity in amplitude, duration, temporal evolution, and spatial structure. This irregularity has been interpreted as resulting from either nonlinear chaotic dynamics of the ocean-atmosphere system or from stochastic forcing by weather noise, including episodic "westerly wind bursts" and other forms of intraseasonal atmospheric variability (*2*).

The life cycles of El Niño and La Niña differ in important details (*10*), one of which is that nonlinear processes favor stronger El Niños than La Niñas (*11*). These differences may account in part for the skewed distribution of ENSO SST anomalies toward larger extreme warm vis-à-vis cold values (Fig. 2). The tendency for more and stronger El Niños than La Niñas from the mid-1970s to the late 1990s has also been cited as evidence for a decadal modulation of ENSO. Interaction with the Pacific decadal oscillation (PDO) (*12*) is one possible explanation, although it could also be simply that the ENSO cycle varies randomly on decadal time scales (*13*, *14*).

There is considerable debate at present about what causes the trade winds to relax at the onset of El Niño. One perspective is that ENSO freely oscillates between warm and cold phases as part of a continuum in which weakening of the trades at the onset of the warm phase results from large-scale deterministic processes operating during previous phases (*15*). Another perspective is that the ocean and atmosphere in the tropical Pacific tend to stably reside in a preferred state that is cold in the east and warm in the west and that El Niños occur only when the system is energized by high-frequency stochastic forcing (*16*). Arguments have been marshaled to support both perspectives, and there is evidence to suggest that the system may alternate between multidecadal epochs of more stable versus freely oscillating dynamics (*13*). This issue has considerable implications not only for our understanding of ENSO but also for our ability to improve ENSO forecast models, because predicting the onset of warm and cold events and their ultimate magnitude while still in the early stages of development may depend on accurate representation of both seasonal and shorter time scale dynamical processes in the ocean and the atmosphere (*17*).

Climate Impacts

Shifts in tropical Pacific precipitation patterns in response to El Niño warming in the central

and eastern Pacific typically bring drought to Australia, Indonesia, and neighboring countries, whereas the island states of the central Pacific and the west coast of South America are often inundated with heavy rains. Changes in the location and intensity of this rainfall and associated latent heat release into the atmosphere also lead to widespread changes in atmospheric circulation and weather patterns outside the tropical Pacific referred to as teleconnections (*3*). The remote effects of ENSO are felt in the North and South Pacific (Fig. 1), in all other ocean basins, on all seven continents (*3*, *18*, *19*), and in the stratosphere (*20*). Strong events like those in 1982–1983 and 1997–1998 have dramatic worldwide consequences, whereas weak events like the one in 2004–2005 (Fig. 2) may have impacts that are muted or even undetectable above the background weather noise of the atmosphere (*21*). La Niña often produces climate impacts that are roughly opposite to those of El Niño, although asymmetries in convective heating of the tropical atmosphere due to warm and cold SST anomalies favor larger atmospheric responses to strong El Niños than to strong La Niñas (*22*).

El Niño and La Niña affect the frequency, intensity, and spatial distribution of tropical storms. In the Atlantic, for example, hurricanes tend to be reduced in number and intensity during moderate to strong El Niño events but stronger and more numerous during La Niña events. These year-to-year changes translate into a 3-to-1 greater likelihood of a major Atlantic hurricane striking the United States during La Niña versus El Niño years, with correspondingly higher economic losses during La Niña years (*23*).

Geographically, the impacts of El Niño and La Niña are most consistent from event to event in the tropical Pacific and bordering areas where the atmosphere responds directly to SST forcing (*3*). Impacts are prominent but less consistent at higher latitudes and in other ocean basins remote from the Pacific because of interference from weather noise or other regional modes of climate variability. Teleconnections may also vary with time because of long-term changes in the structure and amplitude of ENSO SST anomalies or because of changes in atmospheric circulation that affect far-field responses to tropical Pacific SST forcing (*24*, *25*). Thus, although El Niño and La Niña often lead to systematic seasonal shifts in regional weather patterns that favor drought, flood, heat waves, and extreme events, actual impacts may vary from those expected for any given ENSO episode.

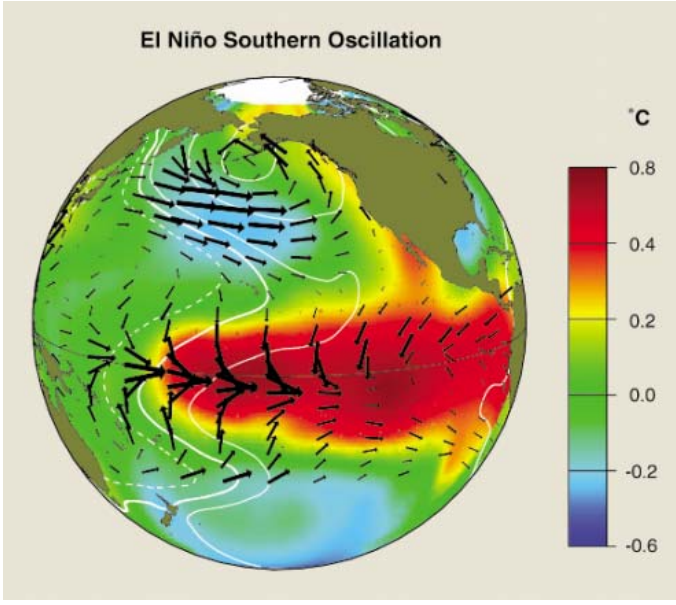

Fig. 1. El Niño anomalies in SST (color shading and scale in °C), surface atmospheric pressure (contours), and surface wind stress (vectors) in the Pacific basin. Pressure contour interval is 0.5 mb, with solid contours positive and dashed contours negative. Wind stress vectors indicate direction and intensity, with the longest vector equivalent to ~1 N m^{-2}. The patterns in this graphic are derived from a linear regression against SST anomalies averaged over 6°N–6°S, 90°W–180° in the eastern and central equatorial Pacific. All quantities scale up or down with the intensity of anomalies in this index region, that is, higher for strong El Niños and lower for weak El Niños. Anomalies of opposite sign apply to La Niña events, although there are some differences in the spatial patterns of El Niño and La Niña that this linear analysis does not capture (*10*, *11*).

Ecosystems

The altered environmental conditions that result from El Niño and La Niña influence global patterns of primary production (the fixation of carbon by plants) (*26*), with effects that ripple through higher levels of the food chain in both marine and terrestrial ecosystems. During El Niño, primary production in the tropical Pacific, which accounts for 10% of the total in the world ocean, significantly decreases in response to weakened upwelling (*27*). This reduced productivity affects the mortality, fecundity, and geographic distribution of marine mammals, sea birds, and commercially valuable fish species (*28*). El Niño's impact on Pacific ecosystems extends from the open ocean to the west coasts of North and South America and involves benthic as well as pelagic communities (*29*). Moreover, atmospheric teleconnections can influence marine ecosystems remote from the tropical Pacific, such as in the Southern Ocean where ENSO affects the abundance and distribution of krill, a keystone species in the Antarctic marine ecosystem (*30*).

Populations decimated by El Niño, particularly at higher trophic levels, may require several years to fully rebound. The collapse of the Peruvian anchovy fishery during the 1972–1973 El Niño is a classic example. The fishery was the largest in the world, with harvests of over 12 million metric tons in the early 1970s. However, a decade of overfishing had reduced the resilience of the anchovy stocks to withstand major environmental disturbances. This set the stage for a catastrophic shift in the ecosystem when sea temperatures warmed and the food chain was disrupted. Anchovy harvests during the subsequent 20 years were reduced by an order of magnitude, a reduction reinforced by a decadal shift toward warmer tropical Pacific temperatures in the mid-1970s (*31*).

Elevated temperatures associated with strong El Niño events lead to bleaching of tropical corals. The most massive and widespread episode of bleaching occurred during the 1997–1998 El Niño, when 16% of the world's reef-building coral died (*32*). Decadal warming trends in tropical ocean temperatures, possibly related to global warming, contributed to this bleaching by elevating background temperatures on which El Niño SST anomalies were superimposed.

ENSO influences terrestrial ecosystems primarily by altering patterns of rainfall, surface temperature, and sunlight availability, which affect primary productivity, plant and animal mortality, and species-specific reproductive strategies. Effects of El Niño and La Niña have been documented in such diverse environments as tropical rainforests, mangrove swamps, boreal forests, deserts, and semiarid shrub lands (*28*, *33*). In the Galapagos Islands, for example, seasons of unusually heavy rainfall associated with El Niños lead to the greening and flowering of an otherwise arid landscape. Sharp increases in the population of Darwin's finches result from the increased availability of seeds and insects, with some species faring better than others depending on body and beak size. Many broods of a reproductively successful finch species can hatch over the course of a strong El Niño event, so the forces of natural selection act to produce evolutionary changes in key physical traits that are passed from one generation to the next. These adaptations provide a unique demonstration of Darwin's theory of evolution (*34*).

Species may respond in unexpected ways to ENSO forcing as a result of biotic interactions involving competition and predator-

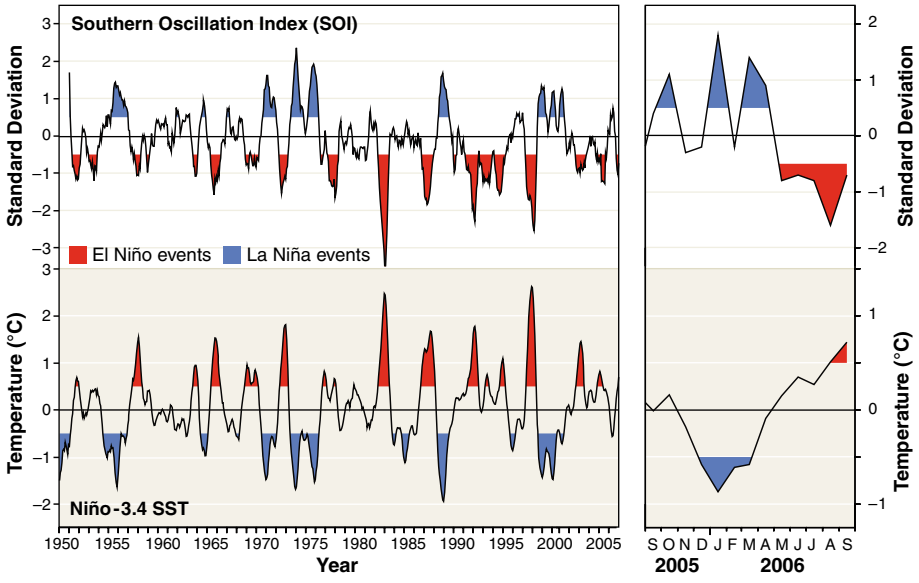

Fig. 2. The Southern Oscillation index (SOI) and Niño-3.4 SST index for January 1950 to September 2006. This plot illustrates the coupled interactions between the ocean and the atmosphere that give rise to ENSO variations. Low SOI values are associated with weaker trade winds and warm sea temperatures (El Niño), whereas high SOI values are associated with stronger trade winds and cold sea temperatures (La Niña). The Niño-3.4 index is computed from monthly SST anomalies in the region 5°N–5°S, 120°–170°W. Positive anomalies >0.5°C indicate El Niño events, and negative anomalies 0.5 are shaded to emphasize the relationship with El Niño and La Niña. In the left panel, values have been smoothed with a 5-month running mean for clarity. The right panel shows the last 13 months of the record (unsmoothed) to highlight developing El Niño conditions in late 2006. Note the different scales for Niño-3.4 SST and SOI in the two panels.

prey relationships (*28*). ENSO impacts may also be exaggerated by land-use practices (*35*) and in some cases may catalyze shifts in ecosystems that persist stably for decades (*33*). Forest fires, like those that burned out of control over large drought-affected regions of Central America, the Amazon, and Indonesia during the 1997–1998 El Niño, result in catastrophic changes in ecosystem structure and function as habitat is destroyed and endemic populations are decimated. Local extinctions that affect biodiversity are also possible as in the case of fig wasps in Borneo, which disappeared as a result of extreme drought associated with the 1997–1998 El Niño (*36*).

Global Carbon Cycle

Year-to-year variability in global atmospheric carbon concentrations is dominated by the ENSO cycle (*37*). The equatorial Pacific is the largest natural oceanic source of carbon to the atmosphere, outgassing about 1 billion metric tons of carbon in the form of CO_2 per year. The source of this carbon is equatorial upwelling, which brings water rich in inorganic carbon from the interior ocean to the surface. During El Niño, equatorial upwelling is suppressed in the eastern and central Pacific, significantly reducing the supply of CO_2 to the surface (*38*). As a result, the global increase in atmospheric CO_2, which is primarily driven by anthropogenic sources, noticeably slows down during the early stages of an El Niño. However, during the later stages of an El Niño, global CO_2 concentrations rise sharply, reflecting the delayed response of the terrestrial biosphere to El Niño–induced changes in weather patterns. Widespread droughts and elevated temperatures in the tropics contribute to an increase in the number and extent of forest fires and to modification of the balance between respiration and photosynthetic uptake of CO_2 in land plants. These processes, which were particularly pronounced during the severe 1982–1983 and 1997–1998 El Niños (*39*), result in an anomalous increase in the supply of CO_2 to the atmosphere sufficient to override the reduction in CO_2 from decreased equatorial upwelling. Forest fires in Indonesia during the 1997–1998 El Niño, because of their scale and duration, released unprecedented amounts of CO_2 into the atmosphere, producing the largest annual increase in concentrations since record-keeping began in 1957 (*40*).

Forecasting ENSO and Its Impacts

Except for the regular progression of the seasons, ENSO is the most predictable climate fluctuation on the planet. Its predictability is based on wind-driven seasonal variations in the amount of heat stored in the upper few hundred meters of the tropical Pacific Ocean. These variations affect sea surface temperatures, which in turn influence the global atmospheric circulation. The ability to predict ENSO was first demonstrated in the mid-1980s using simple dynamical and statistical models (*4*). This was followed by the development of several other forecast systems of increasing sophistication, with skill (a quantitative measure of forecast accuracy) expected for lead times of up to a year. Surprisingly however, weak to moderate strength ENSO-related fluctuations of the early to mid-1990s were not well predicted. Forecast models also failed to predict the onset, rapid growth, ultimate magnitude, and sudden demise of the giant 1997–1998 El Nino with uniform reliability (*41*).

Despite considerable efforts in model and forecast system development, progress in improving prediction skill has been very modest in recent years. Dynamical methods offer the most promise for further improvement in the long term, but they are not at present systematically better than statistical methods (*42*). Virtually all coupled climate models exhibit significant bias errors in the simulation of ENSO variations and the mean tropical Pacific climate (*43*). Coupled model forecasts are also prone to experience "initialization shock," a rapid unphysical adjustment toward the model climatology that can interfere with the ability to correctly evolve real climate signals. Moreover, few if any 3 of these models realistically represent variability associated with westerly wind bursts and other tropical intraseasonal time-scale fluctuations.

In parallel with efforts to reduce model biases, minimize initialization shock, and improve overall model performance, ensemble forecast methods have recently been developed to enhance forecast skill. These methods involve averaging over several individual forecasts from a single model or averaging over the forecasts from several different models (*44*). One such ensemble illustrates SST predictions for the development of an El Niño this year (Fig. 3). Warming is already under way (Fig. 2), although there is uncertainty in the ultimate strength of the event given the spread of the forecasts, which range from weak to moderate in amplitude. It is noteworthy that this ensemble of models did not predict significantly enhanced probabilities of El Nino development until July 2006, more or less coincident with the occurrence of westerly wind bursts in the western Pacific and observed warming in the central Pacific.

From a societal perspective, it is important to predict not only ENSO-related ocean temperature fluctuations but also seasonal climate anomalies throughout the world. Statistical and dynamical modeling approaches are both presently used for this purpose (*45*), and they indicate the likely development of typical El Niño temperature and precipitation anomalies for the 2006–2007 boreal fall and winter season (*46*). However, as with the ultimate magnitude of the event, there is considerable uncertainty at present in the expected severity of its impacts.

Promising methods to improve forecasting of seasonal climate anomalies in the future are under development, including those that combine information from an ensemble of dynamical global climate models weighted according to their relative reliability (*47*).

Practical Applications

ENSO variability affects agriculture, power generation, fresh water resources, public health and safety, forestry, fisheries, transportation, tourism, financial markets, and many other spheres of climate-sensitive human endeavor (*48*). To cite a few specific examples, ENSO-related changes in temperature and precipitation create conditions favorable for the spread of zoonotic, insect-borne, and water-borne diseases such as hantavirus, malaria, dengue fever, and cholera (*49*). As a measure of impact, many of the 22,000 lives lost during the 1997–1998 El Niño were related to disease outbreaks in the developing world (*6*). The unprecedented scale of the Indonesian forest fires (*35*) and the resulting veil of haze and smog throughout Southeast Asia during 1997–1998 also led to widespread respiratory illness (*50*).

Drought as well as flooding can adversely affect both subsistence agriculture and the production of cash crops. ENSO-related shifts in precipitation patterns have affected the production of wheat, rice, maize, sugar cane, and other important crops in far-flung corners of the globe (*48*, *51*, *52*). Historically, drought-related crop failures due to El Niño were a major contributor to famine that would periodically devastate vulnerable populations (*53*).

Current ENSO climate forecasts have modest skill at two- to three-season lead times, although for specific seasons and locations performance is much better (*45*). Thus, even in view of their limitations, ENSO forecasts can provide valuable input to the development of risk-management strategies for many climate-sensitive activities. In addition, although forecasting the precise onset of warm and cold events is problematic, it is known that ENSO SST anomalies during the second half of the calendar year tend to persist for about two seasons. Therefore, once an event is under way, simply being able to observe and describe its evolution can provide valuable information for decision makers.

The predictability of ENSO has prompted many efforts to make practical use of climate analysis and forecast information (*54*). Examples include input to management strategies for public health (*50*, *55*), agriculture and food security (*51*, *52*), fresh water resources (*56*), and fisheries (*57*). ENSO's impacts on storm-generated surface waves and coastal ocean circulation, which affect geological processes such as shoreline erosion and accretion, have been factored into land development and coastal zone management plans at local governmental levels (*58*).

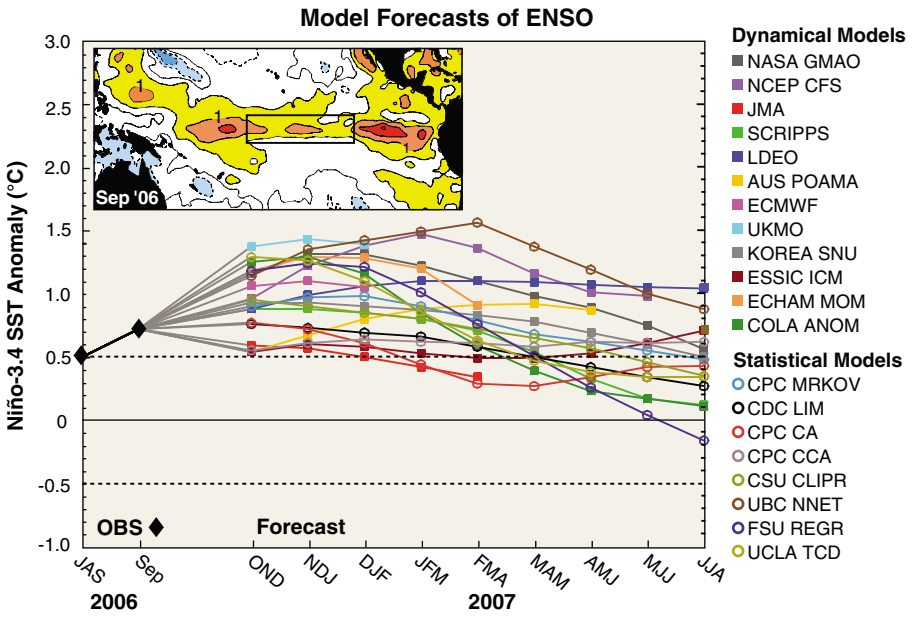

Fig. 3. Statistical and dynamical model forecasts for SST in the Niño-3.4 region (5°N–5°S, 120°–170°W). Forecasts in most cases are from September 2006 initial conditions and are for seasonal averages from October-November-December (OND) 2006 through June-July-August (JJA) 2007 seasonal averages. Most models predict significant warm anomalies (>0.5°C anomaly), indicating the likelihood of a weak to moderate strength El Niño lasting at least into boreal spring 2007. The forecasts represent ensemble means or, for most statistical models, a single deterministic forecast. Institutions involved in issuing the forecasts are indicated by different symbols and listed at right (*80*). Area between the dashed lines at ±0.5°C indicates neutral conditions. Observed values (OBS) for July-August-September (JAS) 2006 and for September 2006 alone are shown as black diamonds. The inset shows observed SST anomalies averaged over 3 to 30 September 2006, with the Niño-3.4 region outlined. Contour interval in the inset is 0.5°C, with warm anomalies in yellow to red colors and cold anomalies in blue. See http://iri.columbia.edu/climate/ENSO/currentinfo/SST_table.html for a description of the various models and the methods by which the forecasts are compiled.

To be of value, seasonal forecasts need to be delivered with sufficient accuracy, timeliness, and detail. Communicating the probabilistic nature of the forecasts and their uncertainties is also essential (*52*) because forecasts are not 100% perfect and outcomes sometimes are at odds with expectations. Despite these challenges, though, prudent use of ENSO forecasts can pay dividends. California, for instance, saved US $1 billion in 1997–1998 as a result of actions taken by individuals, businesses, and government in response to advance warning of El Niño's impending impacts (*59*).

Most efforts to make use of ENSO forecast information have focused on preparing for El Niño events because in the past 25 years they have tended to be more frequent, stronger, and dramatic in terms of impacts than La Niña events. However, predictability can be exploited advantageously for both phases of the ENSO cycle (*60*). Also, it is often the adverse impacts of ENSO variations that receive the most publicity, whereas the benefits, at least for some regions of the globe, are much less understood and appreciated. It is estimated, for example, that the 1997–1998 El Niño resulted in a net benefit of $20 billion to the U.S. economy because of the reduced number of land-falling hurricanes and the unusually warm winter in the Midwest (*59*).

ENSO Past and Future

Evidence from natural climate archives such as corals and lake sediments indicates that ENSO varied significantly in strength in the geologic past. For example, changes in the Earth's radiation balance due to major volcanic eruptions, variations in solar output, and the precession of the Earth about its axis have all affected the ENSO cycle over the past 130,000 years (*9*, *61*, *62*). Further back in time, permanent El Niño–like conditions developed in the tropical Pacific during the warm Pliocene ~3 to 5 million years ago when atmospheric CO_2 levels were comparable to those of today (*63*). Also, evidence suggests a more energetic ENSO cycle during the Eocene "hothouse" ~35 to 55 million years ago when atmospheric CO_2 concentrations approached levels that were twice the pre-industrial values (*64*).

Past climates are not exact analogs for the modern world, but it is reasonable to assume that changes in the radiative balance of the earth due to anthropogenic greenhouse gas emissions could affect climatic conditions in the tropical Pacific. Using this logic, some investigators have interpreted the tendency for stron-

ger and more frequent El Niños than La Niñas since the mid-1970s (Fig. 2) as a manifestation of global warming. This recent behavior is, however, most likely not outside the range expected for natural climate variability (*62*, *65*). Competing hypotheses, such as random fluctuations or interaction with the PDO, are equally plausible (*13*). Thus, there is no definitive evidence from the instrumental record at present for changes in ENSO behavior in response to greenhouse gas forcing.

How future global warming may affect ENSO is open to debate. The consensus outlook from the current generation of global climate models suggests no significant change in ENSO characteristics under various greenhouse gas emission scenarios that presume a doubling of atmospheric CO_2 from preindustrial levels over the next 100 years (*66*). Similarly, there is no clear indication of a significant shift toward either permanent El Niño–like or permanent La Niña–like background conditions in response to doubled CO_2 concentrations (*9*, *66*). However, climate models have known flaws that compromise the reliability of future projections in the tropical Pacific (*67*).

Therefore, we cannot say with confidence at present how global warming will affect either ENSO variability or the background state on which it is superimposed (*9*). Nonetheless, substantial long-term changes in the tropical Pacific, if they were to occur, could amplify global warming (*63*, *68*) and leave regional-scale fingerprints on it by shifting the probability distribution of ENSO-related teleconnections. These changes would affect marine and terrestrial ecosystems, in some cases counterintuitively because of species interactions or other nonlinear biological processes (*33*). Systematic changes in the tropical Pacific would feed back to the global carbon cycle by modifying the balance of carbon sources and sinks in the ocean and on land (*38*). Altered climatic conditions in the tropical Pacific would likewise introduce a wild card into the effects of global warming on hurricane frequency and intensity, currently a topic of hot debate (*69*).

Concluding Remarks

The first years of the 21st century have witnessed a burgeoning interest in the ENSO cycle, its impacts on the Earth system, and its socioeconomic consequences. This interest was stimulated by the powerful 1997–1998 El Niño and enabled by research advances over the previous two decades. ENSO is the strongest and most predictable natural variation of Earth's climate on year-to-year time scales, affecting physical, biological, chemical, and geological processes in the oceans, in the atmosphere, and on land. As a key piece of Earth's complex climate puzzle, it provides a conceptual framework within which to coherently interpret seemingly disconnected events in widely separated parts of the globe. By virtue of their recurrence every few years and their distinctive global pattern of environmental impacts, El Niño and La Niña also provide a unique context for developing testable hypotheses about how various components of the Earth system respond to climate forcing. Knowledge about the ENSO cycle and the ability to forecast its variations, however limited at present, supply valuable information for economic development, public welfare, and responsible stewardship of Earth's limited natural resources. From a broad perspective, therefore, ENSO represents an integrating concept across a range of disciplines in the Earth and related social sciences. Moreover, as a fascinating scientific problem with real-time climate impacts and tangible socioeconomic consequences, ENSO offers an opportunity to educate the public and policy makers about natural climate variability and, by extension, climate change.

References and Notes

1. M. J. McPhaden *et al.*, *J. Geophys. Res.* **103**, 14,169 (1998).
2. J. D. Neelin *et al.*, *J. Geophys. Res.* **103**, 14,261 (1998).
3. K. E. Trenberth *et al.*, *J. Geophys. Res.* **103**, 14,291 (1998).
4. M. Latif *et al.*, *J. Geophys. Res.* **103**, 14,375 (1998).
5. M. H. Glantz, *Current of Change: Impacts of El Niño and La Niña on Climate and Society.* (Cambridge Univ. Press, Cambridge, UK, 2001).
6. It has been estimated that the 1997–1998 El Niño resulted in 22,000 fatalities and US $36 billion in economic losses worldwide (*70*).
7. M. J. McPhaden, *Science* **283**, 950 (1999).
8. According to the Web of Science Citation Index (*71*), during the 5-year period from 2001 to 2005, 4257 publications in the refereed earth science literature appeared with El Niño, La Niña, or ENSO in the abstract, the title, or as a key word. This output represents more than half of all 8128 ENSO-related papers published in the 40 years since 1966 when the first seminal paper on El Niño as a basin-wide phenomenon was published (*72*).
9. M. A. Cane, *Earth Planet. Sci. Lett.* **230**, 227 (2005).
10. N. Larkin, D. E. Harrison, *J. Clim.* **15**, 1118 (2002).
11. S.-I. An, F. F. Jin, *J. Clim.* **17**, 2399 (2004).
12. N. J. Mantua, S. R. Hare, *J. Oceanogr.* **58**, 35 (2002).
13. A. V. Fedorov, S. G. H. Philander, *Science* **288**, 1997 (2000).
14. It has been proposed that the Pacific Decadal Oscillation results from rather than causes the decadal variation of ENSO (*73*).
15. D. Chen, M. A. Cane, A. Kaplan, S. E. Zebiak, D. Huang, *Nature* **428**, 733 (2004).
16. W. S. Kessler, *Geophys. Res. Lett.* **29**, 2125 10.1029/2002GL015924 (2002).
17. High-frequency intraseasonal forcing has often been characterized in terms of purely stochastic noise. However, large-scale seasonally varying background conditions in the tropical Pacific modulate aspects of this forcing, such as seasonal mean variance levels, so there may be a partially deterministic and predictable component to it as well (*74*).
18. ENSO teleconnections to Europe are relatively weak, but there is potentially a predictable signal in European rainfall during boreal spring after the peak SST anomalies in both El Niño and La Niña years (*75*).
19. ENSO impacts in Antarctica are described in (*76*).
20. M. Taguchi, D. L. Hartmann, *J. Clim.* **19**, 324 (2006).
21. The weakness of the 2004–2005 El Niño and its short-lived, limited climatic impacts sparked controversy in the scientific community as to whether the event should even be classified as an El Niño (*77*).
22. M. P. Hoerling, A. Kumar, T. Xu, *J. Clim.* **14**, 1277 (2001).
23. R. A. Pielke Jr., C. N. Landsea, *Bull. Am. Meteorol. Soc.* **80**, 2027 (1999).
24. H. F. Diaz, M. Hoerling, J. K. Eischeid, *Int. J. Climatol.* **21**, 1845 (2001).
25. Many of the confounding factors that affect the robustness of ENSO teleconnections may have been at work in weakening the relationship between ENSO and Indian summer monsoon rainfall during the 1980s and 1990s (*78*).
26. M. J. Behrenfeld *et al.*, *Science* **291**, 2594 (2001).
27. F. P. Chavez *et al.*, *Science* **286**, 2126 (1999).
28. N. C. Stenseth *et al.*, *Science* **297**, 1292 (2002).
29. L. Levin *et al.*, *Prog. Oceanogr.* **53**, 1 (2002).
30. L. B. Quetin, R. M. Ross, *Mar. Ecol. Prog.* **259**, 185 (2003).
31. F. P. Chavez, J. Ryan, S. E. Lluch-Cota, M. Ñiquen, *Science* **299**, 217 (2003).
32. G. R. Walther *et al.*, *Nature* **416**, 389 (2002).
33. M. Holmgren *et al.*, *Front. Ecol. Environ* **4**, 87 (2006).
34. P. R. Grant, B. R. Grant, *Science* **296**, 707 (2002).
35. F. Siegert, G. Ruecker, A. Hinrichs, A. A. Hoffman, *Nature* **414**, 437 (2001).
36. R. D. Harrison, *Proc. R. Soc. London B. Biol. Sci.* **267**, 911 (2000).
37. P. J. Rayner, I. G. Enting, R. J. Francey, R. Langenfelds, *Tellus* **51B**, 213 (1999).
38. R. A. Feely *et al.*, *J. Geophys. Res.* **111**, C08S90, doi: 10.1029/2005JC003129 (2006).
39. S. J. Wright, in *Rain Forests: Past, Present, and Future*, E. Bermingham, C. Dick, C. Moritz, Eds. (Univ. Chicago Press, Chicago, 2005), pp. 295–310.
40. S. E. Page *et al.*, *Nature* **420**, 61 (2002).
41. A. G. Barnston, M. H. Glantz, Y. He, *Bull. Am. Meteorol. Soc.* **80**, 217 (1999).
42. G. J. van Oldenborgh, M. A. Balmaseda, L. Ferranti, T. N. Stockdale, D. L. T. Anderson, *J. Clim.* **18**, 3240 (2005).
43. E. Guilyardi, *Clim. Dyn.* **26**, 329 (2006).
44. T. N. Palmer *et al.*, *Bull. Am. Meteorol. Soc.* **85**, 853 (2004).
45. L. Goddard *et al.*, *Int. J. Climatol.* **21**, 1111 (2001).
46. NOAA, National Weather Service, Climate Prediction Center, ENSO Diagnostic Discussion Archives, www.cpc.ncep.noaa.gov/products/expert_assessment/ENSO_DD_archive.shtml.
47. F. J. Doblas-Reyes, R. Hagedorn, T. N. Palmer, *Tellus* **57A**, 234 (2005).
48. M. H. Glantz, Ed., *Once Burned, Twice Shy: Lessons Learned from the 1997-98 El Niño* (United Nations Univ. Press, Tokyo, 2000).
49. The actual occurrence and severity of disease outbreaks depends not only on climatic influences like ENSO but also on a variety of other socioeconomic factors, such as poverty level, public health and sanitation, exposure risks, and government intervention policies. See (*78*) for a review of ENSO and health.
50. R. S. Kovats, M. J. Bouma, S. Hajat, E. Worrall, A. Haines, *Lancet* **362**, 1481 (2004).
51. R. Naylor, W. Falcon, N. Wada, D. Rochberg, *Bull. Indonesian Econ. Stud.* **38**, 75 (2002).
52. A. Patt, C. Gwata, *Glob. Environ. Change* **12**, 185 (2002).
53. M. Davis, *Late Victorian Holocausts: El Niño Famines and the Making of the Third World* (Verso, London, 2001).
54. It is not so much that social and economic losses associated with weather-related hazards are greater during El Niño or La Niña events but that during these times climate conditions may be predictable with greater accuracy (*79*).
55. M. C. Thomson *et al.*, *Nature* **439**, 576 (2006).
56. F. A. S. Filho, U. Lall, *Water Resour. Res.* **39**, 1307 10.1029/2002WR001373 (2003).
57. K. A. Broad, P. Pfaff, M. H. Glantz, *Clim. Change* **54**, 415 (2002).
58. J. C. Allan, P. D. Komar, G. R. Priest, *J. Coast. Sci.* **38**, 83 (2003).
59. S. A. Changnon, *Bull. Am. Meteorol. Soc.* **80**, 1819 (1999).
60. M. H. Glantz, Ed., *La Nina and Its Impacts* (United Nations Univ. Press, Tokyo, 2002).

61. M. E. Mann, M. A. Cane, S. E. Zebiak, A. Clement, *J. Clim.* **18**, 447 (2005).
62. A. W. Tudhope *et al.*, *Science* **291**, 1511 (2001).
63. A. V. Fedorov *et al.*, *Science* **312**, 1485 (2006).
64. M. Huber, R. Caballero, *Science* **299**, 877 (2003).
65. C. Wunsch, *Bull. Am. Meteorol. Soc.* **80**, 245 (1999).
66. G. J. van Oldenbourgh, S. Y. Philip, M. Collins, *Ocean Science* **1**, 81 (2005).
67. K. AchutaRao, K. R. Sperber, *Clim. Dyn.* **27**, 1 (2006).
68. K. E. Trenberth, J. M. Caron, D. P. Stepaniak, S. Worley, *J. Geophys. Res.* **107**, 4065 10.1029/2000JD000298 (2002).
69. A. Witze, *Nature* **441**, 564 (2006).
70. K. Sponberg, *Compendium of Climatological Impacts*, National Oceanic and Atmospheric Administration, Washington, DC, (1999).
71. Web of Science Citation Index, http://isiknowledge.com
72. J. Bjerknes, *Tellus* **18**, 820 (1966).
73. K. B. Rodgers, P. Friedrichs, M. Latif, *J. Clim.* **17**, 3761 (2004).
74. I. Eisenman, L. Yu, E. Tziperman, *J. Clim.* **18**, 5224 (2005).
75. B. Lloyd-Hughes, M. A. Saunders, *Int. J. Climatol.* **22**, 1 (2002).
76. J. Turner, *Int. J. Climatol.* **24**, 1 (2004).
77. B. Lyon, A. G. Barnston, *U.S. CLIVAR Variations* **3**, 1 (2005).
78. K. K. Kumar, B. Rajagopalan, M. Hoerling, G. Bates, M. A. Cane, *Science* **314**, 115 (2006).
79. L. Goddard, M. Dilley, *J. Clim.* **18**, 661 (2005).
80. Dynamical and statistical models in Fig. 3 are the National Aeronautics and Space Administration Global Modeling and Assimilation Office (NASA GMAO) model, the National Oceanic and Atmospheric Administration (NOAA) National Centers for Environmental Prediction Coupled Forecast System (NCEP CFS) model, the Japan Meteorological Agency (JMA) model, the Scripps Institution of Oceanography (Scripps) model, the Lamont Doherty Earth Observatory (LDEO) model, the Australian Bureau of Meteorology Predictive Ocean Atmosphere Model for Australia (POAMA), the European Centre for Medium-Range Weather Forecasts (ECMWF) model, the United Kingdom Met Office (UKMO) model, the Korea Meteorological Administration (Korea SNU) model, the University of Maryland Earth System Science Interdisciplinary Center Intermediate Coupled Model (ESSIC ICM), European Centre Hamburg Model-Modular Ocean Model (ECHAM MOM), the Center for Ocean-Land-Atmosphere Studies Anomaly (COLA ANOM) model, the NOAA Climate Prediction Center Markov (CPC MRKOV) model, the NOAA Climate Diagnostics Center Linear Inverse Model (CDC LIM), the NOAA Climate Prediction Center Constructed Analog (CPC CA) model, the NOAA Climate Prediction Center Canonical Correlation Analysis (CPC CCA) model, the Colorado State University Climatology and Persistence (CSU CLIPER) model, the University of British Columbia Neural Network (UBC NNET) model, the Florida State University Regression (FSU REGR) model, and the University of California at Los Angeles Theoretical Climate Dynamics (UCLA TCD) model.
81. We acknowledge funding from NOAA's Climate Program Office (M. J. M. and S. E. Z.) and the National Science Foundation (M. H. G.). Special thanks to T. Barnston, S. Tudhope, M. Holmgren, and R. Feely for helpful suggestions and to S. Hare for permission to reproduce Fig. 1. This is PMEL publication 2969.

17 July 2006; accepted 31 October 2006
10.1126/science.1132588

Amphiregulin, a T_H2 Cytokine Enhancing Resistance to Nematodes

Dietmar M. Zaiss,[1] Li Yang,[1] Pranav R. Shah,[1] James J. Kobie,[1]
Joseph F. Urban,[2] Tim R. Mosmann[1]*

Despite improved sanitation, intestinal nematode infections remain a major health threat to humans. Protection against nematodes is mainly mediated by type 2–biased immune responses (*1*), characterized by T helper 2 (T_H2) lymphocytes and other cells secreting a set of cytokines, including interleukin 4 (IL-4), IL-5, IL-10, and IL-13 (*2*). Increased shedding of the epithelium of the caecum of the intestine is also crucially important for clearing the intestinal nematode parasite *Trichuris muris* (*3*). Members of the epidermal growth factor (EGF) family can induce proliferation of the gut epithelium (*4*). GeneChip (Affymetrix, Santa Clara, CA,) analysis of genes induced in different CD4 T cell subsets revealed that in vitro activation through the T cell antigen receptor induced preferential expression of the EGF family member amphiregulin in T_H2 cells, compared with the absence of amphiregulin expression in naïve, $T_H$pp, or T_H1 cells (Fig. 1A). Selective expression in T_H2 cells was confirmed by a GeneChip analysis of T cell subsets from a second mouse strain (*5*) and by a Northern blot and reverse transcription polymerase chain reaction (RT-PCR) analysis (fig. S1).

To test whether amphiregulin was also expressed during a typical type 2 response in vivo, we infected C57BL/6 mice with *T. muris*, and 14 days after infection we analyzed cDNA from mesenteric lymph nodes (MLN) by real-time PCR. Expression of the T_H1 cytokine interferon-γ was reduced, whereas expression of amphiregulin was increased, in parallel with the typical T_H2 cytokines IL-4 and IL-13 (Fig. 1B). Amphiregulin mRNA was also detected by real-time PCR [normalized threshold cycle difference (ΔCt) = 11.5 compared to CD3ε] in the caecal tissue of infected amphiregulin-deficient mice (*6*) that had received CD4 T cells from a *Trichuris*-infected wild-type mouse but was undetectable (ΔCt > 15.9 compared to CD3ε) in nontransferred mice, confirming amphiregulin expression by T cells in the caecal tissue.

The physiological relevance of amphiregulin to parasite infection was tested by comparing amphiregulin-deficient and wild-type C57BL/6 mice after infection with *T. muris*. In these experiments, similar numbers of larvae were detected after 10 days (366 compared to 363), and both wild-type and amphiregulin-deficient mice cleared the parasite by day 19. However, worm clearance at day 14 was significantly delayed in amphiregulin-deficient mice (Fig. 1C). The CD4 T cell–dependent increase in the progression of proliferating epithelial cells up the gut villi, induced by *Trichuris* infection, was also diminished in amphiregulin-deficient mice (fig. S2). However, the infection induced similar IL-4, IL-5, and IL-13 responses in amphiregulin-deficient and wild-type mice (fig. S3).

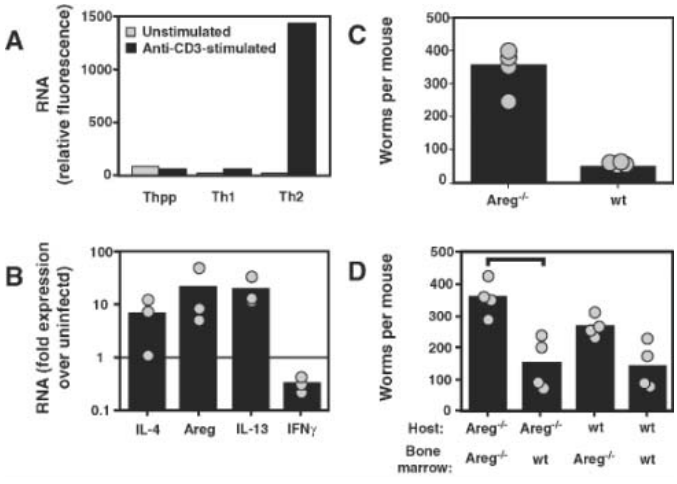

Fig. 1. Amphiregulin (Areg) is expressed by activated T_H2 cells and required for rapid nematode expulsion. (**A**) BALB/c $T_H$pp, T_H1, and T_H2 cell lines were produced as described previously (*5*), and gene expression was measured by using Affymetrix GeneChips before and 9 hours after activation by antibodies specific for CD3 and CD28 (*5*, *7*). (**B**) RNA isolated from MLN of day 14 *Trichuris*-infected C57BL/6 mice was analyzed by real-time PCR. Expression quantities were normalized to CD3ε expression and compared with uninfected mice (baseline of Areg expression being ΔCt = 12.8 compared to CD3ε). (**C**) Female wild-type (wt) or amphiregulin-deficient mice were infected with *T. muris*, and worms in the caecum and upper colon were counted on day 14 by a blinded operator (*6*). (**D**) Irradiated (10 gray) wild-type and amphiregulin-deficient mice were reconstituted with either wild-type or amphiregulin-deficient T cell–depleted bone marrow cells and after 30 days infected with *T. muris.* Worms in the gut were counted blind on day 14.

Clearance of *Trichuris* is independent of mast cells, γ δ T cells, eosinophils, and natural killer T cells (*1*). However, it remained possible that nonlymphoid gut cells might produce amphiregulin that could enhance pathogen clearance. To test whether lymphoid cell-derived amphiregulin was sufficient to accelerate parasite clearance, we infected bone marrow chimeras between amphiregulin-deficient and wild-type mice with *Trichuris* and measured the worm burdens 14 days later. Amphiregulin-expressing bone marrow cells significantly restored parasite clearance in amphiregulin-deficient mice ($P = 0.021$, one-tailed Mann Whitney test, Fig. 1D). Thus, although other pathways (possibly IL-13–dependent) can ultimately expel worms, amphiregulin secreted by hematopoietic (probably T_H2) cells significantly enhances the expulsion of this intestinal parasite.

The expression of amphiregulin by the T_H2 subset of T cells provides a newly recognized link between the type 2 adaptive immune response and the proliferation of gut epithelial cells that aids helminth parasite removal. This response adds to other type 2 effector mechanisms, including edema and smooth muscle contractility (*8*), to provide a concerted attack on the parasites. The coexpression of amphiregulin with the allergy-inducing T_H2 cytokine pattern also raises the intriguing possibility that T_H2 cells contribute to both the tissue hypertrophy and allergic mechanisms that cause asthma.

References and Notes

1. L. J. Cliffe, R. K. Grencis, *Adv. Parasitol.* **57**, 255 (2004).
2. T. R. Mosmann, R. L. Coffman, *Annu. Rev. Immunol.* **7**, 145 (1989).
3. L. J. Cliffe *et al.*, *Science* **308**, 1463 (2005).
4. C. S. Potten *et al.*, *Gut* **36**, 864 (1995).
5. L. Yang, T. Mosmann, *Eur. J. Immunol.* **34**, 1617 (2004).
6. N. C. Luetteke *et al.*, *Development* **126**, 2739 (1999).
7. Materials and Methods are available on *Science* Online.
8. T. Shea-Donohue, J. F. Urban Jr., *Curr. Opin. Gastroenterol.* **20**, 3 (2004).
9. Supported by U.S. Public Health Service grants AI48604 and DFG/ZA280. We thank D. Lee for providing the original amphiregulin-deficient mice.

Supporting Online Material

www.sciencemag.org/cgi/content/full/314/5806/1746/DC1
Materials and Methods
Figs. S1 to S3

10 August 2006; accepted 21 September 2006
10.1126/science.1133715

[1]David H. Smith Center for Vaccine Biology and Immunology and Department of Microbiology and Immunology, University of Rochester, Rochester, NY 14642, USA. [2]Beltsville Human Nutrition Research Center, Agricultural Research Service, U.S. Department of Agriculture, Beltsville, MD 20705, USA.

*To whom correspondence should be addressed. E-mail: Tim_Mosmann@urmc.rochester.edu

P[acman]: A BAC Transgenic Platform for Targeted Insertion of Large DNA Fragments in *D. melanogaster*

Koen J. T. Venken,[1] Yuchun He,[2,3] Roger A. Hoskins,[4] Hugo J. Bellen[1,2,3,5]*

We describe a transgenesis platform for *Drosophila melanogaster* that integrates three recently developed technologies: a conditionally amplifiable bacterial artificial chromosome (BAC), recombineering, and bacteriophage ϕC31–mediated transgenesis. The BAC is maintained at low copy number, facilitating plasmid maintenance and recombineering, but is induced to high copy number for plasmid isolation. Recombineering allows gap repair and mutagenesis in bacteria. Gap repair efficiently retrieves DNA fragments up to 133 kilobases long from P1 or BAC clones. ϕC31-mediated transgenesis integrates these large DNA fragments at specific sites in the genome, allowing the rescue of lethal mutations in the corresponding genes. This transgenesis platform should greatly facilitate structure/function analyses of most *Drosophila* genes.

Drosophila is an important model organism for studying biology and disease, and new tools are continually being developed to facilitate this research (*1*, *2*). A major advance was the development of *P*-element–mediated transformation after the injection of plasmids into *Drosophila* embryos (*3*). Hence, *P*-element vectors have been engineered for numerous applications (*4*). However, *P*-element–mediated transformation has a number of limitations: inability to clone large DNA fragments in available *P*-element vectors, difficulties in manipulating large DNA fragments, inability to transfer large DNA fragments into the fly genome, and failure to target DNA to specific sites in the genome.

Cloning large DNA fragments in high–copy-number plasmids, such as typical *P*-element vectors, is inefficient because large fragments are unstable at high copy number in bacteria. Hence, low–copy-number vectors, including P1 (*5*) and bacterial artificial chromosome (BAC) (*6*) vectors, were developed to stably maintain large cloned DNA fragments. Unfortunately, low–copy-number vectors hamper sequencing, embryo injection, and other manipulations requiring large amounts of plasmid DNA. An elegant solution is a conditionally amplifiable plasmid that has two origins of replication (*ori*'s): *oriS* for low-copy propagation, typical for P1 and BAC vectors; and *oriV*, which can be experimentally induced to high copy number (*7*). Hence, the introduction of conditionally amplifiable BAC features into fly transformation vectors is a first key step to manipulating large DNA fragments in *Drosophila*.

Cloning of large DNA fragments is limited by conventional methods that rely on restriction enzymes and DNA ligases, hampering analyses of large genes and gene complexes. Recently, efficient in vivo cloning technologies using enhanced and regulated recombination systems, commonly known as recombineering, have been developed (*8*). Recombineering greatly facilitates the retrieval of DNA fragments through gap repair and their subsequent site-directed mutagenesis. Because recombineering is based on homologous recombination, restriction enzymes and DNA ligases are not required. Recombineering is widely used by mouse geneticists to generate transgenic and knockout constructs. Recombineering-mediated mutagenesis is much more efficient with low-copy plasmids (*8*). Hence, using recombineering in a conditionally amplifiable BAC should greatly facilitate the gap repair of large DNA fragments and subsequent mutagenesis at low copy number.

P-element–mediated transformation is limited by DNA size, precluding the study of large genes (>40 kb) and gene complexes. In addition, more than 75% of *P* elements insert in regulatory elements of genes (*9*), often disrupting genes in subtle ways (*10*). Moreover, *P* elements are subject to position effects: the effect of a local chromosomal environment on the levels or patterns of transgene expression. This necessitates the generation and characterization of several transgenes for each DNA construct studied. Hence, site-specific integration would greatly facilitate structure-function analysis of transgenes, permitting direct comparison of differently mutagenized DNA fragments integrated at the same site in the genome. Recently, site-specific integration using the integrase of bacteriophage ϕC31 has been demonstrated in *Drosophila* (*11*). ϕC31-integrase mediates recombination between an engineered "docking" site, containing a phage attachment (*attP*) site, in the fly genome, and a bacterial attachment (*attB*) site in the injected plasmid. Three pseudo-*attP* docking sites were identified within the *Drosophila* genome, potentially bypassing desired integration events in engineered *attP* sites. Fortunately, they did not seem receptive to *attB* plasmids, because all integration events were at the desired *attP* sites (*11*). Thus, recovery of large DNA fragments by gap repair into a low-copy plasmid containing an *attB* site, followed by ϕC31-mediated transformation, might allow the integration of any DNA fragment into any engineered *attP* docking site dispersed throughout the fly genome.

Here we describe new vectors that overcome the limitations associated with *P*-element–mediated transgenesis. We developed P/ϕC31 artificial chromosome for manipulation (P[acman]), a conditionally amplifiable BAC vector that contains recognition sites for both *P*-transposase– (*3*) and ϕC31-mediated integration (*11*). P[acman] permits recombineering-mediated cloning of any genomic DNA fragment from *Drosophila* P1 or BAC clones (*12*–*15*) and enables the transfer of large DNA fragments into the fly genome. The ability to easily manipulate these DNA fragments through recombineering and to introduce them into specific sites in the fly genome will greatly facilitate and accelerate in vivo genetic manipulations of *Drosophila*.

Results

Construction of a BAC transgenesis vector for Drosophila. The motivation to construct P[acman] grew from our inability to clone 29- and 39-kb DNA fragments in existing *P*-element vectors for the transformation rescue of mutations in the gene *senseless2* (*16*). We were unable to identify restriction sites for cloning the entire gene. Moreover, recombineering-mediated gap repair in existing high-copy *P*-element vectors was unsuccessful. This was consistent with published data demonstrating that gap repair in high-copy or medium-copy plasmids has an upper size limit of 25 and 80 kb, respectively (*17*). Because high-copy *P* elements have a substantial size, gap repair is limited to fragments of about 20 kb. We hypothesized that a low-copy plasmid might alleviate size limitations and improve the stability of large DNA fragments. Hence, we added *P*-element components to a chloramphenicol-resistant conditionally amplifiable BAC (*7*), resulting in P[acman]-Cm^R (Fig. 1A). The *P*-element components include the 5′*P* and 3′*P* termini required for *P*-transposase–mediated integration, a multiple cloning site (MCS), and the *white*$^+$ marker. The conditionally amplifiable BAC contains two origins of replication: *oriS* and *oriV* (*7*). *oriS* keeps P[acman] at low

[1]Program in Developmental Biology, Baylor College of Medicine, Houston, TX 77030, USA. [2]Department of Molecular and Human Genetics, Baylor College of Medicine, Houston, TX 77030, USA. [3]Howard Hughes Medical Institute, Baylor College of Medicine, Houston, TX 77030, USA. [4]Department of Genome Biology, Lawrence Berkeley National Laboratory, Berkeley, CA 94720–3200, USA. [5]Department of Neuroscience, Baylor College of Medicine, Houston, TX 77030, USA.

*To whom correspondence should be addressed. E-mail: hbellen@bcm.edu

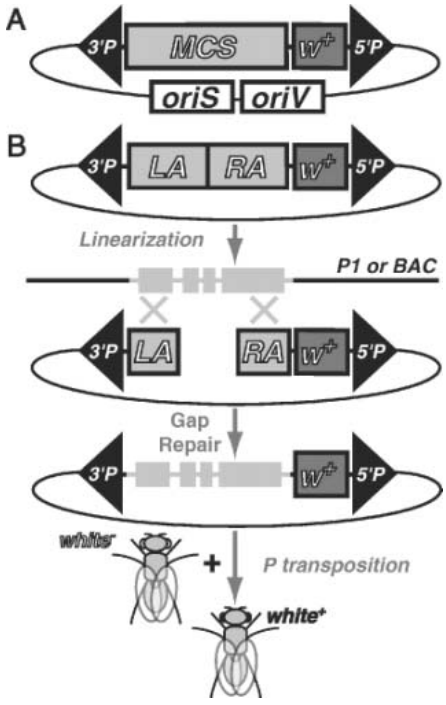

Fig. 1. P[acman]: BAC transgenesis for *Drosophila*. **(A)** P[acman] contains *P*-element transposase sites (3′*P* and 5′*P*), *white*$^{+}$, and an MCS. This *P* element is inserted in the conditionally amplifiable BAC, containing a low-copy origin of replication (*oriS*) and a copy-inducible origin of replication (*oriV*). **(B)** P[acman] is linearized between both homology arms (LA and RA) and transformed into recombineering bacteria containing P1 or BAC clones. Integration into the germ line of *white*$^{-}$ flies is mediated by *P*-element–mediated transformation.

Table 1. Retrieval of genes in P[acman]. Genomic fragments containing genes of interest retrieved by gap repair into P[acman]-Cm^{R} or -Ap^{R} are shown. Donor plasmids, with clone coordinates, are P1, BACs, or ampicillin-modified BACs (BAC-Ap^{R}). Mutations in the corresponding genes were lethal or showed a phenotype. Rescue was obtained for most genes using *P*-element–mediated transformation. NA, not applicable.

Gene	Construct	Size	Donor	Clone	P[acman]	Mutation	Rescue
sens2	sens2-22	22.3 kb	P1	DS05421	Cm^{R}	NA	NA
sens2	sens2-29	28.9 kb	P1	DS05421	Cm^{R}	NA	NA
sens2	sens2-39	38.9 kb	P1	DS05421	Cm^{R}	NA	NA
CG10805	CG10805-S	9.7 kb	P1	DS05421	Cm^{R}	Lethal	Yes
CG10805	CG10805-L	14.7 kb	P1	DS05421	Cm^{R}	Lethal	Yes
dap160	dap160	10.9 kb	P1	DS02919	Cm^{R}	Lethal	Yes
sens	sens-S	12.1 kb	BAC-Ap^{R}	BACR17E13	Cm^{R}	Lethal	Yes
sens	sens-L	18.1 kb	BAC-Ap^{R}	BACR17E13	Cm^{R}	Lethal	Yes
Dalpha7	Da7	29.4 kb	BAC-Ap^{R}	BACR02B03	Cm^{R}	Phenotype	Yes
Drp	Drp	9.4 kb	BAC	BACR30P05	Ap^{R}	Lethal	Yes*
Sec8	Sec8-L	12 kb	BAC	BACR02L23	Ap^{R}	Lethal	No
Eps15	Eps15-L	11.9 kb	BAC	BACR27P17	Ap^{R}	Lethal	Yes

*From (*25*).

copy number for the stability of large cloned inserts and efficient recombineering, whereas *oriV* permits copy-number induction for high-yield DNA preparation for sequencing and embryo injections. We created transgenic flies containing P[acman]-Cm^{R} using *P*-transposase–mediated integration. To facilitate cloning by gap repair from a variety of sources, we also replaced the ampicillin-resistance marker into P[acman]-Cm^{R}, resulting in P[acman]-Ap^{R}. Both plasmids can be used to clone any DNA fragment from a variety of donor vectors.

Recombineering-mediated gap repair into P[acman]. P[acman] was used to retrieve fragments by gap repair. For each gap repair, we designed four primer sets (fig. S1). Two homology arms, located at either end of the DNA fragment, were cloned into P[acman] (fig. 1B). Linearization between both homology arms and the subsequent transformation of the linearized construct into recombineering-competent bacteria containing the necessary genomic clone allow retrieval of the DNA fragment by gap repair. Gap repair was performed with the use of two similar strategies, relying on *Red* recombination functions (fig. S2) (*17*, *18*). Both strategies were used to retrieve DNA fragments ranging from 9.4 to 39 kb, from different donor plasmids (Table 1). Colony polymerase chain reaction (PCR) screening identified correct recombination events at both junctions after gap repair. After plasmid copy-number induction, DNA fingerprinting and sequencing demonstrated that the desired fragment was obtained. Hence, the methodology is reliable and large DNA fragments can easily be retrieved.

To test the functionality of the gap-repaired constructs, we used *P*-mediated transposition. Although germline transformation of the constructs was efficient with small inserts, the efficiency dropped for fragments over 20 kb. Transgenic flies containing the gap-repaired fragments in P[acman] were crossed to flies carrying mutations in the corresponding genes. Eight out of 9 fragments tested fully rescued the lethality or visible phenotype associated with the mutations, in the homozygous or transheterozygous condition (Table 1). One fragment (Sec8-L) did not rescue, although a smaller fragment encompassing the same gene did.

ϕC31-mediated integration of P[acman]. Because *P*-transposase–mediated transformation has size limitations, we explored the possibility of using ϕC31-mediated integration to integrate larger constructs at specific sites within the genome. To combine the power of recombineering with ϕC31, we equipped P[acman] with an *attB* site, resulting in *attB*-P[acman]. To create genomic *attP* docking sites, we introduced an *attP* site and *yellow*$^{+}$ into a minimal *piggyBac* transposon (*19*) (*piggyBac-yellow*$^{+}$*-attP*) and integrated and remobilized this *piggyBac* in the *Drosophila* genome using *piggyBac* transposase. We isolated 34 homozygous viable insertions and determined their exact genomic location (Fig. 2A and table S1). Because *piggyBac* has a more random distribution than *P*-transposase (*9*), *attB*-P[acman] should integrate into both gene-poor and gene-rich regions.

To integrate *attB*-P[acman], we co-injected circular plasmid DNA and mRNA encoding ϕC31-integrase (*11*) into embryos carrying *piggyBac-yellow*$^{+}$*-attP* (Fig. 2B). Integration results in flies with a "yellow^{+}" body color and "white^{+}" eye color phenotype. Because the *attB* site is upstream of the MCS and *white*$^{+}$ is downstream of the MCS, only transgenic flies that are "yellow^{+} white^{+}" should have undergone an integration event containing most of the injected DNA, including the cloned insert (Fig. 2B). Hence, successful integration events can be genetically traced. Moreover, because both transposons (*P*-element and *piggyBac*) are maintained after integration, the inserted DNA can be remobilized using the respective transposases.

We tested whether different *attP* docking sites are equally receptive to *attB*-P[acman]-Ap^{R}. We focused on seven docking sites: two each on chromosomes X, 2, and 3, and one on chromosome 4. As shown in table S2, all but one of these docking sites were receptive, with similar integration efficiencies of 20 to 30%. We occasionally obtained efficiencies as high as 60%, similar to those in a previous report (*11*). However, in general we observed higher survival rates than Groth *et al*. (*11*). In our hands, such efficiencies were higher than the *P*-transposase–mediated integration of similar-sized constructs. Because ϕC31-mediated–integration is site-specific, only a single insertion is needed, and the injection procedure can therefore be scaled down to 50 embryos or less. Integration of *attB*-P[acman]-Ap^{R} in the same docking site led to the same *white*$^{+}$ expression level (fig. S3). This is convenient, because rare events that were not integrated in the proper site exhibited a different eye color and were therefore distinguished from true integration events. Integration of *attB*-P[acman]-Ap^{R} in a single docking site on chromosome 2 consistently caused a patchy red eye phenotype (fig. S3D), indicating position-effect variegation of *white*$^{+}$

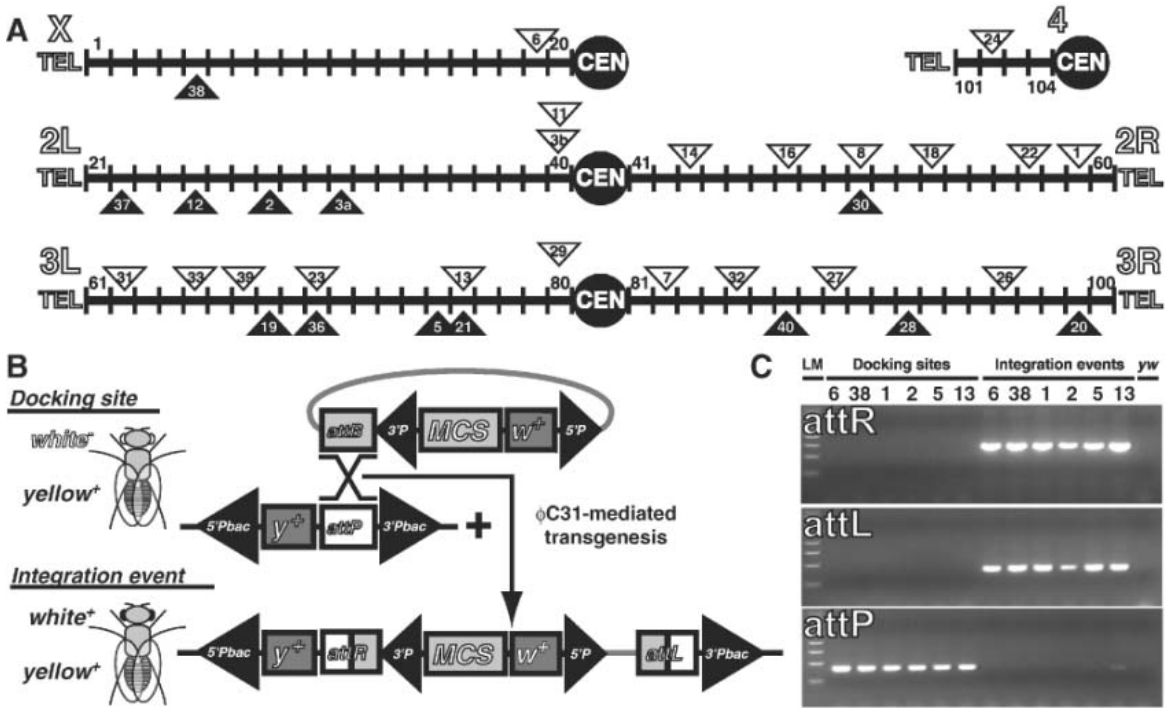

Fig. 2. P[acman] transgenesis in *Drosophila* using the ϕC31 system. **(A)** The *piggyBac-y*$^{+}$*-attP* docking element was transformed or remobilized in the *Drosophila* genome to obtain multiple *attP* docking lines (VK lines). Locations are indicated on a schematic representation of the polytene chromosomes. White triangles represent insertions between, and black triangles within, annotated genes. VK line numbers (table S1) are indicated within the triangles. **(B)** *attB*-P[acman] can integrate at an *attP* docking site in the fly genome. **(C)** Correct integration events in docking sites are PCR-positive for the *attR* and *attL* assays, whereas original docking sites are PCR-positive for the *attP* assay. *yw* served as a negative control. Two docking sites on chromosomes X (VK6 and VK38), 2 (VK1 and VK2), and 3 (VK5 and VK13) were used. LM, length marker.

expression. This was not observed for the *yellow*$^{+}$ marker present at the same docking site. Moreover, the insertion of *attB*-P[acman]-Ap^{R} into different docking sites resulted in different eye color phenotypes, indicating position effects on the expression level of the *white*$^{+}$ marker (fig. S3). The main difference between ϕC31- and *P*-element–mediated integration is that position effects with the ϕC31 system are predictable, allowing for the selection of different but defined expression levels.

To identify correct integration events, we developed PCR assays specific for the *attP*, *attL* (left attachment), and *attR* (right attachment) sites (Fig. 2C). Correct integration events were identified by the loss of the *attP* PCR product (specific for the original docking site) and the appearance of *attL* and *attR* PCR products (specific for the integration event). PCR analysis indicated that all but one of the insertions was correctly integrated. Moreover, correct integration events in homozygous viable docking sites maintained homozygous viability, demonstrating that the insertion does not detrimentally affect the local chromosomal environment. In numerous transformation experiments, in addition to proper integration events, we recovered only one event that converted a homozygous viable docking site into a recessive lethal locus. PCR analysis demonstrated that this event did not result in correct integration. Therefore, ϕC31-mediated integration is very efficient.

Cloning of large DNA fragments into attB-*P[acman].* To clone large DNA fragments into *attB*-P[acman]-Ap^{R}, we performed recombineering-mediated gap repair, as described above. We retrieved fragments up to 102 kb in length from single P1 or BAC clones (Table 2). Multiple genes and gene complexes, including *bancal*, *Dscam*, *teashirt*, and the *Bearded* and *Enhancer of Spl* complexes, were cloned into *attB*-P[acman]-Ap^{R} (Table 2). Unfortunately, some large genes were not contained within a single BAC (*15*). We therefore decided to reconstitute large genes through serial gap repair from two overlapping BAC clones into *attB*-P[acman]-Ap^{R}: In step 1, the smaller part is retrieved from one BAC, which is followed by step 2, retrieving the remainder of the gene (Fig. 3 and fig. S4). This two-step procedure was successful in retrieving a 133-kb fragment encompassing the *Tenascin-major* gene (Table 2).

Table 2. Retrieval of genes in *attB*-P[acman]. Genome fragments containing genes of interest retrieved by gap repair into *attB*-P[acman]-Ap^{R} are shown. Donor fragments are from P1 or BACs, or from PCR. Clone coordinates of the donor clones are indicated. Mutations in all corresponding genes are lethal. Rescue is indicated for *P*-element– or ϕC31-mediated transformation. ND, not determined; NA, not applicable.

Gene	Construct	Size	Donor	Clone	Transgenics			
					P	Rescue	phiC31	Rescue
Sec6	Sec6-S	2.8 kb	PCR	BACR27L09	Yes	No	Yes	ND
miR-4	miR-4	4.5 kb	BAC	BACR02J10	ND	NA	ND	NA
Sec8	Sec8-S	4.9 kb	BAC	BACR02L23	Yes	Yes	ND	NA
Eps15	Eps15-S	10.8 kb	BAC	BACR3B7	ND	NA	Yes	ND
Sec6	Sec6-L	11.5 kb	BAC	BACR27L09	Yes	ND	Yes	ND
sens	sens-L	18.1 kb	BAC	BACR17E13	ND	NA	No	NA
miR-9a	miR-9a	20.1 kb	BAC	BACR01D04	ND	NA	Yes	ND
Tsh	Tsh-1	28.4 kb	BAC	BACR03L08	ND	NA	Yes	Yes
grp	grp	29.8 kb	P1	DS00592	ND	NA	Yes	ND
Brd-C	Brd-C	37.2 kb	BAC	BACR01H12	ND	NA	ND	NA
bancal	bancal	39.5 kb	BAC	BACR33D17	ND	NA	ND	NA
Dscam	Dscam-1	73.3 kb	BAC	BACR26B18	ND	NA	Yes	Yes
E(Spl)-C	E(Spl)-C	77.7 kb	BAC	BACR13F13	ND	NA	Yes	Yes
Tsh	Tsh-2	86.4 kb	BAC	BACR03L08	ND	NA	Yes	Yes
Dscam	Dscam-2	102.3 kb	BAC	BACR26B18	ND	NA	No	NA
ten-m	ten-m	20 kb	BAC	BACR02D04	NA	NA	NA	NA
ten-m	ten-m	133 kb	BAC	BACR22C11	ND	NA	Yes	Yes

ϕC31-mediated integration of large gap-repaired fragments. To obtain transgenic flies with *attB*-P[acman]-Ap^R constructs, we can use either *P*-transposase or ϕC31-integrase. We first tested *P*-transposition for three small fragments. Transgenic animals were obtained for all three (Table 2). Because *P*-transposase–mediated integration is inefficient for fragments larger than 20 kb, we switched to ϕC31-mediated integration. Several injection rounds suggested that the molar DNA concentration was critical. We empirically established that 75 ng of DNA per microliter of injection buffer (ng/μl) is the lower limit for *attB*-P[acman]-Ap^R (~13 kb). Therefore, large (75- to 135-kb) supercoiled plasmid DNA (300 to 750 ng/μl) was co-injected with ϕC31 mRNA (250 to 500 ng/μl) (*11*). As shown in Table 2, we obtained transgenic animals for most constructs, including 73-, 76-, 86-, and 133-kb fragments. In these cases, the transformation efficiency was about 10% for medium (15 to 50 kb) and 2 to 4% for large plasmids (>50 kb). PCR analysis confirmed that all constructs integrated correctly. For two transgenes, 18 and 102 kb in length, we did not obtain transformants, illustrating that optimization for certain constructs might be required. Different gap-repaired fragments inserted in the same docking site differentially affected *white*$^+$ expression, suggesting that DNA context is important. Finally, multiple fragments fully rescued two independent lethal mutations, in the homozygous or transheterozygous condition, in each of the four corresponding genes or gene complexes tested (Table 2). These data show that gap repair permits the cloning of BAC-sized fragments, large transgenes can be integrated site-specifically in the *Drosophila* genome using ϕC31, and mutations in essential genes and entire gene complexes can be rescued by large transgenic fragments.

Discussion

P[acman] provides numerous improvements when compared to current strategies for *Drosophila* transgenesis. First, DNA constructs larger than 100 kb can be retrieved from genomic P1 and BAC clones using recombineering-mediated gap repair. Fragments are retrieved into a plasmid fitted with an inducible *oriV* replication origin that allows easy preparation of large quantities of DNA for sequencing and *Drosophila* transgenesis. The retrieved fragments do not need to be resequenced because they are directly retrieved from the genomic clone without PCR amplification. Second, unlike *P*-transposase, ϕC31-integrase enables the integration of large fragments into the *Drosophila* genome. Because ϕC31-integrase catalyzes recombination between two ectopic attachment sites (*attB* and *attP*), transgenes are integrated at specific docking sites in the fly genome. This largely eliminates the problem of position effects, a highly desirable feature when comparing different mutagenized constructs derived from the same transgene for structure/function analysis. Finally, site-directed mutagenesis via recombineering is much more efficient in low-copy plasmids such as P[acman].

We were able to clone fragments as large as 102 kb from single BACs. Only one report documents the gap repair of a similarly sized fragment from one BAC (*20*). In both cases, gap repair was successful because of the use of a low-copy vector. Indeed, gap repair into high-copy or medium-copy plasmids has an upper size limit of 25 and 80 kb, respectively (*17*). We also reconstituted one of the largest *Drosophila* genes, using serial gap repair, resulting in reconstitution of a 133-kb fragment. One recent report demonstrated a variation of seamless recombination of two large DNA fragments (*20*). The methodology described here may facilitate the cloning of even larger genomic fragments into P[acman], which may not be contained within single BAC clones in the genome tiling path set (*15*).

The numerous docking sites (Fig. 2A and table S1) created in this work will have to be characterized in more detail to determine the expression levels of different genes that are inserted in the same site. It will also be important to determine whether adjacent enhancers or regulatory elements influence gene expression in each of the docking sites in order to identify sites that are as "neutral" as possible, a requirement important for the study of regulatory elements. The neighboring genome environment may also become important when overexpression or RNA interference transgenes are inserted. We feel that *piggyBac-y+-attP* insertions in intergenic regions may be the best candidates for these applications, although this will have to be determined experimentally.

The circular ϕC31 bacteriophage genome is integrated into the linear genome of its host, *Streptomyces lividans*, by ϕC31-integrase (*21*). The genome of ϕC31 is about 41.5 kb, which is larger than standard high-copy plasmids. This fact suggested that ϕC31-integrase would be useful to integrate circular DNA molecules up to 41.5 kb and potentially larger into the *Drosophila* genome. Indeed, we integrated fragments up to ~146 kb at defined sites in the genome, which was previously impossible. Large gap-repaired fragments should complement many molecularly defined deficiencies (*22*), and subsequent mutagenesis should permit the analysis of genes within the deletion, obviating the need to recover mutations using conventional genetic screens or imprecise excision of mapped *P* elements. This approach also opens the road for clonal analysis of any gene that maps close to centromeric heterochromatin, because transgenic constructs for these genes can be recombined onto an *FRT*-containing chromosome. Finally, recombineering will allow the integration of any peptide or protein tag into the genomic rescue constructs to study protein localization and function in vivo.

The methodology proposed here opens up a wide variety of experimental manipulations that were previously difficult or impossible to perform in *Drosophila*. Moreover, it is expected that it should be possible to adapt this methodology to other model organisms, because *piggyBac* transposes in many species, including mammals (*23*), and ϕC31 is operational in many species, including mammalian cells (*24*).

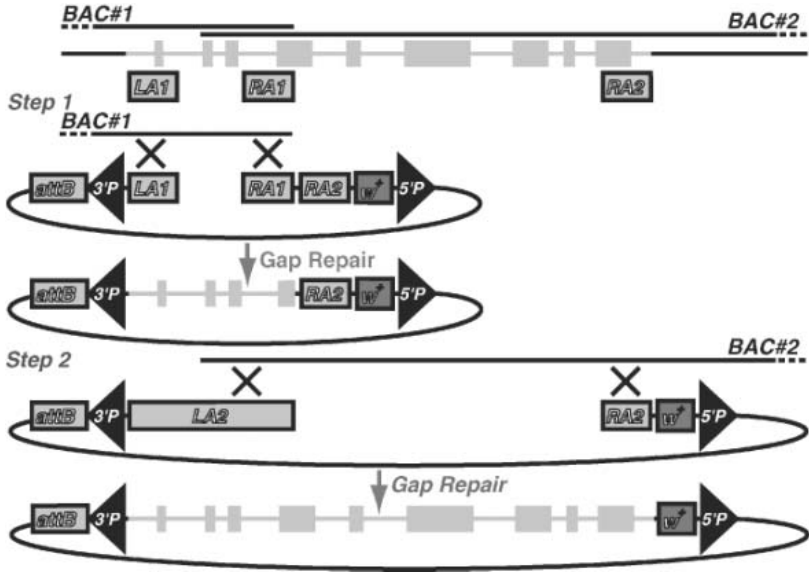

Fig. 3. Reconstitution of large fragments from two overlapping BACs by serial gap repair. Three homology arms are designed: LA1, RA1, and RA2, located at the left end, the region of overlap of the two BACs, and the right end of the desired DNA fragment, respectively. During step 1, the construct is linearized between LA1 and RA1, and the left segment of the gene is obtained from BAC 1, resulting in LA2. In step 2, the construct is linearized between LA2 and RA2, and the remaining segment of the gene is obtained from BAC 2 to reconstitute the entire gene.

References and Notes

1. K. J. Venken, H. J. Bellen, *Nat. Rev. Genet.* **6**, 167 (2005).
2. K. A. Matthews, T. C. Kaufman, W. M. Gelbart, *Nat. Rev. Genet.* **6**, 179 (2005).
3. G. M. Rubin, A. C. Spradling, *Science* **218**, 348 (1982).
4. E. Ryder, S. Russell, *Brief. Function. Genom. Proteom.* **2**, 57 (2003).
5. N. Sternberg, *Proc. Natl. Acad. Sci. U.S.A.* **87**, 103 (1990).
6. H. Shizuya *et al.*, *Proc. Natl. Acad. Sci. U.S.A.* **89**, 8794 (1992).
7. J. Wild, Z. Hradecna, W. Szybalski, *Genome Res.* **12**, 1434 (2002).
8. N. G. Copeland, N. A. Jenkins, D. L. Court, *Nat. Rev. Genet.* **2**, 769 (2001).
9. H. J. Bellen *et al.*, *Genetics* **167**, 761 (2004).
10. K. K. Norga *et al.*, *Curr. Biol.* **13**, 1388 (2003).
11. A. C. Groth, M. Fish, R. Nusse, M. P. Calos, *Genetics* **166**, 1775 (2004).
12. W. Kimmerly *et al.*, *Genome Res.* **6**, 414 (1996).
13. R. A. Hoskins *et al.*, *Science* **287**, 2271 (2000).
14. M. D. Adams *et al.*, *Science* **287**, 2185 (2000).
15. S. E. Celniker *et al.*, *Genome Biol.* **3**, RESEARCH0079 (2002).
16. H. Jafar-Nejad, H. J. Bellen, *Mol. Cell. Biol.* **24**, 8803 (2004).
17. E. C. Lee *et al.*, *Genomics* **73**, 56 (2001).
18. D. L. Court *et al.*, *Gene* **315**, 63 (2003).
19. X. Li, N. Lobo, C. A. Bauser, M. J. Fraser Jr., *Mol. Genet. Genomics* **266**, 190 (2001).
20. G. Kotzamanis, C. Huxley, *BMC Biotechnol.* **4**, 1 (2004).
21. H. M. Thorpe, M. C. Smith, *Proc. Natl. Acad. Sci. U.S.A.* **95**, 5505 (1998).
22. A. L. Parks *et al.*, *Nat. Genet.* **36**, 288 (2004).
23. H. F. Xu *et al.*, *Mol. Genet. Genomics* **276**, 31 (2006).
24. D. A. Sorrell, A. F. Kolb, *Biotechnol. Adv.* **23**, 431 (2005).
25. P. Verstreken *et al.*, *Neuron* **47**, 365 (2005).
26. GenBank accession numbers for the P[acman] vectors are as follows: P[acman]-Cm^R-F-2, EF106977; P[acman]-Ap^R-F-2-5, EF106978; *attB*-P[acman]-Cm^R-F-2, EF106979; and *attB*-P[acman]-Ap^R-F-2, EF106980. We thank the Bloomington Stock Center and Drosophila Genome Resource Center for fly stocks and plasmids, respectively; and M. Calos, J. Carlson, A. Celik, H.-T.Chao, K.-W. Choi, J. Clemens, N. Copeland, D. Court, C. Delidakis, M. Evans-Holm, D. Featherstone, M. Fraser, A. Handler, N. Jenkins, H. Kim, E. Lai, P. Liu, P. Ponsaerts, R. Mann, D. Schmucker, S. Speese, W. Szybalski, U. Tepass, L. Zipursky, and past and present members of the Bellen lab for flies, bacteria, plasmids, help, and/or stimulating discussions. H.J.B is an investigator with the Howard Hughes Medical Institute. This work was supported by NIH (grant GM067858-05) and the Howard Hughes Medical Institute. Plasmids are available through the Drosophila Genome Resource Center. Fly strains are available through the Bloomington Stock Center.

Supporting Online Material

www.sciencemag.org/cgi/content/full/1134426/DC1
Materials and Methods
Figs. S1 to S4
Tables S1 to S4
References

28 August 2006; accepted 9 November 2006
10.1126/science.1134426
Include this information when citing this paper.

Rubidium-Rich Asymptotic Giant Branch Stars

D. A. García-Hernández,[1]*† P. García-Lario,[1,2] B. Plez,[3] F. D'Antona,[4] A. Manchado,[5] J. M. Trigo-Rodríguez[6,7]

A long-debated issue concerning the nucleosynthesis of neutron-rich elements in asymptotic giant branch (AGB) stars is the identification of the neutron source. We report intermediate-mass (4 to 8 solar masses) AGB stars in our Galaxy that are rubidium-rich as a result of overproduction of the long-lived radioactive isotope ^{87}Rb, as predicted theoretically 40 years ago. This finding represents direct observational evidence that the ^{22}Ne(α,n)^{25}Mg reaction must be the dominant neutron source in these stars. These stars challenge our understanding of the late stages of the evolution of intermediate-mass stars and would have promoted a highly variable Rb/Sr environment in the early solar nebula.

Low- and intermediate-mass stars (1 to 8 solar masses $M_\odot$) evolve toward the asymptotic giant branch (AGB) phase (*1*) after the completion of hydrogen and helium burning in their cores, before they form planetary nebulae, ending their lives as white dwarfs. Basically, an AGB star is composed of an inert carbon-oxygen (C-O) core surrounded by a He-rich intershell and an extended H-rich convective envelope. Nuclear energy release is dominated by the H shell and interrupted periodically by thermonuclear runaway He-shell "thermal pulses" that initiate a series of convective and other mixing events. Strong mass loss enriches the interstellar medium (ISM) with the products of the resulting complex nucleosynthesis (*2*). During this thermally pulsing AGB (TP-AGB) phase, stars originally born O-rich (reflecting the ISM composition) can turn C-rich (C/O > 1) as a consequence of the "dredge-up" of processed material from the bottom of the convective envelope to the stellar surface. In AGB stars at the higher end of this range (4 to 8 $M_\odot$), the convective envelope penetrates the H-burning shell, activating the so-called "hot bottom burning" (HBB) process (*3*, *4*). HBB takes place when the temperature at the base of the convective envelope is hot enough ($T \geq 2 \times 10^7$ K) that ^{12}C can be converted into ^{13}C and ^{14}N through the CN cycle, so these AGBs are no longer C-rich and become again or remain O-rich despite the dredge-up. HBB models (*3*, *4*) also predict the production of the short-lived ^{7}Li isotope through the "^{7}Be transport mechanism" (*5*), which should be detectable at the stellar surface. The HBB activation in massive AGB stars is supported by lithium overabundances in luminous O-rich AGB stars of the Magellanic Clouds (*6*, *7*). In our own Galaxy, a small group of stars showing OH maser emission at 1612 MHz (sometimes without an optical counterpart but very bright in the infrared, the OH/IR stars) has recently been found to show strong Li abundances (*8*).

Mixing of protons into the He-rich intershell during the TP-AGB phase leads to reaction chains producing free neutrons, which allow production of neutron-rich elements such as Rb, Sr, Y, Zr, Ba, La, Nd, and Tc by slow neutron capture on iron nuclei and other heavy elements (the s process) (*9*–*11*). There are two possible chains for the neutron production: ^{13}C(α,n)^{16}O and ^{22}Ne(α,n)^{25}Mg. The ^{13}C neutron source operates at relatively low neutron densities ($N_n < 10^7$ cm^{-3}) and temperatures $T < 0.9 \times 10^8$ K (*11*, *12*) in TP-AGB stars during the interpulse period. The ^{22}Ne neutron source operates at much higher neutron densities ($N_n > 10^{10}$ cm^{-3}) and requires higher temperatures ($T > 3.0 \times 10^8$ K), which are achieved only while the convective thermal pulse is ongoing. In the more massive AGB stars (> 4 to 5 $M_\odot$), where these high temperatures are more easily achieved, the s-process elements are expected to form mainly through the ^{22}Ne(α,n)^{25}Mg reaction (*11*, *13*). The ^{22}Ne neutron source also strongly favors the production of the stable isotope ^{87}Rb because of the operation of a branching in the s-process path at ^{85}Kr (*14*) that modifies the isotopic mix between ^{85}Rb and ^{87}Rb (*14*–*17*). Unfortunately, the Rb isotope ratio cannot be measured in stellar sources (*17*) even with the help of very-

[1]ISO Data Centre, European Space Astronomy Centre, Research and Scientific Support Department, European Space Agency, Villafranca del Castillo, Apdo. 50727, E-28080 Madrid, Spain. [2]Herschel Science Centre, European Space Astronomy Centre, Research and Scientific Support Department, European Space Agency, Villafranca del Castillo, Apdo. 50727, E-28080 Madrid, Spain. [3]Groupe de Recherches en Astronomie et Astrophysique du Languedoc, UMR 5024, Université de Montpellier 2, F-34095 Montpellier Cedex 5, France. [4]INAF–Osservatorio Astronomico di Roma, via Frascati 33, I-00040 MontePorzio Catone, Italy. [5]Instituto de Astrofísica de Canarias and Consejo Superior de Investigaciones Científicas, La Laguna, E-38200 Tenerife, Spain. [6]Institute of Space Sciences and Consejo Superior de Investigaciones Científicas, Campus UAB, Facultat de Ciències, Torre C-5, parells, 2ª planta, 08193 Bellaterra, Barcelona, Spain. [7]Institut d'Estudis Espacials de Catalunya, Ed. Nexus, Gran Capità 2-4, 08034 Barcelona, Spain.

*To whom correspondence should be addressed. E-mail: agarcia@astro.as.utexas.edu
†Present address: W. J. McDonald Observatory, University of Texas, Austin, TX 78712, USA.

high-resolution spectra because the lines are too broad, and thus it is difficult to use this parameter as a neutron density indicator. As an alternative, the total Rb abundance can be used. The theoretical prediction is that the relative abundance of Rb to other nearby elements produced by the s process, such as Zr, Y, and Sr, is a powerful indicator of the neutron density at the s-process site and, as such, is a good discriminant of the operation of the ^{13}C versus the ^{22}Ne neutron source in AGB stars (*11*, *15*–*17*).

Our sample is composed of 102 galactic OH/IR stars that we have identified as massive O-rich AGB stars, for which we recently determined their Li and Zr abundances (*8*). These stars are experiencing very strong mass loss rates (up to several times 10^{-5} $M_{\odot}$ year^{-1}) at this stage and, as a consequence, most of them are heavily obscured by thick circumstellar envelopes, making optical observations very difficult. Indeed, 42 stars were found to be too faint at 7800 Å to perform any kind of analysis.

Despite this observational problem, we were able to obtain high-resolution optical echelle spectra (resolving power of ~40,000 to 50,000) for 60 stars in the sample. The observations were carried out with the Utrecht Echelle Spectrograph at the 4.2-m William Herschel Telescope at the Observatorio del Roque de los Muchachos (La Palma, Spain) during three different observing runs in August 1996, June 1997, and August 1997 and the Cassegrain Echelle Spectrograph of the European Southern Observatory 3.6-m telescope at La Silla, Chile in February 1997. Because of the very red colors of the sources observed, the signal-to-noise (S/N) ratios achieved in the reduced spectra can strongly vary from the blue to the red orders (10 to 20 at 6000 Å, >100 at 8000 Å). The AGB stars studied here are quite different from other galactic AGB samples previously studied because they show the coolest temperatures yet observed (effective temperature $T_{\rm eff}$ ~ 2700 to 3300 K) and display peculiar properties. The extremely red spectra are dominated by strong molecular bands mainly due to titanium oxide (TiO). The TiO veiling effect is so intense that it is very difficult to identify individual atomic lines in the spectra of these stars, with the exception of neutral species such as Li I (6708 Å), Ca I (6122 and 6573 Å), K I (7699 Å), Rb I (7800 Å), and a few Fe I lines. From the measurement of the radial velocities, we conclude that the Li and Ca atomic lines, as well as the TiO molecular bands, must be formed in the stellar atmosphere, whereas the K I and Rb I absorption lines usually have circumstellar components with peculiar velocities. For the majority of stars, the difference between the mean radial velocities of the stellar and circumstellar lines is on the order of the expansion velocity of the circumstellar envelope, as derived from the OH maser measurements. In particular, the Rb I resonance line at 7800.3 Å is originated not only in the photosphere of these stars but also in the outer nonstatic layers of the stellar atmosphere and in the expanding circumstellar shell, as our observations confirm.

With the use of state-of-the-art synthetic models appropriate for cool O-rich AGB spectra, we first derived the stellar fundamental parameters (e.g., $T_{\rm eff}$ ~ 2700 to 3300 K, solar metallicity [Fe/H] = 0.0, C/O = 0.5, gravity log g = −0.5, etc.) of these stars (*8*). Then we carried out a chemical abundance analysis on those sources for which a spectrum with enough S/N was obtained in the 7775 to 7835 Å region around the Rb I 7800.3 Å line. For this we constructed a grid of model spectra at different effective temperatures in the 7775 to 7835 Å region, and we used χ^2 minimization to determine which of the model spectra provided the best fit to the observations. The goal was to fit the overall shape of the spectra including the TiO bandheads, which are very sensitive to variations in the effective temperature as well as the Rb abundances, which were derived by fitting the Rb I line. The Rb hyperfine structure (*18*) was considered, for which we assumed a solar Rb isotopic composition (*19*). Note that an extremely different value of the Rb isotope ratio changes the derived Rb abundances only by a maximum of 0.1 dex. A few sample spectra together with the best model fits are presented in Fig. 1. We could obtain reliable Rb photospheric abundances for 22 stars in our sample (Table 1).

The rest of the stars displayed also very strong Rb I lines, but the circumstellar contribution to the line was difficult to quantify, and thus an accurate abundance analysis was not possible. Our analysis yielded a wide variety of Rb abundances ranging from [Rb/Fe]~ −1.0 to +2.6 dex. The overall uncertainty in the derived Rb abundances is estimated to be always less than 0.8 dex. This mainly reflects the sensitivity to changes in the atmospheric parameters adopted for the modeling.

Theoretical models enable us to infer the mass of the stars from the observed nucleosynthesis pattern (*15*–*17*). Values of [Rb/Fe] ≈ −0.3 to +0.6 dex and [Rb/Zr] < 0, generally found in MS, S, and C (N-type) AGB stars in our Galaxy, are usually interpreted as an indication of these stars being low-mass (~1 to 3 $M_{\odot}$) AGB stars and of the $^{13}C(\alpha,n)^{16}O$ reaction being the main neutron source at the origin of s-process nucleosynthesis (*15*, *16*). Instead, most of the stars analyzed in our sample show a strong Rb enhancement ([Rb/Fe] ~ +0.6 to +2.6 dex) in combination with only a mild Zr enrichment, as we determined [Zr/Fe] < 0.5 in our stars (*8*). The high Rb/Zr ratios (~0.1 to 2.1 dex) derived confirm that the stars in our sample belong to the group of more massive (> 4 to 5 $M_{\odot}$) AGB stars in our Galaxy and provide observational evidence that the $^{22}Ne(\alpha,n)^{25}Mg$ reaction is indeed the dominant neutron source in these AGB stars.

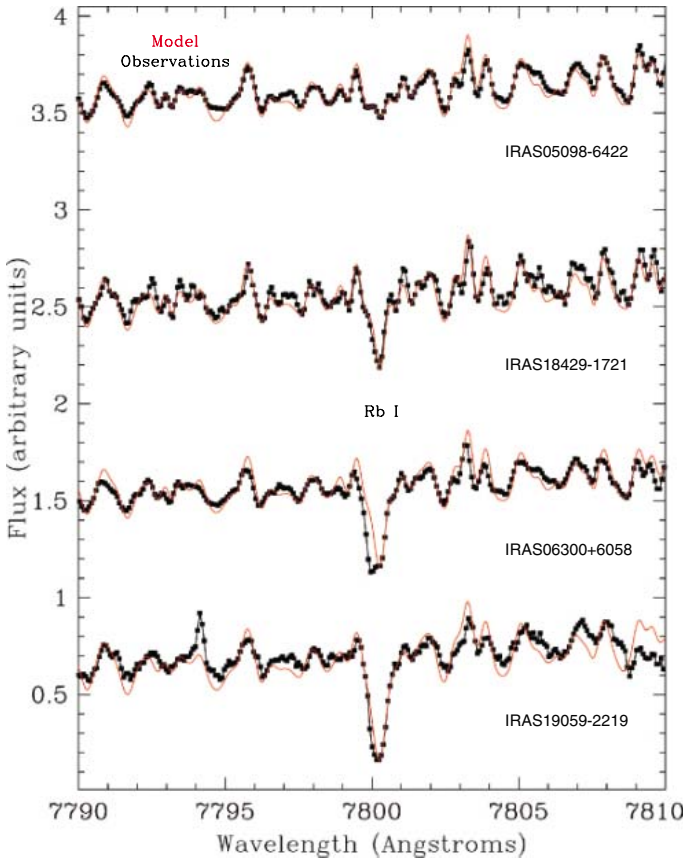

Fig. 1. Best model fit and observed spectra around the Rb I line at 7800.3 Å. Shown are observed spectra (in black) and the best model fit (in red) of four sample stars (IRAS 05098-6422, IRAS 18429-1721, IRAS 06300+6058, and IRAS 19059-2219) with an effective temperature of 3000 K but with very different Rb abundances: [Rb/Fe] = +0.1, +1.2, +1.6, and +2.3 dex, respectively. Note that the Rb I resonance line has a clear "blue-shifted" circumstellar component in the Rb-rich star IRAS 06300+6058.

The expansion velocities derived from the OH masers can also be taken as an additional distance-independent mass indicator (*20*, *21*). Despite the relatively large uncertainties involved, the Rb abundances were found to show a very nice correlation with the OH expansion velocities (Fig. 2). This correlation seems to confirm that the efficiency of the ^{22}Ne neutron source is directly correlated with the stellar mass as a consequence of the higher temperature achieved in the He intershell during the convective thermal pulses, as predicted by the models (*11*–*13*). In Fig. 2 we can clearly distinguish two groups of stars. Those stars in the sample with v_{exp}(OH) below 6 km s^{-1} were identified as non-HBB AGBs (< 4 to 5 $M_{\odot}$) displaying relatively low Rb enhancements; whereas those with v_{exp}(OH) greater than 6 km s^{-1} are suggested to be more massive AGB stars (> 4 to 5 $M_{\odot}$) experiencing HBB (*8*). Indeed, the more extreme stars in our sample, showing the larger Rb enhancements, must represent a class of even higher-mass stars (~6 to 8 $M_{\odot}$). In particular, the extremely Rb-rich star IRAS 19059-2219 is probably the most massive AGB star in our sample, with [Rb/Fe] = +2.6 dex.

The strong Rb overabundances observed, coupled with the lack of strong Zr enhancements in these stars (*8*), are certainly not predicted by current theoretical models, which usually do not consider stars in this very high mass range, nor do these models take into account the very strong mass loss rates that these stars experience during the TP-AGB phase. The above results thus challenge our understanding of the late stages of the evolution of intermediate-mass stars.

Table 1. Spectroscopic effective temperatures and Rb abundances derived. When the Rb I line at 7800.3 Å is resolved in two components (circumstellar and stellar), the abundance estimate corresponds to the photospheric abundance needed to fit the stellar component and it is marked with an asterisk. Stars IRAS 19059-2219 and IRAS 19426+4342 were observed in two different epochs. Note that stars IRAS 10261-5055 and IRAS 19147+5004 are not long-period, Mira-like variables, and as such they are possibly non-AGB stars.

IRAS name	Other	T_{eff} (K)	[Rb/Fe]	S/N at 7800 Å
01085+3022	AW Psc	3000	+2.0	49
04404-7427	SY Men	3000	+1.3*	68
05027-2158	T Lep	2800	+0.4	418
05098-6422	U Dor	3000	+0.1	309
05151+6312	BW Cam	3000	+2.1	161
06300+6058	Ap Lyn	3000	+1.6*	127
07222-2005		3000	+0.6*	30
09194-4518	MQ Vel	3000	+1.1*	25
10261-5055	VZ Vel	3000	< –1.0	595
14266-4211		2900	+0.9	106
15193+3132	VS Crb	2800	–0.3	266
15576-1212	Fs Lib	3000	+1.5	91
16030-5156	V352 Nor	3000	+1.3	86
16037+4218	V1012 Her	2900	+0.6	115
17034-1024	V850 Oph	3300	+0.2	189
18429-1721	V3952 Sgr	3000	+1.2	98
19059-2219	V3880 Sgr	3000	+2.3/+2.6	32/49
19147+5004	TZ Cyg	3000	–0.5	110
19426+4342		3000	+1.0*/+1.0*	19/25
20052+0554	V1416 Aql	3000	+1.5*	47
20077-0625	V1300 Aql	3000	+1.3*	19
20343-3020	RT Mic	3000	+0.9	76

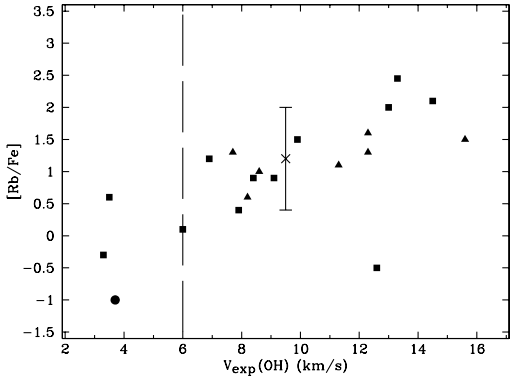

Fig. 2. Observed Rb abundances (squares) versus OH expansion velocity. One upper limit to the Rb abundance is shown with a dot. The abundance estimates that correspond to the photospheric abundance needed to fit the stellar component are shown with triangles. A maximum error bar of ±0.8 dex is also shown for comparison. The star with high OH expansion velocity and no Rb, which does not follow the general behavior observed, is IRAS 19147+5004 (TZ Cyg). This star possibly is a non-AGB star, as it is not a long-period, Mira-like variable.

Remarkably, Rb was found not to be overabundant in the few O-rich massive AGB stars previously studied in the Magellanic Clouds (*6*), contrary to the galactic O-rich AGB stars studied here. The luminous O-rich AGBs of the Magellanic Clouds, in fact, may constitute a sample of stars less massive than the present one, in which the temperature for HBB at the bottom of the convective layers is reached more easily than in the galactic population of AGB stars considered here. Because of their lower metallicity (*22*), they would develop lower temperatures during the helium thermal pulse, and thus would activate only the ^{13}C(α,n)^{16}O neutron chain. The dependence of Rb production and the efficiency of the ^{22}Ne neutron source on parameters such as metallicity and mass loss rate should be fully investigated in the future.

Our work also has implications for meteoritics. If the radioactive chronometer ^{87}Rb is strongly overproduced by the activation of the ^{22}Ne neutron source in HBB AGB stars, the overall nucleosynthesis of this isotope in the galaxy may be significantly affected. Huge amounts of Rb-rich processed material can be transferred to the ISM by massive AGB stars, with relevant implications for the Rb primeval solar nebula abundance. Radioactive dating studies of primitive chondrites assume that the initial conditions are known and that the oldest components of chondrites (calcium- and aluminum-rich inclusions) evolved without external exchange of ^{87}Rb and ^{87}Sr, but our data suggest that the initial ^{87}Rb/^{87}Sr ratio may have been altered by a nearby population of massive AGB stars during the early evolution of our solar system. The presence of these stars in the vicinity of the Sun is also supported by the identification of a few oxide presolar grains for which an intermediate-mass AGB origin has been determined (*23*, *24*). In such an environment, it is very unlikely that a Rb/Sr chondritic ratio could be maintained constant in the protoplanetary disk for the time span in which chondritic meteorites formed, as previously suggested (*25*). Consequently, the ^{87}Rb/^{87}Sr ratio measured in primitive meteorites should be considered only a qualitative measure of antiquity, as was previously pointed out from studies of refractory inclusions in the Allende meteorite (*26*).

References and Notes

1. I. Iben Jr., A. Renzini, *Annu. Rev. Astron. Astrophys.* **21**, 271 (1983).
2. G. Wallerstein, G. R. Knapp, *Annu. Rev. Astron. Astrophys.* **36**, 369 (1998).
3. I.-J. Sackmann, A. I. Boothroyd, *Astrophys. J.* **392**, L71 (1992).
4. I. Mazzitelli, F. D'Antona, P. Ventura, *Astron. Astrophys.* **348**, 846 (1999).
5. A. G. W. Cameron, W. A. Fowler, *Astrophys. J.* **164**, 111 (1971).
6. B. Plez, V. V. Smith, D. L. Lambert, *Astrophys. J.* **418**, 812 (1993).
7. V. V. Smith, B. Plez, D. L. Lambert, D. A. Lubowich, *Astrophys. J.* **441**, 735 (1995).
8. D. A. García-Hernández *et al.*, *Astron. Astrophys.*, in press (http://arxiv.org/abs/astro-ph/0609106).

9. M. Schwarzschild, R. Härm, *Astrophys. J.* **150**, 961 (1967).
10. R. H. Sanders, *Astrophys. J.* **150**, 971 (1967).
11. M. Busso, R. Gallino, G. J. Wasserburg, *Annu. Rev. Astron. Astrophys.* **37**, 239 (1999).
12. O. Straniero *et al.*, *Astrophys. J.* **440**, L85 (1995).
13. J. W. Truran, I. Iben Jr., *Astrophys. J.* **216**, 797 (1977).
14. H. Beer, R. L. Macklin, *Astrophys. J.* **339**, 962 (1989).
15. C. Abia *et al.*, *Astrophys. J.* **559**, 1117 (2001).
16. D. L. Lambert *et al.*, *Astrophys. J.* **450**, 302 (1995).
17. J. Tomkin, D. L. Lambert, *Astrophys. J.* **523**, 234 (1999).
18. A. Banerjee, D. Das, V. Natarajan, *Europhys. Lett.* **65**, 172 (2004).
19. N. Grevesse, A. J. Sauval, *Space Sci. Rev.* **85**, 161 (1998).
20. P. S. Chen, R. Szczerba, S. Kwok, K. Volk, *Astron. Astrophys.* **368**, 1006 (2001).
21. F. M. Jiménez-Esteban, P. García-Lario, D. Engels, in *Planetary Nebulae as Astronomical Tools*, R. Szczerba, G. Stasinska, S. K. Gorny, Eds. (AIP Conference Proceedings, vol. 804, American Institute of Physics, Melville, NY, 2005), pp. 141–144.
22. P. Ventura *et al.*, *Astrophys. J.* **550**, L65 (2001).
23. C. M. O'D. Alexander, *Philos. Trans. R. Soc. London Ser. A* **359**, 1973 (2001).
24. E. Zinner *et al.*, *Geochim. Cosmochim. Acta* **69**, 4149 (2005).
25. K. D. McKeegan, A. M. Davis, in *Meteorites, Planets, and Comets*, A. Davis, Ed., vol. 1 of *Treatise on Geochemistry* (Elsevier-Pergamon, Oxford, 2003), pp. 431–460.
26. F. A. Podosek *et al.*, *Geochim. Cosmochim. Acta* **55**, 1083 (1991).
27. Supported by the Spanish Ministerio de Educación y Ciencia (MEC) grants AYA 2004-3136 and AYA 2003-9499 (A.M. and P.G.L.) and a MEC JdC grant (J.M.T.R.). This work is based on observations obtained at the 4.2-m William Herschel Telescope, operated on the island of La Palma by the Isaac Newton Group in the Observatorio del Roque de Los Muchachos of the Instituto de Astrofisica de Canarias, and on observations obtained with the 3.6-m telescope at ESO–La Silla Observatory (Chile).

Supporting Online Material
www.sciencemag.org/cgi/content/full/1133706/DC1
Fig. S1

10 August 2006; accepted 19 October 2006
Published online 9 November 2006;
10.1126/science.1133706
Include this information when citing this paper.

Heterogeneous Three-Dimensional Electronics by Use of Printed Semiconductor Nanomaterials

Jong-Hyun Ahn,[1,2,3] Hoon-Sik Kim,[5] Keon Jae Lee,[1,3] Seokwoo Jeon,[1,2,3] Seong Jun Kang,[1,2,3] Yugang Sun,[1,2,3] Ralph G. Nuzzo,[1,2,3,4] John A. Rogers[1,2,3,4,5]*

We developed a simple approach to combine broad classes of dissimilar materials into heterogeneously integrated electronic systems with two- or three-dimensional layouts. The process begins with the synthesis of different semiconductor nanomaterials, such as single-walled carbon nanotubes and single-crystal micro- and nanoscale wires and ribbons of gallium nitride, silicon, and gallium arsenide on separate substrates. Repeated application of an additive, transfer printing process that uses soft stamps with these substrates as donors, followed by device and interconnect formation, yields high-performance heterogeneously integrated electronics that incorporate any combination of semiconductor nanomaterials on rigid or flexible device substrates. This versatile methodology can produce a wide range of unusual electronic systems that would be impossible to achieve with other techniques.

Many existing and emerging electronic devices benefit from the heterogeneous integration of dissimilar classes of semiconductors into single systems, in either two-dimensional (2D) or 3D layouts (*1*, *2*). Examples include multifunctional radio-frequency communication devices, infrared imaging cameras, addressable sensor arrays, and hybrid silicon complementary metal oxide semiconductor (CMOS) circuits and nanowire devices (*3*–*7*). In some representative systems, compound semiconductors or other materials provide high-speed operation, efficient photodetection, or sensing capabilities; the silicon CMOS provides digital readout and signal processing in circuits that often involve stacked 3D configurations. Wafer- or chip-scale bonding (*1*, *2*, *6*, *8*–*10*) and epitaxial growth (*3*, *11*, *12*) represent the two most widely used methods for achieving these types of integrated systems.

The bonding processes use fusion processes (*8*, *9*) or layers of adhesives (*6*, *10*) to combine integrated circuits, photodiodes, or sensors formed separately on different semiconductor wafers. This approach works well in many cases, but it has important drawbacks (*1*, *9*), including (i) limited ability to scale to large areas (i.e., larger than the wafers) or to more than a few layers in the third (i.e., stacking) dimension; (ii) incompatibility with unusual materials (such as nanostructured materials) and/or low-temperature materials and substrates; (iii) challenging fabrication and alignment for the through-wafer electrical interconnects; (iv) demanding requirements for planar bonding surfaces; and (v) bowing and cracking that can occur from mechanical strains generated by differential thermal expansion and contraction of disparate materials. Epitaxial growth provides a different approach, which uses molecular beam epitaxy or other means to form thin layers of semiconductor materials directly on the surfaces of wafers of other materials. Although this method avoids some of the aforementioned problems, the requirements for epitaxy place severe restrictions on the quality and type of materials that can be grown, even when buffer layers and other advanced techniques are used (*1*, *13*).

By contrast, nanoscale wires, ribbons, membranes, or particles of inorganic materials, or carbon-based systems such as single-walled carbon nanotubes (SWNTs) or graphene sheets (*14*–*17*), can be grown and then suspended in solvents or transferred onto substrates in a manner that bypasses the need for epitaxial growth or wafer bonding. Recent work has shown the integration of isolated crossed nanowire diodes in 2D layouts formed by solution casting (*18*). Our results show how dissimilar single-crystal inorganic semiconductors (such as micro- and nanoscale wires and ribbons of GaN, Si, and GaAs) can be combined with one another and also with other classes of nanomaterials (such as SWNTs) with the use of a scalable and deterministic printing method to yield complex, heterogeneously integrated electronic systems in 2D or 3D layouts. The capabilities of this process are demonstrated by ultrathin multilayer stacks of high-performance metal oxide semiconductor field-effect transistors (MOSFETs), high electron mobility transistors (HEMTs), thin-film transistors (TFTs), photodiodes, and other components that are integrated into device arrays, logic gates, and actively addressable photodetectors on rigid inorganic and flexible plastic substrates.

Figure 1 illustrates representative steps for producing these types of systems. The process begins with the synthesis of the semiconductor nanomaterials, each on their own source substrate. The devices shown in Fig. 1 allow micro- and nanoscale wires and ribbons of single-crystalline GaN, GaAs, and Si that were formed with the use of wafer-based source materials and lithographic etching procedures (*19*–*23*) to be integrated with each other or with networks of SWNTs that were grown by chemical vapor deposition (*16*, *23*). Scanning electron micrographs at the top of Fig. 1 show these semiconductor nanomaterials after their removal from the source substrates. For circuit fabrica-

[1]Department of Materials Science and Engineering, University of Illinois, Urbana-Champaign, IL 61801, USA. [2]Beckman Institute for Advanced Science and Technology, University of Illinois, Urbana-Champaign, IL 61801, USA. [3]Frederick Seitz Materials Research Laboratory, University of Illinois, Urbana-Champaign, IL 61801, USA. [4]Department of Chemistry, University of Illinois, Urbana-Champaign, IL 61801, USA. [5]Department of Electrical and Computer Engineering, University of Illinois, Urbana-Champaign, IL 61801, USA.

*To whom correspondence should be addressed. E-mail: jrogers@uiuc.edu

tion, these elements remain in the configurations defined on the wafers during the fabrication or growth stage: aligned arrays in the case of the GaN, GaAs, and Si materials, and submonolayer random networks for the SWNTs. High-temperature doping and annealing procedures for ohmic contacts to the GaN, GaAs, and Si can be performed on the source substrates.

The next step involves transferring these processed elements, with the use of an elastomeric stamp–based printing technique (*19*), from the source substrates to a device substrate, such as a sheet of polyimide (PI) (Fig. 1). In particular, laminating a stamp of polydimethylsiloxane against the source substrate establishes soft, van der Waals adhesion contacts to the semiconductor nanomaterial elements. We contacted the "inked" stamp to a device substrate (such as a PI sheet) with a thin, spin-cast layer of a liquid prepolymer (such as polyamic acid) on its surface and then cured the polymer, which left these semiconductor materials embedded on and well adhered to this layer (*19*–*22*) when the stamp was removed. Similar procedures work well with a range of substrates (i.e., rigid or flexible and organic or inorganic) and semiconductor nanomaterials. We used a slightly modified version of this process for the SWNT devices (*23*). The thickness of the interlayer (PI in this case) can be as small as 500 nm and was typically 1 to 1.5 μm for the systems we describe.

After some additional processing—including deposition and patterning of gate dielectrics, electrodes, and interconnects—the transfer printing and device fabrication steps can be repeated, beginning with spin-coating a new prepolymer interlayer on top of the previously completed circuit level. Automated stages specially designed for transfer printing or conventional mask aligners enable overlay registration accuracy of ~2 μm over several square centimeters (fig. S1). The spatial distortions associated with the printing had a mean value of ~0.5 μm (fig. S2). The yields for printing of Si, SWNT, GaAs, and GaN were >99%, >99%, >95%, and >85%, respectively. Defects in these last two cases were associated with fracture and impartial transfer for the relatively wide GaAs ribbons and relatively thick GaN bars, respectively (fig. S3). Layer-to-layer interconnects (*24*) were formed simply by evaporating metal lines over and into openings in the interlayers defined by photopatterning and/or dry etching.

This fabrication approach has several important features. First, all of the processing on the device substrate occurs at low temperatures, thereby avoiding differential thermal expansion and shrinkage effects that can result in unwanted deformations in multilayer stacked systems. This operation also enables the use of low-temperature plastic substrates and interlayer materials, and it helps to ensure that underlying circuit layers are not thermally degraded by the processing of overlying devices. Second, the method is applicable to broad classes of semiconductor nanomaterials, including emerging materials such as SWNTs. Third, the soft stamps enable nondestructive contacts with underlying device layers; these stamps, together with the ultrathin semiconductor materials, can also tolerate surfaces that have some topography. Fourth, the ultrathin device geometries and interlayers allow easy formation of layer-to-layer electrical interconnects by direct metallization over the device structure. These features overcome many of the disadvantages of conventional approaches.

Figure 2 presents three-layer, 3D stacks of arrays of Si MOSFETs fabricated by the general process flow shown in Fig. 1. We used single-crystalline silicon nanoribbons with doped contacts (formed on the source wafer), SiO_2 dielectrics formed by plasma-enhanced chemical vapor deposition, and Cr/Au metallization for the source, drain, and gate electrodes (*25*). Each device uses three aligned nanoribbons, each with length $L = 250$ μm, width $W = 87$ μm, and thickness = 290 nm. Figure 2A shows an optical micrograph of an edge of the system; the layout of the system was designed to reveal separately the parts of the substrate that support one, two, and three layers of MOSFETs. A 90° rotation of the device geometry for the second layer, relative to the first and third, helps to clarify the layout of the system. Schematic cross-sectional and angled views of the stacked structure are shown in Fig. 2B. The sample can be viewed in 3D using confocal optical microscopy. Figure 2C shows top and angled views of such images. (The image quality degrades somewhat with depth because of scattering and absorption from the upper layers). Figure 2D presents electrical measurements of representative devices in each layer. Devices on

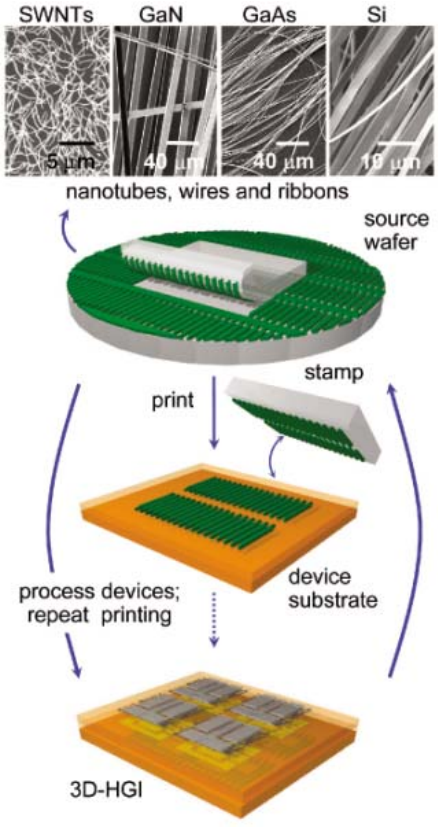

Fig. 1. Schematic illustration of a printed semiconductor nanomaterials–based approach to heterogeneous 3D electronics. The process involves the repetitive transfer printing of collections of nanotubes, nanowires, nanoribbons, or other active nanomaterials, separately formed on source substrates, to a common device substrate to generate interconnected electronics in ultrathin, multilayer stack geometries. HGI, heterogeneous integration.

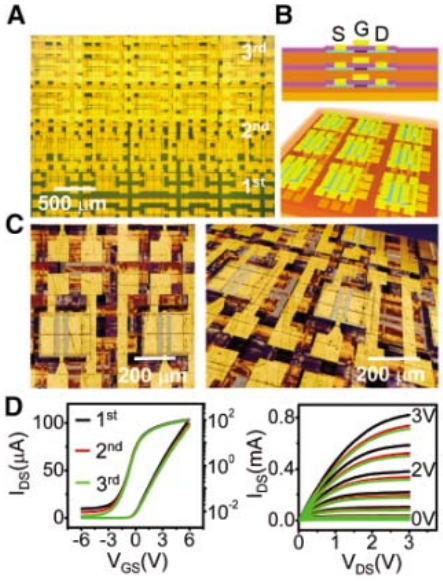

Fig. 2. (**A**) Optical micrograph view of the top of a 3D multilayer stack of arrays of single-crystal silicon MOSFETs that use printed silicon nanoribbons for the semiconductor. The bottom (1st), middle (2nd), and top (3rd) parts of this image correspond to regions with one, two, and three layers of devices, respectively. (**B**) Schematic cross-sectional (top) and angled (bottom) views. S, D, and G refer to source, drain, and gate electrodes (all shown in gold), respectively. The light and dark blue regions correspond to doped and undoped regions of the silicon ribbons; the purple layer is the SiO_2 gate dielectric. (**C**) 3D images (left, top view; right, angled view) collected by confocal microscopy on a device substrate similar to that shown in (A) and (B). The layers are colorized (gold, top layer; red, middle layer; blue, bottom layer; silicon, gray) for ease of viewing. (**D**) Current-voltage characteristics of Si MOSFETs in each of the layers, showing excellent performance (mobilities of 470 ± 30 cm^2/Vs) and good uniformity in the properties. The channel lengths and widths are 19 and 200 μm, respectively. The overlap lengths, as defined by distance that the gate electrode extends over the doped source and drain regions, are 5.5 μm. I_{DS}, drain current; V_{GS}, bias voltage; V_{DS}, drain voltage.

each of the three layers, which are formed on a PI substrate, show excellent properties with linear mobilities of 470 ± 30 cm^2/Vs (where the error is SD), on/off ratios greater than 10^4, and threshold voltages of –0.1 ± 0.2 V; there are no systematic differences between devices in different layers. Additional layers can be added to this system by repeating the same procedures. To investigate issues related to mismatches in coefficients of thermal expansion in these systems, we evaluated the behavior of the devices under thermal cycling (60 times) between room temperature and 90°C. Small changes were observed for the first few cycles followed by stable behavior (fig. S9).

In addition to 3D circuits with a single semiconductor, Fig. 3 illustrates that the capability to combine various semiconductors can be used in multiple layers. We fabricated arrays of HEMTs, MOSFETs, and TFTs—with the use of GaN bars, Si nanoribbons, and SWNT films, respectively, on PI substrates. Figure 3, A and B, shows high-magnification optical and confocal images, respectively, of the resulting devices. The GaN HEMTs on the first layer use ohmic contacts (Ti/Al/Mo/Au, annealed on the source wafer) for the source and drain, and Schottky (Ni/Au) contacts for the gates. Each device uses GaN ribbons (composed of multilayer stacks of AlGaN/GaN/AlN) interconnected electrically by processing on the device substrate. The SWNT TFTs on the second layer use SiO_2 and epoxy for the gate dielectric and Cr/Au for the source, drain, and gate. The Si MOSFETs use the same design as those shown in Fig. 2. Various other devices can be constructed with different combinations of Si, SWNT, and GaN (figs. S4 and S5). Figure 3C presents the current-voltage characteristics of typical devices in the systems of Fig. 3, A and B. In all cases, the properties are similar to those fabricated on the source wafers: The GaN HEMTs have threshold voltages (V_{th}) of –2.4 ± 0.2 V, on/off ratios greater than 10^6, and transconductances of 0.6 ± 0.5 mS; the SWNT TFTs have V_{th} = –5.3 ± 1.5 V, on/off ratios greater than 10^5, and linear mobilities of 5.9 ± 2.0 cm^2/Vs; and the Si MOSFETs have V_{th} = 0.2 ± 0.3 V, on/off ratios greater than 10^4, and linear mobilities of 500 ± 30 cm^2/Vs.

Another interesting aspect of these devices, which follows from the use of thin PI substrates (25 μm), devices (<1.7 μm), and PI interlayers (1.5 μm), is their mechanical bendability. This characteristic is important for applications in flexible electronics, for which these systems might provide attractive alternatives because of their enhanced capabilities compared with those of conventional organic-based devices. We evaluated the effective transconductance (g_{eff}) for the Si, SWNT, and GaN devices in the system of Fig. 3A as a function of bend radius. Figure 3D, which shows these data normalized to the transconductance in the unbent state (g_{0eff}), demonstrates the stable performance for bend radii down to 3.7 mm. To explore the response of devices to operation under various conditions, such as repeated bending and electrical testing, we carried out two sets of experiments. Repeated bending (up to 2000 cycles) resulted in no substantial change in the properties of the devices (fig. S8). Repeated electrical testing showed stable responses (~10% changes in properties, or less) (fig. S11). Figures S12 to S15 present information on variation in device properties.

Electrical interconnections formed between different levels in these devices can create

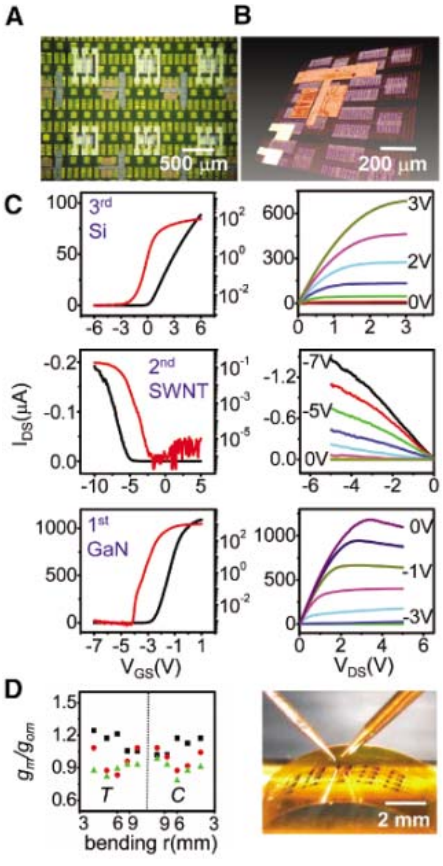

Fig. 3. (**A**) Optical micrograph of 3D heterogeneously integrated electronic devices, including GaN nanoribbon HEMTs, Si nanoribbon MOSFETs, and SWNT network TFTs, in a three-layer stack. (**B**) 3D image collected by confocal microscopy. The layers are colorized (gold: top layer, Si MOSFETs; red: middle layer, SWNT TFTs; pink: bottom layer) for ease of viewing. (**C**) Electrical characteristics of GaN devices on the first layer (channel lengths, widths and gate widths of 20, 170, and 5 μm, respectively, and ribbon thicknesses, widths, and lengths of 1.2, 10, and 150 μm, respectively), SWNT devices on the second layer (channel lengths and widths of 50 and 200 μm, respectively, and average tube diameters and lengths of ~1.5 nm and ~10 μm, respectively), and Si devices on the third layer (channel lengths and widths of 19 and 200 μm, respectively). (**D**) (Left) Normalized transconductances (g_m/g_{0m}) of devices in each layer (black squares, Si MOSFETs; red circles, SWNT TFTs; green triangles, GaN HEMTs) as a function of bending radius of the plastic substrate. *T*, tension; *C*, compression. (Right) Image of the bent system and probing apparatus.

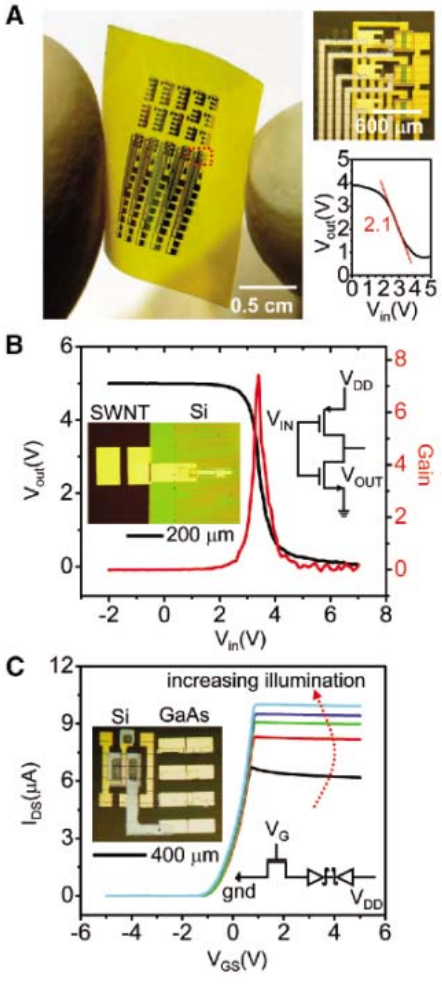

Fig. 4. (**A**) Image of a printed array of 3D silicon n-channel metal oxide semiconductor inverters on a PI substrate. The inverters consist of MOSFETs (channel lengths of 4 μm, load-to-driver width ratio of 6.7, and a driver width of 200 μm) on two different levels, interconnected by electrical via structures. The image on the top right provides a magnified view of the region indicated by the red box in the left frame. The graph on the bottom right shows transfer characteristics of a typical inverter. (**B**) Transfer characteristics of a printed complementary inverter that uses a p-channel SWNT TFT (channel length and width of 30 and 200 μm, respectively) and an n-channel Si MOSFET (channel length and width of 75 and 50 μm, respectively). The insets provide an optical micrograph of an inverter (left) and a circuit schematic (right). (**C**) Current-voltage response of a GaAs MSM (channel length and width of 10 and 100 μm, respectively) integrated with a Si MOSFET (channel length and width of 9 and 200 μm, respectively) at different levels of illumination from dark to 11 μW with an infrared light source at 850 nm. The insets show an optical image (left) and a circuit diagram (right). gnd, ground.

interesting circuit capabilities. The thin polymer interlayers allow robust interconnects to be formed easily by evaporating metal lines over lithographically defined openings. Thermal cycling tests showed no changes in their properties (fig. S10). Figure 4A shows a 3D n-channel metal oxide semiconductor inverter (logic gate) in which the drive (L = 4 μm, W = 200 μm) and load (L = 4 μm, W = 30 μm) Si MOSFETs are on different levels. With a supply voltage of 5 V, this double-layer inverter exhibits well-defined transfer characteristics with gains of ~2, comparable to the performance of conventional planar inverters that use similar transistors. Figure 4B shows an inverter with a complementary design (CMOS) with the use of integrated n-channel Si MOSFETs and p-channel SWNT TFTs, designed to equalize the current-driving capability in both pull-up and pull-down directions. Transfer curves collected with a supply voltage (V_{DD}) of 5 V and gate voltage (input) swept from 0 to 5 V appear in Fig. 4B. The curve shapes and gains (as high as ~7) are qualitatively consistent with numerical circuit simulations (fig. S6). As a third example, we built GaAs metal-semiconductor-metal (MSM) infrared detectors (*26*), integrated with Si MOSFETs on flexible PI substrates, to demonstrate a capability for fabricating unit cells that could be used in active infrared imagers. In this case, printed nanoribbons of GaAs (L = 400 μm, W = 100 μm, and thickness = 270 nm) transferred onto a substrate with a printed array of Si nanoribbon MOSFETs form the basis of the MSMs. Electrodes (Ti/Au) deposited on the ends of these GaAs nanoribbons form back-to-back Schottky diodes with separations of 10 μm. The resulting detector cells exhibit current enhancement as the intensity of infrared illumination increases (Fig. 4C), consistent with circuit simulation (fig. S7). A responsivity of about 0.30 A/W at the 850-nm wavelength is observed from 1 to 5 V. (This value underestimates the true responsivity because it ignores optical reflection). The bendability of this system, which is comparable to that of the devices in Fig. 3, could be useful for advanced systems such as curved focal plane arrays for wide-angle infrared night vision imagers.

Printed semiconductor nanomaterials provide new approaches to 3D heterogeneously integrated systems that could be important in various fields of application, including not only those suggested by the systems reported here but also others such as microfluidic devices with integrated electronics, chemical and biological sensor systems that incorporate unusual materials with conventional silicon-based electronics, and photonic and optoelectronic systems that combine light emitters and detectors of compound semiconductor with silicon drive electronics or microelectromechanical structures. Furthermore, the compatibility of this approach with thin, lightweight plastic substrates may create additional opportunities for devices that have unusual form factors or mechanical flexibility as key features.

References and Notes

1. K. Banerjee, S. J. Souri, P. Kapur, K. C. Saraswat, *Proc. IEEE* **89**, 602 (2001).
2. S. F. Al-Sarawi, D. Abbott, P. D. Franzon, *IEEE Trans. Components Packaging Manufacturing Technol. Part B* **21**, 2 (1998).
3. A. S. Brown *et al.*, *Mater. Sci. Eng. B* **87**, 317 (2001).
4. Y.-C. Tseng *et al.*, *Nano Lett.* **4**, 123 (2004).
5. C. Joachim, J. K. Gimzewski, A. Aviram, *Nature* **408**, 541 (2000).
6. G. Roelkens *et al.*, *Opt. Express* **13**, 10102 (2005).
7. D. B. Strukov, K. K. Likharev, *Nanotechnology* **16**, 888 (2005).
8. Q. Y. Tong, U. Gosele, *Semiconductor Wafer Bonding: Science and Technology* (John Wiley, New York, 1999).
9. M. A. Schmidt, *Proc. IEEE* **86**, 1575 (1998).
10. P. Garrou, *Semicond. Int.* **28**, SP10 (February, 2005).
11. H. Amano, N. Sawaki, I. Akasaki, Y. Toyoda, *Appl. Phys. Lett.* **48**, 353 (1986).
12. T. Kuykendall *et al.*, *Nat. Mater.* **3**, 524 (2004).
13. J. C. Bean, *Proc. IEEE* **80**, 571 (1992).
14. A. M. Morales, C. M. Lieber, *Science* **279**, 208 (1998).
15. M. Law *et al.*, *Science* **305**, 1269 (2004).
16. J. Kong, H. T. Soh, A. M. Cassell, C. F. Quate, H. Dai, *Nature* **395**, 878 (1998).
17. K. S. Novoselov *et al.*, *Science* **306**, 666 (2004).
18. Y. Huang, X. Duan, C. M. Lieber, *Small* **1**, 142 (2005).
19. M. A. Meitl *et al.*, *Nat. Mater.* **5**, 33 (2006).
20. E. Menard, K. J. Lee, D. Y. Khang, R. G. Nuzzo, J. A. Rogers, *Appl. Phys. Lett.* **84**, 5398 (2004).
21. Y. Sun, S. Kim, I. Adesida, J. A. Rogers, *Appl. Phys. Lett.* **87**, 083501 (2005).
22. S.-H. Hur, D.-Y. Khang, C. Kocabas, J. A. Rogers, *Appl. Phys. Lett.* **85**, 5730 (2004).
23. Materials and methods are available as supporting material on *Science* Online.
24. S. Linder, H. Baltes, F. Gnaedinger, E. Doering, in *Proceedings of the 7th IEEE International Workshop on Micro Electro Mechanical Systems*, Oiso, Japan, 25 to 28 January 1994 (IEEE, Piscataway, NJ, 1994), pp. 349–354.
25. J.-H. Ahn *et al.*, *IEEE Electron Devices Lett* **27**, 460 (2006).
26. J. B. D. Soole, H. Schumacher, *IEEE J. Quantum Electron.* **27**, 737 (1991).

27. The research was supported by the U.S. Department of Energy, Division of Materials Sciences under award no. DEFG02-91ER45439, through the Frederick Seitz Materials Research Laboratory (FS-MRL). We thank T. Banks and K. Colravy for help with cleanroom and other facilities at the Frederick Seitz Materials Research Laboratory and H. C. Ko, Q. Cao, P. Ferreira, J. Dong, and E. Menard for help with printing and distortion measurements using facilities and manufacturing approaches developed at the Center for Nanoscale Chemical Electrical Mechanical Manufacturing Systems at the University of Illinois (funded by the NSF under grant DMI-0328162). All imaging and surface analysis was performed at the FS-MRL Center for Microanalysis of Materials at the University of Illinois at Urbana-Champaign, supported by award no. DEFG02-91ER45439.

Supporting Online Material

www.sciencemag.org/cgi/content/full/314/5806/1754/DC1
Materials and Methods
Figs. S1 to S15

12 July 2006; accepted 31 October 2006
10.1126/science.1132394

Quantum Spin Hall Effect and Topological Phase Transition in HgTe Quantum Wells

B. Andrei Bernevig,[1,2] Taylor L. Hughes,[1] Shou-Cheng Zhang[1]*

We show that the quantum spin Hall (QSH) effect, a state of matter with topological properties distinct from those of conventional insulators, can be realized in mercury telluride–cadmium telluride semiconductor quantum wells. When the thickness of the quantum well is varied, the electronic state changes from a normal to an "inverted" type at a critical thickness d_c. We show that this transition is a topological quantum phase transition between a conventional insulating phase and a phase exhibiting the QSH effect with a single pair of helical edge states. We also discuss methods for experimental detection of the QSH effect.

The spin Hall effect (*1*–*5*) has recently attracted great attention in condensed matter physics, not only for its fundamental scientific importance but also because of its potential application in semiconductor spintronics. In particular, the intrinsic spin Hall effect promises the possibility of designing the intrinsic electronic properties of materials so that the effect can be maximized. On the basis of this line of reasoning, it was shown (*6*) that the intrinsic spin Hall effect can in principle exist in band insulators, where the spin current can flow without dissipation. Motivated by this suggestion, researchers have proposed the quantum spin Hall (QSH) effect for graphene (*7*) as well as for semiconductors (*8*, *9*), where the spin current is carried entirely by the helical edge states in two-dimensional samples.

Time-reversal symmetry plays an important role in the dynamics of the helical edge states (*10*–*12*). When there is an even number of pairs of helical states at each edge, impurity scattering or many-body interactions can open a gap at the edge and render the system topologically trivial. However, when there is an odd number of pairs of helical states at each edge, these effects cannot open a gap unless time-reversal symmetry is

[1]Department of Physics, Stanford University, Stanford, CA 94305, USA. [2]Kavli Institute for Theoretical Physics, University of California, Santa Barbara, CA 93106, USA.

*To whom correspondence should be addressed. E-mail: sczhang@stanford.edu

spontaneously broken at the edge. The stability of the helical edge states has been confirmed in extensive numerical calculations (*13*, *14*). The time-reversal property leads to the Z_2 classification (*10*) of the QSH state.

States of matter can be classified according to their topological properties. For example, the integer quantum Hall effect is characterized by a topological integer n (*15*), which determines the quantized value of the Hall conductance and the number of chiral edge states. It is invariant under smooth distortions of the Hamiltonian, as long as the energy gap does not collapse. Similarly, the number of helical edge states, defined modulo 2, of the QSH state is also invariant under topologically smooth distortions of the Hamiltonian. Therefore, the QSH state is a topologically distinct new state of matter, in the same sense as the charge quantum Hall effect.

Unfortunately, the initial proposal of the QSH in graphene (*7*) was later shown to be unrealistic (*16*, *17*), as the gap opened by the spin-orbit interaction turns out to be extremely small, on the order of 10^{-3} meV. There are also no immediate experimental systems available for the proposals in (*8*, *18*). Here, we present theoretical investigations of the type III semiconductor quantum wells, and we show that the QSH state should be realized in the "inverted" regime where the well thickness d is greater than a certain critical thickness d_c. On the basis of general symmetry considerations and the standard band perturbation theory for semiconductors, also called $k \cdot p$ theory (*19*), we show that the electronic states near the Γ point are described by the relativistic Dirac equation in 2 + 1 dimensions. At the quantum phase transition at $d = d_c$, the mass term in the Dirac equation changes sign, leading to two distinct $U(1)$-spin and Z_2 topological numbers on either side of the transition. Generally, knowledge of electronic states near one point of the Brillouin zone is insufficient to determine the topology of the entire system; however, it does allow robust and reliable predictions on the change of topological quantum numbers. The fortunate presence of a gap-closing transition in the HgTe-CdTe quantum wells therefore makes our theoretical prediction of the QSH state conclusive.

The potential importance of inverted band-gap semiconductors such as HgTe for the spin Hall effect was pointed out in (*6*, *9*). The central feature of the type III quantum wells is band inversion: The barrier material (e.g., CdTe) has a normal band progression, with the s-type Γ_6 band lying above the p-type Γ_8 band, and the well material (HgTe) having an inverted band progression whereby the Γ_6 band lies below the Γ_8 band. In both of these materials, the gap is smallest near the Γ point in the Brillouin zone (Fig. 1). In our discussion we neglect the bulk split-off Γ_7 band, as it has negligible effects on the band structure (*20*, *21*). Therefore, we restrict ourselves to a six-band model, and we start with the following six basic atomic states per unit cell combined into a six-component spinor:

$$\Psi = \left(|\Gamma_6, {}^1/_2\rangle, |\Gamma_6, {}^{-1}/_2\rangle, |\Gamma_8, {}^3/_2\rangle, |\Gamma_8, {}^1/_2\rangle, |\Gamma_8, {}^{-1}/_2\rangle, |\Gamma_8, {}^{-3}/_2\rangle\right) \quad (1)$$

In quantum wells grown in the [001] direction, the cubic or spherical symmetry is broken down to the axial rotation symmetry in the plane. These six bands combine to form the spin-up and spin-down (±) states of three quantum well subbands: $E1$, $H1$, and $L1$ (*21*). The $L1$ subband is separated from the other two (*21*), and we neglect it, leaving an effective four-band model. At the Γ point with in-plane momentum $k_{\|} = 0$, m_J is still a good quantum number. At this point the $|E1, m_J\rangle$ quantum well subband state is formed from the linear combination of the $|\Gamma_6, m_J = \pm{}^1/_2\rangle$ and $|\Gamma_8, m_J = \pm{}^1/_2\rangle$ states, while the $|H1, m_J\rangle$ quantum well subband state is formed from the $|\Gamma_8, m_J = \pm{}^3/_2\rangle$ states. Away from the Γ point, the $E1$ and $H1$ states can mix. Because the $|\Gamma_6, m_J = \pm{}^1/_2\rangle$ state has even parity, whereas the $|\Gamma_8, m_J = \pm{}^3/_2\rangle$ state has odd parity under two-dimensional spatial reflection, the coupling matrix element between these two states must be an odd function of the in-plane momentum k. From these symmetry considerations, we deduce the general form of the effective Hamiltonian for the $E1$ and $H1$ states, expressed in the basis of $|E1, m_J = {}^1/_2\rangle$, $|H1, m_J = {}^3/_2\rangle$ and $|E1, m_J = -{}^1/_2\rangle$, $|H1, m_J = -{}^3/_2\rangle$:

$$H_{\text{eff}}(k_x, k_y) = \begin{pmatrix} H(k) & 0 \\ 0 & H^*(-k) \end{pmatrix}, \quad H(k) = \varepsilon(k) + d_i(k)\sigma_i \quad (2)$$

where σ_i are the Pauli matrices. The form of $H^*(-k)$ in the lower block is determined from time-reversal symmetry, and $H^*(-k)$ is unitarily equivalent to $H^*(k)$ for this system (*22*). If inversion symmetry and axial symmetry around the growth axis are not broken, then the interblock matrix elements vanish, as presented.

We see that, to the lowest order in k, the Hamiltonian matrix decomposes into 2 × 2 blocks. From the symmetry arguments given above, we deduce that $d_3(k)$ is an even function of k, whereas $d_1(k)$ and $d_2(k)$ are odd functions of k. Therefore, we can generally expand them in the following form:

$$d_1 + id_2 = A(k_x + ik_y) \equiv Ak_+$$

$$d_3 = M - B(k_x^2 + k_y^2), \ \varepsilon(k) = C - D(k_x^2 + k_y^2) \quad (3)$$

where A, B, C, and D are expansion parameters that depend on the heterostructure. The Hamiltonian in the 2 × 2 subspace therefore takes the form of the (2 + 1)-dimensional Dirac Hamiltonian, plus an $\varepsilon(k)$ term that drops out in the quantum Hall response. The most important quantity is the mass or gap parameter M, which is the energy difference between the $E1$ and $H1$ levels at the Γ point. The overall constant C sets the zero of energy to be the top of the valence band of bulk HgTe. In a quantum well geometry, the band inversion in HgTe necessarily leads to a level crossing at some critical thickness d_c of the HgTe layer. For thickness $d < d_c$ (i.e., for a thin HgTe

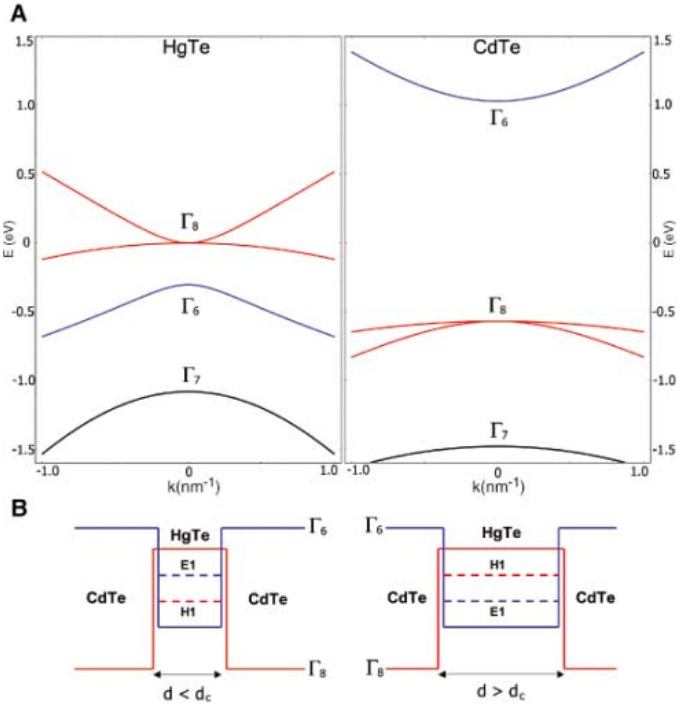

Fig. 1. (**A**) Bulk energy bands of HgTe and CdTe near the Γ point. (**B**) The CdTe-HgTe-CdTe quantum well in the normal regime $E1 > H1$ with $d < d_c$ and in the inverted regime $H1 > E1$ with $d > d_c$. In this and other figures, $\Gamma_8/H1$ symmetry is indicated in red and $\Gamma_6/E1$ symmetry is indicated in blue.

layer), the quantum well is in the "normal" regime, where the CdTe is predominant and hence the band energies at the Γ point satisfy $E(\Gamma_6) > E(\Gamma_8)$. For $d > d_c$, the HgTe layer is thick and the well is in the inverted regime, where HgTe dominates and $E(\Gamma_6) < E(\Gamma_8)$. As we vary the thickness of the well, the $E1$ and $H1$ bands must therefore cross at some d_c, and M changes sign between the two sides of the transition (Fig. 2, A and B). Detailed calculations show that, close to transition point, the $E1$ and $H1$ bands—both doubly degenerate in their spin quantum number—are far away in energy from any other bands (*21*), hence making an effective Hamiltonian description possible. Indeed, the form of the effective Dirac Hamiltonian and the sign change of M at $d = d_c$ for the HgTe-CdTe quantum wells deduced above from general arguments is already completely sufficient to conclude the existence of the QSH state in this system. For the sake of completeness, we also provide the microscopic derivation directly from the Kane model using realistic material parameters (*22*).

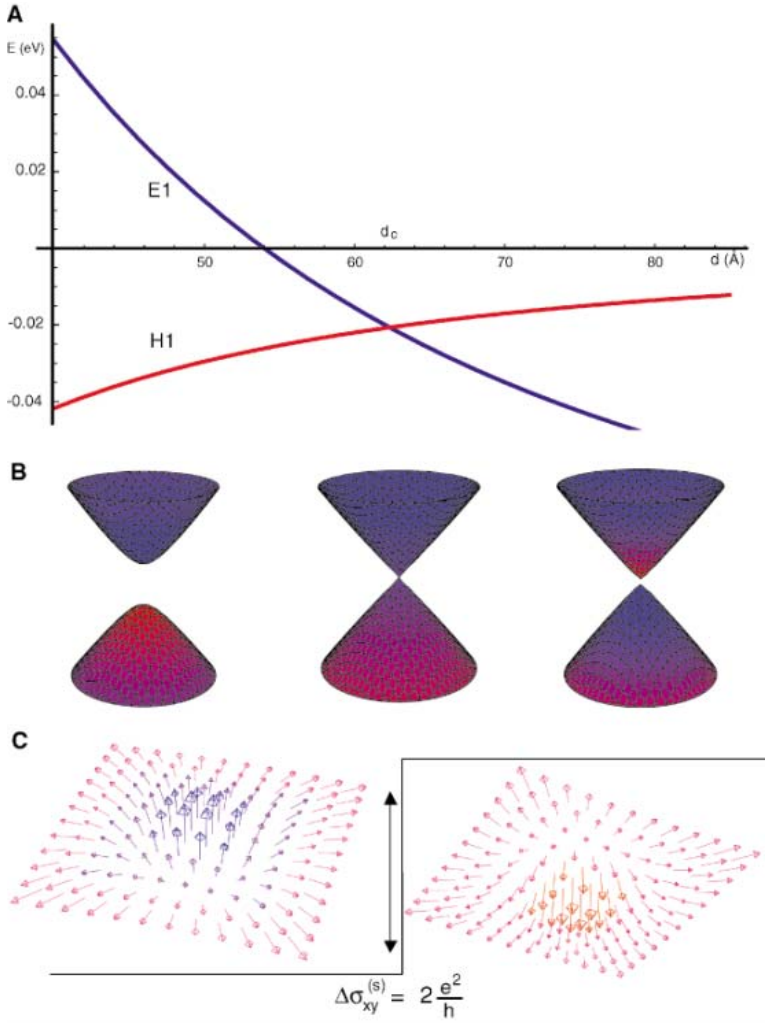

Fig. 2. (**A**) Energy of $E1$ (blue) and $H1$ (red) bands at $k_{||} = 0$ versus quantum well thickness d. (**B**) Energy dispersion relations $E(k_x,k_y)$ of the $E1$ and $H1$ subbands at $d = 40$, 63.5, and 70 Å (from left to right). Colored shading indicates the symmetry type of the band at that k point. Places where the cones are more red indicate that the dominant state is $H1$ at that point; places where they are more blue indicate that the dominant state is $E1$. Purple shading is a region where the states are more evenly mixed. At 40 Å, the lower band is dominantly $H1$ and the upper band is dominantly $E1$. At 63.5 Å, the bands are evenly mixed near the band crossing and retain their $d < d_c$ behavior moving farther out in k-space. At 70 Å, the regions near $k_{||} = 0$ have flipped their character but eventually revert back to the $d < d_c$ farther out in k-space. Only this dispersion shows the meron structure (red and blue in the same band). (**C**) Schematic meron configurations representing the $d_i(k)$ vector near the Γ point. The shading of the merons has the same meaning as the dispersion relations above. The change in meron number across the transition is exactly equal to 1, leading to a quantum jump of the spin Hall conductance $\sigma_{xy}^{(s)} = 2e^2/h$. We measure all Hall conductances in electrical units. All of these plots are for $Hg_{0.32}Cd_{0.68}Te$-HgTe quantum wells.

Figure 2A shows the energies of both the $E1$ and $H1$ bands at $k_{||} = 0$ as a function of quantum well thickness d obtained from our analytical solutions. At $d = d_c \sim 64$ Å, these bands cross. Our analytic results are in excellent qualitative and quantitative agreement with previous numerical calculations for the band structure of $Hg_{1-x}Cd_xTe$-HgTe-$Hg_{1-x}Cd_xTe$ quantum wells (*20*, *21*). We also observe that for quantum wells of thickness 40 Å $< d <$ 70 Å, close to d_c, the $E1\pm$ and $H1\pm$ bands are separated from all other bands by more than 30 meV (*21*).

Let us now define an ordered set of four six-component basis vectors $\psi_{1,\ldots,4} = (|E1, +\rangle, |H1, +\rangle, |E1, -\rangle, |H1, -\rangle)$ and obtain the Hamiltonian at nonzero in-plane momentum in perturbation theory. We can write the effective 4 × 4 Hamiltonian for the $E1\pm$, $H1\pm$ bands as

$$H_{ij}^{\text{eff}}(k_x, k_y) = \int_{-\infty}^{\infty} dz \langle \psi_j | \mathcal{H}(k_x, k_y, -i\partial_z) | \psi_i \rangle \tag{4}$$

where $\mathcal{H}(k_x, k_y, -i\partial_z)$ is the six-band Kane model (*19*). The form of the effective Hamiltonian is severely constrained by symmetry with respect to z. Each band has a definite z symmetry or antisymmetry, and vanishing matrix elements between them can be easily identified. For example,

$$H_{23}^{\text{eff}} = \frac{1}{\sqrt{6}} P k_+ \int_{-\infty}^{\infty} dz \langle \Gamma_6, +1/2(z) | \Gamma_8, -1/2(z) \rangle \tag{5}$$

where P is the Kane matrix element (*19*), vanishes because $|\Gamma_6, +1/2\rangle(z)$ is even in z, whereas $|\Gamma_8, -1/2\rangle(z)$ is odd. The procedure yields exactly the form of the effective Hamiltonian (Eq. 2), as we anticipated from the general symmetry arguments, with the coupling functions taking exactly the form of Eq. 3. The dispersion relations (*22*) have been checked to be in agreement with prior numerical results (*20*, *21*). We note that for $k \in [0, 0.01\ \text{Å}^{-1}]$ the dispersion relation is dominated by the Dirac linear terms. The numerical values for the coefficients depend on the thickness, and values at $d = 58$ Å and $d =$ 70 Å are given in (*22*).

Having presented the realistic $k \cdot p$ calculation starting from the microscopic six-band Kane model, we now introduce a simplified tight-binding model for the $E1$ and $H1$ states based on their symmetry properties. We consider a square lattice with four states per unit cell. The $E1$ states are described by the s-orbital states $\psi_{1,3} = |s, \alpha = \pm 1/2\rangle$, and the $H1$ states are described by the spin-orbit coupled p-orbital states $\psi_{2,4} = \pm(1/\sqrt{2})|p_x \pm ip_y, \alpha = \pm 1/2\rangle$, where α denotes the electron spin. Nearest-neighbor coupling between these states gives the tight-

binding Hamiltonian of the form of Eq. 2, with the matrix elements given by

$$d_1 + id_2 = A[\sin(k_x) + i\,\sin(k_y)]$$

$$d_3 = -2B[2 - (M/2B) - \cos(k_x) - \cos(k_y)]$$

$$\varepsilon(k) = C - 2D[2 - \cos(k_x) - \cos(k_y)] \quad (6)$$

The tight-binding lattice model simply reduces to the continuum model Eq. 2 when expanded around the Γ point. The tight-binding calculation serves dual purposes. For readers uninitiated in the Kane model and $k \cdot p$ theory, this gives a simple and intuitive derivation of our effective Hamiltonian that captures all the essential symmetries and topology. On the other hand, it also introduces a short-distance cutoff so that the topological quantities can be well defined.

Within each 2 × 2 subblock, the Hamiltonian is of the general form studied in (*9*), in the context of the quantum anomalous Hall effect, where the Hall conductance is given by

$$\sigma_{xy} = -\frac{1}{8\pi^2}\iint dk_x dk_y \hat{\mathbf{d}} \cdot \partial_x \hat{\mathbf{d}} \times \partial_y \hat{\mathbf{d}} \quad (7)$$

in units of e^2/h (the square of the charge on the electron divided by the Planck constant), where $\hat{\mathbf{d}}$ denotes the unit $d_i(k)$ vector introduced in the Hamiltonian Eq. 2. When integrated over the full Brillouin zone, σ_{xy} is quantized to take integer values that measure the skyrmion number, or the number of times the unit $\hat{\mathbf{d}}$ winds around the unit sphere over the Brillouin zone torus. The topological structure can be best visualized by plotting $\hat{\mathbf{d}}$ as a function of k. In a skyrmion with a unit of topological charge, the $\hat{\mathbf{d}}$ vector points to the north (or the south) pole at the origin, points to the south (or the north) pole at the zone boundary, and winds around the equatorial plane in the middle region.

Substituting the continuum expression for the $d_i(k)$ vector as given in Eq. 3, and cutting off the integral at some finite point in momentum space, one obtains $\sigma_{xy} = {}^1/_2\ sign\ (M)$, which is a well-known result in field theory (*23*). In the continuum model, the $\hat{\mathbf{d}}$ vector takes the configuration of a meron, or half of a skyrmion, where it points to the north (or the south) pole at the origin and winds around the equator at the boundary. As the meron is half of a skyrmion, the integral Eq. 7 gives $\pm{}^1/_2$. The meron configuration of $d_i(k)$ is depicted in Fig. 2, B and C. In a noninteracting system, half-integral Hall conductance is not possible, which means that other points from the Brillouin zone must either cancel or add to this contribution so that the total Hall conductance becomes an integer. The fermion-doubled partner (*24*) of our low-energy fermion near the Γ point lies in the higher-energy spectrum of the lattice and contributes to the total σ_{xy}. Therefore, our effective Hamiltonian near the Γ point cannot yield a precise determination of the Hall conductance for the whole system. However, as one changes the quantum well thickness d across d_c, M changes sign and the gap closes at the Γ point, leading to a vanishing $d_i(k = 0)$ vector at the transition point $d = d_c$. The sign change of M leads to a well-defined change of the Hall conductance $\Delta\sigma_{xy} = 1$ across the transition. As the $d_i(k)$ vector is regular at the other parts of the Brillouin zone, these parts cannot lead to any discontinuous changes across the transition point at $d = d_c$.

So far, we have only discussed one 2 × 2 block of the effective Hamiltonian H. General time-reversal symmetry dictates that $\sigma_{xy}(H) = -\sigma_{xy}(H^*)$; therefore, the total charge Hall conductance vanishes, and the spin Hall conductance (given by the difference between the two blocks) is finite and given by $\Delta\sigma_{xy}^{(s)} = 2$ in units of e^2/h. From the general relationship between the quantized Hall conductance and the number of edge states (*25*), we conclude that the two sides of the phase transition at $d = d_c$ must differ in the number of pairs of helical edge states by 1, thus concluding our proof that one side of the transition must be Z_2 odd and topologically distinct from a fully gapped conventional insulator.

It is desirable to establish which side of the transition is topologically nontrivial. For this purpose, we return to the tight-binding model Eq. 6. The Hall conductance of this model has been calculated (*25*) in the context of the quantum anomalous Hall effect, and previously in the context of lattice fermion simulation (*26*). Besides the Γ point, which becomes gapless at $M/2B = 0$, there are three other high-symmetry points in the Brillouin zone. The (0,π) and (π,0) points become gapless at $M/2B = 2$, whereas the (π,π) point becomes gapless at $M/2B = 4$. Therefore, at $M/2B = 0$, there is only one gapless Dirac point per 2 × 2 block. This behavior is qualitatively different from the Haldane model of graphene (*27*), which has two gapless Dirac points in the Brillouin zone. For $M/2B < 0$, $\sigma_{xy} = 0$; for $0 < M/2B < 2$, $\sigma_{xy} = 1$. Because this condition is satisfied in the inverted gap regime where $M/2B = 2.02 \times 10^{-4}$ at 70 Å (*22*) and not in the normal regime where $M/2B < 0$, we believe that the inverted case is the topologically nontrivial regime supporting a QSH state.

We now discuss the experimental detection of the QSH state. A series of purely electrical measurements can be used to detect the basic signature of the QSH state. By sweeping the gate voltage, one can measure the two-terminal conductance G_{LR} from the p-doped to bulk-insulating to n-doped regime (Fig. 3). In the bulk insulating regime, G_{LR} should vanish at low temperatures for a normal insulator at $d < d_c$, whereas G_{LR} should approach a value close to $2e^2/h$ for $d > d_c$. Strikingly, in a six-terminal measurement, the QSH state would exhibit vanishing electric voltage drop between the terminals μ_1 and μ_2 and between μ_3 and μ_4, in the zero temperature limit and in the presence of a finite electric current between the L and R terminals. In other words, longitudinal resistance should vanish in the zero temperature limit, with a power-law dependence, over distances larger than the mean free path. Because of the absence of backscattering, and before spontaneous breaking of time reversal sets in, the helical edge currents flow without dissipation, and the voltage drop occurs only at the drain side of the contact (*11*). The vanishing of the longitudinal resistance is one of the most remarkable manifestations of the QSH state. Finally, a spin-filtered measurement can be used to determine the spin Hall conductance $\sigma_{xy}^{(s)}$. Numerical calculations (*13*) show that it should take a value close to $\sigma_{xy}^{(s)} = 2e^2/h$.

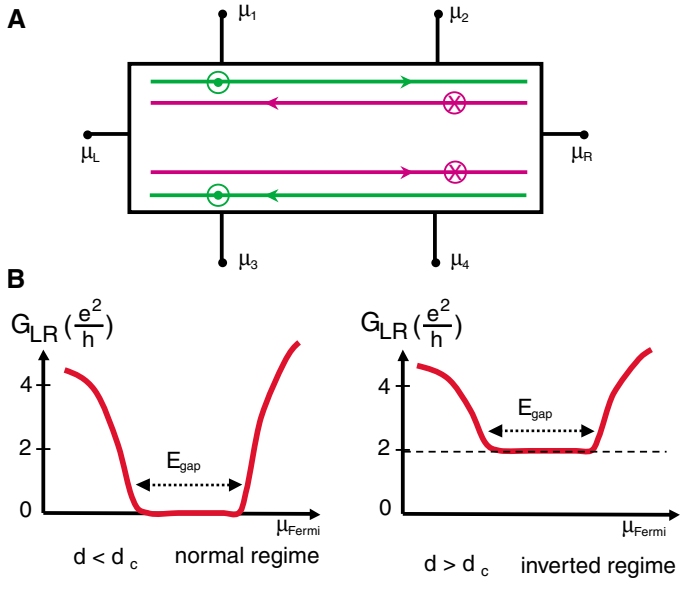

Fig. 3. (**A**) Experimental setup on a six-terminal Hall bar showing pairs of edge states, with spin-up states in green and spin-down states in purple. (**B**) A two-terminal measurement on a Hall bar would give G_{LR} close to $2e^2/h$ contact conductance on the QSH side of the transition and zero on the insulating side. In a six-terminal measurement, the longitudinal voltage drops $\mu_2 - \mu_1$ and $\mu_4 - \mu_3$ vanish on the QSH side with a power law as the zero temperature limit is approached. The spin Hall conductance $\sigma_{xy}^{(s)}$ has a plateau with the value close to $2e^2/h$.

Constant experimental progress on HgTe over the past two decades makes the experimental realization of our proposal possible. The mobility of the HgTe-CdTe quantum wells has reached $\mu \sim 6 \times 10^5$ cm^2 V^{-1} s^{-1} (*28*). Experiments have already confirmed the different characters of the upper band below ($E1$) and above ($H1$) the critical thickness d_c (*20*, *29*). The experimental results are in excellent agreement with band-structure calculations based on $k \cdot p$ theory. Our proposed two-terminal and six-terminal electrical measurements can be carried out on existing samples without radical modification, with samples of $d < d_c \approx 64$ Å and $d > d_c \approx 64$ Å yielding contrasting results. As a consequence, we believe that the experimental detection of the QSH state in HgTe-CdTe quantum wells is possible.

References and Notes

1. M. I. Dyakonov, V. I. Perel, *Phys. Lett. A* **35**, 459 (1971).
2. S. Murakami, N. Nagaosa, S. C. Zhang, *Science* **301**, 1348 (2003).
3. J. Sinova *et al.*, *Phys. Rev. Lett.* **92**, 126603 (2004).
4. Y. Kato *et al.*, *Science* **306**, 1910 (2004).
5. J. Wunderlich, B. Kaestner, J. Sinova, T. Jungwirth, *Phys. Rev. Lett.* **94**, 047204 (2005).
6. S. Murakami, N. Nagaosa, S. C. Zhang, *Phys. Rev. Lett.* **93**, 156804 (2004).
7. C. L. Kane, E. J. Mele, *Phys. Rev. Lett.* **95**, 226801 (2005).
8. B. A. Bernevig, S. C. Zhang, *Phys. Rev. Lett.* **96**, 106802 (2006).
9. X.-L. Qi, Y. S. Wu, S. C. Zhang, *Phys. Rev. B* **74**, 085308 (2006).
10. C. L. Kane, E. J. Mele, *Phys. Rev. Lett.* **95**, 146802 (2005).
11. C. Wu, B. A. Bernevig, S. C. Zhang, *Phys. Rev. Lett.* **96**, 106401 (2006).
12. C. Xu, J. Moore, *Phys. Rev. B* **73**, 045322 (2006).
13. L. Sheng *et al.*, *Phys. Rev. Lett.* **95**, 136602 (2005).
14. M. Onoda, Y. Avishai, N. Nagaosa, http://arxiv.org/abs/cond-mat/0605510.
15. D. J. Thouless, M. Kohmoto, M. P. Nightingale, M. den Nijs, *Phys. Rev. Lett.* **49**, 405 (1982).
16. Y. Yao, F. Ye, X. L. Qi, S. C. Zhang, Z. Fang, http://arxiv.org/abs/cond-mat/0606350.
17. H. Min *et al.*, *Phys. Rev. B* **74**, 165310 (2006).
18. S. Murakami, http://arxiv.org/abs/cond-mat/0607001.
19. E. O. Kane, *J. Phys. Chem. Solids* **1**, 249 (1957).
20. E. G. Novik *et al.*, *Phys. Rev. B* **72**, 035321 (2005).
21. A. Pfeuffer-Jeschke, thesis, University of Würzburg (2000).
22. See supporting material on *Science* Online.
23. A. N. Redlich, *Phys. Rev. D* **29**, 2366 (1984).
24. H. B. Nielsen, M. Ninomiya, *Nucl. Phys. B* **185**, 20 (1981).
25. X. L. Qi, Y. S. Wu, S. C. Zhang, *Phys. Rev. B* **74**, 045125 (2006).
26. M. F. L. Golterman, K. Jansen, D. B. Kaplan, *Phys. Lett. B* **301**, 219 (1993).
27. F. D. M. Haldane, *Phys. Rev. Lett.* **60**, 635 (1988).
28. K. Ortner *et al.*, *Appl. Phys. Lett.* **79**, 3980 (2001).
29. C. R. Becker, V. Latussek, A. Pfeuffer-Jeschke, G. Landwehr, L. W. Molenkamp, *Phys. Rev. B* **62**, 10353 (2000).

30. We thank X. Dai, Z. Fang, F. D. M. Haldane, A. H. MacDonald, L. W. Molenkamp, N. Nagaosa, X.-L. Qi, R. Roy, and R. Winkler for discussions. B.A.B. acknowledges the hospitality of the Kavli Institute for Theoretical Physics at the University of California, Santa Barbara, where part of this work was performed. Supported by NSF grant DMR-0342832 and by the U.S. Department of Energy, Office of Basic Energy Sciences, under contract DE-AC03-76SF00515.

Supporting Online Material

www.sciencemag.org/cgi/content/full/314/5806/1757/DC1
SOM Text
Fig. S1
Table S1
References

10 August 2006; accepted 1 November 2006
10.1126/science.1133734

Photoconductive Coaxial Nanotubes of Molecularly Connected Electron Donor and Acceptor Layers

Yohei Yamamoto,[1] Takanori Fukushima,[1,2]* Yuki Suna,[1] Noriyuki Ishii,[3] Akinori Saeki,[4] Shu Seki,[4] Seiichi Tagawa,[4] Masateru Taniguchi,[4] Tomoji Kawai,[4] Takuzo Aida[1,2]*

Controlled self-assembly of a trinitrofluorenone-appended gemini-shaped amphiphilic hexabenzocoronene selectively formed nanotubes or microfibers with different photochemical properties. In these nanotubes, which are 16 nanometers in diameter and several micrometers long, a molecular layer of electron-accepting trinitrofluorenone laminates an electron-donating graphitic layer of π-stacked hexabenzocoronene. The coaxial nanotubular structure allows photochemical generation of spatially separated charge carriers and a quick photoconductive response with a large on/off ratio greater than 10^4. In sharp contrast, the microfibers consist of a charge-transfer complex between the hexabenzocoronene and trinitrofluorenone parts and exhibit almost no photocurrent generation.

As exemplified by organic photovoltaic devices (*1*–*3*), heterojunction of electron donor and acceptor layers at a macroscopic level allows for the conversion of light energy into electrical energy (*4*, *5*). If one can elaborate a nano-object composed of molecularly conjugated domains of such a redox couple, the resultant material is expected to serve as a nanoscopic energy converter. However, donor and acceptor molecules tend to stack on one another, rather than segregate (*6*–*8*), giving rise to charge-transfer (CT) assemblies (*9*–*11*), in which photochemically generated charge carriers are trapped and readily annihilated through a rapid recombination. Here we report a coaxial nanotubular object formed by controlled self-assembly of trinitrofluorenone (TNF)–appended hexabenzocoronene (HBC) amphiphile **1** (Fig. 1A), in which a molecular layer of electron-accepting TNF laminates an electron-donating graphitic layer of π-stacked HBC (Fig. 2) (*12*). This structure creates an extremely wide interface for the spatially segregated redox couple so that, upon photoirradiation, the electrical conduction has a large on/off ratio (>10^4) that is difficult to attain with other carbon-based materials (*13*–*15*). Such molecularly engineered photoconductive materials with a tubular morphology are unusual and join the few examples of photoconductive nanostructured assemblies that have been reported (*7*, *16*).

HBC derivatives with symmetrically substituted paraffinic side chains form discotic liquid-crystalline materials that exhibit a hole-transport capability through their one-dimensional columnar HBC stacks (*5*, *17*–*21*). Recently, we have discovered that gemini-shaped amphiphilic HBCs (structure **3**, Fig. 1A) can self-assemble to form well-defined nanotubular objects, whose walls consist of a graphitic layer of π-stacked HBC and whose inner and outer surfaces are covered by hydrophilic triethylene glycol (TEG) chains (*22*, *23*). Upon doping with oxidants, the HBC graphitic nanotubes become electrically conductive (*22*, *24*). In the present work, we prepared HBC-TNF **1** and **2**, which bear an electron-accepting 4,5,7-trinitro-9-fluorenone functionality (*25*) at each terminus of either (**1**) and both (**2**) of the TEG chains (Fig. 1A). The energy levels of the highest occupied molecular orbital (HOMO) and the lowest unoccupied molecular orbital (LUMO) of HBC **3** (*22*) and TNF **4** (*26*) (Fig. 1B) were determined by means of square-wave voltammetry and electronic absorption spectroscopy (fig. S1) (*27*). Apparently, photoinduced electron transfer is energetically possible between the HBC and TNF functionalities of **1** and **2**.

Compounds **1** and **2** were synthesized by oxidative cyclization of the corresponding hexaphenylbenzene precursors with $FeCl_3$ in CH_2Cl_2/$MeNO_2$ (*27*). Both compounds in tetrahydrofuran (THF) were colored brown, indicating a CT interaction between the HBC and TNF parts in

[1]Aida Nanospace Project, Exploratory Research for Advanced Technology–Solution Oriented Research for Science and Technology (ERATO-SORST), Japan Science and Technology Agency, National Museum of Emerging Science and Innovation, 2-41 Aomi, Koto-ku, Tokyo 135–0064, Japan. [2]Department of Chemistry and Biotechnology, School of Engineering, and Center for NanoBio Integration, The University of Tokyo, 7-3-1 Hongo, Bunkyo-ku, Tokyo 113–8656, Japan. [3]Biological Information Research Center, National Institute of Advanced Industrial Science and Technology, Tsukuba Central-6, 1-1-1 Higashi, Tsukuba, Ibaraki 305–8566, Japan. [4]Institute of Scientific and Industrial Research, Osaka University, 8-1 Mihogaoka, Ibaraki, Osaka 567–0047, Japan.

*To whom correspondence should be addressed. E-mail: fukushima@nanospace.miraikan.jst.go.jp (T.F.); aida@macro.t.u-tokyo.ac.jp (T.A.)

the ground state. Even under high dilution, their THF solutions displayed broad CT absorption bands above 500 nm (fig. S2). Because a 1:1 mixture of **3** and **4** under identical conditions to those in the above-described experiments did not exhibit such characteristic CT bands, the donor (HBC) and acceptor (TNF) chromophores in compounds **1** and **2** most likely interact intramolecularly rather than intermolecularly. Nevertheless, the CT complexation in THF must be dynamic, given the subtle difference in electrochemical potentials of each of the chromophore parts from the corresponding reference (figs. S1 and S3).

Although HBC **3** not bearing TNF readily self-assembles in THF to give nanotubes (*22*), HBC-TNF **1** and **2** are both highly soluble in THF, and neither of them will form ordered assemblies in this solvent. However, the controlled self-assembly of **1** takes place upon diffusion of a methanol (MeOH) vapor into a THF solution of **1**. Depending on the initial concentration of **1**, either nanotubes or microfibers with different photochemical properties selectively formed. When a THF solution of **1** at a concentration of 0.12 mM was exposed to a MeOH vapor at 25°C, a yellow suspension resulted (Fig. 3A, inset) (*27*). However, when the concentration of **1** in THF was 10 times higher (1.2 mM), the diffusion of a MeOH vapor produced a dark-brown precipitate (Fig. 3C, inset) (*27*).

Scanning electron microscopy (SEM) indicated that the yellow-colored substance in the former case (concentration of **1** = 0.12 mM) is composed of nanotubes that have open-ended hollow spaces inside (Fig. 3A). Transmission electron microscopy (TEM) displayed that the nanotubes are several micrometers long and have uniform diameter and wall thickness of 16 and 3 nm, respectively (Fig. 3B). This size regime is analogous to that of the nanotubes formed from **3** (*22*). On the other hand, as observed by SEM (Fig. 3C) and TEM (Fig. 3D), the brown-colored substance that formed in the latter case (concentration of **1** = 1.2 mM) consists only of solid microfibers without hollow space, whose diameters range from 0.2 to 2 μm. Thus, in order to obtain the nanotubes selectively, the initial concentration of **1** for the vapor diffusion should not be greater than 0.12 mM, otherwise the microfibers form concomitantly with the nanotubes.

The concentration-dependent dual-mode self-assembly, thus observed for **1**, most likely originates from a possible competition of the homotropic assembly of the HBC parts with a CT complexation (heterotropic assembly) between the HBC and TNF functionalities. Indeed, electronic absorption spectroscopy of a yellow-colored cast film of the nanotubes did not display any CT bands but did display two red-shifted bands at 430 and 460 nm, which is characteristic of tubularly assembled HBC (*22*) (Fig. 4A). In sharp contrast, a cast film of the microfibers showed strong CT absorptions at 510 and 640 nm (Fig. 4B).

We also found that tubularly assembled **1** exhibits a much-pronounced x-ray diffraction peak at $2\theta = 25.7°$, assignable to regularly stacked HBC with a *d* spacing of 3.46 Å (fig. S4). Infrared spectroscopy of the nanotubes showed CH_2 stretching vibrations at 2919 (antisymmetric stretching frequency) and 2850 cm^{-1} (symmetric stretching frequency), indicating that the dodecyl chains of **1** are stretched to form a bilayer tape via interdigitation (*22*). These observations allow us to conclude that the HBC and TNF parts are segregated in the nanotubes, in which the former forms the graphitic wall as the self-assembling component, whereas the latter covers the inner and outer surfaces of the graphitic wall (Fig. 2). Unlike **1**, compound **2** did not yield any nanotubular objects under identical self-assembling conditions except for brown-colored irregular aggregates.

Photoconducting properties of the nanotubes and microfibers of self-assembled HBC-TNF **1** were evaluated by a two-probe method that used micrometer-gap electrodes fabricated on a silicon substrate (*27*). Vapor-diffused THF/MeOH suspensions of either nanotubes or microfibers were cast on the electrodes, dried under a reduced pressure, and irradiated at wavelength $\lambda = 300$ to 650 nm (light power density, 70 mW mm^{-2}). The nanotubes exhibited a photocurrent upon irradiation. Current-voltage (*I-V*) profiles of the nanotubes (Fig. 4C) showed that the current is markedly enhanced upon irradiation by a factor of $>10^4$. For example, at an applied voltage of +2 V, the photocurrent and dark current of the nanotubes were 4.2 nA and 0.07 pA, respectively. The photocurrent was nearly proportional to an applied voltage ranging from, for example, –2 to +2 V (Fig. 4C), indicating an ohmic behavior of the electrical conduction. As the power density of the incident light was increased from 3.4 to 150 mW mm^{-2}, the observed photocurrent was linearly enhanced (fig. S5). As shown in the inset of Fig. 4C, the photocurrent switching was prompt and repeatable by turning the light on and off. In sharp contrast, similar irradiation of the microfibers hardly exhibited photocurrent generation (Fig. 4D).

The essentially different photoconducting behaviors of the nanotubes and microfibers were supported by flash-photolysis time-resolved microwave conductivity (FP-TRMC) measurements (*27*, *28*). Upon exposure to a laser pulse ($\lambda = 355$ nm), the nanotubes showed a prompt rise of a transient conductivity $\langle\Delta\sigma\rangle$, which reached a maximum value $\langle\Delta\sigma_{max}\rangle$ of 13 μS m^{-1} in 0.11 μs

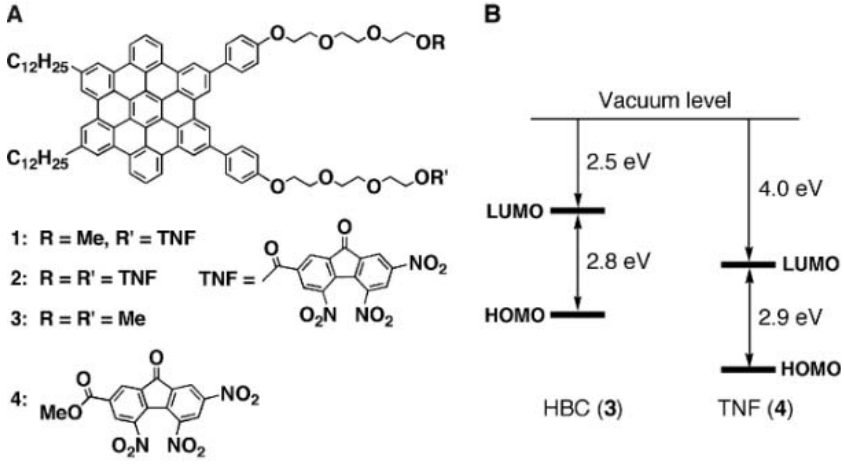

Fig. 1. HBC derivatives for self-assembly. (**A**) Molecular structures of HBC-TNF **1** and **2** and reference compounds **3** and **4**. (**B**) HOMO and LUMO levels of **3** and **4**.

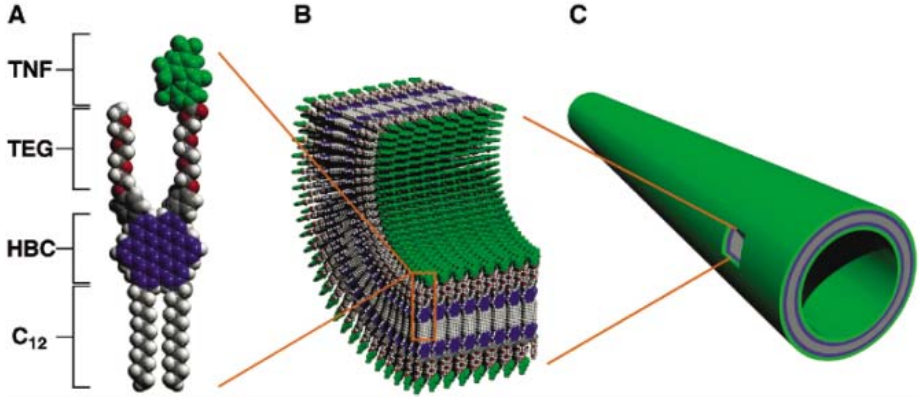

Fig. 2. Self-assembly of HBC-TNF **1**. (**A**) Space-filling model of **1**. C_{12}, dodecyl chain. (**B**) Schematic representation of the nanotube wall. (**C**) Schematic representation of the nanotube with a coaxial donor-acceptor configuration. A molecular layer of electron-accepting TNF (green) laminates an electron-donating graphitic layer of π-stacked HBC (blue).

(Fig. 4E), whereas the microfibers displayed a negligibly small conductivity ($<\Delta\sigma_{max}> = 0.6$ μS m^{-1}) in 0.12 μs (Fig. 4E). Most of the fluorescence from the HBC parts in the nanotubes of **1** was quenched by electron transfer to the TNF pendants (Fig. 4F), where the observed fluorescence quantum yield Φ_{FL} of <0.1% is much smaller than that of tubularly assembled **3** (*22*) without TNF (Φ_{FL} = 6.4%). Time-resolved fluorescence spectroscopy (fig. S6) showed that the averaged fluorescence lifetime of **1** in the nanotubes (0.13 ns) is much shorter than that of tubularly assembled **3** (6.0 ns). The photocurrent action spectrum, obtained by plotting the external quantum efficiency (EQE) of the nanotubes of **1** versus λ of the incident light (*27*), represents the characteristic absorption bands of the tubularly assembled HBC (*22*) (Fig. 4A). Together with the fact that the nanotubes of **3** without TNF, which are analogous to the microfibers of **1**, showed only a negligibly small photoconductivity (fig. S7), photoexcitation of the HBC groups in the nanotubes, resulting in an electron transfer to TNF, is responsible for the photocurrent generation.

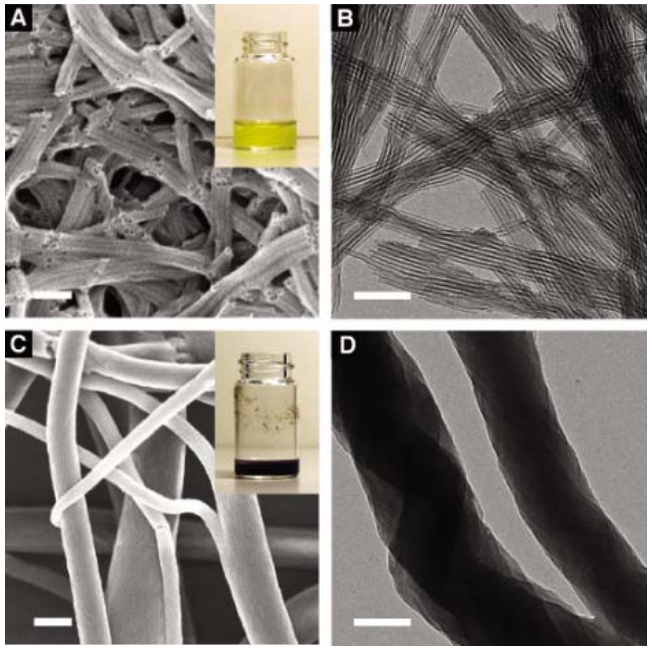

Fig. 3. Electron micrographs of self-assembled nanotubes and microfibers formed from HBC-TNF **1**. (**A**) SEM micrograph of an air-dried suspension of the nanotubes of **1**. Scale bar, 100 nm. (Inset) Photograph of a suspension of the nanotubes of **1**. (**B**) TEM micrograph of an air-dried suspension of the nanotubes of **1**. Scale bar, 200 nm. (**C**) SEM micrograph of an air-dried suspension of the microfibers of **1**. Scale bar, 1 μm. (Inset) Photograph of a suspension of the microfibers of **1**. (**D**) TEM micrograph of an air-dried suspension of the microfibers of **1**. Scale bar, 200 nm.

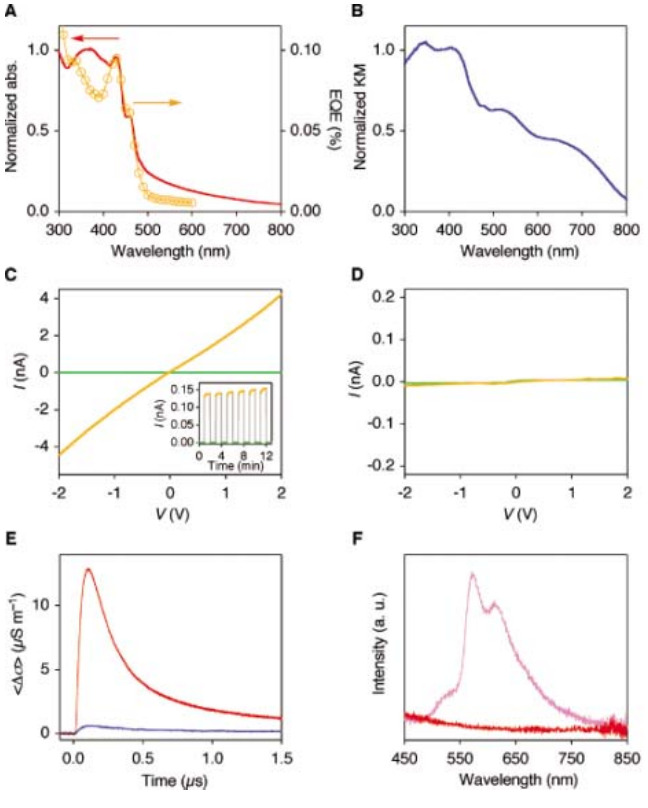

Fig. 4. (**A**) Electronic absorption spectrum normalized at 370 nm (red) and photocurrent action spectrum (orange) of a cast film of the nanotubes of **1** at 25°C. Circles indicate EQE values. EQE is defined as the number of charge carriers flowing in the external circuit per number of incident photons. (**B**) Kubelka-Munk (KM) spectrum normalized at 370 nm of a cast film of the microfibers of **1** converted from its diffuse reflectance spectrum at 25°C. Because of scattering, the sample did not show a reliable absorption spectrum. (**C**) *I-V* profiles at 25°C of a cast film of the nanotubes of **1** with (orange) and without (green) photoirradiation (λ = 300 to 650 nm). (Inset) Change in electric current at 25°C of a cast film of the nanotubes of **1** in response to turning on (orange) and off (green) photoirradiation. The applied light power density and voltage were 5.5 mW mm^{-2} and +2 V, respectively. (**D**) *I-V* profiles at 25°C of a cast film of the microfibers of **1** with (orange) and without (green) photoirradiation (λ = 300 to 650 nm). (**E**) FP-TRMC profiles at 25°C of cast films of the nanotubes (red) and microfibers (blue) of **1** upon photoirradiation at 355 nm. (**F**) Fluorescence spectra at 25°C of cast films of the nanotubes of **1** (red) and **3** (purple) upon photoirradiation at 365 nm. a.u., arbitrary units.

Although hybrid materials composed of individual arrays of electron donor and acceptor molecules are promising advances toward the efficient conversion of light energy into electrical energy, the donor and acceptor arrays have to be connected to allow electron-transfer communication without their CT complexation. We show that a primary donor-acceptor CT complexation, if any, can be switched off in the subsequent assembling stage when the competing homotropic assembly of donor and/or acceptor molecules compensates the energy loss accompanied by the dissociation of the CT complex. The coaxial donor-acceptor configuration of the nanotube of **1** provides an ultimate molecular-design strategy to achieve a wide interface for spatially segregated redox couples. Furthermore, its micrometer-scale one dimensionality, along with the large on/off ratio of the photoconductive response, is highly attractive for optoelectronic applications.

References and Notes

1. C. W. Tang, *Appl. Phys. Lett.* **48**, 183 (1986).
2. G. Yu, J. Gao, J. C. Hummelen, F. Wudl, A. J. Heeger, *Science* **270**, 1789 (1995).
3. J.-L. Brédas, D. Beljonne, V. Coropceanu, J. Cornil, *Chem. Rev.* **104**, 4971 (2004).
4. M. Granström *et al.*, *Nature* **395**, 257 (1998).
5. L. Schmidt-Mende *et al.*, *Science* **293**, 1119 (2001).
6. P. Samorí *et al.*, *J. Am. Chem. Soc.* **126**, 3567 (2004).
7. F. Würthner *et al.*, *J. Am. Chem. Soc.* **126**, 10611 (2004).
8. E. H. A. Beckers *et al.*, *J. Am. Chem. Soc.* **128**, 649 (2006).
9. D. Markovitsi, H. Bengs, H. Ringsdorf, *J. Chem. Soc. Faraday Trans.* **88**, 1275 (1992).
10. V. Percec *et al.*, *Nature* **419**, 384 (2002).
11. W. Pisula *et al.*, *Angew. Chem. Int. Ed.* **45**, 819 (2006).

12. Coaxial (*29*) and concentric (*30*) junctions of donor and acceptor arrays have recently been reported for the molecular design of photoinduced energy and electron-transfer systems, respectively.
13. M. Freitag, Y. Martin, J. A. Misewich, R. Martel, Ph. Avouris, *Nano Lett.* **3**, 1067 (2003).
14. M. E. Itkis, F. Borondics, A. Yu, R. C. Haddon, *Science* **312**, 413 (2006).
15. Y. J. Xing *et al.*, *Appl. Phys. Lett.* **87**, 263117 (2005).
16. A. D. Schwab *et al.*, *Nano Lett.* **4**, 1261 (2004).
17. A. M. van de Craats *et al.*, *Adv. Mater.* **11**, 1469 (1999).
18. M. D. Watson, A. Fechtenkötter, K. Müllen, *Chem. Rev.* **101**, 1267 (2001).
19. A. M. van de Craats *et al.*, *Adv. Mater.* **15**, 495 (2003).
20. C. D. Simpson, J. Wu, M. D. Watson, K. Müllen, *J. Mater. Chem.* **14**, 494 (2004).
21. A. C. Grimsdale, K. Müllen, *Angew. Chem. Int. Ed.* **44**, 5592 (2005).
22. J. P. Hill *et al.*, *Science* **304**, 1481 (2004).
23. W. Jin *et al.*, *Proc. Natl. Acad. Sci. U.S.A.* **102**, 10801 (2005).
24. Y. Yamamoto *et al.*, *Adv. Mater.* **18**, 1297 (2006).
25. R. O. Loutfy, C. K. Hsiao, B. S. Ong, B. Keoshkerian, *Can. J. Chem.* **62**, 1877 (1984).
26. T. Sulzberg, R. J. Cotter, *J. Org. Chem.* **35**, 2762 (1970).
27. Materials and methods are available as supporting material on *Science* Online.
28. A. Acharya *et al.*, *J. Phys. Chem. B* **109**, 20174 (2005).
29. C. Röger *et al.*, *J. Am. Chem. Soc.* **128**, 6542 (2006).
30. W.-S. Li *et al.*, *J. Am. Chem. Soc.* **128**, 10527 (2006).

31. We thank H. Watanabe and K. Suzuki (Hamamatsu) for the measurements of fluorescence quantum yields and time-resolved fluorescence decay profiles and A. Morishima (JASCO Corporation) for the measurement of diffuse reflectance spectroscopy. N.I. performed TEM; M.T. and T.K. constructed the micrometer-gap electrodes; and A.S., S.S., and S.T. made FP-TRMC measurements.

Supporting Online Material

www.sciencemag.org/cgi/content/full/314/5806/1761/DC1
Materials and Methods
Figs. S1 to S7
References

28 August 2006; accepted 1 November 2006
10.1126/science.1134441

A Clathrate Reservoir Hypothesis for Enceladus' South Polar Plume

Susan W. Kieffer,[1]* Xinli Lu,[1] Craig M. Bethke,[1] John R. Spencer,[2] Stephen Marshak,[1] Alexandra Navrotsky[3]

We hypothesize that active tectonic processes in the south polar terrain of Enceladus, the 500-kilometer-diameter moon of Saturn, are creating fractures that cause degassing of a clathrate reservoir to produce the plume documented by the instruments on the Cassini spacecraft. Advection of gas and ice transports energy, supplied at depth as latent heat of clathrate decomposition, to shallower levels, where it reappears as latent heat of condensation of ice. The plume itself, which has a discharge rate comparable to Old Faithful Geyser in Yellowstone National Park, probably represents small leaks from this massive advective system.

Data from the instruments on the Cassini spacecraft (*1*–*6*) prompt a major scientific question: What is the reservoir that produces the plume on Enceladus? The plume erupts from the tectonically active (*1*) and warm (*2*) south polar terrain (SPT); it contains not only H_2O vapor and ice particles (*1*) but also CH_4, N_2, and CO_2 gases (*6*). A highly variable flux of the order of 10^{-7} to 10^{-6} kg s^{-1} m^{-2} (and possibly several orders of magnitude greater, depending on vent conditions at depth) emanates from at least 17 separate vents along the four tectonically active tiger stripes (*6*, *7*). The surface of Enceladus in the SPT is composed of amorphous and crystalline water ice with traces of complexed CO_2 (*4*).

On the basis of the assumption that the reservoir for the plume is a single-component H_2O system, it was hypothesized that the plume erupted from chambers of liquid water at 273 K as close as 7 m to the surface, the "Cold Faithful" model (*1*). However, it has also been argued that the plume composition represents the surface and near-surface composition at the site of outgassing (*6*), in which case the additional gases must be accounted for. Observed CO_2 concentrations could be in aqueous solution at pressures greater than ~24 bars and could help drive geyser eruptions [as on Earth (*8*–*10*)]. However, CH_4, and N_2 are so sparingly soluble in liquid water that these gases could not have originated from a liquid aqueous phase. The solubility of these gases in clathrate hydrates (ices with a cage-like structure in which water ice traps other volatile components), however, is enormous compared with their solubility in liquid water. The observed molar ratio of H_2O vapor to noncondensible gases in the plume is 10:1 (*6*). The similarity between this and the ratio of water to guest molecules in a clathrate (hydration number is 6:1 to 8:1) suggests that the reservoir could consist of clathrates or clathrates plus water ice. The potentially important role of multicomponent clathrates in Enceladus has been pointed out (*11*, *12*); we investigated the possibility that explosive decomposition of a clathrate of this composition could account for the observations summarized above. Relevant decomposition curves for the binary clathrates and a mixed clathrate of the composition corresponding to the plume are shown in Fig. 1A.

In an undisturbed cold region of Enceladus, including undisturbed regions of the SPT, a conductive geotherm centered at the surface temperature (70 to 80 K, Fig. 1B, point A) would intersect either the CO_2 sublimation curve (Fig. 1B, point B) or the clathrate decomposition curve (Fig. 1B, point C) before intersecting the H_2O boiling curve (Fig. 1B, point D). Conductive geotherms centered at higher heat flow regions (Fig. 1B, point E) intersect the boiling curve at tens of meters (Fig. 1B, points near F) but are irrelevant if thermal conduction in pure H_2O ice is not the dominant process of heat transport, which we suggest is the case (Fig. 1B, point D).

Water ice and complexed CO_2 have been detected on the surface of Enceladus (*4*). This observation, coupled with an examination of the phase diagrams of Fig. 1, suggests that the crust consists of a leaky H_2O-CO_2 ice cap "seal" on the order of 3.5-km thickness overlying a clathrate reservoir (*13*) (Fig. 1B). As long as the seal contains only minor leaks, confining pressure is maintained and the clathrate remains stable. Small leaks will tend to be self-sealing, because water vapor rising from depth freezes in the cold ice cap (Fig. 2A). If the seal breaks and confining pressure is lost, as happens repeatedly as the tectonically active cap fractures, the clathrate is exposed to near-vacuum conditions and decomposes, perhaps violently (Fig. 2, B to D). With time, self-sealing resumes, and the system returns to ambient conditions. In this way, vents in Enceladus' ice cap may be opening and closing continually, producing variable fluxes and plumes that reach high above the moon's surface.

We suggest that episodic and frequent formation of new fractures in the SPT repeatedly exposes clathrate reservoirs to near-vacuum conditions. Large fluxes of gas release are always accompanied by massive ejection of ice grains when decompression takes place (*14*, *15*). As these authors discuss, decomposition may be complicated by the low-temperature polymorphic (hexagonal, cubic, amorphous, and nanophase) changes in ice, but these complexities cannot be addressed quantitatively, so we restrict our discussion to clathrate decomposition. We hypothesize that this process produces jets of gas and ice particles in the fractures comparable to jets produced by comets. If the total pressure drops below the vapor pressure of the ice particles, they sublimate to yield water vapor. Whether this occurs at depth in the fracture (Fig. 2B, left) or above the surface in the plume (Fig. 2B, right) depends on the pressure distribution, which we cannot specify.

[1]Department of Geology, University of Illinois at Urbana–Champaign, 1301 West Green Street, Urbana, IL 61801, USA. [2]Department of Space Studies, Southwest Research Institute, 1050 Walnut Street, Suite 400, Boulder, CO 80302, USA. [3]Thermochemistry Facility and Nanomaterials in the Environment, Agriculture, and Technology (NEAT) Organized Research Unit (ORU), University of California at Davis, 1 Shields Avenue, Davis, CA 95616, USA.

*To whom correspondence should be addressed. E-mail: skieffer@uiuc.edu

Clathrate decomposition into a vacuum is self-sustaining, because vapor is the stable phase, but simultaneously self-limiting, because the decomposition is endothermic. In smaller fractures, condensation may lead to rapid self-sealing (Fig. 2A), but in larger fractures condensation may be limited to boundary layers at the walls. Condensation is accompanied by the delivery of latent heat to the walls. The boundary layer thickness is limited by the rate of heat transfer away from the walls, and the net effect may be that larger fractures remain open. Nevertheless, the ice coating will shut off the supply of gases, and the pressure, even in a deep fracture, may drop toward vacuum conditions. When it drops to the vapor pressure of ice at the local temperature, sublimation of ice can begin if there is an adequate heat supply (Fig. 2C). The interplay between these various processes and active tectonics will result in complex and constantly changing fracture networks (Fig. 2D) and could lead to the highly time variable phenomena observed for the plume. We examined whether the magnitudes of the observed gas and vapor fluxes are consistent with the observed thermal constraints and properties of clathrates and ice. Construction of detailed models is neither possible nor warranted by the data available. We could, however, look at two extreme cases: decomposition into a vacuum and into a network of cracks and fractures.

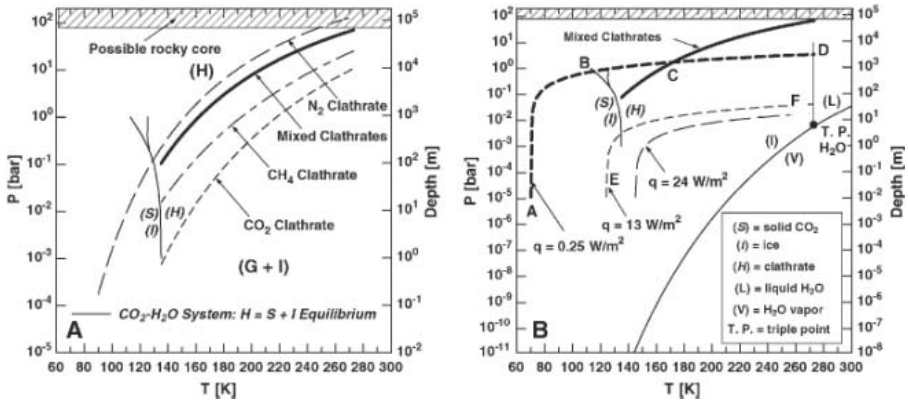

Fig. 1. (**A**) Decomposition curves from clathrate hydrate (H) to gas plus ice (G+I) for the three binary clathrates of interest and for the mixed clathrate proposed for the reservoir on Enceladus (*21*, *22*) and the sublimation curve for CO_2 (*23*). (**B**) Phase relations for H_2O and CO_2 single-component systems, the mixed clathrate system from (A), and some possible shallow thermal profiles. The thermal profile ABC shown is a purely conductive profile for a surface temperature at 1-cm depth of 70 K and a heat flow of 0.25 W m^{-2}. At ambient background conditions on Enceladus, a conductive thermal profile for a density of 1000 kg m^{-3} allows ice to be stable to 3.5 bars pressure and about 3 km depth or the mixed clathrate to be stable at pressure > 1.5 bars (>1.3 km depth). Italicized letters apply only to the CO_2 system.

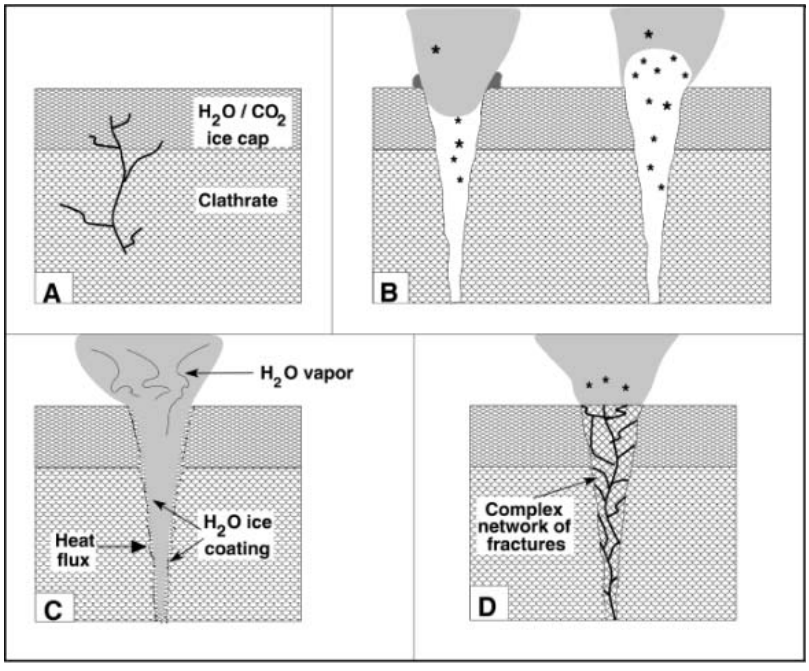

Fig. 2. Schematic illustrations. (**A**) Small self-sealing fractures extending from the clathrate reservoir through the ice cap seal. (**B**) A large fracture venting gas plus ice particles derived from the decomposing clathrate directly to the surface. The white area with snowflakes is composed of the noncondensible gases and ice fragments derived from decomposition of the clathrate. The gray area is gas and sublimated water vapor and ice crystals. The birm on the left fracture schematically shows possible surface redeposition from the plume. (**C**) A fracture into the clathrate with walls coated by H_2O ice, which can sublimate. (**D**) A complex fracture network through the clathrate and ice. We hypothesize that these variations of fracture geometries and processes are occurring at multiple vents in the SPT and that they are time-variable.

A maximum rate of clathrate decomposition into a vacuum can be calculated from the Hertz-Knudsen-Langmuir equation (*16*). For decomposition of the mixed clathrate at 190 K and 0.5 MPa, the limiting rate would be ~ 900 kg s^{-1} m^{-2}. An eruption of this magnitude would pose a notable problem to a spacecraft in low orbit but is unlikely to be maintained long enough for Cassini to have encountered such an event during the short time of observations to date. Rather, we assumed that the Cassini measurements are monitoring lower, more steady-state output from the plumes.

To examine decomposition of clathrate into a network of cracks, we adapted the model (*17*) for depressurization of methane clathrates to gas plus liquid water under terrestrial conditions for decomposition of our hypothesized mixed clathrate to gas plus water ice on Enceladus. The model provides the production rate of the noncondensible gases, which can be tested against the observed fluxes. From the gas flux, estimates of water vapor flux can be made for certain conditions.

The reservoir is represented as a fractured permeable medium. It may be the clathrate itself or a mixture of clathrate and ice or some other solid substance (Fig. 2). Penetration of a fracture initiates a decomposition front that propagates away from the fracture into the clathrate reservoir. Along this front, clathrates decompose at a pressure, P_d, intermediate between the reservoir pressure, P_r, and gas pressure, P_g, in the fracture. Gas production rate is a function of these pressures, temperature, zone permeability, and porosity. We assumed that the heat required for the decomposition 28 kJ mol^{-1} (gas mixture) is available as discussed below. Two plausible cases are discussed; sensitivity studies about the effect of porosity and permeability are provided in Fig. 3 [Supporting Online Material (SOM) text and fig. S1].

We calculated fluxes for one shallow and one deep reservoir to set pressure-temperature boundary conditions. Our nominal shallow cool reservoir has a temperature of 190 K, which is close to that inferred for warm areas (*2*) and ensures there is sufficient enthalpy to accelerate particles to escape velocity if decompressed to 145 K. For the shallow reservoir, we assigned an initial pressure just high enough for clathrate stability at 190 K, 5 bar. We also examined flow from a deeper reservoir at 35 km (41 bar), corresponding to a

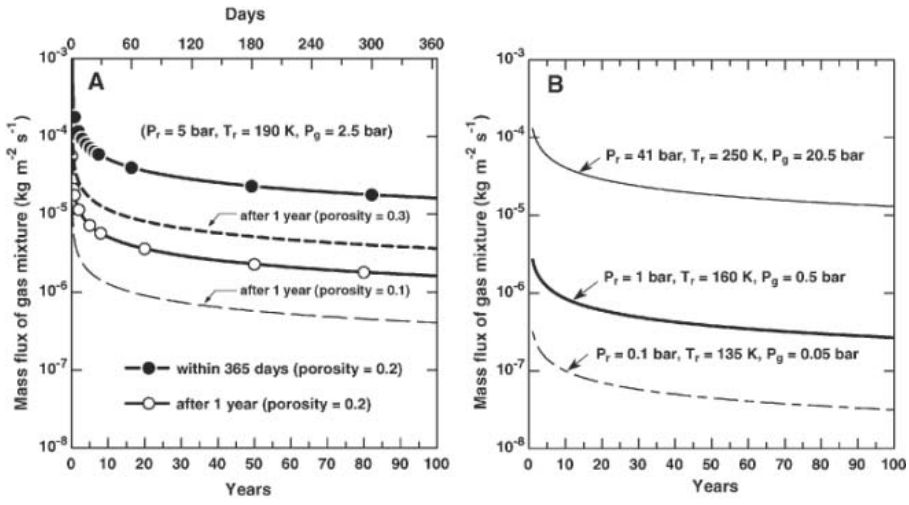

Fig. 3. (**A**) Flux of noncondensible gases calculated according to the model adapted from (*17*) on two different time scales (top and bottom axes). The top axis in days applies only to the top curve in this panel of the figure. Sensitivity to porosity shown by dashed curves. (**B**) Examples of sensitivity to reservoir pressure and temperature.

depth about halfway into the estimated crust, and assigned a temperature of 250 K, corresponding to a plausible geothermal gradient (Fig. 1B). Actual reservoir pressures and temperatures are unknown; these are simply plausible end-members.

Pressures in the active fractures could span the range from reservoir pressure to near-vacuum surface conditions (Fig. 2D). The former is likely at the base of a network of small fractures; the latter, at the base of a single wide fracture. When gas flows in complicated networks, pressure conditions are commonly determined by narrow constrictions where the flow chokes to sonic conditions of pressure, temperature, and flow velocity (Mach number = 1) (*18*). Typically, this pressure is about half of the reservoir pressure (see Fig. 3 for values).

For the shallow reservoir, initial fluxes of the noncondensible gases (G) are ~10^{-1} kg s^{-1} m^{-2} but decrease to ~10^{-4} kg s^{-1} m^{-2} within weeks (Fig. 3A), to ~5×10^{-6} kg s^{-1} m^{-2} within 10 years, and to ~10^{-6} kg s^{-1} m^{-2} within 100 years. Porosity and permeability change these values by about one-half an order of magnitude. Sensitivity tests at even lower pressures and temperatures show that fluxes are in about the same range (Fig. 3B). Fluxes from the deeper reservoir are more than an order of magnitude greater because of both the larger pressure gradient between the reservoir and the fracture and the higher temperature (Fig. 3B).

This model gives the flux of the noncondensible gases, CO_2, N_2, and CH_4. We suggest that these gases entrain small particles of water ice at about the molar ratio of 10:1 (mass ratio of 6:1) and carry them upward in the flow. Upon encountering pressures lower than the vapor pressure either within the fracture or in the atmosphere, these small particles sublimate to produce the observed vapor-to-gas ratio. Therefore, adding in the water vapor component to the observed mass ratio of 6:1 gives a total flux of vapor plus gas of ~7×10^{-4} kg s^{-1} m^{-2} after a few weeks, ~35×10^{-6} kg s^{-1} m^{-2} after a decade, and 7×10^{-6} kg s^{-1} m^{-2} after a century. Given the highly variable fluxes and uncertainties in measurements and modeling, these results imply that clathrate degassing could produce fluxes of the order of magnitude measured for the plume, 10^{-7} to 10^{-6} kg s^{-1} m^{-2}. The rapid decay over a time frame of weeks is similar to the time scale of 1 month that was documented as the decay time for a burst of particles into Saturn's E-ring observed in 2004, as well as the time scale in (*6*). The high fluxes calculated from the model also allow some H_2O and CO_2 to recondense on the walls and near surface to form the low ridges of H_2O with trapped CO_2 observed by (*1*, *4*) (Fig. 2B, left, one schematic rim shown in dark gray).

Alternatively, these calculated fluxes will be reduced by a process known to occur when clathrates degas: Surfaces become coated with water ice, and the reaction slows or ceases (Fig. 2C). In this case, the pressure in the fracture drops to the vapor pressure of the ice, and sublimation can occur if heat is available. After sublimation removes or weakens the ice, the degassing cycle can start again (Fig. 2B).

How much heat is required to produce the plume from the clathrate by this process? We ignored the comparatively small energy required for acceleration and considered larger latent heats of decomposition of the clathrate, ~890 kJ kg^{-1} of noncondensible gas mixture, and the additional heat of sublimation of water ice, ~2800 kJ kg^{-1}. For a total vapor flux of 100 to 350 kg s^{-1}, the energy required to produce the plumes is then 0.3 to 0.9 GW, about one-tenth of the 3 to 7 GW radiated from the SPT. This is consistent with our hypothesis that much of the energy of decomposition and sublimation is transported from depth and redeposited at higher levels as heat of condensation of ice and carbon dioxide and that the plume represents small leaks on a massive advection system.

We conclude that Enceladus' south polar plume consists of numerous relatively small leaks tapping a system of advecting gases, ice, and vapor (*1*, *2*, *6*, *7*). The total discharge of a few hundred kilograms per second from all of the vents contributing to the plume at the south pole of Enceladus is remarkably similar to the discharge of Old Faithful Geyser in Yellowstone National Park (*18*), but the discharge into a vacuum gives the plume its magnificent height and spread. We emphasize that heat transport is not along thermal profiles determined by the thermal conductivity of ice in these regions but rather by advection of vapor and redistribution of latent heats. As an alternative to the shallow boiling water "Cold Faithful" model (*1*), we propose that the south pole of Enceladus is a colder world with a "Frigid Faithful" plume emanating from degassing clathrates. This model accounts in a simple and unified way for the gas composition of the plume and the variability of fluxes over space and time. It provides a plausible advective heat transfer process as heat absorbed as latent heat of decomposition of clathrate is redeposited near the surface as latent heat of condensation of ice.

References and Notes

1. C. C. Porco *et al.*, *Science* **311**, 1393 (2006).
2. J. R. Spencer *et al.*, *Science* **311**, 1401 (2006).
3. C. J. Hansen *et al.*, *Science* **311**, 1422 (2006).
4. R. H. Brown *et al.*, *Science* **311**, 1425 (2006).
5. F. Spahn *et al.*, *Science* **311**, 1416 (2006).
6. J. H. Waite Jr. *et al.*, *Science* **311**, 1419 (2006).
7. F. Tian, A. I. F. Stewart, O. B. Toon, K. M. Larsen, L. W. Esposito, in preparation.
8. X. Lu, thesis, University of Auckland, Auckland, New Zealand (2004).
9. X. Lu, A. Watson, A. V. Gorin, J. Deans, *Geothermics* **34**, 389 (2005).
10. X. Lu, A. Watson, A. V. Gorin, J. Deans, *Geothermics* **35**, 409 (2006).
11. J. I. Lunine, D. J. Stevenson, *Astrophys. J. Suppl. Ser.* **58**, 493 (1985).
12. J. S. Kargel, *Science* **311**, 1389 (2006); and references therein.
13. The mixed clathrate decomposition curve was calculated using the formulation of (*11, 19*).
14. D. Laufer, I. Pat-El, A. Bar-Nun, *Icarus* **178**, 248 (2005).
15. For a summary, H. Hong, M. Pooladi-Darvish, P. R. Bishnoi, *J. Can. Petrol. Technol.* **42**, 45 (2003).
16. J. W. Wilder, D. H. Smith, *J. Phys. Chem. B* **106**, 6298 (2002).
17. C. Ji, G. Ahmadi, D. H. Smith, *Chem. Eng. Sci.* **56**, 5801 (2001).
18. S. W. Kieffer, *Rev. Geophys.* **27**, 28 (1989).
19. S. L. Miller, *Science* **165**, 489 (1969).
20. W. F. Kuhs, B. Chazallon, P. G. Podaelli, F. Pauer, *J. Inclusion Phenom. Mol. Recognition Chem.* **29**, 65 (1997).
21. E. D. Sloan Jr., *Clathrate Hydrates of Natural Gases* (Marcel Dekker, New York, ed. 2, 1997).
22. Nitrogen data from (*20*); methane and carbon dioxide from (*21*).
23. J. Longhi, *J. Geophys. Res.* **111**, E06011 (2006).

24. We thank P. Chakraborty and G. Gioia for many helpful discussions and acknowledge support by NASA grant NAG5-12747 to S.W.K.

Supporting Online Material

www.sciencemag.org/cgi/content/full/314/5806/1764/DC1
SOM Text
Fig. S1

7 August 2006; accepted 27 October 2006
10.1126/science.1133519

The mtDNA Legacy of the Levantine Early Upper Palaeolithic in Africa

Anna Olivieri,[1] Alessandro Achilli,[1] Maria Pala,[1] Vincenza Battaglia,[1] Simona Fornarino,[1] Nadia Al-Zahery,[1,2] Rosaria Scozzari,[3] Fulvio Cruciani,[3] Doron M. Behar,[4] Jean-Michel Dugoujon,[5] Clotilde Coudray,[5] A. Silvana Santachiara-Benerecetti,[1] Ornella Semino,[1] Hans-Jürgen Bandelt,[6] Antonio Torroni[1]*

Sequencing of 81 entire human mitochondrial DNAs (mtDNAs) belonging to haplogroups M1 and U6 reveals that these predominantly North African clades arose in southwestern Asia and moved together to Africa about 40,000 to 45,000 years ago. Their arrival temporally overlaps with the event(s) that led to the peopling of Europe by modern humans and was most likely the result of the same change in climate conditions that allowed humans to enter the Levant, opening the way to the colonization of both Europe and North Africa. Thus, the early Upper Palaeolithic population(s) carrying M1 and U6 did not return to Africa along the southern coastal route of the "out of Africa" exit, but from the Mediterranean area; and the North African Dabban and European Aurignacian industries derived from a common Levantine source.

An "out of Africa" dispersal of modern humans is now widely accepted, together with a model postulating a single "southern route" dispersal from the Horn of Africa to the Persian/Arabian Gulf and further along the tropical coast of the Indian Ocean to Southeast Asia and Australasia (*1*–*3*). Within this model, however, the delayed settlement of most parts of West Eurasia needs an explanation. In contrast with South Asians, East Asians, and Australasians, West Eurasians have only a moderate amount of haplogroup-level diversity within mitochondrial DNA (mtDNA) haplogroups N and R (the early derivative of N) but lack almost completely haplogroup M, which is otherwise dominant in Asia (Fig. 1). The colonization of West Eurasia is thought to have been the result of an offshoot of the colonization along the southern route, followed by a lengthy pause, perhaps at the Persian/Arabian Gulf, until the climate improved and the ancestors of West Eurasians were able to enter first the Levant and then Europe (*2*, *4*, *5*). Paleoenvironmental evidence is crucial to this argument, suggesting that an earlier migration toward the north >50 thousand years ago (ka) would have been impossible given the climate of the time, with desert extending from North Africa to Central Asia (*6*).

In contrast, a clade of M, referred to as M1, is present at high frequencies in the Horn of Africa and appears to be predominantly African-specific (Fig. 1 and table S1). This raises the possibility that M could have arisen in East Africa before the out of Africa exit (*7*, *8*), or M1 might represent a back-migration into East Africa (*9*–*11*).

[1]Dipartimento di Genetica e Microbiologia, Università di Pavia, Via Ferrata 1, 27100 Pavia, Italy. [2]Department of Biotechnology, College of Science, University of Baghdad, Iraq. [3]Dipartimento di Genetica e Biologia Molecolare, Università "La Sapienza," Piazzale Aldo Moro 5, 00185 Rome, Italy. [4]Molecular Medicine Laboratory, Rambam Health Care Campus, Efron 9 Street, Bat Galim, 31096 Haifa, Israel. [5]Centre d'Anthropologie, FRE 2960 CNRS, Université Paul Sabatier, Toulouse III, 37, Allées Jules Guesde, 31073 Toulouse Cedex, France. [6]Department of Mathematics, University of Hamburg, Bundesstrasse 55, 20146 Hamburg, Germany.

*To whom correspondence should be addressed. E-mail: torroni@ipvgen.unipv.it

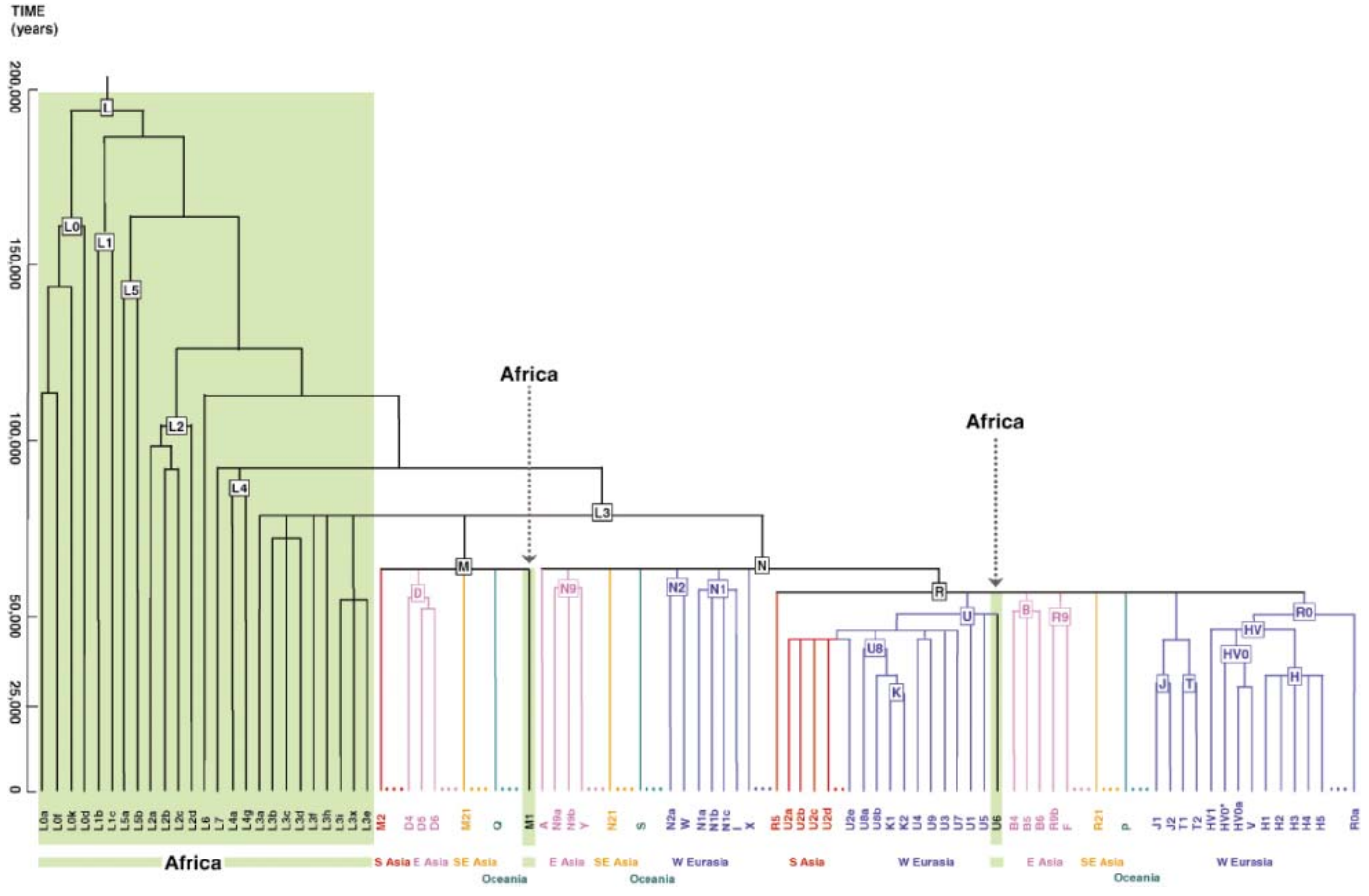

Fig. 1. Schematic representation of the worldwide phylogeny of human mtDNA. African haplogroups are in green and those of other geographical regions are in other colors.

The scenario of a back-migration into Africa is supported by another feature of the mtDNA phylogeny. Haplogroup M's Eurasian sister clade, haplogroup N, which has a very similar age to M and no indication of an African origin, includes R, which in turn embraces haplogroup U (Fig. 1). Haplogroup U is subdivided into numerous clades (U1 to U9) and is characterized by an extremely broad geographical distribution ranging from Europe to India and Central Asia (*12*). However, one of its clades—U6—is mainly found in northern Africans (*13*, *14*) but is also observed in eastern Africans (*11*), a situation that parallels that of M1, with the only difference being that M1 is more common in East Africa than in North Africa.

The hypothesis of a back-migration from Asia to Africa is also strongly supported by the current phylogeography of the Y chromosome variation, because haplogroup K2 and paragroup R1b*, both belonging to the otherwise Asiatic macrohaplogroup K, have been observed at high frequencies only in Africa (*15*, *16*). However, because of the relatively low molecular resolution of the Y chromosome phylogeny as compared to that of the mtDNA, it was impossible to come to a firm conclusion about the precise timing of this dispersal (*15*, *16*).

To shed some light on haplogroups M1 and U6 in Africa, we sequenced mtDNA genomes belonging to M1 (n = 51) and U6 (n = 30) from populations distributed over the geographical range of the two haplogroups. The phylogenies of the M1 and U6 sequences are illustrated in Figs. 2 and 3, respectively.

The average sequence divergence [± standard error computed as in (*17*)] of the 51 M1 coding-region sequences from the root of haplogroup M1 is 7.16 ± 1.38 substitutions (disregarding indels and pathological mutations), which corresponds to a coalescence time estimate of 36.8 ± 7.1 thousand years (ky) for the entire haplogroup M1 (*18*). The M1 tree shows an initial deep split into two sister subclades, M1a and M1b, each containing several independent basal branches, at least seven within M1a and two within M1b (Fig. 2). The M1a branch shows a coalescence time of 28.8 ± 4.9 ky (5.60 ± 0.96 substitutions). The other major branch of the tree, M1b, is also ancient, with an estimated coalescence time of 23.4 ± 5.6 ky (4.55 ± 1.08 substitutions), but in contrast to M1a, which encompasses the entire geographical range of M1, M1b is present only in the Mediterranean area (fig. S1).

Haplogroup U6 is characterized by an overall coalescence time estimate of 45.1 ± 6.9 ky (8.77 ± 1.34 substitutions) (Fig. 3), and U6a (the most represented of its clades) has a coalescence time of 37.5 ± 4.3 ky (7.29 ± 0.83 substitutions). It is worth emphasizing that U6 is a sister clade of the European haplogroup U5 (Fig. 1), which is dated 41.4 ± 9.2 ka (*12*) and was most likely carried by the first European settlers (*19*).

The overall coalescence age estimates for M1 (~37 ky) and U6 (~45 ky) are largely overlapping when standard errors are considered. This supports the scenario that M1 and U6 could have been involved in the same population expansion and dispersal events. Given that the origin of haplogroup U is West Asia and that the presence of U6 in Africa is due to gene flow from that area, the phylogeographic similarities between the two haplogroups indicate that M1 (or its molecular ancestor) is also of western Asian ancestry. This suggests that there was a migration event about 40 to 45 ka that concomitantly affected both haplogroups. An ancient arrival of M1 in Africa (or in its close proximity) is supported by the fact that none of the numerous M haplogroups in Asia (*20*, *21*) harbors any of the distinguishing M1 root mutations, and by the lack of Asian-specific clades within M1 (and U6), as might be expected in the case of a more recent arrival. The arrival of

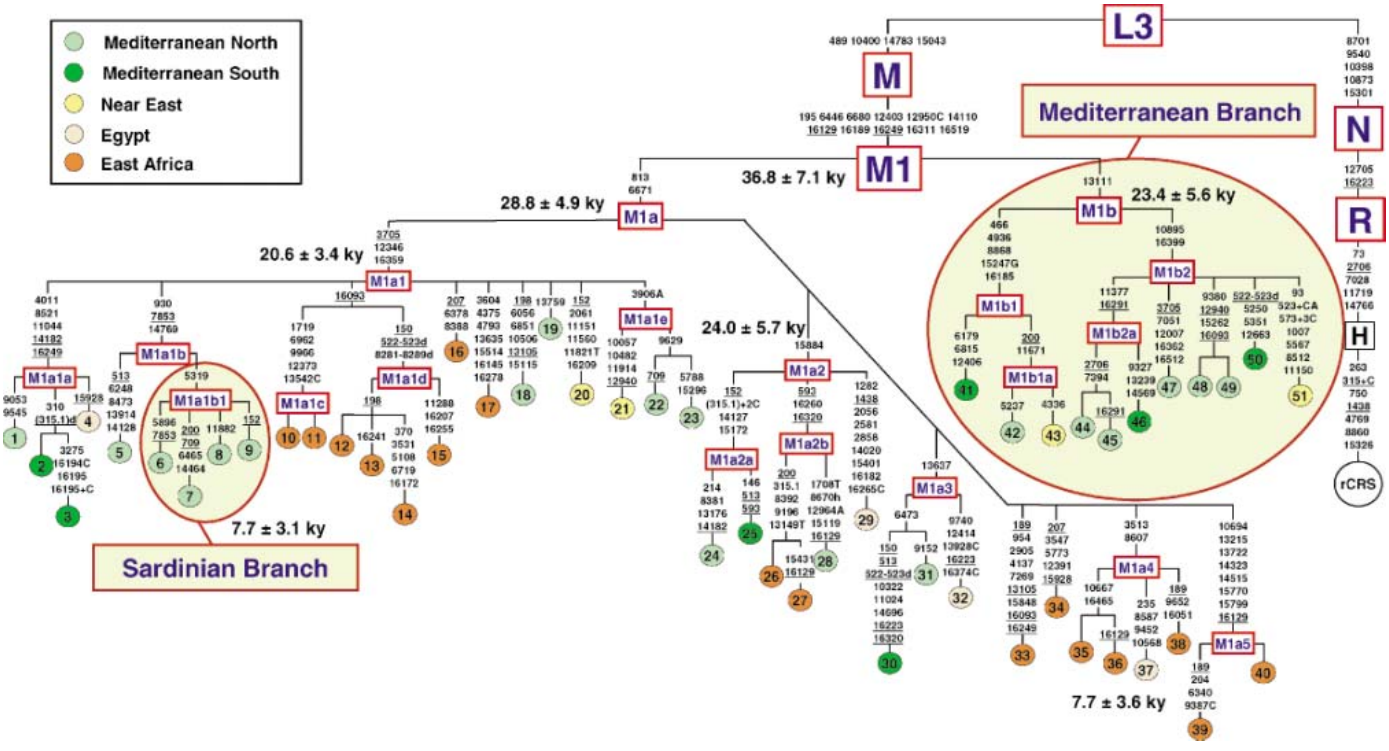

Fig. 2. Tree of 51 mtDNA sequences belonging to haplogroup M1. The tree is rooted using the reference sequence (rCRS) (*27*) as an outgroup. The sequencing procedure and phylogeny construction were performed as described elsewhere (*4*, *28*, *29*). mtDNAs were selected through a preliminary sequence analysis of the control region and a restriction fragment length polymorphism survey in order to include the widest possible range of internal variation of the haplogroup. All M1 sequences are new except for 17, which is the same sample as 25 in Torroni *et al.* (*3*). Mutations are shown on the branches; they are transitions unless a base is explicitly indicated. Suffixes indicate transversions (to A, G, C, or T), indels (+, d) or heteroplasmy (h). Recurrent mutations are underlined; pathological mutations are in italics. The ethnic or geographic origins of mtDNAs are as follows: Italy (1, 5 to 9, 23, 24, 28, 31, 42, 44, 45, and 47 to 49); Berbers of Egypt (2 and 3); Egypt (4, 29, 32, and 37); Ethiopian Jews (10 and 11); Ethiopia (12 to 17, 26, 27, 33 to 35, 38, and 40); Greece (18 and 19); Iraqi Jew (20); Druze (21); American (USA) of European ancestry (22); Berbers of Morocco (25, 30, 46, and 50); Kenya (36); Somalia (39); Mauritania (41); Bedouin, southern Israel (43); and Iraqi (51). For additional information regarding the tree, see the supporting online material (SOM).

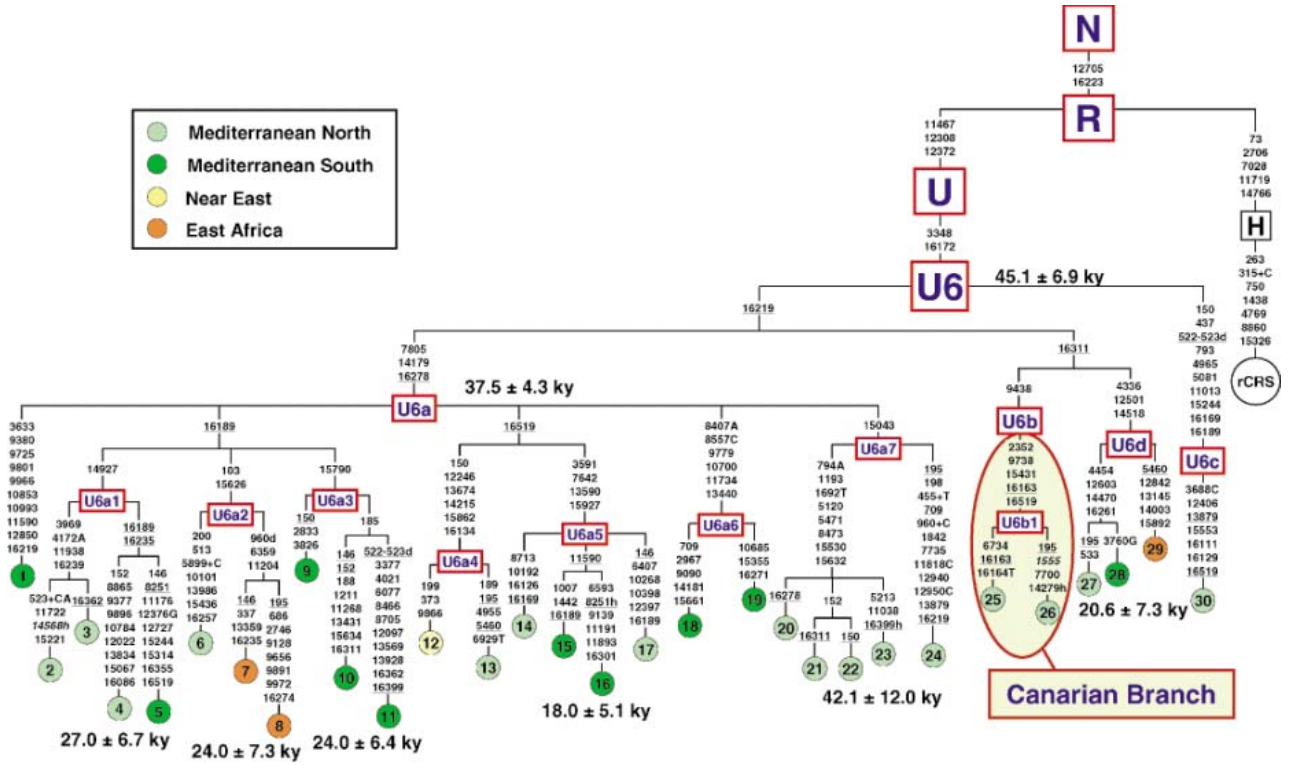

Fig. 3. Tree of 30 mtDNA sequences belonging to haplogroup U6. All U6 sequences are new except for 7 and 25, which are the same samples as 38 and 39 in Achilli *et al.* (*12*). Nomenclature is consistent with (*24*), except that U6a1 has now been narrowed and the motif for U6b1 has been completed. The ethnic or geographic origins of mtDNAs are as follows: Berbers of Morocco (1, 10, 11, 19, and 28); Italy (2 to 4, 6, 13, 14, 17, 20 to 23, 27, and 30); Algeria (5); Ethiopia (7 and 8); Nigeria (9 and 15); Iraq (12); Tunisia (16 and 18); France (24); Dominican Republic (25); Spain (26); and Ethiopian Jew (29). For additional information regarding the tree, see the SOM.

M1 and U6 in Africa 40 to 45 ka would temporally overlap with the event(s) that led to the peopling of Europe by modern humans.

This raises the possibility that the population(s) harboring M1, U6, and U5 (or their close molecular ancestors) were all living in the same broad geographic area of southwestern Asia, possibly in separate regional enclaves, and that they all were affected by an event that led to their expansion and relocation. It has been proposed that a change in climate conditions, fragmenting and reducing the desert areas (*6*), allowed humans to enter first the Levant and then Europe (*4*). However, such a climatic change would also render North Africa equally accessible from the Levant. Thus, while populations bearing U5 took part in the colonization of Europe, populations with M1 and U6 entered North Africa. Such a scenario implies that the population(s) harboring M1 and U6 did not return to Africa along the southern coastal route of the out of Africa exit but from the Mediterranean area. The Greenland Interstadial 12, from ~44 to ~48 ka (*22*, *23*), could have been the main period of dispersal into the Levant and subsequently into North Africa.

Furthermore, the distribution of M1b and most of the U6 clades only in Mediterranean regions indicates that both M1 and U6 differentiated into their major subclades while they were in the Mediterranean area, and only later some subsets of M1a (including its derivatives M1a1 and M1a2), U6a2, and U6d diffused to East Africa, possibly along the Nile Valley. It cannot be excluded that a further late dispersal of M1 and U6 within North and East Africa might have been associated with the diffusion, after the Last Glacial Maximum, of the emerging Afro-Asiatic language family. Indeed, M1 and U6 in Africa are mostly restricted to Afro-Asiatic–speaking areas.

In the Holocene, some of the M1 and U6 clades were involved in subsequent migration and colonization events. For instance, M1a1b1 is found only in Sardinia (Fig. 2), where it is also fairly frequent (1.8%). Its estimated coalescence age of 7.7 ± 3.1 ky suggests that the founding M1a1b mtDNA was brought to Sardinia by the first modern humans that arrived to the island. A similar scenario can be envisioned for U6b1, which was typical of the Guanches (*24*), the ancestral population of the Canary Islands.

Our phylogeographic studies of mtDNA haplogroups reinforce the scenario that the first Upper Paleolithic cultures in North Africa (Dabban) and Europe (Aurignacian) had a common source in the Levant (*14*, *25*, *26*) and in fact spread by migration from some core area in the Levantine Corridor. The dispersal of Levantine people to Europe and North Africa was then marked by the mtDNA haplogroups U5 and U6/M1, respectively.

References and Notes

1. P. Forster, S. Matsumura, *Science* **308**, 965 (2005).
2. P. Mellars, *Science* **313**, 796 (2006).
3. A. Torroni, A. Achilli, V. Macaulay, M. Richards, H.-J. Bandelt, *Trends Genet.* **22**, 339 (2006).
4. V. Macaulay *et al.*, *Science* **308**, 1034 (2005).
5. M. Richards *et al.*, in *Human Mitochondrial DNA and the Evolution of Homo sapiens*, H.-J. Bandelt, V. Macaulay, M. Richards, Eds., vol. 18 of *Nucleic Acids and Molecular Biology* (Springer-Verlag, Berlin, Germany, 2006), pp. 225–265.
6. T. H. van Andel, P. C. Tzedakis, *Quat. Sci. Rev.* **15**, 481 (1996).
7. G. Passarino *et al.*, *Am. J. Hum. Genet.* **62**, 420 (1998).
8. L. Quintana-Murci *et al.*, *Nat. Genet.* **23**, 437 (1999).
9. M. Richards *et al.*, *Am. J. Hum. Genet.* **72**, 1058 (2003).
10. P. Forster, *Philos. Trans. R. Soc. London Ser. B* **359**, 255 (2004).
11. T. Kivisild *et al.*, *Am. J. Hum. Genet.* **75**, 752 (2004).
12. A. Achilli *et al.*, *Am. J. Hum. Genet.* **76**, 883 (2005).
13. J. C. Rando *et al.*, *Ann. Hum. Genet.* **62**, 531 (1998).
14. V. Macaulay *et al.*, *Am. J. Hum. Genet.* **64**, 232 (1999).
15. F. Cruciani *et al.*, *Am. J. Hum. Genet.* **70**, 1197 (2002).
16. J. R. Luis *et al.*, *Am. J. Hum. Genet.* **74**, 532 (2004).
17. J. Saillard *et al.*, *Am. J. Hum. Genet.* **67**, 718 (2000).
18. D. Mishmar *et al.*, *Proc. Natl. Acad. Sci. U.S.A.* **100**, 171 (2003).
19. M. Richards *et al.*, *Am. J. Hum. Genet.* **67**, 1251 (2000).
20. Q.-P. Kong *et al.*, *Hum. Mol. Genet.* **15**, 2076 (2006).
21. C. Sun *et al.*, *Mol. Biol. Evol.* **23**, 683 (2006).
22. N. J. Shackleton, R. G. Fairbanks, Tzu-chien Chiu, F. Parrenin, *Quat. Sci. Rev* **23**, 1513 (2004).
23. W. J. Burroughs, *Climate Change in Prehistory: The End of the Reign of Chaos* (Cambridge Univ. Press, Cambridge, 2005).
24. N. Maca-Meyer *et al.*, *BMC Genet.* **4**, 15 (2003).

25. P. Van Peer, P. M. Vermeersch, in *The Emergence of Modern Humans: An Archaeological Perspective*, P. Mellars, Ed. (Edinburgh Univ. Press, Edinburgh, 1990), pp. 139–159.
26. O. Bar-Yosef, *Annu. Rev. Anthropol.* **31**, 363 (2002).
27. R. M. Andrews *et al.*, *Nat. Genet.* **23**, 147 (1999).
28. A. Torroni *et al.*, *Am. J. Hum. Genet.* **69**, 1348 2001).
29. A. Achilli *et al.*, *Am. J. Hum. Genet.* **75**, 910 (2004).
30. We are grateful to all the donors for providing blood samples and to the people who contributed to their collection. In particular we are grateful to F. El Chennawi, E. Crubézy, A. Baali, M. Cherkaoui, and M. Melhaoui for their help in the collection of the Moroccan and Egyptian samples. The sampling of the Berbers was made within the framework of The Origin of Man, Language and Languages, EUROCORES Programme, and benefited from funding by the Conseil Régiona de Midi-Pyrénées (Toulouse, France), the CNRS, and the European Community Sixth Framework Programme under contract ERASCT-2003-980409. This research received support from Progetti Ricerca Interesse Nazionale 2005 (Italian Ministry of the University) (to R.S. and A.T.), Ministero degli Affari Esteri (to O.S.), Compagnia di San Paolo (to O.S. and A.T.), and Fondazione Cariplo (to A.T.). mtDNA sequences have been deposited in GenBank with accession numbers DQ341082 and EF060313 to EF060362 for M1 sequences, and AY882416 to AY882417 and EF064317 to EF064344 for U6 sequences.

Supporting Online Material

www.sciencemag.org/cgi/content/full/314/5806/1767/DC1
SOM Text
Fig. S1
Table S1
References

26 September 2006; accepted 2 November 2006
10.1126/science.1135566

Nannoplankton Extinction and Origination Across the Paleocene-Eocene Thermal Maximum

Samantha J. Gibbs,[1]* Paul R. Bown,[2] Jocelyn A. Sessa,[3] Timothy J. Bralower,[3] Paul A. Wilson[1]

The Paleocene-Eocene Thermal Maximum (PETM, ~55 million years ago) was an interval of global warming and ocean acidification attributed to rapid release and oxidation of buried carbon. We show that the onset of the PETM coincided with a prominent increase in the origination and extinction of calcareous phytoplankton. Yet major perturbation of the surface-water saturation state across the PETM was not detrimental to the survival of most calcareous nannoplankton taxa and did not impart a calcification or ecological bias to the pattern of evolutionary turnover. Instead, the rate of environmental change appears to have driven turnover, preferentially affecting rare taxa living close to their viable limits.

Modern biodiversity studies predict huge losses of flora and fauna (*1*) associated with anthropogenic carbon emissions and projected climate change (up to ~35% of species by 2050) (*2*). Paleontological records from analog events in geologic history provide a way to test the ecological basis of these predictions. The Paleocene-Eocene Thermal Maximum (PETM) is attributed to a rapid increase in atmospheric CO_2 levels, perhaps caused by the exhumation and oxidation of methane from marine sediments (*3*–*5*). Within less than 10 thousand years (ky) (*6*, *7*), ocean temperatures rose by 5° to 8°C, marine and terrestrial carbon isotope values ($\delta^{13}C$) decreased by 3 to 8 per mil, and the calcite compensation depth (CCD) (*8*) in the deep sea shoaled by up to 2 km (*9*–*12*). Subsequently, $\delta^{13}C$ values returned to near-background levels within 110 to 210 ky (*6*, *13*). The PETM was accompanied by dramatic reorganization in marine and terrestrial ecosystems (*9*, *14*–*19*), with the most extreme response being the catastrophic extinction of 35 to 50% of benthic foraminiferal species (*17*).

To understand biotic change across the PETM more fully, we estimate the rate of evolutionary change within the calcareous nannoplankton; i.e., the number of species that appeared and disappeared through time. Calcareous nannoplankton are ideal for testing the organismal response to the PETM because their surface-water habitat renders them highly sensitive to environmental change. Moreover, their fossil record is exceptionally complete during this time interval, both taxonomically and stratigraphically (*18, 19*). Our records are at a resolution of up to 10 ky, allowing us to resolve patterns on the time scale of environmental disturbance.

Our data come from open-ocean sites in the paleoequatorial Pacific and the Southern Ocean [Ocean Drilling Program (ODP) sites 1209 and 690] and two sections on the New Jersey paleoshelf (U.S. Geological Survey drill hole at Wilson Lake and ODP leg 174AX drill hole at Bass River) (fig. S1). By combining nannofloral data sets with cyclostratigraphic age models (*6*), we calculated species extinction and origination rates per unit depth and per unit time (*20*). Two methods were used to calculate evolutionary rates per unit time. First, we applied the widely used proportional rates method, dividing the number of originations or extinctions by time, normalized for diversity [(*20*), following (*21*)]. Second, per-capita rates were calculated using the natural log of the ratio of taxa that range through a time bin to either those that only cross the bottom boundary of the bin (for extinction) or those that cross the top boundary (for origination) (*20*, *22*, *23*). This latter method has the advantage of removing spurious variation in rates created by unequal duration of time bins (*22*). Both methods return rates per unit time (*24*) and are thus not biased by variation in sediment accumulation (*25*).

At all sites, the pattern of change recorded across the PETM in evolutionary rates and species richness (Figs. 1 and 2 and table S1) is similar, pointing to global rather than local species turnover (*26*). In the ~70 ky before the PETM, origination was low and there were virtually no extinctions, resulting in a gradual increase in species richness. Origination and extinction rates increased during the first 70 ky of the PETM, defined by the interval from the onset to the peak of the carbon isotope excursion (CIE, dark shaded zone in Figs. 1 and 2). During this interval, the inferred rate of CO_2 absorption by the oceans was greatest, and up to 18 species (from a maximum of 84) appeared or disappeared. The synchronous increase in both per-unit-depth and per-unit-time rates demonstrates that the abrupt change in turnover cannot be attributed to changes in sedimentation rate (e.g., section condensation resulting from dissolution at the base of the PETM). At three locations [site 1209, Wilson Lake (WL), and Bass River (BR)], average proportional (per unit time) rates of origination and extinction were 1.6 and 1.7% per 10 ky, respectively (table S1), compared to an average of 0.5 and 0.1% per 10 ky in the pre-event background interval (Fig. 1). At site 690, Maud Rise, Southern Ocean, a more finely resolved record of the CIE is available (*24*), and the evolutionary rate data reveal that proportional origination and extinction rates were 11 and 5% per 10 ky, respectively, during the first 10 ky after the event onset (Fig. 2). During the remainder of the PETM, despite continued environmental perturbation (*9, 10*), origination and extinction rates rapidly returned to pre-event levels, with a maximum of 10 species appearing or disappearing over the next ~150 ky. Proportional rates of origination and extinction in the recovery interval remained low (averaging 0.2 and 0.5% per 10 ky, respectively, table S1) with a gradual drop in species richness (Fig. 1).

In Fig. 3, we compare the rates that we have measured for the PETM with long-term

[1]School of Ocean and Earth Sciences, National Oceanography Centre, Southampton, European Way, Southampton, SO14 3ZH, UK. [2]Department of Earth Sciences, University College London, Gower Street, London WC1E 6BT, UK. [3]Department of Geosciences, Pennsylvania State University, University Park, PA 16802, USA.

*To whom correspondence should be addressed. E-mail: sxg@noc.soton.ac.uk

records of nannofossil diversity binned into 3-million-year (My) intervals (*21*). In the long-term record, the bin containing the PETM [56 to 53 million years ago (Ma)] shows the highest rates of turnover for the Cenozoic, with both origination and extinction rates at 54%. Comparison with the results of our study suggests that much of this turnover was probably focused in the onset of the short-lived PETM event. This finding implies that the importance of geological events marked by rapid evolutionary turnover, such as the PETM, is likely to be systematically underestimated within low-resolution records of biodiversity change.

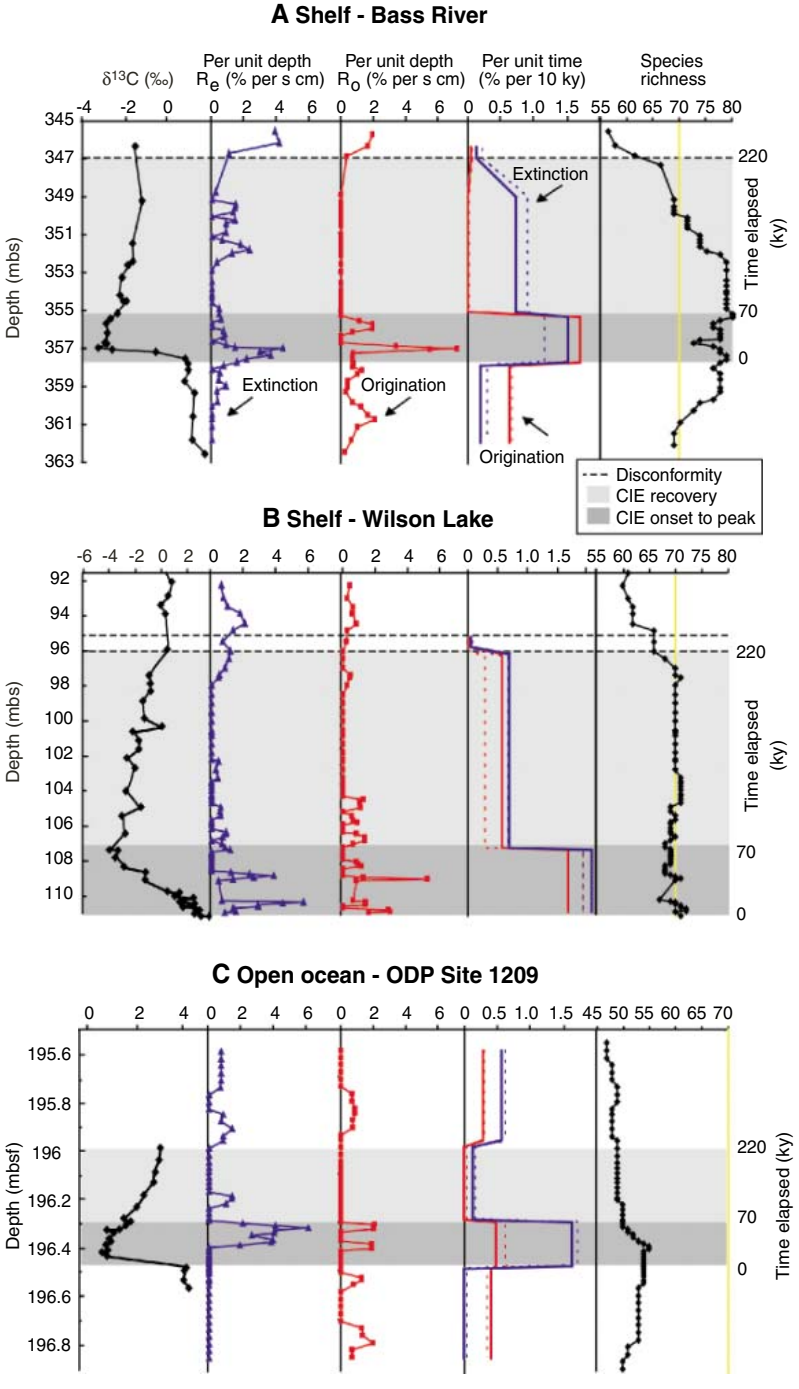

Fig. 1. Per-unit-depth (% per sampling interval) and per-unit-time (proportional and per-capita) evolutionary rates across the CIE for (**A**) BR, (**B**) Wilson Lake, and (**C**) ODP site 1209. Extinction rates (R_e), blue; origination rates (R_o), red; proportional, solid line (% per 10 ky); per capita, dashed line (lineage per 10 ky, using the same scale as the proportional rates but $\times 10^{-2}$). The sampling intervals are described in (*20*). Diversity is expressed as total species present (species richness) per sample with the 70-species level marked on each plot (yellow). The shaded intervals correspond to time elapsed from the onset of the CIE, with dark gray being the onset-to-peak interval and light gray being the recovery interval. Mbsf, meters below sea floor; mbs, meters below surface. At both BR and WL, hiatuses in the uppermost part of the recovery interval artificially elevate rates per unit depth above the disconformities. The sources of the carbon isotope records in Figs. 1, 2, and 4 are detailed in (*20*).

Despite the strong ecological responses of nannofossil assemblages to environmental changes at the PETM (*18, 19*), the pattern of evolutionary reorganization that we see is surprising in two ways. First, the rate of turnover is relatively modest, considering the magnitude of environmental change that has been inferred for the PETM and in light of findings from laboratory culture experiments and ocean acidification models (*27, 28*). Second, the turnover lacks an obvious ecological or calcification bias. Both oligotrophic warm-water–favoring taxa (e.g., several species of *Discoaster* and *Fasciculithus*) and inferred mesotrophic cool-water–favoring taxa (e.g., several species of *Neochiastozygus* and *Prinsius bisulcus*) appear and disappear (table S4). Furthermore, there is no obvious evidence of an evolutionary decrease in lith calcification or an overcompensation in robustness, despite increasing geologic evidence for massive carbonate undersaturation in the oceans (*11*, *12*). Heavily calcified as well as fragile nannofossils both appear and disappear within the interval from the onset to the peak of PETM conditions (Fig. 4, table S4), providing no obvious evidence for geologically sustained inhibition of surface-water calcification. Apparently, surface-water saturation state was not perturbed across the event to a point that was detrimental to the survivorship of most calcareous nannoplankton taxa. On the other hand, taxa that became extinct were rare (<1% abundance in pre-event assemblages) compared to the dominant taxa that survived. Presumably, the rare taxa lived closer to their ecological limits than the more common taxa and were therefore more susceptible to a contraction of population numbers below viable limits (*29*), with originations rapidly filling the empty ecological niches. The lack of ecological bias in our data and the clustering of bioevents at the initiation of the PETM suggest that it was the rate of environmental change that drove evolutionary turnover during this event, rather than change in any given individual environmental factor.

In comparison to many plants and animals, calcareous nannoplankton should be relatively resilient to environmental perturbation because of their planktonic habit, near-cosmopolitan distribution, large population sizes, and short life cycle. Yet our data demonstrate that even these organisms display a prominent acceleration in both origination and extinction rates across the PETM (Figs. 1 to 3). However, the measured present-day rates of CO_2 increase, and those predicted for the coming century are even greater than for the PETM (*30*), with projections of increased surface-water acidity of 0.7 pH units over the next 300 years (*31*),

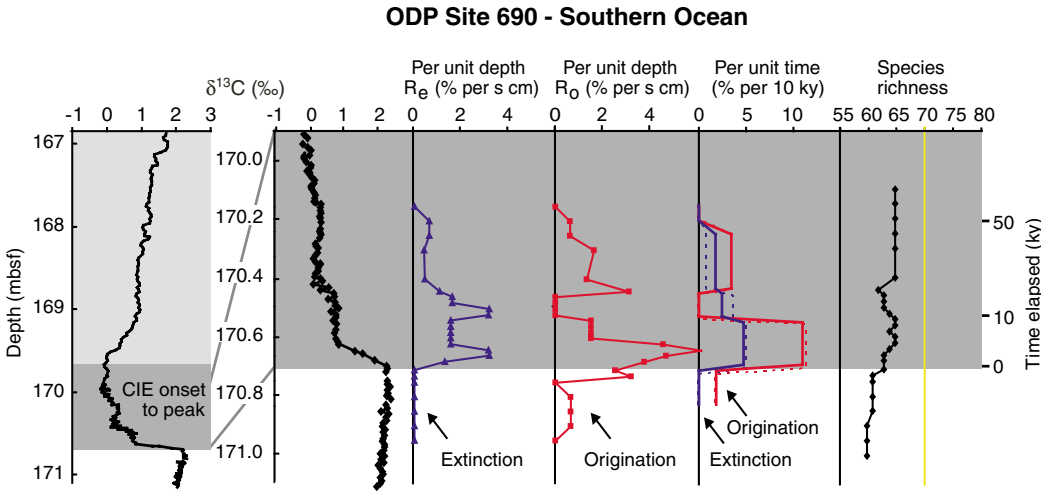

Fig. 2. Per-unit-depth (% per sampling interval) and per-unit-time (proportional, solid; and per-capita, dashed) evolutionary rates across the onset-to-peak interval of the CIE at ODP site 690. Per-capita rates use the same scale as the proportional rates but × 10^{-2}. Abbreviations and symbols are the same as in Fig. 1.

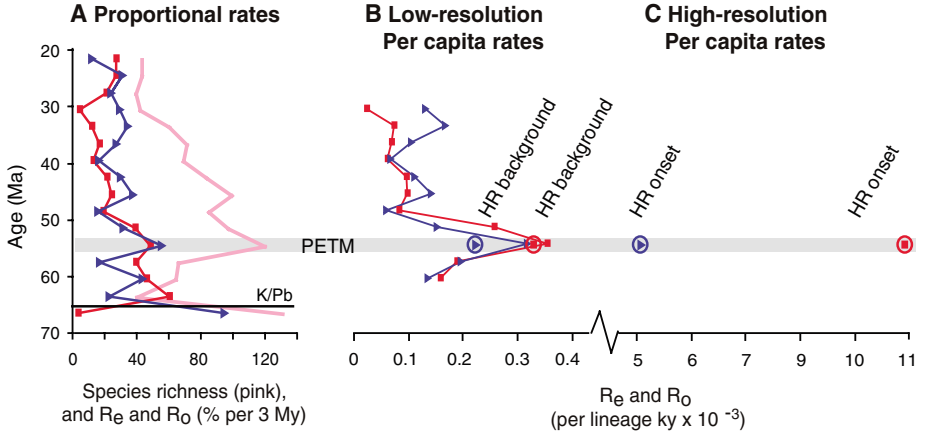

Fig. 3. High-resolution PETM evolutionary rate estimates compared to low-resolution (3 My) Paleogene nannofossil biodiversity. (**A**) Paleogene diversity data replotted from (*22*) at the midpoint of each 3-My time bin. Total nannofossil diversity (pink line) and proportional R_e, blue, and R_o, red, rates per 3-My interval are shown. Evolutionary rates for the interval from 62 to 68 Ma reflect species losses and biotic recovery associated with the Cretaceous-Paleogene boundary (K/Pb). (**B**) Proportional evolutionary rates from 62 to 26 Ma recalculated as per-capita rates (lineage per ky). (**C**) PETM high-resolution (HR) per-capita rates (lineage per ky, circled symbols) from the event onset at site 690 (table S3) and HR per-capita rates for pre- and post-event intervals labeled as background (table S1). Note the break in the per-capita rate scale. This scale applies to both (B) and (C). It is necessary to use per-capita rates rather than proportional rates for comparison of time-interval bins of different durations (*20*, *22*).

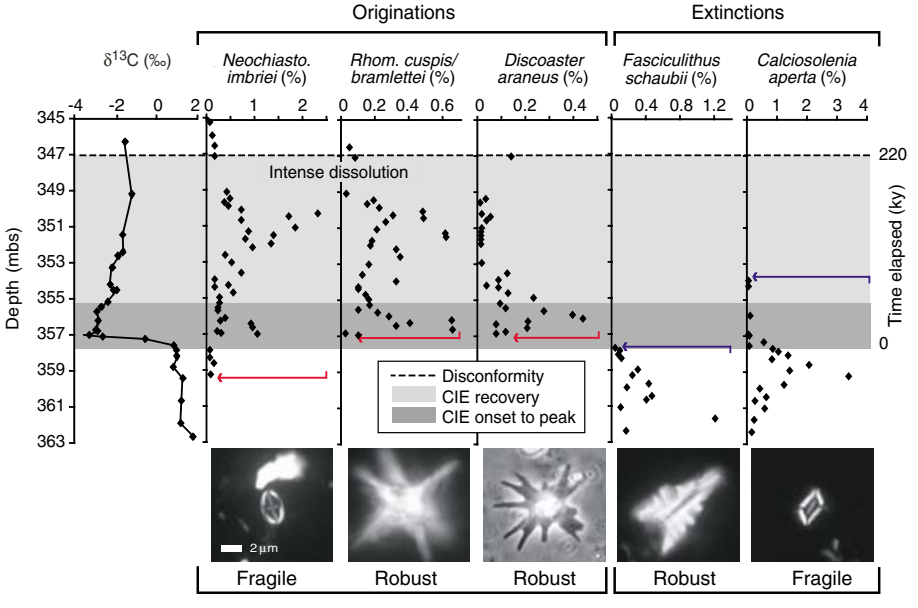

Fig. 4. Examples from BR of species that originated and became extinct during the PETM interval. Abundances are % abundances of total nannofossils. The species illustrated are examples of robust and delicate taxa (table S4). In this context, robust refers to nannofossils that are either relatively large or are constructed of large, blocky calcite units. Fragile refers to nannofossils composed of small and/or thin calcite units. The arrows indicate appearance (red) and disappearance (blue) levels. The light-microscope images are all at the same scale, with the bar representing 2 μm. *Neochiasto.*, *Neochiastozygus*; *Rhom.*, *Rhomboaster*.

possibly even resulting in aragonite undersaturation of the high latitudes by 2050 (*28*). Although there was no catastrophic loss of calcifying plankton at the PETM, the evolutionary rates that we have documented are likely to be modest compared to those that will accompany projected surface-water acidification over coming centuries.

References and Notes

1. E. O. Wilson, *The Diversity of Life* (Penguin, London, 1994).
2. C. D. Thomas *et al.*, *Nature* **427**, 145 (2004).
3. G. R. Dickens, J. R. O'Neil, D. K. Rea, R. M. Owen, *Paleoceanography* **10**, 965 (1995).

4. M. E. Katz, D. K. Pak, G. R. Dickens, K. G. Miller, *Science* **286**, 1531 (1999).
5. H. Svensen *et al.*, *Nature* **429**, 542 (2004).
6. U. Röhl, T. J. Bralower, R. D. Norris, G. Wefer, *Geology* **28**, 927 (2000).
7. Even this massive geological carbon-cycle perturbation is dwarfed by anthropogenic rates of carbon emissions [~0.2 gigatons (Gt) per year for PETM and 8 Gt per year for modern (*30*)].
8. The CCD is the depth at which the rate of calcite input from surface waters equals the rate of dissolution and, in practice, is mapped on the sea floor by the transition from carbonate-bearing (above the CCD) to carbonate-free (below the CCD) sediments.
9. J. P. Kennett, L. D. Stott, *Nature* **353**, 225 (1991).
10. J. C. Zachos *et al.*, *Science* **302**, 1551 (2003).
11. J. C. Zachos *et al.*, *Science* **308**, 1611 (2005).
12. A. B. Colosimo, T. J. Bralower, J. C. Zachos, *Proc. ODP Sci. Res.* **198**, 1 (2006); available at www-odp.tamu.edu/publications/198_SR/112/112.htm.
13. K. A. Farley, S. F. Eltgroth, *Earth Planet. Sci. Lett.* **208**, 135 (2003).
14. G. J. Bowen *et al.*, *Science* **295**, 2062 (2002).
15. P. D. Gingerich, *Geol. Soc. Am. Spec. Pap.* **369**, 463 (2003).
16. S. L. Wing *et al.*, *Science* **310**, 993 (2005).
17. E. Thomas, in *Late Paleocene-Early Eocene Climatic and Biotic Events in the Marine and Terrestrial Records*, M.-P. Aubry, S. G. Lucas, W. A. Berggren, Eds. (Columbia Univ. Press, New York, 1998), pp. 214–235.
18. T. J. Bralower, *Paleoceanography* **17**, 1023 (2002).
19. S. J. Gibbs, T. J. Bralower, P. R. Bown, J. C. Zachos, L. Bybell, *Geology* **34**, 233 (2006).
20. Materials and methods are available as supporting material on *Science* Online.
21. P. R. Bown, J. A. Lees, J. R. Young, in *Coccolithophores–From Molecular Processes to Global Impacts*, H. Thierstein, J. R. Young, Eds. (Springer, Berlin, 2004), pp. 481–508.
22. M. Foote, *Paleobiology* **26** (suppl. to no. 4), 74 (2000).
23. Because the two methods generate similar patterns of turnover, we refer only to proportional rates, which tend to be more intuitive, in the text (but both proportional and per-capita rates are shown in the tables and figures).
24. Our calculated rates of evolutionary turnover are considered to be conservative for a number of reasons. First, the practice of integrating turnover rates over intervals of geological time (binning) necessarily yields rates of evolutionary change that are time-averaged. At BR, WL, and site 1209, the PETM is binned into two intervals: from the onset to the peak CIE (70 ky) and the recovery (150 ky) (*20*). At site 690, the record is resolved into time intervals of about 10 ky (table S3). This higher resolution is possible at site 690 because the cyclostratigraphic age model that we have used (*6*) was developed at this site. Second, there is likely to have been differential postmortem dissolution resulting in the selective removal of some delicate species, both in surface waters (*21*) and in the sediment. This in part accounts for the minor geographic variations in rates, resulting from higher species numbers in shelf and lower-latitude areas as a function of better preservation in shelf areas, and a real increase in species diversity (*20*).
25. We have used the cyclostratigraphic age model of Röhl *et al.* (2000) (*6*) rather than an alternative age model based on extraterrestrial He ($^3He_{ET}$) incorporation in sediments (*13*, *20*). The choice of age model does not substantially alter our findings because the onset-to-peak interval is nearly identical in both age models (table S1 and fig. S2). Values differ for the recovery interval, but this discrepancy is not substantial to our findings because the high-resolution record from site 690 demonstrates that extinction and origination rates returned to near-background levels before carbon isotope values increased from their PETM minimum [marking the start of recovery (*20*)], irrespective of age model (fig. S2).
26. Despite large CCD changes at the PETM, we are confident that the patterns we observed are associated with evolutionary turnover and not dissolution. We have assessed nannofossil preservation through the sections, and where substantial dissolution is present, it is confined to short intervals during the event onset to peak. All samples that exhibited substantial dissolution were excluded (*20*).
27. U. Riebesell *et al.*, *Nature* **407**, 364 (2000).
28. J. C. Orr *et al.*, *Nature* **437**, 681 (2005).
29. R. D. Norris, in *Deep Time: Paleobiology's Perspective*, D. H. Erwin, S. L. Wing, Eds. (Paleontological Society, Lawrence, KS, 2000), pp. 236–258.
30. J. T. Houghton *et al.*, *Climate Change 2001: The Scientific Basis: Contribution of Working Group I to the Third Assessment Report of the Intergovernmental Panel on Climate Change* (Cambridge Univ. Press, Cambridge, 2001).
31. K. Caldeira, M. E. Wicket, *Nature* **425**, 365 (2003).

32. We thank A. Z. Krug and M. Patzkowsky for technical assistance; S. Wing, U. Röhl, T. Tyrell, and L. Lourens for discussion; and M. Foote and others for reviews. This work was supported by NSF grant EAR-0120727 to S.J.G. and T.J.B. and a National Natural Research Council research fellowship to S.J.G. This research used samples and data provided by the ODP and the U.S. Geological Survey.

Supporting Online Material

www.sciencemag.org/cgi/content/full/314/5806/1770/DC1
Materials and Methods
Figs. S1 and S2
Tables S1 to S4
References

15 August 2006; accepted 31 October 2006
10.1126/science.1133902

Biomass, Size, and Trophic Status of Top Predators in the Pacific Ocean

John Sibert,[1]* John Hampton,[2] Pierre Kleiber,[3] Mark Maunder[4]

Fisheries have removed at least 50 million tons of tuna and other top-level predators from the Pacific Ocean pelagic ecosystem since 1950, leading to concerns about a catastrophic reduction in population biomass and the collapse of oceanic food chains. We analyzed all available data from Pacific tuna fisheries for 1950–2004 to provide comprehensive estimates of fishery impacts on population biomass and size structure. Current biomass ranges among species from 36 to 91% of the biomass predicted in the absence of fishing, a level consistent with or higher than standard fisheries management targets. Fish larger than 175 centimeters fork length have decreased from 5% to approximately 1% of the total population. The trophic level of the catch has decreased slightly, but there is no detectable decrease in the trophic level of the population. These results indicate substantial, though not catastrophic, impacts of fisheries on these top-level predators and minor impacts on the ecosystem in the Pacific Ocean.

Industrial fisheries for tunas and associated species extend over most of the tropical and temperate Pacific Ocean and currently produce over 2.5 million tons (*1*) or about 64% of the 2004 global tuna catch (Fig. 1). These fisheries have grown continuously since the 1950s and have removed more than 50 million tonsof large pelagic fish. The fishery targets four primary temperate and tropical tuna species: skipjack (*Katsuwonus pelamis*), yellowfin (*Thunnus albacares*), bigeye (*T. obesus*), and albacore (*T. alalunga*) tuna. Other species, bluefin tuna (*T. orientalis*), billfishes, and oceanic sharks are also taken, but the primary tuna species make up >90% of the total catch by weight. Data derived from these fisheries (including catch, fishing effort, size composition, and tagging data) show a 50-year record of natural variability in and human impacts on open-ocean ecosystems. We analyzed all available data with state-of-the art stock assessment methods to provide estimates of fishery impacts on population biomass, size structure, and trophic status of major top-level predator stocks in the Pacific Ocean: bigeye tuna, yellowfin tuna, skipjack tuna, albacore tuna, and blue shark (*Prionice glauca*) (*2*).

The trajectories of exploited and unexploited (*3*) biomass vary substantially among stocks (Fig. 2). Exploited western Pacific yellowfin and bigeye have declined steadily to levels near the equilibrium biomass that would produce the maximum sustainable yield (MSY) in the fishery. Skipjack tuna and blue shark appear to have increased slightly, whereas albacore have fluctuated in both directions. Current total and adult biomass range, respectively, from 36 to 91% and 12 to 89% of that predicted in the absence of fishing (Table 1 and fig. S1). The variability in biomass over time and among stocks cannot be attributed entirely to fishing. Each stock has a unique recruitment history, some with periods of several years during which recruitment is more than 1 SD above or below the long-term average for the stock (fig. S2).

[1]Joint Institute for Marine and Atmospheric Research, University of Hawaii, Honolulu, HI 96822, USA. [2]Oceanic Fisheries Programme, Secretariat of the Pacific Community, BP D5, Noumea 98848, New Caledonia. [3]Pacific Islands Fisheries Science Center, National Marine Fisheries Service, National Oceanic and Atmospheric Administration, 2570 Dole Street, Honolulu, HI 96822, USA. [4]Inter-American Tropical Tuna Commission, 8604 La Jolla Shores Drive, La Jolla, CA 92037, USA.

*To whom correspondence should be addressed. E-mail: sibert@hawaii.edu

Longline fishing, which selectively removes the largest and oldest individuals, was the primary method of fishing for the first 25 years of the tuna fishery except in some coastal areas. The biomass of tunas larger than 175 cm fork length (measured from the tip of the snout to the center of the fork in the tail) decreased by 40% by the end of the 1970s (Fig. 3A). The current biomass of tunas larger than 175 cm is less than 17% of the biomass expected in the absence of fishing, but this segment of the population never made up more than 5% of the total tuna biomass (fig. S5). The burgeoning purse-seine fishery in the 1980s began to remove smaller fish (~75 cm in length), spreading exploitation to earlier life-history stages (Fig. 3A).

An ontogenetic model relating size to trophic level was applied to the size structure of the catch, exploited population, and unexploited population to estimate trophic levels (*2*). The trophic level of the catch, aggregated across the eight stocks, was about 10% higher than the trophic level in both the exploited and unexploited population in the 1950s and declined steadily to the same level as the exploited population (Fig. 3B). The trophic level of the catch dropped from 4.1 to 4.0 over the past 50 years because of the increased catch of smaller fish, but the trophic level in the exploited population has remained relatively constant at 3.9 (table S3).

Stock assessment is sometimes criticized (*4*) for dependence on unproven assumptions and for producing uncertain results. Integrated stock assessment models are, however, the tools of choice when attempting to accommodate disparate fisheries data as opposed to selecting a single data source [for example, (*5*)]. Our analysis depends mainly on ratios of estimated variables, which are less variable than point estimates (*6*). The analysis, which used all available fisheries data, shows that the biomass of top-level predators has not declined catastrophically in spite of the continuous increase in catches since the 1950s. The biomass of four stocks is greater than 74% of their unexploited potential, and the biomass of the remaining four stocks is 36 to 49% of the unexploited potential, as expected when the catch approaches MSY.

The biomass of several stocks of primary tuna and other top predators (*7*–*10*) has declined to MSY-associated levels. The ecosystem impact of such reductions is unknown, but model studies have shown that fishing all species in an ecosystem at mortality rates yielding single-species MSY may, under some conditions, lead to the erosion of trophic structure and depensa-

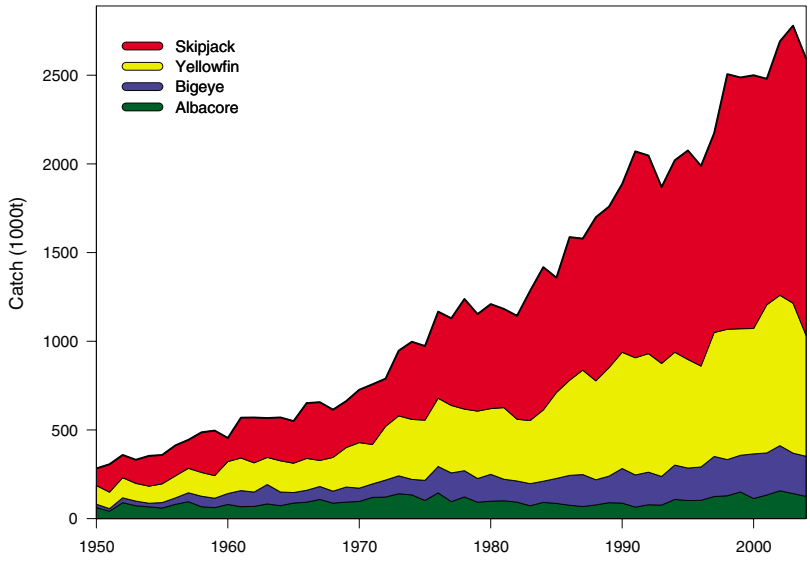

Fig. 1. Catches of major tuna species in the Pacific Ocean from 1950 through 2004 (*1*).

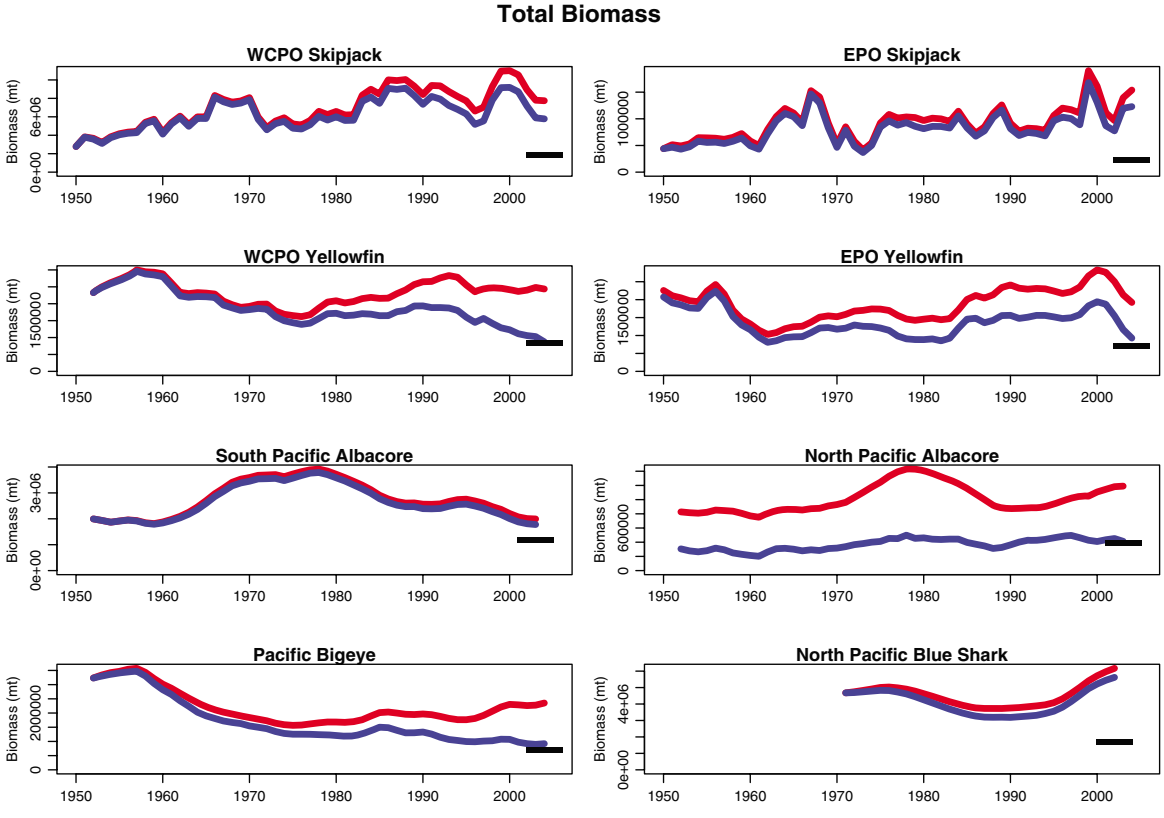

Fig. 2. Trends in total biomass for eight stocks of large predators in the Pacific Ocean, estimated from integrated stock assessment models. Blue lines indicate the biomass estimated from the observed fishing history (the exploited population), and red lines indicate the biomass estimated in the absence of all fishing (the unexploited population). The single black dash indicates the equilibrium biomass corresponding to MSY conditions, assuming current levels of recruitment and distribution of fishing mortality among fisheries. WCPO, western central Pacific Ocean; EPO, eastern Pacific Ocean.

tory effects on recruitment (*11*, *12*). MSY is, nevertheless, enshrined by many national and international fishery management agencies as the target level of catch to which fishery management aspires. More conservative, but ad hoc, reference points, such as maintaining adult populations above 50% of the unexploited adult biomass, may be more appropriate for an ecosystem approach to fisheries management (*13*).

Attempting to establish an unvarying initial reference point or baseline against which to evaluate changes in biomass is misleading. For example, the biomass of yellowfin in the eastern Pacific is currently about 2 times greater than the biomass at the beginning of the data time series, suggesting that the stock is in good condition. The exploited biomass is, however, only 49% of the unexploited biomass, and the current catch is near MSY (*14*). Expressing the impact of fishing as the ratio of exploited to unexploited biomass is a more sensitive indicator than comparison of current biomass to the biomass at some arbitrary date in the past at which the stock is assumed to be in a "pristine" or "virgin" state. The impact of the fishery is detectable in all stocks when the exploited-to-unexploited ratio is used.

The increase in the biomass of certain species, such as blue shark and skipjack, is a potentially important ecosystem response predicted by simple ecosystem models (*15*) and possibly attributable to a reduction in the biomass of other large predators. The possibility that the biomass of rapidly growing predators (such as *Coryphaena hippurus* and *Acanthocybium solandri*) may be also increasing should be examined. Unfortunately, complete fisheries statistics for these species are not available, and they rank low on the list of priority species for stock assessment in fishery management organizations.

Single-species assessment models do not explicitly include the effects of changes in the abundance of one species on the abundance of another. Until assessment models are able to simultaneously analyze multiple species, whether reduced abundance of larger fish has led to an increase in skipjack abundance will remain uncertain. In spite of this limitation, single-species stock assessments have an important role in the ecosystem approach to fisheries. Single-species assessment methods applied to nontarget species, such as blue shark, reveal potentially important ecosystem trends.

The results presented here appear to differ sharply from widely accepted views of the status of large oceanic predatory fish stocks and the ecosystem effects of fishing (*5*, *16*). Our results, however, should be interpreted as extensions of previous work, providing a more realistic (*17*–*22*) appraisal of the effects of fishing on the pelagic ecosystem. Our estimates of biomass trends interpret all available data from all major fishing fleets in the context of well-understood population dynamics processes. The analysis extends the concept of aggregating abundance across species (*5*) by summing biomass according to length across species, concluding that the biomass of fish smaller than 175 cm is near that predicted for stocks at full exploitation and that drastic declines in abundance are detectable only in fish larger than 175 cm. Furthermore, the analysis extends the concept of "shifting baseline" (*23*, *24*) by defining an empirical, quantitative reference base that depends directly on the activity being analyzed, concluding that although some predator populations have declined severely in response to fishing, others have increased. Finally, the analysis extends the notion of examining the impact of fisheries on the trophic level of the catch (*16*) by also examining the trophic level of the population at large, concluding that there is no impact on the trophic level of the population and that the apparent reduction in the trophic level of the catch is caused by the development of purse-seine fisheries targeting smaller tunas; that is, by "fishing through the food web" (*21*).

Fishery scientists have been warning of impending stock conservation problems in Pacific yellowfin and bigeye tuna in the western and central Pacific Ocean since 2001 (*25*), and the relatively depressed condition of the spawning populations of these two species has stimulated fishery managers to attempt to impose constraints on the fishery. The Western and Central Pacific Fisheries Commission and the Inter-American Tropical Tuna Commission have the responsibility to implement conservation regulations in the western and eastern Pacific Ocean, respectively. Scientists in both commissions have recommended management options, including catch and effort limits, restrictions on the use of artificial floating objects by the purse-seine fishery, and time and area closures, to maintain sustainable fisheries for these species on both sides of the Pacific (*26*, *27*). Unfortunately, these options have not been fully implemented, and decreases in fishing mortality have not yet been realized. Commissioners and national delegations to these commissions need to implement effective conservation measures before stocks reach a state where draconian measures, such as complete closures, are required to preserve the fishery and sustain the ecosystem.

Table 1. Comparison of estimated impacts of fishing computed as the ratio of estimated exploited biomass to the estimated unexploited biomass in the last year of the analysis (exploited/unexploited) and as the ratio of estimated exploited biomass in the last year to that in the first year (biomass ratio).

Stock	Exploited/unexploited		Biomass ratio	
	Total	Adult	Total	Adult
North Pacific albacore	0.38	0.12	1.34	0.94
Pacific bigeye	0.39	0.26	0.28	0.19
WCPO yellowfin	0.36	0.27	0.37	0.30
EPO yellowfin	0.49	0.41	2.12	2.27
North Pacific blue shark	0.91	0.89	1.20	1.16
WCPO skipjack	0.74	0.70	2.08	1.84
EPO skipjack	0.79	0.77	2.79	3.12
South Pacific albacore	0.89	0.83	0.89	0.91

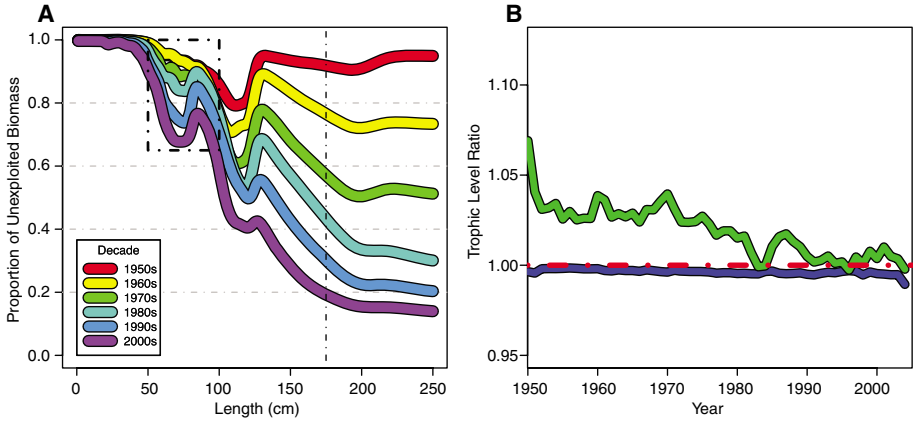

Fig. 3. Two ecosystem indicators of the effects of fishing. (**A**) Impact of fishery on size. The ratio of exploited to unexploited biomass at increasing fork lengths by decade from 1950 through 2004 for all tuna stocks is shown. The dashed box indicates the size range of skipjack caught by the purse-seine fishery. The vertical dashed line indicates 175 cm fork length. (**B**) Impact of fishery on the trophic level of exploited tuna biomass and catch. The blue line is the ratio of the trophic level of exploited biomass to the trophic level of the unexploited biomass, and the green line is the ratio of the trophic level of the catch to the trophic level of the unexploited biomass. The dashed red line indicates 1.0, the relative trophic level in the unexploited biomass.

References and Notes

1. T. Lawson, Ed., *Western And Central Pacific Fisheries Commission Tuna Fishery Yearbook* (Western and Central Pacific Fisheries Commission, Pohnpei, Federated States of Micronesia, 2004), available at www.spc.int/oceanfish/Docs/Statistics/TYB.htm.
2. Background material and analytical methods are available as supporting material on *Science* Online.
3. The "exploited" biomass is defined here as the biomass of the population estimated by the assessment model. The "unexploited" biomass is defined as the biomass that might have existed in the absence of fishing, estimated by setting the fishing mortality parameters to zero in the model. The unexploited population trajectories include the estimated effects of temporal variability in recruitment on the dynamics of the populations, thus incorporating environmental constraints that occurred during the history of the fishery and the estimated effect of the additional recruitment resulting from a larger spawning biomass (*2*).
4. A. Longhurst, *Fish. Res.* **81**, 107 (2006).
5. R. Myers, B. Worm, *Nature* **423**, 280 (2003).
6. M. Labelle, *Fish. Res.* **71**, 311 (2005).
7. P. Kleiber, M. Hinton, Y. Uozumi, *Mar. Freshw. Res.* **54**, 349 (2003).
8. M. Labelle, NOAA Technical Memorandum *NOAA-TM-NMFS-SWFSC-341* (U.S. Department of Commerce, Washington, DC, 2002).
9. M. Hinton, W. Bayliff, *Inter-American Tropical Tuna Commission Stock Assessment Report* **3**, 328 (2002).
10. W. Bayliff, *Inter-American Tropical Tuna Commission Stock Assessment Report* **2**, 247 (2002).
11. C. Walters, V. Christensen, S. Martell, J. Kitchell, *ICES J. Mar. Sci.* **62**, 558 (2005).
12. S. Hall, J. Collie, D. Duplisea, M. Bravington, J. Link, *Can. J. Fish. Aquat. Sci.* **63**, 1344 (2006).
13. C. Walters, J. Kitchell, *Can. J. Fish. Aquat. Sci.* **58**, 39 (2001).
14. S. Hoyle, M. Maunder, *Inter-American Tropical Tuna Commission Stock Assessment Report* **6**, 3 (2005).
15. J. Hinke *et al.*, *Ecol. Soc.* **9**, 10 (2004).
16. D. Pauly, V. Christensen, J. Dalsgaard, R. Froese, F. Torres, *Science* **279**, 860 (1998).
17. J. Hampton, J. Sibert, P. Kleiber, M. Maunder, S. Harley, *Nature* **434**, E1 (2005).
18. T. Polacheck, *Mar. Policy* **30**, 470 (2006).
19. G. Burgess *et al.*, *Fisheries* **30**, 206 (2005).
20. C. Walters, *Can. J. Fish. Aquat. Sci.* **60**, 1433 (2003).
21. T. Essington, A. Beaudreau, J. Wiedenmann, *Proc. Natl. Acad. Sci. U.S.A.* **103**, 3171 (2006).
22. M. Maunder *et al.*, *ICES J. Mar. Sci.* **63**, 1373 (2006).
23. D. Pauly, *Trends Ecol. Evol.* **10**, 430 (1995).
24. J. Jackson *et al.*, *Science* **293**, 629 (2001).
25. *Report of the Fourteenth Meeting of the Standing Committee on Tuna and Billfish* (Secretariat of the Pacific Community, Noumea, New Caledonia, 2001), available at www.spc.int/oceanfish/Html/SCTB/SCTB14/sctb14rep.pdf.
26. J. Hampton *et al.*, *Estimates of Sustainable Catch and Effort Levels for Target Species and the Impacts on Stocks of Potential Management Measures* (WCPFC–SC1 Working Paper SA-WP–10, Western and Central Pacific Fisheries Commission, Pohnpei, Federated States of Micronesia, 2005), available at http://wcpfc.org/sc1/pdf/SC1_SA_WP_10.pdf.
27. M. Maunder, S. Harley, *Bull. Mar. Sci.* **78**, 593 (2006).

28. We thank our colleagues P. Crone, S. Hoyle, A. Langley, M. Ogura, Y. Takeuchi, M. Ichinokawa, and P. Williams, who assembled the data and conducted the stock assessments on which our synthesis is based; B. Bayliff, H. Dewar, G. Dinardo, K. Holland, K. Mason, C. Walters, G. Watters, and three anonymous reviewers for constructive comments on previous drafts of this paper; and D. Fournier for his work in creating the MULTIFAN-CL stock assessment method. This work was funded by Cooperative Agreement NA17RJ1230 between the Joint Institute for Marine and Atmospheric Research and the National Oceanic and Atmospheric Administration, by members of the Secretariat of the Pacific Community and its donor agencies, and by members of the Inter-American Tropical Tuna Commission. Views expressed in the paper do not necessarily represent the views of these agencies, their subagencies, or their member countries.

Supporting Online Material

www.sciencemag.org/cgi/content/full/314/5806/1773/DC1
Materials and Methods
SOM Text
Figs. S1 to S7
Tables S1 to S3
References and Notes

20 September 2006; accepted 8 November 2006
10.1126/science.1135347

A Secreted Serine-Threonine Kinase Determines Virulence in the Eukaryotic Pathogen *Toxoplasma gondii*

S. Taylor,[1]* A. Barragan,[1,2]* C. Su,[1,3]* B. Fux,[1] S. J. Fentress,[1] K. Tang,[1] W. L. Beatty,[1] H. El Hajj,[4] M. Jerome,[5] M. S. Behnke,[5] M. White,[5] J. C. Wootton,[6] L. D. Sibley[1]†

Toxoplasma gondii strains differ dramatically in virulence despite being genetically very similar. Genetic mapping revealed two closely adjacent quantitative trait loci on parasite chromosome VIIa that control the extreme virulence of the type I lineage. Positional cloning identified the candidate virulence gene *ROP18*, a highly polymorphic serine-threonine kinase that was secreted into the host cell during parasite invasion. Transfection of the virulent *ROP18* allele into a nonpathogenic type III strain increased growth and enhanced mortality by 4 to 5 logs. These attributes of ROP18 required kinase activity, which revealed that secretion of effectors is a major component of parasite virulence.

Toxoplasma gondii is a widespread protozoan parasite that chronically infects ~25% of the world's human population (*1*). *T. gondii* is dominated by three widespread, clonal lineages, which rapidly expanded following a severe genetic bottleneck ~10,000 years ago (*2*, *3*). Despite ~98% genetic identity, dramatic differences in virulence exist between *T. gondii* strains (*4*). Type I strains cause lethal infection in all strains of laboratory mice even at low inocula [lethal dose (LD_{100}) ≈ 1] (*4*, *5*), whereas types II and III strains are much less virulent [median lethal dose (LD_{50}) ≥ 10^3] (*4*). Acute virulence is associated with rapid dissemination, high parasite burdens, and overproduction of T helper cell type 1 cytokines (*6*, *7*). Toxoplasmosis has primarily been associated with type II strains, whereas type III strains are rarely associated with disease (*8*, *9*). Although less prevalent, type I can cause severe congenital infections (*10*), ocular toxoplasmosis (*11*, *12*), and encephalitis in AIDS patients (*13*). Acute virulence of *T. gondii* in the mouse model is genetically determined (*14*), although the genes involved in this phenotype are unknown.

The extreme linkage disequilibrium of *T. gondii* populations (*4*, *9*) limits the use of association or population-based studies for identifying virulence genes. Therefore, we used forward genetic mapping to identify genes that determine natural differences in virulence. The recently completed genome map of the 14 chromosomes of the *T. gondii* ~65-megabase haploid genome provided a framework for quantitative trait locus (QTL) mapping with 175 informative genetic markers (*15*, *16*). Genomewide QTL mapping was used to analyze the genetic basis of acute virulence in 34 independent progeny from a genetic cross between the virulent type I strain GT-1 and the nonvirulent type III strain CTG (*14*). These parental strains differ in a number of virulence-related phenotypes including (i) migration under soft agarose, (ii) transmigration across polarized epithelia, (iii) intracellular replication, (iv) acute mortality in the mouse model, and (v) serum response of animals surviving low-dose infection (*17*).

Toxoplasma gondii and related apicomplexan parasites actively invade mammalian cells by using actin-based motility (*18*), which also enables passage across polarized epithelia and through tissues. Migration is enhanced in type I strains, and this may contribute to dissemination and, hence, acute virulence (*19*). In the present study, migration was monitored with two in vitro assays: migration under soft agarose and transmigration across polarized epithelia (*17*, *19*). The progeny from the cross showed correlated responses for migration (MIG) and transmigra-

[1]Department of Molecular Microbiology, Washington University School of Medicine, St. Louis, MO 63130, USA. [2]Swedish Institute for Infectious Disease Control and Center for Infectious Medicine, Department of Medicine, Karolinska Institutet, 141 86 Stockholm, Sweden. [3]Department of Microbiology, University of Tennessee, Knoxville, TN 37996, USA. [4]Unité Mixte de Recherche (Joint Research Unit) CNRS 5539, University Montpellier 2, Place Eugene Bataillon, 34095 Montpellier Cedex 5, France. [5]Department of Veterinary Molecular Biology, Montana State University, Bozeman, MT 59717, USA. [6]Computational Biology Branch, National Center for Biotechnology Information, National Institutes of Health, Bethesda, MD 20894, USA.

*These authors contributed equally to this work.
†To whom correspondence should be addressed. E-mail: sibley@borcim.wustl.edu

tion (TM) ($r = 0.75$ linear regression) that ranged from low levels like those of type III to levels that exceeded the type I parent (Fig. 1, A and B, and table S1).

Acute mortality (MOR) of the progeny was tested in outbred CD1 mice challenged with different doses of parasites by intraperitoneal (i.p.) inoculation (*17*). Although the type III parental strain demonstrated very low cumulative mortality [defined as the number of deaths per number of animals infected (*17*)], type I was uniformly lethal, even at low inocula (Fig. 1C and table S1). Consistent with a multigenic trait, mortality caused by the progeny clones ranged from low levels to 100% (Fig. 1C and table S1). Animals that survived challenge were subsequently tested for serological responses to parasite antigens by Western blot (*14*, *17*). Serum responses (SER) fell into three distinct categories: negative (not infected), weak positive, and strong positive (Fig. 1C and fig. S1). Intracellular growth (GRO) rates for individual progeny (*17*) were correlated with virulence (table S1), which is consistent with previous observations of the parental lines (*20*).

Genomewide scans were used to locate QTLs in the parasite genome that control these quantitative traits (*17*). Remarkably, a single strong primary association was detected for each of the MIG, TM, MOR, and SER phenotypes, which were clustered at the same region of parasite chromosome VIIa (chr VIIa) ($P < 0.001$) (Fig. 2A). A major component of GRO also mapped to the same segment of chr VIIa, although with lesser statistical significance (Fig. 2A). Secondary associations for MOR and SER were also noted on chr Ia, and for GRO on chr XI and XII (Fig. 2A) (*17*). Analyses of two-locus interactions for SER and MOR showed a significant interaction only for the QTLs on VIIa and Ia (Fig. 2A). When we controlled for the major QTL for MOR/SER statistically (*17*), secondary scans did not reveal any other major peaks contributing to these phenotypes. The extremely strong support for the highly clustered QTLs on chr VIIa indicates that a few closely linked genes determine virulence.

Fine mapping of the QTLs on chr VIIa was aided by isolation of additional recombinant progeny (*17*). The primary MOR/SER QTL mapped to a region spanning the CS3 to ST3921 markers with a peak at marker ST3921 (Fig. 2B and table S2). MIG and TM mapped to a broad region of chr VIIa between genetic markers CS12 and CS11 (Fig. 2B), with a peak at markers ST4000 and ST1107 that lie within 28 kilobases (kb) of each other (table S2). Smaller secondary peaks were also observed for MIG and TM, and these partially overlapped with the major SER/MOR QTL (Fig. 2B). These findings indicate that a broad QTL on chr VIIa contributes to MIG/TM, and a second sharper QTL controls MOR/SER (Fig. 2B).

Pinning the QTLs to the sequenced genome scaffolds identified corresponding genomic regions and candidate genes that may control these phenotypes (Fig. 2B and table S2). The MIG/TM QTL contains several excellent candidate genes that may mediate enhanced migration, including two formin homology domain proteins, a calcium-dependent protein kinase (CDPK), and a unique myosin VI–like gene known as MyoK (table S2). The traits MOR/SER map to a distinct QTL of 140 kb containing 21 genes (Fig. 2B and table S2), representing a 10-fold improvement in resolution over previous mapping of this QTL (*14*). Analysis of the 21 genes in this region with the extensive expressed sequence tag (EST) database for *T. gondii* (*21*, *22*) revealed that only *ROP18* contained abundant type I polymorphisms. ROP18 is a member of a family of parasite proteins that are secreted from apical organelles called rhoptries (*23*). The type III and type I alleles of ROP18 differed at 78 positions in a total of 541 residues (~14%) (fig. S2A), compared with the typical ~1% divergence between lineages (*2*, *3*). Microarray and quantitative real-time fluorescence polymerase chain reaction (QPCR) analyses indicated that only *ROP18* showed significant differences in expression; type III was almost undetectable

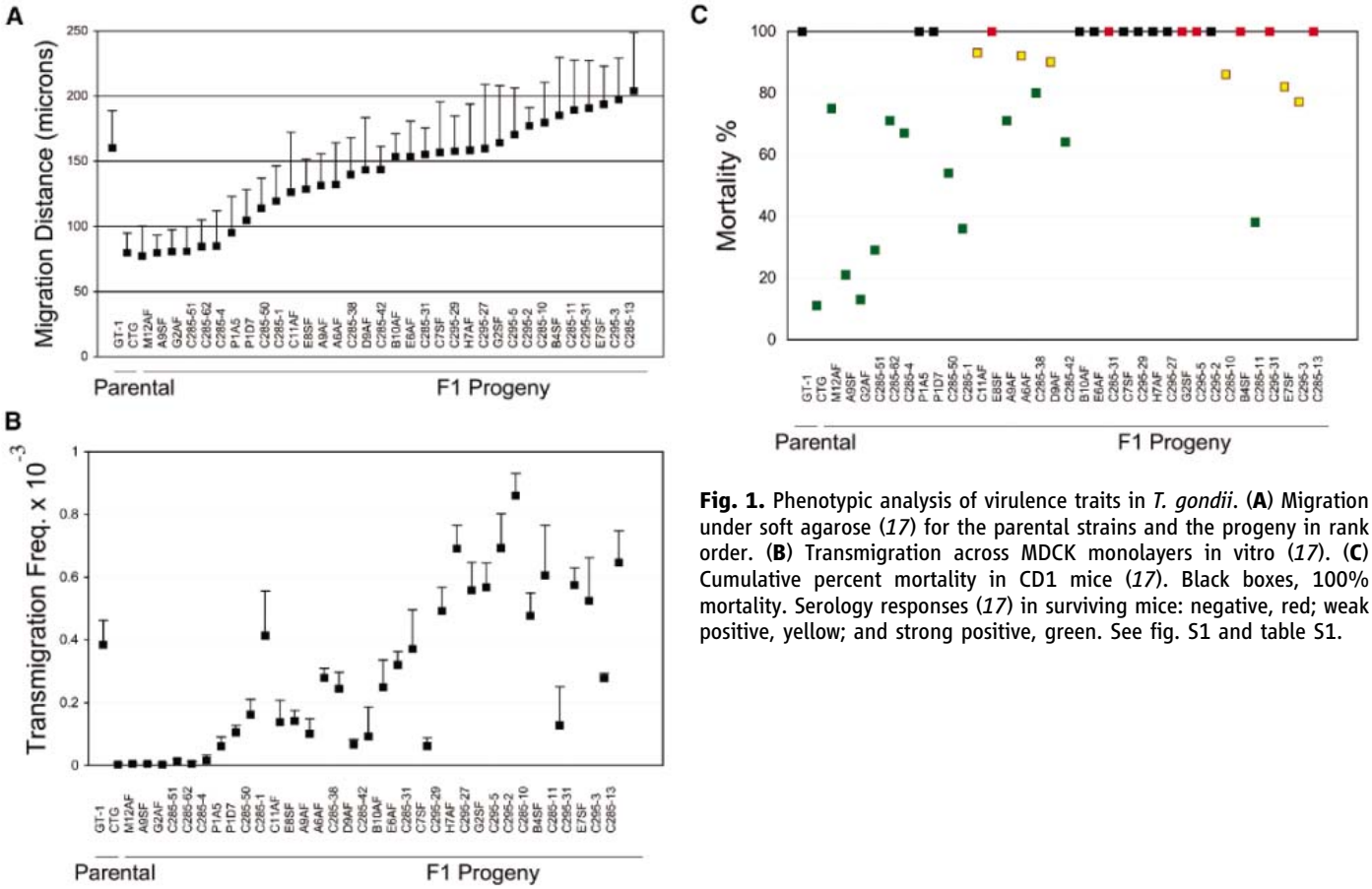

Fig. 1. Phenotypic analysis of virulence traits in *T. gondii*. (**A**) Migration under soft agarose (*17*) for the parental strains and the progeny in rank order. (**B**) Transmigration across MDCK monolayers in vitro (*17*). (**C**) Cumulative percent mortality in CD1 mice (*17*). Black boxes, 100% mortality. Serology responses (*17*) in surviving mice: negative, red; weak positive, yellow; and strong positive, green. See fig. S1 and table S1.

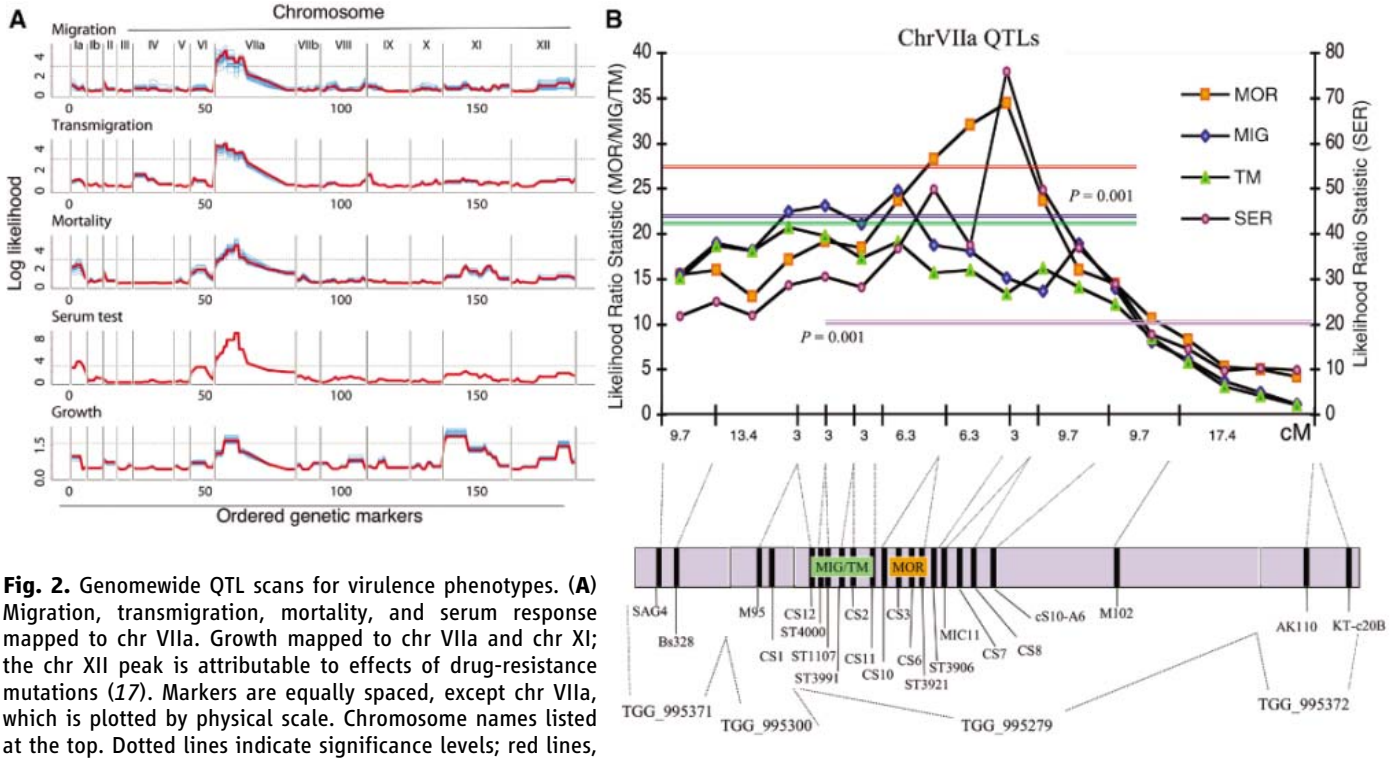

Fig. 2. Genomewide QTL scans for virulence phenotypes. (**A**) Migration, transmigration, mortality, and serum response mapped to chr VIIa. Growth mapped to chr VIIa and chr XI; the chr XII peak is attributable to effects of drug-resistance mutations (*17*). Markers are equally spaced, except chr VIIa, which is plotted by physical scale. Chromosome names listed at the top. Dotted lines indicate significance levels; red lines, log likelihood plots; blue lines, 95% confidence intervals (*17*). (**B**) Fine mapping of QTLs on chr VIIa and positioning on the genome scaffolds. Mortality (MOR) and serum response (SER) showed an overlapping peak at CS3 to ST3921. MIG and TM mapped to a broad region with a peak at ST4000 to ST1170. Markers (black bars) are listed below the sequenced genome scaffolds (gray rectangles with TGG scaffold numbers) and their corresponding positions are shown in centimorgans on the *x* axis.

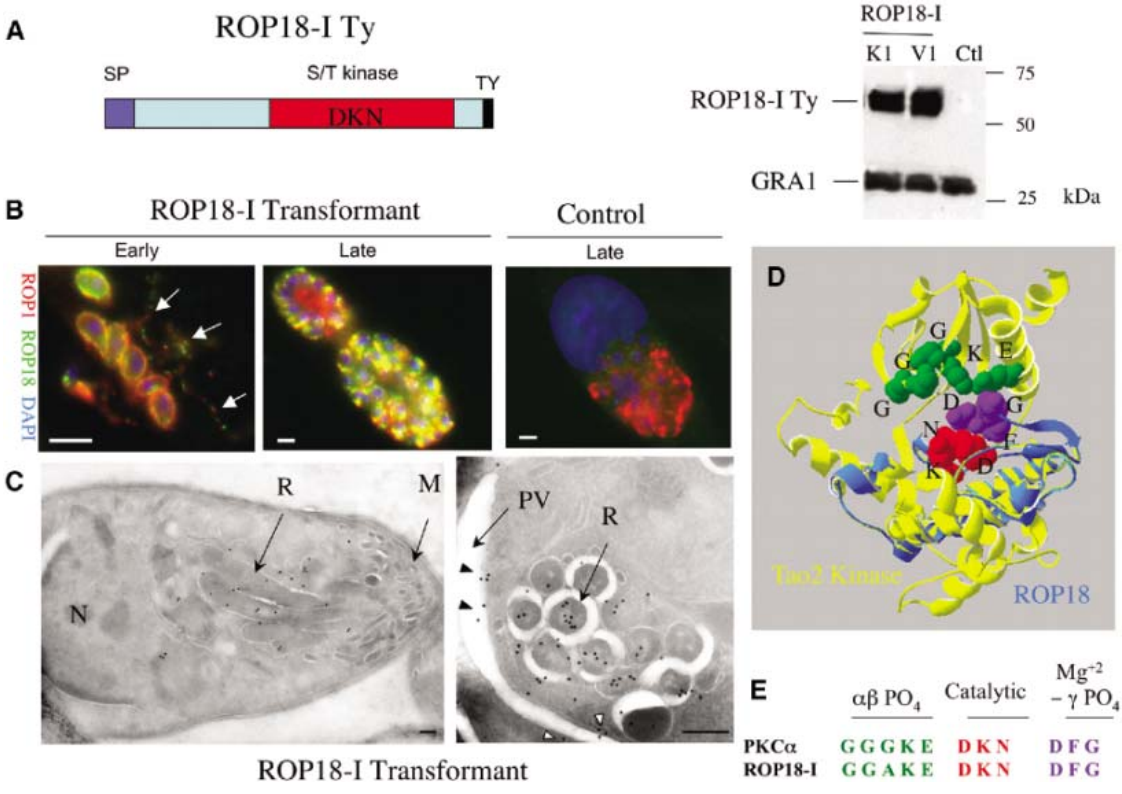

Fig. 3. Localization and homology modeling of ROP18 in *T. gondii*. (**A**) Diagram of ROP18-I Ty construct. Western blot analysis of ROP18-I transformant clones (K1, V1) versus control transformant (Ctl) (*17*). (**B**) Immunofluorescence localization of ROP18-I in transformant (V1 clone) vs. control (*17*). ROP18-I (green) was secreted into early PVs and into vesicles in the cytosol (arrows). In late PVs, ROP18-I accumulated in the rhoptries of mature daughter cells. Rhoptry marker ROP1 (red), nuclei stained with DAPI (4′,6′-diamidino-2-phenylindole) (blue). Scale bars, 5 μm. (**C**) Immuno–electron microscopy localization of ROP18-I in rhoptries (R) but not micronemes (M) or the nucleus (N) (*17*). ROP18-I was secreted into the PV (arrowheads in right image). Scale bars, 200 nm. (**D**) Homology model of ROP18-I (blue) based on Tao2 kinase (yellow) (*17*). (**E**) Conserved active site residues in PKCα and ROP18-I kinase domains.

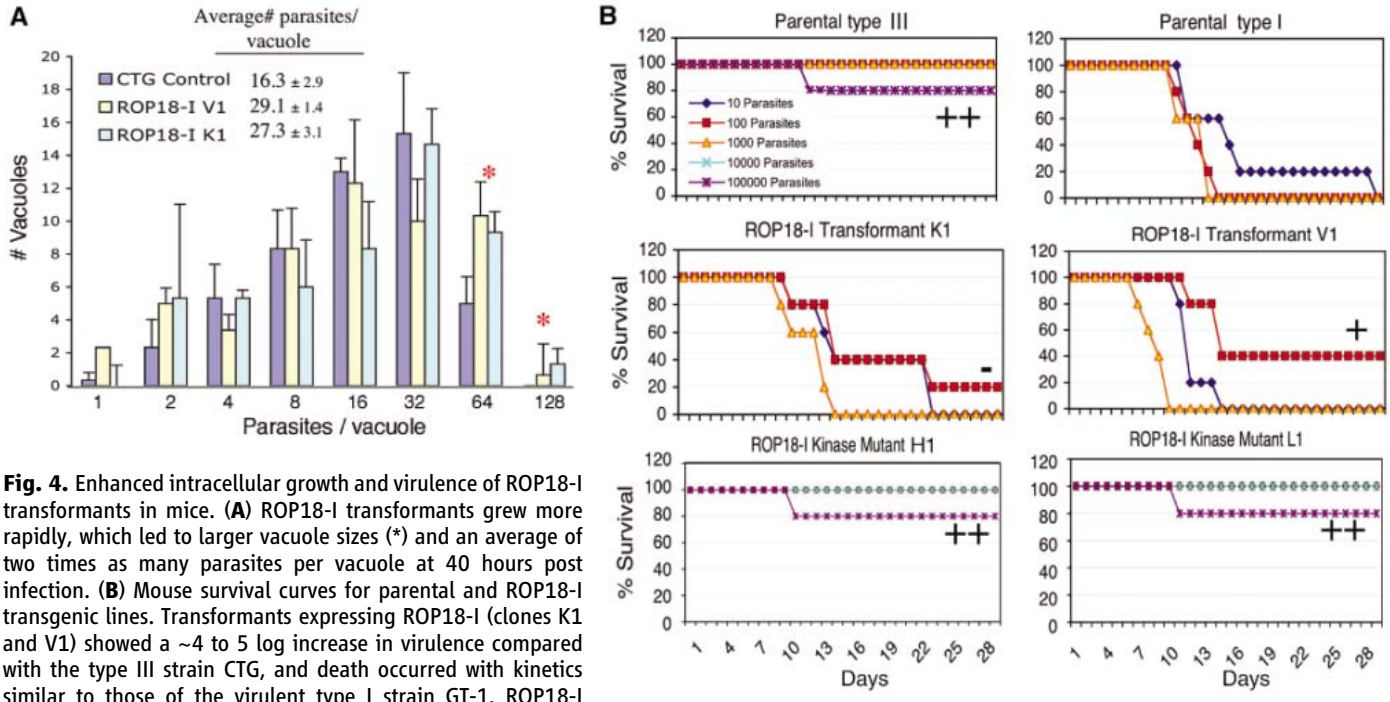

Fig. 4. Enhanced intracellular growth and virulence of ROP18-I transformants in mice. (**A**) ROP18-I transformants grew more rapidly, which led to larger vacuole sizes (*) and an average of two times as many parasites per vacuole at 40 hours post infection. (**B**) Mouse survival curves for parental and ROP18-I transgenic lines. Transformants expressing ROP18-I (clones K1 and V1) showed a ~4 to 5 log increase in virulence compared with the type III strain CTG, and death occurred with kinetics similar to those of the virulent type I strain GT-1. ROP18-I kinase mutants (Asp^{394}Ala) (clones H1, L1) remained avirulent. Serological responses in survivors: negative (–), weak positive (+), strong positive (++).

relative to type I (fig. S2, B and C). The high polymorphism and dramatic difference in expression indicate that ROP18 is the basis for the dramatic difference in acute virulence.

To evaluate the contribution of ROP18 to virulence, we expressed an epitope-tagged copy of the type I allele (*ROP18-I*) in the wild-type III strain CTG, which effectively provides a null background. Two transformants expressing Ty epitope–tagged ROP18-I were selected for comparison with a control expressing only the selectable marker (Fig. 3A). QPCR revealed that *ROP18-I* was expressed in the transgenic lines at levels comparable to those of the wild-type I strain (fig. S2C). Ty epitope–tagged ROP18-I was found in early parasitophorous vacuoles (PVs), where it overlapped with the rhoptry marker ROP1, and in vesicular structures in the host cell cytosol (Fig. 3B, arrows). Cryoimmuno–electron microscopy confirmed that ROP18 was found in rhoptries and released into the PV (Fig. 3C and fig. S3). In the presence of cytochalasin D, which allows apical secretion but blocks parasite entry (*17*, *24*), ROP18-I was secreted abundantly into the host cell cytosol (fig. S4), as are other rhoptry proteins (*24*). Previous studies have indicated that ROP2 (*25*) and ROP5 (*26*) are exposed to the host cell cytosol, which suggests that after secretion into the host cell and targeting to the PV, ROP18 is also in direct contact with the host cell.

To evaluate the contribution of ROP18 to growth, we measured the intracellular replication of ROP18-I transformants in vitro. Expression of ROP18-I in the slower-growing type III CTG strain led to a twofold increase in the average number of parasites per vacuole (Fig. 4A). When extrapolated over an 8- to 10-day period, this difference could account for the much higher tissue burdens following in vivo infection with virulent type I strains (*6*, *7*). Consistent with this, challenge of outbred CD1 mice with CTG transformants expressing ROP18-I revealed a 4 to 5 log increase in virulence when compared with the wild-type III CTG strain (Fig. 4B). Collectively, these results establish that expression of the type I allele of ROP18 in the nonvirulent type III background is sufficient for conferring acute virulence of *T. gondii*. In an accompanying report, Saeij *et al*. demonstrate that ROP18 also contributes to differences in pathogenesis between the less-virulent type II and III strains.

ROP18 is related to the ROP2 subfamily of rhoptry proteins that share a conserved serine-threonine protein kinase domain (*27*). All of the conserved residues important for serine-threonine kinase activity are present in ROP18 and homology modeling revealed that ROP18 contains a typical kinase domain fold, complete with a highly conserved catalytic active site (*17*), similar to the serine-threonine kinases Tao2 and protein kinase Cα (PKCα) (Fig. 3, D and E). To test the role of kinase activity in the phenotype conferred by ROP18, a point mutation disrupting kinase activity (Asp^{394}Ala) (*28*) was expressed as a stable transgene in *T. gondii* (fig. S5). Type III transformants carrying the Asp^{394}Ala mutation of ROP18-I did not show enhanced growth and remained avirulent (Fig. 4B), which demonstrated that ROP18 requires kinase activity for mediating enhanced virulence. Although all three alleles of ROP18 contain the highly conserved active-site residues, the type III allele contains significant changes that may alter substrate binding, regulation, or activity (fig. S2A).

Collectively, our data suggest that, after secretion into the host cell, ROP18 kinase acts on a cellular target to enhance parasite infection. Consequently, ROP18 is a prime candidate for mediating previously reported alterations in host cell signaling (*29*), prevention of apoptosis (*30*), and altered gene expression (*31*), in *T. gondii*–infected cells. Although ROP18 is the major factor controlling acute mortality, ROP18-I transformants did not show enhanced migration (fig. S6), which indicates that other nearby genes mediate this phenotype. The close linkage of these QTLs on chr VIIa is consistent with coadaptation. In the current highly clonal *T. gondii* population structure (*2*, *3*), these coinherited QTLs may underpin the shared acute virulence of type I strains and may also contribute to pathogenesis in strains with mixed or exotic genotypes, which have been implicated in severe ocular toxoplasmosis (*11*, *12*).

Our findings identify a major role for ROP18 in mediating pathogenesis in *T. gondii* and suggest that both expression level and allelic differences contribute to acute virulence. Conserved serine-threonine kinase domains are found in a variety of other rhoptry proteins in *T. gondii* (*27*) and also in secretory proteins in *Plasmodium* (*32*), which implicates secretion of effector proteins into the host cell as a general mechanism of virulence in eukaryotic pathogens.

References and Notes

1. D. H. Joynson, T. J. Wreghitt, *Toxoplasmosis: A Comprehensive Clinical Guide* (Cambridge Univ. Press, Cambridge, 2001).

2. M. E. Grigg, S. Bonnefoy, A. B. Hehl, Y. Suzuki, J. C. Boothroyd, *Science* **294**, 161 (2001).
3. C. Su *et al.*, *Science* **299**, 414 (2003).
4. L. D. Sibley, J. C. Boothroyd, *Nature* **359**, 82 (1992).
5. D. K. Howe, B. C. Summers, L. D. Sibley, *Infect. Immun.* **64**, 5193 (1996).
6. D. G. Mordue, F. Monroy, M. La Regina, C. A. Dinarello, L. D. Sibley, *J. Immunol.* **167**, 4574 (2001).
7. L. C. Gavrilescu, E. Y. Denkers, *J. Immunol.* **167**, 902 (2001).
8. J. C. Boothroyd, M. E. Grigg, *Curr. Opin. Microbiol.* **5**, 438 (2002).
9. D. K. Howe, L. D. Sibley, *J. Infect. Dis.* **172**, 1561 (1995).
10. I. Fuentes, J. M. Rubio, C. Ramírez, J. Alvar, *J. Clin. Microbiol.* **39**, 1566 (2001).
11. M. E. Grigg, J. Ganatra, J. C. Boothroyd, T. P. Margolis, *J. Infect. Dis.* **184**, 633 (2001).
12. A. Khan *et al.*, *Emerg. Infect. Dis.* **12**, 942 (2006).
13. A. Khan *et al.*, *J. Clin. Microbiol.* **43**, 5881 (2005).
14. C. Su, D. K. Howe, J. P. Dubey, J. W. Ajioka, L. D. Sibley, *Proc. Natl. Acad. Sci. U.S.A.* **99**, 10753 (2002).
15. Toxoplasma genome map, http://toxomap.wustl.edu/.
16. A. Khan *et al.*, *Nucleic Acids Res.* **33**, 2980 (2005).
17. Materials and methods are available as supporting material on *Science* online.
18. L. D. Sibley, *Science* **304**, 248 (2004).
19. A. Barragan, L. D. Sibley, *J. Exp. Med.* **195**, 1625 (2002).
20. J. R. Radke *et al.*, *Mol. Biochem. Parasitol.* **115**, 165 (2001).
21. *Toxoplasma gondii* genome resource, http://ToxoDB.org.
22. J. C. Kissinger, B. Gajria, L. Li, I. T. Paulsen, D. S. Roos, *Nucleic Acids Res.* **31**, 234 (2003).
23. P. J. Bradley *et al.*, *J. Biol. Chem.* **280**, 34245 (2005).
24. S. Håkansson, A. J. Charron, L. D. Sibley, *EMBO J.* **20**, 3132 (2001).
25. C. J. M. Beckers, J. F. Dubremetz, O. Mercereau-Puijalon, K. A. Joiner, *J. Cell Biol.* **127**, 947 (1994).
26. H. El Hajj, M. Lebrun, M. N. Fourmaux, H. Vial, J. F. Dubremetz, *Cell. Microbiol.*, published online 31 July 2006 (10.1111/j.1462-5822.2006.00767.x), in press.
27. H. El Hajj *et al.*, *Proteomics* **6**, 5773 (2006).
28. H. El Hajj *et al.*, *PLoS Pathogens*, in press.
29. E. Y. Denkers, B. A. Butcher, L. Del Rio, L. Kim, *Immunol. Rev.* **201**, 191 (2004).
30. C. G. Luder, U. Gross, *Curr. Top. Microbiol. Immunol.* **289**, 219 (2005).
31. I. J. Blader, I. D. Manger, J. C. Boothroyd, *J. Biol. Chem.* **276**, 24223 (2001).
32. C. Doerig, O. Billker, D. Pratt, J. Endicott, *Biochim. Biophys. Acta* **1754**, 132 (2005).

33. Preliminary genomic and/or cDNA sequence data generated by The Institute for Genomic Research or the Sanger Center was accessed via http://ToxoDB.org. We are grateful for the contributions of J. Ajioka, J.–F. Dubremetz, S, Håkansson, E. Groisman, I. Paulsen, D. Roos, A. Schaffer, and J. Suetterlin. Supported by the NIH (AI36629, AI059176, AI44600, and Centers of Biomedical Research Excellence (COBRE), National Centers for Research Resources P20 RR-020185), the intramural program of National Center for Biotechnology Information at NIH, the Burroughs Welcome Fund, the Swedish Research Council, and the Swedish Foundation for Strategic Research. The GenBank accession number for the *ROP18-III* allele is ABI35958.

Supporting Online Material

www.sciencemag.org/cgi/content/full/314/5806/1776/DC1
Materials and Methods
Figs. S1 to S6
Tables S1 to S3
References and Notes

9 August 2006; accepted 3 November 2006
10.1126/science.1133643

Polymorphic Secreted Kinases Are Key Virulence Factors in Toxoplasmosis

J. P. J. Saeij,[1]* J. P. Boyle,[1]* S. Coller,[1] S. Taylor,[2] L. D. Sibley,[2] E. T. Brooke-Powell,[3] J. W. Ajioka,[3] J. C. Boothroyd[1]†

The majority of known *Toxoplasma gondii* isolates from Europe and North America belong to three clonal lines that differ dramatically in their virulence, depending on the host. To identify the responsible genes, we mapped virulence in F_1 progeny derived from crosses between type II and type III strains, which we introduced into mice. Five virulence (*VIR*) loci were thus identified, and for two of these, genetic complementation showed that a predicted protein kinase (ROP18 and ROP16, respectively) is the key molecule. Both are hypervariable rhoptry proteins that are secreted into the host cell upon invasion. These results suggest that secreted kinases unique to the Apicomplexa are crucial in the host-pathogen interaction.

Toxoplasma gondii is an obligate intracellular parasite capable of infecting a wide variety of warm-blooded animals. Infections are widespread in humans and can lead to severe disease in utero or in individuals with a suppressed immune system. The majority of European and North American isolates belong to three distinct clonal lines, referred to as types I, II, and III (*1*, *2*). Types I and III appear to be the result of just one or two matings between an ancestral type II strain and, respectively, one or other of a pair of closely related strains that are distinct from type II (*3*–*6*). The three major *Toxoplasma* lines differ in a number of phenotypes (*7*), the best described of which is virulence in mice: type I strains are the most virulent with a lethal dose (LD_{100}) of one parasite (*8*, *9*), whereas types II and III have values for median lethal dose (LD_{50}) that range from 10^2 to 10^5. There may also be differences in the virulence of the three strains in humans (*10*–*12*).

Previously (*3*), we demonstrated that a cross between a type II and a type III strain produced F_1 progeny (S23 and CL11) that were more virulent (up to 3 logs) than 14 of their siblings (*3*). Because only two of the 16 progeny showed this difference, it was likely that multiple loci controlled virulence in these strains, and to identify these loci, we phenotyped 23 additional recombinant F_1 progeny from II × III crosses (*13*, *14*). Progeny with high virulence were identified by infecting mice with 100 tachyzoites; progeny with very low virulence were identified by infecting mice with 100,000 parasites.

The parental type III clone was significantly less virulent than the parental type II clone, and among the recombinant progeny, a range of distinct phenotypes was observed (table S1). Injection of 100 parasites of some progeny (including strain S23 described above) resulted in uniform acute mortality in mice. There was also a large class of avirulent clones, unable to kill mice even when injected at the high dose (100,000) (table S1). The log-likelihood of association of virulence phenotypes with genetic markers was analyzed for three different phenotypes: (i) "high-dose survivability" ($\log_{10}$ of the survival time after injection of 100,000 parasites); (ii) "avirulence," a binary trait defined as no mortality at any dose; and (iii) "low-dose survivability" ($\log_{10}$ of the survival time after injection of 100 parasites). In the initial genome scan (*15*), two quantitative trait loci (QTLs) were identified: one that was highly significant at the left end of chromosome XII (*VIR1*) and one of borderline significance on chromosome X (*VIR2*) (Fig. 1A). A high logarithm of odds (LOD) score in such analyses, as seen for the chromosome XII QTL, can obscure the contribution of other loci, especially when the number of progeny being analyzed is limited. When the variance associated with the QTL at the beginning of chromosome XII was fixed as a covariate, three additional QTLs emerged as significant (Fig. 1B): one each on chromosomes VIIa (*VIR3*), VIIb (*VIR4*), and toward the right end of chromosome XII (*VIR5*). (See table S2 for a complete summary of all QTLs and their effects.)

Although the genomic regions spanned by the detected QTLs are large [~1 megabase (Mb)], we identified candidate genes on the basis of predicted coding function (*16*, *17*), amount of polymorphism (*5*), and gene expression information [expressed sequence tags (EST) frequencies (*18*) and microarray data (this study)]. Of par-

[1]Department of Microbiology and Immunology, Stanford University School of Medicine, Stanford, CA 94305, USA. [2]Department of Molecular Microbiology, Washington University School of Medicine, St. Louis, MO 63110, USA. [3]Department of Pathology, Cambridge University, Cambridge, CB2 1QP, UK.

*These authors contributed equally to this work.
†To whom correspondence should be addressed. E-mail: john.boothroyd@stanford.edu

ticular interest were polymorphic genes whose products were predicted to interact with the host (i.e., expected to be secreted into and/or beyond the parasitophorous vacuole) and with differences in expression between the type II and type III strains.

The *VIR3* QTL spans a maximum of ~1.1 Mb within which there are 140 predicted proteins (*16*, *17*). *ROP18* stood out as the strongest candidate gene within this interval for a number of reasons. First, it has high homology to the ROP2 family of serine-threonine protein kinases in *Toxoplasma*, which are released from specialized apical secretory organelles, called rhoptries, that are unique to the Apicomplexa. Second, ROP18 was previously identified in our laboratory as part of the rhoptry proteome [ROP2L2 of (*19*)] and has recently been confirmed to be a functional kinase (*20*) that ends up in the parasitophorous vacuole after host cell invasion (*20*, *21*). Third, expression levels of *ROP18* are very different between strains: Initial microarray results indicated that strains having the type III allele expressed significantly less mRNA than those with a type II allele, and quantitative polymerase chain reaction (QPCR) showed this difference to be on the order of 10,000-fold (Fig. 2A and fig. S3A). Analysis of the F_1 progeny showed that this difference cosegregates with the *VIR3* QTL (fig. S1; peak LOD score 4.5, $P < 0.01$). Sequencing the entire *ROP18* gene (including promoter regions) and comparing type I, II, and III strains revealed that type III strains have a 2.1-kb sequence inserted 85 bp upstream of the ATG start codon, which is not present in type I or type II *ROP18*, or anywhere else in the only fully sequenced *Toxoplasma* genome (from a type II strain) (*16*, *17*). It seems likely that this insertion (relative to types I and II) in the 5′-untranslated region (UTR)–promoter of the type III *ROP18* allele is involved in the major difference in expression of this locus in type III strains, although this has not been directly tested. Last, *ROP18* is found in a genomic span that is generally dominated by type II–specific single-nucleotide polymorphisms (SNPs) on the basis of polymorphism maps derived from EST sequences (*5*) and, as predicted by this, the type II *ROP18* allele [(*16*) Gene model 20.m03896] has 11 (0.66%) SNPs in the coding region relative to types I (GenBank accession number CAJ27113) and III (GenBank accession number EF092842) (Fig. 2B). Superimposed on this expected level of polymorphism, however, is a completely unexpected and extremely large number (85; 5.0%) of type III–specific SNPs (64 of which result in amino acid changes) (Fig. 2B).

To determine whether *ROP18* was in fact the *VIR3* QTL, we introduced a type II (ME49) allele of *ROP18* into an avirulent type III background (CEP). This was done by cloning the type II gene (with 588 bp of endogenous promoter and the complete coding region) in frame with a C-terminal hemagglutinin (HA) tag. HA-specific antibody immunofluorescence on the resulting parasites revealed the presence of ROP18-HA in the rhoptries as expected (Fig. 2C), and also in vacuole-like structures within the host cell early after infection (Fig. 2D), similar to those previously observed for other rhoptry proteins (*22*). In BALB/c mice, these type III:$ROP18_{II}$ parasites were at least 4 logs more virulent than the wild type strain (Fig. 3). A second, genetically distinct type III:$ROP18_{II}$ clone (from a different transfection than the clone described in Fig. 3) was isolated that had similarly enhanced virulence in mice.

It is likely that the differences in the expression levels of *ROP18* are enough to account for the large difference in virulence between type III:$ROP18_{II}$ and the wild-type line (CEP), and *ROP18* levels were about eight times as high in the virulent type III:$ROP18_{II}$ as in a type II strain (fig. S3). However, the large number of polymorphisms in the type III coding region could also play a role, and future experiments using strains with allelic replacement of coding and/or promoter sequences will distinguish between these possibilities. Consistent with the results presented here, a separate study examining progeny from a cross between types I and III to determine the genetic basis for the extreme virulence of type I strains, Taylor *et al*. (*21*) found that expression of the type I *ROP18* allele in an avirulent type III strain also dramatically increases virulence in mice. These data confirm that *ROP18* is indeed a virulence gene and is likely the genetic basis for the virulence QTL on chromosome VIIa that was identified in both studies (*9*, *21*).

VIR4 falls within a 0.55-Mb interval on chromosome VIIb. Within this candidate region, one locus, *ROP16*, immediately stood out because of its extreme variability [the type II allele has 39 nonsynonymous SNPs compared with types I and III in ~2100 bp of coding sequence (*23*)], its status as a rhoptry protein kinase (and thus likely injected during invasion), and our recent results demonstrating that this rhoptry protein kinase is injected into the host cell cytosol and is involved in the strain-specific differences in induction of interleukin 12 (IL-12) secretion by mouse macrophages (*23*) [IL-12 is well known to be key in *Toxoplasma* pathogenesis (*24*, *25*)]. To test whether *ROP16* was indeed the *VIR4* QTL, we introduced either a type III or a type I allele of *ROP16* into a type II strain. Both alleles were pursued because our previous studies indicated that the type II allele is recessive (loss of function) to both the type I and type III alleles, and the type I and type III alleles have only three nonsynonymous SNPs

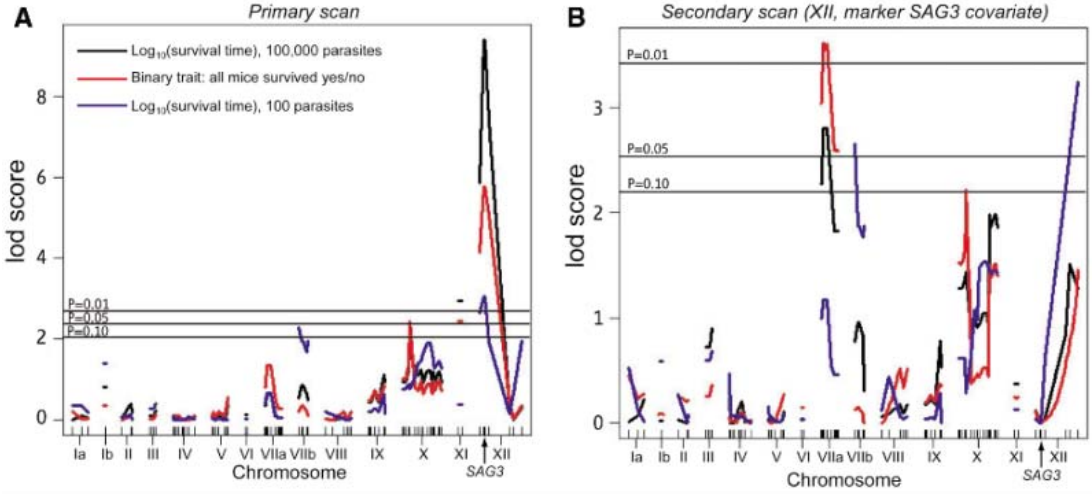

Fig. 1. Genetic mapping of virulence phenotypes of F_1 progeny from II × III crosses. BALB/c and CBA/J mice were infected with 100,000 or 100 tachyzoites from 40 different F_1 recombinant progeny from II × III crosses, and mortality was recorded daily for 40 days. As there were no significant differences between the two different mouse strains, results were pooled. Three phenotypes are represented: (i) "high-dose survivability," $\log_{10}$ survival time (in days) after injection of 100,000 parasites (black line); (ii) "avirulence," a binary trait defined as no mortality at any dose (red line); (iii) "low-dose survivability," $\log_{10}$ survival time (in days) after injection of 100 parasites (blue line). Plots indicate the log-likelihood association of phenotypes with markers aligned across the genome. Marker positions (in cM) are given by tick marks. Significance levels determined by 1000 permutations are indicated by horizontal lines [upper lines are significant; lower line is suggestive ($P = 0.1$)]. Because the significance levels for all three of the phenotypes differed by less than 0.1 LOD unit, only one significance line is drawn for all three. (**A**) Primary genome scan (see text). (**B**) Secondary genome scan after the effect of the major virulence peak on chromosome XII, evident in (A) and cosegregating with the *SAG3* marker, is neutralized by making it a covariate.

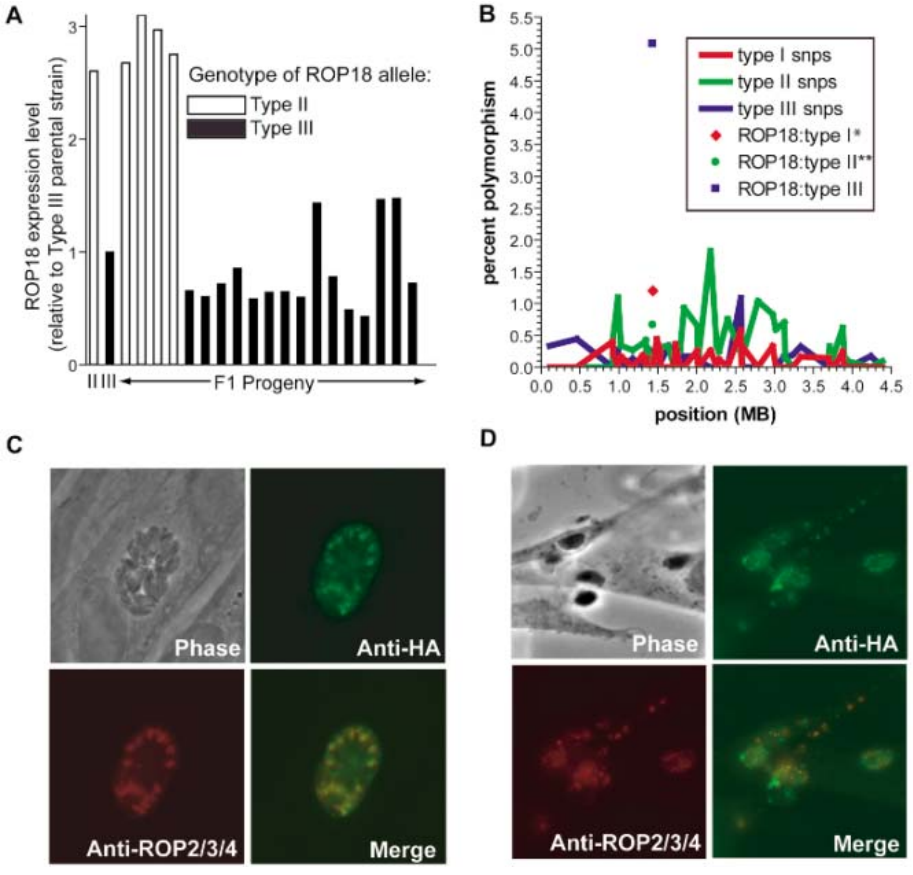

Fig. 2. Expression level, polymorphism analysis, and localization of *ROP18*. (**A**) Expression level of *ROP18* in the parental lines (type II, ME49, and type III, CEP) and 18 F_1 progeny. Data are displayed as fold-difference relative to the type III parent. The genotype for each of the F_1 progeny at the *ROP18* locus is indicated by the bar color (white or black). (**B**) Variation in the percentage of type I, II, and III SNP polymorphisms across chromosome VIIa. The entire chromosome was divided into 10-kb windows, and the number of SNPs of each type in each window [based on EST assemblies; see (*5*)] was divided by the number of sites with data from all three strains to compute a polymorphism percentage. The number of each polymorphism type in the *ROP18* coding region is also shown. *Accession number AM075204 (*28*). **Downloaded from (*16*) (Gene model 20m.03896). (**C**) Immunofluorescence assay of type III:$ROP18_{II}$ showing HA-specific staining (green) of HA-tagged ROP18 colocalizing with the rhoptry marker ROP2/3/4 (red) in human foreskin fibroblasts 40 hours post inoculation. (**D**) Immunofluorescence assay of type III:$ROP18_{II}$ showing HA-specific staining of tagged ROP18 in human foreskin fibroblasts 2 hours post inoculation. Punctate staining indicates the location of ROP18-HA that has been secreted into the infected host cell (*22*). Color scheme same as in (C).

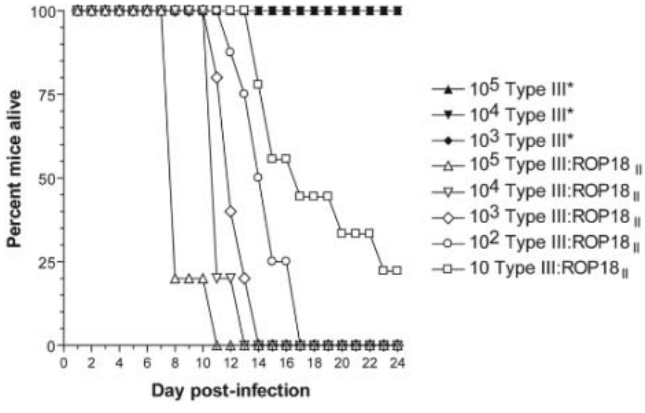

Fig. 3. Effect of expressing the type II allele for *ROP18* in a type III strain background (CEP) on virulence in mice. Mice were infected intraperitoneally with either CEP*Δhxgprt* complemented with *HXGPRT* alone (CEP*) or CEP parasites complemented with the type II allele for *ROP18* along with 588 bp of upstream sequence (type III:$ROP18_{II}$). Infections were verified in all the survivors based on the presence of *Toxoplasma*-specific antibodies, and only seropositive survivors are represented on the graph. Ten mice were used for all strain and dose combinations except for type III:$ROP18_{II}$-100 (eight mice) and type III:$ROP18_{II}$-10 (seven mice).

between them (*23*). The engineered strains were injected into mice, and virulence was compared with that of parental type II. The results (Fig. 4) show a substantial decrease in virulence in the strains carrying either the type I or the type III transgene. This is consistent with our QTL analyses, which indicate that the type III allele is associated with lower virulence (table S1). Obtaining two genetically distinct clones (type II:$ROP16_I$ and type II:$ROP16_{III}$) with identical virulence phenotypes argues against finding the insertion site of the DNA construct to be responsible for the drop in pathogenicity.

The results presented above strongly support the idea that polymorphic rhoptry kinases provide the genetic basis for two of the virulence QTLs mapped here. The identities of the genes contributing to the other three *VIR* loci are not yet known: None had a candidate gene as compelling as *ROP16* and *ROP18* (see supplementary results for a discussion of the other three loci). In no case do any of the five *VIR* loci appear to mediate virulence through an enhancement in growth, because no significant growth phenotype was seen for any of the F_1 progeny strains reported here, with the notable exception of CL15 which, as reported previously, has a substantial growth retardation (*3*). Furthermore, simple growth rate is not likely the basis of the virulence differences, because the parental type III strain has a slight growth advantage compared with the ME49 strain despite its being less virulent (*26*). ROP18 has recently been shown to be an active kinase

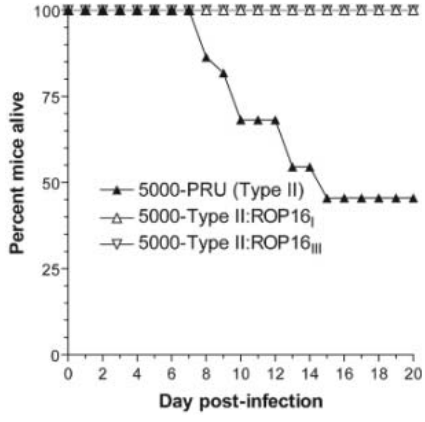

Fig. 4. Effect of expressing the type I and III strain allele of *ROP16* in the type II Prugniaud strain (PRU*Δhxgprt*) on virulence in mice. Mice were infected intraperitoneally with 5000 tachyzoites of type II (PRU*Δhxgprt*) or an engineered version expressing an HA-tagged copy of the *ROP16* allele from the type III CEP strain (type II:$ROP16_{III}$) or the type I RH strain (type II:$ROP16_I$). For PRU*Δhxgprt*, 24 mice were used, 10 for type II:$ROP16_{III}$, and 14 for type II:$ROP16_I$. Infections were verified in all the survivors on the basis of the presence of *Toxoplasma*-specific antibodies. Results from three independent experiments were pooled.

capable of phosphorylating a parasite protein of unknown identity (*20*), and ROP16 has all of the key residues known to be crucial for kinase activity (*23*). In the case of ROP16, we have recently reported that its expression impacts several host transcription pathways, including those mediated by STAT3/6 (*23*). Available evidence, however, suggests that neither STAT3 nor STAT6 is a direct substrate of this kinase, although both are differentially phosphorylated depending on the allele of *ROP16* present in the infecting strain (*23*). Identification of the physiological substrates for ROP16 and ROP18 will yield great insights into their function.

The extreme sequence divergence observed for ROP16 and ROP18 could be a result of immune selection, but it is striking that these proteins are substantially more different among the three strains than the major surface antigens, SAG1 and SAG2 (*3*), which are highly immunogenic (at least in terms of antibodies) and thus are likely to represent an extreme for targets of selective pressure. It could be that ROP16 and ROP18 are subject to immune pressure by T cell responses rather than by antibodies (the major T cell antigens of *Toxoplasma* are not known, but the presence of ROP16 and ROP18 within the infected host cell would make them readily available for antigen presentation). For *ROP18*, pairwise comparisons of nonsynonymous to synonymous SNPs among the three alleles suggests that selection is operating on type I and type II ROP18. All 28 SNPs between them result in amino acid changes; the ratio of nonsynonymous nucleotide substitutions to synonymous nucleotide substitutions (Ka/Ks) is 4.6 (*27*) (fig. S2B). It is less clear how much selection has operated on the type III allele, where 20 of the 85 SNPs specific to this strain are synonymous, which gives Ka/Ks values closer to 1.0 [a ratio expected under a neutral selection model (fig. S2B); Ka/Ks = 1.7 and 1.3 versus type I and type II alleles, respectively]. It is possible that the very low expression of *ROP18* in type III strains makes type III *ROP18* a "null" allele that can more readily accumulate random mutation, although the level of variation in this allele is so atypical for this strain and genomic region (Fig. 2B) (*5*) that both positive selection and neutral drift may have operated on this allele over time. It will be key to sequence the *ROP18* gene in other *T. gondii* isolates to determine the range of selective pressure at this locus in the population. Finally, instead of immune pressure, another possibility is that at least some of the sequence divergence of these genes could be a result of optimization for interaction with specific proteins (e.g., their substrates) in one or more hosts that are central to their transmission. It is difficult to predict what those hosts are or were but *Mus* spp. has probably not played that role for all three strain types, given the very different allele-specific interactions described here. Rather, other species of rodents or birds that are central to the parasite's transmission, perhaps in distinct parts of the world, could be the true, evolutionarily relevant hosts in which selection for different versions of these key genes occurred.

References and Notes

1. D. K. Howe, L. D. Sibley, *J. Infect. Dis.* **172**, 1561 (1995).
2. M. L. Darde, B. Bouteille, M. Pestre-Alexandre, *J. Parasitol.* **78**, 786 (1992).
3. M. E. Grigg, S. Bonnefoy, A. B. Hehl, Y. Suzuki, J. C. Boothroyd, *Science* **294**, 161 (2001).
4. T. Lehmann, C. R. Blackston, S. F. Parmley, J. S. Remington, J. P. Dubey, *J. Parasitol.* **86**, 960 (2000).
5. J. P. Boyle *et al.*, *Proc. Natl. Acad. Sci. U.S.A.* **103**, 10514 (2006).
6. C. Su *et al.*, *Science* **299**, 414 (2003).
7. J. P. Saeij, J. P. Boyle, J. C. Boothroyd, *Trends Parasitol.* **21**, 476 (2005).
8. L. D. Sibley, J. C. Boothroyd, *Nature* **359**, 82 (1992).
9. C. Su, D. K. Howe, J. P. Dubey, J. W. Ajioka, L. D. Sibley, *Proc. Natl. Acad. Sci. U.S.A.* **99**, 10753 (2002).
10. D. K. Howe, S. Honore, F. Derouin, L. D. Sibley, *J. Clin. Microbiol.* **35**, 1411 (1997).
11. S. Honore *et al.*, *Pathol. Biol. (Paris)* **48**, 541 (2000).
12. J. C. Boothroyd, M. E. Grigg, *Curr. Opin. Microbiol.* **5**, 438 (2002).
13. A. Khan *et al.*, *Nucleic Acids Res.* **33**, 2980 (2005).
14. L. D. Sibley, J. C. Boothroyd, *Mol. Biochem. Parasitol.* **51**, 291 (1992).
15. Materials and methods are available as supporting material on *Science* Online.
16. *Toxoplasma* database, www.ToxoDB.org.
17. J. C. Kissinger, B. Gajria, L. Li, I. T. Paulsen, D. S. Roos, *Nucleic Acids Res.* **31**, 234 (2003).
18. L. Li *et al.*, *Genome Res.* **13**, 443 (2003).
19. P. J. Bradley *et al.*, *J. Biol. Chem.* **280**, 34245 (2005).
20. H. El Hajj *et al.*, *PLoS Pathogens*, in press.
21. S. Taylor *et al.*, *Science* **314**, 1776 (2006).
22. S. Hakansson, A. J. Charron, L. D. Sibley, *EMBO J.* **20**, 3132 (2001).
23. J. P. J. Saeij *et al.*, *Nature*, in press.
24. P. M. Robben *et al.*, *J. Immunol.* **172**, 3686 (2004).
25. U. Wille, E. N. Villegas, L. Craig, R. Peach, C. A. Hunter, *Infect. Immun.* **70**, 6940 (2002).
26. L. D. Sibley, A. J. LeBlanc, E. R. Pfefferkorn, J. C. Boothroyd, *Genetics* **132**, 1003 (1992).
27. W. H. Li, *J. Mol. Evol.* **36**, 96 (1993).
28. H. El Hajj, M. Lebrun, M. N. Fourmaux, H. Vial, J. F. Dubremetz, *Cell Microbiol.* published online 10.1111/j.1462-5822.2006.00767.x (2006).

29. This work was supported by grants to J.C.B. from the NIH (AI21423, AI30230, and AI41014) and the Ellison Medical Foundation (a Senior Scholar Award); to L.D.S. from the NIH (AI36629, AI059176); to J.W.A. from the U. K. Biotechnology and Biological Sciences Research Council and the Wellcome Trust; to J.P.J.S from the California Universitywide AIDS Research Program (F04-ST-216); to S.C. from the California Universitywide AIDS Research Program (FT-207-ST); and to J.P.B. from the NIH (F32AI60306). We thank J. D. Dunn for construction of the pGRA-HA-HPT vector; A. Fouts for help with QPCR; K. W. Broman for his many helpful suggestions on using the R/qtl package; P. Bradley and J.-F. Dubremetz for exchange of unpublished data; E. Pfefferkorn for performing the original crosses as part of a collaboration on drug resistance; the U. K. Medical Research Council MRC HGMP for printing the *Toxoplasma* microarrays; and M. White, J. Wootton, and J.-F. Dubremetz for helpful comments on the manuscript. Preliminary genomic and/or cDNA sequence data were accessed from ToxoDB.org and/or www.tigr.org/tdb/t_gondii/. Genomic data were provided by The Institute for Genomic Research (supported by the NIH grant AI05093) and by the Sanger Center (Wellcome Trust). EST sequences were generated by Washington University (NIH grant 1R01AI045806-01A1). The GenBank accession number for the ROP18 sequence from the type III strain CTG is EF092842.

Supporting Online Material

www.sciencemag.org/cgi/content/full/314/5806/1780/DC1
Materials and Methods
SOM Text
Figs. S1 to S3
Tables S1 and S2
References

9 August 2006; accepted 3 November 2006
10.1126/science.1133690

Nitrogen Fixation at 92°C by a Hydrothermal Vent Archaeon

Mausmi P. Mehta* and John A. Baross

A methanogenic archaeon isolated from deep-sea hydrothermal vent fluid was found to reduce N_2 to NH_3 at up to 92°C, which is 28°C higher than the current upper temperature limit of biological nitrogen fixation. The 16*S* ribosomal RNA gene of the hyperthermophilic nitrogen fixer, designated FS406-22, was 99% similar to that of non–nitrogen fixing *Methanocaldococcus jannaschii* DSM 2661. At its optimal growth temperature of 90°C, FS406-22 incorporated $^{15}N_2$ and expressed *nifH* messenger RNA. This increase in the temperature limit of nitrogen fixation could reveal a broader range of conditions for life in the subseafloor biosphere and other nitrogen-limited ecosystems than previously estimated.

Hydrothermal fluids venting from unsedimented deep-sea mid-ocean ridges are low in nitrate and ammonia (*1*), indicating that the microbial community inhabiting the subseafloor (*2*) may be limited by fixed nitrogen. Dissolved N_2 is abundant in hydrothermal vent fluids (*3*), and biological nitrogen fixation has been proposed to explain the depleted $^{15}N/^{14}N$ ratios of low–trophic level animals living around hydrothermal vents (*4*). The nitrogenase enzyme complex, encoded by the *nifHDK* genes, catalyzes nitrogen fixation, i.e., the reduction of N_2 to NH_3. Although *nifH* genes have been detected in hydrothermal vent fluid (*5*), no microorganism isolated from deep-sea vents has, to our knowledge, been reported to fix nitrogen. A wide

School of Oceanography, University of Washington, Seattle, WA 98195, USA.

*To whom correspondence should be addressed. E-mail: mausmi@alum.mit.edu

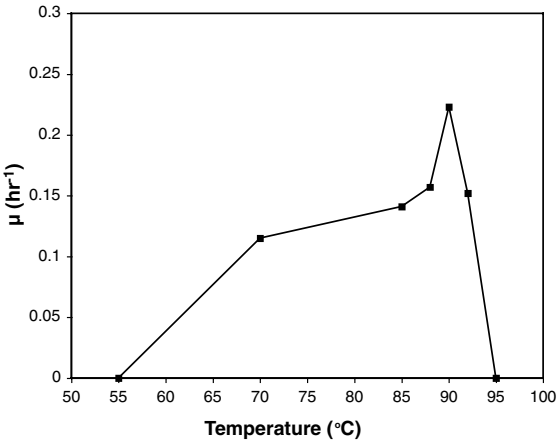

Fig. 1. Growth rate of FS406-22 grown with N_2 as the sole source of nitrogen, as a function of temperature. The specific growth rate (μ) is the average of three determinations of growth rate during exponential phase. Growth was monitored by epifluorescence microscopy (*12*).

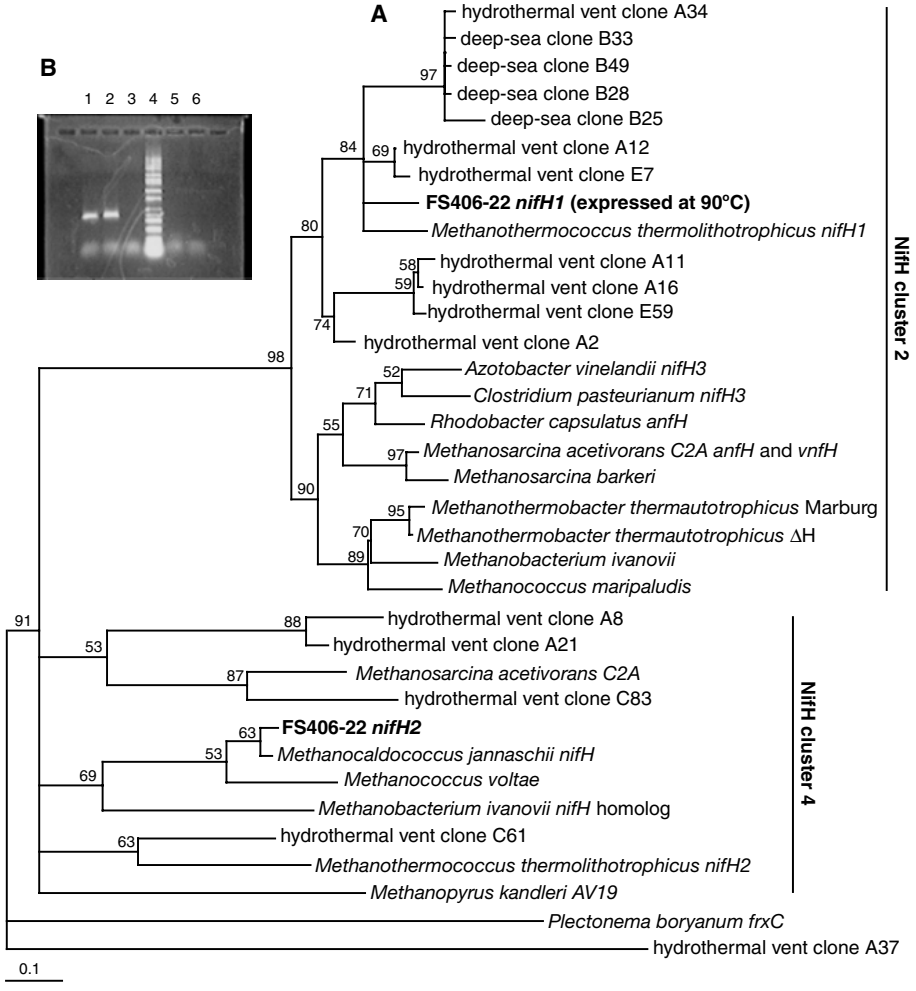

Fig. 2. (**A**) NifH amino acid phylogenetic tree constructed by quartet puzzling maximum likelihood (*12*). Cluster 2 includes molybdenum dinitrogenase reductases from methanogens, as well as alternative vanadium and iron-only dinitrogenase reductases (VnfH, AnfH) from Methanosarcinales and bacteria. Cluster 4 includes paralogous dinitrogenase reductases that are probably not involved in nitrogen fixation. The scale bar indicates the number of amino acid substitutions per site. The tree is outgroup rooted with *Plectonema boryanum frxC*, a dinitrogenase reductase–like protein involved in the light-independent reduction of protochlorophyllide. GenBank ID numbers for tree sequences are listed in table S2, and the alignment is shown in fig. S2. (**B**) Lanes 1 and 2: the product of RT-PCR with *nifH* primers and 2 and 3 μl of RNA extracted from FS406-22 growing on N_2 at 90°C; lane 3: RT-PCR without RNA; lane 4: Hi-Lo DNA ladder; lane 5: *nifH* PCR with 2 μl of RNA; lane 6: *nifH* PCR without RNA. The product in lanes 1 and 2 lies between the 400- and 500-bp bands of the ladder.

range of diverse bacteria, and the methanogenic archaea, are diazotrophic, or capable of nitrogen fixation (*6*). The subseafloor at mid-ocean ridges is bathed in reduced, H_2- and CO_2-rich hydrothermal fluid and thus provides an ideal habitat for methanogens, strict anaerobes that produce methane as a by-product. The methanogen *Methanothermococcus thermolithotrophicus* is currently the most thermophilic microorganism known that fixes nitrogen, at up to 64°C (*7*). *Synechococcus* ecotypes from microbial mats also fix nitrogen at up to 63.4°C (*8*). Here we describe the isolation of a methanogen from deep-sea hydrothermal vent fluid that fixes nitrogen at up to 92°C, which extends the upper temperature limit of biological nitrogen fixation by 28°C.

Axial volcano is located in the northeast Pacific, at the intersection of the Cobb-Eikelberg hotspot and the Juan de Fuca Ridge. The upper 100 m of oceanic crust beneath Axial seamount is estimated to have high porosity (*9*, *10*), and the diverse archaeal community associated with its subseafloor includes thermophilic and hyperthermophilic methanogens, with maximal growth rates from 45° to 80°C and above 80°C, respectively (*11*). During the 2004 New Millennium Observatory cruise to Axial volcano, fluid exiting the subseafloor was sampled from a diffuse vent named marker 113 (*12*). The fluid, which was measured to be 23°C at the point of sampling, was inoculated into a medium designed to select for diazotrophs and incubated anaerobically at 70° and 90°C. The enrichment cultures were positive at both temperatures and transferred into an antibiotic-containing medium to prevent the growth of bacteria. The amount of fixed nitrogen in the medium was reduced over time and then omitted completely (*12*).

The archaeal culture, named FS406-22, was capable of growth from 58° to 92°C with N_2 as the sole source of nitrogen, in a medium containing marine salts and H_2 plus CO_2. Maximal growth occurred at 90°C, and no growth was detected at 55° and 95°C (Fig. 1). Agitation of the culture was necessary for growth on N_2, and clusters of two or more cocci were visible by phase contrast microscopy during exponential growth. To determine the identity of FS406-22, we sequenced its 16*S* ribosomal RNA (rRNA) gene and found it to be 99% identical to the 16*S* rRNA gene from the methanogen *Methanocaldococcus jannaschii* (fig. S1). *M. jannaschii* was isolated from a deep-sea hydrothermal vent chimney on the East Pacific Rise in a nitrogen-rich medium, and grows in a temperature range of 50° to 86°C with an optimum near 85°C (*13*). Our hydrothermal vent isolate FS406-22 produced methane, determined by means of gas chromatography (GC). The specific growth rate of FS406-22 grown with nitrate and ammonium was 0.37 $hour^{-1}$ at 90°C, which is lower than the rate reported for *M. jannaschii* at 85°C, which is ~1.5 $hour^{-1}$ (*13*).

The *nifH* gene, which encodes dinitrogenase reductase, is highly conserved, and its phylogeny is mostly consistent with that of the 16*S* rRNA gene. The *nifD* and *nifK* genes encode a molybdenum-containing dinitrogenase that together with dinitrogenase reductase constitutes the nitrogenase enzyme

complex. Cluster 2 of the *nifH* phylogenetic tree (Fig. 2A) includes molybdenum nitrogenases from methanogens, as well as alternative iron- or vanadium-containing nitrogenases from Methanosarcinales and bacteria (*14*). Cluster 4 of the *nifH* phylogeny consists of paralogous archaeal nitrogenases that are assumed not to fix nitrogen.

Hydrothermal vent isolate FS406-22 has two copies of the *nifH* gene (Fig. 2A), one similar to *M. jannaschii*'s divergent copy (*15*) and another related to the *nifH* from *M. thermolithotrophicus* that is expressed at 64°C (*16*). Some of the *nifH* sequences previously recovered from deep-sea hydrothermal vent fluids (*5*) are more similar to *nifH1* from FS406-22 than from *M. thermolithotrophicus* [Supporting Online Material (SOM) Text]. While growing at 90°C, FS406-22 expresses *nifH1*, which we determined by sequencing the product of the reverse transcription polymerase chain reaction (RT-PCR) (Fig. 2B). To confirm that FS406-22 fixes molecular nitrogen and to estimate its rate of nitrogen fixation, we performed $^{15}N_2$ tracer assays at 90°C by incubating the cultures with $^{15}N_2$ and determining the nitrogen isotope ratios of the microbial biomass with an isotope ratio mass spectrometer (*17*). The control culture without added $^{15}N_2$ had a $\delta^{15}N$ of −4.86 per mil (‰) (versus air), or 0.36 atom %, which reflects the negative isotopic fractionation that results from biological nitrogen fixation. The experimental cultures had $\delta^{15}N$ values from 3650 to 4238‰ (versus air), or 1.68 to 1.89 atom %, and the estimated rate of nitrogen fixation at 90°C by FS406-22 was 0.30 μmol N_2 $liter^{-1}$ $hour^{-1}$ (*12*). Although biological nitrogen fixation has often been invoked to explain the low $\delta^{15}N$ values of deep-sea hydrothermal vent fauna compared to nonvent fauna (*18*), FS406-22 is the first microorganism isolated from the deep sea reported to exhibit diazotrophy.

To further characterize the *nif* operon in FS406-22, we designed PCR primers for *nifD* and sequenced the region downstream of the *nifH* gene (Fig. 3). The P_{II} nitrogen sensor proteins, encoded by *nifI*$_1$ and *nifI*$_2$, are responsible for "ammonia switch-off" or posttranslational regulation of nitrogenase in *Methanococcus maripaludis* (*19*) and were present in FS406-22. Two additional primers designed for *nifD* as well as a primer designed for *nifK*, based on those genes from *M. thermolithotrophicus*, were not successful in FS406-22. A phylogenetic tree of $NifI_1$ and $NifI_2$ proteins from FS406-22 and other archaea is shown in Fig. 3.

Highly conserved genes such as 16*S* rRNA can differ by less than 3%, whereas the prokaryotes they originate from show much greater genomic and physiological variation (*20*). In the case of FS406-22 and *M. jannaschii*, whose 16*S* rRNA genes diverge by only 1%, the former contains a functional *nif* operon and fixes nitrogen, whereas the latter does not. FS406-22 grown with N_2 or fixed nitrogen can grow at 6°C hotter than *M. jannaschii*, but the optimal growth rate of *M. jannaschii* is four times as great as that of FS406-22. To perform a rigorous comparison, however, one would have to cultivate both organisms under identical conditions, which we have not done. We also sequenced a 1550–base pair (bp) region of the FS406-22 genome that included the riboflavin synthase gene (*ribC*) and a putative aldehyde ferredoxin oxidoreductase gene (*aor*) that was 85% similar to the same stretch of DNA in *M. jannaschii*. The cluster 4 *nifH2* from FS406-22 was 87% similar to the only *nifH* from *M. jannaschii* at the nucleotide level and 96% similar at the amino acid level (Fig. 2A).

The revelation of a hyperthermophilic archaeal diazotroph may have implications for the evolutionary history of nitrogenase. Phylogenetic analysis of nitrogenase and chlorophyll iron proteins suggests that an ancestral iron protein duplicated and diverged into molybdenum and iron-only nitrogenases (*nifH* and *anfH*) before the separation of bacteria and methanogenic archaea (*21*). Subsequently, ancient duplications of *nifH* gave rise to the chlorophyll iron proteins, suggesting that nitrogenase predates photosynthesis and the rise of atmospheric oxygen (*21*). Raymond *et al*. detail two scenarios for the evolution of nitrogenase: that it was present in the last universal common ancestor and then lost in many lineages, or that it arose later within methanogenic archaea and was laterally transferred into bacteria (*22*). Given the lack of oxygen in the early Earth's atmosphere (*23*) and that nitrogenase is inactivated by O_2, the first nitrogenase probably arose in an anaerobe.

All methanogenic diazotrophs examined, and several anaerobic bacteria like *Chlorobium tepidum*, *Dehalococcoides ethenogenes*, *Heliobacterium chlorum, Clostridium acetobutylicum*, and *Desulfovibrio gigas*, have the *nifI*$_1$ and *nifI*$_2$ genes (*24*). In all of the archaeal operons, they are located between *nifH* and *nifD*, and the $NifI_1$ and $NifI_2$ proteins form a complex that binds directly to dinitrogenase (*19*). Because $NifI_1$, $NifI_2$ and GlnB/GlnK constitute all three subfamilies of the P_{II} nitrogen sensor family (*25*), the clusters provide a root for each other in an unrooted tree containing all three (*26*). Such phylogenetic analyses, as well as molecular evolutionary studies of other *nif* genes, all place *M. thermolithotrophicus* on a deep, basal branch (*6*, *26*–*28*). The unrooted $NifI_1$ and $NifI_2$ phylogenetic tree in Fig. 3 shows that the FS406-22 and *M. thermolithotrophicus* proteins form a deeply branching group that is basal to all other archaeal proteins, including

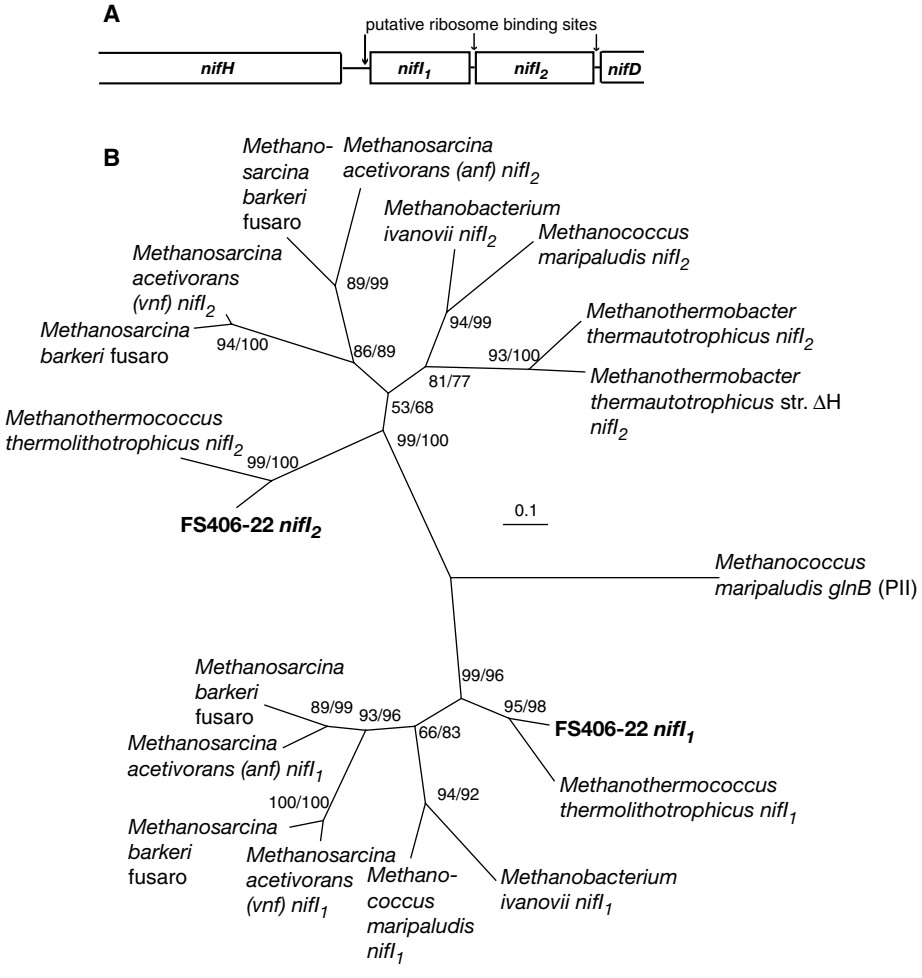

Fig. 3. (**A**) The *nif* genes sequenced from FS406-22: *nifH* (807 bp), *nifI*$_1$ (318 bp), *nifI*$_2$ (387 bp), and *nifD* (141 bp). (**B**) An unrooted $NifI_1$ and $NifI_2$ amino acid phylogenetic tree determined by quartet puzzling maximum likelihood (support values listed first) and by the distance-based Fitch-Margoliash method (bootstrap values listed second). The GlnB protein from *M. maripaludis* is displayed as an outgroup. The maximum-likelihood branch lengths are shown, and the scale bar indicates the number of amino acid substitutions per site. GenBank ID numbers for tree sequences are listed in table S3, and the alignment is shown in fig. S3.

those from alternative nitrogenases. However, the quartet puzzling support and bootstrap values are not high enough to rule out alternative topologies. The maximum-likelihood branch lengths in Fig. 3 suggest that FS406-22 $NifI_1$ and $NifI_2$ are the shortest distance to the internal node that represents the ancestral P_{II} protein. A recent reconstruction of the tree of life with 31 universal gene families supports the hypothesis that the last universal common ancestor lived at high temperatures (*29*). We propose that among diazotrophic archaea, the nitrogenase from FS406-22 might have retained the most ancient characteristics, possibly derived from a nitrogenase present in the last common ancestor of modern life.

References and Notes

1. D. A. Butterfield *et al.*, in *The Subseafloor Biosphere at Mid-Ocean Ridges*, W. S. D. Wilcock, E. F. DeLong, D. S. Kelley, J. A. Baross, S. C. Cary, Eds. (American Geophysical Union, Washington, DC, 2004), vol. 144 of Geophysical Monograph Series, pp. 269–289.
2. M. Summit, J. A. Baross, *Proc. Natl. Acad. Sci. U.S.A.* **98**, 2158 (2001).
3. J. L. Charlou *et al.*, *Chem. Geol.* **171**, 49 (2000).
4. G. H. Rau, *Nature* **289**, 484 (1981).
5. M. P. Mehta, D. A. Butterfield, J. A. Baross, *Appl. Environ. Microbiol.* **69**, 960 (2003).
6. J. P. W. Young, in *Biological Nitrogen Fixation*, G. Stacey, R. H. Burris, H. J. Evans, Eds. (Chapman & Hall, New York, 1992), pp. 43–86.
7. N. Belay, R. Sparling, L. Daniels, *Nature* **312**, 286 (1984).
8. A.-S. Steunou *et al.*, *Proc. Natl. Acad. Sci. U.S.A.* **103**, 2398 (2006).
9. L. A. Gilbert, thesis, University of Washington (2004).
10. M. J. Pruis, H. P. Johnson, *Geophys. Res. Lett.* **29**, 1076 (2002).
11. J. A. Huber, D. A. Butterfield, J. A. Baross, *Appl. Environ. Microbiol.* **68**, 1585 (2002).
12. Materials and methods are available as supporting material on *Science* Online.
13. W. J. Jones, J. A. Leigh, F. Mayer, C. R. Woese, R. S. Wolfe, *Arch. Microbiol.* **136**, 254 (1983).
14. Y.-T. Chien, S. H. Zinder, *J. Bacteriol.* **176**, 6590 (1994).
15. C. J. Bult *et al.*, *Science* **273**, 1058 (1996).
16. N. Souillard, L. Sibold, *Mol. Microbiol.* **3**, 541 (1989).
17. J. P. Montoya, M. Voss, P. Kähler, D. G. Capone, *Appl. Environ. Microbiol.* **62**, 986 (1996).
18. M. C. Kennicutt II, R. A. Burke Jr., in *The Microbiology of Deep-Sea Hydrothermal Vents*, D. M. Karl, Ed. (CRC Press, Boca Raton, FL, 1995), pp. 275–287.
19. J. A. Dodsworth, J. A. Leigh, *Proc. Natl. Acad. Sci. U.S.A.* **103**, 9779 (2006).
20. G. Rocap *et al.*, *Nature* **424**, 1042 (2003).
21. D. H. Burke, J. E. Hearst, A. Sidow, *Proc. Natl. Acad. Sci. U.S.A.* **90**, 7134 (1993).
22. J. Raymond, J. L. Siefert, C. R. Staples, R. E. Blankenship, *Mol. Biol. Evol.* **21**, 541 (2004).
23. J. F. Kasting, J. L. Siefert, *Science* **296**, 1066 (2002).
24. T. Arcondéguy, R. Jack, M. Merrick, *Microbiol. Mol. Biol. Rev.* **65**, 80 (2001).
25. J. A. Leigh, in *Genomes and Genomics of Nitrogen-Fixing Organisms*, R. Palacios, W. E. Newton, Eds. (Springer, the Netherlands, 2005), pp. 7–12.
26. J. A. Leigh, *Curr. Issues Mol. Biol.* **2**, 125 (2000).
27. Y.-T. Chien, S. H. Zinder, *J. Bacteriol.* **178**, 143 (1996).
28. Y.-T. Chien, V. Auerbuch, A. D. Brabban, S. H. Zinder, *J. Bacteriol.* **182**, 3247 (2000).
29. F. D. Ciccarelli *et al.*, *Science* **311**, 1283 (2006).

30. We thank S. Bolton, D. Butterfield, W. Chadwick, the NOAA Vents Program, and the crews of the ROV *ROPOS* and R/V *Thompson* for sample collection and E. Olson for performing GC work and assistance with $^{15}N_2$ tracer assays. Washington Sea Grant (NA 76RG011 9) and the NASA Astrobiology Institute, through the Carnegie Geophysical Institute, supported this research. GenBank accession numbers for FS406-22 sequences are EF079967 to EF079969.

Supporting Online Material

www.sciencemag.org/cgi/content/full/314/5806/1783/DC1
Materials and Methods
SOM Text
Figs. S1 to S4
Tables S1 to S4
References

6 September 2006; accepted 31 October 2006
10.1126/science.1134772

Greater Disruption Due to Failure of Inhibitory Control on an Ambiguous Distractor

Yoshiaki Tsushima,[1] Yuka Sasaki,[2,3] Takeo Watanabe[1]*

Considerable evidence indicates that a stimulus that is subthreshold, and thus consciously invisible, influences brain activity and behavioral performance. However, it is not clear how subthreshold stimuli are processed in the brain. We found that a task-irrelevant subthreshold coherent motion led to a stronger disturbance in task performance than did suprathreshold motion. With the subthreshold motion, activity in the visual cortex measured by functional magnetic resonance imaging was higher, but activity in the lateral prefrontal cortex was lower, than with suprathreshold motion. These results suggest that subthreshold irrelevant signals are not subject to effective inhibitory control.

We experience an overwhelming amount of visual stimuli. However, a great number of the stimuli are not consciously perceived (are invisible) for a number of reasons, including weakness of the stimuli (*1*, *2*), task irrelevance (*3*, *4*), interference by other stimuli (*1*, *5*–*10*), and combinations of these factors. Nevertheless, an invisible stimulus can influence brain activity and task performance (*1*, *2*, *10*–*12*). One would naturally assume that the degree of an invisible stimulus's influence is generally weaker than that of a visible stimulus.

We conducted a series of psychophysical and functional magnetic resonance imaging (fMRI) experiments. During each trial of experiment 1, 15 participants were presented with a sequence of eight items (two digits and six alphabetic letters) at the center of a computer screen. In the background, a dynamic random-dot (DRD) display with coherently moving dots (signal) and randomly moving dots (noise) (*2*, *13*–*15*) was presented (Fig. 1). The participants were instructed to focus on and report the two digits. This task is known as the rapid serial visual presentation (RSVP) task. The background DRD display was thus task-irrelevant (*16*). The ratio of signal dots to the total number of dots (coherence ratio) was varied from trial to trial. A higher motion coherence task-relevant condition strongly activates monkey middle temporal (MT) (*17*) and human MT+ (*18*), which are the visual areas that are largely specialized for motion processing. These findings would naturally lead to the prediction that a higher task-irrelevant motion coherence stimulus would also produce stronger internal signals within the visual system, which either would result in greater disturbance in task performance (*2*, *19*, *20*) or would not influence task performance because of attentional filtering or the suppression of, if weak, irrelevant signals (*21*).

Performance with coherent motion ≥20% did not significantly differ from performance with 0% coherent motion (Fig. 2A). This is consistent with the attention-filtering hypothesis (*21*) in that task-irrelevant motion coherence signals (at least ≥20%) did not influence task performance. However, at 5% coherence ratio, performance was significantly lower than at 0 and 20% coherence ratios. Immediately after the main condition, we conducted a test to measure motion coherence ratio threshold (*16*). The participants were instructed to indicate one of the four coherent motion directions used in the main condition in a

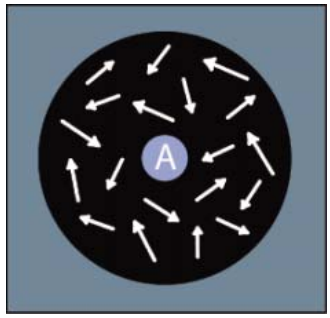

Fig. 1. Stimulus. A sequence of letters and digits was presented in the center while dots moved in the background. The ratio of the number of coherently moving dots to the total number of randomly moving plus coherently moving dots was varied from trial to trial. Arrows represent motion vectors.

[1]Department of Psychology, Boston University, 64 Cummington Street, Boston, MA 02215, USA. [2]Athinoula A. Martinos Center for Biomedical Imaging, Department of Radiology, Massachusetts General Hospital, Charlestown, MA 02129, USA. [3]Exploratory Research for Advanced Technology (ERATO) Shimojo Implicit Brain Function Project, California Institute of Technology, Pasadena, CA 91125, USA.

*To whom correspondence should be addressed. E-mail: takeo@bu.edu

DRD display whose coherent motion ratio was varied in seven steps from trial to trial. The result showed that the 5% coherence ratio produced chance-level performance and therefore can be considered to be a subthreshold motion ratio condition (*2*). Thus, although suprathreshold task-irrelevant signals (e.g., 20%) were successfully filtered out (*21*), those below but near the chance-level threshold led to disturbance of task performance.

In experiment 2, to examine whether the performance dip and motion coherence threshold are correlated, we lowered the luminance contrast of the moving dots (from 65.9 to 2.2 candela/m^2) so that the coherence threshold would considerably increase, while maintaining the same methods used in the previous experiment (n = 10 participants). Both the threshold of coherent motion and the performance dip shifted toward a higher coherence ratio (Fig. 2B).

There is the possibility that task-irrelevant, translating coherent motion may induce eye movements, which could be related to the performance dip. In experiment 3 (n = 6), using the same method as in experiment 1 except that eye movements were monitored, the same pattern of performance was obtained. No systematic difference was observed in eye-movement patterns between coherence ratios (*16*). We also conducted experiment 4 (n = 15) in which signal dots contracted rather than translated, because contracting motion does not elicit major eye movements. Nevertheless, basically the same pattern of results was obtained, including the performance dip at the 5% coherence ratio (*16*). Thus, it does not seem that eye movements are a major factor in the performance-dip effect.

In experiment 5, to investigate the underlying neural mechanism that causes such a paradoxical effect, we measured fMRI activity in six participants, with contracting coherent motion ratios varied between 0, 5, 10, and 20%. The amount of activity of MT+, which reflects the strength of processed motion signals (*18*), was highest for 5% coherence (Fig. 3A, red), at which level the performance dip occurred (Fig. 3A, black). Weak coherent motion that is around the chance-level threshold thus strongly activates MT+ and also impairs task performance. In contrast, the results of the control condition in which motion was task-relevant (*16*) show that the MT+ activity (Fig. 3A, green) and performance increased with increasing coherence ratio, which is in accord with previous findings (*17*, *18*). Thus, the performance dip and highest MT+ activity are related to the fact that motion was task-irrelevant.

In the lateral prefrontal cortex (LPFC), which plays an important role in inhibitory control of inappropriate behavior or irrelevant signals (*22*–*26*), the amount of activity at the 5% coherence ratio showed no significant difference from that at 0% coherence but was significantly lower than at the 10 and 20% coherence levels (Fig. 3B, red) (*27*).

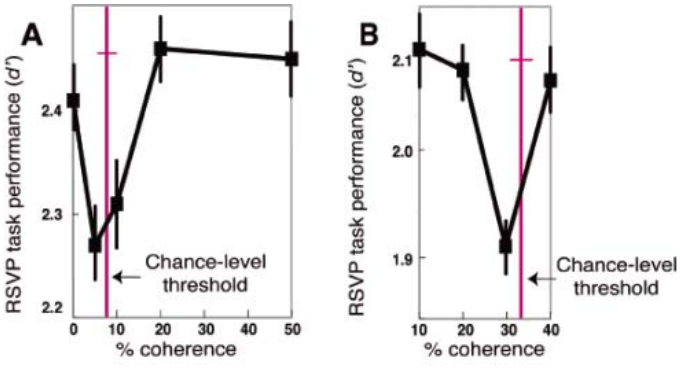

Fig. 2. Results of experiments 1 and 2. (**A**) Results of experiment 1. Mean RSVP task performance (d') as a function of the coherence ratio of background DRD displays is shown. d' at 5% coherence ratio was significantly lower than at 0% coherence ratio ($P < 0.001$, t test with Bonferroni correction) and 20% coherence ($P < 0.001$), indicating a performance dip at 5% coherence ratio. Vertical error bars, ±1 SEM. A vertical pink bar represents the mean chance-level threshold with a horizontal pink bar, ±1 SEM, indicating that 5% coherent motion is under the chance-level threshold. (**B**) Results of experiment 2 in which the dot luminance contrast was lower than in experiment 1. Mean RSVP performance (d') at 30% coherence ratio was significantly lower than at 20% coherence ratio ($P < 0.01$) and 40% coherence ratio ($P < 0.01$). The dip performance (d') as well as the chance-level threshold were shifted. The scales of the y axes in (A) and (B) are not identical.

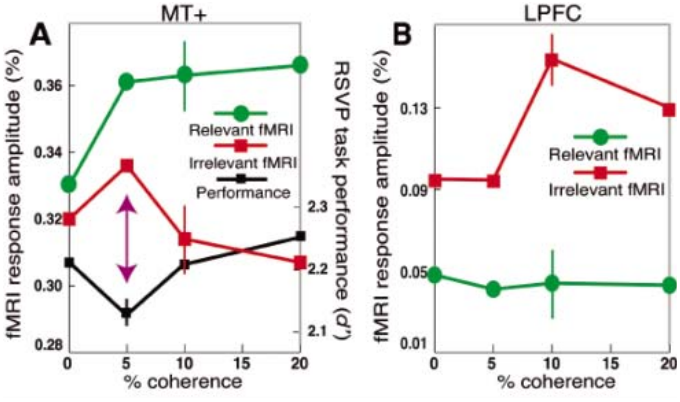

Fig. 3. Results of experiment 5. (**A**) Averaged BOLD signals for area MT+ in the conditions in which coherent motion was task-relevant (green line) and task-irrelevant (red line) and mean RSVP performance (d') in the task-irrelevant condition (black line) are shown. In the task-relevant condition, BOLD signals at 0% coherence ratio were significantly lower than at 5% ($P < 0.05$), 10% ($P < 0.05$), and 20% ($P < 0.05$) coherence ratios. BOLD signals in the task-irrelevant condition and RSVP performance show clear symmetric patterns, as indicated by an arrow. Vertical error bars, ±1 SEM for each condition. (**B**) Averaged BOLD signals for area LPFC in the condition in which coherent motion was task-relevant (green line) and -irrelevant (red line). In the task-irrelevant condition, BOLD signals at the 5% coherence ratio were significantly lower than those at the 10 and 20% ratios ($P < 0.05$ for both) but showed no significant difference from those at 0% coherence ratio. Vertical error bars, ±1 SEM for each condition.

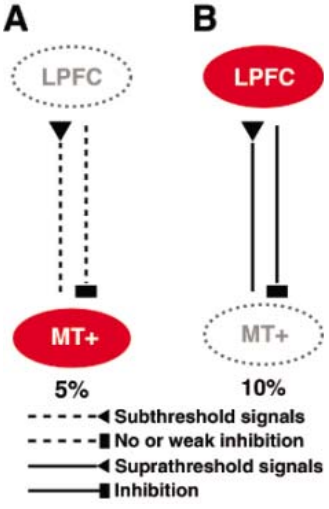

Fig. 4. Schematic illustration of the hypothesized bidirectional interactions between the LPFC and MT+. (**A**) No significant difference between the LPFC activity at 0 and 5% coherence ratios in experiment 5 suggests that the LPFC fails to notice 5% coherent motion signals from MT+ (left dotted flow line). Thus, the LPFC does not provide direct or indirect effective inhibitory control on MT+ (right dotted flow line). Activity in MT+ determines the engagement of the LPFC, which in turn determines inhibitory control on MT+ signals. (**B**) Significantly higher LPFC activity at the 10% coherence ratio than at the 0% coherence ratio in experiment 5 suggests that the LPFC-noticed 10% coherent motion signals from MT+ (left solid flow line) provide direct or indirect inhibitory control (right solid flow line) on MT+. This observed relationship between the LPFC and MT+ is in accord with the observed high negative correlation between task-irrelevance–related activity in the LPFC and MT+ over the four coherence ratios (*28*).

How is the LPFC activity related to the activity in MT+ in the task-irrelevant condition? The correlation coefficient between the task-irrelevance–related activity (*28*) in MT+ and the LPFC was –0.90. This is in accord with the view that when the LPFC is activated, it provides direct or indirect inhibitory control on the activity of MT+.

One might think that the low performance at the 5% coherence ratio was obtained because, despite the instructions to focus on RSVP task performance, the participants may have tried to find a coherent motion direction or to detect whether coherent motion was presented. If these motion tasks are difficult, they may leave fewer resources available for the RSVP task. However, this is not likely. If the participants engaged in the search for motion direction, this task should be hardest at 0% coherence and therefore, the lowest RSVP performance should have occurred at 0% and not at 5% coherence. Second, if the participants engaged in motion detection, this task should be hardest at 5% coherence because indecision may be greatest near the coherent motion threshold, and thus in accordance with the observed RSVP performance result. However, the lowest blood oxygen level–dependent (BOLD) activity was observed at 5% coherence ratio in the LPFC and cannot be directly explained by this possibility.

The results of the present study demonstrate two important points. First, a weak task-irrelevant stimulus feature that is below but near the perceptual threshold more strongly activates the visual area (MT+) that is highly related to the stimulus feature and more greatly disrupts task performance. There was a tendency for activity in the posterior occipitotemporal sulcus (pOTS) (*29*, *30*) and the left angular gyrus (*31*), which are sensitive to letters and words and may be related to the RSVP task, to be lower at the 5% coherence than at the other coherent motion ratios. This contradicts the general view that irrelevant signals that are stronger in stimulus properties have a greater influence on the brain and performance and that the influence of a subthreshold stimulus is smaller than that of a suprathreshold stimulus.

Second, the results may reveal important bidirectional interactions between a cognitive controlling system and the visual system. The LPFC, which has been suggested to provide inhibitory control on task-irrelevant signals (*22*–*26*), may have a higher detection threshold for incoming signals than the visual cortex. Task-irrelevant signals around the threshold level may be sufficiently strong to be processed in the visual system but not strong enough for the LPFC to notice and, therefore, to provide effective inhibitory control on the signals (Fig. 4A). In this case, such signals may remain uninhibited, take more resources for a task-irrelevant distractor, leave fewer resources for a given task (*32*, *33*), and disrupt task performance more than suprathreshold signals. On the other hand, suprathreshold coherent motion may be noticed, may be given successful inhibitory control by the LPFC, and may leave more resources for a task (Fig. 4B) (*22*–*26*). This mechanism may underlie the present paradoxical finding that subthreshold task-irrelevant stimuli activate the visual area strongly and disrupt task performance more than some suprathreshold stimuli. It could also be one of the reasons why subthreshold stimuli often lead to relatively robust effects (*2*, *11*, *14*).

References and Notes

1. S. He, P. Cavanagh, J. Intriligator, *Nature* **383**, 334 (1996).
2. T. Watanabe, J. E. Nanez, Y. Sasaki, *Nature* **413**, 844 (2001).
3. J. K. O'Regan, R. A. Rensink, J. J. Clark, *Nature* **398**, 34 (1999).
4. A. Mack, I. Rock, *Inattentional Blindness* (MIT Press, Cambridge, MA, 1998).
5. M. M. Chun, *J. Exp. Psychol. Hum. Percept. Perform.* **23**, 738 (1997).
6. V. Stuphorn, J. D. Schall, *Nat. Neurosci.* **9**, 925 (2006).
7. R. Blake, R. Fox, *Nature* **249**, 488 (1974).
8. S. H. Lee, R. Blake, D. J. Heeger, *Nat. Neurosci.* **8**, 22 (2005).
9. N. K. Logothetis, J. D. Schall, *Science* **245**, 761 (1989).
10. S. Dehaene *et al.*, *Nature* **395**, 597 (1998).
11. M. Bar, I. Biederman, *Psychol. Sci.* **9**, 464 (1998).
12. J. D. Haynes, G. Rees, *Nat. Neurosci.* **8**, 686 (2005).
13. A. Sahraie, M. Milders, M. Niedeggen, *Vision Res.* **41**, 1613 (2001).
14. A. R. Seitz, T. Watanabe, *Nature* **422**, 36 (2003).
15. M. Niedeggen, A. Sahraie, G. Hesselmann, M. Milders, C. Blakemore, *Brain Res. Cogn. Brain Res.* **13**, 241 (2002).
16. Materials and methods are available as supporting material on *Science* Online.
17. W. T. Newsome, E. B. Pare, *J. Neurosci.* **8**, 2201 (1988).
18. G. Rees, K. Friston, C. Koch, *Nat. Neurosci.* **3**, 716 (2000).
19. J. Stroop, *J. Exp. Psychol.* **18**, 643 (1935).
20. A. M. Treisman, G. Gelade, *Cogn. Psychol.* **12**, 97 (1980).
21. S. R. Friedman-Hill, L. C. Robertson, R. Desimone, L. G. Ungerleider, *Proc. Natl. Acad. Sci. U.S.A.* **100**, 4263 (2003).
22. R. Dias, T. W. Robbins, A. C. Roberts, *Nature* **380**, 69 (1996).
23. J. M. Fuster, *The Prefrontal Cortex: Anatomy, Physiology, and Neurophysiology of the Frontal Lobe* (Lippincott-Raven, New York, ed. 3, 1997).
24. R. T. Knight, W. R. Staines, D. Swick, L. L. Chao, *Acta Psychol. (Amst.)* **101**, 159 (1999).
25. J. G. Kerns *et al.*, *Science* **303**, 1023 (2004).
26. A. W. MacDonald III, J. D. Cohen, V. A. Stenger, C. S. Carter, *Science* **288**, 1835 (2000).
27. In the control condition in which motion was task-relevant (Fig. 3B, green), no significant difference was found between any pair of coherence levels.
28. Task-irrelevance–related activity is defined as a BOLD signal amount in the task-relevant condition subtracted from that in the task-irrelevant condition, for each motion coherence and for each cortical area.
29. M. Ben-Shachar, R. F. Dougherty, G. K. Deutch, B. A. Wandell, *Cereb. Cortex* 10.1093/cercor/bhl071 (2006).
30. S. Dehaene, L. Cohen, M. Sigman, F. Vinckier, *Trends Cogn. Sci.* **9**, 335 (2005).
31. A. M. Callan, D. E. Callan, S. Masaki, *Neuroimage* **28**, 553 (2005).
32. R. Desimone, J. Duncan, *Annu. Rev. Neurosci.* **18**, 193 (1995).
33. E. K. Miller, J. D. Cohen, *Annu. Rev. Neurosci.* **24**, 167 (2001).

34. This study is funded by grants from NIH (R01 EY015980 and R21 EY017737), NSF (BCS-0345746, BCS-0549036, and BCS-PR04-137 Center of Excellence for Learning in Education, Science, and Technology), and the Human Frontier Science Program Organization (RGP18/2004) to T.W., and by grants from National Center for Research Resources (P41RR14075), the Mental Illness and Neuroscience Discovery Institute, the Athinoula A. Martinos Center for Biomedical Imaging, and the ERATO Shimojo Implicit Brain Function project to Y.S. We thank P. Cavanagh, Y. Kamitani, M. Kawato, I. Motoyoshi, J. Nanez, M. Sakagami, S. Shimojo, and the members of Vision Sciences Laboratory at Boston University for their comments on the study and N. Ito and Y. Yotsumoto for technical assistance.

Supporting Online Material

www.sciencemag.org/cgi/content/full/314/5806/1786/DC1
Materials and Methods
Figs. S1 and S2
References

31 July 2006; accepted 20 October 2006
10.1126/science.1133197

Maternal Oxytocin Triggers a Transient Inhibitory Switch in GABA Signaling in the Fetal Brain During Delivery

Roman Tyzio,[1] Rosa Cossart,[1] Ilgam Khalilov,[1] Marat Minlebaev,[1] Christian A. Hübner,[2] Alfonso Represa,[1] Yehezkel Ben-Ari,[1]* Rustem Khazipov[1]

We report a signaling mechanism in rats between mother and fetus aimed at preparing fetal neurons for delivery. In immature neurons, γ-aminobutyric acid (GABA) is the primary excitatory neurotransmitter. We found that, shortly before delivery, there is a transient reduction in the intracellular chloride concentration and an excitatory-to-inhibitory switch of GABA actions. These events were triggered by oxytocin, an essential maternal hormone for labor. In vivo administration of an oxytocin receptor antagonist before delivery prevented the switch of GABA actions in fetal neurons and aggravated the severity of anoxic episodes. Thus, maternal oxytocin inhibits fetal neurons and increases their resistance to insults during delivery.

Delivery is a stressful event associated with high risks to the fetal brain (*1*); however, whether the fetal brain prepares for delivery remains largely unknown. We addressed this issue by studying γ-aminobutyric acid (GABA)–mediated (GABAergic) signaling in the

rat hippocampus. GABA is the principal inhibitory neurotransmitter in the adult brain. However, during fetal and postnatal periods GABA has a depolarizing action (*2*–*4*) and provides the major, and often the only, excitatory synaptic input to immature neurons (*5*). Excitatory action of GABA is due to elevated intracellular chloride and depolarized value of the GABA type A ($GABA_A$) reversal potential (E_{GABA}) (*6*–*10*). Excitatory GABA is pivotal in control of neuronal firing, generation of the primitive patterns of activity, intracellular calcium signaling, and neuronal development (*2*, *3*). GABA signaling is therefore expected to be an essential element in physiological adaptation to stress during delivery.

To characterize the properties of GABA signaling during the perinatal period, we used cell-attached recordings from fetal and neonatal rat hippocampal slices [from embryonic day (E) 18 to postnatal day (P) 5; term is E21] (*11*). During fetal (E18 and E19) and postnatal periods (P1 to P5), activation of $GABA_A$ receptors increased the firing of action potentials in the majority of CA3 pyramidal cells [Fig. 1A; also (*6*, *7*, *12*)]. However, during a brief period extending from E20 to day of birth (P0), the proportion of cells excited by GABA sharply decreased. The loss of the excitatory effect of GABA peaked at E21 [~1 to 2 hours before delivery (Fig. 1A)].

The action of GABA depends on the direction of the transmembrane current elicited by GABA, its driving force (DF_{GABA}) being the difference between E_{GABA} and resting membrane potential (E_m). Positive values of DF_{GABA} determine excitatory actions of GABA in immature neurons (*2*, *3*, *6*, *7*). To estimate DF_{GABA}, we used cell-attached recordings of single $GABA_A$ channels (*10*) (Fig. 1, B to D), which affect neither E_{GABA} nor E_m. With 1 μM GABA in the pipette solution, $GABA_A$ channels were observed in ~90% of patches (n = 553) but not in the presence of the $GABA_A$ receptor antagonist picrotoxin [100 μM; n = 25 (Fig. 1B)]. We found that DF_{GABA} is strongly depolarizing in fetal and postnatal periods (Fig. 1D). However, DF_{GABA} negatively shifted during a brief near-term period (from E20 to P0), switching to a hyperpolarizing value of –8.4 ± 2.5 mV at term [mean ± SEM, n = 34 (Fig. 1D)]. Thus, the disappearance of GABA-mediated excitation at term (Fig. 1A) coincides with a switch in polarity of GABA signals.

The perinatal changes in DF_{GABA} could be due to a negative shift of E_{GABA} or to a depolarizing shift of E_m. By using cell-attached recordings of single *N*-methyl-D-aspartate (NMDA) channels as voltage sensors (*12*, *13*), we found that during early fetal and postnatal periods E_m is –78.7 ± 1.9 mV (n = 42; pooled data for E18 and E19 and P1 to P5) [also (*13*, *14*)], but near term there is a small hyperpolarizing shift to –85.4 ± 1.5 mV [n = 14 at birth (Fig. 1E)]. Knowing DF_{GABA} and E_m, we calculated E_{GABA} (E_{GABA} = DF_{GABA} + E_m) and found that E_{GABA} switches from –40 mV at E18 to –92 mV at E21 and then returns to depolarizing values shortly after birth (Fig. 1F). This corresponds to a decrease in $[Cl^-]_i$ (intracellular chloride concentration) from 18 mM to 4 mM (Fig. 1F).

Because GABA-induced depolarization raises $[Ca^{2+}]_i$ (*12*, *15*–*18*), we used a multibeam two-photon microscope to monitor $[Ca^{2+}]_i$ changes in hundreds of CA3 neurons in slices loaded with the calcium indicator fura 2-AM (Fig. 2). The $GABA_A$ receptor agonist isoguvacine (10 μM) elicited a robust increase of $[Ca^{2+}]_i$ in the majority of neurons at E18 and at P2 to P4 [average of 56 ± 3%, n values of 7 movies and 931 cells (Fig. 2, B to D)]. In contrast, at E21 to P0, $[Ca^{2+}]_i$ increased in only 31 ± 6% (n values of 10 movies and 1546 cells, $P < 0.01$) cells. Isoguvacine also decreased the frequency of spontaneous calcium

[1]Institut de Neurobiologie de la Méditerranée, INSERM U29, Université de la Méditerranée, Campus Scientifique de Luminy, Boite Postale 13, 13273 Marseille Cedex 09, France. [2]Institut für Humangenetik, Universitätsklinikum Hamburg-Eppendorf, 20251 Hamburg, Germany.

*To whom correspondence should be addressed. E-mail: ben-ari@inmed.univ-mrs.fr

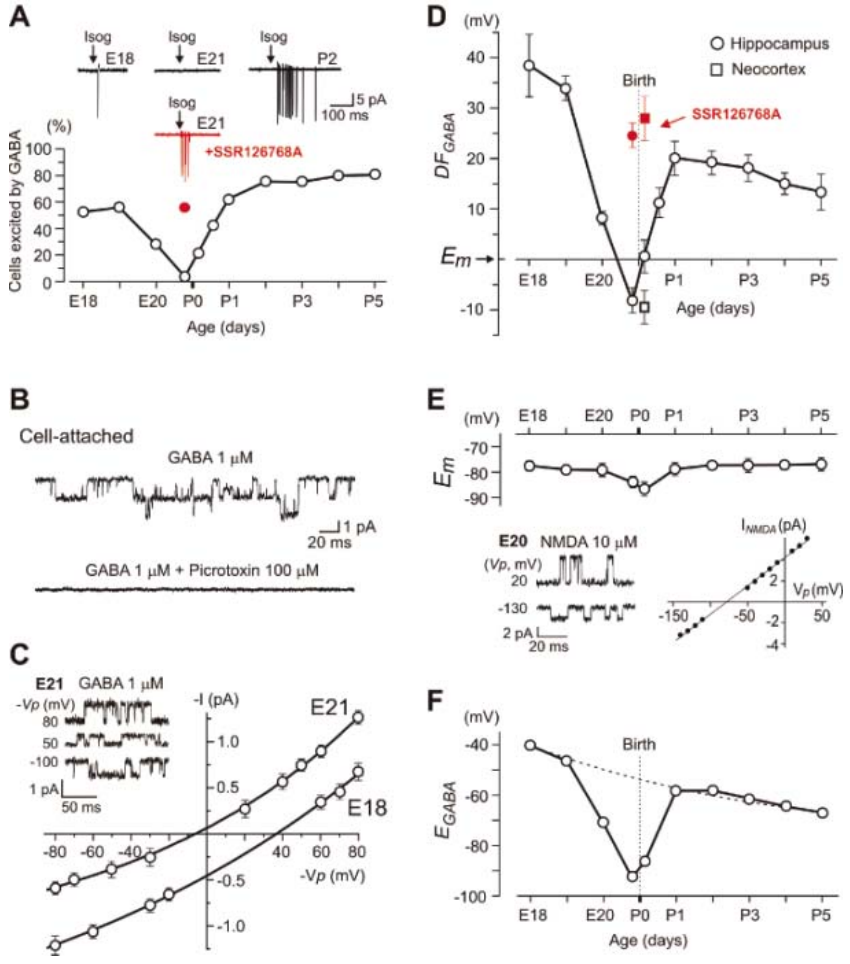

Fig. 1. Transient perinatal loss of the $GABA_A$-mediated excitation. (**A**) Responses of CA3 pyramidal cells recorded in cell-attached mode to the $GABA_A$ agonist isoguvacine. Below, summary plot of the proportion of cells excited by isoguvacine during the perinatal period. There is a transient loss of the excitatory effect of isoguvacine near term. Red corresponds to the fetuses whose mothers received SSR126768A. [E21 corresponds to the early phase of delivery (1 to 2 hours before birth); P0 is the day of birth; pooled data from 146 neurons.] (**B**) Cell-attached recordings of single $GABA_A$ channels with 1 μM of GABA in patch pipette (top trace); the channels were not observed in the presence of the $GABA_A$ antagonist picrotoxin (100 μM; bottom trace). (**C**) *I-V* relationships of the currents through $GABA_A$ channels in two cells at E21 and E18; their reversal potential corresponds to DF_{GABA}. (**D**) Summary plot of the age dependence of DF_{GABA} inferred from single $GABA_A$ channels recordings [mean ± SEM; 209 CA3 pyramidal cells (○) and 17 neocortical pyramidal cells (□); 6 to 24 patches for each point]. Red indicates pretreatment with SSR126768A (n values are 25 hippocampal and 9 neocortical patches). (**E**) Age dependence of the resting membrane potential (E_m) of CA3 pyramidal cells inferred from the reversal of single NMDA channels recorded in cell-attached mode (n = 84 cells; 4 to 12 patches for each point). (**F**) Age dependence of the $GABA_A$ reversal potential (E_{GABA} = E_m + DF_{GABA}). There is a transient hyperpolarizing shift of E_{GABA} near birth.

events in many neurons near term [9 ± 2% (Fig. 2)]. Thus, during delivery, the ability of GABA to increase $[Ca^{2+}]_i$ is significantly reduced.

What underlies the near-term switch in GABA actions? Because this phenomenon is not observed in fetal neurons grown in culture (*8*, *9*), we hypothesized that it is related to parturition and in particular to maternal hormones released during delivery. Parturition is initiated by a massive release of oxytocin (*19*). In addition to its pivotal role in parturition, there are also indications that oxytocin exerts multiple effects in the adult central nervous system (*19*–*25*). Maternal oxytocin easily crosses the placenta to reach the fetus (*26*), suggesting that oxytocin may be responsible for the hyperpolarizing switch in action of GABA in fetal neurons during delivery. With selective antibodies, we found a high density of oxytocin receptor immunoreactivity in the hippocampus and neocortex during the perinatal period (Fig. 3A and figs. S1 and S2). During cell-attached recordings from slices at E18 and P2, applications of oxytocin (1 μM) induced a negative shift in DF_{GABA} (Fig. 3, C and D) and suppressed GABA-mediated excitation (Fig. 3B). The effects of oxytocin were completely prevented by bath application of the selective oxytocin receptor antagonist atosiban (AT, 1 to 5 μM) (Fig. 3D). At term, application of oxytocin did not cause a significant effect on the hyperpolarizing DF_{GABA} (Fig. 3D), suggesting that the effects of exogenous oxytocin are occluded by the endogenous hormone. In keeping with this hypothesis, we found that atosiban switched DF_{GABA} from hyperpolarizing to depolarizing at term but not in fetal and postnatal neurons (Fig. 3D). Moreover, intracardial perfusion of E21 fetuses with artificial cerebrospinal fluid (ACSF, to wash out endogenous hormone) produced a similar shift of DF_{GABA} from hyperpolarizing to depolarizing (fig. S3). Addition of 1 μM oxytocin at the end of the perfusion restored hyperpolarizing values of DF_{GABA} (fig. S3). Therefore, endogenous oxytocin is present in slices at term and provides tonic activation of oxytocin receptors, leading to the shift of DF_{GABA}. We also found that the negative shift in DF_{GABA} from 38.4 ± 6.2 mV (n = 8) to –7.2 ± 2.2 mV (n = 18) occurred in E18 fetuses obtained from mothers treated with oxytocin (50 μg/kg) during 2 hours before cesarean delivery.

To directly measure the effects of oxytocin on $[Cl^-]_i$, we used two-photon chloride imaging in slices loaded with a chloride-sensitive dye, MQAE (Fig. 3, E and F) (*27*). In E18 and P4 slices, oxytocin (1 μM) produced a significant increase in the baseline fluorescence signal in half of the imaged cells, indicating a strong reduction of $[Cl^-]_i$ [average of 43 ± 4%, n values of 10 movies and 1792 cells (Fig. 3F)], and the effect was prevented by atosiban (5 μM; reduction of $[Cl^-]_i$ in 5 ± 3% cells, n values of 2 movies and 435 cells). Furthermore, incubation of P4 slices with oxytocin reversed the effect of isoguvacine on spontaneous calcium events [59 ± 17% imaged cells not activated by isoguvacine, n values of 3 movies and 228 cells (fig. S4)]. Thus, the effects of oxytocin fully matched the changes in GABA signaling occurring at term. This result indicates that oxytocin is sufficient to trigger changes of $[Cl^-]_i$.

To determine whether endogenous oxytocin is necessary for the near-term switch in the action of GABA, we treated pregnant rats orally with the selective oxytocin receptor antagonist SSR126768A (*28*) (1 mg/kg, starting from E20) and measured the consequences at term. Cell-attached recordings revealed major differences between treated and age-matched control pups, including strongly depolarizing values of DF_{GABA} (Fig. 1D, red circle) and a high proportion of cells excited by GABA (Fig. 1A, red circle). Similar effects were also observed in neocortical neurons, in which DF_{GABA} was –9.4 ± 3.4 mV in control rat pups (n = 8) and 28.3 ± 3.7 mV (n = 9) in pups of mothers pretreated with SSR126768A (Fig. 1D). Thus, maternal oxytocin is necessary and sufficient to trigger the near-term switch in GABA action in the hippocampus and neocortex.

What are the mechanisms underlying the oxytocin-mediated reduction of $[Cl^-]_i$ at term? Because the NKCC1 chloride inward cotransporter is responsible for elevated $[Cl^-]_i$ in immature neurons (*4*, *7*, *29*, *30*), we tested the effects of the selective NKCC1 antagonist bumetanide. We found that bumetanide (10 μM) produces a robust negative shift of DF_{GABA} and occludes the effects of oxytocin (fig. S5). The short latency of oxytocin actions (Fig. 3F) and the observation that blockade of oxytocin receptors does not alter chloride transporters gene expression (fig. S6) suggest that the hormone down-regulates NKCC1 activity.

Hypoxic-ischemic brain damage is a principal cause of newborn death and neurological impairment (*1*). We hypothesized that the excitatory-to-

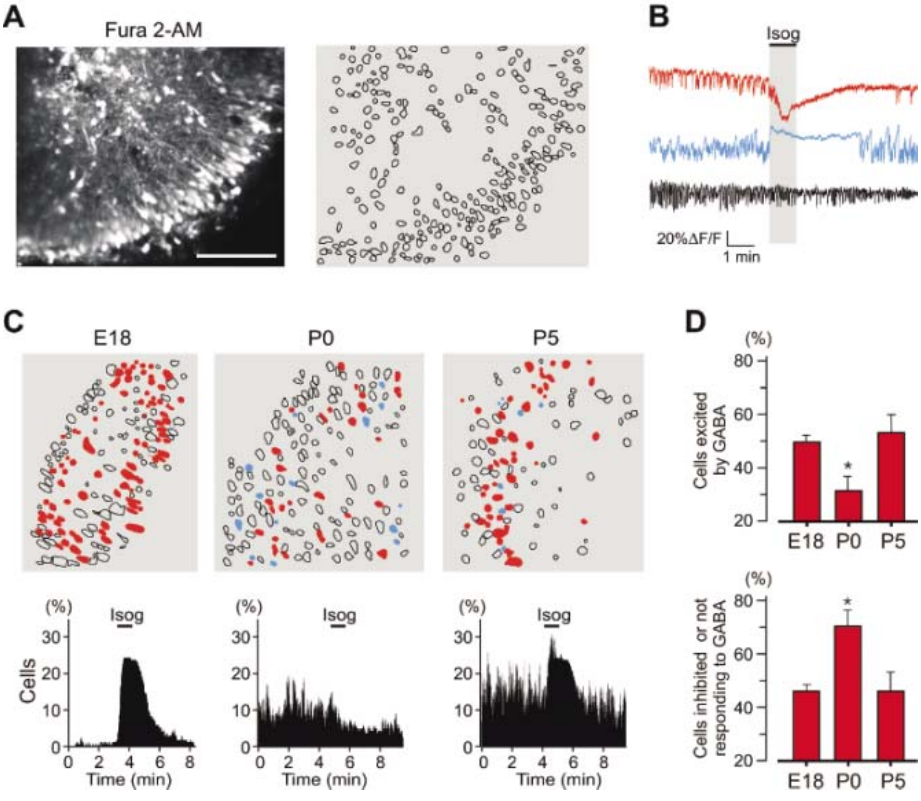

Fig. 2. Perinatal effects of $GABA_A$ receptors activation on $[Ca^{2+}]_i$ in CA3 neurons. (**A**) Two-photon $[Ca^{2+}]_i$ fluorescence image of the CA3 region from a P0 hippocampal slice loaded with fura 2-AM; scale bar indicates 100 μm. (Right) Automatically detected contours of the cells. (**B**) Three types of $[Ca^{2+}]_i$ responses ($\Delta F/F$) to bath application of the $GABA_A$ agonist isoguvacine (10 μM, 1 min): excited (red), inhibited (blue), or not affected (black) by isoguvacine (Isog). (**C**) Contour maps representing the distribution of different cellular responses to isoguvacine at E18, P0, and P5: excited (red), inhibited (blue), and not affected (open contours). Bottom histograms show the percentage of cells that are detected as being active on each movie frame corresponding to the above contour plots (140 ms per frame). Isoguvacine application (10 μM) produces a significant increase in the fraction of active neurons at E18 and P5, whereas it slightly decreased the activity at birth. (**D**) Histograms of the averaged fraction of imaged neurons excited (top) or inhibited or nonaffected (bottom) by isoguvacine at different ages (for P0, n values of 10 movies and 1546 cells; for E18, n values of 2 movies and 375 cells; and for P5, n values of 3 movies and 328 cells; *P < 0.01). Error bars indicate SEM.

inhibitory switch in GABA signaling reduces neuronal activity and metabolic demand, thus helping to protect fetal neurons from hypoxic insults (*31*). Episodes of anoxia and aglycemia were induced by superfusion with a solution in which oxygen was substituted for nitrogen and glucose was substituted for sucrose. The onset of anoxic depolarization (AD) that is an electrophysiological marker of neuronal death (*31*, *32*) was measured by using extracellular field potential recordings in the intact hippocampi of E21 rats in vitro after various treatments in vivo to the mother and/or to the fetuses intracardially before the in vitro experiment (Fig 4). In control fetuses, AD occurred after 55.6 ± 1.4 min (n = 30) of perfusion with the anoxic-aglycemic solution (Fig. 4). In the hippocampi prepared from the fetuses intracardially perfused with atosiban (5 μM; n = 15) or from the fetuses whose mothers received SSR126768A (1 mg/kg; n = 19), AD onset was significantly accelerated to 44.1 ± 1.1 min (n = 34; $P < 0.01$). Bumetanide (10 μM) applied in the presence of the oxytocin receptor antagonists delayed AD to the control values (53.4 ± 1.7 min; n = 18; $P < 0.01$). Bumetanide (10 μM)

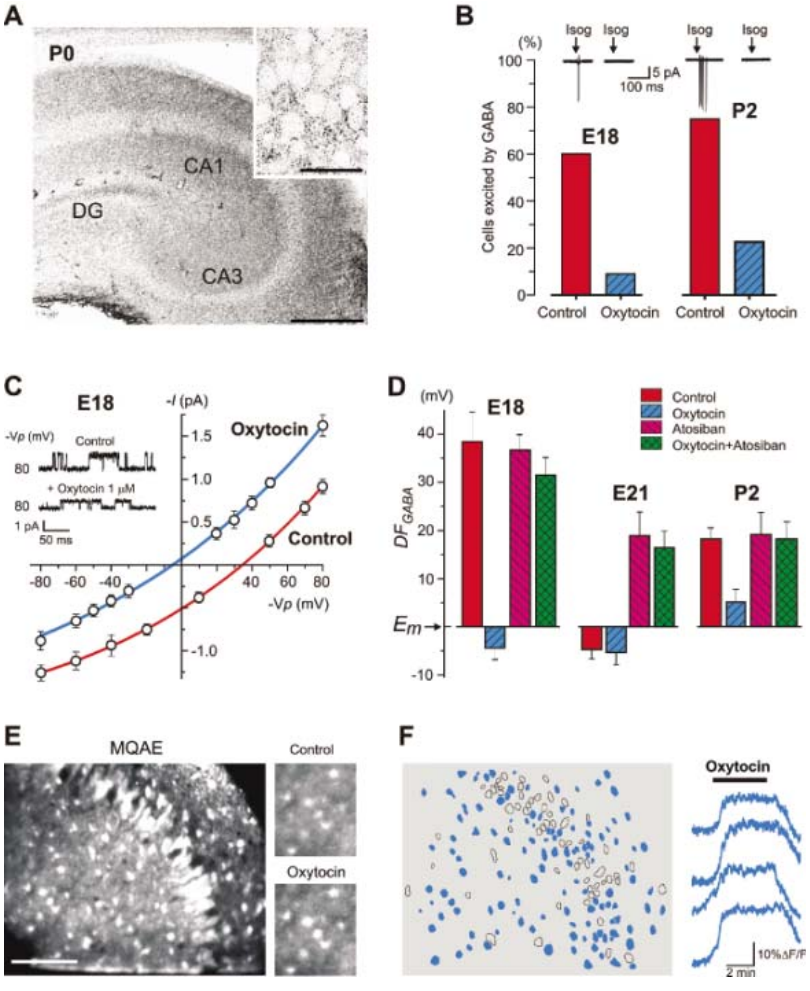

Fig. 3. Oxytocin causes a switch in $GABA_A$ signaling from depolarizing to hyperpolarizing. (**A**) Oxytocin-receptor immunostaining of a P0 rat hippocampus; (inset) CA3 pyramidal cells layer. Bars, 200 μm and (inset) 20 μm. (**B**) Histograms of the proportion of cells excited by brief application of isoguvacine (Isog) in control and in the presence of oxytocin (1 μM) at E18 and P2 (n = 57 cells). (**C**) *I-V* relationships of the currents through single $GABA_A$ channels recorded from two CA3 pyramidal cells at E18 in control and after addition of oxytocin (1 μM). (**D**) Histograms of DF_{GABA} measured at E18, E21, and P2 in control conditions and in the presence of oxytocin (1 μM), antagonist of oxytocin receptors atosiban (1 to 5 μM), and oxytocin plus atosiban (n = 187 cells). (**E**) Two-photon imaging of $[Cl^-]_i$ in P4 hippocampal slice loaded with Cl^- indicator MQAE. Scale bar, 100 μm. (Right) $[Cl^-]_i$ fluorescence change produced by oxytocin application. The intensity of the fluorescence signal increases, and $[Cl^-]_i$ decreases, in the illustrated region. (**F**) Automatically detected contours of the cells imaged in (E), indicating the distribution of cells in which oxytocin application produced a significant decrease in $[Cl^-]_i$ (blue filled contours). On the right, chloride fluorescence changes ($\Delta F/F$) in four representative neurons. Time resolution is 100 ms per frame.

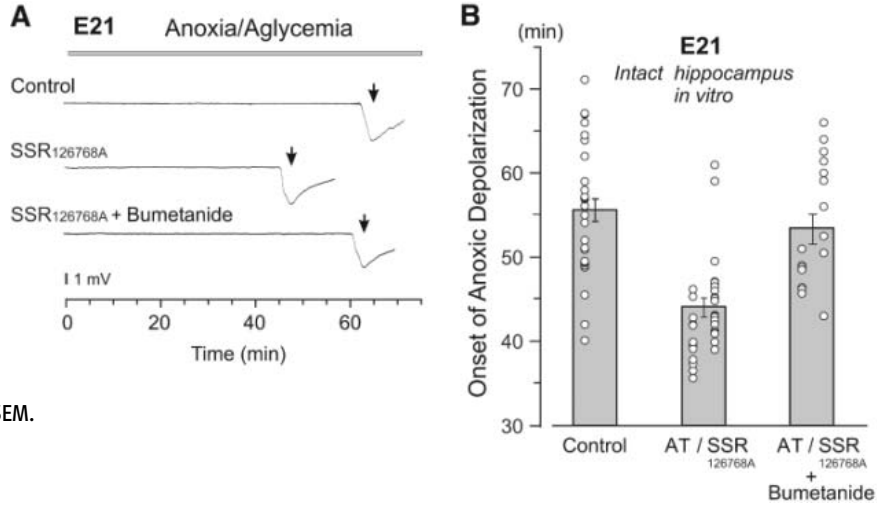

Fig. 4. Blockade of oxytocin receptors decreases fetal brain resistance to anoxia-aglycemia at birth. (**A**) Representative traces to illustrate the effects of anoxic-aglycemic solution on extracellular field potential recordings from E21 intact hippocampi. Arrows indicate terminal AD that marks neuronal death. AD occurs earlier in the presence of SSR126768A (middle trace). Addition of bumetanide (10 μM) occludes the effects of the antagonist and restores the initial delay (bottom trace). (**B**) Summary plot of the onset of AD in control, in the presence of the oxytocin receptors antagonists atosiban (AT, 5 μM, fetal intracardial perfusion and SSR126768A (1 mg/kg to the mother), and after further addition of bumetanide (10 μM). Each circle corresponds to one hippocampus (n = 82 intact hippocampi at E21). Error bars indicate SEM.

occluded the effects of the oxytocin receptor antagonists and restored the control delays (53.4 ± 1.7 min, $n = 18$; $P < 0.01$). These data indicate that maternal oxytocin exerts a neuroprotective action on fetal neurons during parturition and that this action is likely due to a reduction of $[Cl^-]_i$.

Our results suggest that oxytocin, in addition to its well-established role in labor and lactation and its multiple effects in the adult central nervous system (*19*–*25*), also exerts a powerful action on fetal neurons. This mechanism adds a previously unknown facet to the plasticity of GABA signaling via modulation of $[Cl^-]_i$ (*4*, *33*). The dual action produced by a single messenger in the mother and fetus enables a perfect timing for adaptation of fetal neurons to delivery.

References and Notes

1. J. J. Volpe, *Neurology of the Newborn* (Saunders, Philadelphia, ed. 4, 2000).
2. Y. Ben Ari, *Nat. Rev. Neurosci.* **3**, 728 (2002).
3. D. F. Owens, A. R. Kriegstein, *Nat. Rev. Neurosci.* **3**, 715 (2002).
4. J. A. Payne, C. Rivera, J. Voipio, K. Kaila, *Trends Neurosci.* **26**, 199 (2003).
5. R. Tyzio *et al.*, *J. Neurosci.* **19**, 10372 (1999).
6. Y. Ben-Ari, E. Cherubini, R. Corradetti, J.-L. Gaïarsa, *J. Physiol.* **416**, 303 (1989).
7. C. Rivera *et al.*, *Nature* **397**, 251 (1999).
8. D. F. Owens, L. H. Boyce, M. B. Davis, A. R. Kriegstein, *J. Neurosci.* **16**, 6414 (1996).
9. G. Chen, P. Q. Trombley, A. N. van den Pol, *J. Physiol.* **494**, 451 (1996).
10. R. Serafini, A. Y. Valeyev, J. L. Barker, M. O. Poulter, *J. Physiol.* **488**, 371 (1995).
11. Materials and methods are available as supporting material on *Science* Online.
12. X. Leinekugel, I. Medina, I. Khalilov, Y. Ben-Ari, R. Khazipov, *Neuron* **18**, 243 (1997).
13. R. Tyzio *et al.*, *J. Neurophysiol.* **90**, 2964 (2003).
14. D. Maric *et al.*, *Eur. J. Neurosci.* **10**, 2532 (1998).
15. J. A. Connor, H. Y. Tseng, P. E. Hockberger, *J. Neurosci.* **7**, 1384 (1987).
16. R. Yuste, L. C. Katz, *Neuron* **6**, 333 (1991).
17. J. J. LoTurco, D. F. Owens, M. J. Heath, M. B. Davis, A. R. Kriegstein, *Neuron* **15**, 1287 (1995).
18. O. Garaschuk, E. Hanse, A. Konnerth, *J. Physiol.* **507**, 219 (1998).
19. G. Gimpl, F. Fahrenholz, *Physiol. Rev.* **81**, 629 (2001).
20. A. Argiolas, G. L. Gessa, *Neurosci. Biobehav. Rev.* **15**, 217 (1991).
21. M. Raggenbass, *Prog. Neurobiol.* **64**, 307 (2001).
22. K. Tomizawa *et al.*, *Nat. Neurosci.* **6**, 384 (2003).
23. M. Kosfeld, M. Heinrichs, P. J. Zak, U. Fischbacher, E. Fehr, *Nature* **435**, 673 (2005).
24. D. T. Theodosis *et al.*, *Mol. Cell. Neurosci.* **31**, 785 (2006).
25. D. Huber, P. Veinante, R. Stoop, *Science* **308**, 245 (2005).
26. A. Malek, E. Blann, D. R. Mattison, *J. Matern. Fetal Med.* **5**, 245 (1996).
27. N. Marandi, A. Konnerth, O. Garaschuk, *Pflugers Arch.* **445**, 357 (2002).
28. C. Serradeil-Le Gal *et al.*, *J. Pharmacol. Exp. Ther.* **309**, 414 (2004).
29. J. Yamada *et al.*, *J. Physiol.* **557**, 829 (2004).
30. V. I. Dzhala *et al.*, *Nat. Med.* **11**, 1205 (2005).
31. V. Dzhala, Y. Ben-Ari, R. Khazipov, *Ann. Neurol.* **48**, 632 (2000).
32. P. Lipton, *Physiol. Rev.* **79**, 1431 (1999).
33. H. Fiumelli, L. Cancedda, M. M. Poo, *Neuron* **48**, 773 (2005).

34. We thank I. Jorquera, I. Chudotvorova, D. Diabira, and C. Pellegrino for technical assistance; K. Krnjevic, M. Milh, I. Medyna, J. L. Gaiarsa, A. Ivanov, and C. Hammond for helpful comments on the manuscript; and Sanofi-Synthelabs for the gift of SSR126768A. This work was supported by INSERM, Fondation pour la Recherche Médicale, L'Agence Nationale de la Recherche, Federation pour la Recherche sur le Cerveau and Rotary International, Conseil régional Provence-Alpes-Côte d'Azur, and European Community grant LSHB-CT-2004-503467.

Supporting Online Material

www.sciencemag.org/cgi/content/full/314/5806/1788/DC1
Materials and Methods
Figs. S1 to S6
References

31 July 2006; accepted 9 November 2006
10.1126/science.1133212

ATP Release Guides Neutrophil Chemotaxis via P2Y2 and A3 Receptors

Yu Chen,[1]* Ross Corriden,[1,2]* Yoshiaki Inoue,[1] Linda Yip,[1] Naoyuki Hashiguchi,[1] Annelies Zinkernagel,[4] Victor Nizet,[4] Paul A. Insel,[2,3] Wolfgang G. Junger[1]†

Cells must amplify external signals to orient and migrate in chemotactic gradient fields. We find that human neutrophils release adenosine triphosphate (ATP) from the leading edge of the cell surface to amplify chemotactic signals and direct cell orientation by feedback through P2Y2 nucleotide receptors. Neutrophils rapidly hydrolyze released ATP to adenosine that then acts via A3-type adenosine receptors, which are recruited to the leading edge, to promote cell migration. Thus, ATP release and autocrine feedback through P2Y2 and A3 receptors provide signal amplification, controlling gradient sensing and migration of neutrophils.

Neutrophils are primary phagocytic cells with important roles in host defense and tissue repair. However, activated neutrophils damage host tissues and contribute to chronic inflammatory diseases, including rheumatoid arthritis, inflammatory bowel disease, and asthma (*1*). A key feature of neutrophils is their ability to detect and migrate to compromised tissues by following a concentration gradient of chemotactic substances released from microbial pathogens or injured cells.

[1]Department of Surgery, University of California San Diego, San Diego, CA 92103, USA. [2]Department of Pharmacology, University of California San Diego, La Jolla, CA 92093, USA. [3]Department of Medicine, University of California San Diego, La Jolla, CA 92093, USA. [4]Department of Pediatrics, University of California San Diego, La Jolla, CA 92093, USA.

*These authors contributed equally to this work.
†To whom correspondence should be addressed. E-mail: wjunger@ucsd.edu

Neutrophils can respond to chemoattractant gradients that differ in concentration by as little as 1% across the length of the cell body (*2*). Chemotaxis must involve signal amplification because a strongly polarized distribution of intracellular signal-transduction components is observed even in shallow gradients. The mechanisms of signal amplification are unclear (*3*, *4*). We identified the polarized release of adenosine triphosphate (ATP), the activation of P2Y2 receptors, and the translocation and activation of A3 adenosine receptors as key mechanisms of signal amplification that control cell orientation and direct the migration of neutrophils.

Membrane deformation caused by mechanical or osmotic stress induces the release of cellular ATP from mammalian cells; however, detailed information on the underlying mechanisms is lacking (*5*, *6*). Because cell migration also involves membrane deformation, we tested whether the stimulation of human neutrophils with the chemoattractant *N*-formyl-Met-Leu-Phe (FMLP) causes ATP release. Treatment of cells (10^7 cells in 250 μl of solution) with 100 nM FMLP rapidly tripled extracellular ATP concentrations in bulk media (Fig. 1, A and B) by inducing the release of ~0.5% of their ATP pool. Concentrations of extracellular ATP and its hydrolytic products adenosine monophosphate (AMP) and adenosine peaked 5 min after FMLP stimulation; but while the concentration of ATP returned to basal levels after 15 min, AMP and adenosine concentrations remained >5–fold above baseline (Fig. 1B), which is consistent with the presence of ecto–adenosine triphosphatases (ecto-ATPases) (*7*, *8*). Neutrophils completely hydrolyzed exogenous ATP (5 μM) within 2 min after ATP addition, which suggests that they have potent ecto-ATPase activity (Fig. 1C).

Because membrane deformation occurs predominantly at the leading edge closest to the chemoattractant source, we hypothesized this region to be the principal site of ATP release. Fluorescent microscopy that was used to visualize ATP release [based on conversion of nicotinamide adenine dinucleotide phosphate ($NADP^+$) to its reduced form NADPH] revealed that neutrophils discharge ATP within seconds after FMLP stimulation (Fig. 1D and movies S1 to S3), with ATP release highest near the cell membrane with the greatest degree of protrusion (Fig. 1D, inset).

Extracellular ATP and adenosine modulate neutrophil functions, including chemotaxis (*8*, *9*). We tested the effect of apyrase, which hydrolyzes ATP, on chemotaxis in a trans-well system composed of upper wells with neutrophils and lower wells with 1 nM FMLP separated by a filter with 3-μm pores. Addition of apyrase to the upper wells reduced chemotaxis by nearly 100% (Fig. 2A).

Apyrase also inhibited FMLP-induced superoxide formation, implying that FMLP-promoted responses require ATP. Addition of apyrase to the lower wells reduced chemotaxis only by ~40%, which suggests that ATP release is essential for the initiation of chemotaxis but not for maintaining migration once it is initiated. Microscopic analysis of neutrophil chemotaxis toward the tip of a micropipette filled with 100 nM FMLP confirmed this conclusion: Although 79% of control cells migrated toward FMLP with <60° angular deviation from a straight path, the addition of apyrase (10 U/ml) diminished the proper orientation of cells so that only 17% migrated correctly to the chemotactic source (Fig. 2B and movies S4 and S5). Other ATP-hydrolytic enzymes (e.g., ATPase and alkaline phosphatase) had similar effects (fig. S1, A and B), confirming ATP release to be crucial for gradient sensing and cell orientation.

Using the trans-well assay, we found that the nonhydrolyzable ATP analog adenosine 5′-*O*-(3-thiotriphosphate) (ATP-γ-S) increased FMLP-promoted chemotaxis and cell migration in the absence of FMLP, regardless of whether ATP-γ-S was added to the upper or lower well (Fig. 2B), which indicates that extracellular ATP induces chemokinesis (random cell migration) but is not chemotactic. Uniformly added ATP-γ-S (100 μM) impaired chemotaxis to a point source of FMLP, with only 31% of cells migrating along the correct path (Fig. 2C and movie S6), which implies that ATP-γ-S treatment obscures polarized ATP released from the cells and interferes with gradient sensing and proper cell orientation.

Adenosine and ATP are respective ligands of a family of four P1 adenosine (A1, A2a, A2b, and A3) and 15 P2 nucleotide receptors that include ionotropic P2X (P2X1-7) and G protein–coupled P2Y (P2Y1, 2, 4, 6, 11, 14) subtypes (*10*, *11*). We used the general P2-receptor antagonist suramin to test the role of P2 receptors in chemotaxis. Suramin reduced chemotaxis by 80% (Fig. 2D), whereas the P2X-selective antagonists 1-[*N*,*O*-bis(5-isoquinolinesulphonyl)-*N*-methyl-L-tyrosyl]-4-phenylpiperazine (KN-62) and oxidized ATP did not (fig. S1C), implying that P2Y receptors are involved in neutrophil chemotaxis.

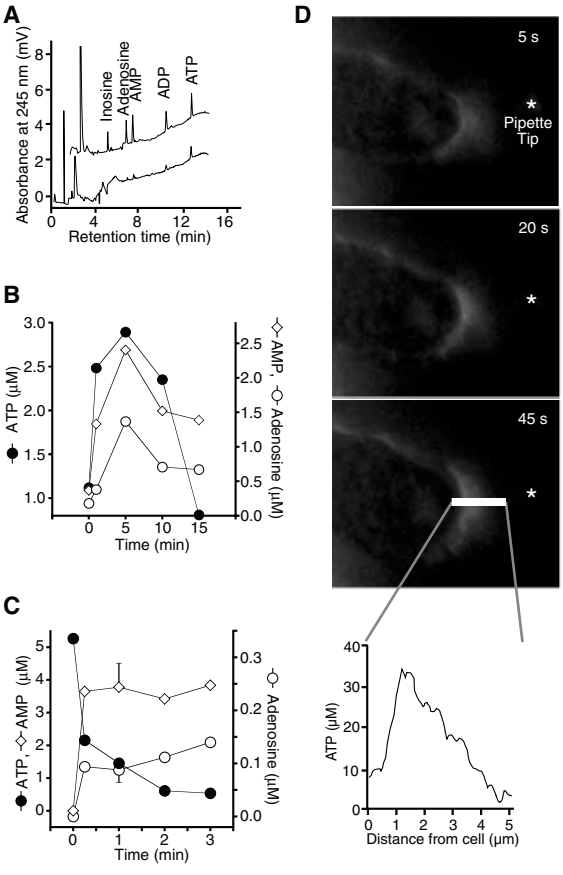

Fig. 1. Release of ATP by FMLP-stimulated neutrophils and formation of adenosine. (**A**) ATP released in response to FMLP was determined with high-performance liquid chromatography (HPLC) analysis of extracellular ATP and its breakdown products. A pair of chromatograms shows ATP and its hydrolytic products in the extracellular environment of neutrophils before (lower trace) or after (upper trace) stimulation with 100 nM FMLP. ADP, adenosine diphosphate. (**B**) Extracellular concentrations of ATP, AMP, and adenosine measured with HPLC analysis at different time points after stimulation of neutrophils with 100 nM FMLP. (**C**) Extracellular ATP, AMP, and adenosine at different times after addition of exogenous ATP to isolated neutrophils. Error bars indicate SD of triplicate determinations. (**D**) Release of ATP from living cells stimulated in a gradient field of FMLP generated with a micropipette (asterisks) was visualized with the use of a two-enzyme assay system that catalyzes the conversion of $NADP^+$ to NADPH in the presence of ATP. The generation of NADPH was monitored in real time by means of fluorescence microscopy (excitation wavelength, 340 nm; emission wavelength, 460 nm). Images were captured at 12 frames per minute. (**Inset**) Extracellular ATP concentrations based on calibration of gray values with a known ATP standard.

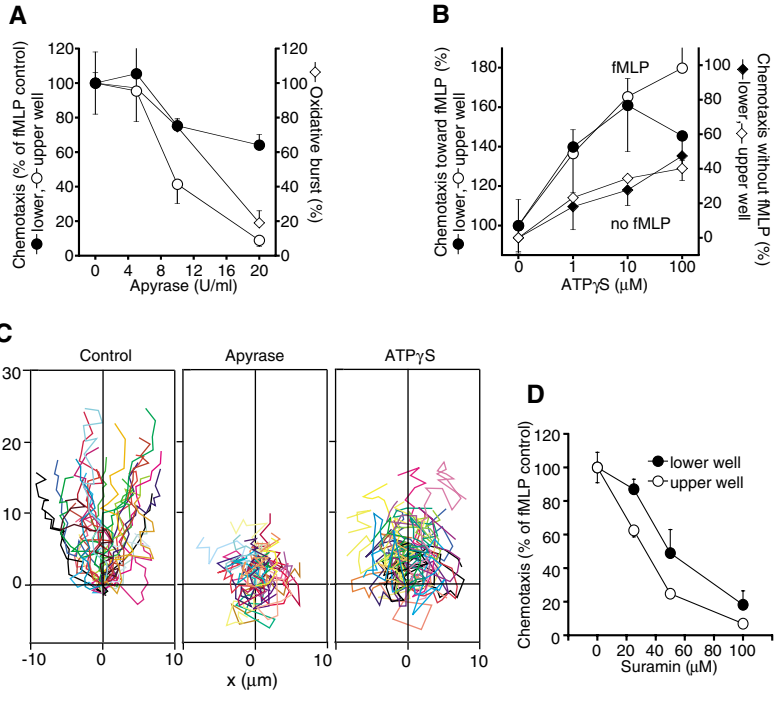

Fig. 2. Effect of exogenous ATP on neutrophil chemotaxis. Trans-well assays with neutrophils in upper wells separated from lower wells containing 1 nM FMLP by a filter with 3-μm pore size were used to assess chemotaxis. (**A**) Effect of apyrase added to the lower or upper well on neutrophil chemotaxis and on FMLP-induced oxidative burst. Cell responses are expressed as a percent of the response to FMLP in the absence of apyrase. (**B**) Treatment with ATP-γ-S in the presence (circles) or absence (diamonds) of FMLP. (**C**) Cell migration studied under the microscope was analyzed by tracing the paths of cells migrating toward a micropipette tip containing 100 nM FMLP in the absence (left) or presence (middle) of 10 U/ml of apyrase or 100 μM ATP-γ-S (right). The *y* axis of the traces represents the direction toward the chemoattractant source, and the *x* axis shows the deviation from the straight path. Cell traces were arranged to show their origins at $x = y = 0$. (**D**) Effect of the P2-receptor antagonist suramin on FMLP-induced cell migration. Error bars in (A), (B), and (D) indicate SD of triplicate determinations.

Real-time reverse transcription polymerase chain reaction (RT-PCR) analysis suggests that neutrophils and human promyelocytic HL60 cells express predominantly A2a-, P2Y2-, and A3-receptor–derived mRNA (Fig. 3, A and B). Immunostaining showed that A3 receptors, but not A2a or P2Y2 receptors, are concentrated at the leading edge of polarized cells (fig. S2, A and B), which suggests that A3 receptors may be involved in chemotaxis. In the trans-well assay, adenosine (1 nM to 1 μM) enhanced chemotaxis, particularly when added in the lower wells along with FMLP (Fig. 4A). Higher concentrations of exogenous adenosine slightly diminished chemotaxis (Fig. 4A and fig. S3A), likely by either activating A2a receptors, which are widely recognized for their inhibitory effects on neutrophils (*8*–*12*) or obscuring endogenous adenosine generated at the leading edge of migrating cells. Removal of extracellular adenosine with adenosine deaminase (ADA), which converts adenosine to inosine, or inhibition of A3 receptors with 3-ethyl-5-benzyl-2-methyl-4-phenylethynyl-6-phenyl-1,4-(±)-dihydropyridine-3,5-dicarboxylate (MRS 1191) inhibited chemotaxis toward FMLP (Fig. 4, B and E), platelet-activating factor, 3% autologous zymosan-activated serum, interleukin-8, and live bacteria (fig. S3, B to D). Inosine generated by ADA did not affect chemotaxis (fig. S3E).

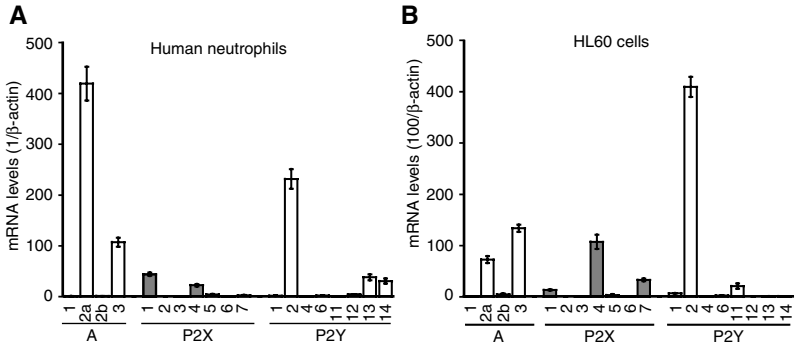

Fig. 3. P1- and P2-receptor expression in neutrophils (**A**) and HL60 cells (**B**). P1- and P2-receptor mRNA expression in human neutrophils and HL60 cells was estimated with real-time RT-PCR analysis and expressed in relation to β-actin. Error bars in (A) and (B) indicate SD of triplicate determinations.

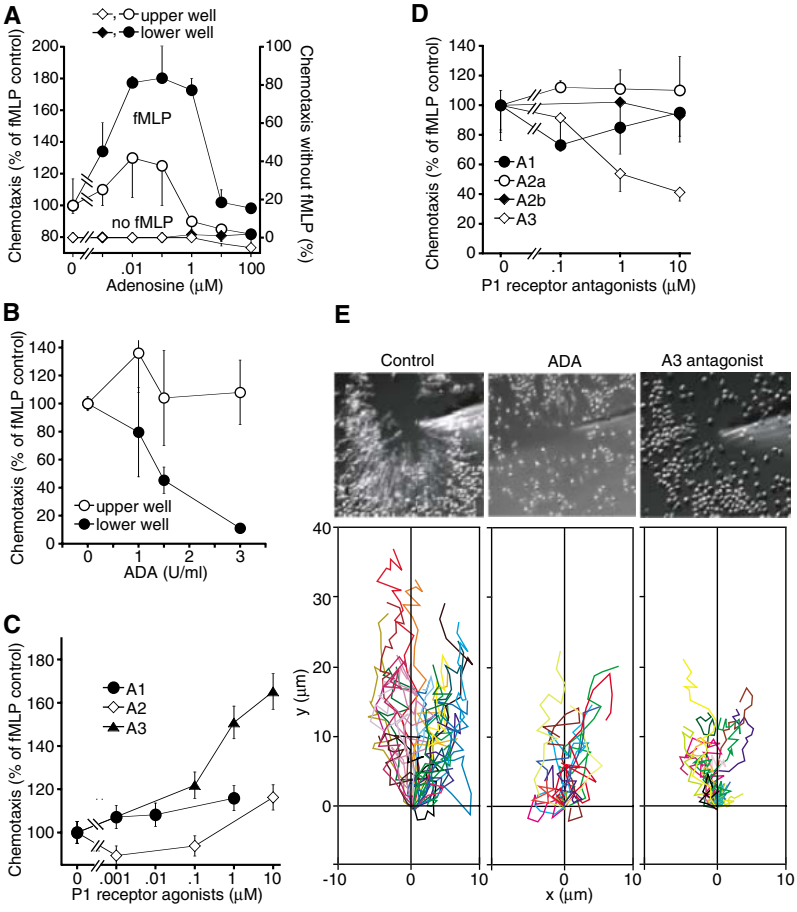

Fig. 4. Role of adenosine and P1 receptors in neutrophil migration. (**A**) The effect of exogenous adenosine added to the lower or upper wells on neutrophil chemotaxis was assessed with the trans-well assay in the presence (circles) or absence (diamonds) of FMLP. (**B**) Effect of ADA on FMLP-induced chemotaxis. (**C**) Effects of the A3-receptor–selective agonist *N*(6)-(3-iodobenzyl) adenosine-5'-*N*-methylcarboxamide (IB-MECA) and of the A2- and A1-receptor–selective agonists 2-*p*-[2-carboxyethyl] phenethylamino-5'-*N*-ethylcarboxamidoadenosine hydrochloride (CGS 21680) and *N*6-cyclopentyl-adenosine (CPA), respectively, on chemotaxis toward FMLP. (**D**) Effects of A3-receptor–selective antagonist MRS 1191 and antagonists of other P1 receptors on chemotaxis toward FMLP. (**E**) Composite images and cell migration traces of cells migrating toward a micropipette tip containing 100 nM FMLP in the absence or presence of 10 U/ml of ADA or 10 μM MRS 1191. Error bars in (A) to (D) indicate SD of triplicate determinations.

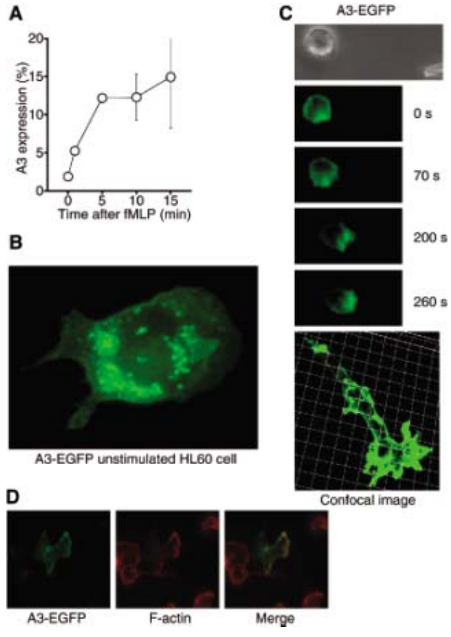

Fig. 5. Localization of A3 receptors to the leading edge of migrating cells. (**A**) The cell surface expression of A3 receptors of human neutrophils at different time points after stimulation of cells with 100 nM FMLP was assessed with flow cytometry and a primary antibody recognizing an extracellular domain of the receptor. Error bars indicate SD of triplicate determinations. (**B**) Fluorescent image of an unstimulated HL60 cell expressing an A3-EGFP fusion protein. (**C**) HL60 cell expressing an A3-EGFP fusion protein migrating toward a micropipette tip containing 100 nM FMLP (bright field image on top). The confocal image at the bottom shows an HL60 cell migrating from the top left to the bottom right corner. (**D**) Colocalization of A3-EGFP fusion protein and actin in cells globally stimulated with 100 nM FMLP.

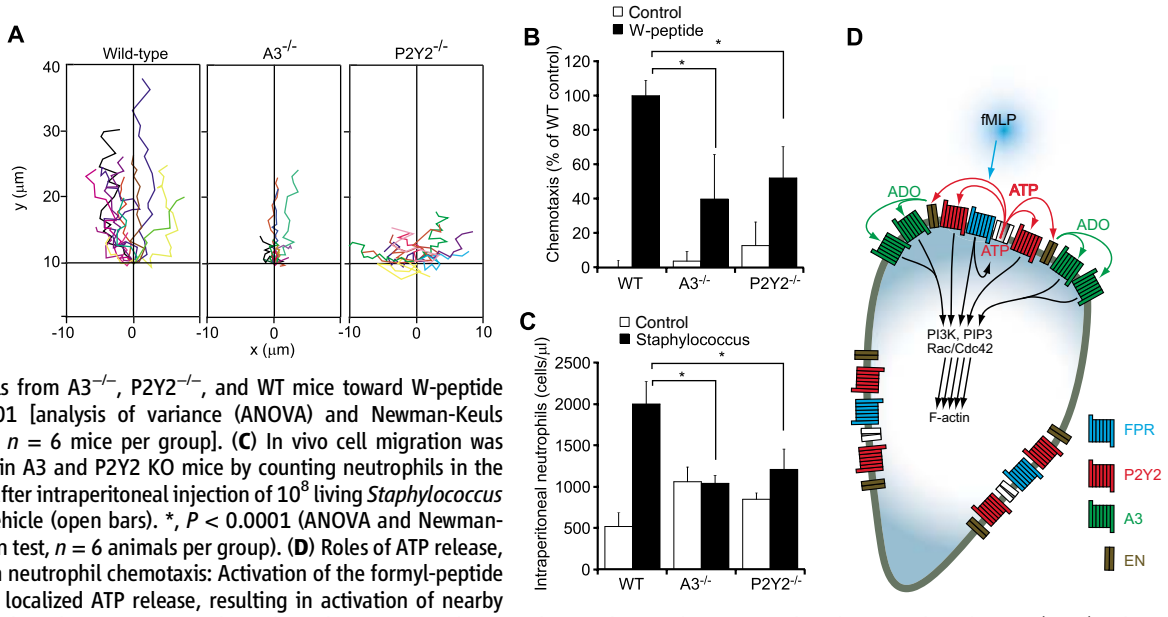

Fig. 6. P2Y2 and A3 receptors control neutrophil chemotaxis in vitro and in vivo. (**A**) Migration paths of neutrophils [isolated from the bone marrow of wild-type (WT) mice and mice deficient of A3 and P2Y2 receptors] migrating toward the FMLP-receptor ligand W-peptide (100 nM). (**B**) Trans-well chemotaxis assays of neutrophils from $A3^{-/-}$, $P2Y2^{-/-}$, and WT mice toward W-peptide (100 nM). *, $P < 0.0001$ [analysis of variance (ANOVA) and Newman-Keuls multiple-comparison test, $n = 6$ mice per group]. (**C**) In vivo cell migration was assessed in WT mice and in A3 and P2Y2 KO mice by counting neutrophils in the peritoneal cavity 4 hours after intraperitoneal injection of 10^8 living *Staphylococcus* bacteria (solid bars) or vehicle (open bars). *, $P < 0.0001$ (ANOVA and Newman-Keuls multiple-comparison test, $n = 6$ animals per group). (**D**) Roles of ATP release, P2Y2, and A3 receptors in neutrophil chemotaxis: Activation of the formyl-peptide receptor (FPR) stimulates localized ATP release, resulting in activation of nearby P2Y2 receptors that amplify chemotactic signals and gradient sensing by stimulating the production of phosphoinositide 3-kinase (PI3K), phosphatidylinositol 3,4,5-trisphosphate (PIP3), and recruitment of Rac, Cdc42, and F-actin to the leading edge. Translocation of A3 receptors to the leading edge, adenosine (ADO) formation by ecto-ATPases/nucleotidases (EN), and autocrine activation of A3 receptors facilitate directed migration. Error bars in (B) and (C) indicate SD.

The finding that the agonists and the antagonist of A3 receptors (but not of other P1-receptor subtypes) affected neutrophil chemotaxis further suggested a special role for A3 receptors in chemotaxis (Fig. 4, C and D). To determine whether A3 receptors control gradient sensing or migration speed, we examined the effect of MRS 1191 on neutrophil chemotaxis under the microscope. MRS 1191 (10 μM) reduced the migration speed of cells toward FMLP from 2.4 ± 1.0 to 0.5 ± 0.7 μm/min (Fig. 4E and movies S7 and S8), whereas gradient sensing seemed largely unaffected. Thus, A3 receptors appear to be the key adenosine receptors that regulate neutrophil chemotaxis by controlling cell migration.

Flow cytometric analysis revealed that FMLP stimulation rapidly increases surface expression of A3 receptors in human neutrophils (Fig. 5A). This finding was confirmed with HL60 cells stably transfected with an A3 receptor–enhanced green fluorescent protein (EGFP) construct and differentiated with dimethyl sulfoxide to induce a neutrophil-like phenotype capable of chemotaxis (*13*, *14*). A3 receptors in resting cells were predominantly localized in cytosolic granules (Fig. 5B). Upon exposure to an FMLP gradient, A3 receptors, but not P2Y2 receptors, rapidly translocated to the cell surface near the leading edge, accumulated on filopodia-like protrusions, and colocalized with F-actin (Fig. 5C and movies S9 and S10), a marker for the leading edge of polarized cells (*15*).

We further studied the chemotaxis of neutrophils from bone marrow of A3- and P2Y2-receptor knockout (KO) mice ($A3^{-/-}$ and $P2Y2^{-/-}$) using the murine chemotactic peptide Trp-Lys-Tyr-Met-Val-Met-NH_2 (W-peptide) (*16*). Chemotaxis of neutrophils from both KO mouse strains was less than that of wild-type mice (Fig. 6, A and B). Neutrophils lacking A3 receptors showed correct directionality but diminished speed, whereas cells without P2Y2 receptors showed a loss in gradient sensing. We confirmed the importance of both receptors for neutrophil chemotaxis in vivo by assessing cell recruitment to the peritoneal cavity of KO mice intraperitoneally injected with 1 nM W-peptide or 10^8 *Staphylococcus aureus* bacteria (Fig. 6C).

Our results lead to a model in which polarized ATP release, in response to chemotactic receptor stimulation, facilitates gradient sensing by activating multiple adjacent P2Y2 receptors that control cell orientation in a chemotactic gradient. Adenosine formation and A3-receptor accumulation at the leading edge likely constitute a second stage of autocrine signal amplification that facilitates chemotaxis by controlling migration speed (Fig. 6D). Other receptors, such as A2a receptors, may contribute to chemotaxis by facilitating membrane retraction at the receding end. This system may help neutrophils locate bacteria and damaged tissues, which also generate extracellular ATP (*17*). In view of their importance for cell migration, P2Y2 and A3 receptors are potential therapeutic targets for the treatment of inflammatory diseases (*18*, *19*).

Chemotaxis in *Dictyostelium discoideum* is controlled by extracellular signaling systems that use cyclic AMP (cAMP) production and the activation of cAMP receptors (*20*–*22*). The results shown here define an analogous mammalian navigation system based on polarized ATP release and purinergic receptor activation in neutrophils.

References and Notes

1. S. J. Weiss, *N. Engl. J. Med.* **320**, 365 (1989).
2. S. H. Zigmond, *J. Cell Biol.* **75**, 606 (1977).
3. A. J. Ridley *et al.*, *Science* **302**, 1704 (2003).
4. P. J. Van Haastert, P. N. Devreotes, *Nat. Rev. Mol. Cell Biol.* **5**, 626 (2004).
5. P. Bodin, G. Burnstock, *Neurochem. Res.* **26**, 959 (2001).
6. G. Yegutkin, P. Bodin, G. Burnstock, *Br. J. Pharmacol.* **129**, 921 (2000).
7. H. Zimmermann, *Naunyn-Schmiedebergs Arch. Pharmakol.* **362**, 299 (2000).
8. B. B. Fredholm, *Gen. Pharmacol.* **28**, 345 (1997).
9. Y. Chen, A. Shukla, S. Namiki, P. A. Insel, W. G. Junger, *J. Leukocyte Biol.* **76**, 245 (2004).
10. G. Burnstock, G. E. Knight, *Int. Rev. Cytol.* **240**, 31 (2004).
11. B. B. Fredholm, A. P. Ijzerman, K. A. Jacobson, K. N. Klotz, J. Linden, *Pharmacol. Rev.* **53**, 527 (2001).
12. Y. Zhang, J. Palmblad, B. B. Fredholm, *Biochem. Pharmacol.* **51**, 957 (1996).
13. A. B. Hauert, S. Martinelli, C. Marone, V. Niggli, *Int. J. Biochem. Cell Biol.* **34**, 838 (2002).
14. G. Servant *et al.*, *Science* **287**, 1037 (2000).
15. G. P. Downey, *Curr. Opin. Immunol.* **6**, 113 (1994).
16. J. K. Seo *et al.*, *J. Immunol.* **158**, 1895 (1997).
17. A. la Sala *et al.*, *J. Leukocyte Biol.* **73**, 339 (2003).
18. D. Knight *et al.*, *J. Leukocyte Biol.* **62**, 465 (1997).
19. B. A. Walker *et al.*, *Am. J. Respir. Cell Mol. Biol.* **16**, 531 (1997).
20. A. R. Kimmel, R. A. Firtel, *Curr. Opin. Genet. Dev.* **14**, 540 (2004).
21. A. J. Ridley *et al.*, *Science* **302**, 1704 (2003).
22. M. Maeda *et al.*, *Science* **304**, 875 (2004).

23. This study was supported in part by National Institute of General Medical Sciences grants R01 GM-51477, GM-60475 (W.G.J.), and GM-66232 (P.A.I.), and by Congressionally Directed Medical Research Program grant PR043034 (W.G.J.).

Supporting Online Material

www.sciencemag.org/cgi/content/full/314/5806/1792/DC1
Materials and Methods
Figs. S1 to S3
Table S1
References
Movies S1 to S10

17 July 2006; accepted 31 October 2006
10.1126/science.1132559

Multi-Functional Imager

The Dyversity multi-functional imager can now rapidly detect 0.5 ng of Sypro Ruby stained protein in less than a second. This new application makes Dyversity a suitable system for high-throughput gel-based proteomics. Dyversity can acquire small amounts of fluorescently labeled protein rapidly because it has a 90-µm resolution, 16-bit charge-coupled device camera. This provides a fast capture time per channel and makes the instrument an alternative to a laser-based scanner.

Syngene For information 800-686-4407 www.2dymension.com

MultiLink-HRP Detection Kit

BioGenex's Super Sensitive MultiLink-HRP Detection System represents state-of-the-art technology in the visualization of antigen–antibody binding reactions, such as in immunohistochemistry (IHC) staining procedures. This detection system is designed to provide savings in time and effort in demanding immunostaining conditions in which optimal detection performance is required to achieve accurate and clean IHC staining results.

Biogenex For information 800-421-4149 www.biogenex.com

Grinding Resin

Molecular Grinding Resin has been developed for effectively grinding biological samples for extraction of DNA, RNA, and proteins. Made of high tensile microparticles, the resin effectively disrupts nuclei and other cell organelles. The resin will not bind protein or nucleic acids.

G-Biosciences/Genotech For information 800-628-7730 www.GBiosciences.com

Protein Stain

LabSafe GEL Blue is a sensitive Coomassie-dye–based protein stain that is environmentally safe. As little as 4 ng bovine serum albumin can be detected without any need for destaining. A ready-to-use format produces rapid protein band visualization on gels following electrophoresis. After a brief wash step, the user simply adds LabSafe GEL Blue directly to the protein gel.

G Biosciences/Genotech For information 314-991-6034 www.GBiosciences.com

Comparator Balance

The XP56C Comparator offers a resolution of 52 million points. In the field of metrology, comparators are used to determine the mass of weights or samples to the highest degree of accuracy. The XP56C Comparator is designed to meet this challenge with a continuous weighing range of 52 g and a readability of 1 µg. The included hanging weighing pan eliminates corner load errors. The WeighCom application guides the user step-by-step through the mass determination process and a user-friendly color touchscreen display enables convenient and error-free operation.

Mettler Toledo For information 614-438-4932 www.mt.com

Literature

Assay Development and Clinical Trial Testing Services from the Experts in Rare Cell Analysis is a brochure offering drug developers a partnership opportunity to accelerate their programs using circulating tumor cells (CTCs), circulating endothelial cells (CECs), and molecular biomarkers in clinical trials. The services include assay development services to format the client's targeted marker to Immunicon's rare cell format; collaboration on clinical trial design using rare cells; testing services such as counting and characterizing CTCs and CECs in drug development programs; and enrichment for downstream molecular analysis.

Immunicon For information 215-830-0777 www.immunicon.com

Fluorometer

The MultiFrequency Phase Fluorometer (MFPF) is a frequency-domain luminescence monitor for measurement of luminescence lifetime, phase, and intensity. The MFPF makes use of LED excitation, avalanche photodiode detection, and filter-based wavelength selection for simple experimental set-up and control. When used with Ocean Optics Oxygen Sensors, it helps to mitigate index effects, eliminate ambient light, and improve system stability in dissolved oxygen applications. The MFPF is especially useful for oxygen-sensing applications in which sensitivity to drift is important and sample set-ups must be undisturbed for long periods of time. Because it makes use of phase-shift technology, the MFPF is invariant to fiber bending and stray light, has a broad dynamic range, generates very little optical and electronic crosstalk, and has low drift and phase noise. Built-in pressure and temperature measurement capabilities also make the MFPF suitable for luminescence sensor design, testing, and calibration. The MFPF was developed by TauTheta Instruments.

Ocean Optics and TauTheta Instruments For information 727-733-2447 www.tautheta.com and www.OceanOptics.com

Newly offered instrumentation, apparatus, and laboratory materials of interest to researchers in all disciplines in academic, industrial, and government organizations are featured in this space. Emphasis is given to purpose, chief characteristics, and availability of products and materials. Endorsement by *Science* or AAAS of any products or materials mentioned is not implied. Additional information may be obtained from the manufacturer or supplier by visiting www.science.labvelocity.com on the Web, where you can request that the information be sent to you by e-mail, fax, mail, or telephone.

POSITIONS OPEN

FACULTY POSITION
MARINE EVOLUTIONARY BIOLOGIST

The Biological Sciences Department at California State Polytechnic University, Pomona, invites applications for a tenure-track, **ASSISTANT PROFESSOR** position in evolutionary biology, beginning September 2007. A Ph.D. in biology or a related field is required and postdoctoral experience is preferred. The candidate will teach a senior level course in evolution, a general education course in marine biology that includes a field-based laboratory, and is expected to teach upper-division and/or graduate-level courses related to his or her area of expertise. Participation in team-teaching of introductory courses may be expected in the future. We seek applicants who study the evolution of marine organisms with a combination of modern field and molecular approaches. Candidates must be strongly committed to teaching, mentoring of undergraduate and graduate (M.S.) students, and developing an externally funded research program. Cal Poly Pomona is a comprehensive Master's level University with a diverse student body. The successful candidate will have demonstrated ability to be responsive to the educational equity goals of the University and its increasing ethnic diversity and international character. Applicants should mail (1) curriculum vitae, (2) statement of teaching philosophy, (3) proposed plan of research, (4) reprints of three representative publications, and (5) the names and contact information of three references to: **Chair, Marine Evolutionary Biologist Search Committee, Biological Sciences Department, California State Polytechnic University, 3801 West Temple Avenue, Pomona, CA 91768-4132.** Review of applications will begin on January 29, 2007. Official transcripts and three letters of reference will be required of all finalists. For further information, visit the Department **website: http://www.csupomona.edu/~biology.** As required by the Clery Disclosure Act, the University's annual security report is available at **website: http://www.csupomona.edu/~public_safety.**

California State Polytechnic University, Pomona, is an Equal Opportunity, Affirmative Action Employer. Cal Poly Pomona subscribes to all state and federal regulations and prohibits discrimination based on gender, race, sexual orientation, national origin, disability, marital status, age, religion, or veteran status. The University hires only individuals lawfully authorized to work in the United States.

ASSISTANT PROFESSOR IN MICROBIOLOGY
Department of Biology
California State University, Northridge

The Department of Biology at California State University, Northridge, seeks a **MICROBIOLOGIST** to fill a tenure-track Assistant Professor position to begin August 2007. Candidates with documented interest in mechanisms of prokaryotic pathogenesis, which may include genomic, metabolomic, or bioinformatics approaches, are strongly desired. The successful candidate is expected to exhibit potential for excellence in teaching, establish a vigorous research program involving undergraduate and Master's degree students, and provide effective instruction to students of diverse backgrounds in a multicultural setting. External funding of research is strongly encouraged. Teaching responsibilities will include general microbiology, graduate seminars, and may include general biology or specialty courses in microbiology. Candidates must have a Ph.D. or equivalent with microbiology emphasis and postdoctoral training. Applicants should send an application letter, curriculum vitae, statement of teaching philosophy, statement of research interests, reprints of up to three publications, and should arrange for three letters of recommendation to be sent to: **Chair, Department of Biology, California State University, 18111 Nordhoff Street, Northridge, CA 91330-8303.** Applications in PDF-format are preferable **(e-mail: larry.allen@csun.edu).** Review of completed applications will begin January 15, 2007, and will continue until the position is filled.

California State University, Northridge, is an Equal Opportunity Employer committed to excellence through diversity.

POSITIONS OPEN

UMBI SHADY GROVE

TENURE-TRACK FACULTY POSITION IN METABOLOMICS
University of Maryland Biotechnology Institute, Shady Grove
Center for Advanced Research in Biotechnology
Center for Biosystems Research

Applications are invited for a tenure-track faculty position at the **ASSISTANT, ASSOCIATE, or PROFESSOR** level. The successful candidate will be expected to develop a rigorous, externally funded research program in the field of metabolomics using advanced analytical methods.

The Shady Grove Campus of the University of Maryland Biotechnology Institute (UMBI) is developing an integrated research program in molecular systems biology, bridging the interests of the Center for Advanced Research in Biotechnology (CARB, **website: http://carb.umbi.umd.edu/),** a partnership with the National Institute of Standards and Technology (NIST) and the Center for Biosystems Research (CBR, **website: http://www1.umbi.umd.edu/~cbr/).** Research areas at the Shady Grove Campus include chemical biology, mass spectrometry, structural biology, bioinformatics, experimental and computational biophysics, systems modeling, plant and insect biology. Several new faculty hires are anticipated over the next two years, and a new 140,000 square-feet research building equipped with state-of-the-art facilities has recently opened.

Qualifications: Ph.D. in biochemistry or related field, postdoctoral experience, and knowledge skills in metabolomics. Areas of interest include but are not limited to: metabolite changes in response to disease or environmental stress; applications in functional genomics; metabolic networks; medicinal plant metabolism; development of metabolomic databases. We are particularly interested in applicants who are seeking a highly collaborative research environment.

Applicants should submit their curriculum vitae (referencing position 300879), a summary of future research plans, and names of three references (PDF file) electronically to **e-mail: carbsrch@umbi.umd.edu** or by mail to: **Metabolomics Search Committee, University of Maryland Biotechnology Institute, Shady Grove, 9600 Gudelsky Drive, Rockville, MD 20850.**

Review of candidates will begin January 1, 2007, and continue until the position is filled.

UMBI is an Equal Employment Opportunity/ADA/Affirmative Action Employer.

ASSOCIATE/FULL PROFESSOR
Histology/Cell Biology/Tenure or Tenure-track
Comparative Biomedical Sciences

Department of Comparative Biomedical Sciences, with numerous funded investigators in cell and molecular biology (including cancer biology), seeks a faculty person in histology/cell biology. Requirements: Ph.D. or equivalent degree in biological/biomedical sciences or related field; postdoctoral experience; research background in cell/molecular biology; ability to teach histology and coordinate a team-taught course in cell biology and histology in the professional curriculum; have (or will have) extramural funding. Responsibilities: establishes and maintains an extramurally funded research program; teaches in the professional curriculum; contributes to the graduate program. Salary and rank will be commensurate with qualifications. *An offer of employment is contingent upon a satisfactory pre-employment background check.* Application deadline is January 12, 2007, or until candidate is selected. Submit letter of application and resume (including e-mail address) to: **Dr. George M. Strain, Professor, Department of Comparative Biomedical Sciences, School of Veterinary Medicine, Louisiana State University, Reference #000490, Baton Rouge, LA 70803, telephone: 225-578-9758, e-mail: strain@lsu.edu.**

Louisiana State University is an Equal Opportunity/Equal Access Employer

Positions @ NIH
THE NATIONAL INSTITUTES OF HEALTH

Developmental Signal Transduction

A postdoctoral position is available in the Laboratory of Cell and Developmental Signaling (LCDS), Center for Cancer Research (CCR) to study the role of Eph receptor and ligand signaling pathways affecting cell movement and cell fate. A combination of molecular, cell biological and biochemical techniques are applied in amphibian and mammalian developmental systems. (See Nature Cell Biology 8: 55-63, 2006; Developmental Cell 6: 55-67, 2004). Please visit our website for more information: http://ccr.cancer.gov/Staff/staff.asp?profileid=5575.

Our laboratory is located at the NCI-Frederick campus and offers state-of-the-art facilities in an exciting environment for postdoctoral research. The NCI offers competitive postdoctoral stipends. A strong background in molecular, cellular, or developmental biology is required. Interested candidates should have a Ph.D. and/or an M.D. and have less than 5 years postdoctoral experience. Fellows from abroad may be eligible for J-1 visa sponsorship. Stipend is commensurate with education and research experience, with a range of $43,200-$55,500. Please submit a cover letter, CV including bibliography, and contact information for three references to: **Ira Daar, PhD., LCDS, NCI-Frederick, Building 560, Room 22-3, Frederick, MD 21702, E-mail: daar@ncifcrf.gov**.

Deputy Director
Division of Extramural Activities

The Department of Health and Human Services (DHHS), National Institutes of Health (NIH), National Cancer Institute, (NCI) is seeking a Deputy Director, Division of Extramural Activities (DEA) to assist in directing an approximately 3.5 billion dollar grant review program. The DEA administers and directs the institute's grant, cooperative agreement, and contract review and referral activities. In addition, the DEA provides information about the NCI's peer review and grants policies as well as committee management and advisory board activities. The Deputy Director, DEA will be appointed at a salary commensurate with his/her qualifications and experience. Full federal benefits include leave, health and life insurance, retirement saving plan (401K equivalent) and relocation expenses.

Qualifications Required: Applicants must have a doctoral level degree (Ph.D., M.D. or equivalents) and have experience in laboratory, clinical or public health research administration that includes budget formulation and management as well as grants and contract development. Consideration is limited to U.S. citizens, resident aliens, or nonresident aliens with a valid employment authorized visa.

How to Apply: Applicants should send a brief biography, curriculum vitae and the names and addresses of four references to:

Bridgette Tobiassen, Administrative Resource Center Manager, Division of Cancer Biology/Division of Extramural Activities, National Cancer Institute, 6130 Executive Boulevard, Room 5052, Rockville, MD 20852. If you need additional information, please call **Bridgette Tobiassen at (301) 496-2871**.

DEADLINE FOR RECEIPT OF APPLICATIONS: January 15, 2007

DIRECTOR, OFFICE OF NIH HISTORY AND MUSEUM

The Office of Intramural Research of the National Institutes of Health (NIH) in Bethesda, Maryland is seeking an outstanding individual to serve as Director of the Office of NIH History (ONH). The Director, ONH, oversees and coordinates scholarly activities relating to the history of the NIH. The Director personally writes books and/or articles about specific NIH research activities and about biomedical research policy and oversees the work of the staff and contractors who perform similar work. The Director collaborates with national and international specialists and helps organize conferences, symposia, and other meetings; advises the Director, NIH, and other senior staff and administrators about historical records, artifacts, and preservation. The Director is also responsible for the ONH web site and on-campus exhibits produced by the Stetten Museum of Biomedical Research. The Director oversees an office of about six staff members and one or two post-doctoral fellows. Further details about ONH and its specific programs can be found at www.history.nih.gov

Candidates are required to have a 4 year course of study in an accredited college or university leading to a bachelor's degree or higher that included a major field of study in History or related field that included at least 18 semester hours in history. The salary range is $107,521-$139,774 and a full package of benefits is included. A detailed vacancy announcement with the mandatory qualifications and application procedures can be found on USAJOBS at **www.usajobs.gov (announcement number OD-07-146557) and NIH website at http://www.jobs.nih.gov**. Questions on application materials may be addressed to **Laurie Steinman at (301) 594-5335**. Applications must be received by midnight eastern standard time on **January 26, 2007**.

Department of Health and Human Services
National Institutes of Health
Clinical Center

Tenure-track Physician
Clinical Center/Nuclear Medicine Department

This position is located in The Warren G. Magnuson Clinical Center, Nuclear Medicine Department (NMD).

We are seeking a research-oriented physician for a possible tenure-track position. An M.D. or M.D. /PhD with U.S. Nuclear Medicine Board certification and CT training is needed to provide diagnostic and therapeutic nuclear medicine procedures as well as to participate in clinical research protocols of the NIH Intramural Program. U.S. citizenship or permanent residency status is required.

Please submit your curriculum vitae, bibliography, and a letter describing your clinical, research, and management experience to: **Mrs. Veronica Olaaje, HR Specialist, DHHS, NIH, OD/CSD-E, 2115 E. Jefferson Street, Rm. 2B209 MSC-8503, Bethesda, MD 20892-8503. Phone: 301-435-4748. Email: volaaje@mail.nih.gov**.

Salary is commensurate with experience. This appointment offers a full benefits package (including retirement, health, life and long term care insurance, Thrift Savings Plan participation, etc.). Application packages should be submitted as early as possible, but no later than **December 31, 2006**.

Selection for this position will be based solely on merit, without discrimination for non-merit reasons such as race, color, religion, sex, national origin, politics, marital status, sexual orientation, physical or mental handicap, age or membership or non-membership in an employee organization.

WWW.NIH.GOV

Health Scientist Administrator
National Institute of Dental and Craniofacial Research (NIDCR)

The National Institute of Dental and Craniofacial Research (NIDCR), National Institutes of Health (NIH), Department of Health & Human Services (DHHS) is seeking applicants for a supervisory Health Scientist Administrator position in the Center for Integrative Biology and Infectious Diseases (CIBID). The position advertised is for the Chief of the Translational Genomics Research Branch. The Branch coordinates the development and implementation of the NIDCR extramural basic and translational genomics research program related to NIDCR-relevant human and microbial genetics and genomics. To this end, areas of basic and applied research in the NIDCR mission include: infectious diseases such as dental caries and periodontal diseases, microbiology, molecular and cellular neuroscience, developmental biology, mineralized tissue and salivary gland physiology, immunology and immunotherapy, epithelial cell regulation and transformation, as well as biomaterials, biomimetics and tissue engineering, and behavior, health promotion and environment. In addition, there are cross-cutting programs involving clinical trials and comprehensive centers of discovery.

The incumbent will direct and oversee the administration of a portfolio of research projects employing translational genetics and genomics research strategies targeted to NIDCR-relevant diseases and will stimulate interest in and provide advice to the extramural community regarding the respective research portfolio. In addition, the incumbent will participate in funding decisions, policy development, as well as implementation and coordination with other programs both within and outside of the NIDCR.

The salary range for this position is $107,521 to $139,774 per annum, commensurate with qualifications and professional experience. A full benefits package is available, which includes retirement, Thrift Savings Plan participation, health, life and long-term care insurance.

Applications will be accepted through **February 15, 2007**. For qualifications required, evaluation criteria, and application instructions, view the vacancy announcements at: **http://jobsearch.usajobs.opm.gov/a9nih.asp** . Refer to announcement **# NIDCR-07-162498-DE or NIDCR-07-162738-MP.** Please contact **Elan Ey at 301-594-2320 or eye@mail.nih.gov** if you have questions.

INVESTIGATOR RECRUITMENT in COMPUTATIONAL LINGUISTICS/TEXT MINING

Computational Biology Branch
National Center for Biotechnology Information
National Library of Medicine

The National Center for Biotechnology Information (NCBI) performs research in computational biology and creates and maintains information systems and computational tools for the biomedical research community. The Computational Biology Branch (CBB) at the NCBI invites applications to fill an Investigator (tenure-track) or tenured Senior Investigator position. The position is for a creative, interactive scientist addressing new challenges in the field of computational linguistics/biomedical text mining. Candidates should hold a doctorate degree with a substantial publication record. The successful candidate will join a diverse, collegial group of investigators within the CBB and will have the opportunity to develop software methods to search PubMed (a widely used electronic repository of biomedical literature) and other linked NCBI databases. To further these goals, interactions between the several NCBI branches would be encouraged. Excellent computational facilities and resources for the rapid achievement of research goals are available. Salaries and benefits are competitive and commensurate with education and experience. Interested applicants should send a letter of interest, curriculum vitae, bibliography, a three-page description of proposed research, and three letters of recommendation to:

W. John Wilbur, M.D. Ph.D., Chair, Search Committee, Computational Biology Branch, National Center for Biotechnology Information, National Library of Medicine, National Institutes of Health, Building 38A, Room 6S606, Bethesda, MD 20894.

Specific questions regarding the recruitment can be directed to **Dr. John Wilbur (Search Chair) at wilbur@ncbi.nlm.nih.gov**.

The deadline for receipt of applications is **April 30, 2007** but candidates will be interviewed as they become available.

Selection for this position will be based solely on merit, without discrimination for non-merit reasons such as race, color, religion, sex, national origin, politics, marital status, sexual orientation, physical or mental handicap, age, or membership or non-membership in an employee organization.

THE UNIVERSITY OF HONG KONG

香 港 大 學

The University of Hong Kong is at the international forefront of higher learning and research, with more than 100 teaching departments and sub-divisions of studies, and more than 60 research institutes and centres. It has over 20,000 undergraduate and postgraduate students from 48 countries. English is the medium of instruction. The University is committed to international standards for excellence in scholarship and research.

School of Biological Sciences
(Re-advertisement)

Applications are invited for appointments as: **(1) Director of the School of Biological Sciences (at Chair level) (Ref.: RF-2006/2007-15); and (2) Professor/Chair of Biological Sciences (Ref.: RF-2006/2007-16)**, on tenured terms, or on a three-year fixed-term basis, tenable from July 1, 2007 or as soon as possible thereafter.

The newly formed School of Biological Sciences aspires to become a top research school in Asia with world-class research and teaching. The School has excellent research facilities and resources, and is supported by a dedicated team of experienced academic and research staff. The areas of expertise include biotechnology, molecular and cell biology, comparative endocrinology, human nutrition, food technology, ecology and biodiversity, marine biology and environmental toxicology.

Applicants should possess a distinguished research and teaching profile, proven academic leadership and a strong commitment to high-quality teaching. The Faculty seeks academic leaders of international stature to undertake research of the highest quality in their fields, and to play a prominent role in academic leadership in undertaking and encouraging interdisciplinary and collaborative research, helping to foster a highly productive and supportive research culture in the Faculty, and enhancing the Faculty's profile both locally and internationally as a centre of excellence in research and teaching. Research start-up funds will be available. For the position of Director, management experience would be an advantage. Applicants who have responded to the previous exercise which closed on October 31, 2006 need not re-apply. Their candidature will be considered together with that of the applicants of this round.

Starting annual salary (superannuable (for tenured terms), or attracting contract-end gratuity and University contribution to a retirement benefits scheme, totalling up to 15% of basic salary) for a Chair is within the non-clinical professorial range, the minimum of which is circa HK$1.1M, and that for a Professorship is around HK$803,700 (approximately US$1 = HK$7.8) (subject to review from time to time at the entire discretion of the University).

The University offers a highly competitive remuneration package inclusive of annual leave, sabbatical leave, housing benefits, medical and dental benefits etc. At current rates, salaries tax does not exceed 16% of gross income.

Further particulars and application forms (272/302 amended) can be obtained at https://www.hku.hk/apptunit/; or from the Appointments Unit (Senior), Human Resource Section, Registry, The University of Hong Kong, Hong Kong (**fax**: (852) 2540 6735 or 2559 2058; **e-mail**: apptunit@hkucc.hku.hk). Questions about the posts should be addressed to Professor S. Kwok, Dean, Faculty of Science (**fax**: (852) 2858 4620); **e-mail**: sunkwok@hku.hk). **Closes January 31, 2007**.

The University is an equal opportunity employer and is committed to a No-Smoking Policy

NIMS

National Institute for Materials Science, a Japanese national institute specializing in research on materials science, employs 550 people, including 400 researchers, and 50 engineers.

RESEARCHER POSITIONS

- Nano-Biotechnology, Molecular Biology, Cellular Biology
- Spintronics Materials and Devices

For more details:
http://www.nims.go.jp/eng/employment/index.html

Senior Professor

University of California San Diego
Section of Ecology, Behavior and Evolution
Division of Biological Sciences
http://www-biology.ucsd.edu/biosections/ebe.html

The Section of Ecology, Behavior, and Evolution, in the Division of Biological Sciences, invites applications for a senior ecologist and/or evolutionary biologist at the rank of tenured full Professor. In addition to Professorial duties it is expected that the successful candidate will be able to assume a term as Section Chair.

The area of scholarship is open, but we seek candidates with proven outstanding records of research, teaching, service, and extramural support who have the leadership qualities to develop further the Section's existing strengths in evolution and ecology. The Section currently consists of a group of a dozen active members and is slated for several upcoming faculty hires. The successful candidate will be expected to have excellent communication and collaboration skills and to be able to work with the current faculty to create a vision and plan for the growth and development of the Section. Level of appointment will be commensurate with qualifications and experience.

Review of applications will begin **February 1, 2007** and will continue until position is filled. We will only accept electronic submissions in the form of a single pdf file. Complete applications should contain copies of CV, list of three referees, statements of research and teaching interests, and synopsis of applicant's goals or vision as a Chair. The complete application should be sent as a single PDF file attachment by email to **ebesearchb@ucsd.edu** with EBE Chair Search as the subject line.

Applicants are welcome to include in their cover letters a personal statement summarizing leadership efforts and/or contributions to diversity. UCSD is an Equal Opportunity-Affirmative Action Employer with a strong institutional commitment to the achievement of diversity among its faculty and staff. Qualified minority and women are especially encouraged to apply.

FACULTY POSITION in BIOCHEMISTRY

Department of Biochemistry
The University of Iowa
Roy J. and Lucille A. Carver College of Medicine

The Department of Biochemistry of the University of Iowa seeks highly qualified applicants for one or more tenure track faculty positions at any rank. The department has broad interests (**www.biochem.uiowa.edu**) and current faculty have strong collaborative interactions with colleagues throughout the Carver College of Medicine and the University. They participate in many interdisciplinary training programs including the Center for Biocatalysis and Bioprocessing, Genetics, Molecular Biology, Molecular Parasitology and the Medical Scientist Training Program. Outstanding new and renovated research space with excellent shared instrumentation is available. We are building in the area of molecular biophysics, proteomics and structural biology, and with special emphasis on candidates who apply NMR and mass spectroscopy to biomedical problems. All applicants must have a relevant graduate degree (Ph.D., M.D., or the equivalent) and productive research experience. They will be judged on their potential to initiate and maintain a vigorous, independent research program, to teach and to train students and postdoctoral fellows.

Applications should include a CV, a 3-page summary of research accomplishments and future plans, and a brief statement of teaching interests. These should be sent as a single pdf file to **biochemsearch@uiowa.edu**, with the applicant's last name in the filename; reprints in pdf format may be sent with the application. Senior applicants should provide names of 3 references. Applicants for the rank of Assistant Professor should ask three scientists familiar with their qualifications to submit letters of reference to **biochemsearch@uiowa.edu**. Consideration of completed applications will begin on **February 1, 2007**. Questions may be directed to: **Prof. Peter Rubenstein, Chair of the Faculty Search Committee, or Prof. John E. Donelson, Head, Dept. of Biochemistry, Roy J. and Lucille A. Carver College of Medicine, Univ. of Iowa, Iowa City, IA, 52242-1109, phone 319-335-7933, fax 319-335-9570**.

The University of Iowa is an Equal Opportunity and Affirmative Action Employer.

MAX-PLANCK-GESELLSCHAFT

The University of Konstanz and the Max Planck Society invite applications for a

Chair of Ornithology
(Full Professor - W3)

at the Department of Biology at the University of Konstanz
and

Director at the Max Planck Institute for Ornithology

The chair holder will have a double appointment as a university professor and as a Scientific Member of the Max Planck Society and director of a new department at the Max Planck Institute for Ornithology, Seewiesen, with its branch institute (Vogelwarte/bird station) at Radolfzell (Bodensee/Lake Constance).

Ideally, applicants would work on topics in the field of **Ecological Immunobiology of Birds** such as the ecology of disease transmission, the consequences of infection on health and behaviour or the ecological adaptations of the avian immune system. The new Department of the Max Planck Institute for Ornithology would complement current lines of research of the Department of Behavioural Ecology & Evolutionary Genetics and of the Department Behavioural Neurobiology, both of which are working with bird model systems. The new department preferably integrates activities of the Radolfzell branch of the institute into the research program. The latter has extensive expertise and infrastructure in monitoring bird migration and breeding biology.

The future chair holder is expected also to complement the scientific profile of the Department of Biology in Konstanz, and to participate in its teaching program.

Promising candidates will be invited to a scientific colloquium to be held in Konstanz in spring 2007.

Application deadline: 01.02. 2007.

Both, the University of Konstanz and the Max Planck Society are equal opportunity employers. Applications by qualified female scientists are especially welcome. Hiring priority will be given to disabled candidates with equal qualifications.

Applications comprising a curriculum vitae, publication list, reprints of the five most important publications, a list of grants and awards, details of teaching experience, as well as statements of current research topics, future research directions and interests should be sent to:

Prof. Dr. Bernhard Schink, Prorektor für Forschung, Fachbereich Biologie, D-78457 Konstanz, Germany www.uni-konstanz.de/FuF/Bio/

and to

Prof. Dr. Manfred Gahr, Managing Director of the Max Planck Institute for Ornithology, 82319 Seewiesen, Germany (http://orn.mpg.de)

Boehringer Ingelheim

Boehringer Ingelheim ranks among the world's 20 leading pharmaceutical corporations. With almost 37,500 employees in 47 countries we are a global team sharing knowledge and ambition to foster a healthier life.

Boehringer Ingelheim Austria is home to the corporation´s dedicated drug discovery center for oncology. More than 200 scientists, technicians, and support staff drive our efforts to identify innovative cancer medicines. We currently have an opening for a post-doctoral scientist within our Department of Pharmacology.

Post-Doctoral Scientist (m/f)
MR Imaging / in vivo Pharmacology

Your responsibilities:

- Responsibility for the MRI lab, equipped with a Bruker Pharmascan 70/16 MR system
- Contribution to multiple drug discovery programs by designing, performing and evaluating MRI studies, e.g. to characterize mechanisms of drug action or validate pharmacodynamic biomarkers

Your qualifications:

- PhD-level degree in the life sciences
- Familiar with MRI techniques
- Research/drug discovery experience specifically in the field of tumor biology/cancer pharmacology would be of advantage
- Team spirit and excellent communication skills
- English is our working language, German language skills would be of advantage

If this position has drawn your attention and you feel qualified, please apply online:
www.boehringer-ingelheim.at

Informal inquires may be directed to Dr. Frank Hilberg (telephone: +43-1-80105-2351, e-mail: frank.hilberg@vie.boehringer-ingelheim.com).

Reference number: 261

Boehringer Ingelheim Austria GmbH
Human Resources
Personnel Development & Recruiting
Dr. Boehringer-Gasse 5-11
A-1121 Vienna, Austria

www.boehringer-ingelheim.at

BESTE ARBEITGEBER ÖSTERREICH 2006

IN 2007

CNRS IS RECRUTING

MORE THAN 400 TENURED RESEARCHERS IN ALL SCIENTIFIC FIELDS*

*Mathematics; Physics; Nuclear and High-Energy Physics; Chemistry; Environmental Sciences ; Life Sciences; Humanities and Social Sciences; Engineering Sciences; Earth Sciences and Astronomy; Communication and Information Technology and Sciences.

This recruitment campaign is open to junior and senior researchers from all over the world. One of the major objectives of this campaign is to encourage international scientists to apply to CNRS.

CNRS researchers work in an enriching scientific environment:
›› numerous large-scale facilities
›› highly-skilled technical support
›› multiple networks throughout Europe and across disciplines
›› access to university research and teaching
›› lab-to-lab and international mobility

At CNRS, the long-term vision of excellence in basic research provides a solid foundation for cutting-edge technological research. Successful candidates to the CNRS benefit from the dynamics, stability and stimulation of belonging to a major research organization.

Application deadline: January 15th 2007

www.cnrs.fr

CENTRE NATIONAL DE LA RECHERCHE SCIENTIFIQUE

PENNSTATE
University Park

The Department of Biology at The Pennsylvania State University (**http://www.bio.psu.edu/**) invites applications for a tenure-track Assistant Professor position in Microbial Ecology. We seek candidates who are developing independent research programs in any system within the broad field of microbial ecology, to address ecology, evolution, and genetics of microbes. Academic excellence will be the primary criterion for evaluation. Joint appointments between colleges and/or departments across the university are possible. The successful candidate will develop an externally funded research program and contribute to teaching at the undergraduate and graduate levels. A separate search for an Earth Systems Ecologist in the College of Earth and Mineral Sciences is part of a coordinated effort to strengthen ties between the life and earth sciences at PSU.

Applicants should submit a letter of interest, curriculum vitae, statements of research and teaching interests, and have three letters of reference sent to: **Search Committee Chair, Microbial Ecology Search, Box G, Department of Biology, 208 Mueller Laboratory, University Park, PA 16802**. Review of applications will begin on **February 15, 2007** and will continue until the position has been filled.

Women and minorities are encouraged to apply. Penn State is committed to Affirmative Action, Equal Opportunity, and the diversity of its workforce.

9 Senior Research Positions at Swedish Universities

The Swedish Research Council announces nine Senior Research Positions within natural and engineering sciences. The positions are intended for scientists who have obtained a Ph.D., where the date of exam, with a few exceptions, is not older than ten years prior to the end of the application period. The positions are financed for a maximum of six years.

There is one position each within the following areas:

- Assembly of Biological Supramolecular Systems
- Cellular Biology and Biophysics in Microfabricated Environments
- Epigenetics
- Multiscale Modelling of Engineering Materials
- Non-Linear Problems and Dynamics
- Quantum Engineering
- Methods of Theoretical Chemistry
- Palaeozoic Palaeobiology, Faunal Diversification and Extinction Events
- Theory of Strongly Correlated Material

The proposal must be approved by a Swedish host university or a Swedish host institution engaged in research.

Apply at www.vr.se no later than February 14, 2007
Application form and instructions can be found at www.vr.se.

Vetenskapsrådet

MICHIGAN STATE UNIVERSITY

Department of Biochemistry and Molecular Biology Chairperson

Michigan State University invites applications and seeks nominations for a Chairperson of the Department of Biochemistry and Molecular Biology. An outstanding scientist is sought to provide leadership that capitalizes on, but is not limited to, existing areas of research strength in genes and signaling, plant biochemistry, and structural and computational biology. Evidence of leadership in interdisciplinary research is an important qualification. It is anticipated that the candidate will contribute to and build upon the highly collaborative research atmosphere within the department and among the science departments, many of which are located in adjacent buildings. A growing medical science community offers additional research opportunities. State-of-the-art support facilities are available to enhance the new chairperson's research program.

The selected individual will be an experienced scholar with a vigorous well-funded research program and creative ideas for strengthening undergraduate and graduate programs (the department has 300 undergraduate majors and more than 100 graduate students). More information about the department is available at **http://www.bmb.msu.edu**.

Applications will start being reviewed on **January 15, 2007**, and will continue to be considered until a suitable candidate is identified. Send cover letter and C.V., including names of three individuals that could be contacted for a recommendation, to:

Lee Kroos
Chairperson Search Committee
Biochemistry and Molecular Biology
Michigan State University
East Lansing, MI 48824-1319
bmbsrch@msu.edu

Women and minorities are encouraged to apply.

Dean of the Graduate School of Biomedical Sciences

The Medical College of Wisconsin invites nominations and applications for the position of Dean of the Graduate School of Biomedical Sciences (www.mcw.edu/gradschool/). The College seeks a strong and dynamic leader with a distinguished record of research, teaching, and service including experience with issues facing graduate education in a medical school environment. The successful candidate will provide leadership for a graduate school that comprises approximately 175 faculty members and currently enrolls 164 PhD, 135 MPH, 105 MS, and 44 MA students. The Dean will have primary responsibility for the Graduate School's existing academic programs and for building new programs of national and international distinction. The successful candidate must hold a doctoral degree and possess academic credentials for a tenured appointment at the rank of Professor. It is expected that the appointee will have experience as a graduate mentor and will have played a leadership role in a graduate program. The successful candidate is encouraged to maintain an active research program (50% time), and a development package and research space commensurate with that effort will be provided.

The Dean provides the educational vision for the Graduate School and reports directly to the President of the College. The appointee will work closely with the Dean and Executive Vice President of the Medical College and Department Chairs to establish, implement and annually review the academic policies of the College. In addition, the appointee will work closely with the Division of Sponsored Research and the Research Foundation to advocate for graduate education both within the College and with external constituencies. The appointee will oversee the administration of the Graduate School with respect to its missions of graduate education, governance, program reviews, graduate faculty coordination, and graduate student services.

The Medical College of Wisconsin (www.mcw.edu) is the largest private research institution in Wisconsin, conducting over $130 million annually in funded research. Over the past several years the College has been among the fastest growing medical schools in the United States in terms of NIH funding. The College is completing major new research facilities. In addition, The Scientist magazine ranked the Medical College of Wisconsin in the top 5 academic institutions for postdoctoral training and in the top 50 best academic centers at which to be a scientist. This appointment is expected to build on the success of our graduate programs, which have trained nationally and internationally recognized scholars.

The Medical College is conveniently located in suburban Milwaukee and is part of an academic medical center that includes nationally distinguished children's and adult hospitals that employ over 13,000 people. The College is located 8 miles west of Lake Michigan with easy access to surrounding communities, lakes, and parks.

The position is available July 1, 2007. Salary and other considerations will be competitive and consistent with the College's commitment to recruiting the best-qualified individual. The Search Committee will begin screening candidates in December (2006) and will continue to review applications until the position is filled. Applicants should provide a curriculum vitae, a statement of interest, and the names and contact information of three references.

Address applications or nominations to:
Robert J. Deschenes, Ph.D.
Joseph F. Heil Professor and Chair of Biochemistry
Chair, Graduate School Dean Search Committee
Department of Biochemistry
Medical College of Wisconsin
8701 Watertown Plank Rd
Milwaukee, WI 53226
For further information, contact
Mary Beth Drapp, Executive Assistant at
414-456-4403 or at mdrapp@mcw.edu

MEDICAL COLLEGE OF WISCONSIN

The Medical College of Wisconsin is an Equal Opportunity/Affirmative Action employer.

WEILL CORNELL
MEDICAL COLLEGE IN QATAR

FACULTY POSITIONS

In a pioneering international initiative, Weill Medical College of Cornell University established the Weill Cornell Medical College in Qatar (WCMC-Q) with the sponsorship of the Qatar Foundation for Education, Science and Community Development. WCMC-Q is located in Doha, Qatar, and in its fifth year of operation, Weill Cornell seeks candidates for faculty positions to teach in Doha in:

NEUROPHYSIOLOGY

Following a two-year Pre-medical Program, the inaugural class has now completed the second year of the traditional four-year education program leading to the Cornell University M.D. degree, which they will receive in May 2008. The medical program at WCMC-Q replicates the admission standards and the innovative problem-based curriculum, which includes, among other things, integrated, multidisciplinary basic science courses that are the hallmark of the Weill Medical College of Cornell University.

Faculty, based in Doha, will be expected to teach their specialty and to contribute to the academic life of the Medical College. This unique program provides the successful applicant with the opportunity to leave his/her mark on a pioneering venture. A state of the art research program, to be housed in WCMC-Q and focused on genetics and molecular medicine and women and children's health will be initiated within the next year. Teaching and research facilities are situated within a brand new building designed to Cornell specifications and located in Education City in Doha amongst other American universities.

All faculty members at WCMC-Q are appointed by the academic departments at Weill Cornell.

Further details regarding the WCMC-Q program and facilities can be accessed at:

www.qatar-med.cornell.edu.

Candidates should have a M.D., Ph.D. or M.D./Ph.D. or equivalent terminal degree. The successful candidate will have strong teaching credentials and experience in teaching medical students. Salary is commensurate with training and experience and is accompanied by an attractive foreign-service benefits package.

Qualified applicants should submit a letter of interest outlining their teaching and research experience and curriculum vitae to:

facultyrecruit@qatar-med.cornell.edu

***Please quote Faculty Search #06-009-sci on all correspondence**

Cornell University is an equal opportunity, affirmative action educator and employer.

The screening of applications will begin immediately and continue until suitable candidates are identified.

Please note, due to the high volume of applications, only short-listed candidates will be contacted.

Does your next career step need direction?

For a career in science, I turn to Science

With thousands of job postings, it's a lot easier to track down a career that suits me

I got the offer I've been dreaming of

Now what?

ScienceCareers.org

We know science

AAAS

I have a great new research idea. Where can I find more grant options?

I want a career, not just a job

You know, ScienceCareers.org is part of the non-profit AAAS

That means they're putting something back into science

There's only one place to go for career advice if you value the expertise of *Science* and the long experience of AAAS in supporting career advancement - ScienceCareers.org. The pages of *Science* and our website ScienceCareers.org offer:

- Thousands of job postings
- Career advice articles and tools
- Funding information
- Networking opportunities

www.sciencecareers.org

NANYANG TECHNOLOGICAL UNIVERSITY

A Global University of Excellence

SCHOOL OF PHYSICAL & MATHEMATICAL SCIENCES

Professor of Chemistry
Professor of Physics
Professor of Mathematical Sciences

Nanyang Technological University (NTU), a top research university in Asia-Pacific, is building its science school rapidly and is seeking outstanding candidates for appointment as Professors of Chemistry or Physics or Mathematical Sciences. The areas of emphasis are as follows:

Chemistry & Biological Chemistry

- Synthesis Methodology and Catalysis
- Bioorganic, Bioinorganic, Bioanalytical and Biophysical Chemistry
- Medicinal Chemistry
- Green Chemistry
- Theoretical & Computational Chemistry

Physics & Applied Physics

- Condensed Matter Physics, Soft Condensed Matter Physics and Biophysics
- Nanoscience, Surface Science and Low Dimensional Systems
- Laser Physics, Photonics and Atom Optics
- Semiconductor Physics, Spintronics and Organic Electronics

Mathematical Sciences

- Computational Mathematics & Applications
- Interdisciplinary Science with significant mathematical content
- Discrete Mathematics & Applications
- Probability, Statistics & Applications

We seek candidates with distinguished achievement in research and who also excel in teaching. Singapore has multiple sources for competitive research funding and NTU provides the environment for cutting edge interdisciplinary research.

Candidates with potential for distinction may also apply to be considered for tenure-track positions at the **Assistant Professor or Associate Professor** level.

Further information at: **http://www.spms.ntu.edu.sg/home/vacancies**

Closing date: 31 March 2007

Enquiries to: **Search Committee**
School of Physical & Mathematical Sciences
E-mail: claire@ntu.edu.sg

THE UNIVERSITY OF TEXAS SOUTHWESTERN MEDICAL CENTER

ASSISTANT PROFESSORS: The Department of Physiology invites outstanding scientists with Ph.D., M.D., or equivalent degrees to apply for tenure-track assistant professor positions. Candidates who use innovative optical, mechanical, electrical, molecular biological or computational methods with important applications to physiological systems, ranging from individual genes and proteins to cells and organs are encouraged to apply.

These positions are part of the continuing growth of the Department at one of the country's leading academic medical centers and will be supported by significant laboratory space on our new campus, competitive salaries, and exceptional start-up packages. The UT Southwestern is the scientific home to four Nobel Prize laureates, 17 members of the National Academy of Sciences and 19 members of the Institute of Medicine. More than 2,000 research projects are supported by $300 million grant funding annually at UT Southwestern.

Applicants should submit curriculum vitae, a brief statement of research plans, and arrange to have three letters of reference sent to: **James Stull, Ph.D., c/o Gena McElyea, Department of Physiology, The University of Texas Southwestern Medical Center, 5323 Harry Hines Boulevard, Dallas, TX 75390-9040**.

UT Southwestern strongly encourages applications from women, minorities, and people with physical challenges. An Equal Opportunity Employer.

Universität Karlsruhe (TH)

Forschungsuniversität · gegründet 1825

The **DFG-Research Center for Functional Nanostructures** (CFN) at the Universität Karlsruhe (TH) invites applications for two positions of

Junior Research Group Leaders

in the area of **„Nanobiology"**.

The positions will become available in 2007 within the framework of the **Cluster of Excellence**. The groups will be funded at least until June 2009, with the possibility for an extension up to a maximum total duration of 5 years. The Junior Research Groups are expected to contribute to and participate in CFN projects related to "Nanobiology" (www.cfn.uni-karlsruhe.de), where groups from molecular biology, physics, chemistry, biochemistry, and electrical engineering already collaborate. Possible research topics of the Junior Research Groups may include biophotonics, mechanochemical sensors, artificial membranes, or bio-assembly of nanomaterials.

The applicants are expected to be outstanding young researchers in one or more fields related to nanobiology. Their competence should be firmly established by publications in international scientific journals, and they should hold their doctorate degree for not more than 5 years. The CFN will support the groups with sufficient funding, start-up investments and additional personnel.

Further information can be obtained from Prof. Anne Ulrich (anne.ulrich@ibg.fzk.de) or from Prof. Martin Bastmeyer (bastmeyer@bio.uka.de).

The Universität Karlsruhe (TH) aims to increase the representation of women among the staff and therefore explicitly encourages applications from female scientists. Universität Karlsruhe (TH) is an equal opportunity employer and will give preference to disabled candidates having the same qualifications as their competitors.

Applications including a short project outline (past and future research), CV, copies of degree certificates, a list of publications, and copies of the five most important publications should be submitted by **8.1.2007** to the CFN coordinator, **Prof. Dr. M. Wegener, Universität Karlsruhe (TH), Institut für Angewandte Physik, Wolfgang-Gaede-Straße 1, D-76131 Karlsruhe, Germany**.

CATIE Centro Agronómico Tropical de Investigación y Enseñanza

DIRECTOR GENERAL

El Centro Agronómico Tropical de Investigación y Enseñanza, CATIE, es un centro científico regional para la agricultura y el manejo de los recursos naturales dedicado al desarrollo rural sostenible y a la reducción de la pobreza en América Tropical. Su misión es contribuir a la reducción de la pobreza rural promoviendo una agricultura y manejo de los recursos naturales competitivos y sostenibles, a través de la educación superior, investigación y cooperación técnica.

Requisitos:

- Doctorado en Agricultura, Recursos Naturales, Ciencias Sociales o campos afines.
- Amplia experiencia en investigación y en instituciones de educación superior.
- Experiencia en manejo institucional de financiamiento en agricultura y/o el sector de recursos naturales renovables, en niveles nacionales e internacionales.
- Prestigio internacional reconocido.
- Ciudadano de un país miembro del sistema interamericano.
- Completamente bilingüe español e inglés.
- Disponibilidad para residir con su familia en la Sede Central del CATIE.
- Preferiblemente ciudadano de uno de los países miembros de CATIE.

Proceso de aplicación: Las personas interesadas deberán enviar en un sobre rotulado Confidencial, carta de aplicación, curriculum vitae, lista de publicaciones, tres referencias personales y tres referencias profesionales relacionadas con el trabajo gerencial y científico, a la siguiente dirección: **Adriana Arce Mena, Área de Recursos Humanos, 7170 CATIE, Turrialba, Costa Rica; aarce@catie.ac.cr; Teléfono: 558-2654, Fax: 558-2506. Fecha límite de recepción: 30 marzo 2007** a las 16 horas

EL CATIE BUSCA ENRIQUECER SU PERSONAL EN TÉRMINOS DE GÉNERO; POR TANTO, INSTA A HOMBRES Y MUJERES EN IGUALDAD DE CONDICIONES A PARTICIPAR. EL CATIE NO HACE DISCRIMINACIÓN POR ORIGEN ÉTNICO, CREDO RELIGIOSO O POLÍTICO.

ST. THOMAS UNIVERSITY

"Developing Leaders For Life"

FACULTY – BIOLOGY

St. Thomas University invites applications for a continuing track position in biology at the Assistant, or Associate Professor level, depending on experience, starting August 2007. A PhD and three years postdoctoral laboratory research experience required. Applicants at the Associate level must have an established and funded research program.

We are searching for an individual who will thrive in a liberal arts environment that combines a strong commitment to teaching and research. Mentoring of undergraduate research students is expected. Candidates with research interests that complement the developing cell science program are particularly encouraged to apply. Specifically, research involving microbial physiology and developmental genetic models will be given preference. The successful candidates will be expected to teach at all levels of the curriculum and establish an externally funded research program that provides rigorous collaborative research projects for undergraduates. Opportunities exist for research collaboration within the developing biomedical research community spawned by the newly forming Scripps Research Institute in South Florida.

Research laboratory space and infrastructure will be provided in our new building. Lab facilities include molecular, histological and microscopy cores.

The department is a multi-discipline unit consisting of 20 full-time and adjunct faculty members. We offer Bachelor of Arts degrees in biology, computer science, and computer information systems in addition to our pre-nursing and pre-engineering programs.

Located in Miami Gardens, Florida, St. Thomas University is a Catholic university with rich cultural and international diversity. Our community includes more than 2600 students and 105 full-time faculty members. Further information is available at **http://www.stu.edu/**.

Completed applications received by **February 1, 2007** will receive full consideration with later applications as needed until position is filled. Send letter of application, curriculum vitae, undergraduate and graduate transcripts (unofficial copies are acceptable initially), statement of research interests, statement of teaching philosophy, and a list of at least three references to: **Lenore Prado, Associate Director of Human Resources, St. Thomas University, 16401 NW 37 Ave., Miami Gardens, FL 33054. Email: facsearch@stu.edu. Fax: (305) 628- 6510**.

St. Thomas University is an Equal Opportunity Employer.

UM PACE

THE UNIVERSITY OF MONTANA

PArtnership for Comprehesive Equity

Project PACE functions as a catalyst to facilitate faculty and administrative gender diversity goals in the sciences.

The University of Montana

ADVANCE

337 & 340 North Corbin Hall
The University of Montana
Missoula, MT 59812
Tel: 406.243.PACE
PACE@mso.umt.edu
http://www.umt.edu/pace

UNIVERSITY OF MARYLAND

Center for Bioinformatics and Computational Biology/UMIACS
Department of Computer Science
Assistant, Associate, and Full Professor

The University of Maryland invites applications for faculty positions at the assistant, associate, and full professor level in the Center for Bioinformatics and Computational Biology (**www.cbcb.umd.edu**), to be appointed jointly with the Computer Science Department (**www.cs.umd.edu**). The University has committed the resources to recruit several new tenured and tenure-track faculty for the Center, directed by Dr. Steven Salzberg, in order to establish a world-class location for research in bioinformatics, computer science, applied mathematics, statistics, molecular biology, genetics, and genomics.

Senior candidates will be expected to lead internationally prominent research programs in computational aspects of genomics and bioinformatics. All applicants are expected to have publications and research experience with strong components of biological science and computing. Experience in interdisciplinary collaboration is an important asset. Exceptional candidates from areas outside of computer science are also encouraged to apply.

The faculty will be housed in contiguous space dedicated to the Center, and will have access to significant high-end computing infrastructure through the University of Maryland Institute for Advanced Computer Studies. The University of Maryland is located near the nation's capital in Washington, D.C., and offers excellent potential for collaboration with other outstanding bioinformatics and genomics research groups nearby, in organizations such as the NIH, The Institute for Genomic Research, the University of Maryland Biotechnology Institute, and the Smithsonian Institution.

Applicants are asked to apply online at **https://www.cbcb.umd.edu/hiring/online/2007**, or by following the link from **http://www.cbcb.umd.edu/aboutus/jobs.shtml**. For best consideration applications should be received by **January 15, 2007**, but applications may be accepted until the position is filled.

The University of Maryland is an Affirmative Action, Equal Opportunity Employer. Women and minorities are encouraged to apply.

FACULTY POSITION

Department of Molecular Pathology
The University of Texas
M. D. Anderson Cancer Center

The **Department of Molecular Pathology at The University of Texas M. D. Anderson Cancer Center** invites applications for tenure/tenure-track faculty positions at the ASSISTANT PROFESSOR and PROFESSOR levels. We are seeking outstanding investigators with special emphasis on molecular mechanisms of solid tumor stem cell involvement in cancer and application to diagnosis and therapy. Ph.D. or M.D. scientists with appropriate research experience should submit curriculum vitae, a short summary of research interests and three letters of reference to:

Dr. Ralph B. Arlinghaus, c/o Ms. Alice Powell
Department of Molecular Pathology (Unit 951)
The University of Texas M. D. Anderson Cancer Center
P.O. Box 301429, Houston, TX 77230-1429
E-mail:apowell@mdanderson.org.

THE UNIVERSITY OF TEXAS
MD ANDERSON
CANCER CENTER
Making Cancer History®

M. D. Anderson Cancer Center is an equal opportunity employer and does not discriminate on the basis of race, color, national origin, gender, sexual orientation, age, religion, disability or veteran status except where such distinction is required by law. All positions at The University of Texas M. D. Anderson Cancer Center are security sensitive and subject to examination of criminal history record information. Smoke-free and drug-free environment.

UNC
SCHOOL OF MEDICINE

Chair
Department of Microbiology

The School of Medicine of the University of North Carolina at Chapel Hill is initiating a search for a Chair to lead its Department of Microbiology. The selected individual will be expected to provide effective academic and administrative leadership for the research and teaching programs of this fine department, one that has strong collaborative relationships with many of the other departments, research centers, and institutes within the University.

Minimum qualifications for this position include a Ph.D. and/or an M.D. degree, a distinguished record of scientific research and extramural funding, evidence of administrative skills, and a commitment to student and post-graduate education. Candidates should have demonstrated ability to lead and manage a multifaceted academic department. Consideration of candidates will begin immediately and will continue until the search has come to a successful conclusion.

Letters nominating qualified candidates are requested and may be sent to:

Richard Boucher, MD
Chair, Microbiology Chair Search Committee
Office of the Dean, School of Medicine
University of North Carolina at Chapel Hill
CB# 7000, 4060 Bondurant Hall
Chapel Hill, N.C. 27599-7000
ATTN: Jennifer Nall
microchairsearch@med.unc.edu

Interested individuals should submit a cover letter, a current Curriculum Vitae, and the names, addresses, and contact information (e-mail addresses and phone numbers) of four or more references. These documents can best be submitted by logging on to the following website: **http://www.med.unc.edu/chairsearch**

The University of North Carolina at Chapel Hill is an Equal Opportunity Employer.

American Cancer Society®

Postdoctoral Fellowship Awards in the Early Detection of Cancer

CANARY FOUNDATION
Stopping Cancer Early – The Best Possible Investment

Canary Foundation, in partnership with the American Cancer Society, is extending its postdoctoral fellowship program focused on studies in the tools and technologies for developing strategies for the early detection of cancer. Research should be directed at new approaches to improve clinical methods for the screening of primary tumors and/or metastases.

Awards will be 3 years with stipends of $42,000, $44,000, and $46,000 per yr, plus an annual $4,000 institutional allowance. Based upon availability of funds and scientific merit of the applications, it is anticipated that up to 3 awards will be made. To restrict funding to full 3 year fellowships, applicants may, at the time of application, have had no more than 2 years of research experience beyond their terminal degree (MD or PhD). Applicants must be US citizens or permanent residents working with an accomplished mentor at a non-profit institution. Awardees will be asked to attend the "Realizing the Promise" Early Detection Symposium May 22-24, 2007.

Deadlines: Letter of intent: **January 16, 2007**; Application: **February 20, 2007**. For information regarding policies, submission of the letter of intent, or to obtain an application, go to the ACS website **www.cancer.org/research**. To learn about the Canary Foundation, visit **www.canaryfoundation.org**. For inquiries, contact **William Phelps, PhD** at **404-929-6835** (**william.phelps@cancer.org**) or **Christopher Widnell** at **404-329-7552** (**Christopher.widnell @cancer.org**)

WEILL CORNELL
MEDICAL COLLEGE IN QATAR

FACULTY POSITIONS

In a pioneering international initiative, Weill Medical College of Cornell University established the Weill Cornell Medical College in Qatar (WCMC-Q) with the sponsorship of the Qatar Foundation for Education, Science and Community Development. WCMC-Q is located in Doha, Qatar, and in its fifth year of operation, Weill Cornell seeks candidates for faculty positions to teach in Doha in:

BIOCHEMISTRY

Following a two-year Pre-medical Program, the inaugural class has now completed the second year of the traditional four-year education program leading to the Cornell University M.D. degree, which they will receive in May 2008. The medical program at WCMC-Q replicates the admission standards and the innovative problem-based curriculum, which includes, among other things, integrated, multidisciplinary basic science courses that are the hallmark of the Weill Medical College of Cornell University.

Faculty, based in Doha, will be expected to teach their specialty and to contribute to the academic life of the Medical College. This unique program provides the successful applicant with the opportunity to leave his/her mark on a pioneering venture. A state of the art research program, to be housed in WCMC-Q and focused on genetics and molecular medicine and women and children's health will be initiated within the next year. Teaching and research facilities are situated within a brand new building designed to Cornell specifications and located in Education City in Doha amongst other American universities.

All faculty members at WCMC-Q are appointed by the academic departments at Weill Cornell.

Further details regarding the WCMC-Q program and facilities can be accessed at:
www.qatar-med.cornell.edu.

Candidates should have a M.D., Ph.D. or M.D./Ph.D. or equivalent terminal degree. The successful candidate will have strong teaching credentials and experience in teaching medical students. Salary is commensurate with training and experience and is accompanied by an attractive foreign-service benefits package.

Qualified applicants should submit a letter of interest outlining their teaching and research experience and curriculum vitae to:

facultyrecruit@qatar-med.cornell.edu

***Please quote Faculty Search #06-008-sci on all correspondence**

Cornell University is an equal opportunity, affirmative action educator and employer.

The screening of applications will begin immediately and continue until suitable candidates are identified.

Please note, due to the high volume of applications, only short-listed candidates will be contacted.

POSITIONS OPEN

TENURE-TRACK FACULTY POSITION IN PATHOBIOLOGY
University of Maryland Biotechnology Institute, Shady Grove
Center for Advanced Research in Biotechnology
Center for Biosystems Research

The University of Maryland Biotechnology Institute (UMBI) invites applications from exceptional candidates for a tenure-track faculty position at the level of **ASSISTANT PROFESSOR.** This position is part of an effort to increase the integration of current programs among the Center for Biosystems Research **(website: http://www1.umbi.umd.edu/~cbr),** the Center for Advanced Research in Biotechnology **(website: http://carb.umbi.umd.edu/)** and the National Institute of Standards and Technology (NIST). The successful candidate will be expected to develop a competitive and externally funded research program in the field of pathobiology advanced analytical methods.

UMBI Shady Grove recently opened a 140,000 square-feet research facility with new capabilities to accommodate diverse research programs requiring biocontainment (BL3), small animals, plant growth needs (growth chambers and greenhouse) and transgenesis (insects and plants). These facilities add to outstanding resources for conducting bioinformatics, X-ray crystallography, nuclear magnetic resonance spectroscopy and biophysical measurements. UMBI Shady Grove is located in the Baltimore/Washington area's biotechnology corridor with convenient access to the National Institutes of Health, NIST, and the U. S. Department of Agriculture research campuses.

Qualifications: Ph.D. in biochemistry or related field, postdoctoral experience, and knowledge skills in pathobiology. Applicants with research interests and proven accomplishments in areas broadly related to pathobiology will be considered. Candidates with interests in plant or animal pathogens, parasites, vectors or the responses of hosts to infection are encouraged to apply, especially those that may interact with scientists in structural biology, biophysics and molecular interactions, genomics and proteomics, or computational biology at UMBI Shady Grove.

Applicants should submit their curriculum vitae (referencing position 300880), a summary of future research plans, and names of three references (PDF file) electronically to **e-mail: carbsrch@umbi.umd.edu** or by mail to: **Pathobiology Search Committee, University of Maryland Biotechnology Institute, Shady Grove, 9600 Gudelsky Drive, Rockville, MD 20850.**

Review of candidates will begin January 1, 2007, and continue until the position is filled.

UMBI is an Equal Employment Opportunity/ADA/Affirmative Action Employer.

PROTEOMIC CANCER RESEARCH POSITION
Eastern Virginia Medical School

A position is available in the Center for Biomedical Proteomics at the Postdoctoral level. The research involves the application of mass spectrometry in cancer-related translational and basic research. The successful applicant will utilize state-of-the-art proteomics tools and molecular techniques housed within well-equipped modern laboratories. The position requires a Ph.D. with expertise in protein chemistry, mass spectroscopy, or molecular biology. Interested individuals should send curriculum vitae and three letters of recommendation to:

O. John Semmes, Ph.D.
Department of Microbiology and Molecular Cell Biology
Eastern Virginia Medical School
700 West Olney Road
Norfolk, VA 23507-1696
E-mail: semmesoj@evms.edu

Eastern Virginia Medical School is an Equal Opportunity, Affirmative Action Employer and a drugfree workplace.

EARTH SCIENCES CURATOR/ PALEONTOLOGIST
University of Alaska, Fairbanks

The University of Alaska Museum of the North and the Department of Geology and Geophysics at the University of Alaska, Fairbanks, invite applications for a tenure-track, **ASSISTANT PROFESSOR** position as Curator of Earth Sciences. We seek a dynamic individual who will instill his/her enthusiasm for paleontology in both students and the public. Applicants who can successfully implement their vision for using natural history collections on the leading edge of science are especially encouraged to apply.

Applicants must have an earned Ph.D. in paleontology or a closely related field prior to hire. Teaching, curatorial, and postdoctoral experience is preferred. The successful candidate is expected to establish a vigorous, externally funded research program; curate and expand the Museum's Earth Sciences collections; collaborate with existing faculty with interests in sedimentology, stratigraphy, geochronology, Quaternary geology, evolutionary biology, and paleoclimatic or paleoenvironmental reconstruction; teach at least one course per year; and advise undergraduate, M.S., and Ph.D. students. Preferred applicants will have a strong background in developing, managing, and using museum collections, and in a specialized research area in paleontology, which is flexible. Experience working with or teaching diverse student populations is desirable. A newly expanded museum, collections laboratory, startup funds, and supercomputer facilities are available. Further information about both the Department and Museum is available at **website: http://www.uaf.edu/geology and www.uaf.edu/museum.**

Interested applicants should apply online at **website: http://www.uakjobs.com** by completing an application form and uploading curriculum vitae, three letters of reference, copies of key publications, and separate statements summarizing experience and long-term goals in research, curation, and teaching . Screening of applications will begin on January 1, 2007, and continue until the position is filled. Questions about this announcement can be addressed to **Molly Lee (e-mail: ffmcl@uaf.edu).** *The University of Alaska is an Affirmative Action/Equal Opportunity Employer. Women and minorities are encouraged to apply.*

POSTDOCTORAL RESEARCH PARTICIPATION POSITION
Nanotechnology-Based Targeted Anti-Viral Therapeutics Air Force Research Laboratory
Wright Patterson Air Force Base, Dayton, Ohio

The Air Force Research Laboratory at Wright-Patterson Air Force Base, in collaboration with Wright State University, has an immediate postdoctoral position for an outstanding **VIRAL, CELLULAR, or MOLECULAR BIOLOGIST** to join a research team working in the nanotechnology area. You will conduct research on how metallic nanomaterials interact with and inhibit viral proteins and particles, using cell-based in vitro model systems to evaluate antiviral effects and host cell toxicity. For more information on how to apply, **e-mail: jeffrey.johnson@orau.org.**

Christopher Newport University (CNU), Department of Biology, Chemistry, and Environmental Science seeks tenure-track **ASSISTANT PROFESSOR** in biology starting August 2007. Will teach/conduct research in fish biology and aquatic ecology and teach introductory biology courses. Ph.D. in appropriate field by June 1, 2007 for tenure-track appointment. All-but-dissertation candidates may be considered for nontenure-track instructor appointment. CNU, a young, selective state-supported liberal arts and sciences University of 4,800 students, is located on the Virginia Peninsula between Williamsburg and Virginia Beach. Full job posting (number 8089)/application details at **website: http://hr.cnu.edu/vacancies/index.html.** Deadline: January 15, 2007. *Equal Opportunity Employer.*

TENURE-TRACK FACULTY POSITION IN STRUCTURAL BIOLOGY
University of Maryland Biotechnology Institute, Shady Grove
Center for Advanced Research in Biotechnology
Center for Biosystems Research

As part of a major new expansion, the University of Maryland Biotechnology Institute (UMBI) invites applications for a tenure-track faculty position **(ASSISTANT PROFESSOR)** in structural biology (X-ray crystallography or nuclear magnetic resonance spectroscopy [NMR]). The successful candidate will be expected to develop a competitive and externally funded research program using structural biology approaches to address contemporary biological questions.

The Shady Grove Campus of UMBI includes scientists from the Center for Advanced Research in Biotechnology (CARB, **website: http://carb.umbi.umd.edu/),** the Center for Biosystems Research (CBR, **website: http://www1.umbi.umd.edu/~cbr/),** and the National Institute of Standards and Technology (NIST). The campus is located in the heart of a major biotechnology community with easy access to the National Institutes of Health and NIST. The successful candidate will benefit from existing strengths in structural biology, biophysical chemistry, and computational biology at CARB, and from research into complex biological systems and pathobiology at CBR. State-of-the art facilities and support for X-ray crystallography and NMR are available at Shady Grove.

Qualifications: Ph.D. in biochemistry or related field, postdoctoral experience and knowledge skills in structural biology. Applicants will be considered who have research interests in any area of contemporary structural biology, including biomedical, plant, or insect biology. Applicants should submit their curriculum vitae (referencing position 300881), a summary of future research plans, and names of three references (PDF file) electronically to **e-mail: carbsrch@umbi.umd.edu** or by mail to: **Structural Biology Search Committee, University of Maryland Biotechnology Institute, Shady Grove, 9600 Gudelsky Drive, Rockville, MD 20850.**

Review of candidates will begin January 1, 2007, and continue until the position is filled.

UMBI is an Equal Employment Opportunity/ADA/Affirmative Action Employer.

FACULTY POSITION
University of Minnesota

In response to the University of Minnesota's Presidential Initiative on Biocatalysis, the Department of Biochemistry, Molecular Biology, and Biophysics and the Biotechnology Institute seek to hire an outstanding faculty member in the area of microbial biochemistry and genomics. The position will be in the Division of Microbial Biochemistry and Biotechnology and is expected to be at the tenure-track **ASSISTANT PROFESSOR** level, but open to outstanding candidates at any level. Review of applications will continue until the position is filled. All candidates must have a Ph.D. degree and a strong publication record. Postdoctoral or equivalent experience is desired. To apply please send curriculum vitae and statements of research and teaching interests, and arrange to have sent three letters of recommendation that consider both teaching and research potential to: **BMBB Search Committee Chair, c/o Kristi Iskierka, Department of Biochemistry, Molecular Biology, and Biophysics, 1479 Gortner Avenue, Saint Paul, MN 55108 U.S.A.** An application sent by e-mail to **e-mail: bti@umn.edu** should be followed by a hard copy sent to the address above. *The University of Minnesota is an Equal Opportunity Educator and Employer.*

NanoScience Technology Center Faculty Positions

University of Central Florida

We seek outstanding candidates for full or associate professor positions in the NanoScience Technology Center (NSTC) at UCF (**www.nanoscience.ucf.edu**) to lead interdisciplinary nanoscience research in the broad areas of photonics, imaging, quantum information, materials, biomolecular science and energy. Exceptional junior candidates in theoretical nanoscience will also be considered for tenure-track positions. The NSTC is a recently established Center with 13 faculty and 32 graduate students working in 20,000 square feet of state-of-the-art laboratory space.

Applicants who have an interest in commercial applications of their work or existing commercial ventures are encouraged to apply. UCF supports such activities through the UCF Technology Incubator which was awarded the 2004 NBIA Technology Incubator of the Year. Competitive packages and customized laboratories will be offered to successful candidates. There are ample opportunities to collaborate with researchers in UCF's other centers such as optics (CREOL), advanced materials (AMPAC), biomolecular science (BMSC) and energy (FSEC) as well as the academic departments. UCF has about 47,000 students and is located in Orlando, a dynamic and progressive metropolitan region that is an excellent place to live and work.

Review of candidates will begin on **January 15, 2007** and will continue until all positions are filled. Please send curriculum vitae, summary of research and teaching plans, and list of three or more references to: **Ms. Rajeswari Natarajan, Program Coordinator, NSTC, 12424 Research Parkway, Suite 400, Orlando, FL 32826 (rnataraj@mail.ucf.edu)**. Electronic applications are encouraged.

UCF is an Affirmative Action Employer. Women and minorities are encouraged to apply. UCF makes all application materials, including transcripts, and all search materials available for public review upon request, in accordance with Florida Statutes.

Scientific Program Director

American Cancer Society®

The American Cancer Society (ACS) is seeking a Scientific Program Director to lead the Society's extramural research and training effort in the areas of clinical cancer research, epidemiology, hematology and immunology. The position is located at the National Home Office in Atlanta, Georgia.

The responsibility of this position is to assure unbiased, rigorous, peer review of grant applications. This involves ensuring ACS requirements are met, assigning applications to appropriate committee members, conducting site visits when necessary and administering awarded grants. In addition, the Program Director will identify and recruit qualified scientists to serve on the peer review committees. The Program Director will serve as an expert source of information on advances in cancer research and the ACS grant programs to Society volunteers, staff, donors and national organizations and agencies, and advise about promising future areas of investigation in his or her specific area of expertise. He or she will also play a significant role in promoting the Society's Research and Training Program, and in that capacity will be called upon to convey the achievements of the Program to professional and lay audiences, and to support the fund-raising efforts of the Society. Depending on personal interest, there is the potential for involvement in the Society's cancer control and health promotion programs.

Minimum requirements are an MD or equivalent degree, 5-years experience as an established investigator, and well-published in the peer reviewed literature. Familiarity with clinical trials is desirable. Excellent communication skills are essential, including the ability to make presentations on cancer research topics to non-scientific audiences. Salary is commensurate with the candidate's qualifications and experience. Candidates should submit a CV and letter of interest, the names of three references, and an indication of salary requirements to: **John Stevens, MD, Vice President for Extramural Grants, Research Department, American Cancer Society, 1599 Clifton Road, NE, Atlanta, GA 30329**; email: **john.stevens@cancer.org**. Interviewing will start immediately until the position is filled.

Los Alamos NATIONAL LABORATORY

The Los Alamos National Laboratory is a premier basic and applied science laboratory, specializing in multidisciplinary research to meet national security needs. LANL is one of the largest research institutions in the world, with an annual budget of approximately $2.1 billion. To create and foster innovations in science, technology, and engineering, the Laboratory employs the best and brightest people and provides an environment to deliver system solutions for our country's national security, now and in the future. The Laboratory is currently seeking:

BIOSCIENCE DEPUTY DIVISION LEADER

Bioscience Division supports national security missions by performing basic research and integrating emerging technologies into functional systems. The principal mission focus is to address issues in environmental stewardship and public health that impact national security. To meet this goal, the Division employs 250 individuals including a Division Leader and Deputy Division Leader who work together to provide leadership, strategic/tactical planning and management for high quality research and development. The Division's R&D is performed in a collaborative environment involving technical staff from throughout the Laboratory as well as external collaborators. The Division is seeking a dynamic Deputy Division Leader with a distinguished research record and excellent leadership skills whot wishes to join our management team to provide strategic direction for the Division and to develop world-class, multidisciplinary research. A Ph.D. and strong research record in a bioscience-related area are required. In addition, a track record of working with sponsors such as the DOE Office of Science, Department of Homeland Security, and other federal agencies, as well as past collaborations with academic institutions are desired. **Job# 213745**

GENOME CENTER DIRECTOR

LANL is one of the partner institutions of the Department of Energy's Joint Genome Institute (DOE-JGI), and specializes in high throughput genomic sequencing and genomic research in support of DOE's missions in energy, environment and national security. While leading and managing the operation of the JGI-LANL, the Genome Center Director will participate in the management and leadership of the overall JGI partnership. The Center Director will also develop the scientific vision for JGI-LANL and how its roles and contributions in the JGI partnership will meet future needs of the Institute and user community in both genomic science and production sequencing. A Ph.D. in Biology, Biochemistry, Microbiology, Computer Sciences, or the equivalent is required. Proven success in a leadership role, project management skills, and familiarity with technology development for high throughput research tools for biological research are desired. **Job# 213622**

ADDITIONAL OPENING

We anticipate an upcoming search for a Group Leader position for a newly-formed Bioenergy and Environmental Sciences Group in the Bioscience Division. The research conducted in this group will be focused primarily on environmental microbiology and bioenergy production in support of DOE mission areas in bioenergy, carbon cycling, and bioremediation. As such, we will expect a successful Group Leader candidate to have research expertise in the same areas, and preference will be given to individuals with experience incorporating genomic and metagenomic approaches to their research. In this role, the Group Leader will be responsible for leading and supporting scientific missions, managing resources and personnel, and serving as an interface between the group and upper management, sponsors and customers. For this position only, send a letter of interest and resume to **resnick@lanl.gov** referencing "B&ES GL" in the subject line.

Applicants for the above positions must have the ability to obtain a DOE Q clearance, which normally requires U.S. citizenship. For full job descriptions and to apply, click on the following link: **www.lanl.gov/jobs** and search for applicable job number. AA/EOE

Los Alamos NATIONAL LABORATORY

www.lanl.gov/jobs

POSITIONS OPEN

Sidwell FRIENDS SCHOOL

SCIENCE DEPARTMENT CHAIR
Sidwell Friends School

Sidwell Friends, a coeducational Quaker day school in Washington, D.C., seeks seasoned Educator to serve as Chair of its Science Department (grades five to 12). The Chair is responsible for maintaining and enriching the School's Science Program and, with the Middle and Upper School Principals, evaluates science faculty and curriculum. Master's or Ph.D. in an appropriate discipline, seven or more years of classroom teaching, administrative experience in leading a challenging and cutting-edge science program, and the ability to communicate clearly and effectively with diverse constituencies are required. This ten-month position begins August 2007. Send cover letter, resume, and names of three references to: **Human Resources, Sidwell Friends School, 3825 Wisconsin Avenue N.W., Washington, DC 20016; fax: 202-537-2418; website: http://www.sidwell.edu; e-mail: hr@sidwell.edu.** *Equal Opportunity Employer.*

THEORETICAL POPULATION GENETICS
University of California, Davis

The College of Biological Sciences, University of California, Davis, invites applications and nominations for a position in the Section of Evolution and Ecology at the tenure-track **ASSISTANT, ASSOCIATE or FULL PROFESSOR** level. Candidates must have a Ph.D. (or equivalent) in the biological sciences or related fields. Candidates should have a strong record of research in theoretical population genetics, focusing on questions related to evolutionary and population genomics. We stress that applicants at all levels will be given serious consideration. The successful candidate will be expected to teach an undergraduate course in introductory biology or evolution and to participate in the core course required of all first-year graduate students in the population biology graduate group. Applicants should submit application materials online at **website: http://www2.eve.ucdavis.edu/jobs/.** These will include: curriculum vitae, description of current and projected research, summary of teaching interests and experience, and up to five publications. Applicants should also arrange to have three references references submit supporting letters online at the above website. Closing date: Open until filled, but all application materials, including letters of recommendation, must be received by January 17, 2007, to assure full consideration. Administrative contact, nominations: **Barbara Shaneyfelt (e-mail: bashaneyfelt@ucdavis.edu).** *The University of California is an Equal Opportunity/Affirmative Action Employer with a strong institutional commitment to the development of a climate that supports equality of opportunity and respect for differences.*

The University of Chicago is seeking qualified applicants for full-time **RESEARCH ASSOCIATE (ASSISTANT PROFESSOR)** position. The primary activity of the Research Associate is academic research in association with a faculty member or team. Qualified applicants are required to possess a doctorate degree in cancer biology, molecular genetics, immunology or related fields, and at least five years of postdoctoral experience. Applicants should possess excellent knowledge of molecular biology methods, including generation of transgenic constructs, viruses and TAT-fusion proteins. Compensation is dependent on qualifications. The University provides a generous package of fringe benefits.

Electronic applications must include as attachments, current curriculum vitae and bibliography, a statement of research interests and goals, and three letters of reference.

E-mail requested information to **e-mail: eboyd@medicine.bsd.uchicago.edu.**

The University of Chicago is an Affirmative Action/Equal Opportunity Employer.

POSITIONS OPEN

FACULTY POSITION
QUANTITATIVE MARINE ECOLOGIST

The Hawaii Institute of Marine Biology (HIMB) is inviting applications for a full-time, 11-month, tenure-track research position in quantitative marine ecology, at the rank of **ASSISTANT RESEARCHER.** HIMB is part of the School of Ocean and Earth Science and Technology (SOEST), at the University of Hawaii at Manoa. Starting date for the position is expected to be 1 September 2007, but is subject to negotiation. The successful candidate will be expected to develop extramurally funded research programs and to mentor graduate students. We seek an applicant whose research is process-oriented and complements the expertise of our existing faculty. Individual qualifications and academic excellence, rather than a specific research discipline, will be the most important criteria in selecting the successful candidate. Areas of interest include (but are not limited to) marine ecosystem function and modeling, community structure, trophic interactions and energy flux, early life history biology and development of autonomous techniques for observing organisms, communities, and biological processes in the sea. It is essential that applicants have a strong background in statistical methods and/or modeling techniques.

Minimum qualifications: A Ph.D. degree in marine biology, oceanography, zoology, or related discipline and a demonstrated capability for creative, high-quality research. Apply in writing with supporting materials including (i) curriculum vitae, (ii) concise statement of research accomplishments and future goals and their pertinence to HIMB, (iii) three representative publications, and (iv) the names and addresses of three references.

Send application to: **Quantitative Marine Ecologist Search, The Hawaii Institute of Marine Biology, P.O. Box 1346, Kaneohe, HI 96744.** Application deadline is 15 February 2007. Questions may be addressed to the: **Search Committee Chair, Dr. Kim Holland, Hawaii Institute of Marine Biology, telephone: 808-236-7410, e-mail: kholland@hawaii.edu.**

The University of Hawaii is an Equal Opportunity/Affirmative Action Employer.

DEPARTMENT OF MEDICINE, University of California, San Francisco. The Department of Medicine at the University of California, San Francisco (UCSF), is recruiting for **PHYSICIAN SCIENTISTS** engaged in molecular medicine research. Candidates must have demonstrated potential to lead a first-rate independent research program and must be certified by the American Board of Internal Medicine. Appointment will be made at the **ASSISTANT/ASSOCIATE/PROFESSOR** level in the In-Residence series, depending upon qualifications. Send curriculum vitae via e-mail to: **Joanne Engel, M.D., Ph.D., Chair, Molecular Medicine Search Committee, e-mail: joanne.engel@ucsf.edu.** *UCSF seeks candidates whose experience, teaching, research, or community service has prepared them to contribute to our commitment to diversity and excellence. The University is an Equal Opportunity/Affirmative Action Employer. All qualified applicants are encouraged to apply, including minorities and women.*

ASSISTANT PROFESSOR, the University of Texas of the Permian Basin (UTPB). Biology, tenure track, fall 2007. Ph.D. in a biological field required. **CELLULAR/MOLECULAR BIOLOGIST** preferred. Teaching responsibilities include general biology, undergraduate, and graduate courses in specialty area. Must develop a research program involving undergraduate and Master's students and seek external funding. Submit curriculum vitae, brief statements of teaching philosophy and research interests, and the names and contact information for three references to: **Douglas Henderson, University of Texas of the Permian Basin, 4901 East University, Odessa, TX 79762. Telephone: 432-552-2270. Fax: 432-552-3230. E-mail: henderson_d@utpb.edu.** Screening of applicants begins February 1, 2007. *UTPB is an Affirmative Action, Equal Opportunity Employer.*

POSITIONS OPEN

CDC

RESEARCH MICROBIOLOGIST
Assay Development and Cell Culture Team
Laboratory Branch, Division of Viral Hepatitis
Centers for Disease Control and Prevention

The Centers for Disease Control and Prevention (CDC), Division of Viral Hepatitis (DVH), Atlanta, Georgia, is seeking applications for a Senior Level Laboratory Scientist or Medical Officer with hepatitis experience to serve as a Senior Scientist in the Assay Development and Cell Culture Team. The DVH serves as a World Health Organization Collaborating Center for Reference and Research on Viral Hepatitis. The position provides leadership and direction to a staff of seven including full-time equivalents, regular fellows, and guest researchers. Applicants must be qualified to oversee a comprehensive investigative agenda that includes the development of immunoassays and molecular assays for the detection of important markers of all viruses causing hepatitis, A-E, as well as new and potentially pathogenic viruses. In addition, candidates will be strongly considered if they have existing skills in cell culture and antiviral resistance studies, and/or interest in developing cell culture-based assays to support a research effort on antiviral resistance. The Team works closely with other three teams in the Branch (Reference Diagnostics, Developmental Diagnostics, and Experimental Pathology) and also with the Epidemiology and Prevention Branches to accomplish the overall mission of the DVH. The candidate must possess a broad range of scientific knowledge and laboratory skills relating to the molecular biology, pathogenesis, virology and immunology of hepatitis viruses, expertise in the propagation of viruses in cell culture, and a comprehensive knowledge of the extant literature pertaining to hepatitis as well as scientific approaches taken by professional peers in government, industry, and academia. Candidates for the position must meet qualifications for the GS-13 level for the federal civil service and/or have a doctoral degree in medicine, microbiology, biology, or other appropriate field. Salary is commensurate with experience.

For more information contact **Howard Fields, Ph.D.** at **e-mail: hfields@cdc.gov (telephone: 404-639-3803),** or **Wendi Kuhnert, Ph.D.,** at **e-mail: wdk1@cdc.gov (telephone: 404-639-3103).**

CDC is an Equal Opportunity Employer.

EXECUTIVE DIRECTOR
Ocean Biogeographic Information System

The web-based, international Ocean Biogeographic Information System (OBIS) Secretariat at Rutgers University, seeks an Executive Director. OBIS is the global portal for distributional data on all marine species, with regional nodes in a dozen countries. The applicant must be highly organized, with excellent communication (verbal, written, and editorial) and coordination skills. Demonstrated successful management of software development projects would be an important qualification. A degree in ecology, oceanography, biogeography or taxonomy would also be advantageous. Applicants must apply online with cover letter, application, curriculum vitae, and references at **website: http://uhr.rutgers.edu/jobpostings/APS/Detail.asp?id=06-001472.** For further information, visit **website: http://iobis.org/news_items.** *Rutgers is an Affirmative Action/Equal Opportunity Employer. Employment eligibility verification required.*

RESEARCH SCIENTIST. Will apply knowledge of protein biochemistry, including protein purification and characterization of plasma proteins, as well as precipitation methods, chromatography, assay development, particularly related to coagulation and fibrinolysis system. Must have Ph.D. in biology or related field, and three years of experience in the job or related experience. Apply by resume to: **Bobby Russell, Biolex Incorporated, 158 Credle Street, Pittsboro, NC 27312.**

POSITIONS OPEN

The Department of Biological Sciences at Marshall University seeks a qualified person to fill a tenure-track position at the **ASSISTANT PROFESSOR** level beginning in the fall of 2007. Responsibilities include teaching undergraduate biology courses, establishing an extramurally funded research program, and participating in departmental and University service. The successful candidate will have research interests that complement departmental strengths. Research activities in invertebrate physiology, entomology, and/or molecular systematics are of particular interest, but not exclusive. Candidates who are able and willing to teach introductory human physiology will be given special consideration. Qualified applicants must have earned a Ph.D. in biology or a closely related discipline and have postdoctoral research experience. Please send a cover letter, current curriculum vitae, statement of teaching goals, a statement of research interests and goals, selected reprints, and three letters of reference (sent directly to the address below). All application materials should be addressed to: **Dr. David Mallory, Chair, BSC Search Committee, Department of Biological Sciences, Marshall University, One John Marshall Drive, Huntington, WV 25755.** Review of completed applications begins on January 15, 2007, and will continue until the position is filled. *Marshall University is an Affirmative Action/Equal Employment Opportunity Employer and values diversity. It is also an NSF ADVANCE institutional transformation University, working to advance the careers of women faculty, especially in the science and engineering disciplines.*

VISITING ASSISTANT PROFESSOR OF BIOLOGY

The Biology Department at the University of the South, also known as Sewanee, invites applications for a Visiting Assistant Professor for the 2007-2008 academic year. The successful candidate will teach in the Department's introductory ecology/evolution/biodiversity class, in biology classes for nonmajors, and possibly in upper-division classes in their area of specialty (nine contact hours per week teaching time). Candidates should be enthusiastic about working in the context of the liberal arts tradition in education. The University, with an undergraduate enrollment of about 1,400, has a highly selective program, and is located on a biologically diverse 10,000-acre campus on Tennessee's Cumberland Plateau. Review of applicants will begin 19 January 2007, and applications will be accepted until a suitable replacement is found. Send a letter of application, curriculum vitae, statements of teaching and research interests, transcripts, and three letters of reference to: **Dr. David Haskell, Chair, Biology Department, 735 University Avenue, The University of the South, Sewanee, TN 37383.** E-mailed applications are not accepted. **Website: http://www.sewanee.edu/biology/top.html.** *The University of the South is an Equal Opportunity Employer. Minorities and women are encouraged to apply.*

CHAIR, DEPARTMENT OF INTEGRATED NATURAL SCIENCES
Arizona State University

Arizona State University (ASU) seeks a Chair for the Department of Integrated Natural Sciences. This new Department of 15 faculty members is strongest in biology, but also has faculty and undergraduate teaching responsibilities in chemistry and physics.

We seek an academic leader to further develop this diverse Department. The Chair will be expected to be effective in the professional development of faculty, to garner external funds to support research and education programs, to encourage recruitment and retention of a diverse student population, and to develop community-based partnerships and internships.

The position is available beginning July 1, 2007. Full applications/qualification information are available at **website: http://www.west.asu.edu/dins/chair.** Consideration of complete applications will begin on March 1, 2007; if position is not filled, completed applications will be considered on the first and fifteenth of each month thereafter until the search is closed. *ASU is an Equal Opportunity/Affirmative Action Employer.*

POSITIONS OPEN

The California NanoSystems Institute (CNSI) is a research center at University of California, Los Angeles (UCLA), whose mission is to encourage University collaboration with industry and to enable the rapid commercialization of discoveries in nanosystems. CNSI members who are on the faculty at UCLA represent a multidisciplinary team of some of the world's preeminent scientists. The work conducted at the CNSI represents world-class expertise in five targeted areas of nanosystems-related research including energy, environment and nanotoxicology, nanobiotechnology and biomaterials, nanomechanical and nanofluidic systems and nanoelectronics, photonics and architectonics.

UCLA's California NanoSystems Institute (CNSI) is pleased to announce the creation of two new fellowship programs with a focus on nanoscience and nanotechnology: the CNSI Graduate Student Pioneer Fellowship Program and the CNSI Postdoctoral Pioneer Fellowship Program.

Applications for the Pioneer Fellowships at UCLA are being solicited from CNSI faculty members in the Departments of Bioengineering, Chemistry and Biochemistry, Civil and Environmental Engineering, Microbiology, Immunology, and Molecular Genetics, Molecular Cell and Developmental Biology, Physics and Astronomy.

GRADUATE STUDENT FELLOWS: Receive an additional $5,000 above the support they receive from their home Departments per year for four years; deadline for applications is January 15, 2007.

POSTDOCTORAL FELLOWS: Receive an additional $10,000 above their postdoctoral salary, per year for up to two years; applicants will be considered during the following time periods: January 2007, April 2007, and September 2007; researchers currently employed by UCLA, or with a Ph.D. awarded by UCLA, are not eligible for this award

For specific details, guidelines, and online application for either the graduate or postdoctoral-level fellowship program please visit the CNSI Pioneer Fellowship **website: http://www.cnsi.ucla.edu/fellowships/.**

UCLA is an Equal Employment Opportunity/Affirmative Action Employer

POSTDOCTORAL POSITIONS
Molecular Mycology and Pathogenesis

Postdoctoral research training positions are available in multiple areas of fungal research. These positions are supported by an NIH training grant that includes 25 principal investigators at three neighboring Institutions: Duke University, North Carolina State University, and the University of North Carolina at Chapel Hill. Collectively, these faculty members offer the opportunity to acquire experience in several areas of mycological research, including molecular mechanisms of human or plant fungal pathogenesis, fungi as model system organisms, fungal genomics, molecular systematics, population genetics, chemotherapy, and clinical mycology. Potential applicants may review the participating faculty and their research programs at **website: http://mgm.duke.edu/microbial/training/mmptp.htm.** Postdoctoral Fellows receive NIH-level stipends commensurate with their years of postdoctoral experience, and travel funds to participate in scientific meetings. *Only U.S. citizens or permanent residents are eligible.* Prospective applicants should contact one or more participating faculty to explore the training options and develop a research plan. The completed application should include a cover letter and the applicant's curriculum vitae, a letter from the prospective mentor(s), two letters of recommendation, and a one-page synopsis of the proposed research project. Submit inquiries and applications to: **T.G. Mitchell, P.O. Box 3803, Duke University Medical Center, Durham, NC 27710,** or **e-mail: tom.mitchell@duke.edu.**

POSITIONS OPEN

DEPARTMENT OF PSYCHIATRY, Massachusetts General Hospital (MGH), Harvard Medical School (HMS). The Massachusetts General Hospital Department of Psychiatry, rated the number one Psychiatry Department by *U.S. News and World Report* for the past 11 years, is seeking a senior, well-established investigator in neuroimaging, with a successful track record of mentorship of fellows, junior, and mid-level faculty, along with demonstrated leadership skills and the ability to direct multidisciplinary teams. The candidate must have an excellent record of peer-reviewed federal funding and high-impact publications. Brain imaging research expertise must be broad in scope, covering an array of contemporary neuroimaging techniques (e.g. functional MRI, MR spectroscopy, and/or PET). Extensive experience collaborating with clinical investigators is required.

The candidate is sought for the position of **DIRECTOR** of Neuroimaging Research in the Department of Psychiatry at MGH, and may include a joint appointment in the Department of Radiology if appropriate. The successful candidate would serve at the HMS professorial level or at the **ASSOCIATE PROFESSOR** level with a trajectory toward promotion to Professor. The position will involve oversight of over a dozen extramurally funded faculty members along with numerous trainees who are currently conducting brain imaging research within the Division. In addition to commensurate space at the Charlestown Navy Yard campus of MGH, the Psychiatric Neuroimaging Research Program has access to dedicated scanning time on state-of-the art 3T MRI devices, as well as access to higher field strength magnets, magneto-encephalography, and PET, in conjunction with the Martinos Center for Biomedical Imaging.

Interested individuals should apply directly to: **Jerrold F. Rosenbaum, M.D., Psychiatrist-in-Chief, Massachusetts General Hospital, 55 Fruit Street, Boston, MA 02114.** *The Massachusetts General Hospital is an Affirmative Action/Equal Opportunity Employer. Minorities and women are strongly urged to apply.*

POSTDOCTORAL RESEARCH FELLOW POSITIONS in tissue engineering and regenerative medicine, two to three immediate openings at the University of Michigan in the areas of (1) bone and cartilage regeneration and (2) hepatocyte culture, liver regeneration, and metabolisms. Candidates must have Ph.D. or M.D. in related field of biological sciences or biomedical engineering. Research projects will focus on biological aspects of regeneration, collaborating with biomedical engineers, and biomaterials scientists in the laboratory. Experience and publications in tissue culture, histology, biochemistry, and molecular biology required. Experience in stem cells and animal implantation are pluses. Interested candidates should provide curriculum vitae with publication list and three to five reference names and contact information to: **Ms. Elizabeth Rodriguiz, Department of Biologic and Materials Sciences, University of Michigan, 1011 N. University Avenue, Ann Arbor, MI 48109-1078. E-mail: earodrig@umich.edu.**

ENVIRONMENTAL FELLOWS AT HARVARD UNIVERSITY

The Harvard University Center for the Environment will award six two-year postdoctoral research fellowships to start September 2007 to outstanding scholars in any field related to the environment. Each Environmental Fellow will work with a host faculty member in his or her Department and participate in an interdisciplinary program at the Center. The fellowship will provide a generous salary and benefits. Applications are due January 15, 2007. Details, including information about the 2006 Fellows, are posted at **website: http://environment.harvard.edu.**

Harvard University Center for the Environment
24 Oxford Street, 3rd Floor
Cambridge, MA 02138

Harvard is an Equal Opportunity/Affirmative Action Employer.

POSITIONS OPEN

ASSISTANT/ASSOCIATE PROFESSOR OF BIOLOGY

The College of Sciences at the University of Findlay is seeking candidates for a tenure-track appointment in biology at an Assistant or Associate Professor level. Applicant review will begin immediately and the position will start in August of 2007. The candidate must have a Ph.D. in biology or a specialization in molecular physiology. A strong focus in molecular and/or genetic techniques is preferred. College teaching experience is desirable, and a commitment to excellence in teaching and scholarly activity is expected. Rank and salary will be commensurate with qualifications. Teaching responsibilities will include zoology and anatomy and physiology. The ability to teach a range of upper-level courses in microbiology, genetics, cell biology, or immunology is highly desirable. The biology area provides instruction to over 1,600 students per year to students majoring in biology, pre-veterinary studies, pharmacy, forensics, environmental science, and other health science areas. Facilities include a newly created life science laboratory for teaching and research. The University of Findlay is a comprehensive Master's degree Institution which has grown from 1,500 to more than 4,500 students in the last twenty years, and is now the largest private University in northwest Ohio. Applicants should submit a letter of application, curriculum vitae, statement of teaching philosophy and the names of three references to: **Mary Jo Geise, Dean of the College of Sciences, The University of Findlay, 1000 North Main Street, Findlay, OH 45840,** or via **e-mail: geise@findlay.edu** on or before February 28, 2007. *The University of Findlay is an Equal Opportunity Employer and Educator.*

BIOLOGICAL AND ENVIRONMENTAL SCIENCES. ASSISTANT PROFESSOR (two positions, full-time, tenure track) beginning August 1, 2007.

CELL BIOLOGIST/ PLANT PHYSIOLOGIST. Teaching responsibilities include cell biology, plant physiology, introductory genetics, introductory biology lecture and laboratory, and possible development of advanced courses in field of expertise.

ENTOMOLOGIST/ INVERTEBRATE ZOOLOGIST. Teaching responsibilities include entomology, invertebrate zoology, introductory biology lecture and laboratory, and possible development of advanced courses in field of expertise. Experience or interest in teaching parasitology is a plus. Ph.D. required and postdoctoral research experience desired. Commitment to teaching excellence, responsiveness to student needs, and effective communication skills essential. Scholarly activities, and a research program that involves undergraduate and graduate students expected. Preference given to candidates with demonstrated excellence in College or University teaching. Screening will begin on January 3, 2007, and will continue until the position is filled. Submit curriculum vitae, transcripts, and three current reference letters to: **Dr. Timothy J. Gaudin, Acting Head, Department of Biological and Environmental Sciences, 615 McCallie Avenue, 2653, The University of Tennessee at Chattanooga, Chattanooga, TN 37403, telephone: 425-423-4341.**

The University of Tennessee at Chattanooga is an Affirmative Action/Equal Opportunity Employer/Title VI+IX/Section 504/ADA/ADEA Institution.

The Office of Science, Department of Energy is seeking a motivated and highly qualified individual to serve as the **ASSOCIATE DIRECTOR,** Office of Biological and Environmental Research. As such, you will provide leadership and direction in establishing vision, strategic plans, goals, and objectives for the research activities supported. You may apply through two different methods, one is for a **SENIOR EXECUTIVE SERVICE** appointment and the second is for an **INTERGOVERNMENTAL PERSONNEL ACT** appointment. The announcement number is SES-SC-HQ-005. The announcement opens on November 6, 2006, and closes on December 21, 2006. Visit **website: http://www.usajobs.opm.gov/** for more information and for instructions concerning application procedures.

POSITIONS OPEN

UNIVERSITY OF PENNSYLVANIA

NIH-sponsored Postdoctoral training in cell/molecular basis of urological diseases: Division of Urology invites applications from prospective **POSTDOCTORAL FELLOWS** (Ph.D., D.V.M.-Ph.D., M.D.-Ph.D., or D.V.M. with residency training in pathology) with background in physiology, cell/molecular biology, or biochemistry. This training program differs from the conventional postdoctoral training in exposing the Postdoctoral Fellows to clinical problems, while carrying out cell/molecular biology research. The Fellows will have exposure and opportunities to translate basic science information into new diagnostic, preventive, and therapeutic strategies. The rapid and effective translation of basic scientific discoveries is greatly facilitated by mentoring from basic and clinical scientists.

The current research interests in the Division of Urology at the University of Pennsylvania Medical Center include (1) alterations of intracellular kinases, phosphatases, and anchoring proteins in smooth muscle urological diseases, (2) smooth muscle signaling mechanisms and regulation in diabetes and smooth muscle remodeling, (3) study of the cell/molecular basis of urinary incontinence, and voiding dysfunction, (4) connective tissue matrix remodeling, and (5) prostate and bladder cancer. However, the program is flexible and any other topics related to urogenital system may be accommodated by recruiting mentors with appropriate expertise from Penn's biomedical science community. Trainees will receive stipend at NIH level, health insurance, and tuition for courses in molecular biology, gene therapy, and urology. Successful applicants should be highly motivated and have a (1) recent doctoral degree (obtained within last three years) in biomedical sciences from a U.S. or foreign University and (2) *U.S. citizenship or immigrant status.* Interested candidates should forward their curriculum vitae and the names of two references to**: Dr. Samuel K. Chacko, Director of Basic Urological Research, 3010 Ravdin-Courtyard, HUP, University of Pennsylvania, 3400 Spruce Street, Philadelphia, PA 19104. Fax: 215-349-5026; e-mail: chackosk@mail.med.upenn.edu.** Start date January 1, 2007. *An Affirmative Action/Equal Opportunity Employer.*

The Division of Social Medicine and Health Inequalities is seeking a full-time junior faculty member at the **ASSISTANT PROFESSOR** level in the area of infectious disease epidemiology, transmission dynamics, and the impact of control interventions. An M.D. or Ph.D./Sc.D. in a related field is required. Qualified candidates should demonstrate an interest in infectious diseases of global health importance and in bio-social approaches to infectious disease research. Applicants should have a record of publication in peer-reviewed journals and have demonstrated an ability to obtain extramural funding. Preference will be given to candidates who have teaching experience. Send statement of interest, curriculum vitae, a brief description of research goals and accomplishments, a summary of current and past grant support, names of three references, and representative reprints of two to five articles/reports to:

Martin S. Hirsch, M.D.
Chair, DSMHI Search Committee
Attn: Jennifer Moltoni
Harvard Medical School
Department of Social Medicine
641 Huntington Avenue, 2nd Floor
Boston, MA 02115

Deadline: January 15, 2007

Brigham and Women's Hospital/Harvard Medical School are Equal Opportunity/Affirmative Action Employers actively committed to increasing the diversity of our faculty: women and members of underrepresented minority groups are therefore strongly encouraged to apply.

POSITIONS OPEN

TWO POSITIONS, MOLECULAR GENETICIST AND BIOCHEMIST

The Biology Department of Franklin and Marshall College invites applications for **TWO VISITING ASSISTANT PROFESSOR** positions, starting July 2007. Candidates should have a Ph.D., demonstrated strength in teaching and research, and ability to engage undergraduates in research.

(1) Molecular Geneticist, three year position: Teaching responsibilities include lecture and laboratory sections of a junior-level core course in molecular genetics and an upper-level elective in molecular biology. The successful candidate may occasionally contribute to the general education curriculum.

(2) Biochemist, one-year position (pending administrative approval): Teaching responsibilities include lecture and laboratory sections of a junior-level biochemistry course emphasizing metabolism and either a sophomore-level core course in physiology and development of plants and animals or an elective in the area of specialization.

Franklin and Marshall College has a tradition of excellence in science and student research; a new life sciences building will open in summer 2007. In addition to the biology major, we offer interdisciplinary majors in biochemistry and molecular biology and in biological foundations of behavior. Applicants should arrange to have letters sent from three references and should submit curriculum vitae, plans for actively engaging undergraduates through teaching and research, and undergraduate and graduate transcripts. Priority will be given to completed applications received by January 15, 2007 (Geneticist), and February 16, 2007 (Biochemist). Electronic submissions will not be accepted. Send applications to: **Professor Ira Feit (Geneticist)** or **Professor Peter Fields (Biochemist), Department of Biology, Franklin and Marshall College, Lancaster, PA 17604-3003. Telephone: 717-291-4118; fax: 717-358-4548; e-mail: cindy.mcintyre@fandm.edu; website: http://www.fandm.edu/biology.xml.**

Franklin and Marshall College is a highly selective liberal arts College with a demonstrated commitment to cultural pluralism. Equal Opportunity Employer.

ASSISTANT PROFESSOR, INVERTEBRATE BIOLOGY, University of Wisconsin, River Falls (UWRF). The Department of Biology seeks a Ph.D. **FIELD BIOLOGIST** with specialization in freshwater or terrestrial invertebrate biology. This is a full-time, nine-month, tenure-track faculty position available August 2007. We are looking for someone who is knowledgeable about multispecies assemblages in nature, and who is willing to learn our local invertebrate species. The successful candidate will teach undergraduate lecture and laboratory courses; these may include general biology, zoology, entomology, ecology, and/or others. Other expectations include advising, research, and service. Evidence of successful teaching and ongoing research is desirable. Review of applications will begin on January 15, 2007, and continue until the position is filled. Application procedures and complete information are available at **website: http://www.uwrf.edu/** (link to employment, faculty/staff opportunities). *UWRF is an Equal Employment Opportunity/Affirmative Action Employer.*

The Biology Department of Rutgers University in Camden, New Jersey, seeks a broadly trained **EXPERIMENTAL GENETICIST** for a tenure-track **ASSISTANT PROFESSOR** position beginning fall 2007. Research interests in systems or computational/integrative biology are desirable. Ph.D. required and postdoctoral experience preferred. This position entails teaching undergraduate and graduate courses in the area of the applicant's expertise and participation in introductory biology courses. Please send curriculum vitae, statement of research interests, and three letters of recommendation to: **Dr. J.V. Martin, Biology Department, Rutgers University, Camden, NJ 08102.** Review of applications will begin January 17, 2007, and continue until the position is filled. *Rutgers is an Equal Opportunity/Affirmative Action Employer. Women and minorities are encouraged to apply.*

POSITIONS OPEN

ASSOCIATE RESEARCH SCIENTIST
(Requisition Number 53395)

The Department of Emergency Medicine at the University of Iowa Hospitals and Clinics is recruiting for a full-time Associate Research Scientist to conduct laboratory research in the fields of cardiovascular disease, diabetes, lipid biochemistry, inflammation and/or opioids. Position requires a Ph.D. degree in the biological or biomedical sciences or professional equivalent (M.D., D.D.S., or D.V.M.), three years of prior postdoctoral research experience or equivalent, and excellent oral and written communication skills. Desirable: One or more years of progressive experience and evidence of developing a reputation as a leader in the fields of cardiovascular disease, diabetes, lipid biochemistry, inflammation and/or opioids; previous track record of independent research work in the form of first author publications in peer-reviewed journals as part of an overall publication record that is current and increasing; and demonstrated success in obtaining grant funding. Highly desirable: two to three years of prior experience with isolation and characterization of primary cardiovascular cells and five years of prior postdoctoral research experience or equivalent. To see a complete position description and/or apply for this position visit our **website: http://jobs.uiowa.edu,** requisition number 53395. The University of Iowa offers a comprehensive salary and benefits package. Initial screening of applicants will begin immediately. Applicable background and credential checks will be conducted. *The University of Iowa is an Equal Opportunity/Affirmative Action Employer. Women and minority candidates are encouraged to apply.*

The Waksman Institute at Rutgers, the State University of New Jersey invites applications for multiple tenure-track faculty positions at the **ASSISTANT, ASSOCIATE, and FULL PROFESSOR** levels.

The Waksman Institute maintains diverse areas of research, with strengths in developmental biology, cell biology, neurobiology, microbiology, protein biochemistry, structural biology, molecular machines, signal transduction, and plant genomics/bioinformatics. The faculty at the Institute use a range of different animal, plant, and microbial model organisms in their genetic research and would welcome a variety of experimental approaches. Demonstrated excellence in research is more important than the area of research. The successful applicant will be expected to develop and maintain an externally funded research program and to teach at the undergraduate and graduate level. Preference will be given to individuals whose interests are synergistic with ongoing research programs at the Institute. Applicants should submit their credentials through our secure web-based application form at **website: http://waksmansearch.rutgers.edu/apply/.**

Applicants should have a Ph.D., Pharm.D., M.D., or equivalent degree and relevant postdoctoral experience. Consideration of applications will begin on January 15, 2007, but these positions will remain open until filled.

STREAM ECOLOGIST
Illinois Natural History Survey

The Illinois Natural History Survey (INHS) seeks a Stream Ecologist at the **ASSISTANT PROFESSIONAL SCIENTIST** level who can develop a strong, externally funded research program emphasizing benthic macroinvertebrates, community or ecosystem-scale ecology, conservation biology, riparian-stream interactions, or watershed-scale issues. Candidates must possess a Doctorate in aquatic ecology or a related discipline. Postdoctoral research experience is preferred. INHS is part of the Illinois Department of Natural Resources and is an affiliated agency of the University of Illinois at Urbana-Champaign. For complete position description and application requirements, visit our **website: http://www.inhs.uiuc.edu/opportunities.** Direct technical questions to **Dr. Walter Hill, e-mail: wrhill@uiuc.edu, telephone: 217-244-2103.** Application deadline: February 1, 2007.

POSITIONS OPEN

University of Massachusetts Medical School
UMASS

POSTDOCTORAL POSITIONS
Biomarker Development
University of Massachusetts Medical School

The Biomarker Development Laboratory, University of Massachusetts Medical School, has several immediate openings for Postdoctoral scientists with experiences of value in the development of biomarker, including synthetic organic and radiopharmaceutical chemistry, molecular biology, optical in vivo imaging, early clinical trials, et cetera. These individuals will join a growing multidisciplinary team emphasizing bench and bedside research primarily in novel applications of DNA and other oligomers as nuclear and optical biomarkers for antisense, pretargeting, and other applications related to the molecular imaging of cancers, infections, and other disease states. A track record in biomarker development would be highly advantageous. The Laboratory is well funded through multiple NIH/Department of Defense two to five-year grants and several grants from industry. Salaries are commensurate with experience and are consistent with NIH guidelines. Applications will be accepted until the positions are filled. Please respond with resume, names and addresses of three references, and a short statement of research interests to: **Dr. D. J. Hnatowich, Department of Radiology, University of Massachusetts Medical School, Worcester, MA 01655 (e-mail: donald.hnatowich@umassmed.edu, telephone: 508-856-4256, fax: 508-856-4572).**

YALE UNIVERSITY
SCHOOL OF MEDICINE
Department of Genetics

The Department of Genetics at the Yale University School of Medicine is seeking to recruit one or more outstanding candidates to become **ASSISTANT PROFESSOR OF GENETICS.** Successful applicants will be provided generous startup funds and space, and will establish strong independent research programs; areas of particular interest include genetics and genomics of vertebrate model organisms, cancer and other human diseases, and computational genomics. We strongly encourage applications from women and minority candidates. Curriculum vitae, a concise statement of research plans, and three letters of recommendation should be sent electronically and with hard copy to:

Richard P. Lifton, M.D., Ph.D.
Chairman
Department of Genetics
Yale University School of Medicine
P.O. Box 208005
New Haven, CT 06520-8005
E-mail: genadm@email.med.yale.edu

An Equal Opportunity/Affirmative Action Employer.

Two **POSTDOCTORAL POSITIONS** in mTOR signaling are available immediately for highly motivated scientists to explore a role of the mTOR pathway in cancer development (see *Science* **307:**1098, 2005). Please send resume and names of three references to: **Dos D. Sarbassov, Ph.D., Department of Molecular and Cellular Oncology, The University of Texas M. D. Anderson Cancer Center, 1515 Holcombe Boulevard, Houston, TX 77030,** or by **e-mail: dsarbass@mdanderson.org.**

The M. D. Anderson Cancer Center is an Equal Opportunity Employer and does not discriminate on the basis of race, color, national origin, gender, sexual orientation, age, religion, disability, veteran status, except, where such distinction is required by law. All positions at the University of Texas M. D. Anderson Cancer Center are security-sensitive and subject to Texas Education Code 51-215, which authorizes the employer to obtain criminal history record information. Smokefree environment.

POSITIONS OPEN

HEALTH SCIENTIST ADMINISTRATOR POSITIONS (TWO)
Health and Science
Office of Research Integrity

The Division of Investigative Oversight (DIO) within the Office of Research Integrity (ORI) is seeking two experienced scientists or physicians with research/clinical experience to serve under the Director, DIO, as **INVESTIGATOR/SCIENTISTS.** DIO's primary task is to conduct oversight reviews of institutional investigations of research misconduct. Applicants should be experienced in running a research program, supervising students and postdoctoral fellows, successfully competing for federal extramural or intramural funds, and peer-reviewing manuscripts and grant applications. Applications with a broad range of experience and scientific interests are preferable because of the wide range of topics that ORI deals with. Good oral and written communication skills are essential.

Please apply online at **website: http://usajobs.opm.gov/** and go to job announcement HHS-OS-2007-0096. Applications must be received by January 2, 2007. If you need assistance, contact **Human Resources Specialists Ms. Anita Ford, telephone: 301-443-1455, e-mail: anita.ford@psc.gov** or **Ms. Beverly White, telephone: 301-443-0803, e-mail: beverly.white@psc.hhslgov.** For additional information about the position, contact **John Dahlberg** at **telephone: 240-453-8800 (e-mail: jdahlberg@osophs.dhhs.gov).** Both positions are at the GS-14 level ($91,407 to $118,828), with the actual salary commensurate with experience. These positions offer full benefits including retirement, health insurance, life and long-term health care insurance, thrift-saving plan participation (matched up to five percent of your salary), et cetera.

Selection will be based on merit and without consideration for race, color, religion, sex, national origin, politics, marital status, sexual orientation, physical handicap, or membership or nonmembership in an employee organization.

TWO TENURE-TRACK
FACULTY POSITIONS
One Each in Ichthyology and Fish Ecology
The College of William and Mary
Virginia Institute of Marine Science
School of Marine Science

The Department of Fisheries Science is seeking candidates for two tenure-track positions, one each in ichthyology and fish ecology. A Ph.D. in ichthyology, vertebrate systematics and evolution, fish ecology, vertebrate ecology, or a related field is required. Postdoctoral research experience is preferred. For the ichthyology position, we seek candidates with expertise in taxonomy/systematics of teleosts and collection-based research that combines morphological and molecular approaches. For the fish ecology position, we seek individuals with expertise in one or more of the following areas: life history and ecology of fishes; quantitative fisheries ecology; survey-based assessment of elasmobranch abundance and diversity. The successful candidates will be expected to develop rigorous externally funded research programs, teach graduate-level courses in ichthyology and fish ecology, mentor M.S. and Ph.D. graduate students, and provide advice to state and federal management agencies. We are seeking relatively recent graduates and will make appointments at the level of **ASSISTANT PROFESSOR.** Only electronic applications will be accepted. Apply at **website: http://www.fisheries.vims.edu/.** Review will begin on February 1, 2007, and continue until the positions are filled. For additional information, contact**: Dr. John E. Olney, Chair, Department of Fisheries Science, Virginia Institute of Marine Science, The College of William and Mary, Gloucester Point, VA 23062. (E-mail: olney@vims.edu, telephone: 804-684-7334.)**

The College of William and Mary is an Equal Opportunity/Affirmative Action Employer. Members of underrepresented groups (including people of color, persons with disabilities, Vietnam veterans, and women) are encouraged to apply.

COURSES & TRAINING

MBL Biological Discovery in Woods Hole

Founded in 1888 as the Marine Biological Laboratory

2007 Microscopy Courses

ANALYTICAL & QUANTITATIVE LIGHT MICROSCOPY
May 9 - May 18, 2007
Application Deadline: January 24, 2007

This comprehensive course provides an in-depth examination of the theory of image formation and the application of video methods for exploring subtle interactions between light and the specimen.

OPTICAL MICROSCOPY & IMAGING IN THE BIOMEDICAL SCIENCES
October 9 - October 18, 2007
Application Deadline: June 29, 2007

This course will enable the participant to obtain and interpret microscope images of high quality to perform quantitative optical measurements and to produce video and digital records for documentation and analysis.

For further information & applications, visit:
www.MBL.edu/education

or contact: Admissions Coordinator
admissions@mbl.edu, (508)289-7401

Women and minorities encouraged to apply.

The MBL is an EEO/Affirmative Action Institution.

Director, ACS Green Chemistry Institute
AMERICAN CHEMICAL SOCIETY

Improving people's lives through the transforming power of chemistry

The American Chemical Society, a federally chartered, non-profit organization, with a multidisciplinary membership of more than 158,000 chemists and chemical engineers, seeks a Director for the ACS Green Chemistry Institute to establish and lead the strategic direction for the Institute, as well as the daily operations of the organization; build its brand and reputation; expand its sources of funding; and lead the development of short- and long-term strategies for the success of the ACS GCI. For more details about GCI, visit its home page at **www.greenchemistryinstitute.org**.

The Director provides the vision necessary to ensure a forward looking approach to challenges and stimulates new initiatives that will effectively advance Green Chemistry and fulfill the Institute's mission. To enhance the image and implementation of Green Chemistry and Engineering, the incumbent will represent ACS GCI in its relationships with major constituencies and stakeholders, the global scientific and engineering communities, and the public. The Director will coordinate efforts throughout the Society on issues related to Green Chemistry and Green Engineering. The Director will develop funding partnerships that will enable the Institute to leverage the Society's investments. The Director will manage ACS GCI operations and staff, assuring that goals are met in a timely and cost-effective manner, and that the Institute serves the stakeholders in an appropriate umbrella role that complements their activities.

Qualifications: In light of these responsibilities, the successful candidate will be a recognized leader in the Green Chemistry and Green Engineering field who is involved in outreach; a creative thinker; a passionate and effective communicator; an enthusiastic articulator; a strategic leader; comfortable with creating and implementing the big-picture; forward-looking, bold, and capable of developing and pursuing an innovative vision to inspire changes in how chemistry is taught; experienced and comfortable working in a visible, high-energy position; and capable of understanding, working with, listening to, and building consensus and collaborating across diverse constituencies. S/he will have an advanced degree or other advanced leadership experience in the area of green chemistry and/or engineering as evidenced by the development of programs, teaching materials, publications, presentations, and/or grant materials in green chemistry. The Director will have successful program development skills, as demonstrated by the inception and creation of new governmental, academic, or private sector programs related to Green Chemistry or similar environmental programs. An excellent track record of development and fund raising is important. Salary is commensurate with experience. Applicants may submit their résumé by either email, (**employment@acs.org**); fax: (**202-872-4077**); or U.S. mail (**1155 16th Street, NW Washington, DC 20036 Attn: Human Resources**) no later than **January 31, 2007**.

ACS is a drug-free, smoke-free, Equal Opportunity Employer.

ANNOUNCEMENTS

NATIONAL CANCER INSTITUTE

Bridge the Gap Between Discovery and Clinical Testing

Access the National Cancer Institute's (NCI) vast resources free of charge to help move therapeutic agents for cancer to the clinic. The National Cancer Institute invites the submission of proposals to:

Rapid Access to Intervention Development

RAID

RAID is *not* a grant program. Successful applicants instead will receive products or information generated by NCI contractors to aid the applicant's development of novel therapeutics towards clinical trial. The goal of RAID is the rapid movement of novel molecules and concepts from the laboratory to the clinic for proof-of-principle clinical trials. RAID will assist investigators by providing any (or all) of the preclinical development steps that may be obstacles to clinical translation. These may include, for example, production, bulk supply, GMP manufacturing, formulation and toxicology.

- **The next deadline for receipt of applications is February 1, 2007. Full applications should be submitted electronically**
- Investigators must register for a certificate for electronic filing
- Further information about RAID and electronic filing of applications can be found at: **http://dtp.nci.nih.gov**
- Inquiries can be made to the RAID Program Coordinator by telephone at 301-496-8720 or by e-mail at RAID@dtpax2.ncifcrf.gov

RAID
Developmental Therapeutics Program
National Cancer Institute
6130 Executive Blvd., RM 8022
Rockville, MD 20852
Tel: 301-496-8720; Fax: 301-402-0831
raid@dtpax2.ncifcrf.gov

NATIONAL INSTITUTES OF HEALTH

POSITIONS OPEN

DIRECTOR
(Microscopy Center)
Comparative Biomedical Sciences

A Director is needed for state-of-the-art microscopy center (fee for service) that houses transmission and scanning electron microscopes, confocal microscope, laser-capture microdissection, fluorescence microscopes, freeze fracture device, and numerous other imaging microscopes such as phase contrast, differential interference contrast, and bright field microscopes. Requirements: Master of Science degree (Ph.D. preferred) in biomedical/biological sciences or related field; ability to operate various light and electron microscopes; knowledge of optical physics. Responsibilities: manages the daily affairs of the microscopy center including operation of instruments; supervises the microscopy staff; assists faculty and staff with imaging needed for research projects; trains individuals to use imaging equipment; performs routine maintenance of imaging instruments. Salary and faculty rank (nontenure track) will be commensurate with qualifications. Application deadline is January 12, 2007, or until candidate is selected. Submit letter of application and resume (including e-mail address) to: **Dr. Steven A. Barker, Professor, Department of Comparative Biomedical Sciences, School of Veterinary Medicine, Louisiana State University, Reference Log #0822, Baton Rouge, LA 70803, telephone: 225-578-3602, e-mail: sbarker@vetmed.lsu.edu.**

Louisiana State University is an Equal Opportunity/Equal Access Employer.

ECOLOGIST

The Department of Biological Sciences, University of New Orleans (UNO), invites applications for a tenure-track position at the rank of **ASSISTANT PROFESSOR.** We seek an Ecologist who uses modeling and/or experimental approaches to understand ecological processes and patterns in wetland plant communities/ecosystems. Applicants must have a Ph.D. and postdoctoral experience. Successful candidates will develop extramurally funded research programs, direct graduate students, and teach at the graduate and undergraduate levels. The candidate will assume an active role in the Ph.D. program in conservation biology and participate in a new interdisciplinary program in wetlands conservation and restoration.

Submit a letter of application, curriculum vitae, statement of research and teaching interests, and three letters of recommendation to **Steve Johnson (e-mail: sgjohnso@uno.edu)** or mail to: **Ecology Search Committee, Department of Biological Sciences, University of New Orleans, LA 70148, telephone: 504-280-6307, fax: 504-280-6121.** Review of applications will begin January 8, 2007. For more information about the Department of Biological Sciences see **website: http://biology.uno.edu/.** *UNO is an Affirmative Action/Equal Opportunity Employer.*

POSTDOCTORAL RESEARCH SCIENTIST
Columbia University

A Postdoctoral Research Scientist position is available in the Department of Medicine at Columbia University Medical Center to develop novel methods for the detoxification of nerve agents. Research will include themutagenesis and modification of artificial bacterial enzymes for enhanced stability and immune evasion.

The candidate must have a Ph.D. with a background in biochemistry or related field. Experience in bacterial protein expression and purification, site-directed mutagenesis, enzyme kinetics, protein cross-linking, high performance liquid chromatography, and basic antibody protocols such as western-blotting, immunoprecipitation, and enzyme-linked immunosorbent assay preferred. Basic organic chemistry skills and experience with organic peptide synthesis would also be advantageous.

Qualified applicants should e-mail curriculum vitae to: **Joanne Macdonald (telephone: 212-342-5610), e-mail: jm2236@columbia.edu.**

Columbia University is an Equal Opportunity/Affirmative Action Employer. Minorities and women are encouraged to apply.

POSITIONS OPEN

Minnesota State University, Mankato, seeks an energetic and dynamic leader for the position of **DEAN,** College of Science, Engineering and Technology. The Dean is the Chief Administrator and Executive Officer who provides vision and leadership for the College and reports directly to the Vice President for Academic Affairs. The Dean is responsible for academic and administrative planning; overseeing nine departments and five applied research centers; program reviews and external accreditations; budgeting; administration of collective bargaining agreements; implementation of college and university policies; promoting, developing, and encouraging cultural diversity and affirmative action initiatives; recruitment, development, and evaluation of faculty; student relations; fundraising and grant activities; maintaining and developing external, public and private partnerships; and overseeing all equipment and facilities assigned to or owned by the College.

Priority consideration will be given to complete applications received by January 15, 2007. The position begins July 1, 2007. For a complete description and application information visit **website: http://www.mnsu.edu/humanres/employment.** A member of the Minnesota State Colleges and Universities System. *Minnesota State Mankato is an Affirmative Action/Equal Opportunity University.*

ECOSYSTEM ECOLOGIST

The Institute of Ecology invites applicants at the **ASSISTANT PROFESSOR or ASSOCIATE PROFESSOR** level for a full-time, tenure-track, nine-month appointment beginning August 2007. As part of a comprehensive new strategic plan to integrate ecological sciences, the Institute seeks an individual who will develop an outstanding externally funded research program in ecosystem ecology. The ideal candidate should have (1) considerable quantitative and modeling expertise, aimed at understanding and forecasting ecosystem dynamics in the context of global and regional environmental change; and (2) a strong commitment to excellence in teaching, which would include a core introductory undergraduate course, participation in graduate courses in their area of specialty, and research that involves M.S. and Ph.D. students.

Applications should be sent by e-mail as a single PDF file that includes a cover letter, curriculum vitae, and statements of research and teaching interests to **e-mail: ecosys@uga.edu.** Applicants should also arrange for three letters of recommendation to be sent as PDF files to this e-mail address. Screening of applications will begin on January 15, 2007. Applications received by that date are assured full consideration with an anticipated start date of August 2007. *The University of Georgia is an Equal Opportunity/Affirmative Action Institution and is committed to having a diverse faculty.*

The U.S. Geological Survey's Patuxent Wildlife Research Center in Laurel, Maryland **(website: http://www.pwrc.usgs.gov/),** seeks a **RESEARCH BIOLOGIST** to concentrate on threatened and endangered species, and work with Patuxent's captive flock of breeding whooping cranes. Experience working with cranes is not required. Research results will contribute to advancements in the conservation of threatened and endangered species through captive breeding, restoration techniques, management of restored populations, or other aspects of the ecology and biology of imperiled species. Specific research expertise for this work may come from a range of organismal and ecological disciplines; one can qualify through the Office of Personnel Management standards as a **PHYSIOLOGIST, ZOOLOGIST, or ECOLOGIST.** Apply online before 21 December 2006, at **website: http://www.usgs.gov/ohr/oars/.** Details on the position and application are provided at the website.

POSITIONS OPEN

ASSISTANT PROFESSOR
Biomolecular Sciences, Fall 2007 (Number C07-075)

Central Connecticut State University (CCSU)'s Department of Biomolecular Sciences seeks applications for a full-time, tenure-track Assistant Professor who will use cellular and molecular approaches to study problems in molecular biology and/or developmental biology.

Qualifications: Candidates must have a Ph.D. in molecular biology or a related field, experience teaching at the undergraduate and graduate (Master's) level, and a demonstrated ability for creative research.

Review of applications will begin January 16, 2007, and will continue until a qualified applicant is selected. To be considered, please submit a cover letter, narrative descriptions of the applicant's teaching and research philosophies, current curriculum vitae, and three letters of reference to: **Biomolecular Sciences Search Committee, c/o Maureen Renock, Central Connecticut State University, 1615 Stanley Street, New Britain, CT 06053 (e-mail: renockmad@ccsu.edu).** Full text of ad can be found at **website: http://www.ccsu.edu/jobs/Jobs_teaching.html.**

CCSU aggressively pursues a program of Equal Employment and Educational Opportunity and Affirmative Action. Members of all underrepresented groups, women, veterans, and persons with disabilities are invited and encouraged to apply.

ASSISTANT PROFESSOR

The Department of Anatomy and Pathology of Joan C. Edwards School of Medicine invites applications for a tenure-track Assistant Professor position to teach human gross anatomy, including laboratory instruction, and to contribute to an evolving graduate program **(website: http://www.bms.marshall.edu).** The successful applicant will have prior experience in teaching gross anatomy, a Ph.D. in a relevant field, and a record of publications. Candidates will be expected to develop and maintain an externally funded research program. Candidates should send an introductory letter stating their teaching experience and philosophy, research accomplishments and future research plans, curriculum vitae, and arrange for at least three letters of reference to be sent to: **Faculty Search Committee for Gross Anatomy, Section of Anatomy, 1542 Spring Valley Drive, Marshall University JCESOM, Huntington, WV 25704-9388.** E-mail submission of applications to **e-mail: rhoten@marshall.edu.** Screening of applications will begin January 5, 2007. *Marshall University is an Equal Opportunity/Affirmative Action/ADA Employer and especially encourages applications from women and members of minority groups.*

MOLECULAR GENETICIST. Tenure-track **ASSISTANT PROFESSOR** in the Biology Department at State University of New York (SUNY), Fredonia. Candidates must have a Ph.D. and postdoctoral experience. Teaching duties are genetics, plus majors and general education courses. A research program that promotes scholarship and involves students is expected. The complete list of application materials is listed on the Department website. Review of completed applications starts on January 15, 2007. Send materials to: **Genetics Search Committee, Department of Biology, State University of New York Fredonia, Fredonia, NY 14063.** See **website: http: www.fredonia.edu/humanresources/faculty.htm** for full ad. *An Affirmative Action/Equal Opportunity Employer, SUNY Fredonia encourages and actively seeks applications from minorities, women, and people with disabilities.*

MARKETPLACE

Receive a **FREE** copy of our New Video
"Primary Cell Culture: Leading Methods and Techniques"
www.cambrex.com/promotion/CB9606

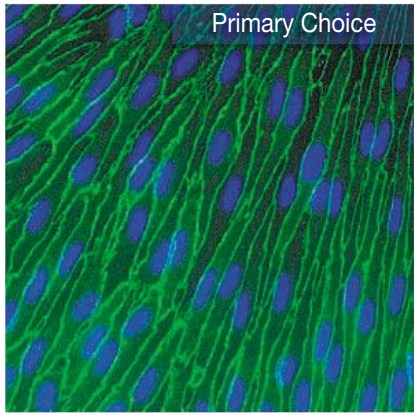

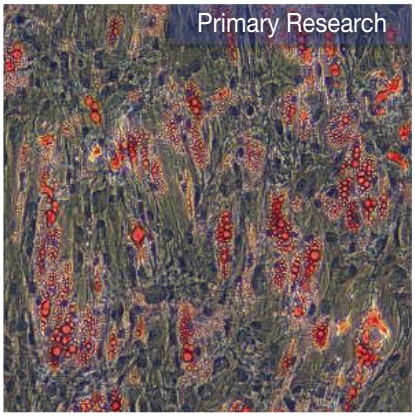

Primary Cells for Pioneering Research

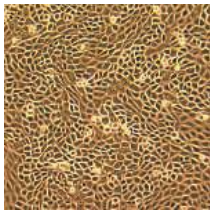

Clonetics® Chemically Defined Keratinocyte Growth Media System

NEW

The Clonetics KGM-CD is:

- Chemically defined – Contains no plant and animal extracts.
- Serum free – Minimize interference from unknown components.
- Optimized for growth and proliferation of human primary keratinocytes.
- Offered in a BulletKit® format – Basal media and required growth supplements.
- Flexible and convenient – Add or subtract components as needed.

Minimize experimental variation and eliminate costly and time-consuming testing or qualifying serum or growth supplements.

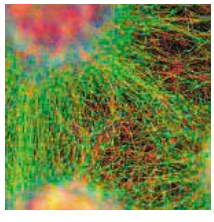

Poietics™ Stem Cells and Media

Human Hematopoietic Progenitor Cells

- Progenitors include CD34+, CD133+, mononuclear cells, and erythroid progenitors isolated from mobilized and normal peripheral blood, bone marrow, and umbilical cord blood.

Human Mesenchymal Stem Cells

- Multipotent, MSC cells and media kits tested and guaranteed for osteogenic, chondrogenic, and adipogenic lineages.

Human Bone, Adipose, and Neural Cells and Media Kits

- Functionally active osteoclast precursors, subcutaneous and visceral preadipocytes, and neural progenitors upon differentiation.
- Media kits for their growth and differentiation.

Cambrex, the source for Clonetics® and Poietics™ Cell Systems, BioWhittaker™ Classical Media, SeaPlaque® and NuSieve® Agarose, and PAGEr® *Precast Gels.*

For more information contact us at:
www.cambrex.com
U.S. **800-638-8174** | Europe **32 (0) 87 32 16 11**

Cambrex Bio Science Walkersville, Inc.
8830 Biggs Ford Road | Walkersville, MD 21793

CAMBREX
Innovation. Experience. Performance.